



UNIVERSIDAD
DE MÁLAGA

Universidad de Málaga
Facultad de Ciencias
Departamento de Química Orgánica

Tesis Doctoral

**SYNTHESIS, FUNCTIONALIZATION AND
CHARACTERIZATION OF DENDRIMERIC STRUCTURES.
BIOIMAGING AND TISSUE REGENERATION
APPLICATIONS**

Programa de Doctorado: Química y Tecnologías Químicas. Materiales y
Nanotecnología

Directores: Dr. Ezequiel Perez-Inestrosa y Dra. Yolanda Vida


Noemi Molina Cabeza

2020





AUTOR: Noemi Molina Cabeza

 <http://orcid.org/0000-0002-8645-3419>

EDITA: Publicaciones y Divulgación Científica. Universidad de Málaga



Esta obra está bajo una licencia de Creative Commons Reconocimiento-NoComercial-SinObraDerivada 4.0 Internacional:

<http://creativecommons.org/licenses/by-nc-nd/4.0/legalcode>

Cualquier parte de esta obra se puede reproducir sin autorización pero con el reconocimiento y atribución de los autores.

No se puede hacer uso comercial de la obra y no se puede alterar, transformar o hacer obras derivadas.

Esta Tesis Doctoral está depositada en el Repositorio Institucional de la Universidad de Málaga (RIUMA): riuma.uma.es



UNIVERSIDAD DE MÁLAGA

Universidad de Málaga

Facultad de Ciencias

Departamento de

Química Orgánica



Centro Andaluz de

Nanomedicina y

Biotecnología

**SYNTHESIS, FUNCTIONALIZATION AND
CHARACTERIZATION OF DENDRIMERIC STRUCTURES.
BIOIMAGING AND TISSUE REGENERATION
APPLICATIONS.**

Síntesis, funcionalización y caracterización de estructuras
dendriméricas. Aplicaciones en bioimagen y regeneración tisular.

Doctoral thesis presented by

Noemí Molina Cabeza

in order to apply to the Doctor of Philosophy in Chemistry

Malaga, 2020





D. Ezequiel Pérez de Inestrosa Villatoro, Catedrático de Química Orgánica y **Dña. Yolanda Vida Pol**, Profesora Titular del Departamento de Química Orgánica de la Universidad de Málaga

CERTIFICAN:

Que la memoria adjunta, titulada “SYNTHESIS, FUNCTIONALIZATION AND CHARACTERIZATION OF DENDRIMERIC STRUCTURES. BIOIMAGING AND TISSUE REGENERATION APPLICATIONS”, que para optar al grado de Doctora (Doctorado Internacional) presenta Noemí Molina Cabeza, ha sido realizada bajo nuestra dirección, en los laboratorios del Departamento de Química Orgánica de la Universidad de Málaga y en los laboratorios del Centro Andaluz de Nanomedicina y Biotecnología (BIONAND).

Considerando que constituye un trabajo de Tesis Doctoral, autorizamos su presentación en la Facultad de Ciencias de la Universidad de Málaga.

Y para que conste, firmamos el presente certificado en Málaga, a marzo de 2020.

Fdo. Dr. Ezequiel Pérez-Inestrosa

Fdo. Dra. Yolanda Vida



Este trabajo no habría sido posible sin la dirección de los profesores Yolanda Vida y Ezequiel Perez-Inestrosa. Desde que comencé a trabajar en el grupo (allá por 2011), primero haciendo un trabajo dirigido, después con una beca de colaboración, durante el máster y finalmente realizando la tesis doctoral, habéis sido unos magníficos profesores a los que siempre he podido acudir en busca de ayuda. Sin duda, sois las figuras que más me han influenciado a la hora de convertirme en investigadora.

Casi igual de importante en la realización de este trabajo han sido los miembros del Laboratorio de Dendrímeros Biomiméticos y Fotónica, tanto los que forman ahora el grupo como los que han pasado por él: Paco, Dani, José María, Antonio, Isa, Pablo, Nekane, Anjara, Carlos, Desi, Violeta, Vladimir y Elsa. En particular, quiero resaltar y agradecer el trabajo del profesor Paco Nájera en los estudios de Simulación de Dinámica Molecular. Siempre dispuestos a echar una mano, han hecho que todos estos años de trabajo hayan sido mucho más llevaderos. Gracias a vosotros me llevo innumerables buenos momentos tanto fuera como dentro del laboratorio. Por último, no puedo terminar este párrafo sin darle las gracias en especial a Anjara, experta en apoyos técnicos y morales, cuyos consejos siempre busco.

Me gustaría agradecer también a los miembros de los grupos de investigación con los que hemos colaborado durante la realización de esta tesis. Al grupo de Cristian Strassert, por acogerme durante tres meses en su laboratorio en introducirme a la química de complejos de platino, y en especial a Marvin con quien trabajé codo con codo durante mi estancia. Al grupo de José Becerra, en particular a Leonor y Ana, por todo el trabajo realizado en materia de regeneración tisular. También quiero agradecer el trabajo del grupo de José María Pomares, especialmente de Juan Antonio, en el estudio de bacterias incubadas con compuestos sintetizados a lo largo de esta tesis y a Luis Díaz y Diego Romero del Departamento de Microbiología, encargados de los estudios de crecimiento de bacterias.

Al Departamento de Química Orgánica de la Universidad de Málaga, en especial a sus profesores, por la docencia recibida durante todos estos años y que sin duda ha contribuido a mi interés por la Química Orgánica.

Cualquier trabajo de investigación necesita de infraestructuras y apoyo técnico, es por eso por lo que quiero agradecer la gran labor realizada por todo el personal de Bionand, tanto técnicos, como administración y mantenimiento. En especial me gustaría dar las gracias a Marisa, John, Juan Félix, Carmen y María, de la unidad de Nanoimagen, por su ayuda en técnicas de Resonancia Magnética y Microscopía. También quiero mostrar mis agradecimientos al personal de los Servicios Centrales de Apoyo a la Investigación de la Universidad de Málaga, en particular a los servicios de Espectrometría de Masas, Espectroscopía XPS y Espectroscopías Electrónicas. Así como al Ministerio de Educación, Cultura y Deporte por la concesión de una beca FPU para la realización de esta tesis.

Quiero dar las gracias a todas aquellas personas que, aunque no han participado de manera directa en este proyecto, han sido parte de mi día a día durante esta etapa, en especial a Maribel, Amene y Patri.

Por último, me dirijo a las personas más importantes, mis padres y mi hermana. Gracias por vuestra paciencia, vuestros apoyos y consejos, todo lo que consiga es gracias a vosotros.

A mis padres,

A mi hermana.

List of Abbreviations

^1H NMR	Proton nuclear magnetic resonance
APTMS	3-Aminopropyltrimetoxysilane
AXO	Amoxicilloyl
BAPAD	2,2-Bis(aminoalkyl)propanamide Dendrimer
Bis-MPA	2,2-bis(methylol)-propionic acid
BnBr	Benzyl bromide
Boc	<i>Tert</i> -butoxycarbonyl
CDI	1,1'-Carbonyldiimidazole
CPP	Calcium phosphate phases
CuAAC	Copper-Assisted Azide-Alkyne Cycloaddition
DCC	Dicyclohexylcarbodiimide
DCM	Dichloromethane
DCU	Dicyclohexylurea
DIC	Diisopropylcarbodiimide
DIPEA	<i>N,N</i> -Diisopropylethylamine
DMAP	4-(Dimethylamino)pyridine
DMF	Dimethylformamide
DMSO	Dimethyl sulfoxide
DOSY	Diffusion-Ordered Spectroscopy
ECAD	Electrochemically assisted deposition
ECM	Extracellular matrix
EDA	Ethylenediamine
EDCI	<i>N</i> -(3-Dimethylaminopropyl)- <i>N'</i> -ethylcarbodiimide hydrochloride
EDX	Energy-dispersive X-ray spectroscopy
EtOAc	Ethyl acetate
EtOH	Ethanol
FLIM	Fluorescence lifetime imaging microscopy
HA	Hydroxyapatite

List of Abbreviations

HSA	Human serum albumin
HOBt	1-Hydroxybenzotriazole hydrate
HSQC	Heteronuclear single-quantum correlation spectroscopy
ILCT	Intraligand charge transfer
LLCT	Ligand-to-ligand charge transfer
LMCT	Ligand-to-metal charge transfer
LMMCT	Ligand-to-metal-metal charge transfer
MeCN	Acetonitrile
MeOH	Methanol
MLCT	Metal-to-ligand charge transfer
MLLCT	Metal-to-ligand-ligand charge transfer
MMLCT	Metal-metal-to-ligand charge transfer
MSCs	Mesenchymal stem cells
NHS	<i>N</i> -Hydroxysuccinimide
OPE	One-photon excitation
PAMAM	Polyamidoamine dendrimers
PLGA	Poly(lactic-co-glycolic acid)
PLIM	Phosphorescence lifetime imaging microscopy
PLL	Poly-L-lysine
POPAM	Polypropylenamine
PPI	Poly(propylene imine)
R_f	Retention factor
RGD	Arginine-glycine-aspartic acid
SBF	Simulated body fluid
SPAAC	Strain Promoted Azide-Alkyne Cycloaddition
TBTA	Tris(benzyltriazolylmethyl)amine
TEC	Thiol-Ene Click Reaction
TEG	Triethylene glycol
THF	Tetrahydrofuran

List of Abbreviations

THPTA	Tris(3-hydroxypropyltriazolylmethyl)amine
TPA	Two-photon absorption
TPE	Two-photon excitation
TPEF	Two-photon-excited fluorescence
TYC	Thiol-Yne Click Reaction

TABLE OF CONTENTS

CHAPTER I. INTRODUCTION	19
I.1 Definitions and General Structure	21
I.2 Historical Background	23
I.3 Synthesis of Dendrimers	31
<i>I.3.1 Divergent Synthesis</i>	32
<i>I.3.2 Convergent Synthesis</i>	33
I.3.3 New approaches	35
I.4 Peptide Chemistry Applied to the Synthesis of Dendrimers	37
<i>I.4.1 Amino Protection/Deprotection Strategy</i>	38
<i>I.4.2 Carboxylic Acid Protection/Deprotection Strategy</i>	38
<i>I.4.3 Amide-forming Reactions</i>	38
I.5 Click Chemistry Applied to Dendrimer Synthesis	39
<i>I.5.1 Copper-assisted azide-alkyne cycloaddition (CuAAC)</i>	40
<i>I.5.2 The Thiol-Ene (TEC) and Thiol-Yne (TYC) Click Reactions</i>	40
<i>I.5.3 Synthesis of Dendrimers via Click Chemistry</i>	40
I.6 Applications of Dendrimers	42
<i>I.6.1 Drug Delivery</i>	43
<i>I.6.2 Gene Delivery</i>	44
<i>I.6.3 Imaging</i>	44
<i>I.6.4 Immunoassays</i>	45
CHAPTER II. OBJECTIVES	47
CHAPTER III. SYNTHESIS OF NEW AMINO TERMINAL DENDRITIC STRUCTURES	51
III.1 Introduction	53
III.2 Synthesis of Amino Terminal Dendrimers by Click Chemistry	56
<i>III.2.1 Synthesis of the Azide Building Block (2)</i>	58
<i>III.2.1.1 Synthesis of 3,3'-diazidopivalic acid (1)</i>	58
<i>III.2.1.2 Synthesis of Benzyl 3,3'-diazidopivaloate (2)</i>	59
<i>III.2.2 Synthesis of dG1</i>	60
<i>III.2.2.1 Synthesis of Benzyl 3,3'-diaminopivaloate (3)</i>	60
<i>III.2.2.2 Synthesis of Benzyl 3,3'-bis(tert-butoxycarbonyl) aminopivaloate (4)</i>	61
<i>III.2.2.3 Synthesis of 3,3'-bis(tert-butoxycarbonyl)aminopivalic Acid (5)</i>	62
<i>III.2.2.4 Synthesis of N-propargil-3,3'-bis(tert-butoxycarbonyl)amino pivalamide, dG1</i>	63
<i>III.2.3 Synthesis of dG2</i>	64
<i>III.2.3.1 Synthesis of dG2-CO₂Bn</i>	66
<i>III.2.3.2 Synthesis of dG2-CO₂H</i>	68
<i>III.2.3.3 Synthesis of dG2</i>	70



III.2.4 Synthesis of dG3	71
III.2.4.1 Synthesis of dG3-CO₂Bn	72
III.2.4.2 Synthesis of dG3-CO₂H	77
III.2.4.3 Synthesis of dG3	79
III.2.5 Synthesis of a Family of Dendrimers, G1_{EDA}NH₂ , G2_{EDA}NH₂ and G3_{EDA}NH₂ .	82
III.2.5.1 Synthesis of 1,2-diazidoethane (6)	85
III.2.5.2 Synthesis of G1_{EDA}NHBoc	86
III.2.5.3 Synthesis of G1_{EDA}NH₂	88
III.2.5.4 Synthesis of G2_{EDA}NHBoc	88
III.2.5.5 Synthesis of G2_{EDA}NH₂	91
III.2.5.6 Synthesis of G3_{EDA}NHBoc	91
III.2.5.7 Synthesis of G3_{EDA}NH₂	94
III.2.6 Synthesis of Dendrimers with Aromatic Cores, G3_{3AB}NH₂ and G3_{4AB}NH₂	99
III.2.6.1 Synthesis of 1,3,5-tris(azidomethyl)benzene (7)	99
III.2.6.2 Synthesis of G3_{3AB}NHBoc	99
III.2.6.3 Synthesis of G3_{3AB}NH₂	102
III.2.6.4 Synthesis of 1,2,4,5-tetrakis(azidomethyl)benzene (8)	104
III.2.6.5 Synthesis of G3_{4AB}NHBoc	105
III.2.7 Synthesis of a Fluorescent Dendrimer, G3_{Naph}NH₂	106
III.2.7.1 Synthesis of N-(3-azidopropyl)-4-((3-azidopropyl)amino)-1,8-naphthalimide (10).	106
III.2.7.2 Synthesis of G3_{Naph}NHBoc	108
III.2.7.3 Synthesis of G3_{Naph}NH₂	111
III.2.8 Mass spectroscopy	113
III.2.9 Electrophoresis	113
III.2.10 DOSY Experiments	114
III.2.11 Molecular Dynamic Simulations	117
III.2.12 Photophysical characterization of G3_{Naph}NH₂	125
III.2.12.1 Studies with <i>E. coli</i> Bacteria (gram-negative)	127
III.2.12.2 Studies with <i>P. subtilis</i> Bacteria (gram-positive)	129
III.2.12.3 Bactericidal test	129
CHAPTER IV. SYNTHESIS OF PLATINUM-DOPED DENDRITIC STRUCTURES	133
IV.1 Introduction	135
IV.2 Synthesis of a water-soluble platinum complex (21)	138
V.2.1 Synthesis of the dendritic structure (18)	142

IV.2.2 Synthesis of the platinum-doped dendritic structure (21)	148
IV.3 Photophysical characterization	152
IV.3.1 Two Photon Excitation Studies	156
IV.4 Biological studies	157
IV.4.1 Studies with <i>E. coli</i> Bacteria (gram-negative)	158
IV.4.2 Studies with <i>P. subtilis</i> Bacteria (gram-positive)	161
IV.4.3 Bactericidal test	162
CHAPTER V. FUNCTIONALIZATION OF TITANIUM SURFACES WITH RGD-DENDRITIC STRUCTURES	165
V.1 Introduction	167
V.2 Functionalization of the Titanium disks	173
V.3 Functionalization of the titanium disks with the cell recognition pattern RGD	176
V.4. Monitorization of the derivatization process	178
V.5 Essays of RGD-functionalized titanium surfaces with pre-osteoblastic cells	180
CHAPTER VI. CONCLUSIONS	183
CHAPTER VII. EXPERIMENTAL SECTION	187
VII.1 Reagents, solvents and analytical techniques	189
VII.2 General Procedures	194
VII.2.1 General procedure for click reactions	194
VII.2.2 General procedure for deprotection of amines	194
VII.2.3 Quantitation of Free Primary Amine Groups (Ninhydrin Test)	194
VII.3 Synthesis of new dendritic structures <i>via click</i> chemistry	195
VII.4 Synthesis of platinum-doped dendritic structure	220
VII.5 Functionalization of titanium surfaces	228
CHAPTER VIII. REFERENCES	233
APPENDIX. SPECTRA	257
DOSY spectra	317
RESUMEN	323

CHAPTER I

INTRODUCTION

I.1 Definitions and General Structure

The term ‘dendrimer’ comes from the Greek words *δένδρον* (dendron) which means "tree" and *μέρος* (méros) that translates into “part”. The name is a clear reference to its geometry, resembling the branches of a tree. They possess a fractal geometry, as many other structures found in nature.

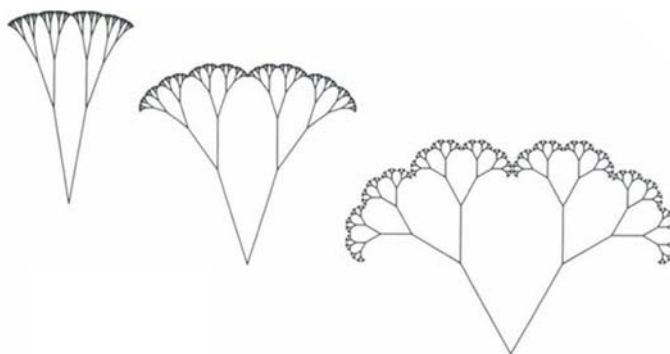


Figure 1. Fractal umbrella trees.¹

Dendrimers can be defined as polymeric molecules with highly regular and branched structures that generally display properties characteristic of monodisperse compounds.² The main difference with other highly branched polymers is their controlled synthesis, in a step by step iterative fashion, resulting in defect-free structures. However, the synthesis of polymers normally occurs in one polymerization step.³

Dendrimers are defined by three components: a multi-functional central core, the branches that grow from the central unit, and an exterior surface with functional end groups. Each subsequent step of growing a new layer represents a new generation of the dendrimer. The branched structures linked in the form of segments to the central unit are termed dendrons (Figure 2).

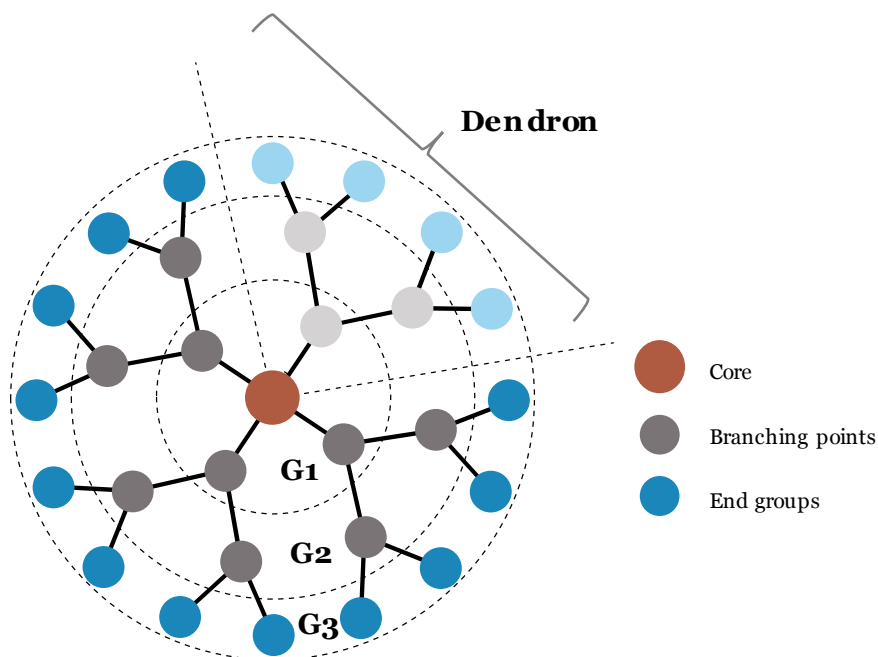


Figure 2. Schematic dendrimer scaffold with four dendrons.

The core unit can be an atom or a molecule. The number of branches that can be bonded to it will influence the multiplicity (and size) of the final structure. It can also exercise a function by itself. A remarkable example is the metallodendrimers in which a ferrocene as core unit confers redox properties to the compound.⁴

The flexibility/rigidity parameters of a dendrimer are conditioned by the choice of the branching units and the end groups. POPAM (polypropylenamine)⁵ and PAMAM⁶ dendrimers can be set as an example of flexible dendrimeric structure, while dendrimers with polyarene⁷ and phenylacetylene⁸ based branching units present a high rigidity.

The end groups are on the periphery of the dendrimer. The number of these groups is determined by the dendrimer generation and the number of reactive groups of the core and branching units. By selecting the proper groups,

properties such as stability, solubility or viscosity can be modified and molecules with specific characteristics, such as biological activity, can be attached to the surface of the dendrimer.

Above a certain generation, the perfect structure of the dendrimer is no longer possible since there is no space for the new terminal groups. The subsequent growing reactions will be hindered by steric effects, resulting in structural defects and polydisperse molecules. This phenomenon is also known as *starburst limit effect*.⁹

There is a gradual transition from an open structure of lower generations of dendrimers to an almost globular form of the higher generations. This phenomenon leads to a lower viscosity of the dendrimers in solution than expected, since their viscosity doesn't increase linearly with molar mass but reaches a maximum and then decreases again at higher generations (*dendrimer effect*).²

I.2 Historical Background

The origins of interest in three dimensional highly branched polymers can be traced back to the network theory of Flory^{9,10,11} and Stockmayer.^{13,14} However, the synthesis of a potentially perpetual multi-branched compound by iterative growth steps was first reported by Vögtle in 1978.¹⁵ It involved iterative reactions of two-fold Michael addition of an amine with acrylonitrile, leading to the dinitrile, and the subsequent reduction of the nitrile groups to obtain the corresponding terminal diamine. The repetition of these two steps of Michael addition and reduction was named *cascade synthesis* and the compounds thus obtained *cascade molecules* (Figure 3). However, this methodology resulted in low yields and product isolation difficulties. It wasn't until the nineties that two research groups presented independently an improved approach to prepare poly(propyleneimine) (PPI) dendrimers.^{16,17}

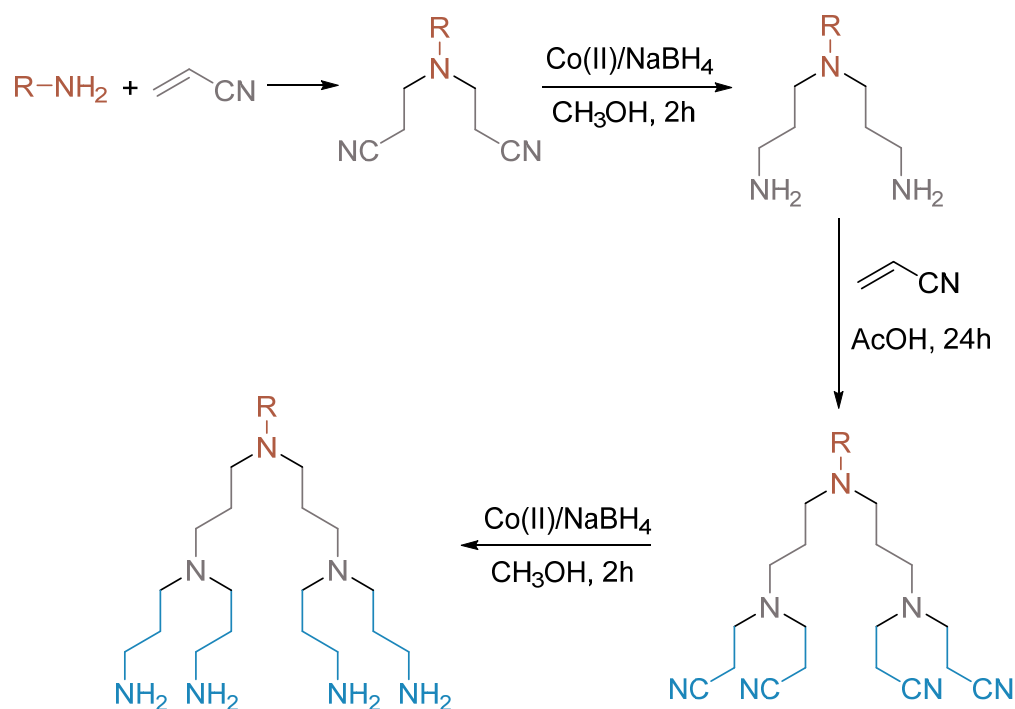


Figure 3. Synthesis of *cascade molecules*.

In 1981, Denkenwalter patented the synthesis of polylysine dendrimers using iterative protection/deprotection steps of amino groups and the formation of amide bonds.¹⁸ Due to the structure of lysine, these molecules possessed unsymmetrical branch lengths (Figure 4).

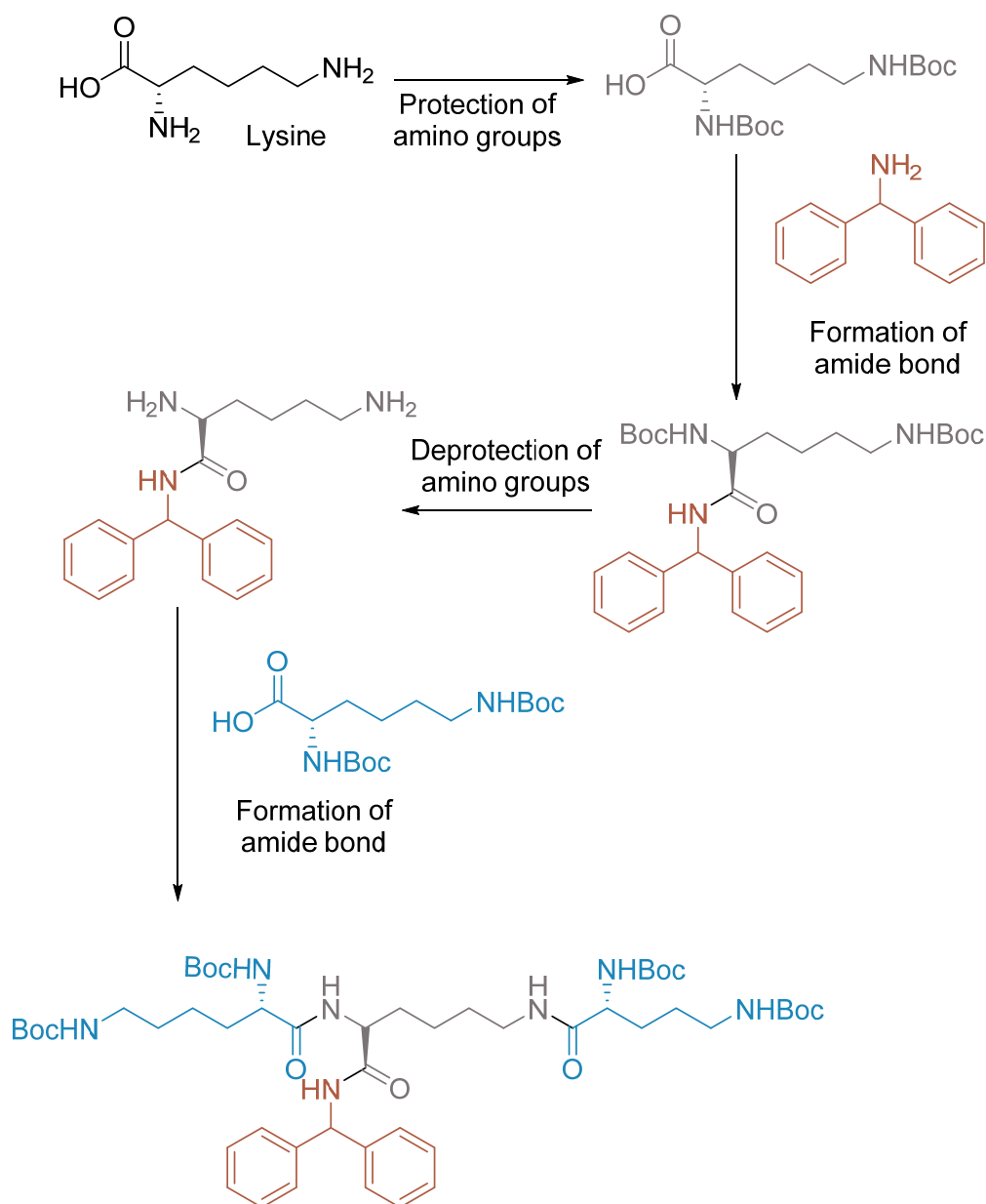


Figure 4. Synthesis of polylysine dendrimers.

In 1985 Tomalia described the synthesis of macromolecular poly(amidoamines) (PAMAM) dendrimers, which he designated as *starburst dendrimers*.^{6,19} Following a similar methodology to Vögtle,¹⁵ this synthesis also relies in the Michael addition (methyl acrylate instead) but the difference lies in the next step of amidation (Figure 5). These amide bonds confer to the molecule solubility in polar solvents such as dichloromethane and short-chain alcohols and make these structures stable to hydrolysis. The ester stages were designated by Tomalia Group as generation 0.5, generation 1.5, and so on.⁶

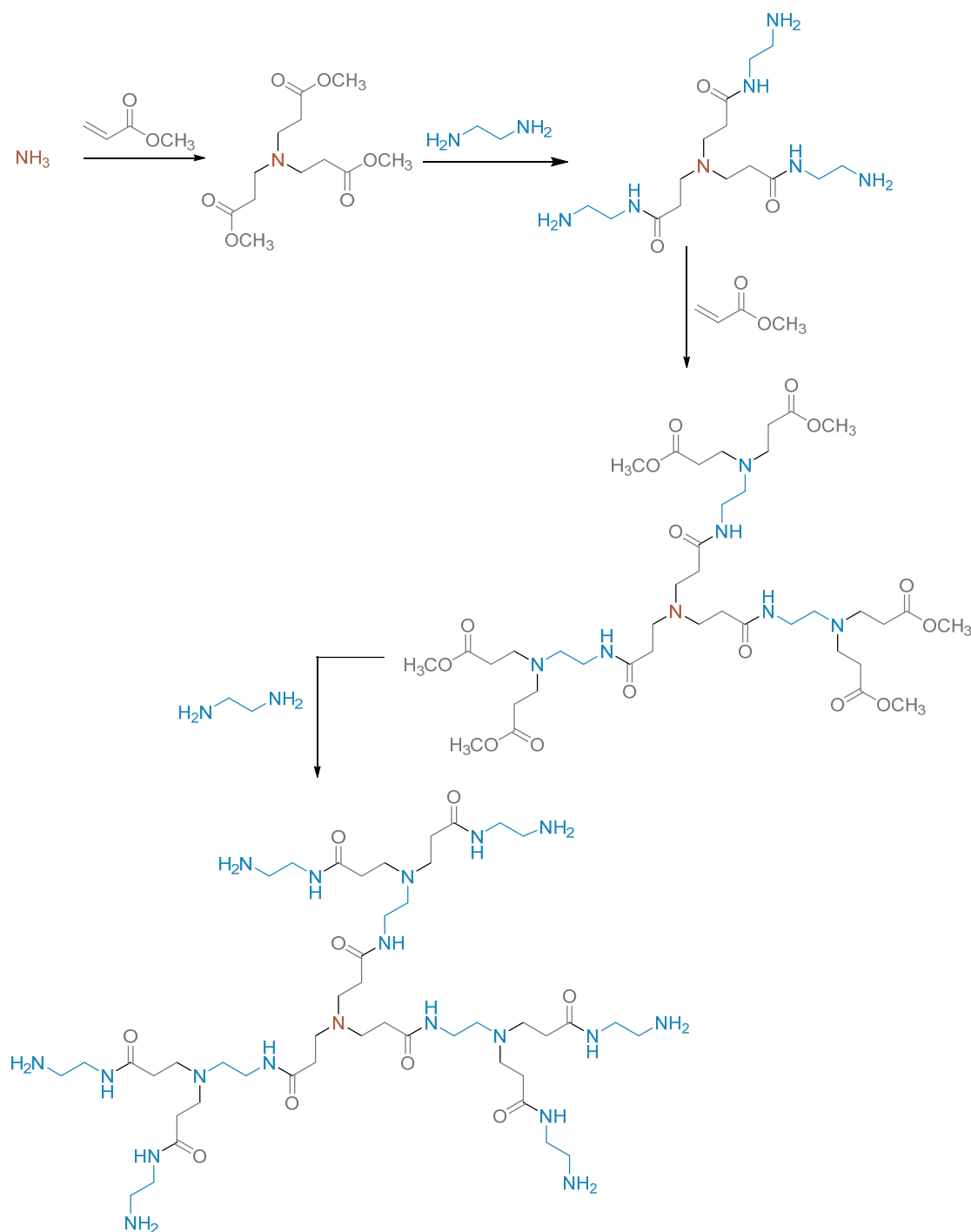


Figure 5. Synthesis of PAMAM dendrimer.

In the same year, Newkome published a divergent synthesis to *arborol systems* (named after the Latin word *arbor* which means ‘tree’). This approach consists of two steps, the treatment of an alkyl halide with the sodium anion of triethyl methanetricarboxylate, which results in a polyester, and the subsequent

amidation reaction with tris(hydroxymethyl)aminomethane to produce the dendritic macromolecules (Figure 6).²⁰

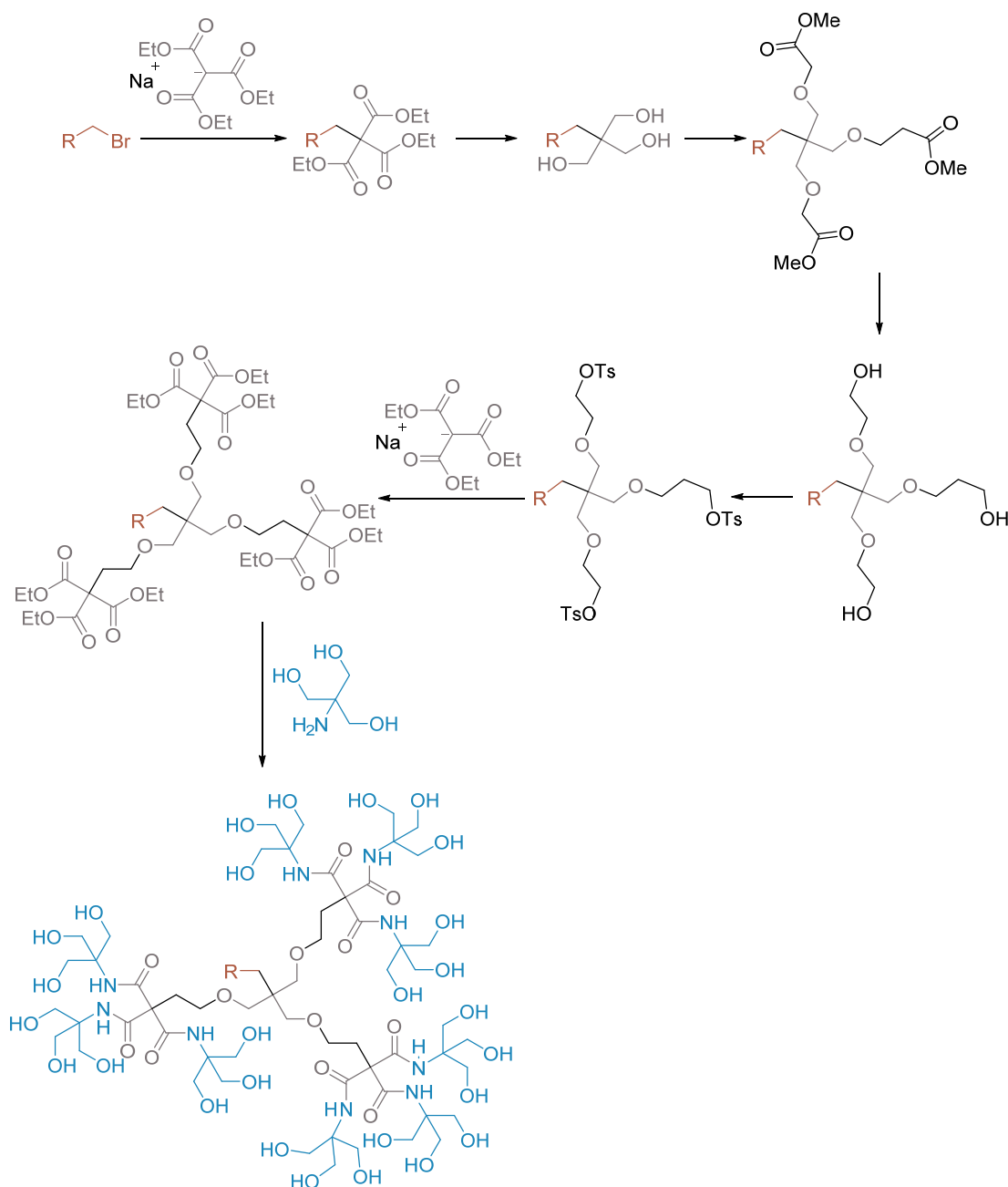
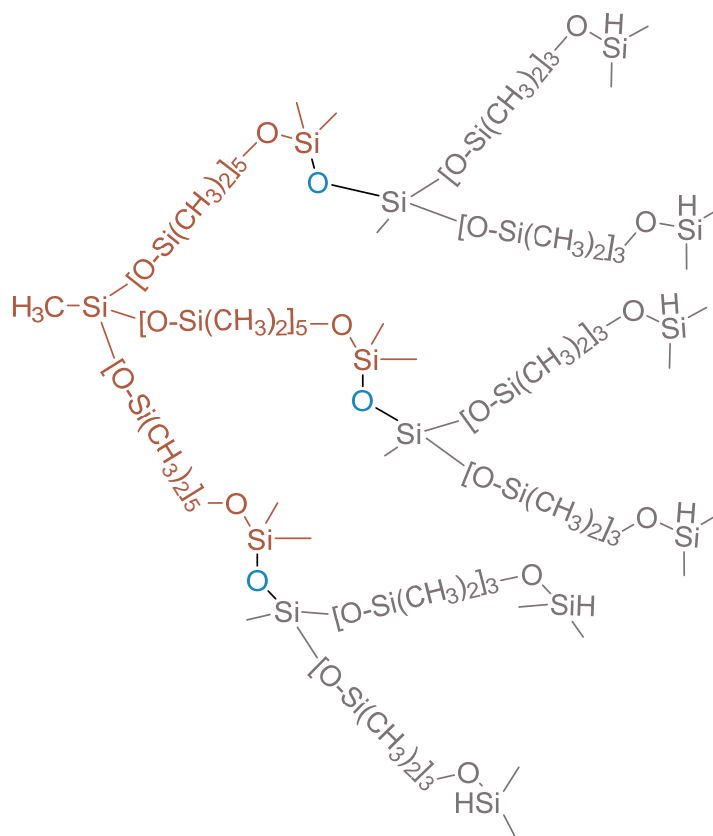


Figure 6. Synthesis of arborols.

At the beginning of 1990, Tomalia's exhaustive review 'Starburst dendrimers: molecular-level control size, shape, surface chemistry, topology and flexibility from atoms to macroscopic matter' popularized the basic concepts of dendrimer chemistry.²¹ In the same year, Fréchet and Hawker published the 'Convergent synthesis' approach²² which would broaden the field of dendrimer

synthesis. In this decade, also notable contributions are the double stage convergent growth schemes²³ and innovative supramolecular self-assembly schemes^{24,25} for synthesizing supramolecular dendrimers. In the same decade, the creation of new dendrimers with different heteroatoms were reported, expanding thus the horizon of synthesis for these structures. In 1990 the first synthesis of silicone-based dendrimers was published²⁶ and in 1994 the first synthesis of neutral phosphorus-based dendrimers was reported.²⁷

a)



b)

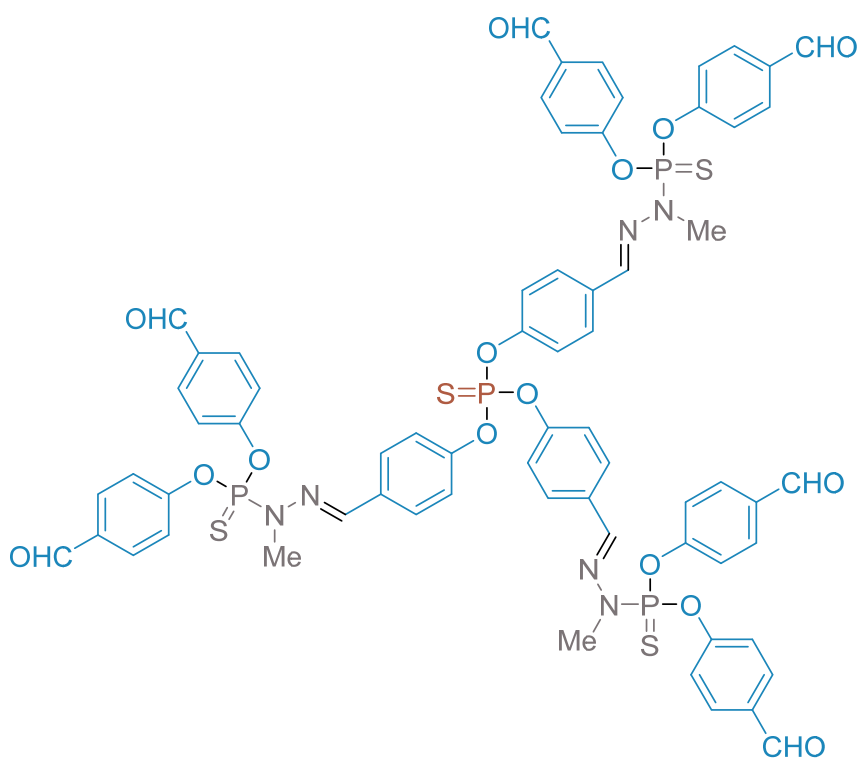


Figure 7. Synthesis of **a)** Silicone dendrimers and **b)** Phosphorus dendrimers.

Since then, a variety of major new dendrimers construction trends has been reported during the past decade.²⁸ Worth noticing are the development of new synthesis strategies based on *click* chemistry (see section I.4), the hybridization of dendrimeric architectures with inorganic nano-building blocks²⁹ and the synthesis of amphiphilic dendrons³⁰ which opened new research areas in the synthesis of *Janus*-type dendrimers (dendrimers constituted of two dendrimeric wedges and terminated by two different functionalities).

Our group has published in 2015 the synthesis of a new kind of polyamide dendrimers, coined BAPAD (Bis-Aminoalkyl-PolyAmide-Dendrimers).³¹ These architectures are based on the iterative use of 3,3'-diazidopivalic acid as building block. The subsequent reduction of the azides to amine groups is followed by a growth step involving the condensation of these amines with two units of building block through the formation of amide bonds (Figure 8).

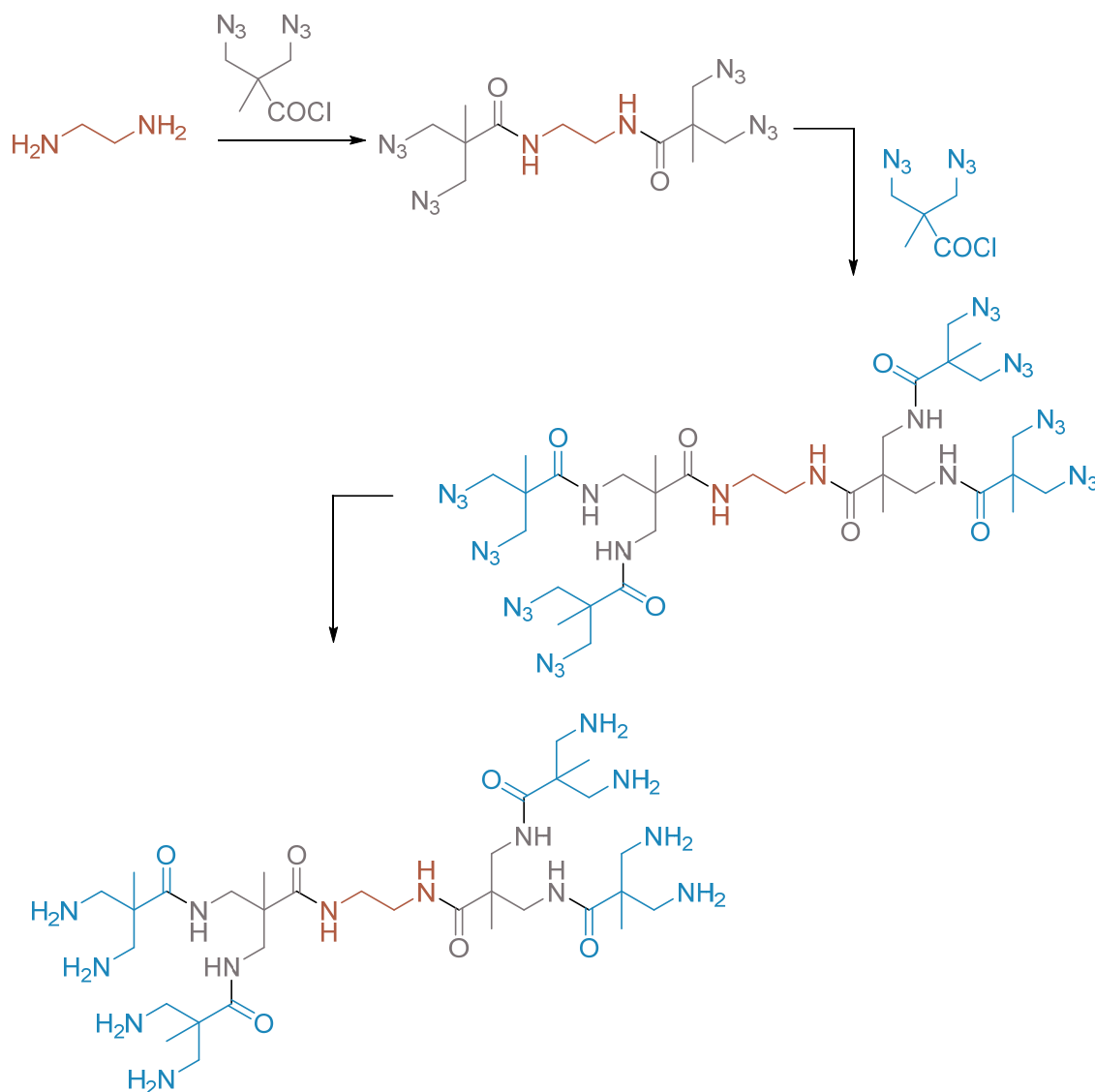


Figure 8. Synthesis of BAPAD dendrimers.

I.3 Synthesis of Dendrimers

Dendrimers are normally synthesized using an iterative sequence of reaction steps that will create different 'layers' or generations. Historically, there are two main approaches for the synthesis of dendrimeric architectures, namely divergent and convergent synthesis.

I.3.1 Divergent Synthesis

According to this strategy, the dendrimer is built from the core outwards *via* the subsequent addition of monomer building blocks (Figure 9). When using this methodology, polyfunctional cores react with monomers. The most widely used monomers belong to the group AB_n ($n \geq 2$), where A and B represent two different functional groups. In order to accomplish a controlled growth, A must be a reactive functional group whereas B must be a non-reactive or protected group. The number of B groups present in the monomer will determine the ramifications of the final dendrimer. Among the different monomers, AB_2 type is the most commonly used.^{32,33} When AB_n is coupled with the polyfunctional core (C_x), a number of x covalent bonds are generated. Thus, a first-generation dendrimer is formed. The second generation is obtained after the deprotection of the B groups and the subsequent coupling of these with new monomers AB_n (through the reaction with A). Iterative steps of deprotection/coupling will provide higher generations of dendrimers.

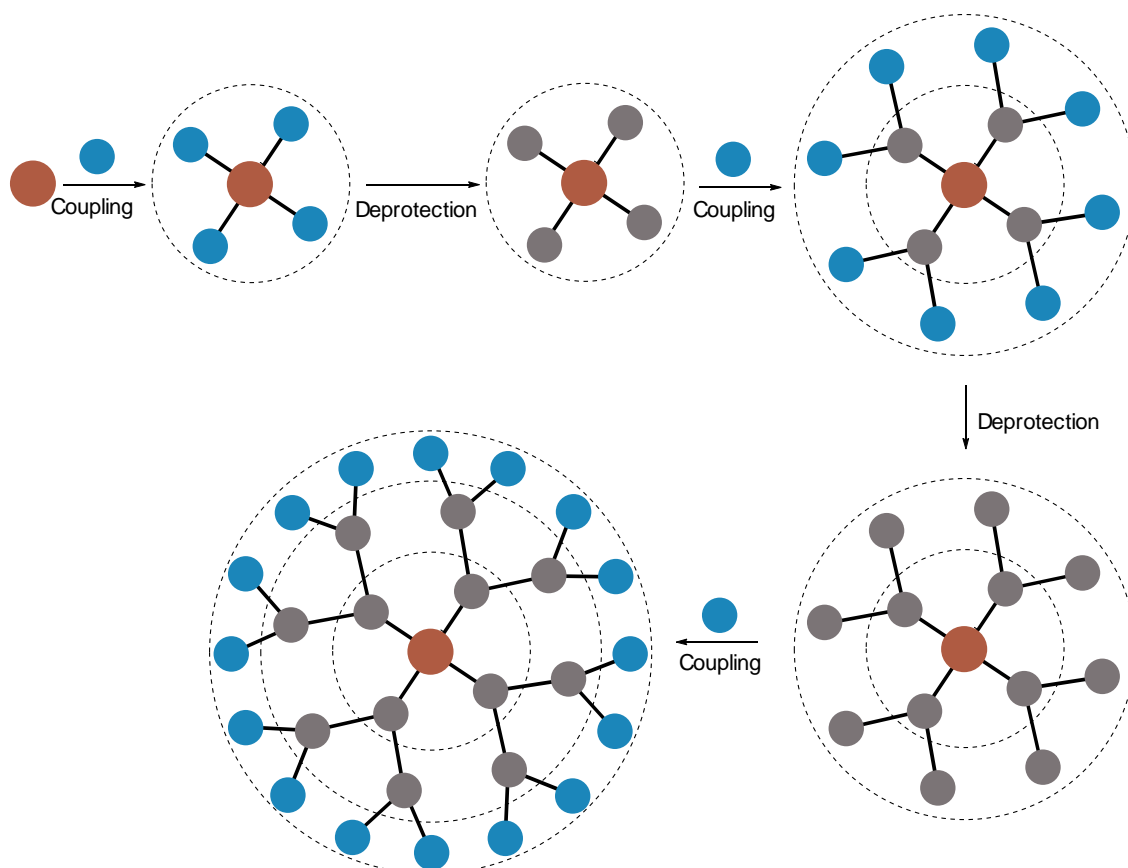


Figure 9. Example of divergent synthesis of dendrimers using AB_2 monomers.

The divergent approach was used in the first published works of synthesis of dendrimers. It was first reported in 1978 in the synthesis of *cascade molecules*¹⁵ and was also used in the synthesis of PAMAM⁶ and polylysine dendrimers.¹⁸ Divergent methodology provides good results, making possible the synthesis of dendrimeric structures at high scale and, in some cases, the automatization of the iterative steps. Moreover, using this strategy, different generations can be synthesized, since the growth reaction sequence can be halted at any point.

However, as the generation increases, so does the number of formed bonds in only one reaction step, which can translate in the appearance of defects in the structure (*starburst limit effect*).¹⁹ Moreover, in order to enforce the complete growth of the dendrimer, an excess of monomer needs to be used which can hinder the purification process and make them tedious and time-consuming. Normally, after each growth step a purification process is needed in order to remove by-products, monomer excess and defect dendrimers. The removal of the latter can become extremely difficult due to the structural similarity with the desired compound.

Due to these limitations, it has been reported that for the fifth generation of PAMAM dendrimer, only 29% of the dendrimer will be defect-free.³⁴ In the case of BAPAD dendrimers, the higher generation obtained was a dendrimer of third generation with 16 peripheral amino groups.³¹ This can be explained by the decrease in the reactivity of the azido groups caused by the backfolding of these surface groups. This effect has been previously observed, being more pronounced in those dendrimers synthesized using a divergent methodology.³⁵

1.3.2 Convergent Synthesis

In the convergent approach, first introduced by Fréchet,²² the end groups are the starting point of the synthesis and the dendrimer is synthesized from the periphery inwards. Following this methodology, dendrons are synthesized and later coupled to a polyfunctional core to obtain the corresponding dendrimer. During the dendron synthesis, monomers AB_n are employed. In contrast with the divergent approach, in this case, B represents the reactive groups whereas A is a protected functional group. Iterative growth steps lead to larger dendrons with a

Unlike the divergent methodology where the number of bonds to be formed increases with each generation, this strategy only involves a constant number of coupling processes at each stage of the synthesis and they can be carried out with only a slight excess of monomer.³⁶ Among the most valued advantages of this approach are the ability to selectively functionalize the focal point and to synthesize asymmetrical dendrimers through the coupling of different dendrons to the core. When coupling the dendrons to the core unit to obtain the final dendrimer, there can be functional sites of the central unit that doesn't react with the dendrons, giving as result defect dendrimers. However, the marked size difference between the final dendrimer and the partially functionalized compounds makes purifications step notably easier than in divergent methodologies.³⁷

However, this methodology is used to synthesize relatively low generation dendrimers since steric hindrance can lead to structural defects when attaching voluminous dendrons to a high-multifunctional core.³⁸ For that reason, it



requires highly effective coupling reactions and sometimes even the use of a spacer in the dendron core.

1.3.3 New approaches

New methods that combine both traditional synthetic approaches have been developed since the 1990s in order to minimize the steps to obtain higher generations.

The hypermonomer strategy, first used by Fréchet,³⁹ employs monomers with more functional groups than the traditional AB_2 , typically AB_3 , AB_4 or AB_8 (Figure 11). Since each monomer possesses more functional groups, the number of steps needed to reach a certain number of peripheral groups decreases. However, normally this hypermonomers are low generation dendrons whose synthesis requires several steps, making the whole synthetic route laborious.

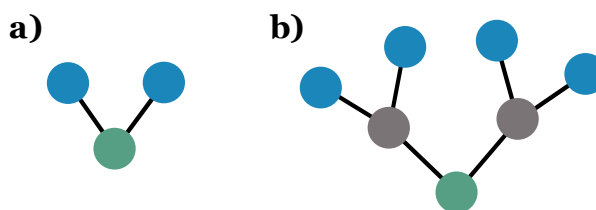


Figure 11. a) Conventional monomer (AB_2); **b)** Hypermonomer (AB_4).

Using the double stage convergent approach, the focal points of the monodendrons are coupled in a divergent manner to the periphery of a low generation dendrimer or hypercore prepared by convergent or divergent growth (Figure 12).⁴⁰ This approach has not been extensively used because the dendrons and hypercore are usually synthesized using conventional methods which can make the whole process tedious.

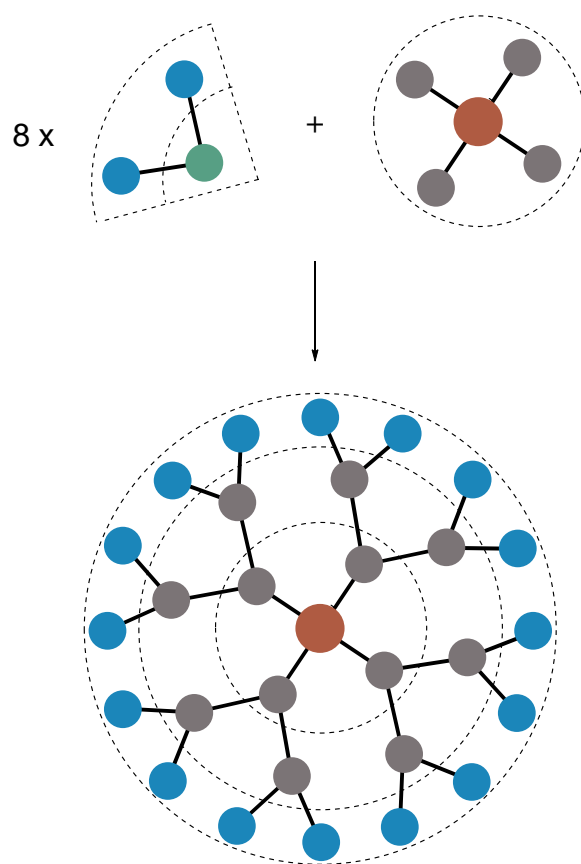


Figure 12. Example of double stage convergent synthesis of dendrimers using AB_2 monomers.

The double exponential growth strategy is based on the synthesis of dendrons of low generation with both, the peripheral group and the focal point, protected. After the selective deprotection of one of these groups, these low generation dendrons are coupled together to obtain higher generations of fully protected dendrons. The final steps include the activation of the focal point, the coupling with the core and the subsequent deprotection of the peripheral groups. This methodology was first employed in 1995⁴¹ and was fully developed in the synthesis of 2,2-bis(methylol)-propionic acid (bis-MPA) dendrimers.⁴²

Recently, great efforts have been carried out in the synthesis of new types of dendrimers that possess different end groups and monomers in their structure. These new macromolecules can be grouped according to their structural characteristics into layer-block dendrimers, segment-block dendrimers or surface-block dendrimers.^{43–47} Belonging to the last two blocks, Janus dendrimers conform a group of dendrimers that possess at least two different functionalities in their surface. This type of dendrimers with multifunctional

surfaces has arisen great interest due to the possibility of combining different properties in one single structure.

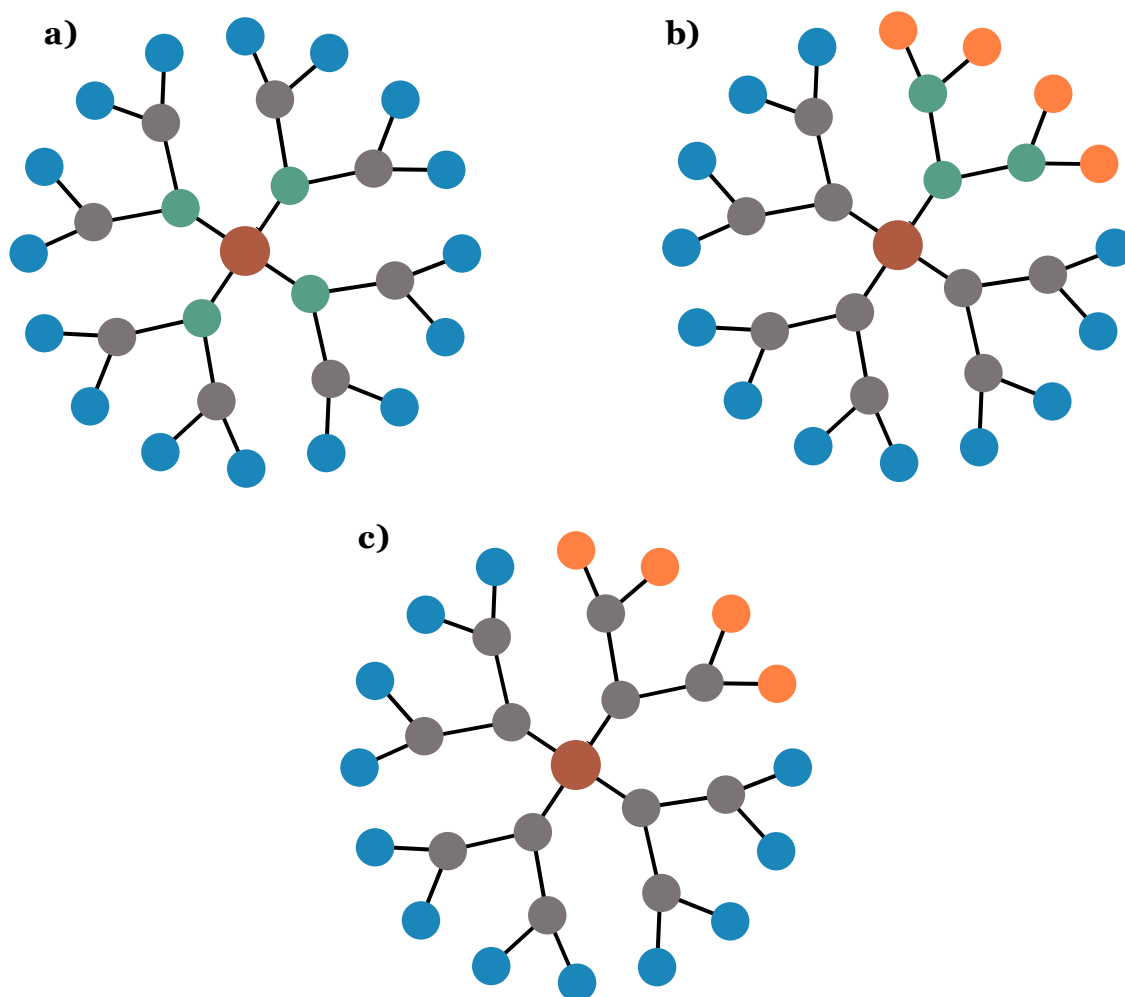


Figure 13. a) Layer-block, b) Segment-block and c) Surface-block dendrimers.

I.4 Peptide Chemistry Applied to the Synthesis of Dendrimers

Peptide synthesis is based upon the proper combination and manipulation of temporary and permanent protecting groups, as well as the choice of efficient coupling reagents for the controlled formation of the peptide bond.⁴⁸ Since a wide variety of dendrimers employ amide bonds, some of them have already been described in previous sections,^{6,18,20} a knowledge of protection/deprotection strategies and coupling methods is desirable. Here, only the methods most relevant to the synthesis of the dendrimers presented in this work are discussed.⁴⁹

I.4.1 Amino Protection/Deprotection Strategy

Protecting groups are crucial to avoid side products when a multifunctional molecule is to react with only one group while maintaining the others inert.

The *tert*-butoxycarbonyl (Boc) group is extensively used in the protection of amines. The method was independently developed by Carpino⁵⁰ and McKay⁵¹ and provides an amino protecting group resistant to hydrogenation and strong alkali medium, which makes it an ideal partner for the benzyl ester, a carboxylic protective group, that can be removed by hydrogenation.

Deprotection can be carried out *via* acids such as trifluoroacetic acid, which generates few side products during deprotection, or hydrochloric acid in dioxane, which is prepared by bubbling a stream of hydrogen chloride gas into dioxane.⁵²

I.4.2 Carboxylic Acid Protection/Deprotection Strategy

Carboxylic acids need to be protected when the acidic proton can interfere with base-catalyzed reactions or to prevent nucleophilic addition reactions.⁵² The protection of a carboxylic acid compound can be carried out under mild conditions using Cs_2CO_3 as base and benzyl bromide.⁵³ This group is stable under acidic conditions, so it can resist the conditions for Boc cleavage. On the other hand, benzyl esters can be cleaved by hydrogenolysis using a palladium catalyst such as Pd/C, $\text{Pd}(\text{OAc})_2$ or $\text{Pd}(\text{OH})_2$ (Pearlman's catalyst). Boc groups are totally stable under these conditions, making both protecting groups perfectly compatible for protection/deprotection synthesis.

I.4.3 Amide-forming Reactions

When forming an amide bond, a proper activation of the carboxylic or amine moiety is needed to carry out the coupling, although the carboxyl activation is the one being used in almost all the recent peptide coupling. A description of the most common used methods for carboxyl activation is given below.

a) *Acid chloride and fluoride methods.* They were first introduced by Fischer⁵⁴ in 1901 in the synthesis of the first dipeptide. Generally, reactants such as thionyl chloride or phosphorus pentachloride are employed to generate the acid chloride that will react with amines to form amides.

b) *Carbodiimide methods.* Carbodiimides were the first coupling reagents to be synthesized. Dicyclohexylcarbodiimide (DCC) has been widely used for coupling since first reported in 1955 by Sheehan and Hess.⁵⁵

The by-product formed, dicyclohexylurea (DCU) is insoluble in most solvents and can be removed by filtration. In the absence of an amino compound the *o*-acylisourea reacts with a second carboxyl component, forming a symmetrical anhydride. As a side reaction rearrangement in the *O*-acylisourea can occur, yielding the *N*-acylurea derivative. To solve this, DCC is often used alongside additives like *N*-hydroxysuccinimide (NHS) or 1-hydroxybenzotriazole hydrate (HOBt), which reduces dramatically racemization or other side reactions by reacting very rapidly with the *O*-acylisourea to give an acylating agent which is still reactive enough for aminolysis.⁵⁶

Since then, other carbodiimides have been synthesized to activate carboxylic acids and favor the creation of amide bonds. Some of them are widely used such as diisopropylcarbodiimide (DIC), 1-ethyl-3-(3-dimethylaminopropyl) carbodiimide (EDCI).

c) *Acylimidazoles using CDI.* Carbonyl diimidazole (CDI) is a useful coupling reagent that allows one-pot amide formation.⁵⁷ The creation of the amide bond is generated *via* acylimidazole as activated species. CDI is added to the carboxylic acid and after the generation of the activated species is ensured, the amine compound is added.⁵⁸

1.5 Click Chemistry Applied to Dendrimer Synthesis

The *click* chemistry paradigm was first published in 2001 and it described reactions that presented certain characteristics: modular, high enthalpy, high yields, stereospecific, atom economy and environmental safety.⁵⁹

I.5.1 Copper-assisted azide-alkyne cycloaddition (CuAAC)

This reaction is based on the Huisgen [2+3] cycloaddition between an alkyne and an azide.⁶⁰ The presence of Cu(I) prevents the formation of the 1,5-triazole, which during Huisgen cycloaddition results in around 50% of the products,^{61,62} making the reaction regioselective and enabling to carrying it out at room temperature.

However, when using this reaction for dendrimer synthesis some problems may arise, being the most common the possible metal complexation by the dendrimer and the deactivation of the Cu(I) catalyst to Cu(0) or Cu(II).⁶³ When aiming for the application of the dendrimers in biomedical fields, the copper contamination can be a concern due to its *in vivo* toxicity.⁶⁴ Most common methods for the removal of copper includes NH₄Cl/NH₄OH washes,⁶⁵ EDTA washes,⁶⁶ KCN washes,⁶⁷ dialysis⁶⁸ or the use of a chelated source of copper⁶⁹ such as tris(3-hydroxypropyltriazolylmethyl)amine (THPTA) and tris(benzyltriazolylmethyl)amine (TBTA). Another option is the copper-free *click* reaction, based on cycle tension release of a cyclooctyne to activate the alkyne. This method is also called Strain promoted azide-alkyne cycloaddition (SPAAC).⁷⁰ Because its orthogonality with CuAAC, it has been used to synthesize Janus dendrimers.⁷¹

I.5.2 The Thiol-Ene (TEC) and Thiol-Yne (TYC) Click Reactions

It consists in the reaction between terminal alkene or alkyne and a thiol.^{72,73} Its main benefits are its mild reaction conditions, since the reaction can be initiated with light ($\lambda=350-365$ nm), and its orthogonality with other reactions such as CuAAC and Michael Addition.

I.5.3 Synthesis of Dendrimers via Click Chemistry

Although the scientific community has expressed a great interest in the synthesis of dendrimers, problems such as the considerable number of reaction steps until higher generations are achieved, the tedious purifications in

each step and the increasing cost with each generation, have hindered transfer from academia to industry. *Click* chemistry can solve some of these problems since it can present yields over 99% and good orthogonality.

Click chemistry reactions can be carried out to couple the final dendrons to the core, to grow the dendrimer as branching points or to modify the periphery of the structures.³⁷

The first report of a dendrimer synthesis employing this chemistry⁷⁴ was carried out using an AB₂ monomer, in which B was acetylene groups and A a chloride group. After the *click* reaction between B and an azido group, the chloride was easily substituted by an azido moiety, making possible the reaction with another AB₂ monomer (Figure 14). The dendrons thus synthesized were finally coupled to different core units.

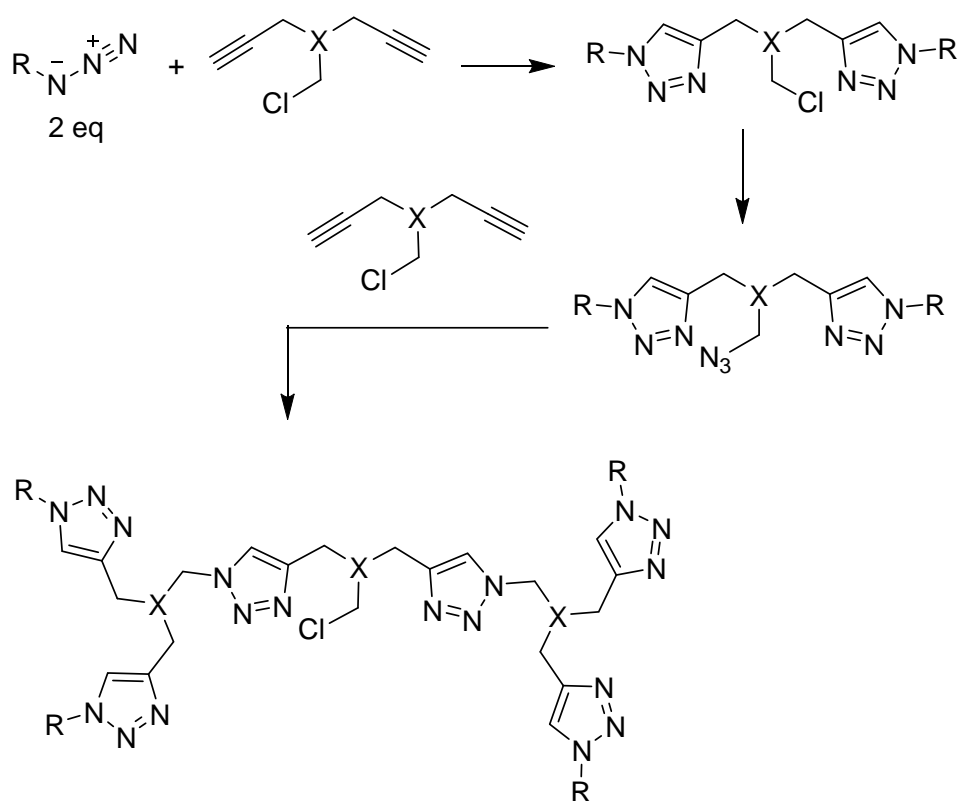


Figure 14. General synthesis of triazole dendrimers.

In recent years, *click* reactions have been used in the synthesis of high molar mass dendrimers,⁷⁵ to functionalized dendrimeric structures with complex

molecules such as peptides⁷⁶ or DNA,⁷⁷ in the synthesis of unsymmetrical,⁷⁸ Janus⁷⁹ and 3-Face dendrimers⁸⁰ or in the layer-block dendrimers.⁸¹

I.6 Applications of Dendrimers

A great number of applications of dendrimers are based in their multivalency, since their structures possess multiple peripheral sites for use. In addition, their 'core-shell' architecture has been exploited for the encapsulation of molecules that are incompatible with the environment external to the dendrimer.⁸²

A modification in the external media conditions (polarity, pH...) can cause a change in the conformation of the dendrimers, which will result in different shape and density. A great number of studies has focused on this knowledge in an attempt to tailor the encapsulation and release properties of dendrimers, for example in drug delivery applications.⁸³

Dendrimeric structures can provide at the core a microenvironment somehow different from the external medium, making possible their use as nanoscale containers.⁸⁴⁻⁸⁶ Dendrimers compile both homo- and heterogeneous catalysts characteristics since they have nanoscopic dimensions, but can also be molecularly dissolved.⁸⁷ Since their first use in catalysis,⁸⁸ the number of works focused on the use of dendrimers as catalyst has increased widely.⁸⁹⁻⁹²

In addition, light-emitting dendrimers present characteristic features such as site isolation effect which prevents the quenching of the luminescent core,⁹³ the antenna effect which increases the core emission through energy transfer from the peripheral chromophores,⁹⁴ and the high glass transition temperature which leads to stable devices.⁹⁵ The study of these properties and their application has made possible the synthesis of highly efficient phosphorescent dendrimers,^{96,97} phosphorescent dendrimers host-free OLEDs,⁹⁸ and dendrimers with high efficiency for red electrophosphorescence.⁹⁹

New advances in Medicine are focused in the use of nanoscience to unite diagnostic and therapeutic applications.¹⁰⁰ Certain features of dendrimeric architectures make them interesting candidates for these medical applications.

Their low polydispersity, the fact that the size and shape of high-generation dendrimers simulate those of proteins and multiple binding sites in their periphery make dendrimers appealing for pharmacochemist since they can act as multifunctional platforms.¹⁰¹ Bioactive substances can be encapsulated or chemically attached to the periphery of the dendrimer. In addition, great efforts have been made in the study of the applications of dendrimers in the field of magnetic resonance imaging (MRI).³⁴

The medical applications of these structures will strongly depend upon not being toxic, injurious or not causing immunological rejection. Other desirable features include that they should be easily excreted and that the time frame of degradation must be that so as to avoid cellular accumulation. PAMAM dendrimers are degradable by solvolysis of the amide backbone under heating conditions.¹⁰² However, ester-based dendrimers are more easily degraded by hydrolysis and their use as tissue adhesive has been studied.¹⁰³⁻¹⁰⁴ An innovative class of dendrimeric structures are the so called “self-immolative” dendrimers, which possess in their structure a trigger that can initiate the fragmentation of the compound into the building blocks.¹⁰⁵ So far, there are no studies that associate intrinsically “toxic” or “not toxic” properties to dendrimers.¹⁰⁶

Toxicity is closely related to the nature of the dendrimer’s end groups. It has been demonstrated that dendrimers with primary amino groups in their periphery, such as PAMAM or PPI, are more toxic and hemolytic than those presenting neutral or anionic end groups. The toxicity of these cationic dendrimers can be lessened by modifying the periphery with anionic or neutral groups.¹⁰⁷

1.6.1 Drug Delivery

The optimization of some drug’s features such as solubility, circulation half-life, drug dose or selectivity can be carried out by means of attaching a carrier to the drug. Dendrimers have been studied for this purpose. Drugs can be either attached covalently to the structure of the dendrimer or encapsulated in its voids. Drug delivery has opened a research field about “cleavable dendrimers”, focused on the study of external stimulus such as pH, photochemistry, redox reaction, etc.

to induce structural changes or the fragmentation of the dendrimeric structures, causing the release of the drug.¹⁰⁸

Drug delivery systems based on dendrimers have been studied for a great variety of applications such as antibacterial,¹⁰⁹ anti-inflammatory,¹¹⁰ anti-cancer,¹¹¹ pulmonary delivery,¹¹² treatment of ocular diseases¹¹³ or treatment of psoriasis¹¹⁴ among many others.

I.6.2 Gene Delivery

Gene therapy is a crucial tool in the treatment of hereditary diseases through the correction of genetic defects by transferring healthy or modified genetic material into the damaged cells. DNA complexes can be formed using cationic dendrimers such as PAMAM. Their transfection to cultured cells is carried out with lower toxicities and higher efficiency than with conventional agents.¹¹⁵ However, *in vivo* studies show that the toxicity of these compounds is related to the cationic charge, limiting their use. For this reason, works in gene transfer have been reported using modified PAMAM structures.¹¹⁶

I.6.3 Imaging

The earliest works on the application of dendrimers in this field consisted on the functionalization of dendrimers with a Gd (III) complex.¹¹⁷ These works showed proton relaxation enhancement in the presence of paramagnetic ions, making them a very promising tool in Magnetic Resonance Imaging (MRI). Since then, the importance of dendrimeric structures in imaging has increased and numerous research lines are focused on applications such as the employment of dendrimeric structures functionalized with organic dyes as fluorescent probes for specific biomolecule labeling.¹¹⁸ The use of dendrimers as coating agents of metalnanoparticles has shown potential advantages in Computer Tomography (CT) imaging over classical iodinated contrast agents.¹¹⁹

I.6.4 Immunoassays

The amplified substrate binding of dendrimers has been used to develop immunoassays because their sensitivity is increased by means of high concentration of antigen content.¹²⁰ Our group has focused on the employment of dendrimers as carrier proteins since these compounds exhibit advantages such as a well-defined structure and therefore a precise density of binding sites compared to conventional peptide carriers conjugates like human serum albumin (HSA) or poly-L-lysine (PLL).¹²¹

PAMAM dendrimers have been functionalized with β -lactam antibiotics (amoxicillin and benzylpenicillin) and their role as hapten-carrier conjugate for the recognition of IgE antibodies in *in vitro* tests has been studied.^{121–123} Our group has also developed new materials for the study of adverse immunological responses. The functionalization of cellulose discs¹²⁴ and zeolites¹²⁵ with benzylpenicilloylated PAMAM dendrimers and silica nanoparticles¹²⁶ coated with amoxicilloylated PAMAM dendrimers was carried out. In both cases, the reproducibility of the materials was demonstrated, and they were successfully used to recognize the corresponding IgEs.

CHAPTER II

OBJECTIVES

In accordance with our group research experience in the study of commercial dendrimers to potentially emulate endogenous carrier proteins,^{123,122} and act as linkers in the immobilization of bioactive molecules,^{127,128} as well as in the synthesis of new dendrimeric structures,¹²⁹ we have proposed for this thesis the following objectives:

1.- The preparation of new dendritic structures through the design of a versatile synthetic route that will enable the adjustment of the number of terminal groups in the periphery of the structures, as well as the incorporation of certain functionalities by choosing the proper core units.

2.- The synthesis of dendritic structures with free amino groups in their periphery and a pyridine as focal point and insertion into tailored Pt(II) complexes with the aim to solve typical limitations of these compounds, like aggregation and low solubility in aqueous media.

3.- The modification of titanium surfaces through covalent binding of the RGD tripeptide. For that purpose, we propose the synthesis of a new BAPAD derivative dendron with a carboxylic acid as focal point and four terminal amino

groups that will make possible the immobilization of the tripeptide *via* thiol-maleimide *click* reaction.

CHAPTER III

**SYNTHESIS OF NEW AMINO TERMINAL
DENDRITIC STRUCTURES**

III.1 Introduction

The research group has developed in recent years the following research lines based on the study of dendrimers:

1) Synthesis and functionalization of dendrimers to potentially emulate endogenous carrier proteins which will form the hapten-carrier conjugate, that is, the antigen responsible for the allergic process. For this purpose, the group has maintained close collaborations with allergology researchers from Malaga University Regional Hospital (Hospital Regional Universitario de Málaga, HRUM) and is part of the Spanish Telematic Net of Cooperative Research of Adversed Reactions to Allergens and Drugs (Red Telemática de Investigación Cooperativa de Reacciones Adversas a Alérgenos y Fármacos en España, RIRAAF). The group carried out studies where commercially available PAMAM dendrimers were employed^{122,123} but also reported the optimized synthesis of dendrimers based on the 3,3'-diazidopivalic acid scaffold (Figure 15) that could be used for this purpose.¹²⁹

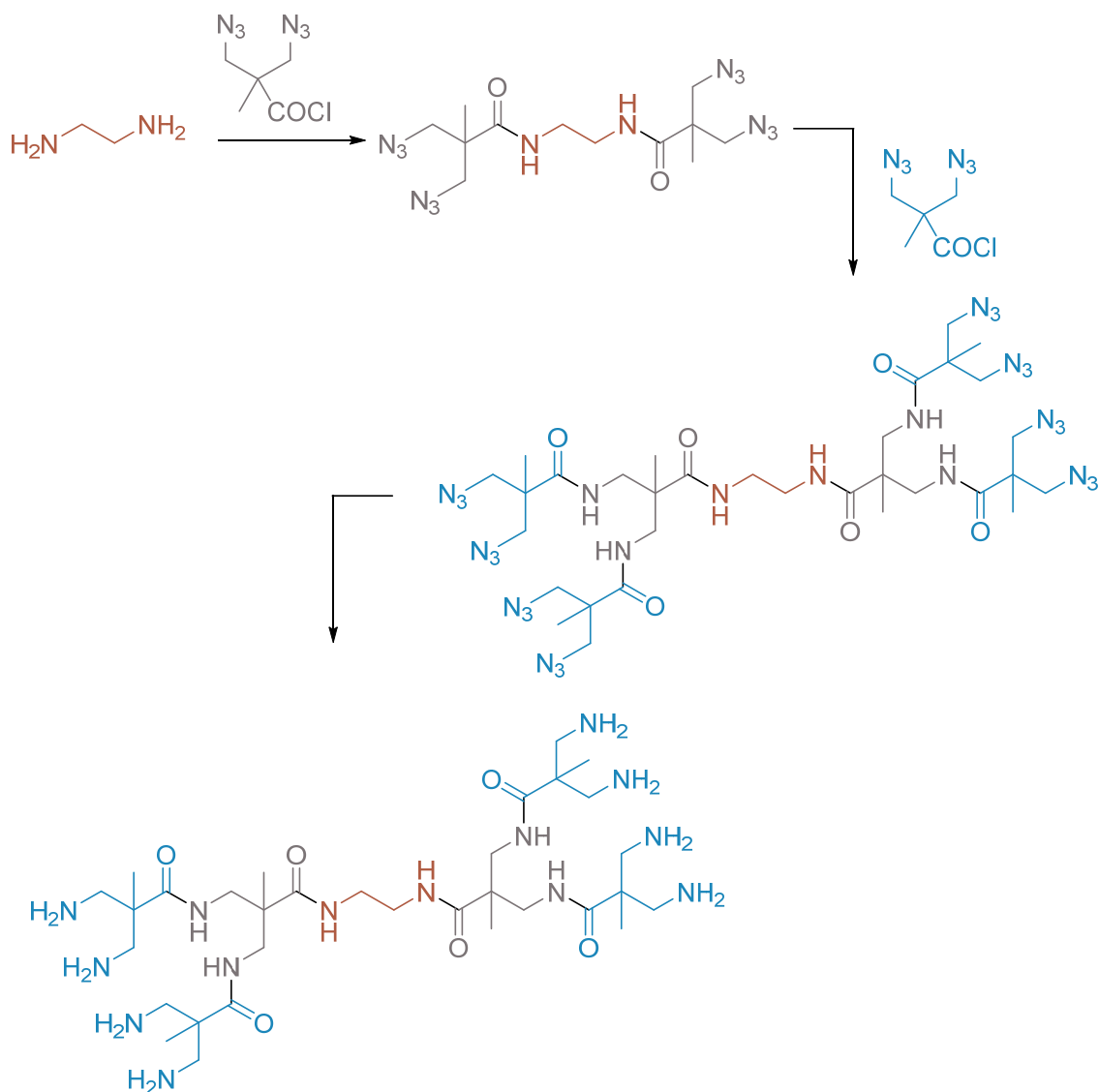


Figure 15. Synthesis of BAPAD dendrimers.

However, one of the major drawbacks of these structures was the fact that the higher generation that could be obtained is a third generation, with 16 peripheral amino groups.³¹

Following this divergent synthetic route, the synthesis of dendrons with a thiol group as focal point was also carried out. These dendrons were functionalized in their periphery with amoxicilloyl (AXO) groups and used in different works. They were attached to a gold surface for the development of a new plasmonic biosensor for the detection of IgE antibodies in amoxicillin allergic patients.¹³⁰ They were also modified with a naphthalimide derivative to study the *in vitro* internalization of these compounds in human dendritic cells.¹³¹

2) Synthesis and application of dendritic structures in tissue regeneration processes, in collaboration with research groups from Centro de Investigación Biomédica en Red (CIBER) in the subject area of Bioengineering, Biomaterials and Nanomedicine (CIBER-BBN). See Chapter V.

For these research lines, amino terminal dendrimers are an excellent alternative, since this functional group reacts easily with a great number of bioactive molecules. The most suitable and available amino terminal dendrimers are Vögtle's polypropylenimine (PPI),¹⁵ Denkwalter's poly(L-lysine) (PLL),¹³² Tomalia's polyamidoamine (PAMAM),^{6,21} and more recently a modification proposed by Malkoch from Hult's polyester (bis-MPA).¹³³ While these dendrimers are characterized by their symmetrical branching, PLL differs in their asymmetry.¹³⁴

Nevertheless, limitations regarding synthesis, quality or stability of those dendrimers have been reported. The most extended used is PAMAM, the first commercially-available even for high generations. However, the stability and quality of PAMAM dendrimers have been previously questioned.¹³⁵ For instance, defects are reported to be present in their structure due to retro-Michael additions and intramolecular lactam formation. Similarly, PPI dendrimer growth can be limited by retro-Michael reactions or intramolecular amine cyclization.³⁴

Another aspect to take into account for certain applications is the high basicity of PAMAM and PPI. The conformation of both dendrimers is strongly affected by low pH due to electrostatic repulsion of the protonated internal tertiary amines.³⁴ On the other hand, polyester (bis-MPA) dendrimers can be synthesized and purified more efficiently and also post-functionalized to display terminal amino groups up to generation five.¹³³ However, the lack of stability due to the well reported hydrolysis of the ester bond may be a problem for certain applications where the steadiness of the dendrimer is required.¹³³

In order to further develop these research lines, stable and water-soluble amino terminal dendritic structures are needed. Due to the positive results obtained so far, we have focused on the design of a versatile synthetic route that will enable the adjustment of the number of terminal groups in the periphery of the dendritic structures as well as the incorporation of certain functionalities by choosing the proper core units.

III.2 Synthesis of Amino Terminal Dendrimers by Click Chemistry

The divergent approach has been successfully employed for the synthesis of dendrimers widely used like PAMAM⁶ or PPI¹⁵, however, higher generations involve lower percentages of defect-free dendrimers. The convergent methodology introduced by Frechet²² involves a limited number of reactive sites in each growing step but presents the disadvantage of steric hindrance in the final coupling steps when the dendrons thus synthesized are voluminous. In the case of the BAPAD dendrimers previously synthesized by our group, the higher generation defect-free structures achieved by the divergent methodology was third generation with 16 terminal amino groups in its surface.^{31,35}

In the present work, we have proposed the synthesis, using a convergent approach, of new stable water-soluble dendritic structures with terminal amino groups making use of the reactive orthogonality of protection/deprotection chemistry and *click* reactions between the focal point and the periphery of the structures.

From a previously synthesized¹²⁹ structure based on the pivalic acid (**1**), a building block was designed, benzyl 3,3'-diazidopivalate (**2**). This compound would react through the azido groups while maintaining the carboxylic acid protected, thus avoiding possible secondary reactions. Also based on these kinds of structures, the first generation dendron, **dG1**, is prepared. This dendron possesses a terminal acetylene group and two boc-protected amino groups. Thus, the first growing step would take place between the terminal acetylene group of **dG1** and the azido groups present in **2** (Figure 16).

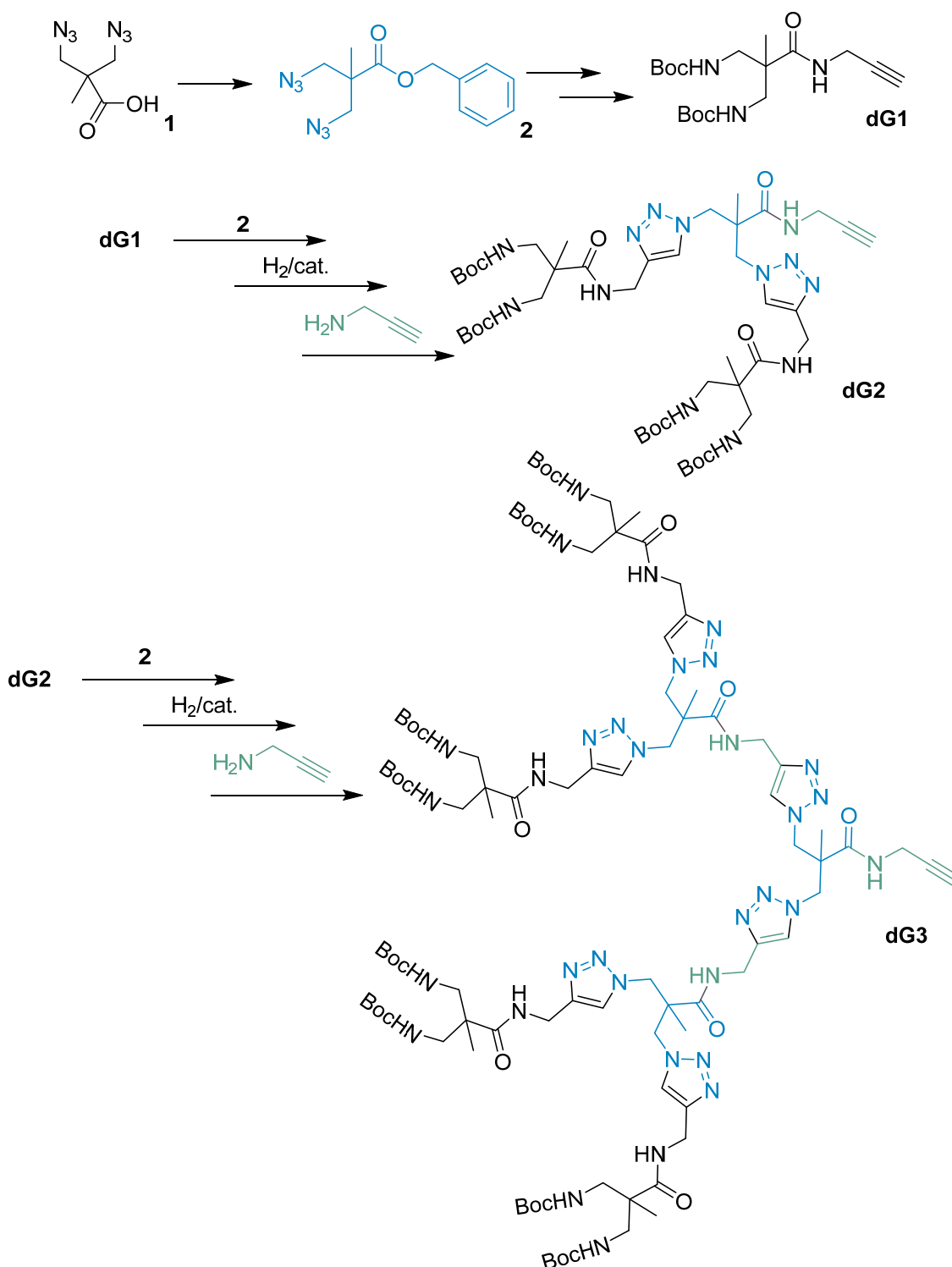


Figure 16. Synthetic scheme for the synthesis of dendrons.

After the deprotection of carboxylic acid and the following reaction with propargylamine, a new dendritic structure with a triple bond as focal point and four Boc-protected amino groups is obtained (**dG2**). Thus, to increase dendron

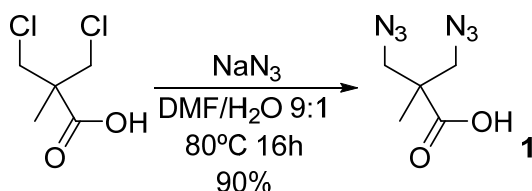
generation (Figure 16), 3 synthetic steps are involved: click reaction, deprotection (hydrogenation) and amide formation.

The goal of this synthetic strategy relies in the versatility of the methodology. Different generations of dendrimers can be synthesized carrying out *click* reactions between the dendrons and a core functionalized with azide groups. With a particular generation dendron it is possible the construction of dendrimers with different size, shape or amount of amino terminal groups by choosing the appropriate core. By changing the multiplicity and functionality of the core, we can design and prepare stable amino terminal dendrimers with a specific ability, size or shape for a particular application. In this work, we have proposed the synthesis of a family of three different generations of dendrimers with ethylene as the core (**G1EDANH₂**, **G2EDANH₂**, **G3EDANH₂**), a set of dendrimers using a third generation dendron with rigid tri- and tetrafunctional cores respectively (**G3_{3AB}NH₂**, **G3_{4AB}NH₂**) and a dendrimer with a fluorescent core (**G3_{Naph}NH₂**). The easy and efficient synthesis of the dendrimer was carried out in one step using click chemistry to couple alkyne-bearing dendrons to azide cores.

III.2.1 Synthesis of the Building Block (2)

III.2.1.1 Synthesis of 3,3'-diazidopivalic acid (1)

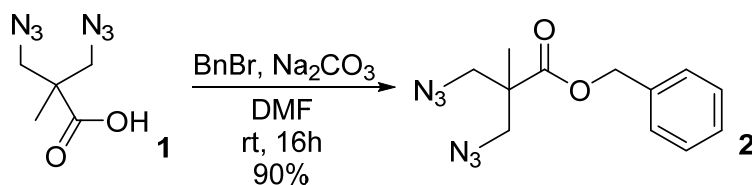
The first step of the synthesis of **2** was the substitution of the chlorides in 3,3'-dichloropivalic acid for azido groups. The reaction was carried out adding an excess of sodium azide to a solution of the starting material. At first, we used only DMF as solvent but the low solubility of the sodium azide in this solvent resulted in lower yields than if a small proportion of water was added. Finally, the reaction was carried out using a solvent mixture of DMF/H₂O 9:1 (Figure 17). The reaction mixture was heated at 80°C for 16 hours and afterwards, the solvent was removed under reduced pressure. EtOAc was then added to precipitate the excess of sodium azide. The compound **1** was thus synthesized with a yield of 90% in a multigram scale.

Figure 17. Synthesis of **1**.

The compound was fully characterized using nuclear magnetic resonance and mass spectroscopy, where the molecular anion M^- can be seen at m/z 183.06. When comparing the ^1H NMR spectrum of **1** (Figure 122) with that of the starting material, a shift upfield can be seen in the doublet signals corresponding to the methylene groups (from 3.89 and 3.75 ppm in the spectrum of the starting material to 3.63 and 3.52 ppm respectively) and the singlet corresponding to the methyl group (from 1.43 to 1.27 ppm).

III.2.1.2 Synthesis of Benzyl 3,3'-diazidopivaloate (**2**)

The second and last step in the synthesis of this building block was the protection of the carboxylic acid group in compound **1**. For that purpose, the formation of the benzyl ester was carried out using benzyl bromide, sodium carbonate as base and DMF as solvent. The mixture was then stirred at room temperature for 16 hours (Figure 18). After purification, **2** was obtained as a colorless oil in a 90% yield.

Figure 18. Synthesis of **2**.

The compound was fully characterized using nuclear magnetic resonance mass and infrared spectroscopy. In the mass spectroscopy spectrum, the peak associated to $[M + \text{Na}]^+$ was found at m/z 297.11, while the most relevant result of the infrared spectra is the existence of the band at 2095 cm^{-1} corresponding to

the azide groups. In the ^1H NMR spectrum (Figure 124), the appearance of a singlet at 5.19 ppm, corresponding to the methylene of the benzyl groups, and a multiplet at 7.42 – 7.32 ppm in the aromatic region, corresponding to the benzene moiety, confirm the successful synthesis of **2**.

III.2.2 Synthesis of **dG1**

For the synthesis of **dG1** the following synthetic route was designed, using amino and carboxylic acid protection/deprotection strategies described previously (Figure 19):

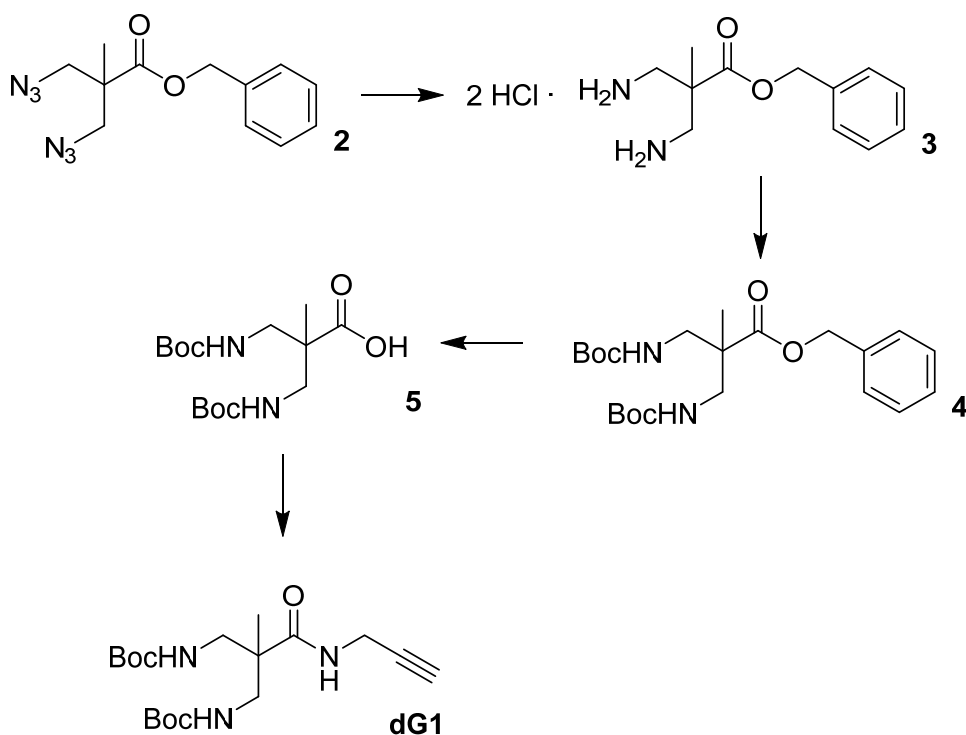


Figure 19. Scheme for the synthesis of **dG1**.

III.2.2.1 Synthesis of Benzyl 3,3'-diaminopivaloate (**3**)

The reduction of the azide groups was carried out using the Staudinger reaction conditions with triphenylphosphine (PPh_3).¹³⁶ Staudinger reaction was chosen over other azide reduction methods like hydrogenolysis, to preserve the benzyl ester moiety. A solution of PPh_3 in THF was added dropwise to an ice-cooled solution of **2** in THF. After the addition was completed, the reaction

mixture was heated under reflux for 16 hours. Then, water was added, and the mixture was left another 16h under reflux (Figure 20). After the removal of the solvent under reduced pressure, the residue was dissolved in HCl 1M and washed with DCM to obtain compound **3** as a colorless solid in a 98% yield with no need of purification.

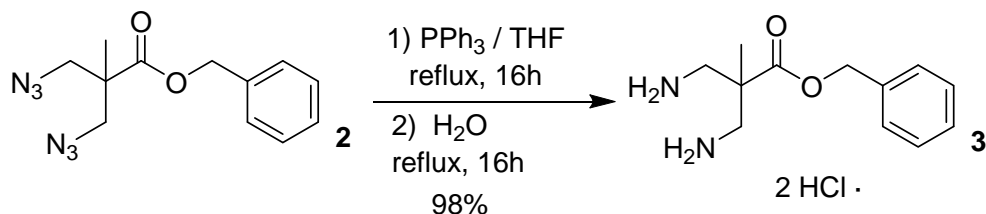


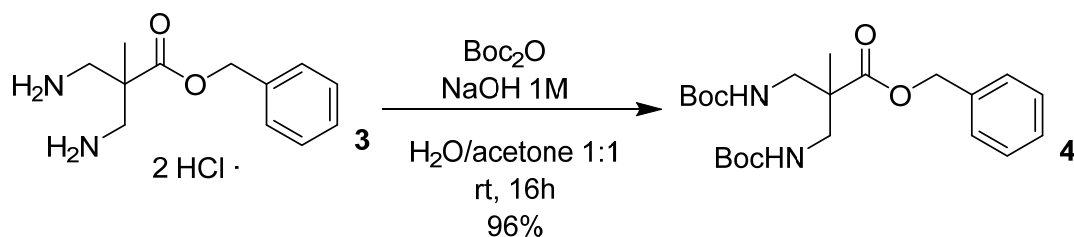
Figure 20. Synthesis of **3**.

Compound **3** was characterized using nuclear magnetic resonance techniques (^1H and ^{13}C) as well as mass spectroscopy in which the peak corresponding to $[\text{M} + \text{H}]^+$ could be found at m/z 223.14.

The ^1H NMR spectrum (Figure 126) shows a singlet signal at 1.49 ppm corresponding to the methyl group, two doublets corresponding to the methylene groups next to the amino groups at 3.29 and 3.45 ppm respectively, a singlet signal corresponding to the methylene group of the benzyl moiety at 5.35 ppm and finally, the aromatic protons appear as a multiplet at around 7.52 ppm.

III.2.2.2 Synthesis of Benzyl 3,3'-bis(*tert*-butoxycarbonyl) aminopivaloate (4**)**

The next step was the protection of the amino groups of compound **3**. Following an orthogonal protection strategy, we chose the *tert*-butoxycarbonyl (Boc) group for the protection of the amino groups since it can resist the subsequent catalytic hydrogenolysis reaction needed to remove the benzyl ester, deprotecting, thus, the carboxylic acid moiety.

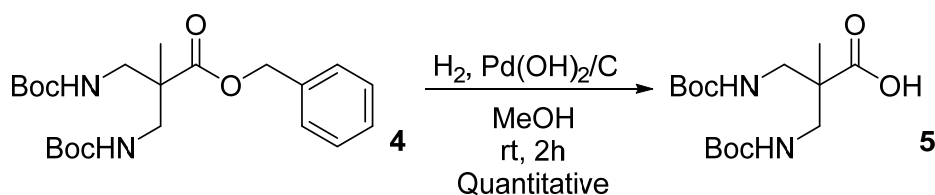
Figure 21. Synthesis of **4**.

Compound **3** was dissolved in an ice-cooled solution of H₂O/acetone 1:1 and NaOH 1M was added dropwise until basic pH was reached. Then, Di-*tert*-butyl dicarbonate was added and the reaction mixture was left stirring for 16 hours at room temperature (Figure 21). After the reaction time had elapsed, acetone was removed, and the product was extracted from the reaction mixture with DCM. No further purification techniques were needed and **4** was obtained as a colorless solid with a 96% yield.

The compound was characterized using ¹H and ¹³C NMR techniques. In the ¹H spectrum (Figure 128), a new signal at 1.43 ppm appears, as well as three new signals in ¹³C NMR at 156.7, 79.4 and 24.4 ppm respectively, corresponding to the Boc groups (Figure 129). In mass spectroscopy, the peak corresponding to [M + Na]⁺ can be found at *m/z* 445.23.

III.2.2.3 Synthesis of 3,3'-bis(*tert*-butoxycarbonyl)aminopivalic Acid (**5**)

The deprotection of the carboxylic acid was carried out *via* hydrogenolysis in the presence of Pearlman's catalyst.¹³⁷ Palladium catalysts are the most widely used catalysts for the hydrogenolysis of organic substrates. Pt and Raney nickel catalysts are also effective for hydrogenolysis in many cases but are used much less frequently than palladium.^{138,139}

Figure 22. Synthesis of **5**.

The catalyst was added to a solution of **4** in MeOH and the reaction took place in an hydrogenator for 2 hours at room temperature, under a hydrogen pressure of 50 bar. The catalyst was removed from the reaction mixture by filtration over celite. Compound **5** was obtained as a colorless oil in quantitative yield (Figure 22).

The reaction was monitored by ^1H NMR (Figure 130), where the complete disappearance of the benzyl signals (a singlet at 5.14 ppm corresponding to the methylene and a multiplet around 7.34 ppm corresponding to the aromatic moiety) can be appreciated. In mass spectroscopy, the peak corresponding to $[\text{M} + \text{Na}]^+$ can be found at m/z 355.18.

III.2.2.4 Synthesis of *N*-propargil-3,3'-bis(*tert*-butoxycarbonyl)aminopivalamide, **dG1**

The final step to obtain **dG1** was the formation of the amide bond between the carboxylic acid **5** and propargylamine. It was achieved by the activation of the carboxylic acid group of **5** with 1,1'-carbonyldiimidazole (CDI) in MeCN and the subsequent addition of the amine. The reaction mixture was left stirring at room temperature for 16 hours (Figure 23). Afterwards, the solvent was removed, and the reaction crude was dissolved in DCM and washed with HCl 0.05M. Finally, **dG1** was obtained as a colorless solid with a yield of 83%.

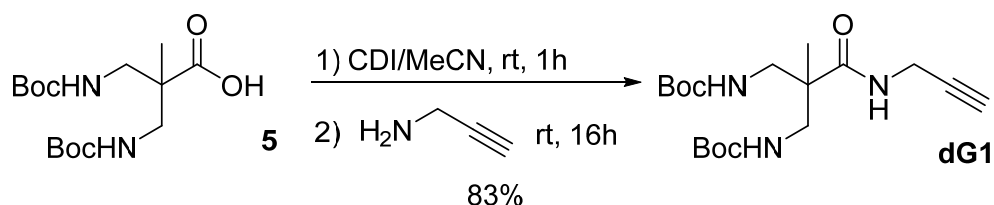
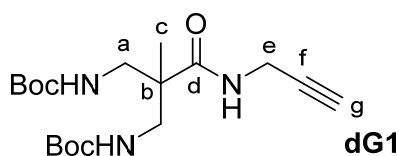


Figure 23. Synthesis of **dG1**.

The compound was fully characterized using ^1H and ^{13}C NMR. In the ^1H NMR spectrum (Figure 36, Figure 132), the new signals corresponding to the acetylene moiety can be seen at around 3.07 and 3.80 ppm as shown in the following table:



Position	¹ H NMR (ppm)	¹³ C NMR (ppm)
CH ₃ (Boc)	1.37 (s, 18 H)	28.2
a	3.14-3.01 (m, 5 H)	47.6
c	0.95 (s, 3 H)	18.5
e	3.80 (dd, <i>J</i> = 4.8, 2.1 Hz, 2 H)	28.4
g	3.14-3.01 (m, 5 H)	72.7

Table 1. ¹H and ¹³C NMR correlation table of **dG1**

Moreover, in mass spectroscopy, the peak corresponding to [M + Na]⁺ can be found at *m/z* 392.22.

III.2.3 Synthesis of **dG2**

The convergent synthesis of the second-generation dendron was achieved by a *click* reaction between the acetylene moiety of the first generation dendron, **dG1**, the azido groups of the building block (**2**). The subsequent deprotection of the carboxylic acid and the reaction with propargylamine resulted in the second-generation dendron, **dG2** (Figure 24).

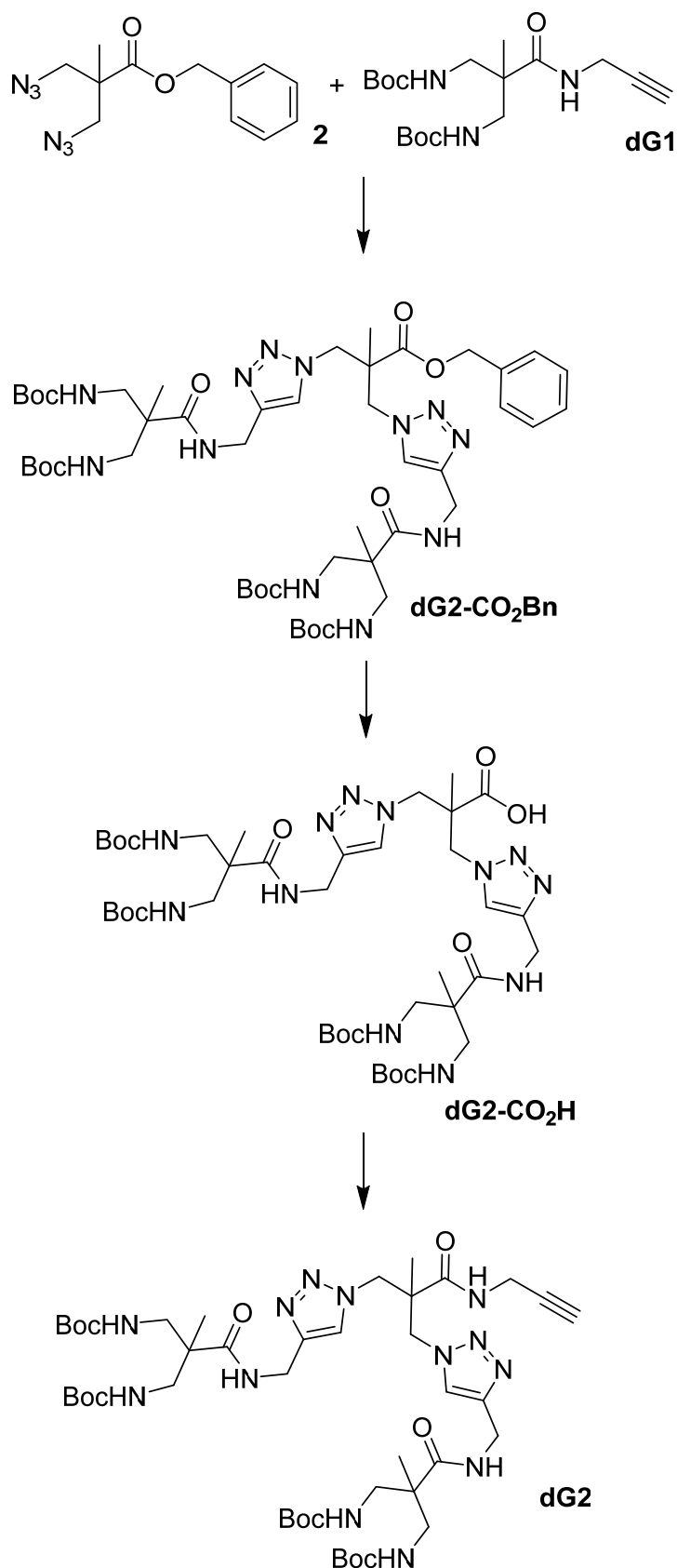


Figure 24. Scheme for the synthesis of **dG2**.

III.2.3.1 Synthesis of **dG2-CO₂Bn**

Different conditions for the *click* reaction between **dG1** and **2** were tested. At first, tris(benzyltriazolylmethyl)amine (TBTA)¹⁴⁰ was used as catalyst and although the reaction was successful, the removal of the catalyst turned out to be problematic since its *R_f* was similar to the product's, making difficult the purification process and significantly decreasing the final yield. For this reason, we decided to set the reaction without the catalyst, which resulted in longer reaction times but a purification with no need of chromatography, resulting in higher reaction yields.

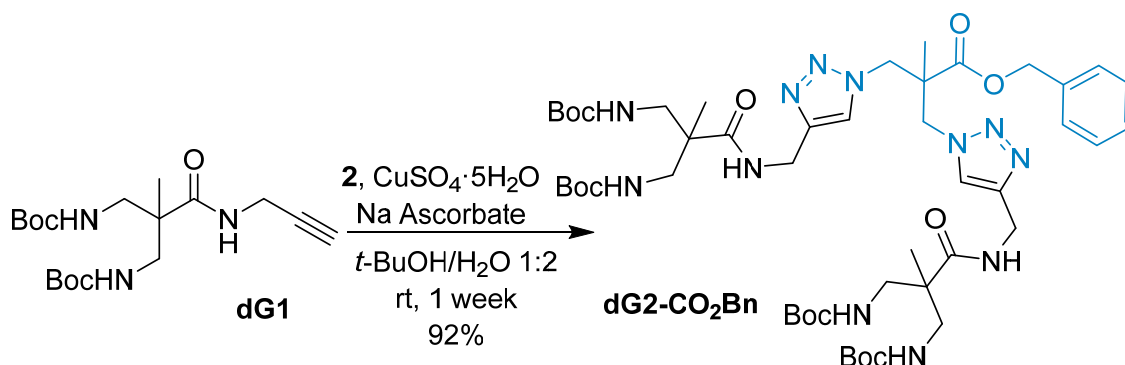


Figure 25. Synthesis of **dG2-CO₂Bn**.

The reaction was carried out as follows: **dG1**, **2**, copper (II) sulphate 5-hydrate and L(+)-ascorbic acid sodium salt were dissolved in *tert*-butanol/water 1:2 and the mixture was stirred at room temperature for one week (Figure 25). Afterwards, the solvent was removed, the mixture dissolved in DCM and washed with NH₄OH. The aqueous phase was extracted with DCM and the combined organic layers were washed with a mixture of NH₄OH/Brine 1:1. After the drying and the removal of the solvent from the organic layer, the product was purified by precipitation in hexane to obtain **dG2-CO₂Bn** as a colorless powder in a 92% yield.

To ensure the complete reaction between **dG1** and **2** that no traces of imperfect dendron were left, infrared spectroscopy measurements were carried out. In Figure 26, the disappearance of the band at 2095 cm⁻¹ (typical of azides) can be seen. This indicates that all azide groups of **2** have reacted and thus, a perfect dendritic structure has been obtained.

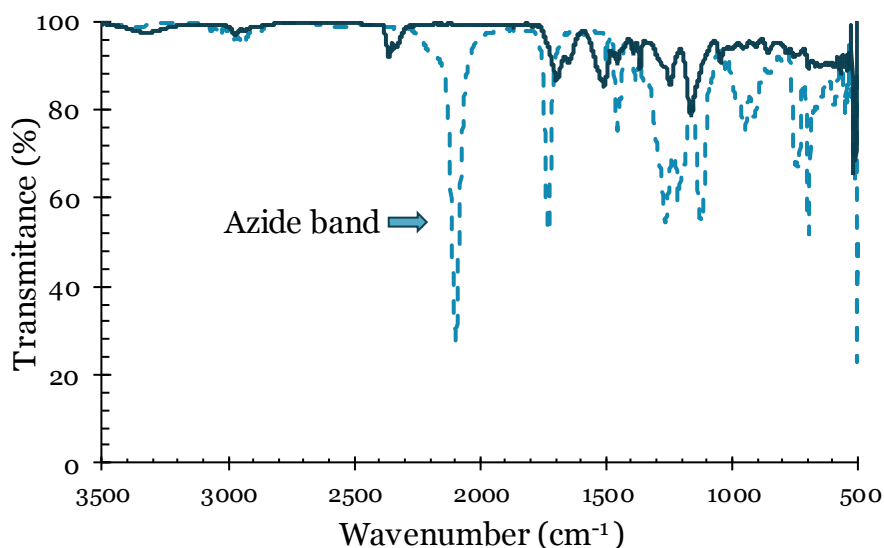


Figure 26. IR spectra of **dG2-CO₂Bn** (solid line) and compound **2** (dotted line).

NMR techniques were used to fully characterize the compound. In the ¹H NMR spectrum, it is worth noting the appearance of the signal at 7.79 ppm that corresponds to the proton of the 1,2,3-triazole cycle. On the other hand, we can corroborate that the signals corresponding to the Boc groups (1.35 ppm) and the benzyl ester (5.09, 7.37 ppm) are still present (Figure 27, Figure 134).

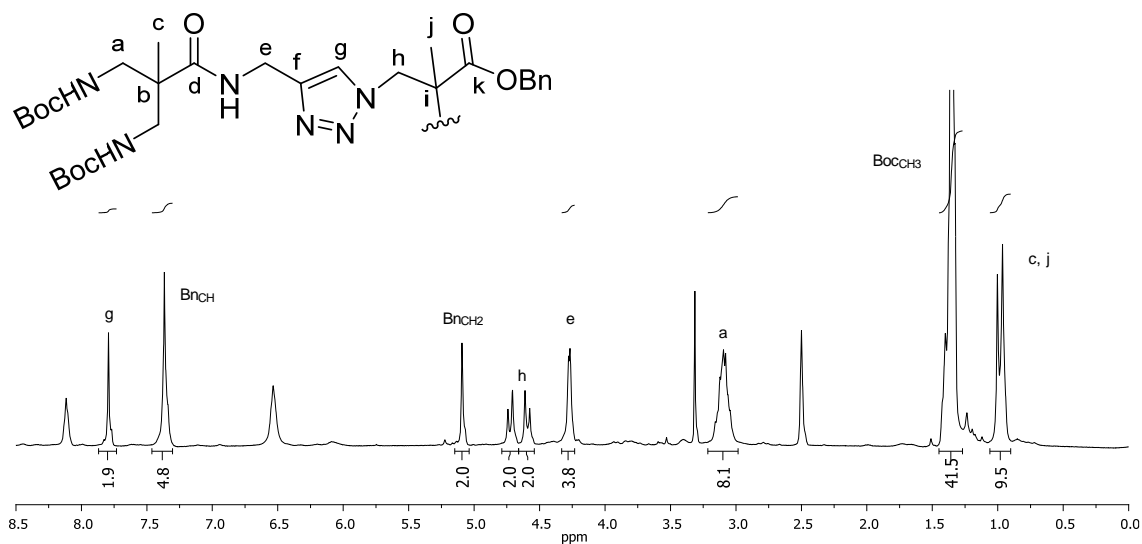


Figure 27. ¹H NMR spectra of **dG2-CO₂Bn** in DMSO.

The ^{13}C NMR spectra (Figure 135) showed the signals of the carbons corresponding to the 1,2,3-triazole cycle at 145.0 and 124.2 ppm plus de signals corresponding to **2** and **dG1** moieties.

In order to facilitate the assignment of NMR spectra, bi-dimensional experiments were carried out. Heteronuclear single-quantum correlation spectroscopy (HSQC) spectra can be found in Appendix (Figure 136). The correspondence of ^1H and ^{13}C assignments are laid out in the following table:

Position	^1H NMR (ppm)	^{13}C NMR (ppm)
BocCH ₃	1.35 (s, 36 H)	28.1
a	3.16-3.04 (m, 8 H)	44.4
c	1.00 (s, 6 H)	18.4
e	4.27 (d, $J = 4.8$ Hz, 4 H)	34.6
g	7.79 (s, 2 H)	124.2
h	4.72 (d, $J = 14.1$ Hz, 2 H) 4.59 (d, $J = 14.1$ Hz, 2 H)	53.4
j	0.96 (s, 3 H)	17.7
BnCH ₂	5.09 (s, 2 H)	66.8
BnCH	7.40-7.32 (m, 5 H)	128.4, 128.1, 128.0

Table 2. ^1H and ^{13}C NMR correlation table of **dG2-CO₂Bn**.

In mass spectroscopy, the peak corresponding to $[\text{M} + \text{H}]^+$ can be found at m/z 1013.58.

III.2.3.2 Synthesis of dG2-CO₂H

The deprotection of the carboxylic acid was carried out similarly to synthesis of **5**. The removal of the benzyl ester was achieved by hydrogenolysis in the presence of Pearlman's catalyst (Figure 28). The compound, a colorless solid, was obtained in quantitative yield.

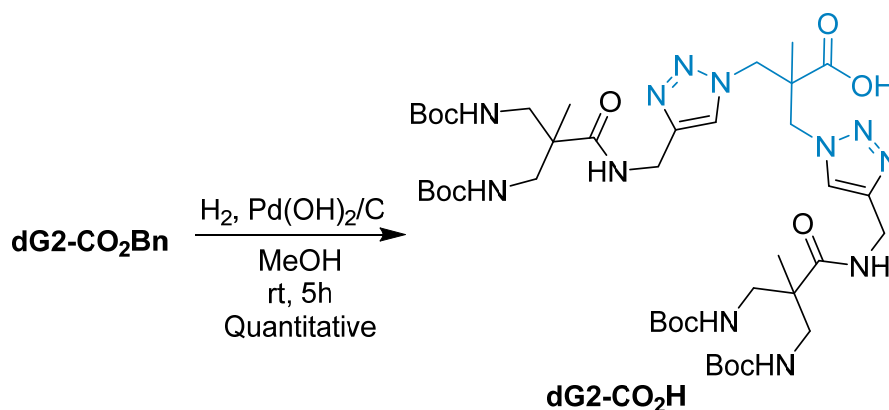


Figure 28. Synthesis of **dG2-CO₂H**.

The reaction was monitored using NMR techniques, the reaction went to completion after five hours, when the fully disappearance of the signals correspondent to the benzyl moiety (singlet at 5.09 ppm corresponding to the methyl group of the benzyl moiety and a multiplet at around 7.37 corresponding to the aromatic protons) can be observed (Figure 29, Figure 137).

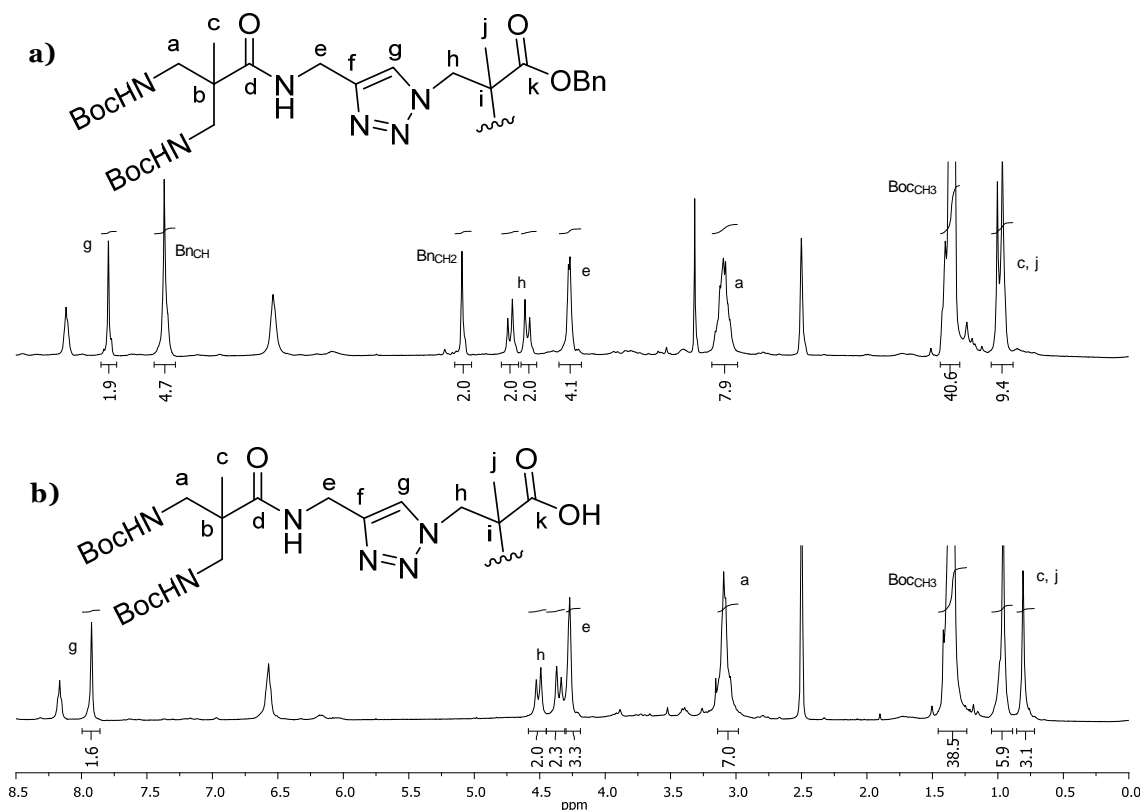


Figure 29. ¹H NMR spectra of **a)** **dG2-CO₂Bn** and **b)** **dG2-CO₂H** in DMSO.

Moreover, in mass spectroscopy, the peak corresponding to $[M + Na]^+$ can be found at m/z 945.51.

III.2.3.3 Synthesis of **dG2**

The final step in the synthesis of the second-generation dendron is the formation of an amide bond between the carboxylic moiety of **dG2-CO₂H** and commercial propargylamine (Figure 30). The same reaction conditions were used as in the synthesis of **dG1**, to obtain a solid with 85% yield.

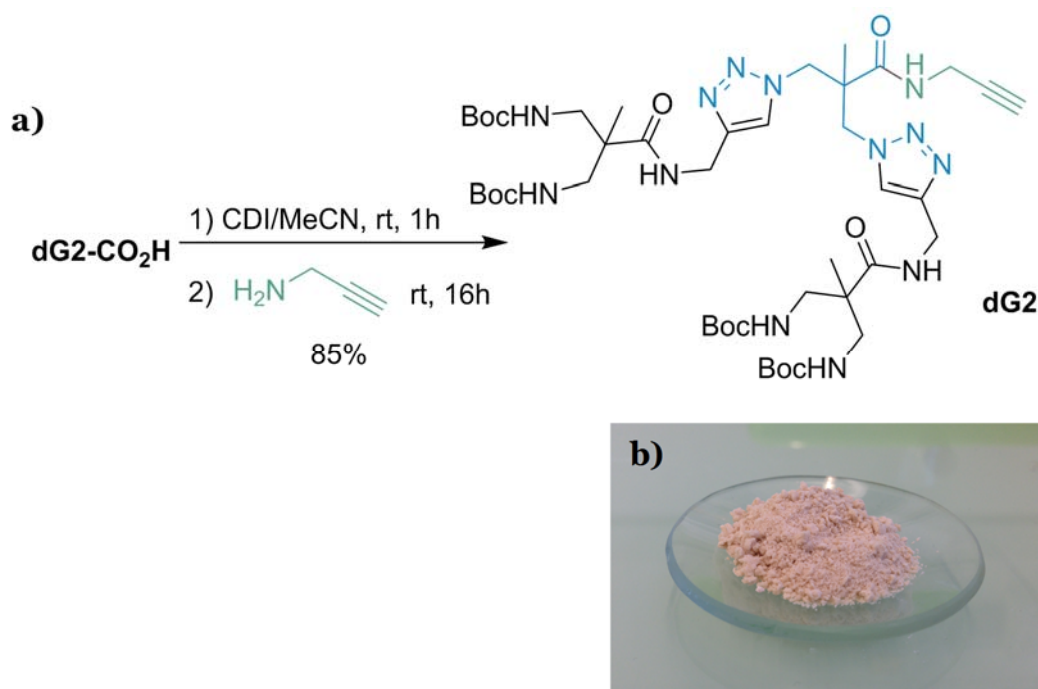
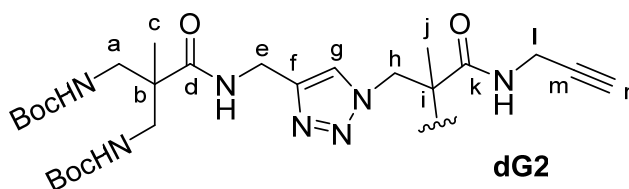


Figure 30. **a)** Synthesis of **dG2**; **b)** picture of **dG2**.

The compound was fully characterized using ^1H and ^{13}C NMR. In the ^1H NMR spectrum (Figure 36, Figure 140), the new signals corresponding to the methylene groups and the terminal proton of the acetylene moiety can be seen at around 3.83 (doublet) and 1.76 ppm (singlet) respectively.

Table 3 resumes the assignments of ^1H NMR and their corresponding ^{13}C NMR signals:



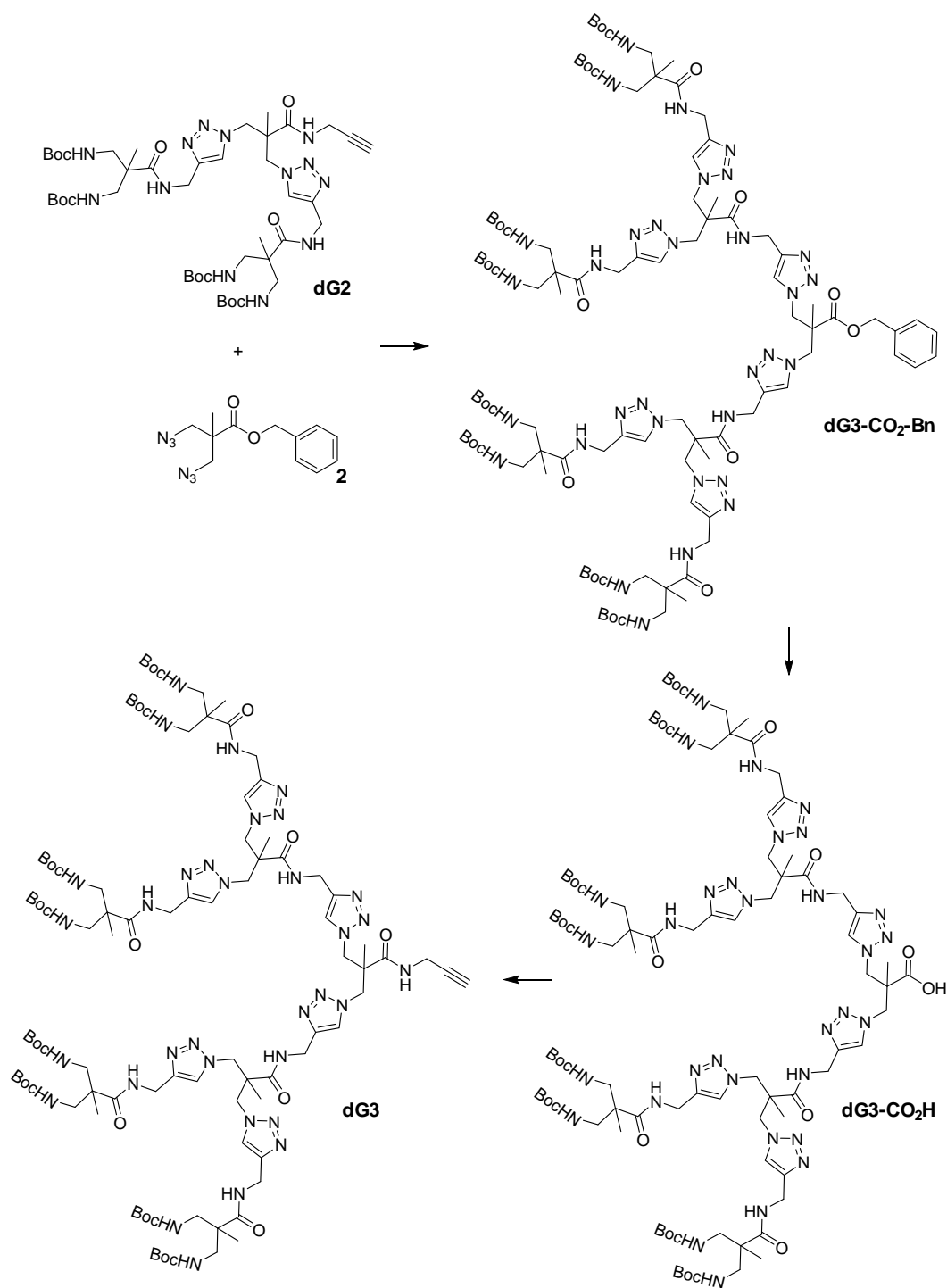
Position	^1H NMR (ppm)	^{13}C NMR (ppm)
BOCCH ₃	1.36 (s, 36 H)	28.1
a	3.12-3.07 (m, 8 H)	44.4
c	0.96 (s, 6 H)	18.4
e	4.27 (s, 4 H)	34.6
g	7.72 (s, 2 H)	123.9
h	4.66 (d, $J=14.1$ Hz, 2 H) 4.52 (d, $J=14.1$ Hz, 2 H)	53.9
j	0.93 (s, 3 H)	17.4
l	3.83 (d, $J=2.7$ Hz, 2 H)	28.6
n	1.76 (s, 1H)	73.1

Table 3. ^1H and ^{13}C NMR correlation table of **dG2**.

In mass spectroscopy, the peak corresponding to $[\text{M} + \text{Na}]^+$ can be found at m/z 982.54.

III.2.4 Synthesis of **dG3**

Following the same steps of growing, deprotecting and amidation as in the synthesis of **dG2**, the synthesis of the third-generation dendron was successfully carried out from the second-generation dendron **dG2** and the azido building block **2**.



III.2.4.1 Synthesis of dG3-CO₂Bn

Click reaction between **dG2** and **2** was carried out using the optimized conditions for the synthesis of **dG2-CO₂Bn**. The desired product was obtained as a colorless solid in 90% yield. However, the formation of higher generations required longer reaction times, probably due to steric hindrance.

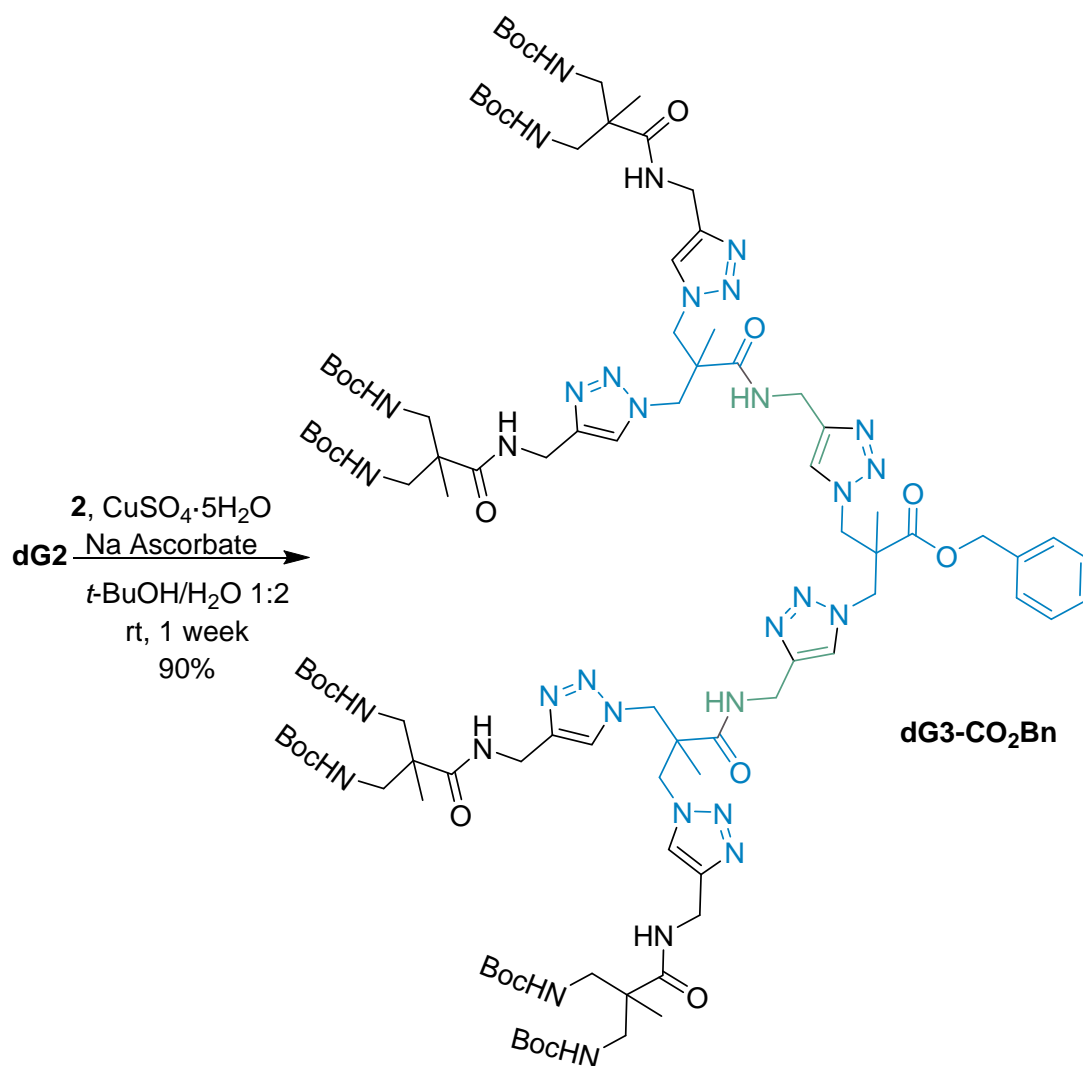


Figure 31. Synthesis of **dG3-CO₂Bn**.

The disappearance of the band at 2095 cm^{-1} (typical of azides) in the infrared measurements indicate that all azide groups have reacted obtaining a dendrimeric structure without imperfections (Figure 32).

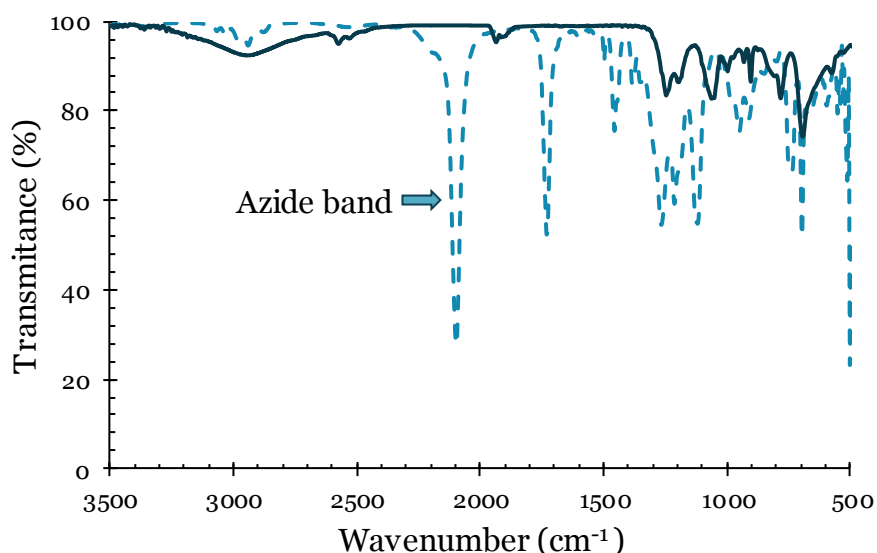
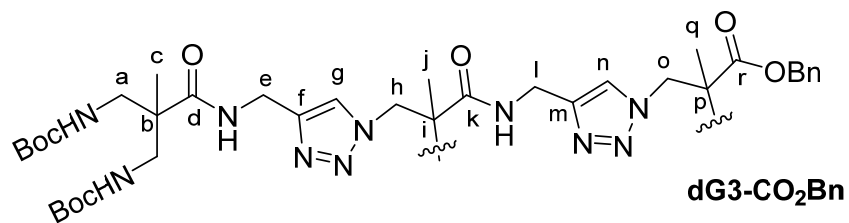
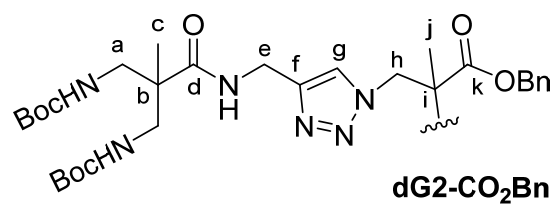
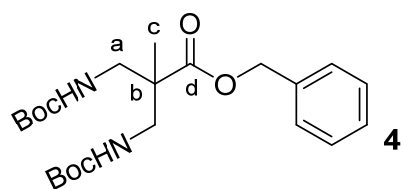


Figure 32. IR spectra of **dG3-CO₂Bn** (solid line) and compound **2** (dotted line).

The compound was further characterized using NMR techniques such as ^1H , ^{13}C , COSY and HSQC. New signals corresponding to the formation of the 1,2,3-triazole cycle can be seen in the aromatic region of the ^1H NMR spectrum (Figure 34, Figure 143) at around 7.80 ppm as well as new signals corresponding to compound **2**. It's noteworthy the appearance of the signals corresponding to the benzyl moiety at 5.10 ppm (singlet, methylene) and at around 7.34 ppm (multiplet, aromatic ring). These signals appear in the ^{13}C spectrum (Figure 144) at around 144 and 125 ppm for the triazole ring, for the benzyl moiety at 135.3, 128.4, 128.1, 128.0 ppm (aromatic ring) and 66.8 ppm (methylene).

In table 4, we present a comparison of the assignment of ^1H NMR signals of the three generations of dendrons, that is, **4**, **dG2-CO₂Bn** and **dG3-CO₂Bn** where a similar pattern in the assignments can be observed.



Position	¹ H NMR (ppm)		
	4	dG2-CO₂Bn	dG3-CO₂Bn
BocCH ₃	1.43 (s, 18 H)	1.35 (s, 36 H)	1.35 (s, 72 H)
a	3.48 (dd, <i>J</i> = 14.4, 8.6 Hz, 2 H) 3.12 (dd, <i>J</i> = 14.4, 8.6 Hz, 2 H)	3.16-3.04 (m, 8 H)	3.18-3.04 (m, 16 H)
c	1.14 (s, 3 H)	1.00 (s, 6 H)	0.96-0.93 (m, 21 H)
e		4.27 (d, <i>J</i> = 4.8 Hz, 4 H)	4.31-4.18 (m, 12 H)
g		7.79 (s, 2 H)	7.94-7.75 (m, 6 H)
h		4.72 (d, <i>J</i> = 14.1 Hz, 2 H) 4.59 (d, <i>J</i> = 14.1 Hz, 2 H)	4.65 (d, <i>J</i> = 14.2 Hz, 4 H) 4.51 (d, <i>J</i> = 14.0 Hz, 2 H)
j		0.96 (s, 3 H)	0.96-0.93 (m, 21 H)
l			4.31-4.18 (m, 12 H)
n			7.94-7.75 (m, 6 H)
o			4.80 (d, <i>J</i> = 14.2 Hz, 2 H) 4.44 (d, <i>J</i> = 13.7 Hz, 2 H)
q			0.96-0.93 (m, 21 H)
BnCH ₂	5.14 (s, 2 H)	5.09 (s, 2 H)	5.10 (s, 2 H)
BnCH	7.39-7.30 (m, 5 H)	7.40-7.32 (m, 5 H)	7.36-7.32 (m, 5 H)

Table 4. ¹H NMR signals assignments of **4**, **dG2-CO₂Bn** and **dG3-CO₂Bn** in DMSO.

In mass spectroscopy, the peak corresponding to [M + Na]⁺ can be found at *m/z* 2216.23.

III.2.4.2 Synthesis of dG3-CO₂H

The deprotection of the carboxylic acid was carried out similarly to synthesis of **5** and **dG2-CO₂H**. The removal of the benzyl ester was achieved by hydrogenolysis in the presence of Pearlman's catalyst (Figure 33). The compound, a colorless solid, was obtained in quantitative yield.

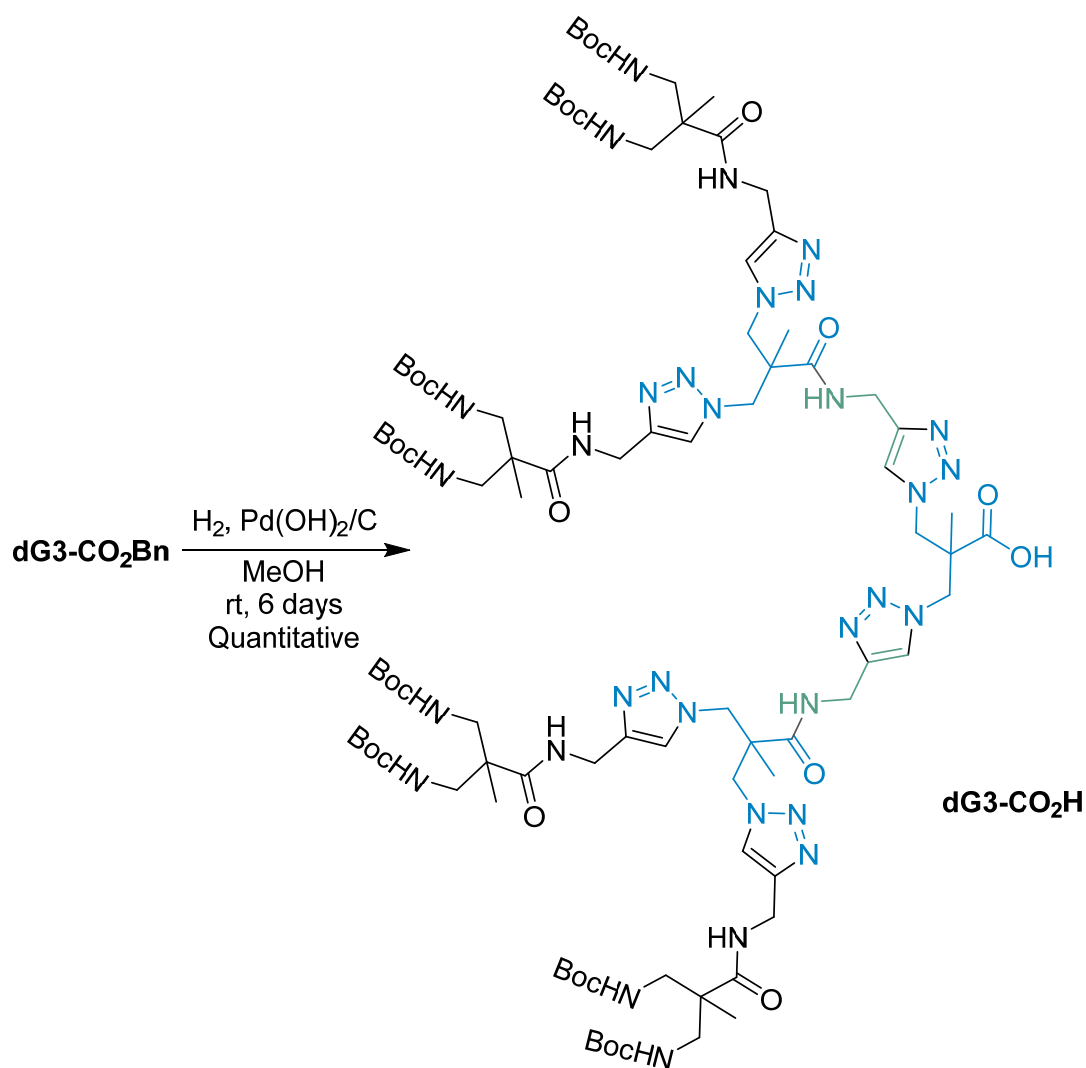


Figure 33. Synthesis of **dG3-CO₂H**.

The reaction was monitored using NMR techniques, where a complete disappearance of the signals correspondent to the benzyl moiety can be observed (Figure 34). The compound was fully characterized using NMR techniques such as ^1H and ^{13}C NMR and HSQC (Figure 146, Figure 147, Figure 148). In mass spectroscopy, the peak corresponding to $[\text{M} + \text{H}]^+$ can be found at m/z 2013.17.

However, it is worth noticing how the reaction time increases with higher generations due to steric hindrance. For the synthesis of **5** barely two hours were needed, in the case of the second-generation analogue, the time needed is more than double (five hours) and finally the reaction time of the hydrogenolysis of the third-generation dendron increases to several days.

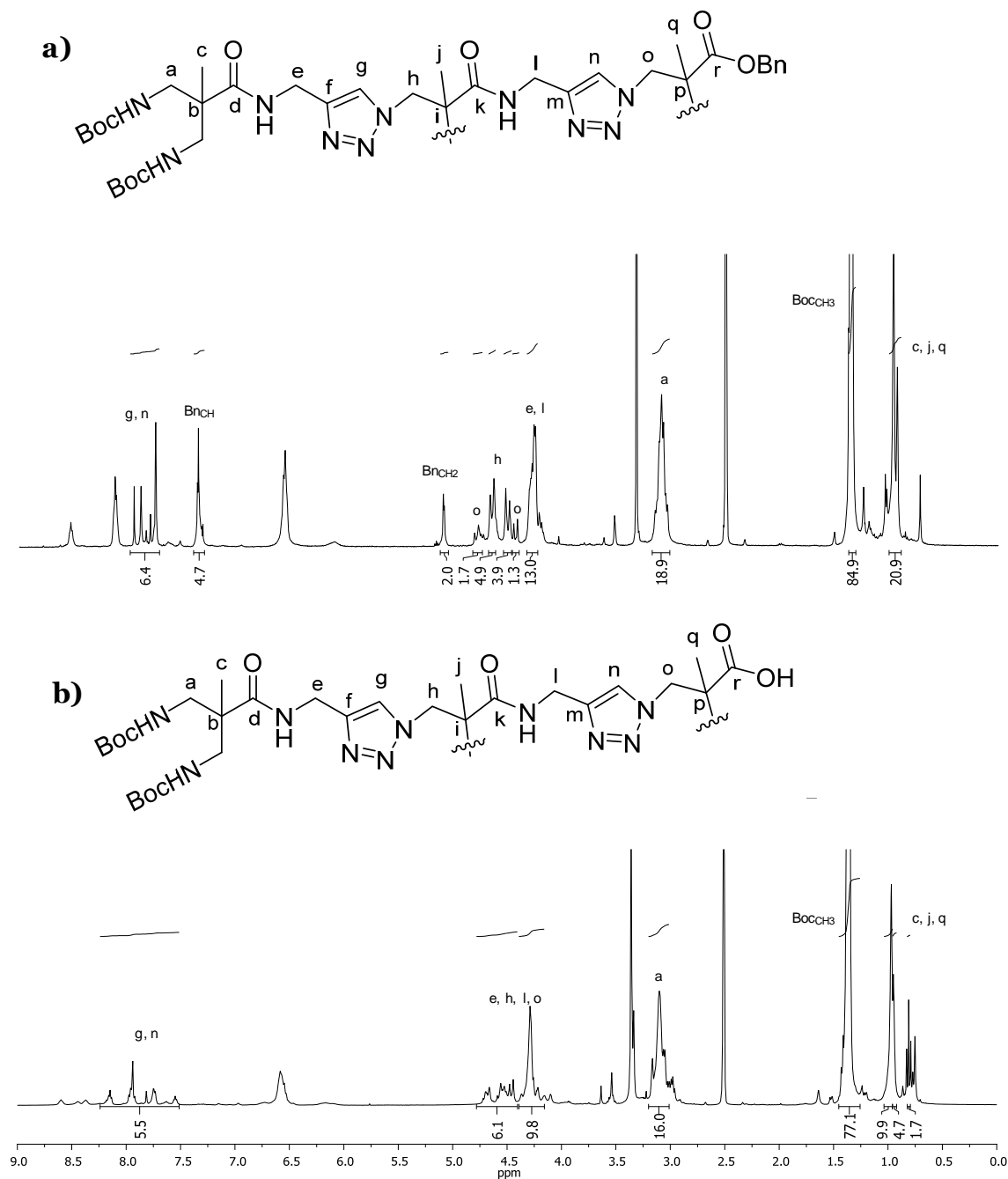


Figure 34. ^1H NMR spectra of **a)** $\text{dG3-CO}_2\text{Bn}$ and **b)** $\text{dG3-CO}_2\text{H}$ in DMSO.

III.2.4.3 Synthesis of dG3

The amidation reaction between the carboxylic moiety of **dG3-CO₂H** and commercial propargylamine to synthesize **dG3** was carried out following the optimized reaction conditions used in the synthesis of **dG1** and **dG2** (Figure 35). The compound was obtained as a solid with 68% yield.

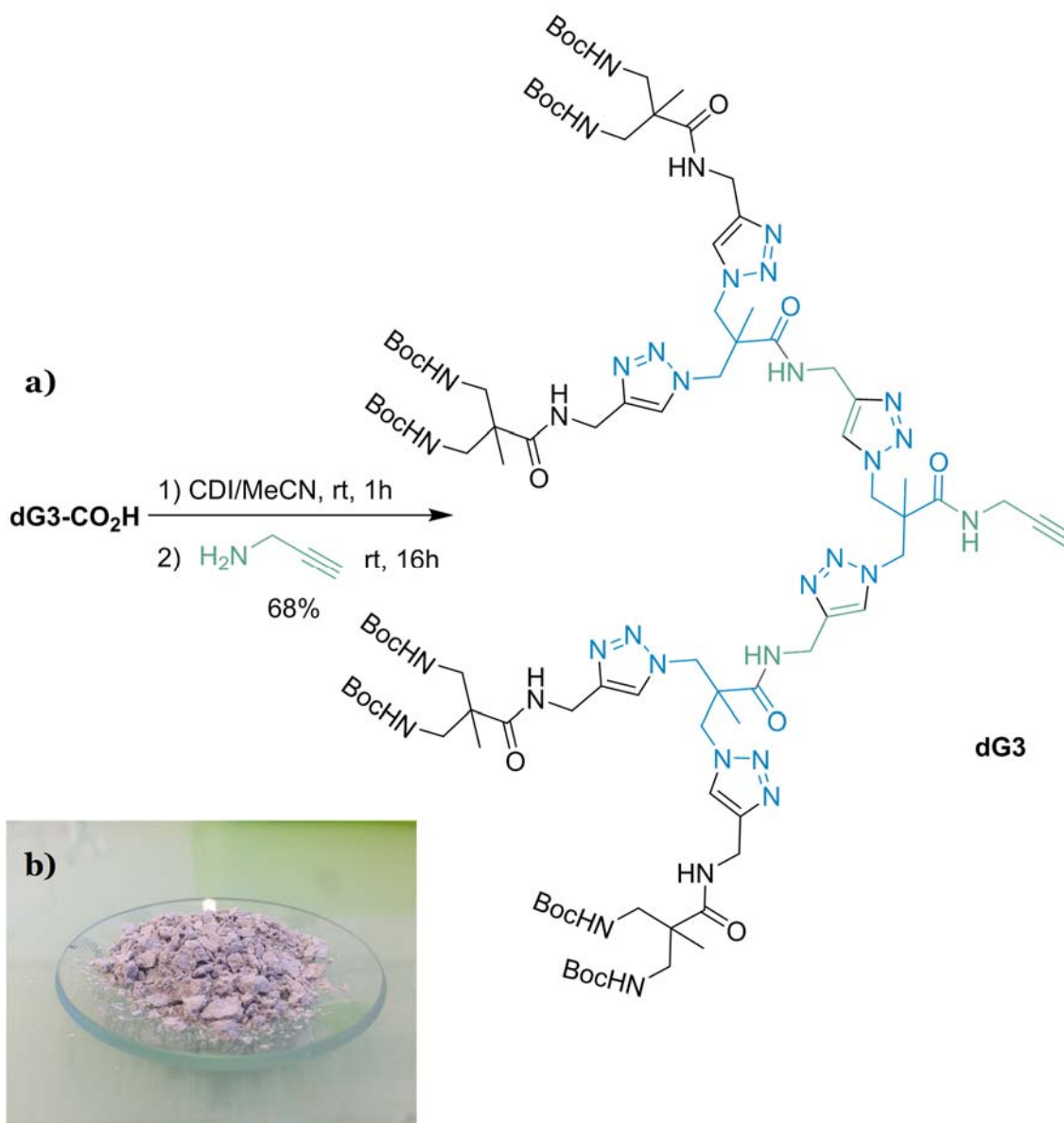


Figure 35. a) Synthesis of **dG3**; **b)** picture of **dG3**.

In ^1H NMR (Figure 36, Figure 149) new signals appear at 3.83 and 1.74 ppm and in ^{13}C NMR (Figure 150) at 79.6, 73.1 and 28.6 ppm corresponding to the introduction of the acetylene moiety in the molecular structure.

If we compare the NMR spectra of the different generation dendrons (Figure 36), we can find a pattern of assignation in the signals. In table 5, the assignation of the proton signals of the three dendrons (**dG1**, **dG2** and **dG3**) is resumed.

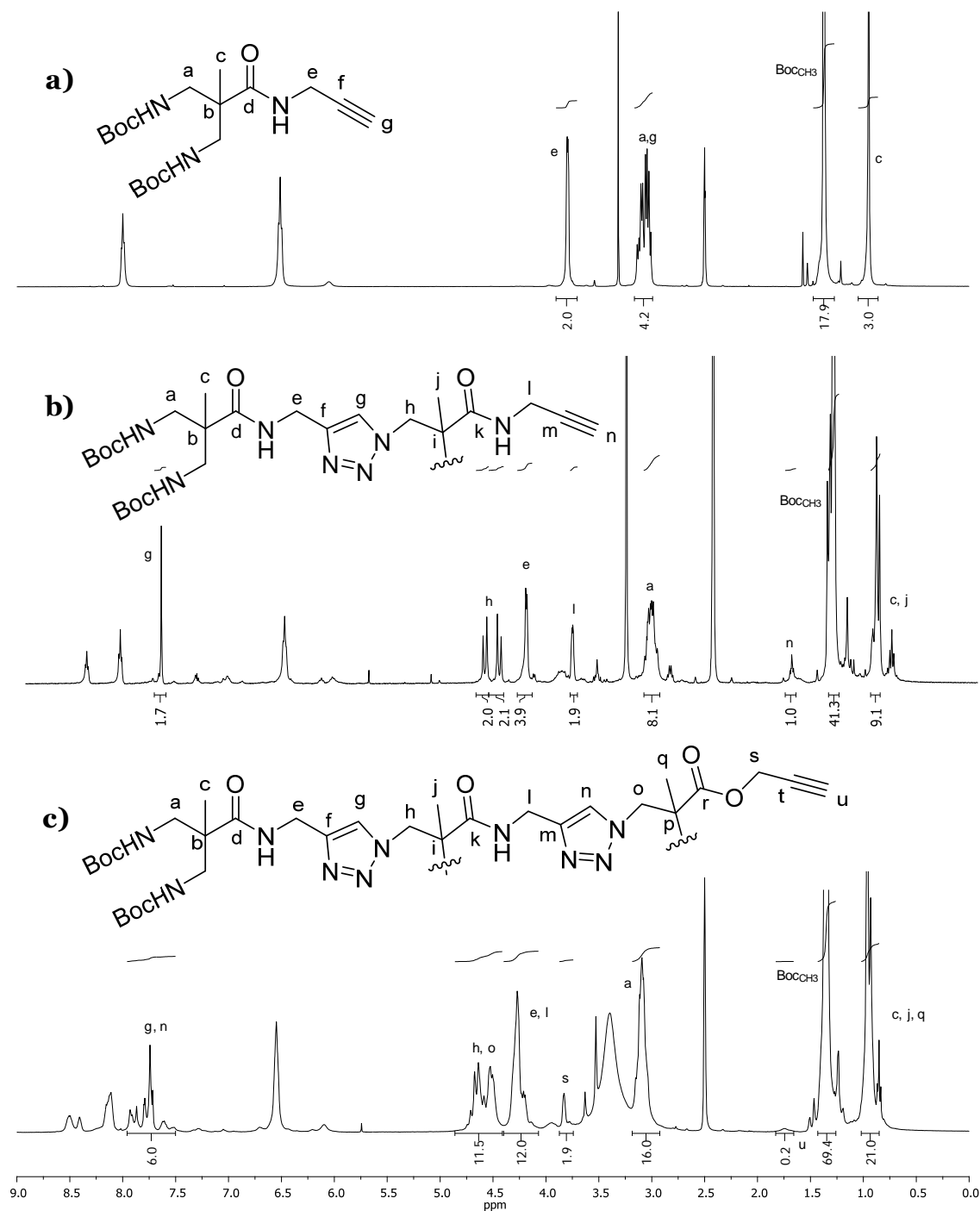


Figure 36. ¹H NMR spectra of **a) dG1**, **b) dG2** and **c) dG3** in DMSO.

Position	¹ H NMR (ppm)		
	dG1	dG2	dG3
BOCCH ₃	1.37 (s, 18 H)	1.36 (s, 36 H)	1.35 (s, 72 H)
a	3.14-3.01 (m, 5 H)	3.12-3.07 (m, 8 H)	3.20-2.95 (m, 16 H)
c	0.95 (s, 3 H)	0.96 (s, 6 H)	0.96-0.93 (m, 21 H)
e	3.80 (dd, <i>J</i> = 4.8, 2.1 Hz, 2 H)	4.27 (s, 4 H)	4.39-4.15 (m, 12 H)
g	3.14-3.01 (m, 5 H)	7.72 (s, 2 H)	7.93-7.54 (m, 6 H)
h		4.66 (d, <i>J</i> = 14.1 Hz, 2 H) 4.52 (d, <i>J</i> = 14.1 Hz, 2 H)	4.71-4.53 (m, 12 H)
j		0.93 (s, 3 H)	0.96-0.93 (m, 21 H)
l		3.83 (d, <i>J</i> =2.7 Hz, 2 H)	4.39-4.15 (m, 12 H)
n		1.76 (s, 1H)	7.93-7.54 (m, 6 H)
o			4.71-4.53 (m, 12 H)
q			0.96-0.93 (m, 21 H)
s			3.83 (s, 2 H)
u			1.74 (s, 1 H)

Table 5. ¹H NMR signals assignments of dG1, dG2 and dG3 in DMSO.

From this table some practical conclusions can be drawn to facilitate and predict the future signal assignment of higher-generation dendrons: methyl groups, (c, j, q...) appear at around 0.95-1 ppm, the methylene groups more

proximate to the amino protected groups, *a*, appear at higher field (3.00-3.10 ppm) than those more internal (*h*, *o*...) (4.50-4.70 ppm), the closest methylenes to the 1,2,3-triazole cycle (*e*, *l*...) can be seen at around 4.30 ppm while the proton corresponding to this cycle (*g*, *n*...) appears in the aromatic region of the spectra, finally, the two characteristic signals of the acetylene moiety can be found at around 3.80 ppm for the methylene and at around 1.75 ppm for the terminal proton.

III.2.5 Synthesis of a Family of Dendrimers, **G1_{EDA}NH₂**, **G2_{EDA}NH₂** and **G3_{EDA}NH₂**.

The efficiency of the proposed methodology for the construction of different generation dendrimers was evaluated using 1,2-diazidoethane as core. Using the different generations of dendrons synthesized, we have carried out the synthesis of a family of dendrimers with an ethylene moiety in its core. After the *click* reaction between the dendron and the core unit, a final step of deprotection of the amine groups is needed to obtain the desired dendrimeric structures.

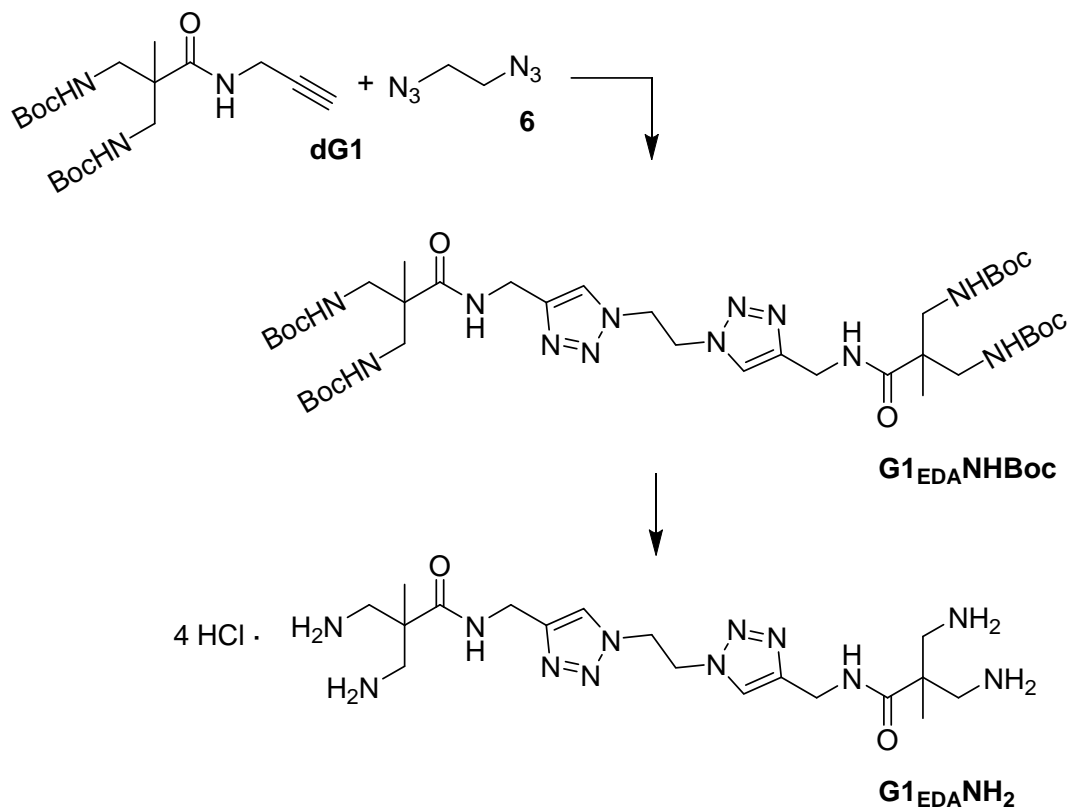


Figure 37. Scheme for **G1_{EDA}NH₂**.

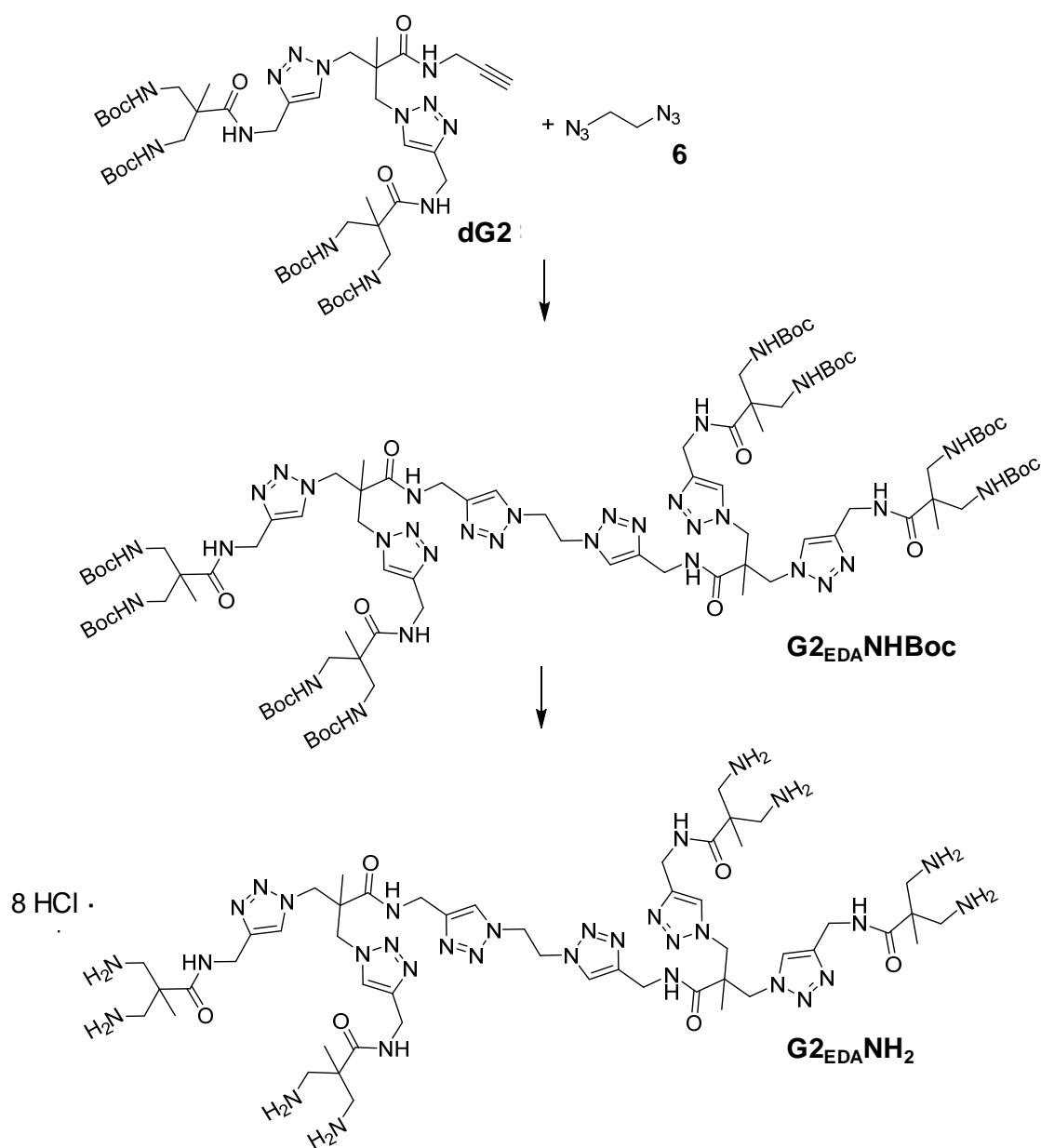
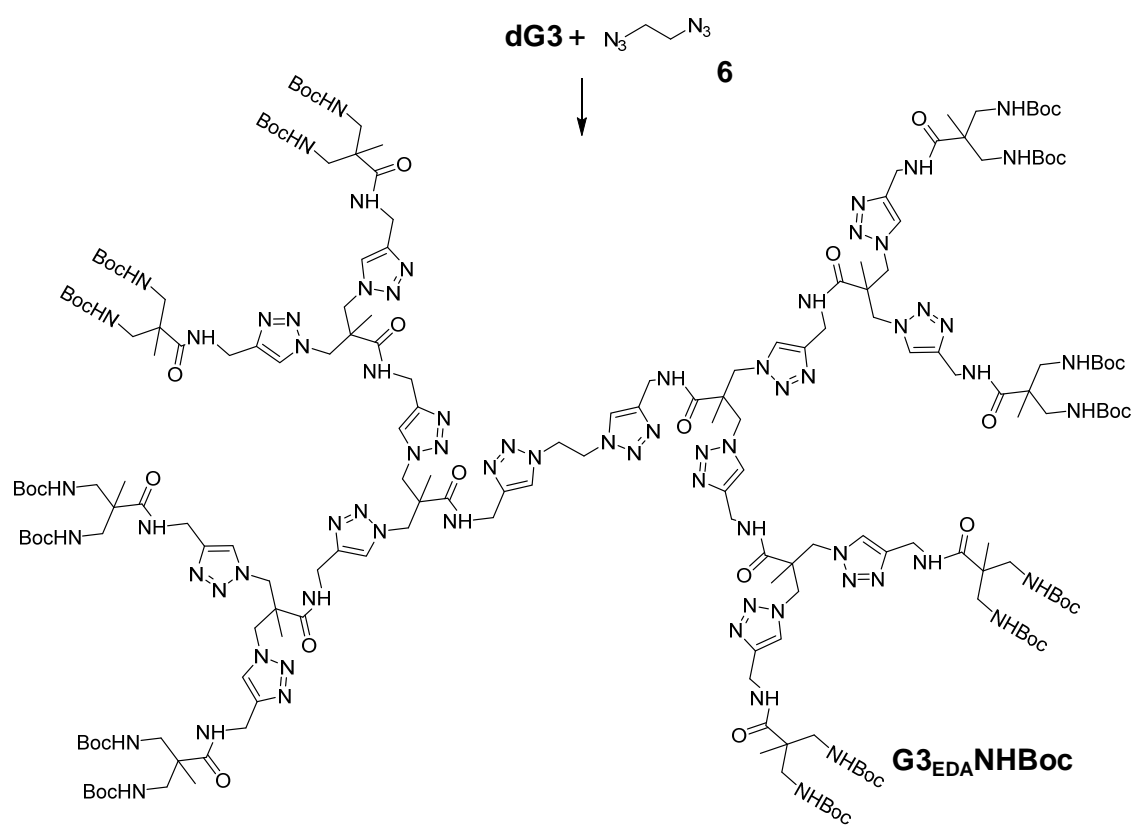


Figure 38. Scheme for $G2_{EDA}NH_2$.



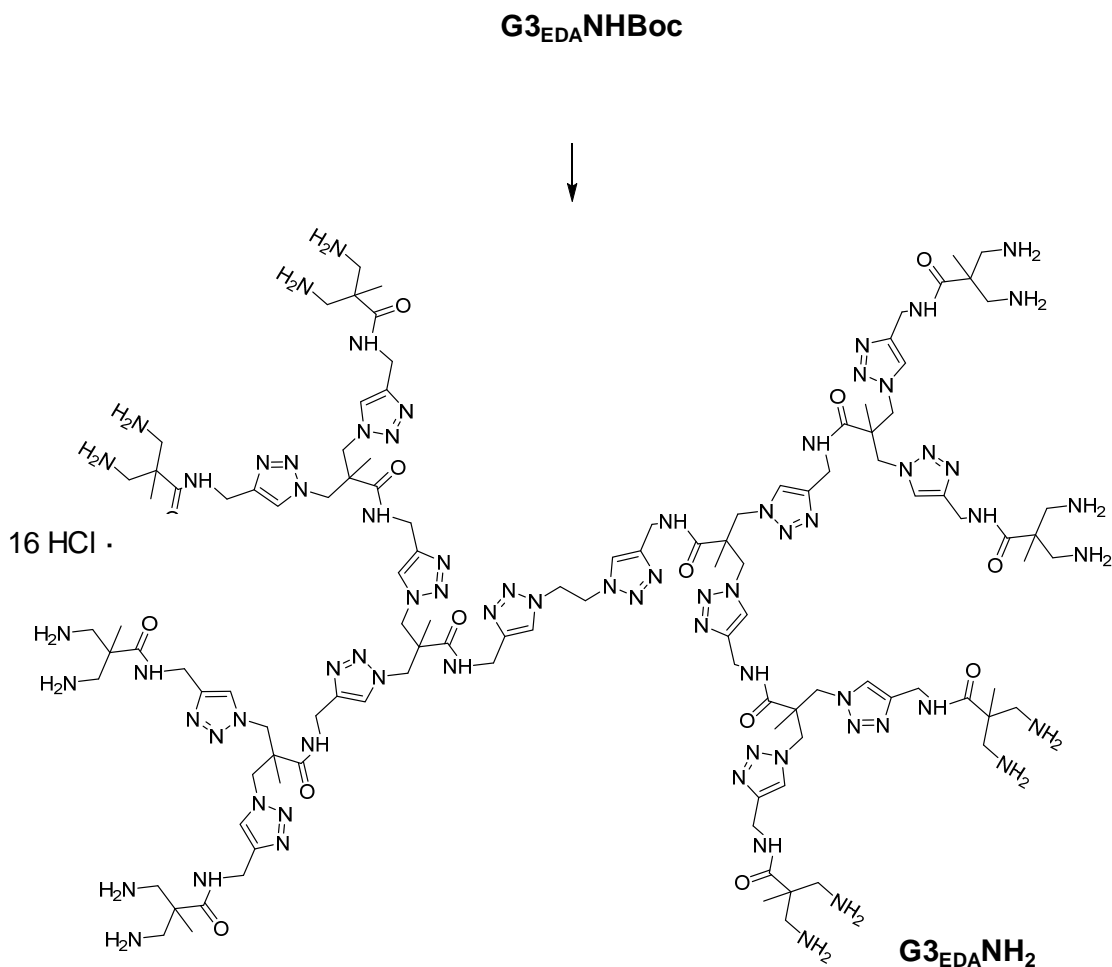


Figure 39. Scheme for **G3_{EDA}NH₂**.

III.2.5.1 Synthesis of 1,2-diazidoethane (**6**)

Synthesis of **6** was carried out following the general procedure to obtain diazidoalkanes described by Blumenstein.¹⁴¹ To a solution of 1,2-dibromoethane in DMF, sodium azide was added (Figure 40). The resulting solution was heated at 50°C overnight. Afterwards, hexane was added, and the mixture was washed with water. The organic phase was dried, filtered and concentrated under reduced pressure to obtain **13** as a colorless oil with 43% yield.

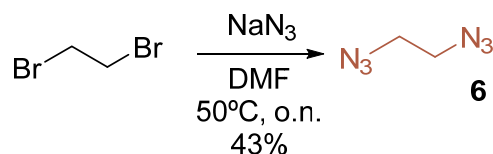


Figure 40. Synthesis of **6**.

The ^1H NMR spectrum (Figure 152) shows a single signal (singlet) at 3.46 ppm corresponding to the methylene groups.

III.2.5.2 Synthesis of $\text{G1}_{\text{EDA}}\text{NHBoc}$

The *click* reaction between dG1 and **6** resulted in the first-generation dendrimer with four protected amino groups in its surface (Figure 41). The same reaction conditions as in the synthesis of $\text{dG2-CO}_2\text{Bn}$ and $\text{dG3-CO}_2\text{Bn}$ were used: **6**, dG1 , copper (II) sulphate 5-hydrate and L(+)-ascorbic acid sodium salt were dissolved in *tert*-butanol/water 1:2 and the mixture was stirred at room temperature for one week (Figure 41). Afterwards, the solvent was removed, the mixture dissolved in DCM and washed with NH_4OH . The aqueous phase was extracted with DCM and the combined organic layers were washed with a mixture of NH_4OH /Brine 1:1. After the removal of the solvent from the organic layer, the product was purified by precipitation in hexane to obtain $\text{G1}_{\text{EDA}}\text{NHBoc}$ as a colorless oil in a 92% yield.

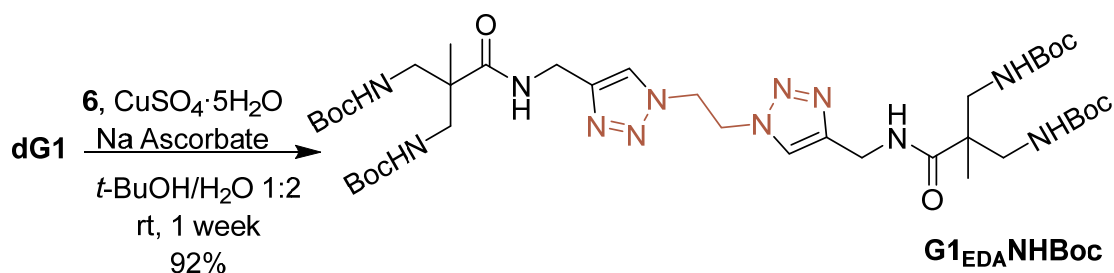


Figure 41. Synthesis of $\text{G1}_{\text{EDA}}\text{NHBoc}$.

IR spectrum of $\text{G1}_{\text{EDA}}\text{NHBoc}$ (Figure 42) shows the disappearance of the typical azide band at 2095 cm^{-1} when compared to the spectrum of compound **6**. There are no traces of the azido compound in the reaction mixture, resulting in defect-free dendrimeric structures.

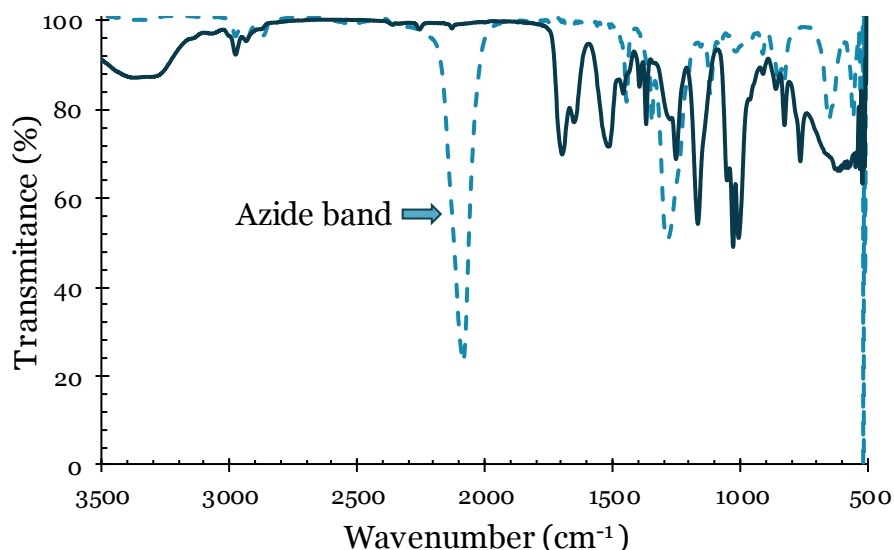


Figure 42. IR spectra of **G1EDANHBOC** (solid line) and compound **6** (dotted line).

The ^1H NMR spectrum (Figure 43, Figure 154) shows the typical signal of the 1,2,3-triazole cycle in the aromatic region (a singlet at 7.76 ppm) and another singlet at 4.82 ppm corresponding to the methylene from the core. The rest of the signals correspond to the **dG1** moiety: methylene groups next to the 1,2,3-triazole cycle form a doublet at 4.24 ppm, methylene groups next to boc appear as a multiplet at around 3.10 ppm, boc signals can be seen at 1.36 ppm and the methyl group appears as another singlet at 0.96 ppm.

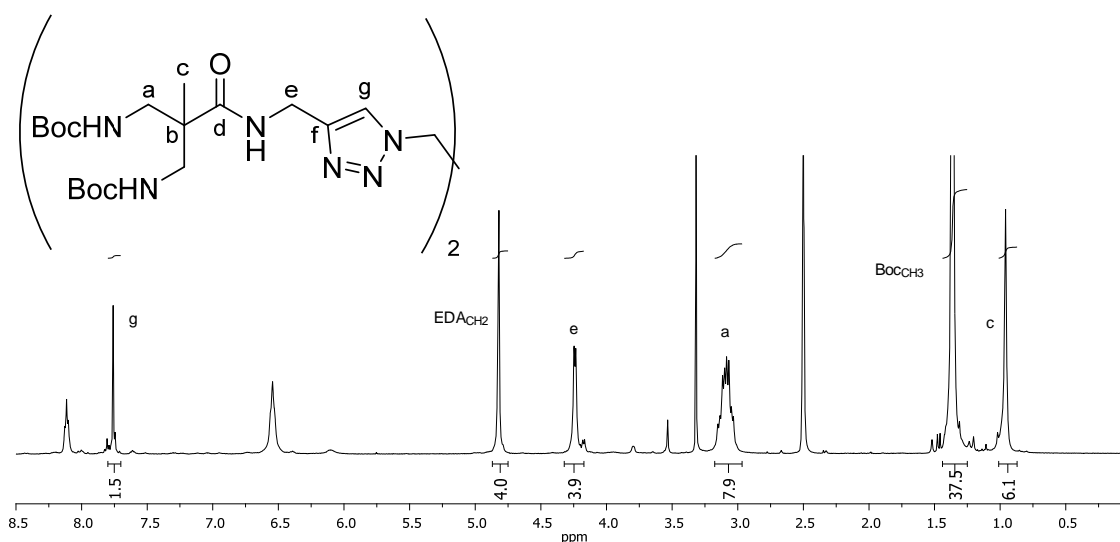


Figure 43. ^1H NMR spectrum of **G1EDANHBOC** in DMSO.

III.2.5.3 Synthesis of $G1_{EDA}NH_2$

The deprotection of the amino groups was carried out dissolving $G1_{EDANHBoc}$ in THF and cooling the solution in an ice-water bath. HCl 4M in dioxane was added dropwise and the mixture was stirred for 16 hours (Figure 44). Afterwards, the solvent was evaporated under vacuum. The compound was purified by exclusion chromatography using a sephadex column to result in the desired product as a white solid in quantitative yield.

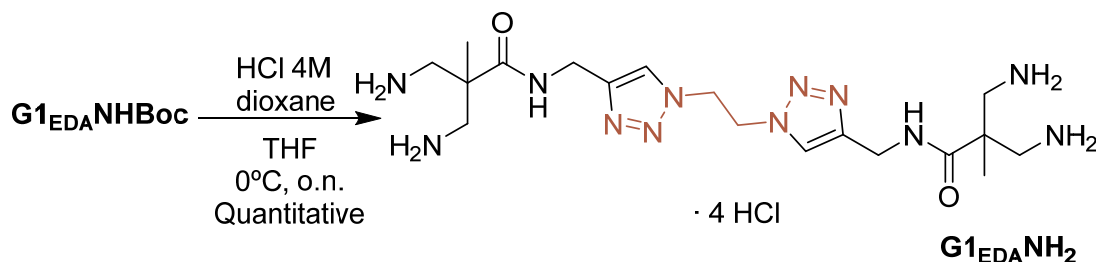


Figure 44. Synthesis of $G1_{EDANH_2}$.

The compound was fully characterized using NMR techniques such as ^1H , ^{13}C and HSQC NMR (Figure 157, Figure 158 and Figure 159, respectively). In ^1H NMR spectrum (Figure 53, Figure 157) is worth noticing the disappearance of the signal at 1.35 ppm corresponding to the methyl groups of the Boc groups. The rest of the signals are present: singlet at 7.85 ppm corresponding to the proton of the 1,2,3-triazole ring, singlet at 4.94 ppm corresponding to the methylene groups of the core unit, singlet at 4.49 ppm corresponding to the methylene groups next to the 1,2,3-triazole ring, two doublets at 3.34 and 3.15 ppm corresponding to the methylene groups next to the amines and a singlet at 1.36 ppm corresponding to the methyl group.

III.2.5.4 Synthesis of $G2_{EDANHBoc}$

The second-generation of this family of dendrimers was achieved by a *click* reaction between the second-generation dendron, **dG2**, and the core, **6** (Figure 45). The reaction condition as well as the subsequent work up and purification was the same as in the synthesis of the first-generation dendrimer analogue. $G2_{EDANHBoc}$ was obtained as a colorless solid in 80% yield.

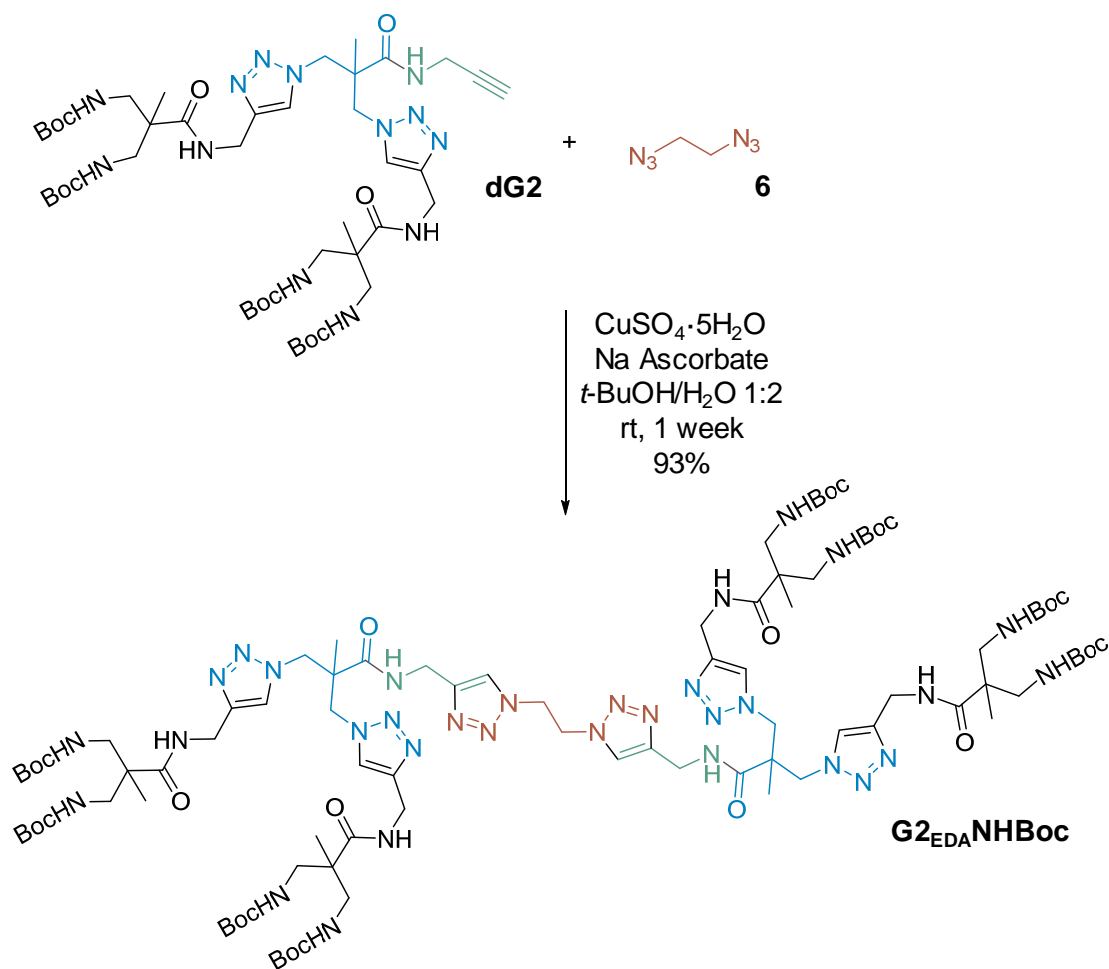


Figure 45. Synthesis of **G₂_{EDANHBoc}**.

IR spectrum (Figure 46) shows no presence of azido groups, as the azide band (2095 cm^{-1}) disappears when comparing it to the spectrum of the starting material **6**.

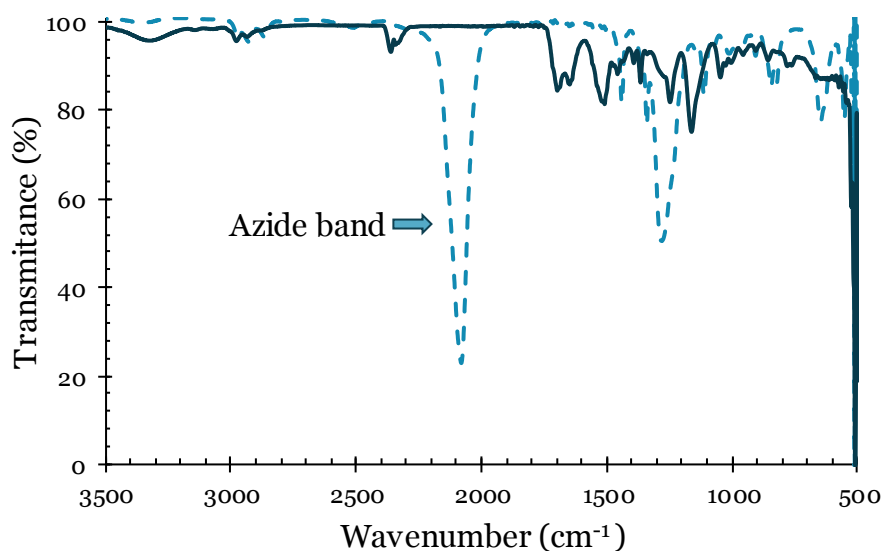


Figure 46. IR spectra of **G2_{EDA}NHBOC** (solid line) and compound **6** (dotted line).

The signals corresponding to the dendrimeric moiety as well as the one corresponding to the core are present in the ^1H NMR spectrum (Figure 47, Figure 16O). The formation of two new 1,2,3-triazole rings in dendrimers was confirmed by the appearance of triazole proton, as a multiplet at around 8.10 ppm, and the adjacent methylene, as a multiplet at around 4.20 ppm.

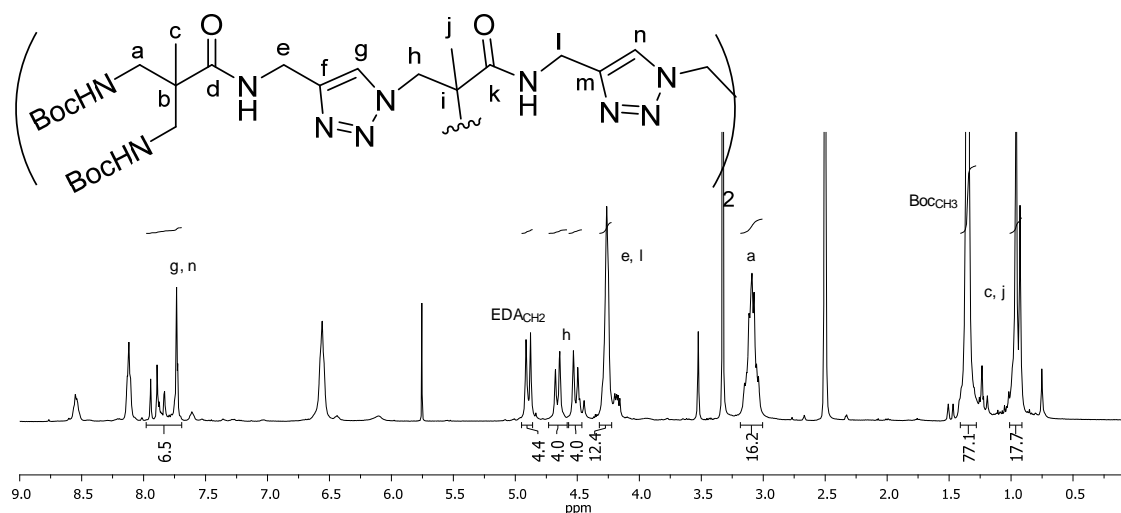


Figure 47. ^1H NMR spectrum of **G2_{EDA}NHBOC** in DMSO.

III.2.5.5 Synthesis of $G2_{\text{EDA}}\text{NH}_2$

The deprotection of the amino groups (Figure 48) was carried out following the same reaction conditions as in the synthesis of $G2_{\text{EDA}}\text{NH}_2$ and was obtained as a colorless solid in quantitative yield.

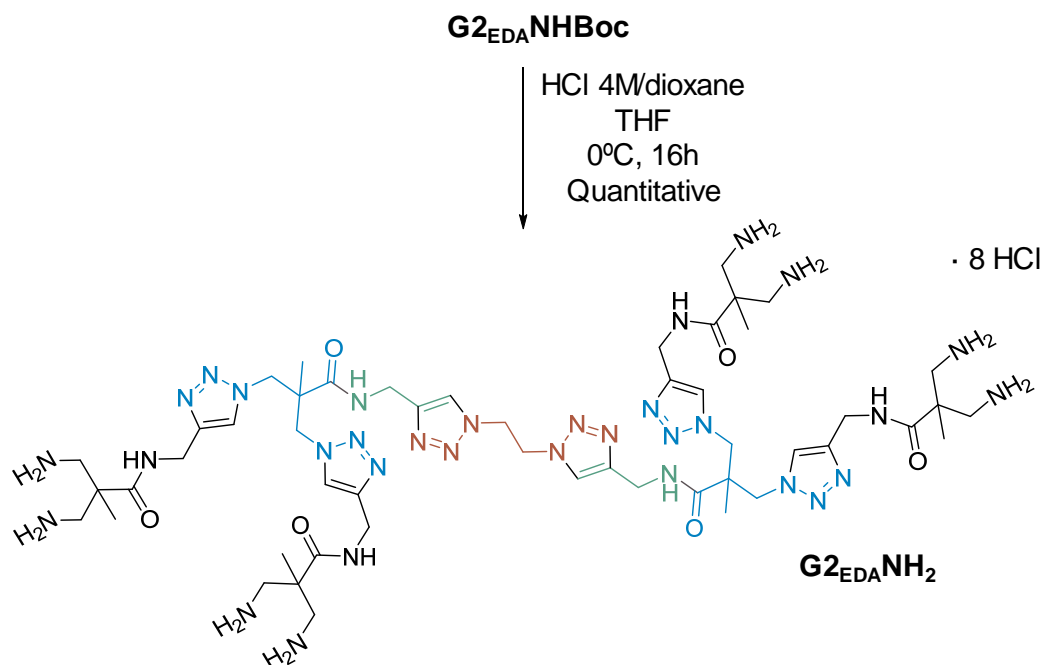


Figure 48. Synthesis of $G2_{\text{EDA}}\text{NH}_2$.

After purification by exclusion chromatography using a sephadex column, no signal of the protecting groups could be appreciated in the ^1H NMR spectra (Figure 53, Figure 163). The protons corresponding to the triazole rings are present in the aromatic region at around 7.80 ppm, the methylene groups of the unit core appear at around 5.00 ppm, the methylene groups adjacent to the triazole rings (e, l) form a multiplet at around 4.50 ppm, methylene groups next to the amines appear as doublets at around 3.80 ppm while the signals corresponding to the methyl groups are shown between 1.00-1.50 ppm.

III.2.5.6 Synthesis of $G3_{\text{EDA}}\text{NH}^+\text{Boc}^-$

Finally, the coupling of the third-generation dendron, **dG3**, and **6** resulted in a dendrimeric structure with sixteen protected amino groups (Figure 49). The *click* reaction was carried out in the presence of copper (II) sulphate 5-hydrate

and L(+)-ascorbic acid sodium salt during one week. The product was purified by precipitation in hexane to obtain it as a colorless solid in 93% yield.

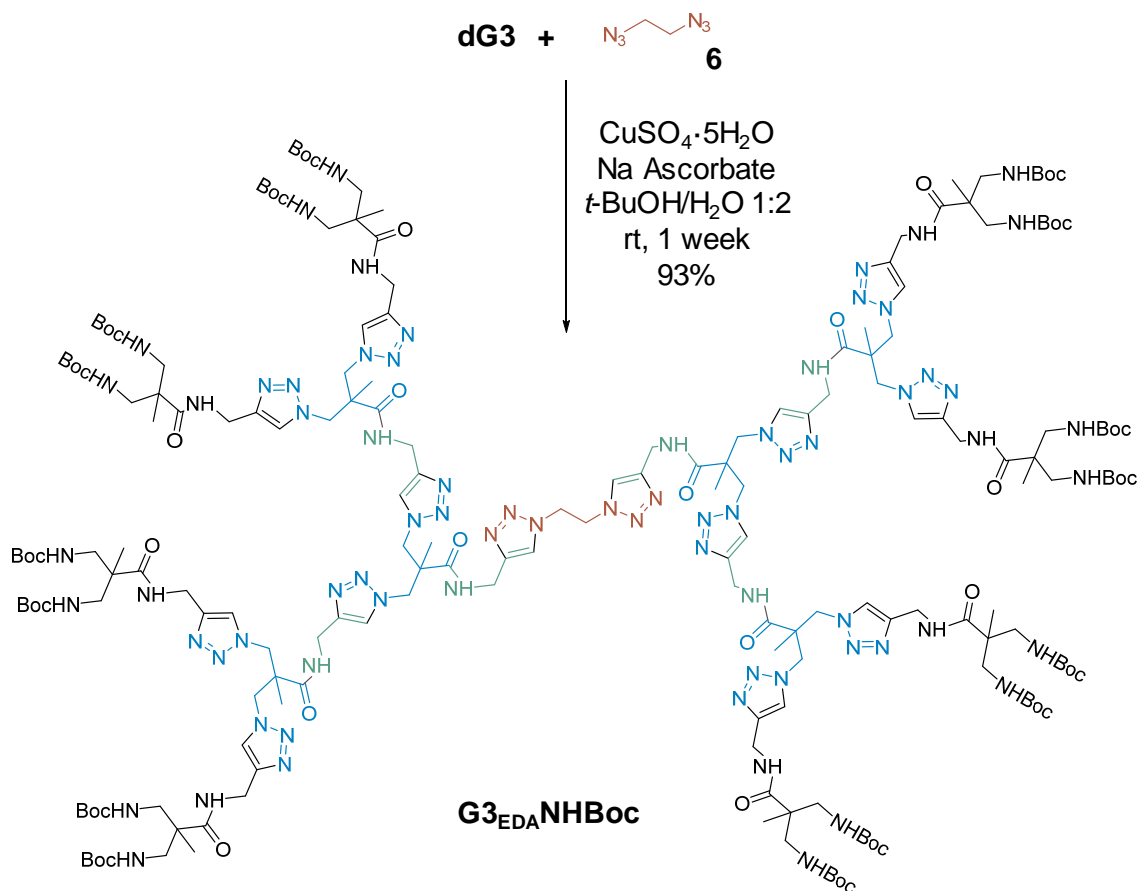


Figure 49. Synthesis of **G3_{EDA}NHBoc**.

Once again, the IR measurements (Figure 50) show the complete disappearance of the azide band at 2095 cm⁻¹, indicating that all azide groups of the starting material **6** have reacted successfully.

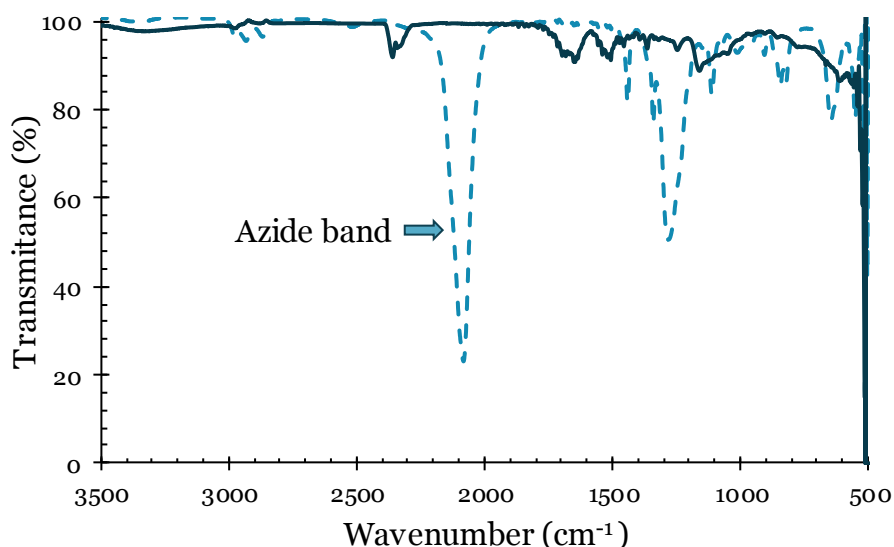


Figure 50. IR spectra of **G3EDANHoc** (solid line) and compound **6** (dotted line).

The compound was also characterized using NMR techniques such as ^1H and ^{13}C NMR and bi-dimensional experiments (HSQC) in order to assign the signals correctly (Figure 166, Figure 167 and Figure 168, respectively). The protons corresponding to the triazole rings are present as a multiplet in the aromatic region at around 7.80 ppm, the methylene groups of the unit core appear below 5.00 ppm, the methylene groups adjacent to the triazole rings (e, l, s) form a multiplet at around 4.25 ppm, methylene groups next to the boc groups appear at around 3.20 ppm while the signals corresponding to the methyl groups are shown between 1.00-1.50 ppm (Figure 51, Figure 166).

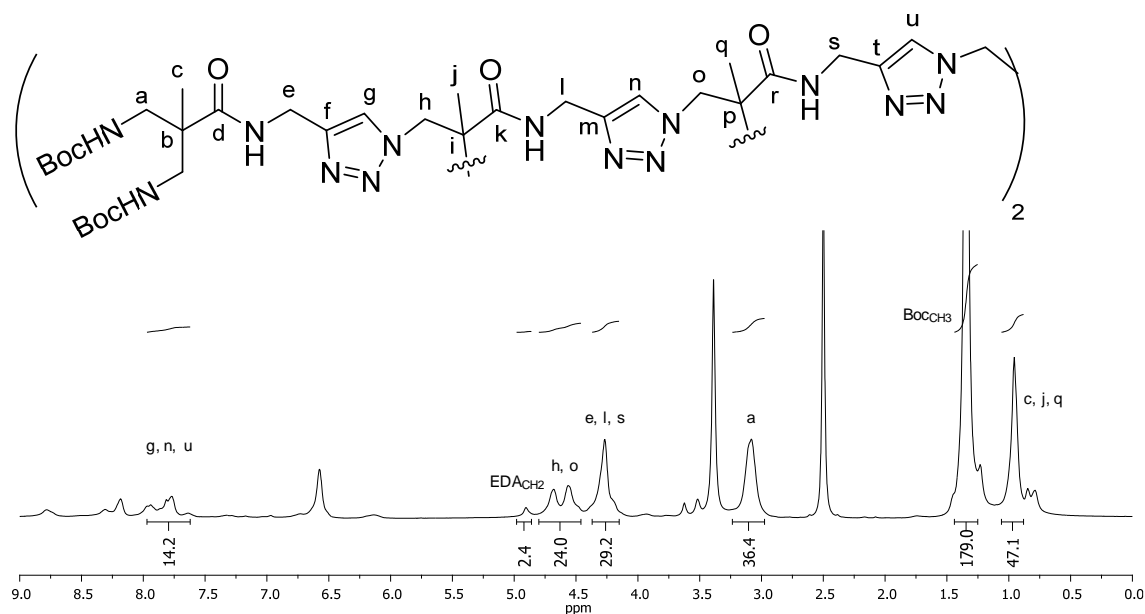


Figure 51. ^1H NMR spectrum of $\text{G3}_{\text{EDANH Boc}}$ in DMSO.

III.2.5.7 Synthesis of $\text{G3}_{\text{EDANH}_2}$

After the deprotection of the amine groups in acidic medium (Figure 52) and subsequent purification of the product by sephadex column, $\text{G3}_{\text{EDANH}_2}$ was successfully obtained as a white solid in quantitative yield.

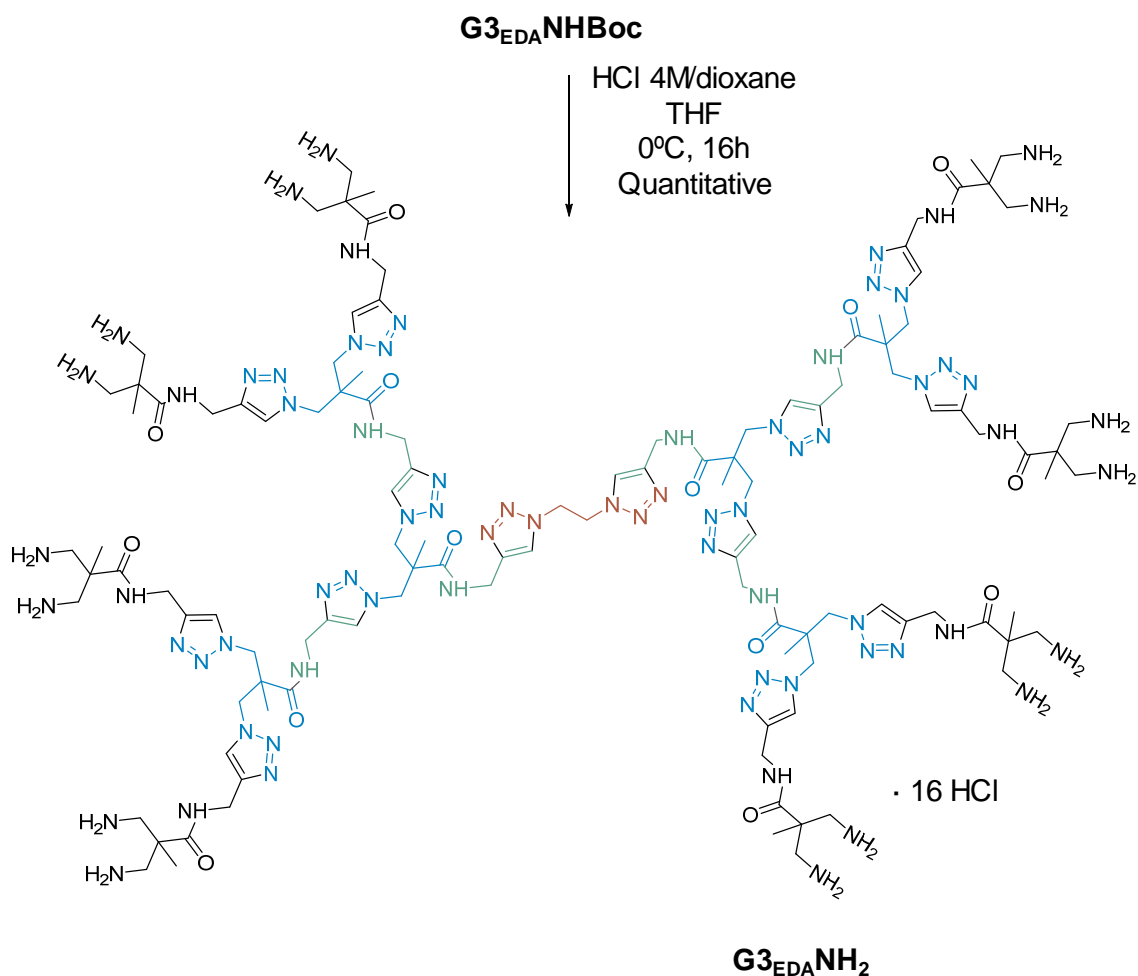
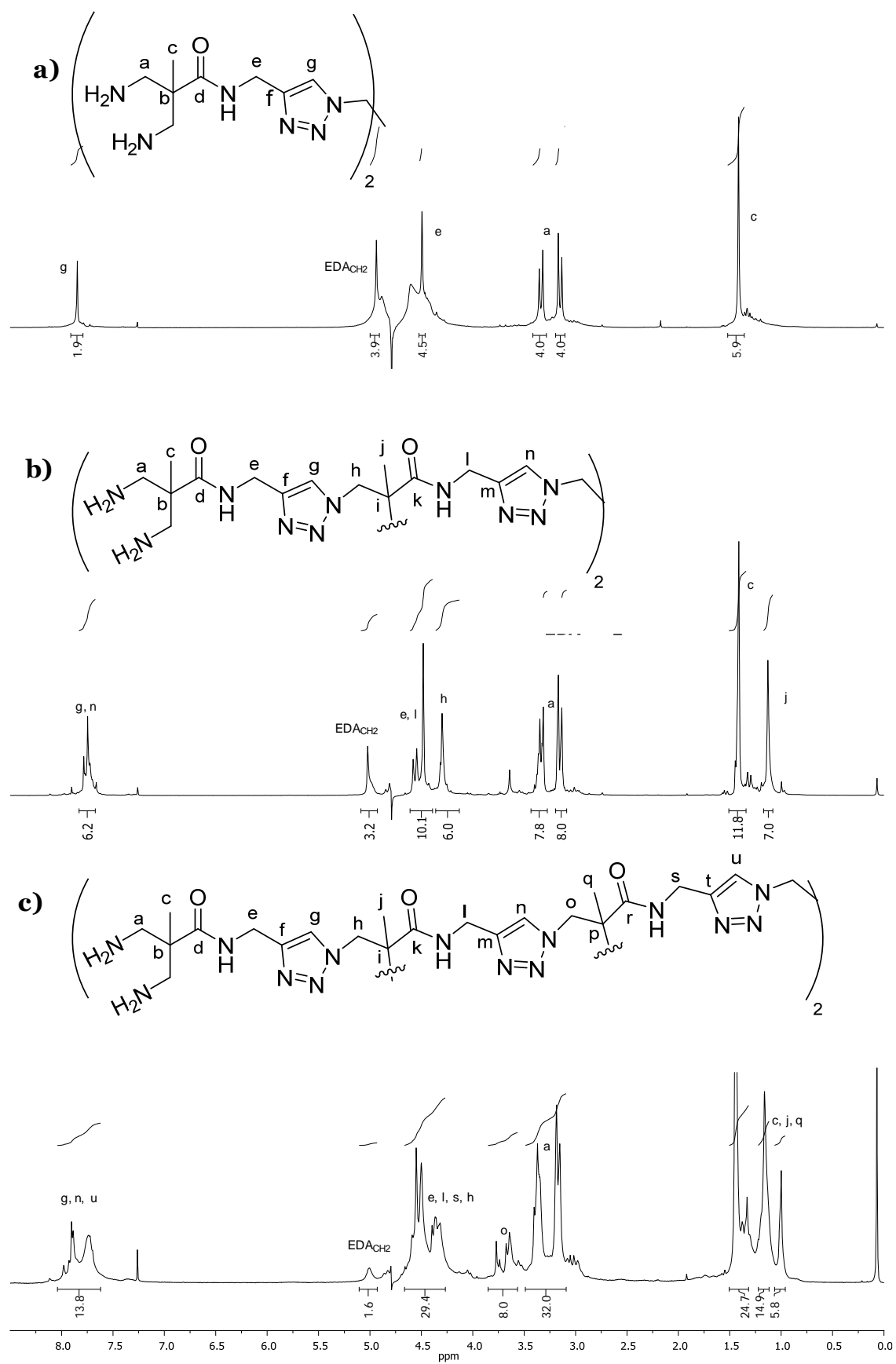


Figure 52. Synthesis of **G3_{EDA}NH₂**.

NMR experiments showed no traces of protecting group signals, indicating that all amino groups were successfully deprotected.

If we compare the NMR spectra of the different generation dendrimers (Figure 53), we can find a pattern of assignation in the signals. Table 6 summarizes the assignation of ¹H NMR signals for the three-generations dendrimers, **G1_{EDA}NH₂**, **G2_{EDA}NH₂** and **G3_{EDA}NH₂**. From table some conclusions can be drawn: the protons of the 1,2,3-triazole cycle (*g*, *n*, *u*) are found at low field in the aromatic region, the signals corresponding to the methylenes of the core (*EDA*CH₂) appear between 4.50-5.00 ppm. As the generation grows, the difficulty to discern the signals increases, obtaining in the spectrum of the third-generation dendrimer multiplets corresponding to variety

of signals. In general, peripheral methylenes (*a*) appear at higher field than those internal (*h*, *o*). Finally, methyl groups are found between 1.50-1.00 ppm.


 Figure 53. ^1H NMR spectra of **a)** G_1EDANH_2 , **b)** G_2EDANH_2 and **c)** G_3EDANH_2 in D_2O .

Position	¹ H NMR (ppm)		
	G1_{EDANH₂}	G2_{EDANH₂}	G3_{EDANH₂}
a	3.34 (d, $J = 13.5$ Hz, 4 H) 3.15 (d, $J = 13.5$ Hz, 4 H)	3.33 (d, $J = 13.5$ Hz, 8 H) 3.15 (d, $J = 13.5$ Hz, 8 H))	3.44-3.09 (m, 32 H)
c	1.42 (s, 6 H)	1.41 (s, 12 H)	1.45 (s, 24 H)
e	4.49 (s, 4 H)	4.58-4.43 (m, 12 H)	4.66-4.20 (m, 44H)
g	7.85 (s, 2 H)	7.78-7.66 (m, 6 H)	8.04-7.62 (m, 14 H)
h		4.31 (s, 8 H)	4.66-4.20 (m, 32H)
j		1.13 (s, 6 H)	1.16 (s, 12 H)
l		4.58-4.43 (m, 12 H)	4.66-4.20 (m, 44H)
n		7.78-7.66 (m, 6 H)	8.04-7.62 (m, 14 H)
o			3.85-3.56 (m, 8 H)
q			1.00 (s, 6 H)
s			4.66-4.20 (m, 44H)
u			8.04-7.62 (m, 14 H)
EDACH ₂	4.94 (s, 4 H)	5.02 (s, 4 H)	4.55 (s, 4 H)

Table 6. ¹H NMR signals assignments of **G1_{EDANH₂}**, **G2_{EDANH₂}** and **G3_{EDANH₂}** in D₂O.

III.2.6 Synthesis of Dendrimers with Aromatic Cores, **G3_{3AB}NH₂** and **G3_{4AB}NH₂**

Making use of the convergent methodology, we proposed the synthesis of dendrimers with 24 and 32 superficial amino groups in only one *click* reaction. For that purpose, tri- and tetra- azido cores were synthesized (**7** and **8**) and reacted with **dG3**. Aromatic cores were choosing to introduce a rigid core in the molecules.

III.2.6.1 Synthesis of 1,3,5-tris(azidomethyl)benzene (**7**)

The compound was synthesized as described previously.¹⁴² 1,3,5-tris(bromomethyl)benzene was dissolved in DMF and sodium azide was added. The reaction mixture was stirred for at 85°C for 16 hours (Figure 54). After cooling, water was added, and the mixture was extracted with CH₂Cl₂. The combined organic phases were dried, filtered and concentrated to provide compound **7** in 98% yield.

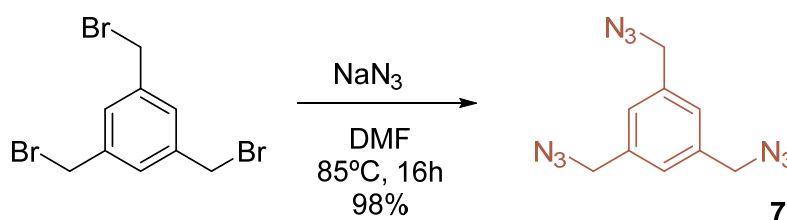


Figure 54. Synthesis of compound **7**.

The ¹H NMR spectrum (Figure 172) shows a singlet at 7.25 ppm corresponding to the aromatic protons and a singlet at 4.40 ppm corresponding to the methylene groups.

III.2.6.2 Synthesis of **G3_{3AB}NHBoc**

G3_{3AB}NHBoc was achieved by *click* reaction of **dG3** and **7** in the presence of copper (II) sulphate 5-hydrate and L(+)-ascorbic acid sodium salt for one week (Figure 55). After purification by precipitation in hexane, the desired product was obtained as a colorless solid in 59% yield.

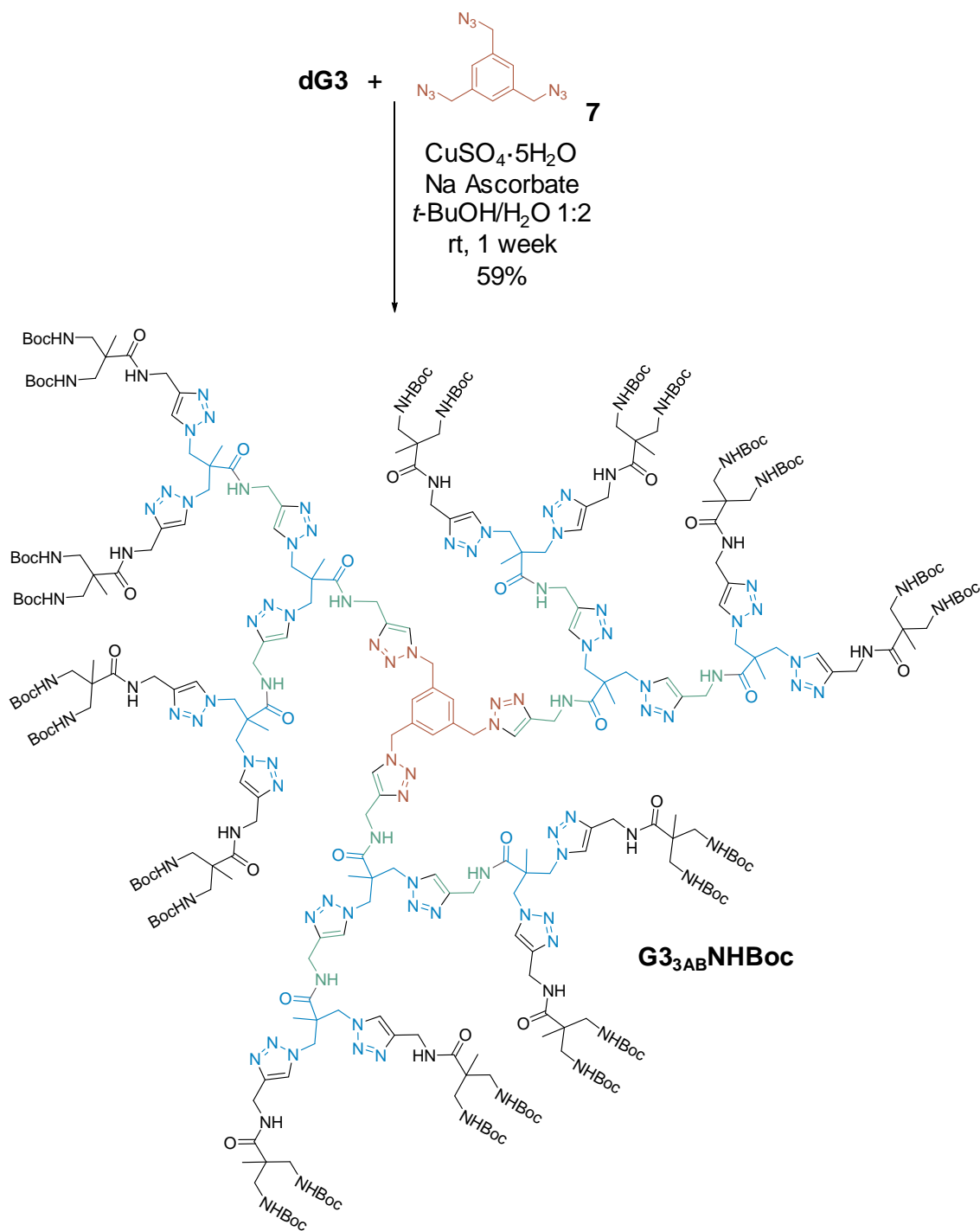


Figure 55. Synthesis of **G_{3AB}NHBoc**.

When comparing **G_{3AB}NHBoc** IR spectrum with that of compound **7** (Figure 56), the disappearance of the azide band (2095 cm^{-1}) is confirmed.

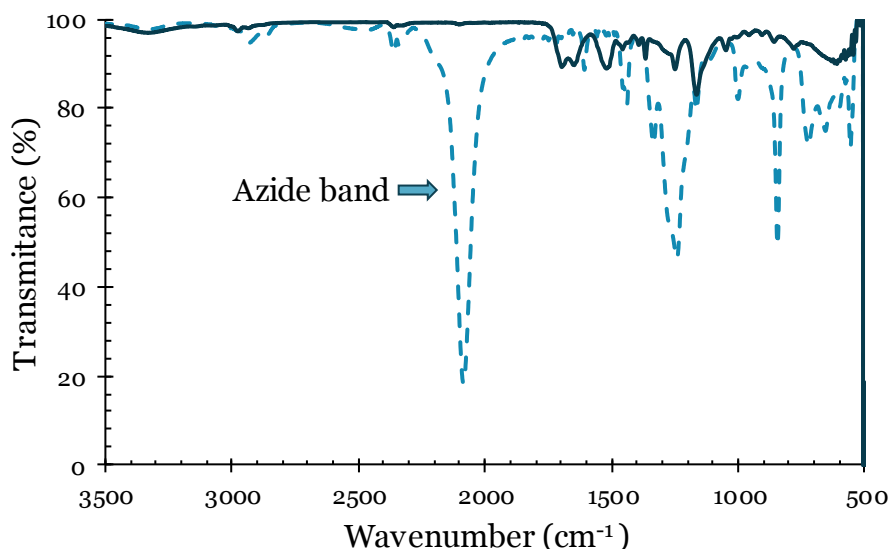


Figure 56. IR spectra of **G3_{AB}NHBoc** (solid line) and compound **7** (dotted line).

As above mentioned, as the dendrimer's size increases, the NMR signals are less defined, and the assignation of these signals becomes more challenging. However, there are resemblances to the NMR spectra of other smaller dendrimers already synthesized. The protons corresponding to the triazole rings and the aromatic core are present as a multiplet in the aromatic region at around 7.80 ppm, the methylene groups of the unit core appear at around 5.60 ppm, the methylene groups adjacent to the triazole rings (e, l, s) form a multiplet at around 4.25 ppm, methylene groups next to the boc groups appear at around 3.20 ppm and the rest of the methylene groups (h, o) form a multiplet at around 4.60 ppm. The signals corresponding to the boc groups appear at 1.34ppm and the methyl groups are shown as multiplet at around 1.00 ppm (Figure 57, Figure 173).

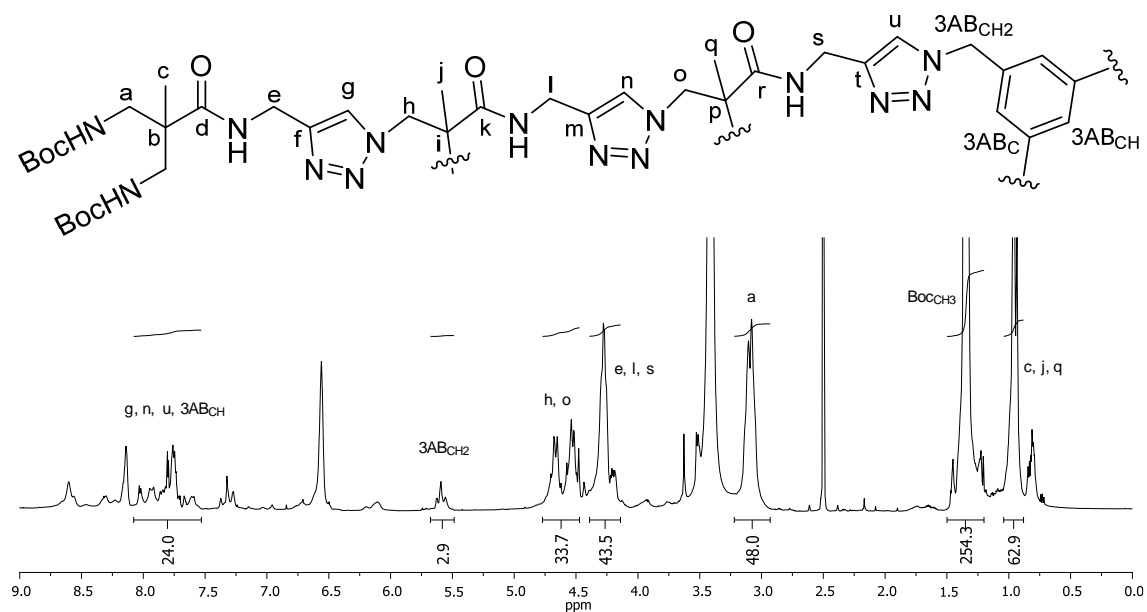


Figure 57. ^1H spectrum of $G_{3AB}NH\text{Boc}$ in DMSO.

III.3.6.3 Synthesis of $G_{3AB}NH_2$

The deprotection of the amino groups was carried out in presence of HCl (Figure 58). The product was purified by sephadex column to obtain a white solid in quantitative yield.

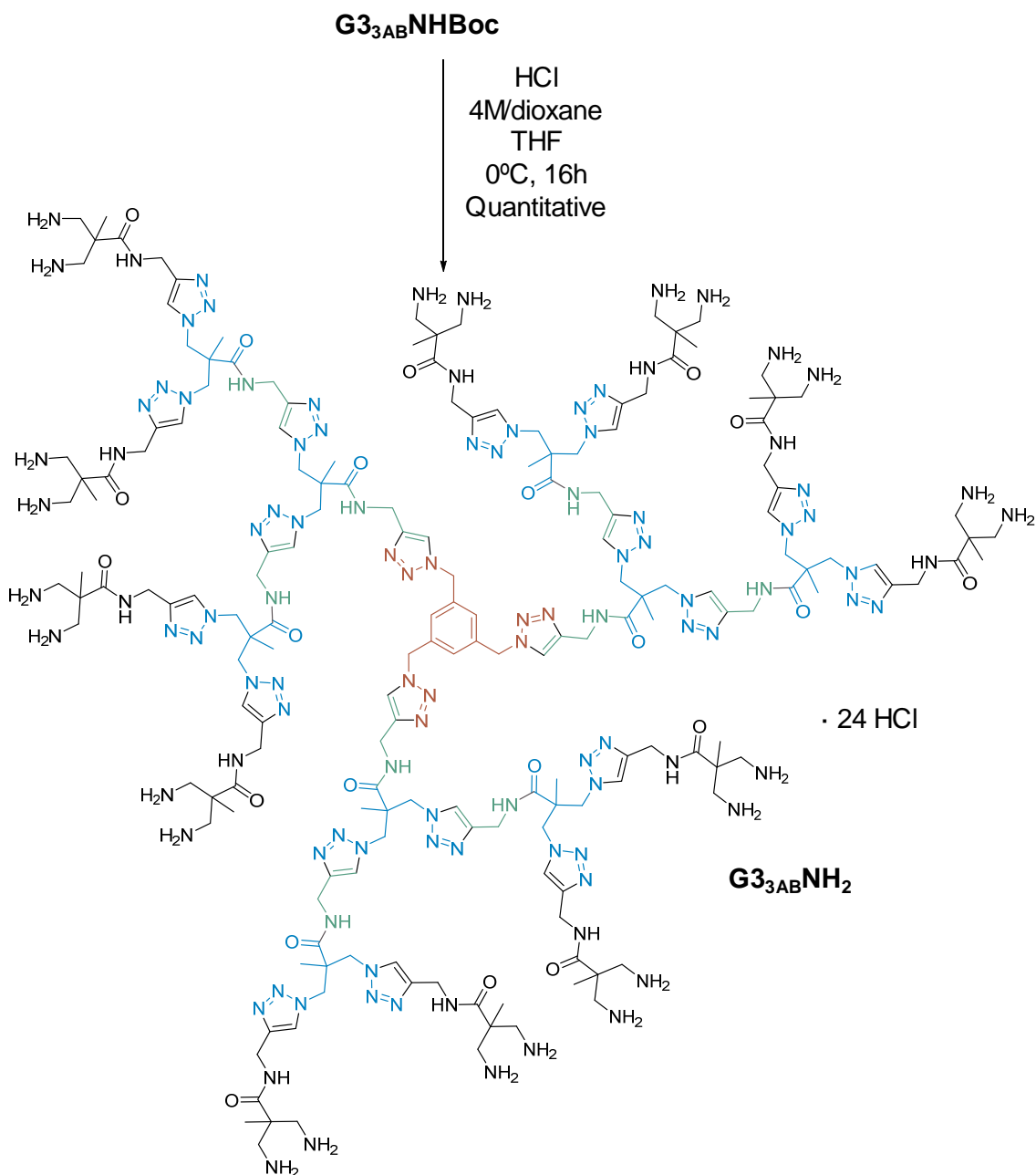


Figure 58. Synthesis of **G₃_{AB}NH₂**.

¹H NMR spectrum in deuterated water (Figure 59, Figure 176) shows the disappearance of the signal corresponding to the methyl groups of Boc as well as the shift to higher field of the *o* methylenes.

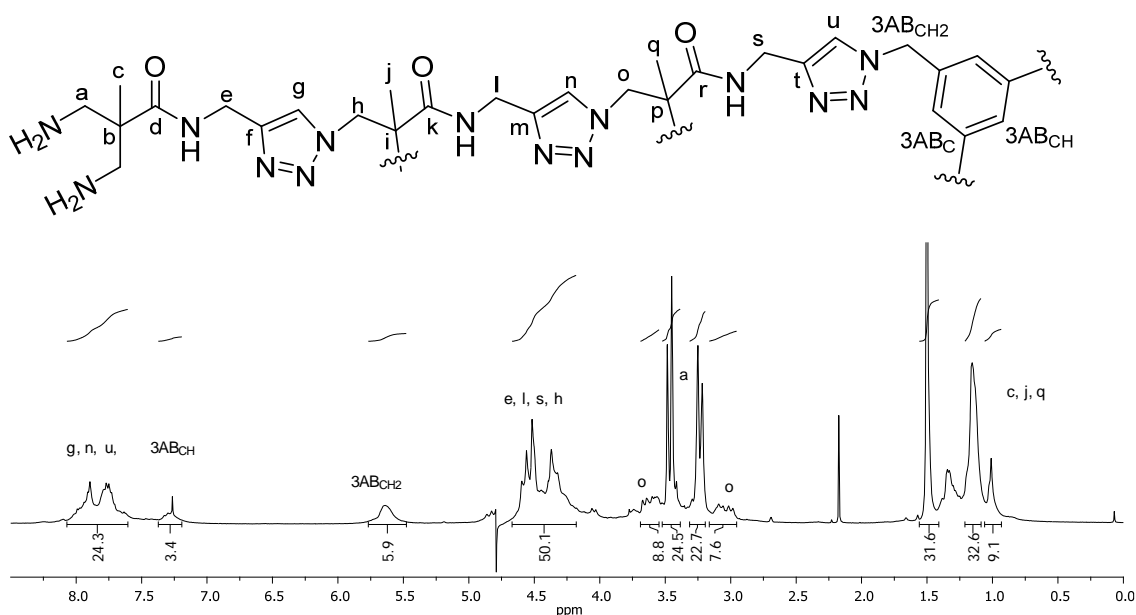


Figure 59. ^1H spectrum of $\text{G3}_{3\text{AB}}\text{NH}_2$ in D_2O .

III.2.6.4 Synthesis of 1,2,4,5-tetrakis(azidomethyl)benzene (**8**)

The compound was synthesized using the same reaction conditions described previously¹⁴² and for the synthesis of **7**. 1,2,4,5-tetrakis(bromomethyl)benzene was dissolved in DMF and sodium azide was added. The reaction mixture was stirred for at 85°C for 16 hours (Figure 60). After cooling, water was added, and the mixture was extracted with CH_2Cl_2 . The combined organic phases were dried, filtered and concentrated to provide compound **8** in 98% yield.

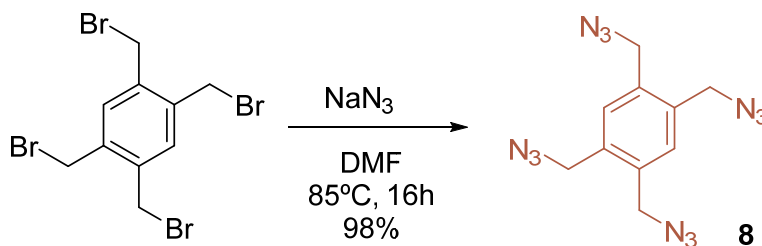


Figure 60. Synthesis of compound **8**.

The ^1H NMR spectrum (Figure 179) shows a singlet at 7.39 ppm corresponding to the aromatic protons and a singlet at 4.46 ppm corresponding to the methylene groups.

III.2.6.5 Synthesis of $G_{34AB}NHBoc$

Once again, a *click* reaction between **dG3** and **8** was carried out in the presence of copper (II) sulphate 5-hydrate and L(+)-ascorbic acid sodium salt for one week to synthesize $G_{34AB}NHBoc$ (Figure 61). However, the formation of the desired product was not possible using these conditions. IR experiments showed residues of the azide band which seemed to indicate that the core was not fully functionalized.

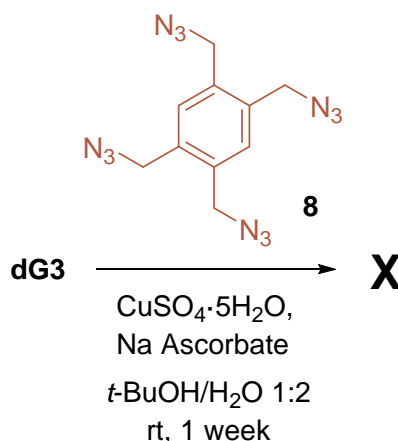


Figure 61. Synthesis of $G_{34AB}NHBoc$.

To solve this problem, we decided making use of the Microwave-assisted organic synthesis since it has become an indispensable tool for bond-forming reactions.¹⁴³ In general, microwave irradiation results in increased reaction rates and yields.¹⁴⁴ The microwave-assisted reaction between **dG3** and **8** was carried out employing CuSO_4 and sodium ascorbate at 85°C . After one hour of irradiation, the azide band at 2095 cm^{-1} was still observed in IR experiments. The reaction was put under irradiation for two more hours but no disappearance of the azide band was achieved. The results indicate that the fully functionalization of the core was unattainable, probably due to steric hindrance (Figure 62).

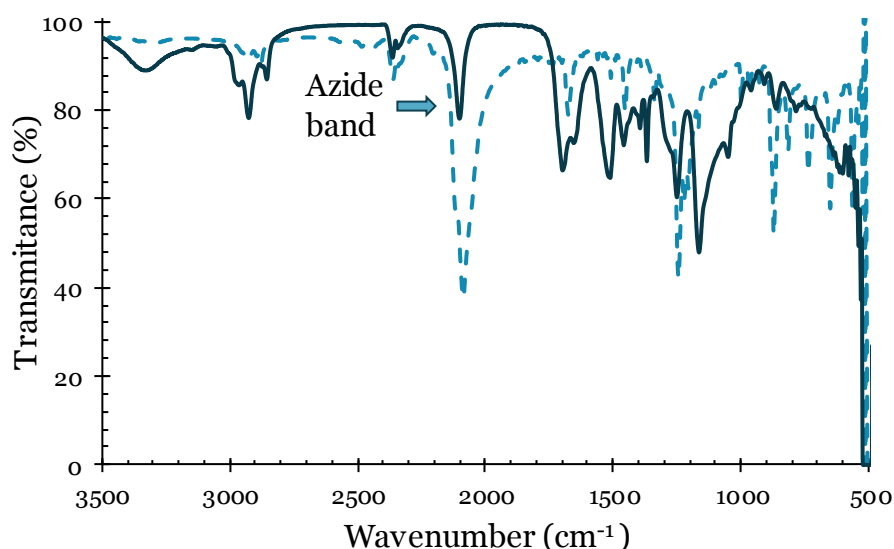


Figure 62. IR spectrum of the reaction between **DG3** and **8** after microwave irradiation for 3 hours (solid line) and compound **8** (dotted line).

III.2.7 Synthesis of a Fluorescent Dendrimer, **G3_{Naph}NH₂**

In order to introduce a functional core, a fluorescent naphthalimide derivative were chosen, since it is well known the potential applications of emissive dendrimer.^{118-119,145-146} Due to our group antecedents,¹³¹ we proposed the introduction of a 4-amino-1,8-naphthalimide moiety, owing to their excellent luminescent properties.

III.2.7.1 Synthesis of *N*-(3-azidopropyl)-4-((3-azidopropyl)amino)-1,8-naphthalimide (**10**).

We proposed the synthesis of a 4-amino-1,8-naphthalimide molecule conveniently functionalized with azido groups (Figure 63) to enable a *click* reaction with the acetylene moiety of **dG3**.

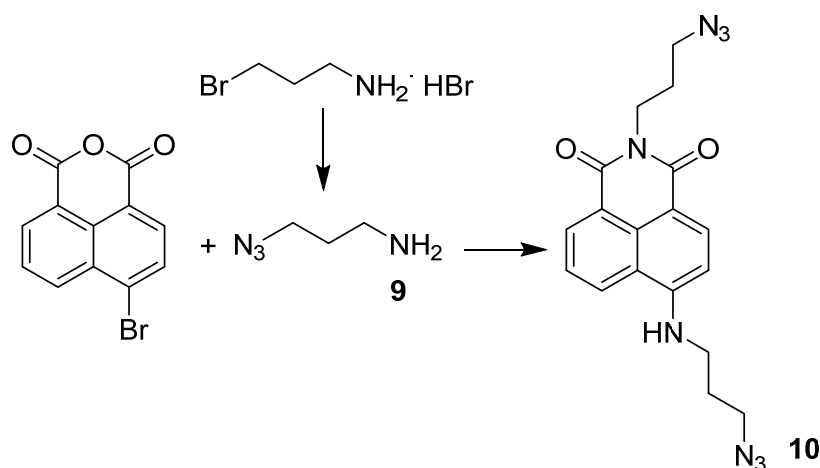


Figure 63. Scheme for **10**.

The first step was the synthesis of 3-azidopropylamine (**9**) from the commercially available compound 1-bromo-3-aminopropane hydrobromide (Figure 64). The starting material was dissolved in water and sodium azide was added. The reaction was stirred during three days at 80°C. The mixture was cooled in an ice-water bath and ether was added. KOH pellets were added until basic pH was attained. The organic layer was separated, and the aqueous phase was extracted with ether. The combined organic layer was dried and concentrated to obtain the product as a colorless oil in 50% yield.

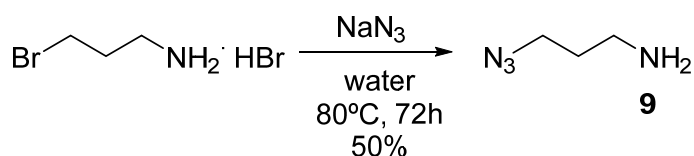
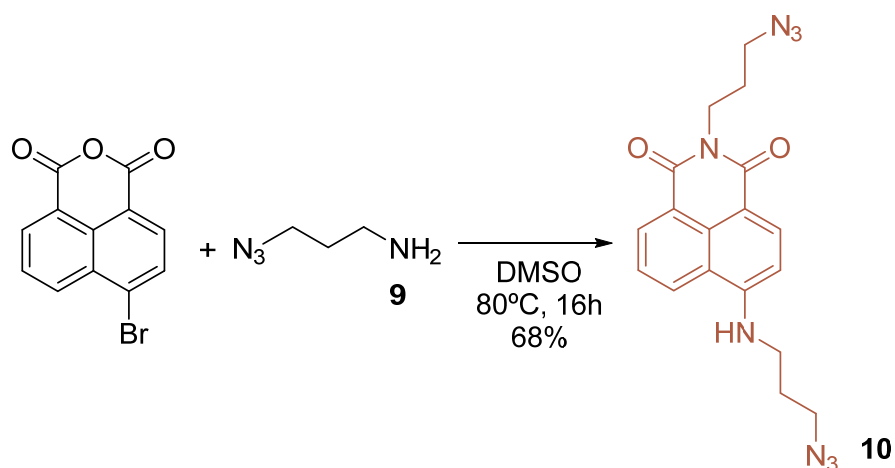


Figure 64. Synthesis of compound **9**.

The ^1H NMR spectrum (Figure 180) shows a triplet at 3.67 ppm corresponding to the methylene group adjacent to the amine, another triplet at 3.24 ppm corresponding to the methylene group adjacent to the azide and a multiplet at 2.11 ppm corresponding to the central methylene of the chain.

The introduction of the azido moiety into the 4-amino-1,8-naphthalimide structure was carried out in DMSO at 80°C, for 16 hours (Figure 65). The compound was purified by silica gel column chromatography to obtain the product as a yellow solid in 68% yield.

Figure 65. Synthesis of **10**.

^1H NMR spectrum (Figure 181) shows the successful introduction of the azido functionality into the naphthalimide structure since new signals corresponding to the alkyl chain appear at 4.25, 3.57, 3.41 and 2.06 ppm.

III.2.7.2 Synthesis of $G3_{\text{Naph}}\text{NHBoc}$

Click reaction between **dG3** and **10** resulted in a fluorescent dendrimer with sixteen protected amino groups in its surface and a naphthalimide core (Figure 66). The desired product was obtained as a yellow solid in 58% yield.

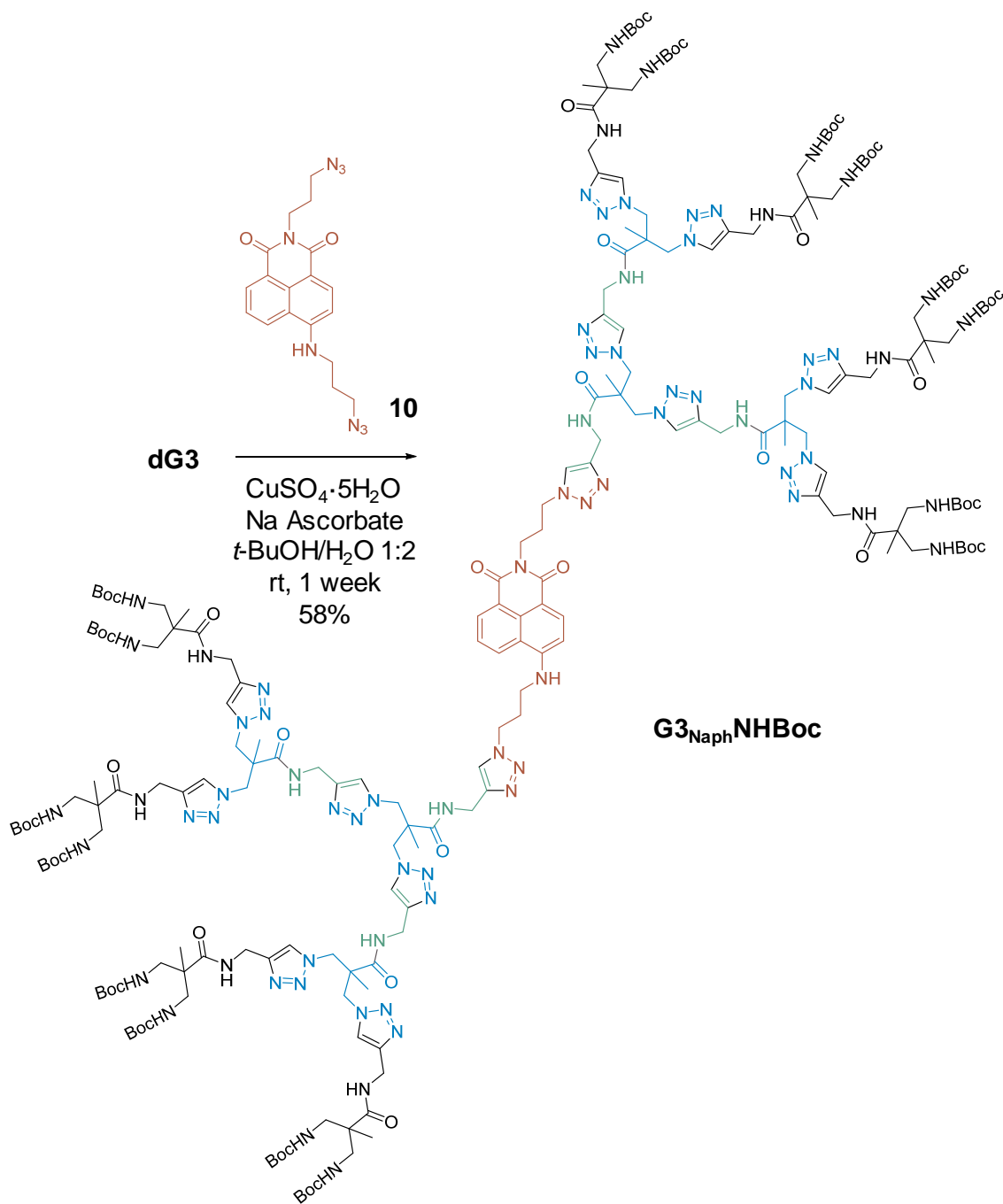


Figure 66. Synthesis of **G3_{Naph}NHBoc**.

IR spectrum of **G3_{Naph}NHBoc** (Figure 67) showed no sign of the azide band (2095 cm^{-1}) present in the spectrum of the starting material, **10** and a new band appears at around 2350 cm^{-1} corresponding to the naphthalimide moiety.

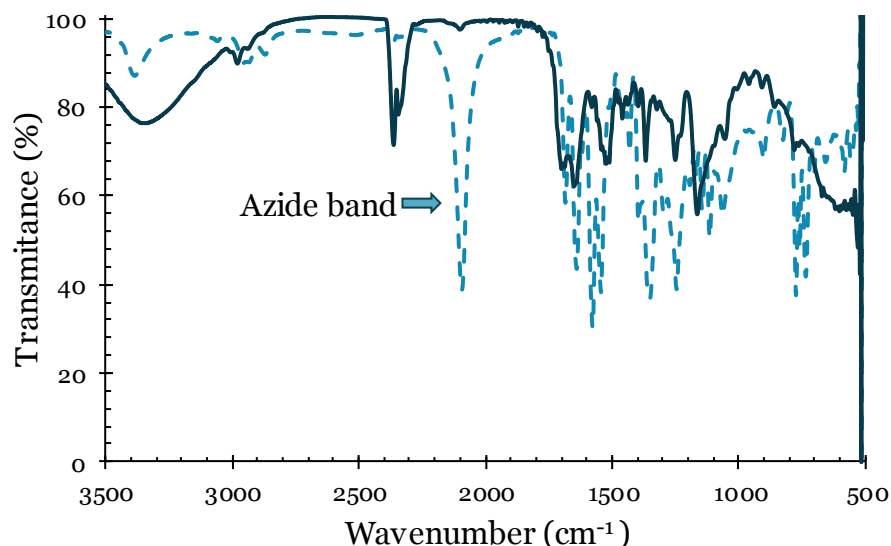


Figure 67. IR spectra of **G3_{Naph}NHBoc** (solid line) and compound **10** (dotted line).

The compound was fully characterized using NMR techniques. ^1H NMR spectrum (Figure 68, Figure 184) shows the typical signals of these dendrimeric structures plus the signals corresponding to the naphthalimide derivative core unit. In the aromatic region between 8.14 and 7.59 ppm the protons corresponding to the triazole rings and the aromatic core can be found. The methylene groups o and h, all the methylene groups adjacent to the triazole rings as well as some of the methylene groups from the chains of the core appear between 4.77 and 4.04 ppm. The rest of the methylene groups from these chains appear at around 3.52, 3.15, 2.20 and 2.10 ppm. The methylene groups next to boc appear in the multiplet at around 3.15 ppm. The singlet at 1.35 ppm corresponds to the boc group and all methyl groups appear between 1.08 and 0.88 ppm.

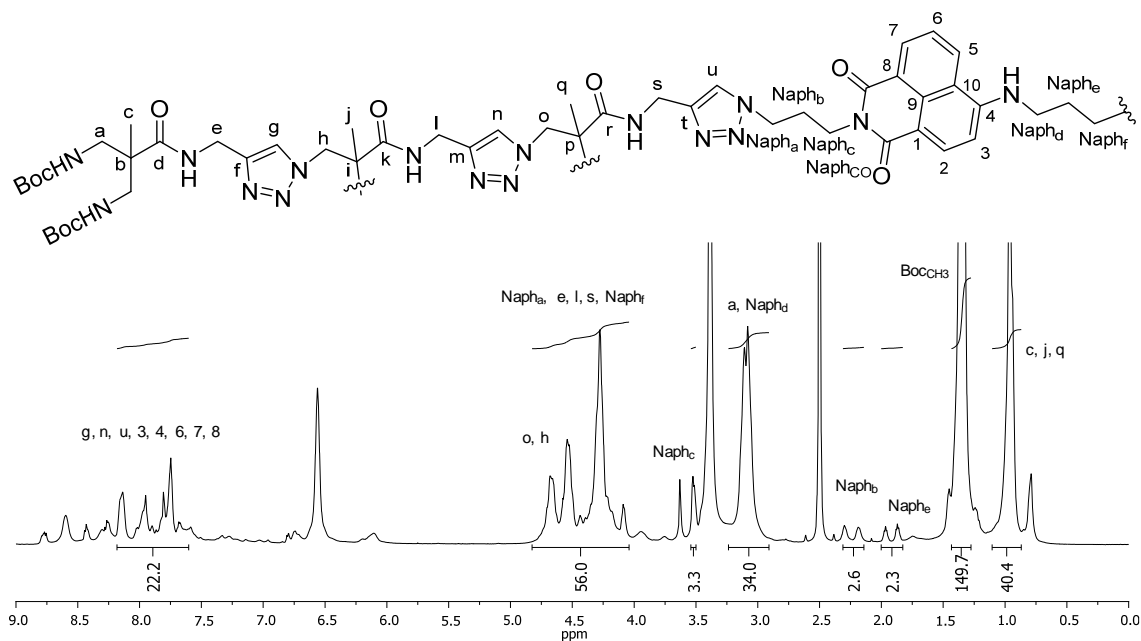


Figure 68. ^1H spectrum of $\text{G3}_{\text{Naph}}\text{NHBoc}$ in DMSO.

III.2.7.3 Synthesis of $\text{G3}_{\text{Naph}}\text{NH}_2$

Finally, the deprotection of the amino groups was carried out in the presence of HCl (Figure 69). After purification by sephadex column, $\text{G3}_{\text{Naph}}\text{NH}_2$ was obtained as a bright yellow solid in quantitative yield.

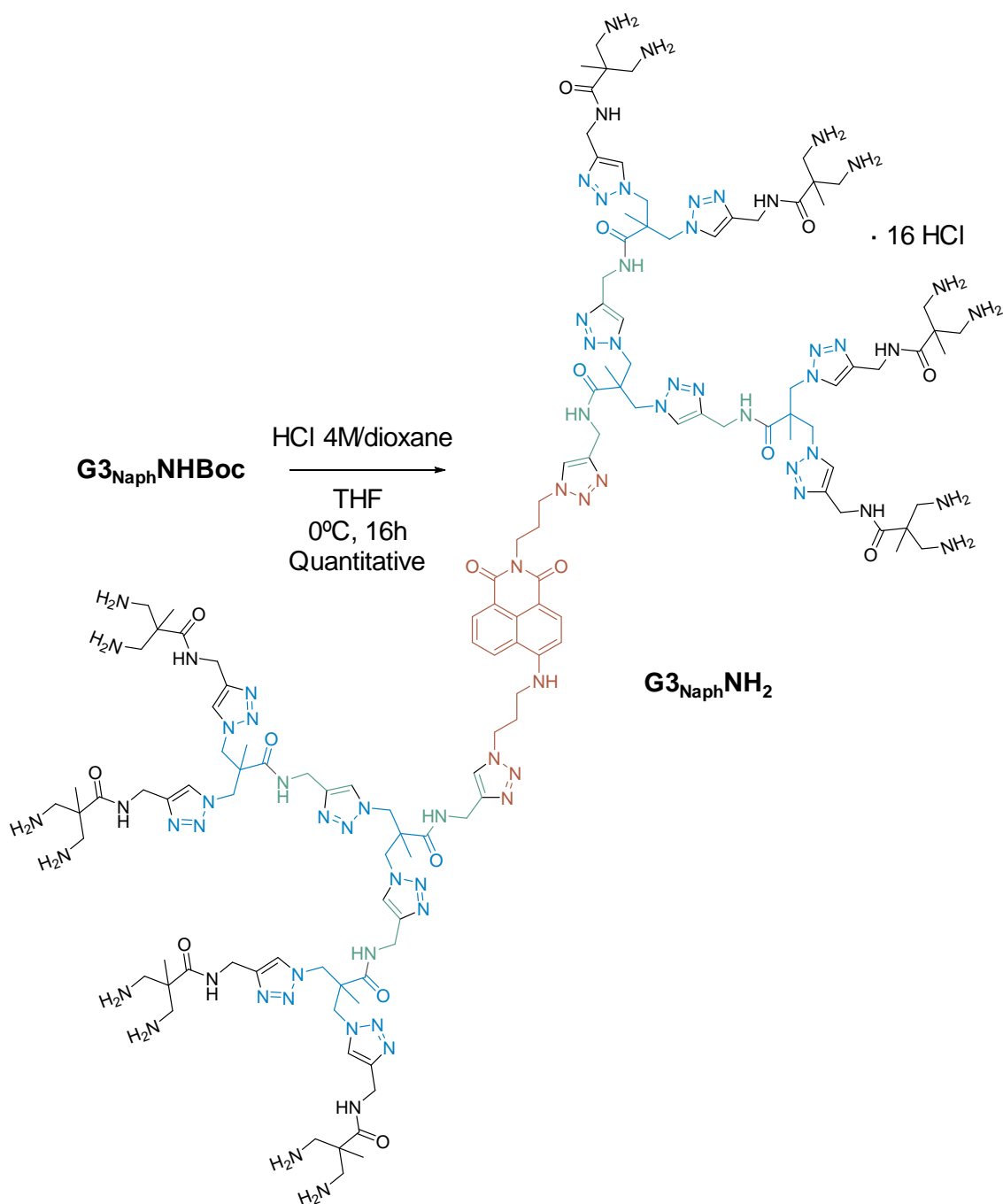


Figure 69. Synthesis of $\text{G3}_{\text{Naph}}\text{NH}_2$.

^1H NMR spectrum (Figure 70, Figure 187) showed the disappearance of the signal corresponding to the Boc protective groups. The protons corresponding to the triazole rings, as well as to the aromatic moiety of the central core, appear between 8.05 and 7.62 ppm. The methylene groups are present between 4.65 and 2.89 ppm and the methyl groups between 1.46 and 1.00 ppm.

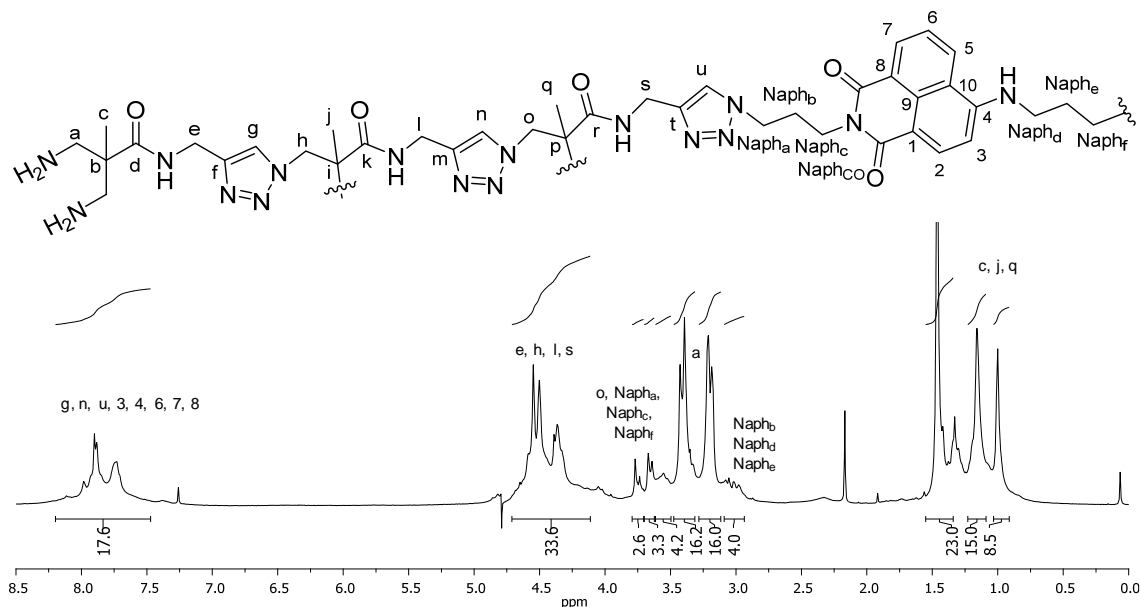


Figure 70. ^1H spectrum of **G3_{Naph}NHBoc** in D_2O .

III.2.8 Mass spectroscopy

All amino terminal dendrimers were purified by size exclusion chromatography, and their structures confirmed by NMR. As previously reported, characterization of dendrimers with high molecular weights and charges by MALDI-TOF is extremely difficult.^{147,148} No mass spectrum could be obtained for the described dendrimers, probably as a result of the lability of the *tert*-butoxycarbonyl (BOC) protecting groups (in **G_nxNH-Boc** derivatives) and the high degree of positive charges (in **G_nxNH₂** derivatives) during measurements.

III.2.9 Electrophoresis

As an alternative, in order to characterize the molecular weight and ensure the homogeneity of each generation of dendrimers, we used polyacrylamide gel electrophoresis (PAGE). Due to the structural similarity between dendrimers and basic proteins, the former can migrate on electrophoresis gels and be stained by reagents commonly used in PAGE.^{149,150} These studies were made in collaboration

with the group of Dr. Guadix and Dr. Perez-Pomares from the Animal Biology Department, University of Malaga.

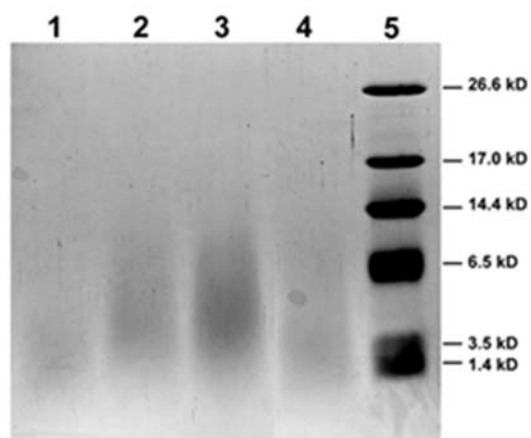


Figure 71. Electrophoresis of amine-terminated dendrimers. Electrophoresis was performed on 20% polyacrylamide gel for 160 min at 125 V. Lane 1: **G₂EDANH₂**; Lane 2: **G₃EDANH₂**; Lane 3: **G₃₃ABNH₂**; Lane 4: **G₃NaphNH₂**; Lane 5: Polypeptide SDS-PAGE Standards (BIO-RAD). The injected sample solution was 20 µg for each dendrimer. All den-drimers and Polypeptide SDS-PAGE Standards were stained uniformly with Coomassie Blue G-250 stain

Figure 71 shows the electropherogram of the amino terminal dendrimers, **G₃EDANH₂**, **G₃₃ABNH₂** and **G₃NaphNH₂**, obtained on a 20% polyacrylamide gel. **G₁EDANH₂** has not been included in the analysis since its molecular weight is relatively small for the standards used. It can be clearly seen in Figure 128 that the bands of all dendrimers (lanes 1, 2, 3 and 4) appear in the gel according to their molecular weight (Table 7) and in all cases resembles the homogeneity of the sample.

III.2.10 DOSY Experiments

Diffusion-Ordered Spectroscopy (DOSY) experiments provided accurate molecular diffusion measurements. DOSY NMR is a two-dimensional NMR technique, in which the signal decays exponentially due to the self-diffusion behaviour of individual molecules.¹⁵¹ The diffusion coefficient thus obtained is dependent on properties such as aggregation, size, mass, charge as well as on environmental properties such as temperature. First diffusion experiments

dealing with dendrimers (poly(propyleneimine) dendrimers) showed that diffusion coefficients decreased with increasing molecular size, and with a decreasing temperature.¹⁵² As expected, the diffusion coefficient obtained increase inversely proportional to the dendrimer's generation.

The amino-dendrimers synthesized in this work were examined by diffusion NMR techniques. DOSY experiments were carried out observing that the decays of all signals are monoexponential, resulting in a linear Stejskal-Tanner plot (Figure 213, Figure 214, Figure 215, Figure 216 and Figure 217). This indicates that only one specie is diffusing, which proves that our dendrimers are monodisperse.¹⁵³

Diffusion coefficients (D) can be determined from the slope of Stejskal-Tanner plot according to the following equation:

$$\ln\left(\frac{I}{I_0}\right) = -\gamma^2 \delta^2 G^2 \left(\Delta - \frac{\delta}{3}\right) D$$

Where G is the gradient field strength (Gauss/cm), I is the integral of the peak area at a given G value, I_0 is the integral of the peak area at $G=0$, γ is the magnetogyric constant of the nucleus ($2.675 \times 10^8 \text{ T}^{-1} \text{ s}^{-1}$ for ^1H), δ is the diffusion gradient length parameter (4.0 ms), Δ is the diffusion delay (100.0 ms), and D is the diffusion coefficient.¹⁵⁴

D can be used to estimate the size of all dendrimers in solution, by calculating the hydrodynamic radius (R_h) using the Stokes-Einstein equation:^{154,155}

$$R_h = \frac{k_B T}{6\pi\eta D}$$

where k_B is the Boltzmann constant, T is the temperature (in K), and η is the viscosity of the solution ($\sim 9.7 \text{ cP}$ for D_2O at 30°C).¹⁵⁴

Table 7 gathers the data obtained by these DOSY experiments as well as other parameters determined by Molecular Dynamic Simulations (See section III.2.11)

Dendrimer	G1EDANH ₂	G2EDANH ₂	G3EDANH ₂	G3 _{3AB} NH ₂	G3NaphNH ₂
Molecular Formula	C ₁₈ H ₃₄ N ₁₂ O ₂	C ₅₀ H ₈₆ N ₃₂ O ₆	C ₁₁₄ H ₁₉₀ N ₇₂ O ₁₄	C ₁₇₇ H ₂₈₈ N ₁₀₈ O ₂₁	C ₁₂₈ H ₂₀₀ N ₇₄ O ₁₆
Terminal -NH ₂ groups	4	8	16	24	16
M. W. (gmol ⁻¹)	450.55	1231.46	2793.26	4264.99	3031.51
<i>D</i> (m ² s ⁻¹)	3.80·10 ⁻¹⁰	3.01·10 ⁻¹⁰	1.93·10 ⁻¹⁰	1.72·10 ⁻¹⁰	2.19·10 ⁻¹⁰
<i>R_h</i> (Å)	5.27	6.66	10.38	11.65	9.15
<i>R_g</i> (Å)	4.17 ± 0.06	6.79 ± 0.09	10.51 ± 0.15	11.37 ± 0.16	9.93 ± 0.14
<i>I_x/I_y</i>	1.22 ± 0.07	1.20 ± 0.03	1.08 ± 0.03	1.27 ± 0.02	1.08 ± 0.03
<i>I_x/I_z</i>	1.62 ± 0.10	2.71 ± 0.16	3.79 ± 0.23	2.35 ± 0.12	2.85 ± 0.19
<i>δ</i>	0.019 ± 0.004	0.066 ± 0.006	0.103 ± 0.006	0.052 ± 0.005	0.073 ± 0.007

Table 7. Data of prepared dendrimers. Diffusion coefficients (*D*) and hydrodynamic radius (*R_h*) determined by NMR experiments. Radius of gyration (*R_g*), aspect ratios (*I_z/I_x* and *I_z/I_y*) and asphericities (*δ*) calculated by MDS.

Larger structures diffuse more slowly, showing smaller diffusion constants. As expected, the dendrimer radius increases with generation in dendrimers with the same core (**G_nEDANH₂**). This correlation is not so clear when comparing generation 3 dendrimers, probably due to a folding of the structure. **G3_{Naph}NH₂** shows a slightly higher diffusion constant than **G3EDANH₂**, which can be translated into a smaller size of the dendrimer. However, the inclusion in the structure of a third dendron (**G3_{3AB}NH₂**), which implies a considerable increase in molecular weight, does not translate into a significant increase in the size of the dendrimer (Table 7). It is important to note that **G3-NH₂** dendrimers are built from different cores, whose structures and multiplicities influence not only the number of amino terminal groups but also the shape, morphology and size of the final dendrimers.

III.2.11 Molecular Dynamic Simulations

To obtain some information about the structure of these dendrimers, molecular models were created and simulated in water as explicit solvent using molecular dynamics (Figure 72). Dendrimers are composed of three different residues: the core (COR) for the corresponding dendrimers, the repetitive 3,3'-[(4-(aminomethyl)-1*H*-1,2,3-triazol-1-yl)]-2-methylpropanoyl units (REP), and the terminal end 3,3'-diamoniopivaloyl unit (TAM) (Figure 73).

For all of these residues the cap region was removed before connecting to another residue. For the 1,4-substituted triazole group we used the parameter described before.¹⁵⁶ The values (bonds, angle torsions, or van der Waals parameters) not included in the parm99 force field, were obtained from the general AMBER force field (GAFF).¹⁵⁷ The minimum energy conformation was submitted to B3LYP/6-31G(d) basis set calculation using Go9,¹⁵⁸ (capped COR and REP residues were optimized *in vacuum*, while capped TAM residue was optimized employing PCM-B3LYP/6-31G(d) with water as solvent).¹⁵⁹ The restrained potential (RESP) method was used for charge fitting.¹⁶⁰ Total cap atom charge was constrained to zero during charge calculation and the overall full residue charge was also set to zero except for the protonated residue (TAM), which was kept at +2. Decapped residues were created using the Antechamber module of AmberTools12,¹⁶¹ and used to build the desired dendrimer generation for the **G_nEDANH₂** with the Dendrimer Building Tool (DBT).¹⁶² The **G₃ABNH₂** and **G₃NaphNH₂** dendrimers were built with AmberTools12 and the LEaP package.

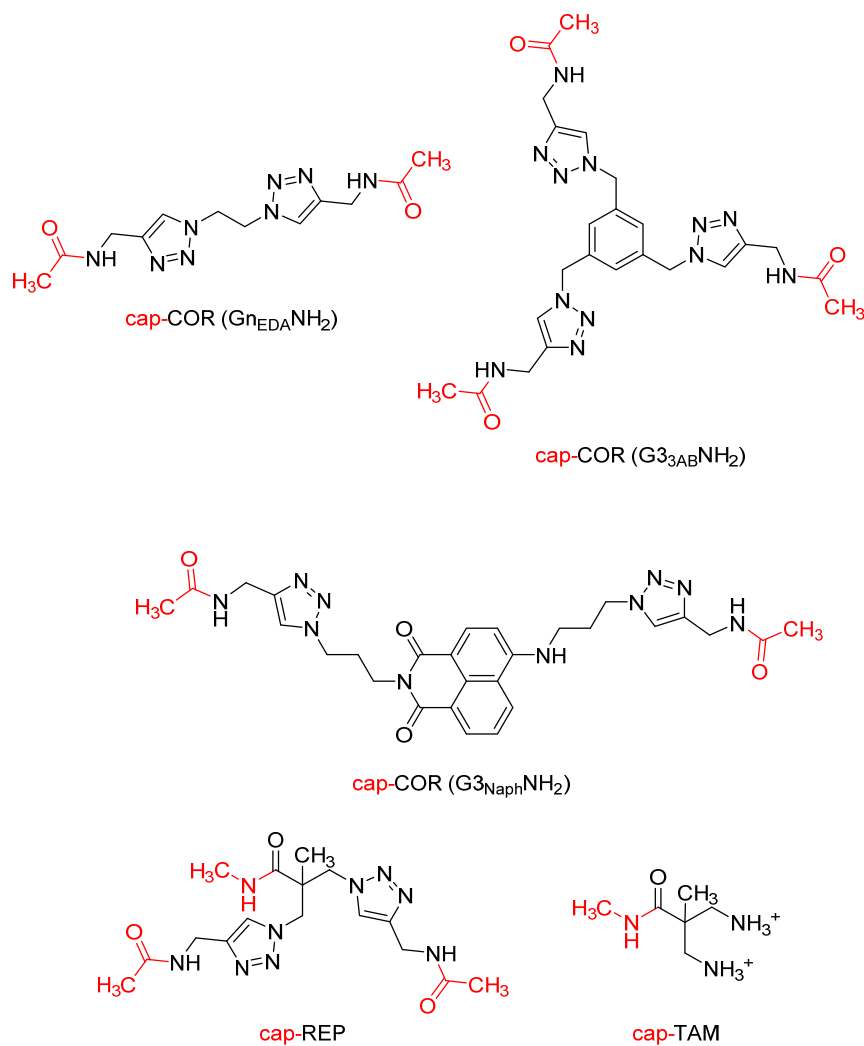


Figure 72. Residues selection for the dendrimers. Cap atoms are in red.

For the simulations we used the AMBER 12 MD software package for all calculations.¹⁶¹ An appropriate number of Cl^- counterions were added, to preserve overall charge, and the molecules hydrated, using the TIP3P water model,¹⁶³ in truncated octahedral cells. In all cases, a minimum 10 Å solvation shell around the dendrimer structure were chosen to provide the dimensions of these cells.

Dendrimer	N_{den}	N_{Cl^-}	N_{solvent}	N_{total}	$V(\text{\AA}^3)$
G1EDANH₂	70	4	8013	8087	93214
G2EDANH₂	182	8	12756	12946	150013
G3EDANH₂	406	16	16479	16901	102339
G3NaphNH₂	440	16	25008	25464	288741
G3₃ABNH₂	618	24	25422	26064	301943

Table 8. Initial properties of dendrimers and simulation details. N_{den} , N_{Cl^-} , N_{solvent} and N_{total} are, respectively, the number of dendrimer atoms, chloride ions, atoms in solvent molecules and the total number of atoms. V is the initial octahedral box volume.

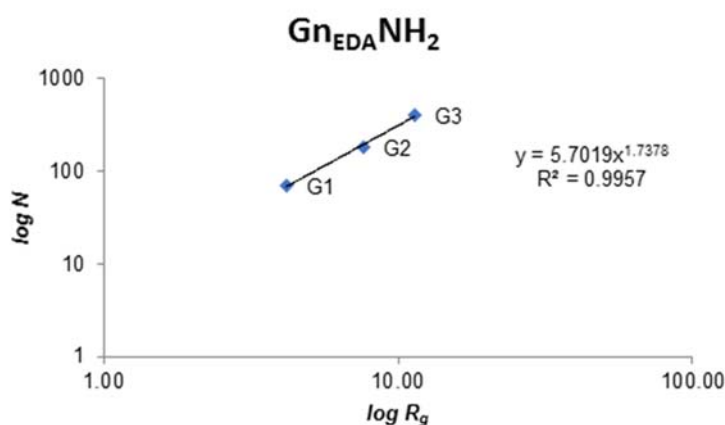
Solvated structures were minimized as described previously.¹²⁹ Briefly, the molecules were optimized using six cycles of conjugated gradient minimization. In the initial cycle, dendrimers were kept in their starting conformation with a harmonic constraint force. Then, was followed by another five periods of minimization decreasing the harmonic restraint force constant from 20 kcal/mol-Å² to zero.

The minimized structures were heated from 0 to 300 K with three steps of 40 ps of MD, the first of them under conditions of constant volume-constant temperature (NVT) and the rest under constant pressure-constant temperature (NPT) conditions. Finally, we carried out an unconstrained MD simulation (2ns) in NPT ensemble to equilibrate the system at 300 K. The motion equation was solved using the Verlet leapfrog algorithm,¹⁶⁴ with an integration step of 2 fs. The SHAKE algorithm was used to constrained the bond lengths involving bonds to hydrogen.¹⁶⁵

Finally, production runs of 20 ns trajectories were done under an NPT ensemble. Temperature regulation was achieved using the Berendsen weak coupling.¹⁶⁶ The particle-mesh Ewald (PME) algorithm was employed to treat long-range electrostatic interactions,¹⁶⁷ with a real space cut off of 9 Å. The same cutoff was used for Van der Waals interactions. For the structural analyses (R_g , RDF, *etc.*) the last 1 ns equilibrated trajectory was used. Amber modules *ptraj* and *cpptraj* were used to accomplish these analyses. VMD software was used for the calculation of molecular surfaces.¹⁶⁸

The equilibrated structures of these molecules have also been analyzed and several properties calculated (Table 7), such as the Radius of gyration (R_g), the aspect ratio and their asphericities.

We found that the size of these molecules for the **Gn_{EDA}NH₂** series increases with each generation, as quantified from the DOSY experiments, and their values are in good agreement with the calculated radius of gyration (R_g) (Table 7). The fractal dimensionality (d_f) value for these compounds can be inferred from the relation between R_g and the number of the dendrimer's atoms (N) and has a value of 1.74 (Figure 73). This indicates that these dendrimer generations do not form perfect spheres since the fractal dimension for a perfectly spherical smooth surface is 3.¹⁶⁹



$$N \sim R_g^{1.74}$$

Figure 73. Relationship between the number of atoms (N) of the **Gn_{EDA}NH₂** dendrimers and their R_g values.

The values of the three principal moments of inertia (I_x , I_y , I_z in decreasing order) can give information about the structural characteristics of these dendrimers. The ratios (I_x/I_y) and (I_x/I_z) are measures of the dendrimer's ellipsoid shape eccentricity. **Gn_{EDA}NH₂** dendrimers showed I_x/I_y and I_x/I_z ratios between 1.22-1.08 and 1.62-3.79 respectively (Table 7). The increase in the gap between the I_x/I_y and I_x/I_z values implies that the ellipsoidal shape is favored when the generation increases. This is corroborated by their asphericity values (Figure 74).

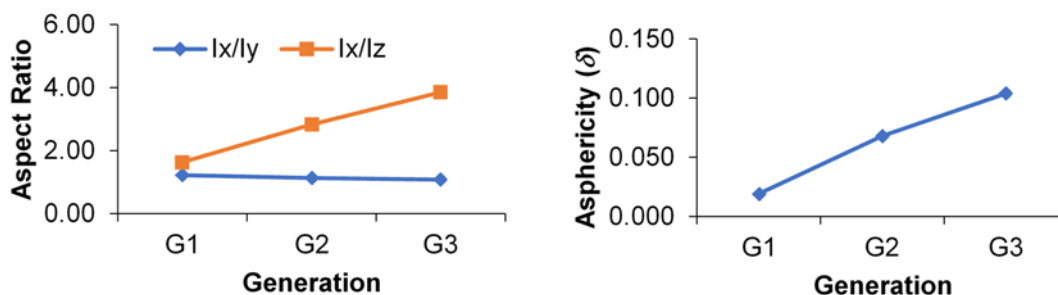


Figure 74. Aspect ratios and asphericity values for **GnEDANH₂** dendrimers as function of their generation.

The atoms distribution within the dendrimers can be described using radial density profiles. Those corresponding to **GnEDANH₂** dendrimer generations are shown in Figure 75. The maximum density is found to be close to the core of the dendrimers, decaying toward the edge. Second and third generation **GnEDANH₂** dendrimers have a plateau corresponding with the distribution of the repetitive unit (REP) and decaying slowly toward the end of the molecule. This shows a region with low atom mobility, high localization and therefore with a dense dendrimer shell pattern. The number of terminal monomers (TAM) doubles with each generation, so the terminal amine groups extend over the molecule, always with increasing density toward the outer region of the dendrimer, but with a higher degree of terminal monomer backfolding when the generation increases (Figure 75).

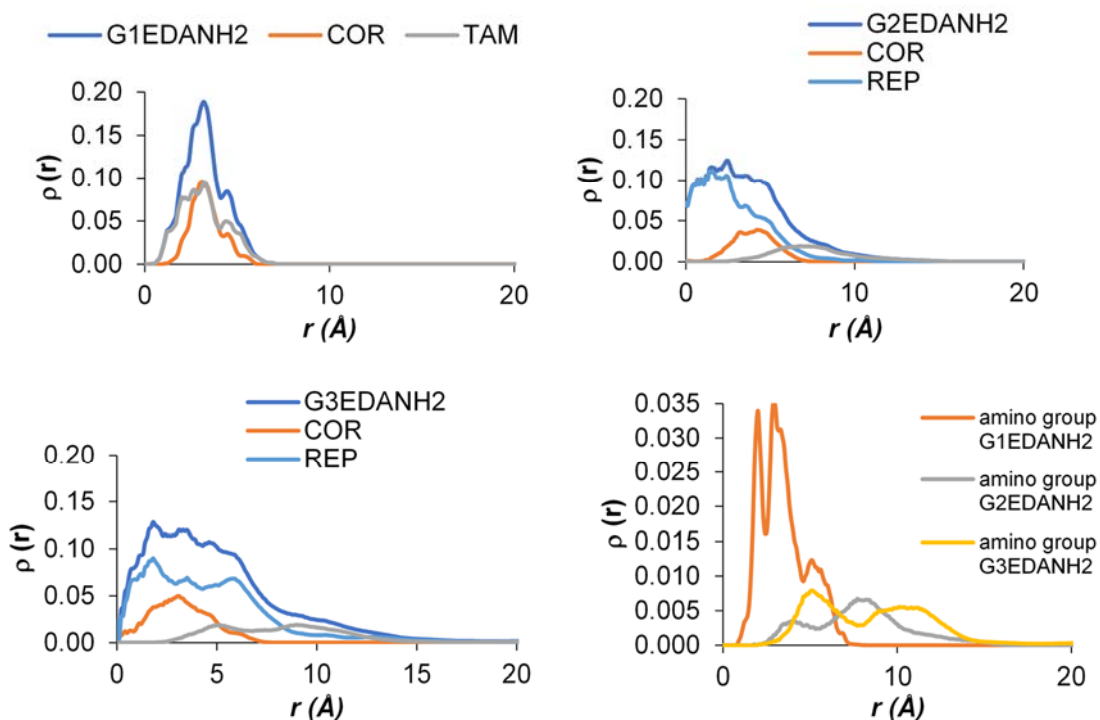


Figure 75. Radial distribution function of the $G_n\text{EDANH}_2$ dendrimers and its monomers using dendrimer center of mass as reference. The unit value for $\rho(r)$ is expressed in atoms/Å³.

To get more insight into how different cores affect the properties of these dendrimers, we have analyzed the calculated parameters for the $G_3\text{-NH}_2$ generations. The R_g of these dendrimers are similar and their values are within 1 Å and reproduce the experimental values (Table 7). The ellipsoid shape eccentricity displays I_x/I_y and I_x/I_z ratios between 1.08, 1.08, 1.27 and 3.79, 2.85, 2.35 for the EDA, Naph and 3AB cores, respectively (Table 7).

The gap decreases between the I_x/I_y and I_x/I_z values implies that a more globular structure is favored when the number of atoms in the dendrimers increases, this is validated by the asphericity values (Table 7, Figure 76).

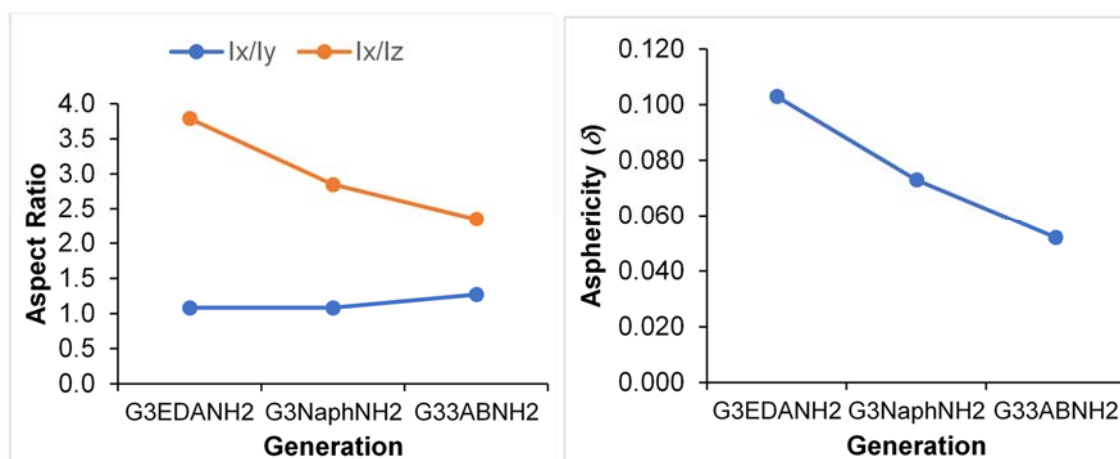


Figure 76. Aspect ratios and asphericity values for **G3-NH₂** dendrimers as function of their generation.

The radial density profiles for the G3-NH₂ dendrimers are shown in Figure 78. In these profiles, density is maxima around the core of the dendrimers. For EDA core-dendrimers, the density shows a plateau with a good correlation with the distribution of the repetitive unit REP and implies a dense dendrimer pattern. For 3AB and Naph core-dendrimers this plateau is smaller. The terminal amine groups are extended from the middle of the molecules toward the outside region of the dendrimer, except for the molecule with the 3AB core, which presents a high degree of back-folding and the TAM residue can be found along all the molecule (Figure 77). From all these dendrimers, the molecule with the Naph core has the least back-folding (Figure 78).

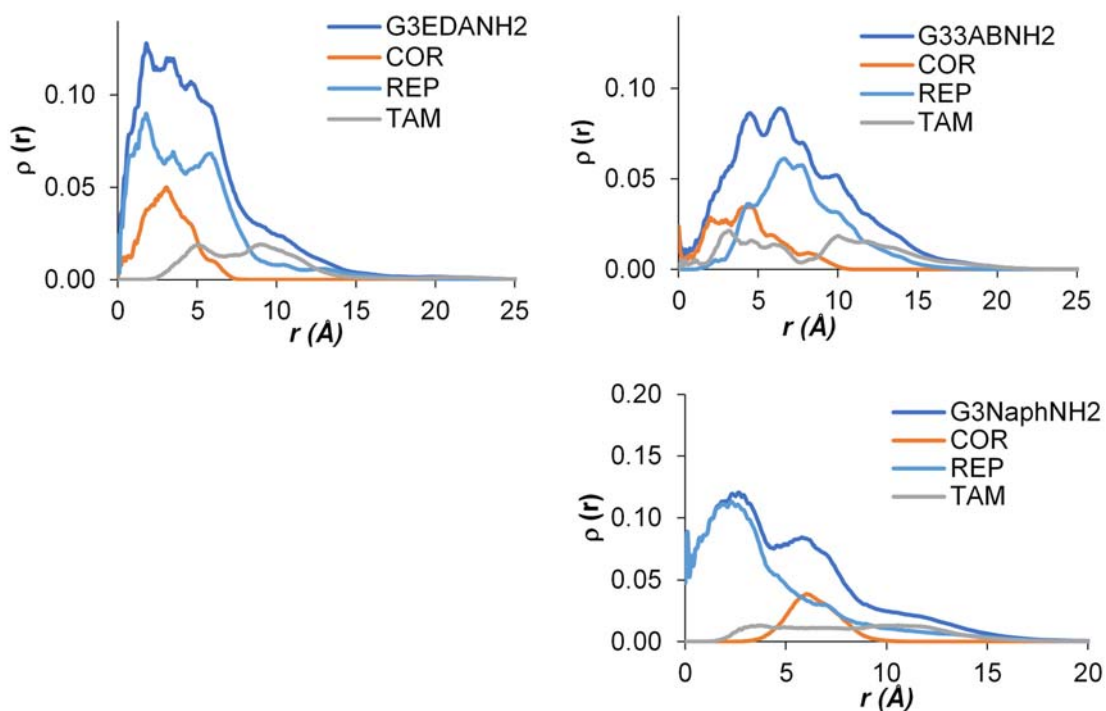


Figure 77. Radial distribution function of the **G3-NH₂** dendrimers and its monomers using dendrimer center of mass as reference. The unit value for $\rho(r)$ is expressed in atoms/Å³.

Comparing the family **Gn_{ED}NH₂** with others amino-terminal dendrimers (PAMAM,¹⁶⁹ PPI¹⁷⁰ and BAPAD³¹), the dendrimers of equivalent generation are similar in size, but differs in shape. While for PAMAM, PPI and BAPAD dendrimers are spheroids in shape when the generation grows, an ellipsoidal shape is favored when the generation of **Gn_{ED}NH₂** increases.

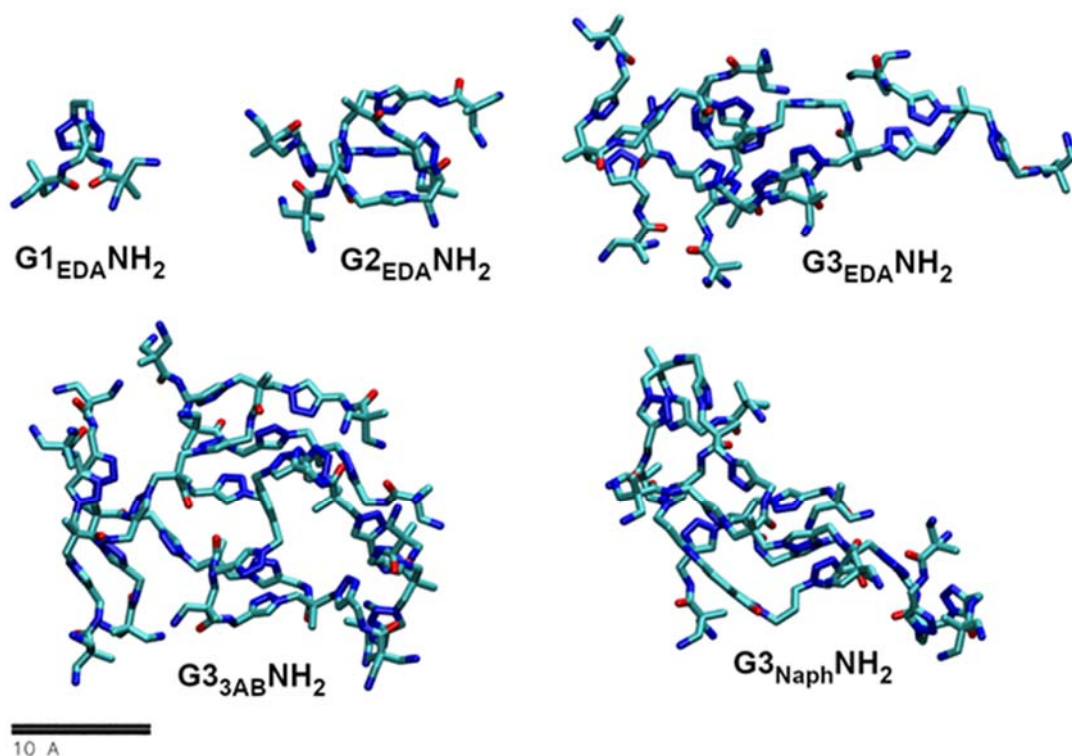


Figure 78. Snapshots from Molecular Dynamic Simulations of **G1_{EDA}NH₂**, **G2_{EDA}NH₂**, **G3_{EDA}NH₂**, **G3_{AB}NH₂** and **G3_{Naph}NH₂**; (to simplify the picture, carbon atoms are depicted in cyan, oxygen atoms in red, nitrogen atoms in blue and hydrogens atoms are omitted).

III.2.12 Photophysical characterization of **G3_{Naph}NH₂**

The photophysical properties of naphthalimide derivatives depend greatly on the substituents on the aromatic ring. The nature of these substituents (electron donor or acceptor) can induce a polar charge-transfer (CT) excited stated.¹⁷¹ Especially important is the substituent at the C-4 position. It has been described how the introduction of halogen groups generate colorless compounds with blue fluorescence¹⁷² while the substitution with amino groups in that position will originate rather yellow compounds with green fluorescence.¹⁷³

G3_{Naph}NH₂ was characterized spectroscopically. The UV-visible absorbance spectrum presented the following bands: λ_{max} nm (ϵ): 259 (4709), 284 (4125) and 447 (3209), (10^{-5} M, Figure 79).

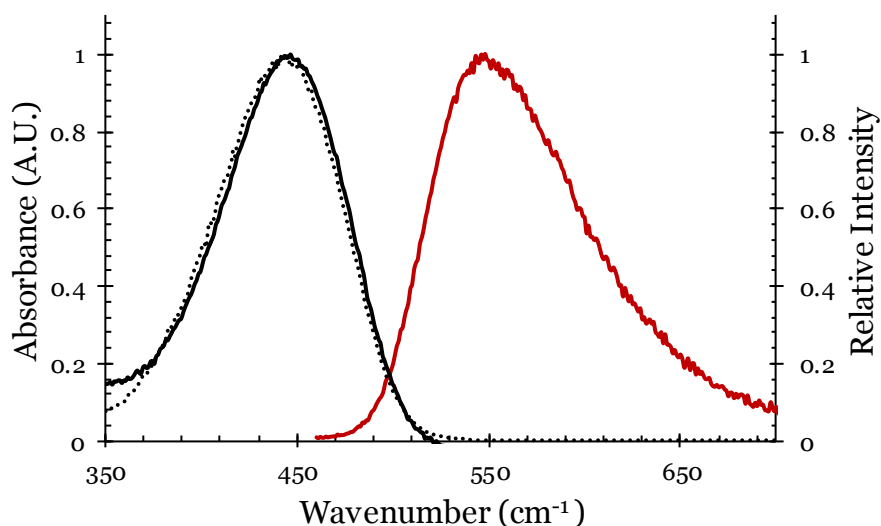


Figure 79. Normalized absorbance (black solid line), excitation (black dotted line) and emission (red line) spectra of **G3_{NaphNH₂}** (10^{-5} M) in water.

G3_{NaphNH₂} exhibits an intense fluorescence emission centered at 550 nm in aqueous solution (10^{-5} M, Figure 79) with an excited state lifetime of 7.5 ns (λ_{em} = 550 nm). Although it has a quantum yield of 26 %, this value is unexpectedly considering an aqueous solution.

Excitation and emission spectra acquired under two photon excitation (TPE) conditions were also recorded. TPE requires the absorption of two lower energy photons to excite the molecule. In this case, the resulted emission occurs at higher energy than each of the photons absorbed. This process is especially useful in bioimaging, since the energy needed to excite the fluorophore is lower and closer to the infrared than in OPE conditions, causing less damage to cells.

The emission observed using an excitation wavelength of 880 nm coincides with the one obtained in the one-photon excitation (OPE) regime (Figure 80).

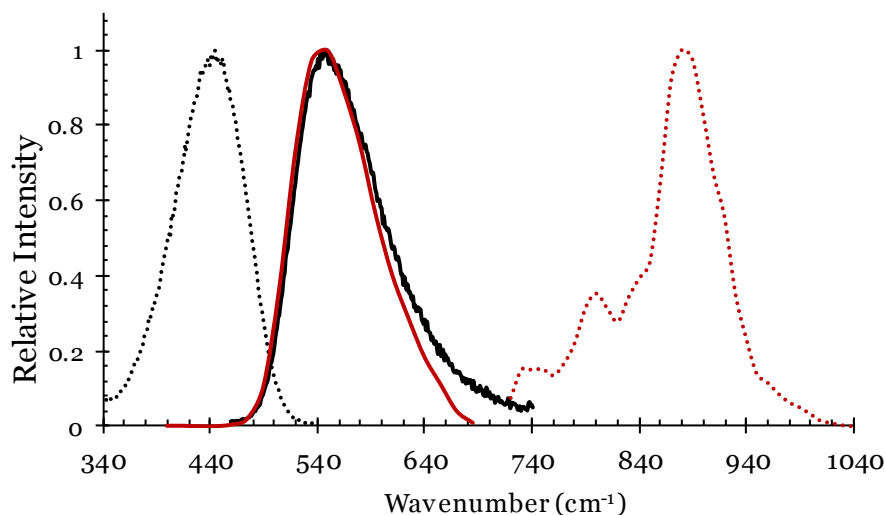


Figure 80. Normalized excitation (dotted line) and emission (solid line) spectra of **G3_{Naph}NH₂** upon one-photon (black) or two-photon (red) excitation (450 and 880 nm, respectively).

G3_{Naph}NH₂ becomes therefore an excellent tool for bioapplications where luminescence is required. The molecule combines the excellent properties of amino terminal dendrimers with a chromophore widely supported by its excellent photo-physical properties.¹⁷⁴

III.2.12.1 Studies with *E. coli* Bacteria (gram-negative)

To evaluate the use of **G3_{Naph}NH₂** as a multichannel fluorescent marker for biological samples, a strain of *E. coli* bacteria was employed as a model target. These studies were made in collaboration with Dr. Guadix and Dr. Perez-Pomares from the Animal Biology Department, University of Malaga. Bacteria (*E.coli*) were grown in 100 mL of LB Broth₃₇ at 37°C in a rocking incubator (18 hours). Then, culture contents were split into two 50 mL vials, centrifuged (5000g, 10 minutes), one of the bacterial pellets was resuspended in 5 mL of PBS with a 10⁻⁴ M solution of compound **G3_{Naph}NH₂**, while the other one was resuspended in 5 mL of only PBS. A 2 hours incubation step in a rocking incubator at 37°C followed. After incubation both samples were centrifuged (5000g, 10 minutes) and washed twice in 10 mL of PBS. Finally, each bacterial sample was resuspended in 500 µL of PBS.

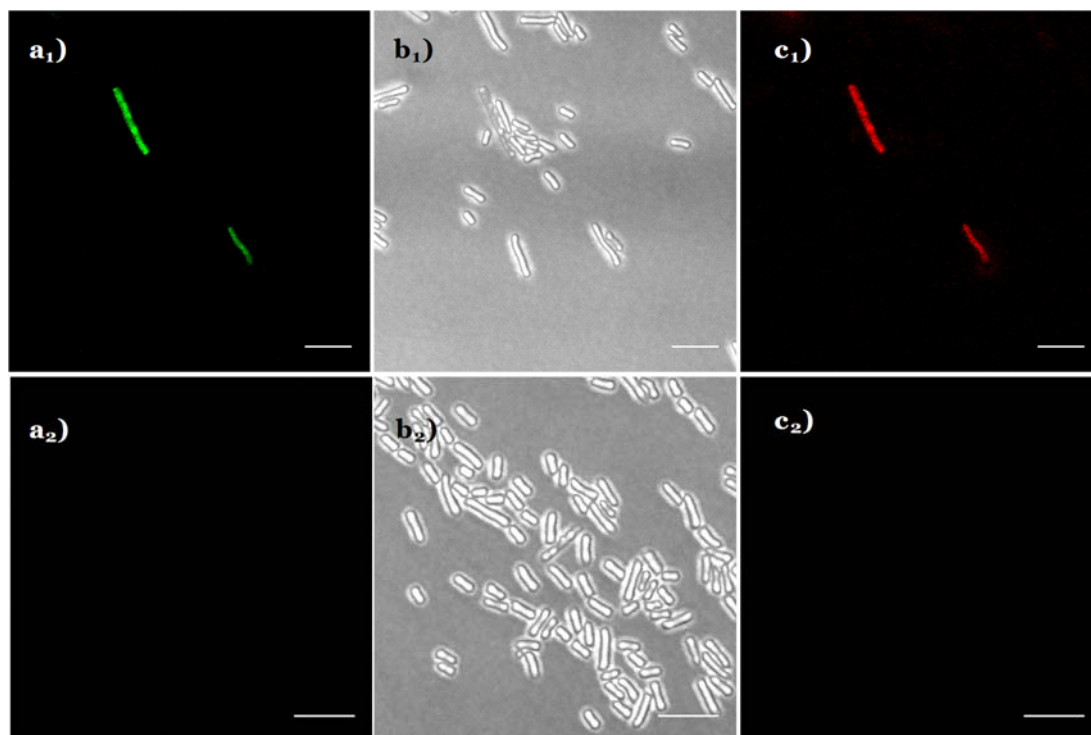


Figure 81. Confocal micrographs of *E. coli* incubated (18h) with (upper row) or without (lower row) **G3_{NaphNH₂}**: **a)** recorded emission under one photon excitation (λ_{exc} = 450 nm; collected through 500-600 nm); **b)** bright field images; **c)** recorded emission under two photon excitation (λ_{exc} = 880 nm; collected through 500-550 nm). Scale bars: 5 μ m

The amino terminal groups of **G3_{NaphNH₂}** provide an effective binder to bacterial surface, owing to their capacity for hydrogen bonds and electrostatic interaction.¹⁷⁵ After incubation with a solution of the dendrimer, **G3_{NaphNH₂}** effectively labeled the *E. coli* cells as can be seen in Figure 81 (10^{-4} M). The outer surface of some bacteria shows an intense fluorescence under both OPE or TPE conditions, thus confirming the adhesion of the dendrimer to the bacterial wall. To further confirm that the origin of this fluorescence derives from the intrinsic emission of the naphthalimide core of the dendrimer, and to rule out biological sample autofluorescence and background noise,¹⁷⁶ specific controls were set up. In un-treated bacteria no autofluorescence is observed under OPE or TPE conditions (the capture settings and image processing are identical).

III.2.12.2 Studies with *P. subtilis* Bacteria (gram-positive)

After the encouraging results obtained using gram negative bacteria, studies were also carried out in order to confirm the adhesion of the compound **G3_{Naph}NH₂** to the wall of gram-positive bacteria. The images taken under both OPE and TPE conditions show the successful marking of the *P. subtilis* (Figure 82). No differences in the marking of both bacteria (*E. coli* and *P. subtilis*) were observed under these conditions.

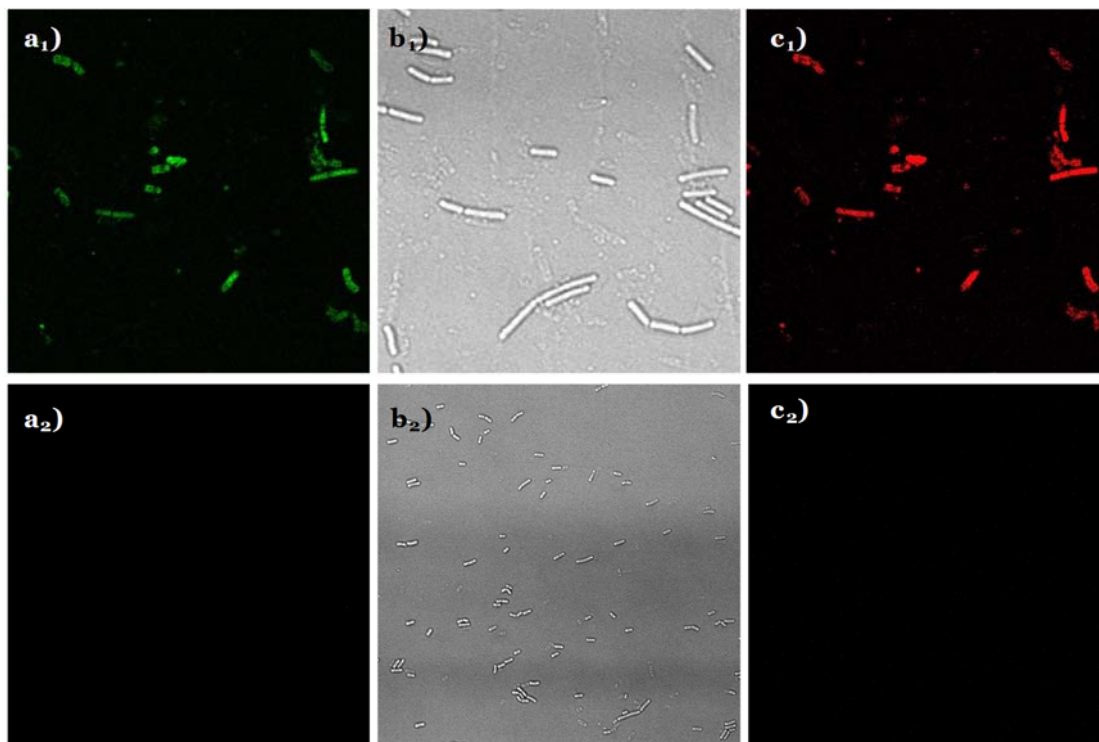


Figure 82. Confocal micrographs of *P. subtilis* incubated (18h) with (upper row) or without (lower row) **G3_{Naph}NH₂**: **a)** recorded emission under one photon excitation (λ_{exc} = 450 nm; collected through 500-600 nm); **b)** bright field images; **c)** recorded emission under two photon excitation (λ_{exc} = 880 nm; collected through 500-550 nm).

III.2.12.3 Bactericidal test

These experiments were carried out by Dr. Díaz-Martínez and Dr. Romero from the Microbiology Department, University of Málaga. The dynamics of bacterial growth was monitored in liquid LB medium originally inoculated with 4×10^6 *E. coli* and *P. subtilis* and incubated in the presence (10 or 100 μ M) or absence of **G3_{Naph}NH₂**. No significant *E. coli* and *P. subtilis* growth delay was recorded with increasing **G3_{Naph}NH₂** concentration from 10 to 100 μ M (Figure 83).

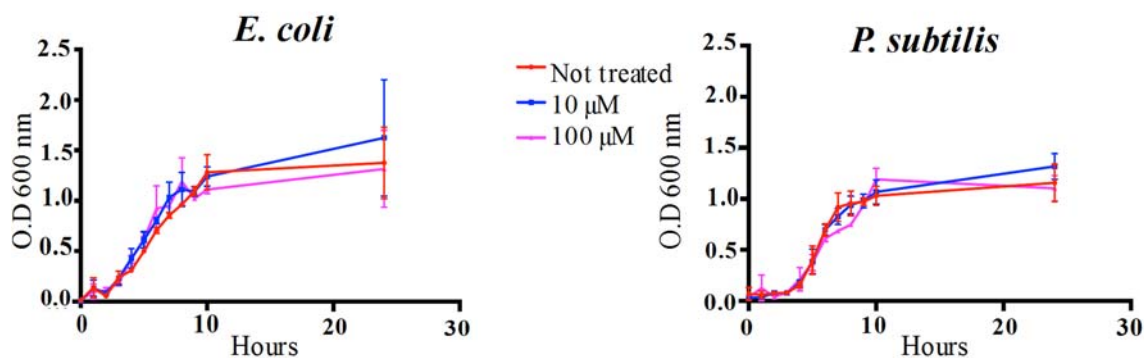


Figure 83. Bacterial growth of *E. coli* and *P. subtilis* when non-incubated (red) and incubated with a solution 10 μM (blue) or 100 μM (purple) of compound **G3**_{NaphNH₂}

In this chapter, a new family of dendrimers has been obtained from a pivalic based monomer using a totally different approach. In this convergent design, **dG3** dendron was prepared taking the advantages of the copper-catalyzed azide-alkyne cycloaddition, resulting in an effective synthesis where **dG3** can be obtained in large quantities with yields higher than 85% in all steps and with easy purification procedure. Different dendrimers have been obtained in two steps from our highly versatile dendron. With this new methodology, it is possible to increase the number of amino terminal groups by choosing the appropriate multiplicity of the core. The size and shape of obtained dendrimers have been evaluated by NMR techniques. The data observed by DOSY experiments is well supported by fully atomistic Molecular Dynamic Simulations. The chemical structure of the core influences the shape and morphology of the final dendrimers, obtaining ellipsoidal shape from dendrimers with an alkyl core and a more globular shape in dendrimers with aromatic cores.

Although no mass spectra could be obtained for the final dendrimers, the data gathered from the different techniques used in their characterization confirms that the desired structures were synthesized. Information obtained from ^1H and ^{13}C NMR spectra is consistent with what could be expected. IR spectra, recorded after each click reaction, shows no traces of the azido compounds. This observation, along with the results of DOSY experiments that indicated the monodispersity of the samples, points to the synthesis of defect-free

dendrimers. Moreover, this is supported by the data collected from Molecular Dynamic Simulations and Electrophoresis experiments.

We demonstrate that this effective dendron can be combined with suitable cores of different multiplicity, thus providing a powerful tool for the rapid assembly of amino terminal dendrimers, with the desired molecular weight, shape and number of amino terminal groups. The chemical stability of these aliphatic-imidazole-amide dendrimers make them excellent candidates for biomedical applications. Moreover, inherent fluorescent dendrimer can be obtained in good yields, completely aqueous soluble and with the amino terminal groups intact. We also demonstrate the application in bioimaging of such dendrimers using both OPE and TPE conditions.¹⁷⁷

CHAPTER IV

**SYNTHESIS OF PLATINUM-DOPED DENDRITIC
STRUCTURE**

IV.1 Introduction

Platinum(II) complexes have aroused interest due to their unique photophysical properties,¹⁷⁸ such as their photostability, their significant Stoke-shift,¹⁷⁹ or the possibility to tune their luminescence to blue, green, red or white by means of ligand design.^{180–183} Moreover, the ability of Pt(II) complexes to emit upon two-photon excitation (TPE) affords the possibility of *in vivo* imaging in tissues. Their long luminescence lifetimes allows the possibility of performing phosphorescence lifetime imaging microscopy (PLIM) that offers advantages over traditional fluorescence lifetime imaging microscopy (FLIM).¹⁸⁴ While FLIM is limited to nanosecond changes in emission lifetimes, PLIM allows lifetime imaging in the microsecond range. This makes possible the recording of lifetime imaging avoiding autofluorescence, the natural emission of light that occurs normally in the nanosecond scale and that constitute a major problem in bioimaging.¹⁷⁶ However, despite these qualities, their application in the field of bioimaging is still limited due to solubility and quenching phenomena in aqueous environments. These extraordinary luminescent properties have encouraged us to study the insertion of a dendritic structure into a Pt(II) complex as a solution for their limitations regarding solubility and quenching in aqueous media.

The photophysical properties of heavy-metal complexes are intimately related to the metal centers, ligand structures, local environment and

intermolecular interaction. Their excited states usually include metal-to-ligand charge transfer (MLCT), ligand-to-ligand charge transfer (LLCT), intraligand charge transfer (ILCT), ligand-to-metal charge transfer (LMCT), metal-metal-to-ligand charge transfer (MMLCT), ligand-to-metal-metal charge transfer (LMMCT) and metal-to-ligand-ligand charge transfer (MLLCT) states.¹⁸⁵

Pt(II) has a d^8 electronic configuration which results in complexes with a square-planar geometry, providing these compounds with unique chemical properties.¹⁸⁶ Interaction between the dz^2 orbitals, normal to the coordination plane, leads to the easy formation of aggregates. The assembly of these compounds can be controlled, for example, by means of proper tailoring of coordinated ligands.¹⁸⁷ The aggregation of complexes that bear a planar ligand, and therefore prone to stacking, can be avoided by inserting a bulky ancillary ligand.¹⁸⁸ Self-assembly of Pt(II) can be exploited to obtain aggregate-induced emission,^{189–191} white organic light emitting diodes (WOLED),^{192–194} luminescent liquid crystals^{195–197} and emissive gels.^{198,199} However, aggregation represents a strong limitation for some applications that require color purity like imaging.

In platinum complexes, the excimeric luminescence from aggregates is attributed to metal-metal-to-ligand charge transfer states ($^3\text{MMLCT}$), whereas monomeric species emit from triplet ligand-centered (^3LC) excited states with sizeable metal-to-ligand charge transfer ($^3\text{MLCT}$) character.

This metal-perturbed ligand-centered ($^3\text{MLCT}$) luminescence is usually quenched by triplet dioxygen in solution ($^3\text{O}_2$), leading to shortened emission lifetimes, reduced luminescence intensities and reactive oxygen species (ROS) such as singlet dioxygen ($^1\text{O}_2$).²⁰⁰ The photoproduction of ROS can be detrimental for optical imaging, where high luminescence intensities are necessitated and cytotoxicity is to be avoided.²⁰¹ Thus, it is necessary to suppress diffusional quenching by shielding the luminophoric complex. Adequate ligands surrounding the metal center can control the alignment of the core and tune π - π staking in solution or in solid media, where the formation of aggregates can be favored or hindered on demand.^{188,202}

It has been recently reported that the adsorption of compact clusters of Pt(II) complexes at the interface of bovine serum albumin, which are intrinsically

shielded from molecular oxygen, allows a time-gated separation of their phosphorescence from background autofluorescence. While these clusters can even act as donors in energy transfer processes, the free monomeric species in solution are non-emissive.²⁰³ Moreover, it has been shown that self-assembled micelles based on tailored copolymers doped with Pt(II) complexes can be tracked by optical and electron microscopy, due to their oxygen-insensitive luminescence and contrast enabled by the high atomic number. The resulting dual readout was employed to track their uptake and localization in eukaryotic cells with high spatiotemporal resolution.²⁰⁴

The synthesis of water-soluble platinum complexes can open new potential applications in bioimaging, where the imaging agents need to show a significant Stoke shift, be photostable, soluble in water and biocompatible. In cell imaging, the uptake and localisation of the luminophore are important aspects to consider. These cells are usually incubated in an aqueous buffer solution, so the luminophore solubility must be sufficient to allow the uptake by the cells. *Passive transport* (diffusion across the membrane) is favoured by cationic compounds and localisation can be manipulated through the selection of groups that react specifically with target species or controlling properties such as polarity.²⁰⁵

Solubilization in aqueous media of similar platinum complexes has been achieved in some cases by modifying the ancillary ligand with TEG chains, although in these cases the formation of hydrogels is favoured and no emission of the monomeric specie is observed at room temperature.²⁰⁶

Prof. Strassert's research group from the Center for Nanotechnology (University of Muenster), is focused in the development of photosensitizing nanoarchitectures and NIR-absorbing optoacoustic labels. The synthesis and fundamental understanding of metal-organic electroluminescent (nano)materials is one of their research lines, focusing on the synthesis and characterization of tailored Pt(II) complexes.^{202,207,208} However, some of the problems related with these complexes are aggregation and low solubility and quenching in aqueous media.

Solubility in aqueous media and shielding of the luminophores from diffusional quenching are two key aspects to be tackled. In this sense, dendrimers

(dendrons) constitute appealing tools. A few dendritic structures have been able to encapsulate and to isolate the emitting core Pt(II) complexes, thus decreasing intermolecular interaction in organic solvents.^{209–211}

This work has been made in collaboration with Prof. Strassert's research group during a predoctoral research stay in their laboratories, where it was proposed the use of alkyl chain-based dendritic structures to protect the emitting core of a Pt(II) complex. These structures should not affect its photophysical properties, due to the non-conjugated nature of the encapsulating array, while the functional groups in the periphery would control the solubility. Moreover, the dendritic structure could effectively avoid aggregation while protecting the emitting core from quenching by molecular oxygen. We propose to combine the unique excited state characteristics of Pt(II) complexes with the features of water-soluble dendrimers. Additionally, as a proof of concept, we will study the ability of such luminophore to act as a biosensor, labeling the cells with a green phosphorescence that can be used for two-photon excitation microscopy.

IV.2 Synthesis of a water-soluble platinum complex (21)

The dendritic structure will be prepared by coupling compounds **3** and **5** through an amide formation reaction and performing the subsequent deprotection of the carboxylic acid group to insert of an acetylene moiety (Figure 84).

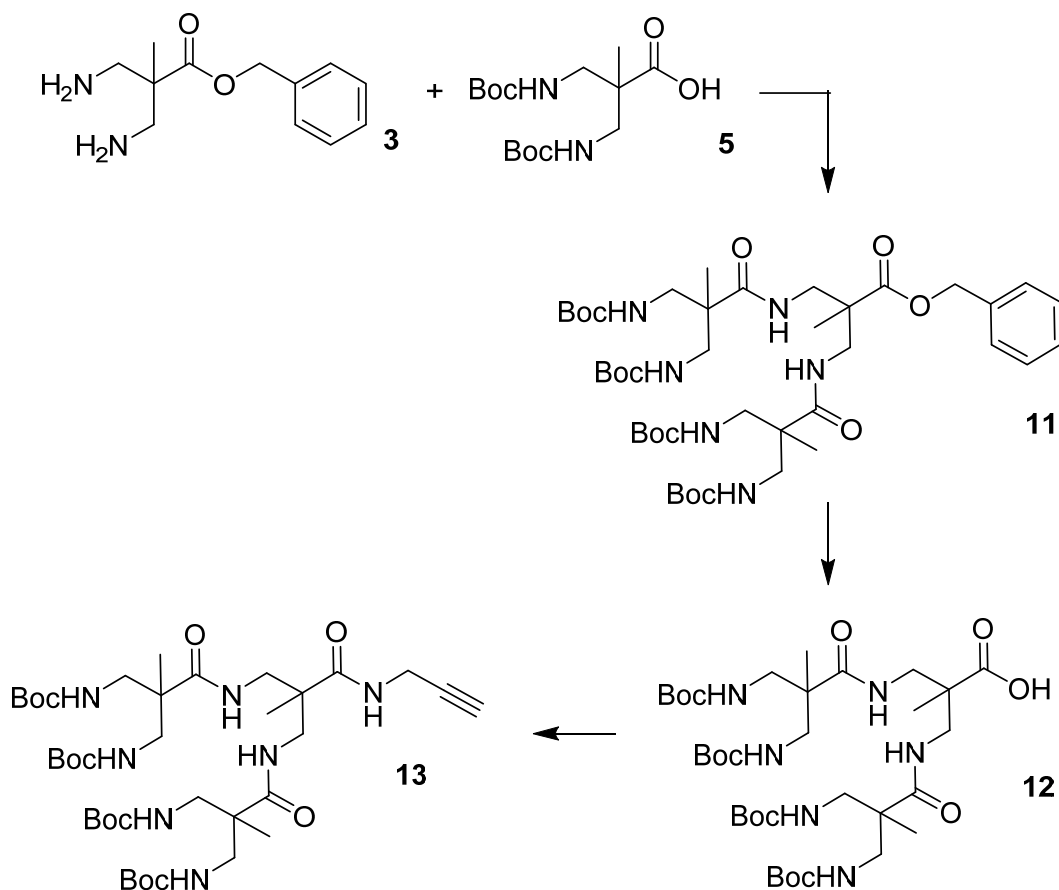


Figure 84. Scheme for **13**.

Due to the experience of Prof. Strassert's research group, a derivative of pyridine (Figure 85) was proposed as anchoring point between the dendrimer and the Pt(II) core, as the bond between the nitrogen of the pyridine moiety and the platinum had been already well established by the group.²¹² First, a bromide derivative of pyridine was synthesized following the procedure described previously.²¹³ The commercial available compound 3,5-pyridine dicarboxylic acid was esterified (**14**) and then reduced to obtain the 3,5-Bis(hydroxymethyl)pyridine (**15**). The bromation was carried out using concentrated aqueous HBr to obtain **16**. The last step was the substitution of the bromide groups for azides to obtain **17**.

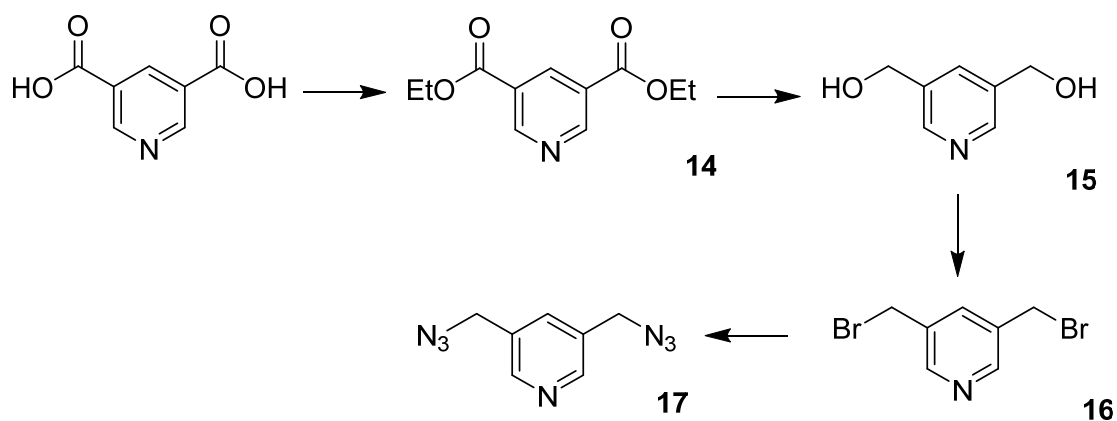


Figure 85. Scheme for 17.

The synthesis of the platinum-doped dendritic structure follows the next scheme (Figure 86):

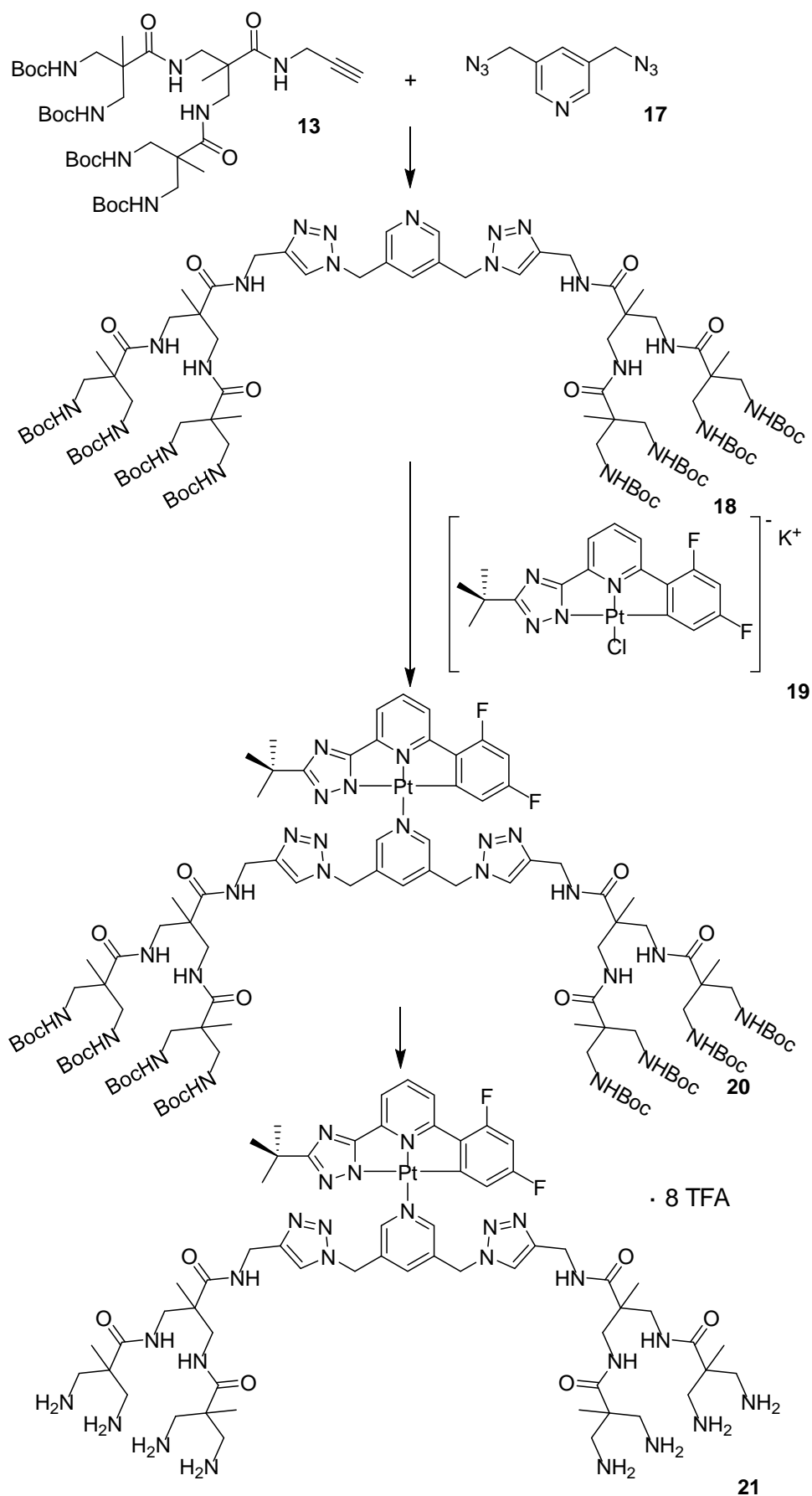


Figure 86. Scheme for **21**.

V.2.1 Synthesis of the dendritic structure (**18**)

Making use of compounds already synthesized, we proposed the synthesis of a novel dendron based on amide bonds. For that purpose, the carboxylic moiety of **5** was conveniently activated by CDI and reacted with the amino groups of **3**. Thus, a dendron with four protected amino groups and a protected carboxylic moiety as focal point was achieved (Figure 87). The chemical orthogonality of both protecting groups will permit us the selective deprotection of each moiety. The desired product was obtained as a colorless solid in 83% yield.

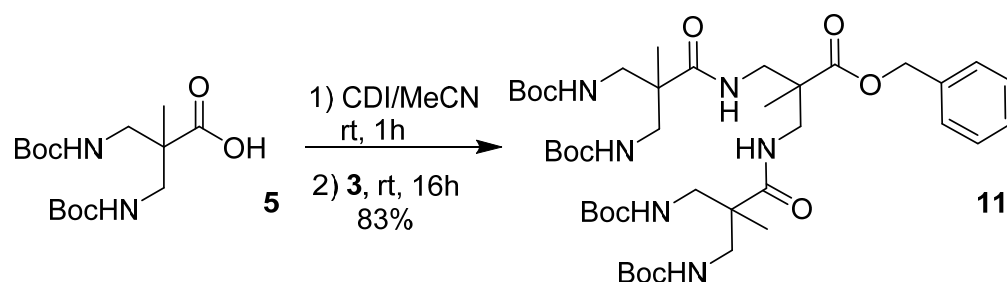
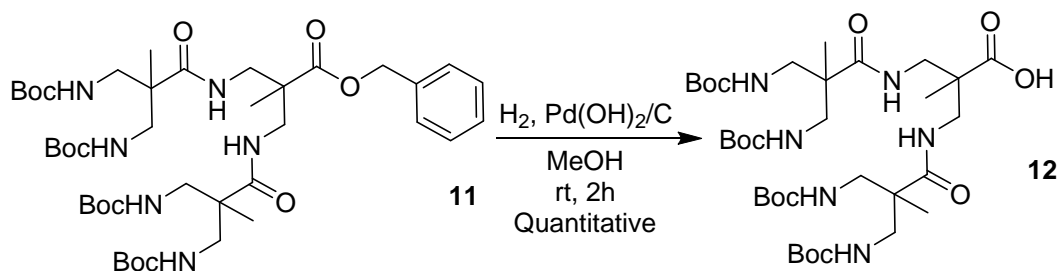


Figure 87. Synthesis of **11**.

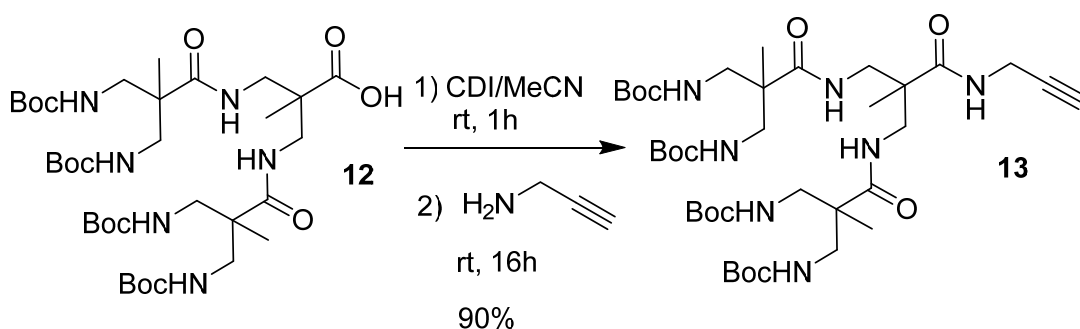
The compound was fully characterized using NMR techniques such as ^1H , ^{13}C NMR and HSQC (Figure 190, Figure 191 and Figure 192, respectively). The ^1H NMR (Figure 190) shows the signals of the benzyl ester moiety at 7.36 and 5.15 ppm while the methylenes of the dendrimeric structure appear as a multiplet at 3.31 ppm. Methyl groups are found between 1.00-1.50 ppm. Mass spectroscopy showed the molecular ion $[\text{M} + \text{Na}]^+$ at m/z 392.22.

Deprotection of the carboxylic acid group took place by hydrogenolysis of **11** in the presence of Pearlman's catalyst (Figure 88). Compound **12** was successfully obtained as a colorless solid in a quantitative yield.

Figure 88. Synthesis of **12**.

The reaction was monitored by ^1H NMR (Figure 193) until no signal of benzyl ester could be detected. Mass spectroscopy spectrum presented the peak $[\text{M} + \text{Na}]^+$ at m/z 783.45

The insertion of the acetylene moiety was carried out activating first the carboxylic acid of **12** with CDI and adding later propargylamine to the reaction mixture (Figure 89). The desired product was obtained as a colorless solid in 90% yield.

Figure 89. Synthesis of **13**.

Mass spectroscopy showed the molecular peak $[\text{M} + \text{Na}]^+$ at m/z 873.49. NMR techniques allowed us to fully characterize the compound. The methylene group adjacent to the triplet bond appears at around 3.80 ppm while the rest of the methylene groups and the proton of the triple bond appear as a multiplet between 3.23 and 2.84 ppm. The singlet at 1.36 corresponds to the methylene of the boc groups and the signal at around 1.00 ppm is associated to the methyl groups of the dendron (Figure 196).

For the synthesis of the azido derivative of pyridine, first, a bromide derivative (**16**) was synthesized following a procedure described previously.²¹³ The commercially available compound 3,5-pyridine dicarboxylic acid was esterified to obtain **14** (Figure 90). Concentrated sulfuric acid was introduced dropwise into a solution of 3,5-pyridine dicarboxylic acid in absolute ethanol. After 16h reflux, ethanol was evaporated under vacuum. Ice water was then added to the reaction crude and was then neutralized with Na₂CO₃ until basic pH. The aqueous phase was extracted with diethyl ether and the organic phase was concentrated to obtain **14** as a yellow oil in 67% yield.

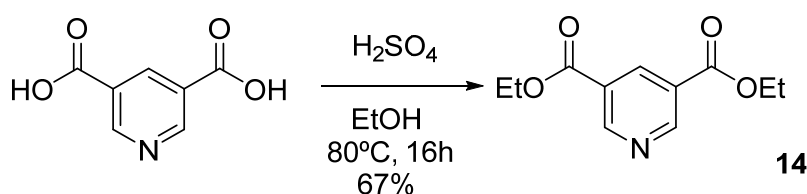
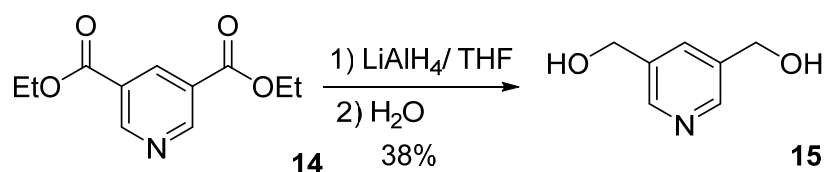


Figure 90. Synthesis of compound **14**.

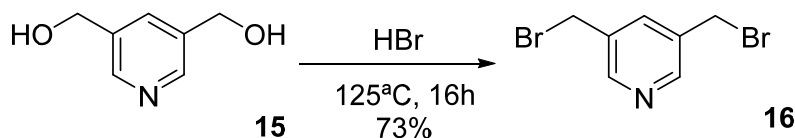
The compound was characterized by ¹H NMR (Figure 199). Its spectrum shows a doublet and triplet in the aromatic region, at 9.36 and 8.86 ppm respectively, corresponding to the protons of the aromatic ring. The methylene groups of the alkyl chain appear as a quadruplet at 4.45 ppm and the methyl groups at 1.43 ppm as a triplet.

Compound **14** was then reduced to obtain the 3,5-bis(hydroxymethyl)pyridine (**15**). A solution of **14** in THF was added dropwise under vigorous stirring to a suspension of LiAlH₄ in THF under a nitrogen stream (Figure 91). Afterwards, water was slowly added, and the white pastry precipitate was filtered. The filtrate was evaporated under vacuum and the compound was purified by column chromatography to obtain **15** in 38% yield.

Figure 91. Synthesis of compound **15**.

^1H NMR spectrum (Figure 200) shows a doublet and multiplet in the aromatic region, at 8.38 and at around 7.66 ppm respectively, corresponding to the protons of the aromatic ring. The methylene groups appear as a doublet at 4.53 ppm.

The substitution of the hydroxy groups by bromide was carried out using concentrated aqueous HBr to obtain **16**. The mixture was heated at 125 °C for 16 h and then cooled to room temperature (Figure 92). The resulting residue was dissolved in H_2O and Na_2CO_3 was added. The aqueous solution was extracted with CH_2Cl_2 and the solvent removed to obtain **24** in 73% yield.

Figure 92. Synthesis of compound **16**.

In the ^1H NMR spectrum (Figure 201) the signals corresponding to the protons of the aromatic ring appear as a doublet and multiplet in the aromatic region, at 8.54 and at around 7.75 ppm respectively, and the methylene groups appear as a singlet at 4.45 ppm.

The last step was the substitution of the bromide groups for azides, this was carried out following a previously described procedure,²¹⁴ in order to obtain **17**. To a solution of **16** in DMF, NaN_3 was added. The mixture was heated at 85°C for 16 hours and then cooled to room temperature (Figure 93). H_2O was added

and the resulting aqueous solution was extracted with CH_2Cl_2 to obtain **17** in 83% yield.

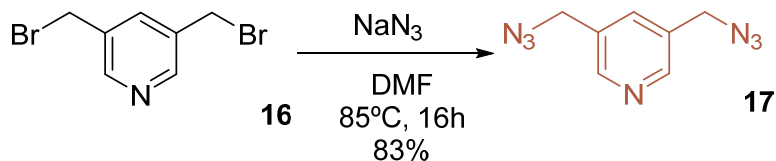


Figure 93. Synthesis of compound **17**.

In the ^1H NMR spectrum (Figure 202) the signals corresponding to the protons of the aromatic ring appear as a doublet and multiplet in the aromatic region, at 8.54 and at around 7.75 ppm respectively, and the methylene groups appear as a singlet at 4.45 ppm.

The *click* reaction between the dendron **13** and the pyridine derivative **17** was carried out using the same conditions designed earlier (Figure 94). The desired product (**18**) was obtained as a colorless solid in 83% yield.

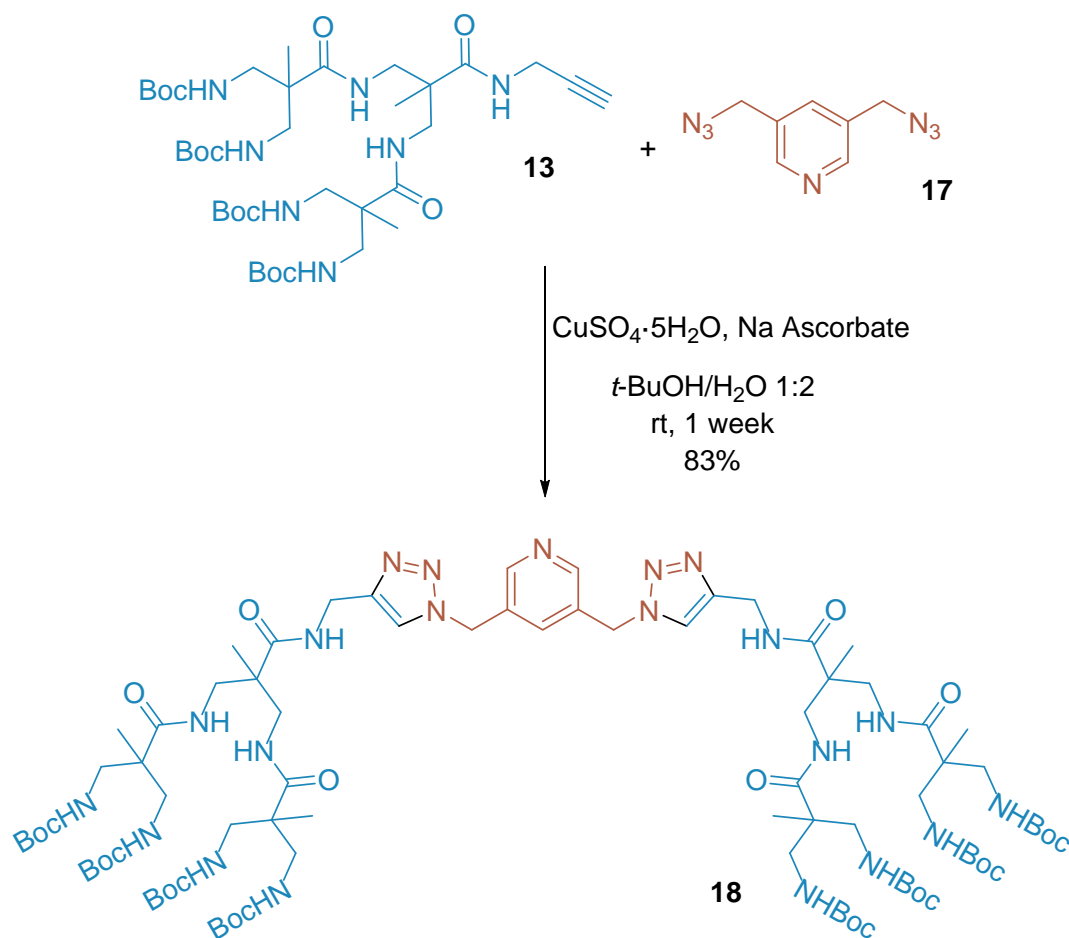


Figure 94. Synthesis of **18**.

Mass spectroscopy showed the molecular peak $[\text{M} + \text{Na}]^+$ at m/z 1785.07. In the ^1H NMR spectrum (Figure 95, Figure 205), the shift to lower field of the methylenes *i* from 3.80 ppm to 4.27 ppm indicates that the click reaction has taken place successfully. It's worth noticing the appearance of signals in the aromatic region, corresponding to the pyridine moiety and the 1,2,3-triazole cycles.

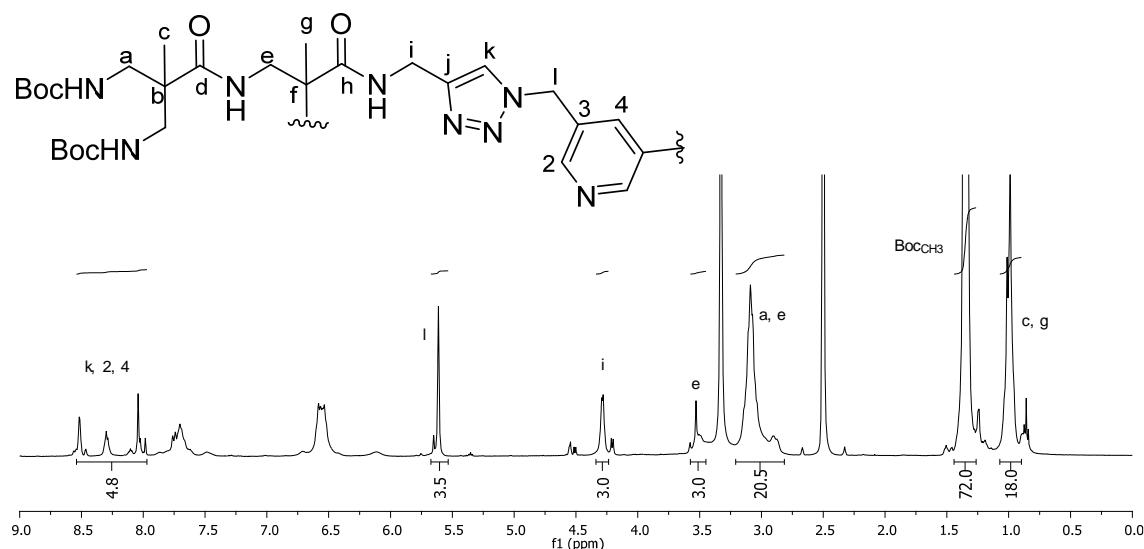


Figure 95. ^1H NMR spectrum of **18** in DMSO.

IR spectrum of **18** (Figure 96) shows the disappearance of the typical azide band (2095 cm^{-1}) indicating the effective formation of both triazole cycles. The band at 2030 cm^{-1} in **18** is typical of pyridine, verifying that the pyridine moiety has been successfully integrated in the dendritic structure.

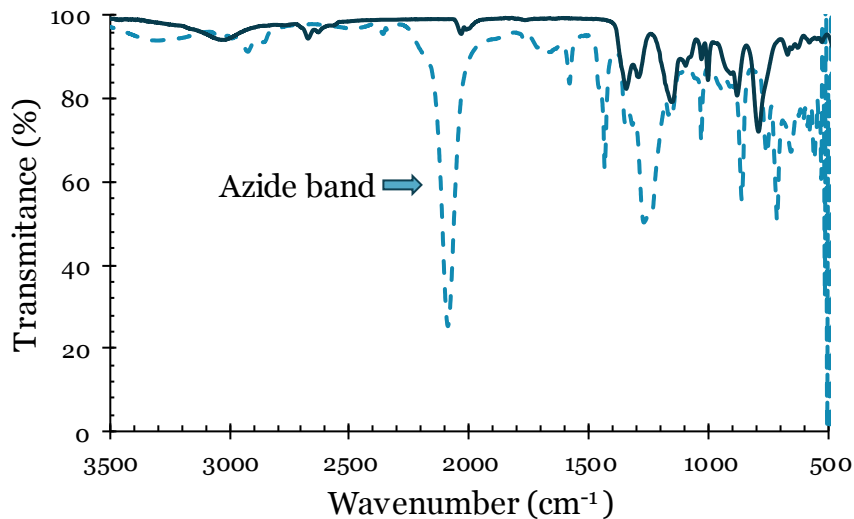


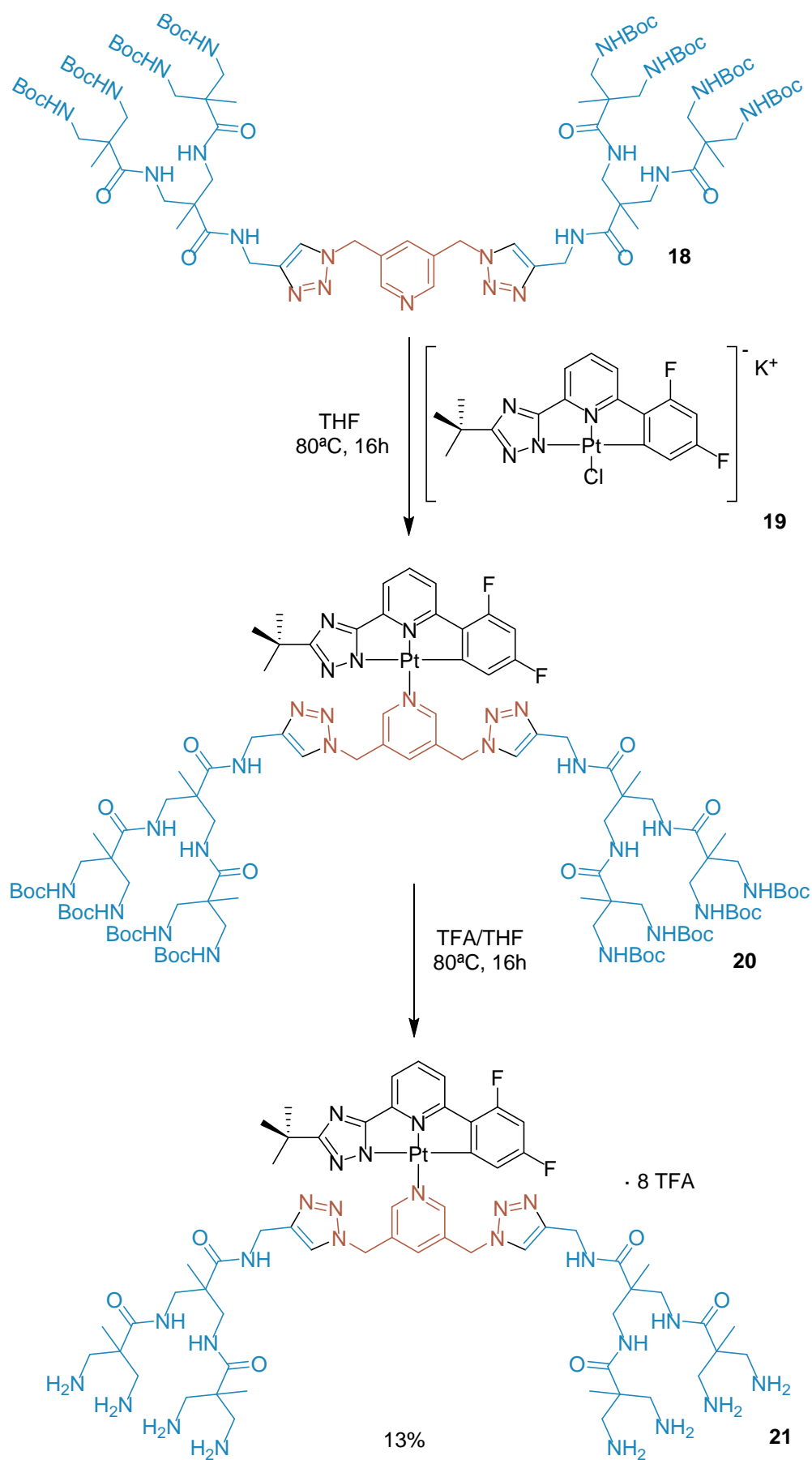
Figure 96. IR spectra of compound **17** (dotted line) and compound **18** (solid line).

IV.2.2 Synthesis of the platinum-doped dendritic structure (**21**)

The platinum-doped dendritic structure was obtained by exchange reaction of the chloride ligand in the ancillary position. The reaction took place

between the dendrimeric structure, **18**, and the platinum compound²⁰² (**19**) supplied by Dr. Strassert research group during my stay at the University of Münster. It was carried out in THF at reflux for 16 hours. Afterwards, the solvent was removed and the deprotection of the amine groups in the presence of TFA was carried out without further purification (Figure 97). The final product, **21**, was purified by sephadex column, obtaining the desired product as a yellow solid in a 13% yield.

The platinum-doped dendritic structure resulted completely soluble in aqueous media. The terminal amino groups provide the molecule with solubility in aqueous media as well as biological activity (such as promoting the adhesion to bacteria) and an interesting reactivity that can lead to the modification of the periphery of the molecule with a wide range of structures.

Figure 97. Synthesis of **21**.

NMR experiments were carried out to confirm the presence of **21**. The addition of new signals in the aromatic region to the ones corresponding to the dendrimeric structure confirms the successful ligand exchange reaction (Figure 98, Figure 208). Broad signals between 0 and 4 ppm are the characteristic of the dendritic moiety together with two singlets at 4.44 and 5.69 ppm, corresponding to the methylene groups adjacent to the triazole ring. The presence of the Pt core is confirmed by the signal between 7.5 and 9 ppm.

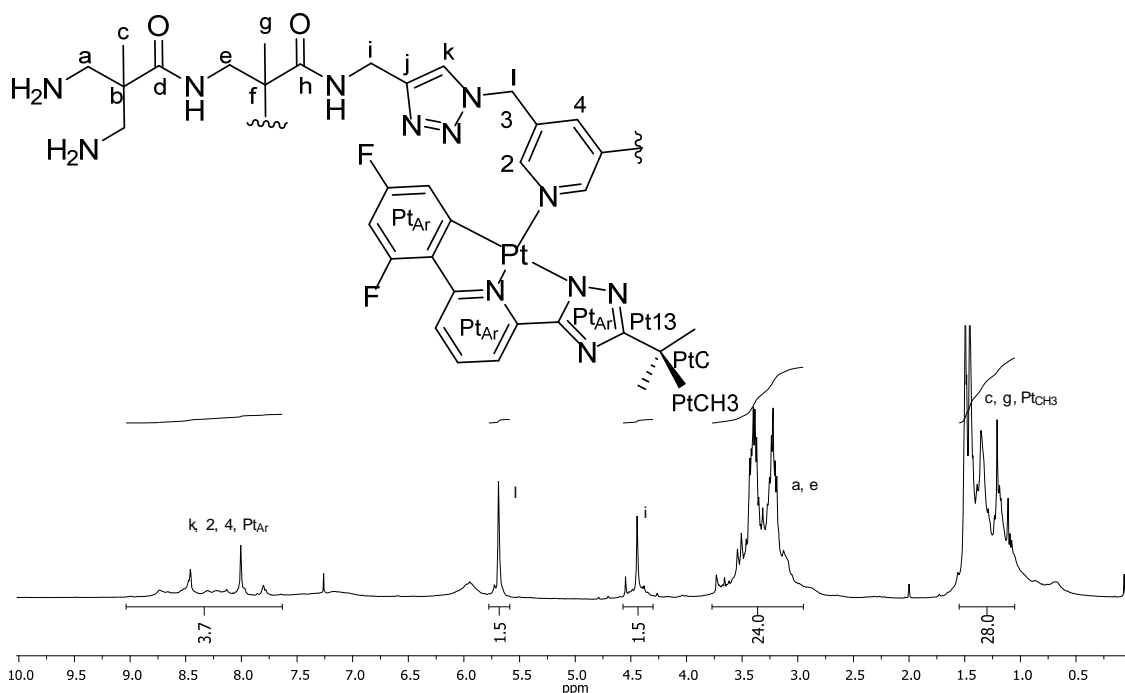


Figure 98. ^1H NMR spectrum of **29** in D_2O .

No mass spectrum was obtained, probably due to the lability of the Pt-N bond of the ancillary ligand.

Diffusion ordered spectroscopy experiments were carried out. DOSY experiments performed on an aqueous solution of **21** at a concentration of 10^{-3} M show a monoexponential decay of the signal and a value for the diffusion coefficient of $2.062 \times 10^{-10} \text{ m}^2/\text{s}$ (Figure 99). This results in a linear Stejskal-Tanner plot, showing that diffusion of a monodisperse molecule is monitored, which excludes any aggregation (Figure 99).^{215,155}.

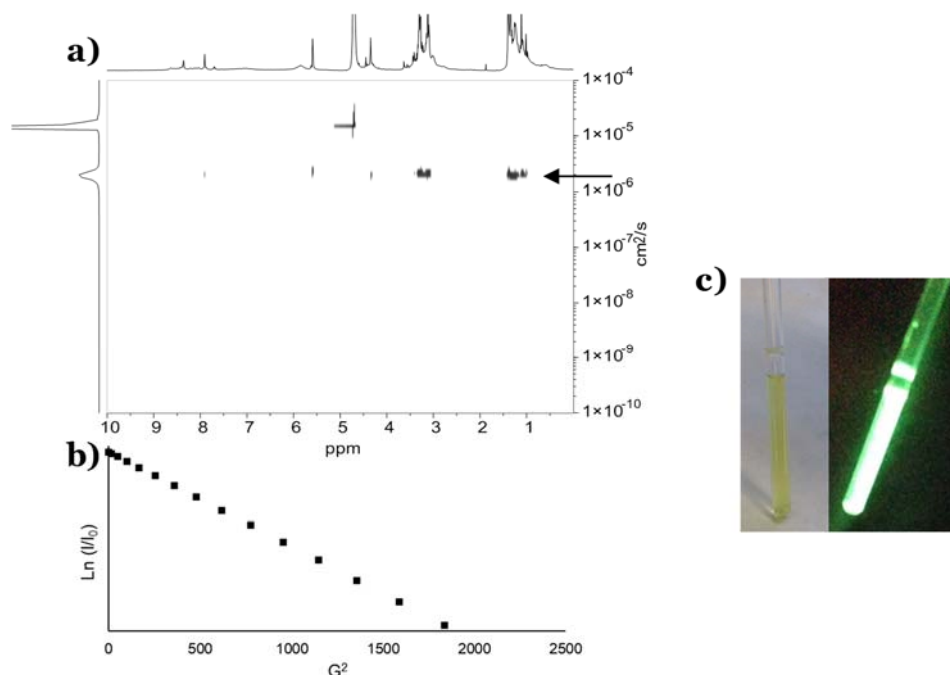


Figure 99. a) DOSY NMR experiment for compound **29**; b) Stejskal-Tanner plot; c) picture of the NMR tube under visible light (left) and excitation at 365 nm (right).

IV.3 Photophysical characterization

The photophysical properties of **21** in aqueous solution (10^{-5} M) were studied. Absorption spectrum showed a band at around 250 nm, which can be assigned to π - π^* excitations, as well as a broad band around 350 nm that can be ascribed to a transition with mixed MLCT/LC character (Figure 100).²⁰² In agreement with the results observed in the DOSY experiments, no signs of ground state aggregation are observed.

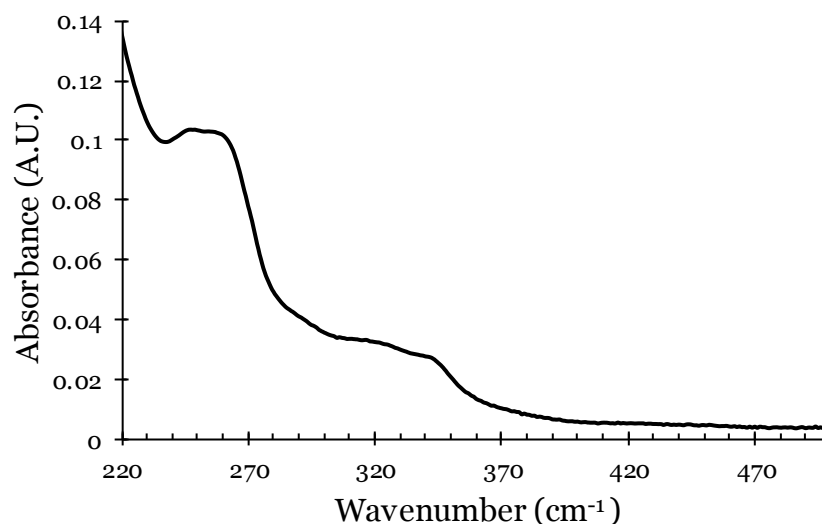


Figure 100. Absorption spectrum of **21** in water.

The complex exhibits a green luminescence, $\lambda_{\text{max}} = 500 \text{ nm}$ ($\lambda_{\text{exc}} = 350 \text{ nm}$), with a luminescent quantum yield of 0.12 and a lifetime of 16 μs under deoxygenated conditions (Figure 101, Table 9). Such luminescence is partially quenched by molecular oxygen, decreasing the luminescent quantum yield to 0.05 and the lifetime to 5 μs under air-equilibrated conditions (Table 9). In fact, both the photoluminescence quantum yields and the amplitude-weighted average lifetimes are diminished by a factor of roughly 3 (Table 9).

Air-equilibrated		deoxygenated	
$\phi_L \pm 0.02$	$\tau \pm 0.01 / \mu\text{s}$	$\phi_L \pm 0.02$	$\tau \pm 0.01 / \mu\text{s}$
0.05	9.8 (28%); 3.1 (78%); [5.0]	0.12	19.0 (57%); 11.1 (43%); [15.5]

Table 9. Luminescent quantum yield (ϕ_L) and lifetime (τ) ($\lambda_{\text{em}} = 500 \text{ nm}$) of a 10^{-5} M aqueous solutions of **21** (fractional amplitudes in parentheses, amplitude-weighted average lifetimes in brackets).

The profile of the emission band corresponds to a monomeric specie. When increasing the concentration (up to 10^{-4} M), no significant contribution of aggregates is observed at around 650 nm, (Figure 101).

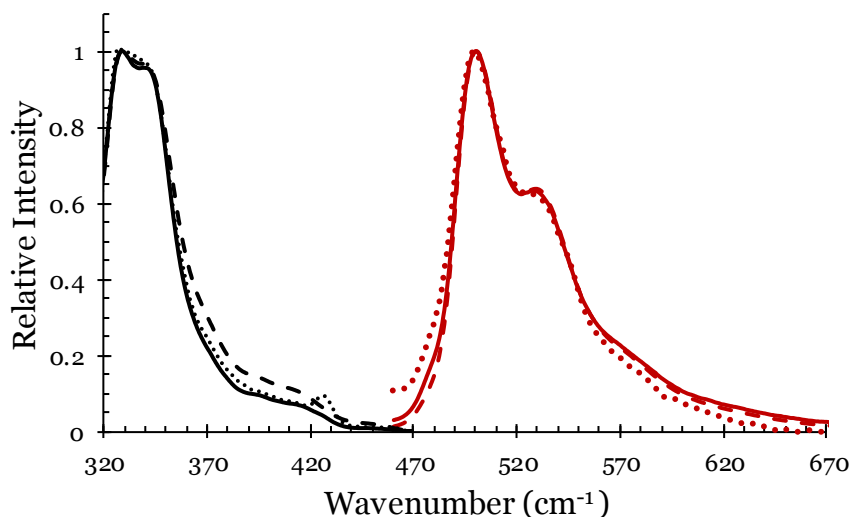


Figure 101. Normalized excitation (left, $\lambda_{\text{em}} = 500$ nm) and emission spectra (right, $\lambda_{\text{exc}} = 350$ nm) of **21**, in aerated aqueous solutions at 10^{-6} M (dotted line), 10^{-5} M (solid line) and 10^{-4} M (dashed line).

Compound **21** is luminescent in aqueous environments without the need of complex carriers, such as proteins, micelles or polymers. However, stability is critical particularly if the biomarker is to be stored for any length of time or to make sure that the photophysical properties of the compounds are not modified during the incubation time with the cells. In order to confirm the photostability of the compound, emission and excitation spectra of a 10^{-5} M solution of **21** in PBS were recorded for two days (Figure 102). No major differences are perceived in any of the experiments carried out which proves that the compound is stable in a standard solution for cell culture at least for 48 hours at room temperature.

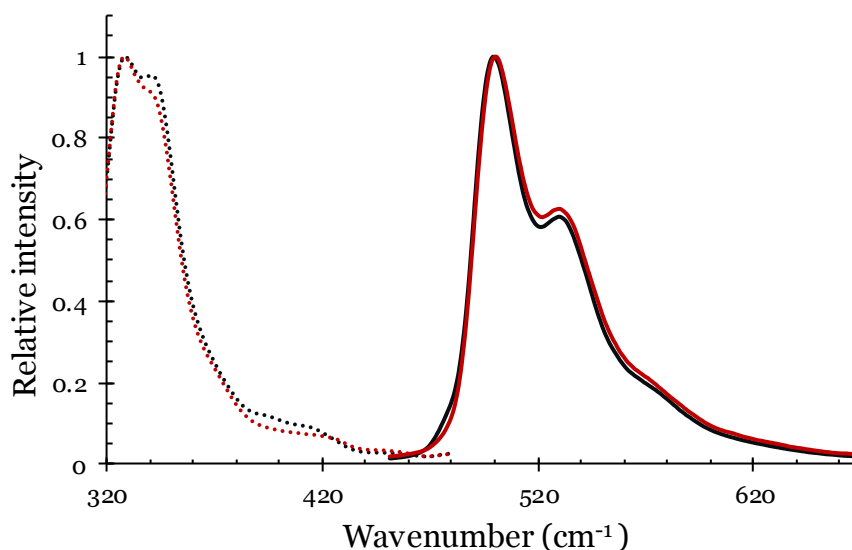


Figure 102. Normalized excitation (left, $\lambda_{em} = 500$ nm) and emission (right, $\lambda_{exc} = 350$ nm) spectra of **21** in aqueous solution at 10^{-5} M freshly prepared (black) and after 48 hours (red).

When comparing these results with similar Pt(II) complexes possessing the same C[^]N[^]N luminophore, a clear influence of the dendritic moiety can be observed,²⁰² as both the quantum yield and the lifetime appear enhanced in fluid environments but without traces of excimeric emission. When the ancillary ligand is a 4-substituted pyridine, a broad red-shifted emission band (around 600 nm) appears at higher concentrations, which can be associated to stacked species. The wavelength of such emission (normally from ³MMLCT states) depends on the bulkiness of the ancillary ligand and its tilt angle with respect to the coordination plane.²⁰²

Similar Pt (II) complexes have been also modified using a 4-substituted pyridine with tetraethylene glycol chains as the ancillary ligand. In that case, solubility in aqueous solution was partially achieved, observing ground state aggregation at concentrations above 10^{-4} M. Above this concentration emission of the aggregates was observed at 580 nm as well, and luminescence of the monomeric species was not observed at any concentration at room temperature.²⁰⁶

The bulky dendritic ligand **18** prevents intermolecular interactions even in aqueous media. Only absorption and emission due to the monomeric species is observed in aerated aqueous solutions of **21**, showing higher luminescence

quantum yields than similar complexes.^{202,206} The long lifetimes observed for **21** indicate that the dendritic structure protects the platinum core against the environment, partially avoiding quenching of the luminescence by molecular oxygen. This is a key feature for imaging, as suppresses the formation of cytotoxic reactive oxygen species.

IV.3.1 Two Photon Excitation Studies

Excitation and emission spectra acquired under TPE conditions were also recorded. The emission obtained by excitation at 720 nm coincides with the one obtained under OPE conditions (Figure 103).

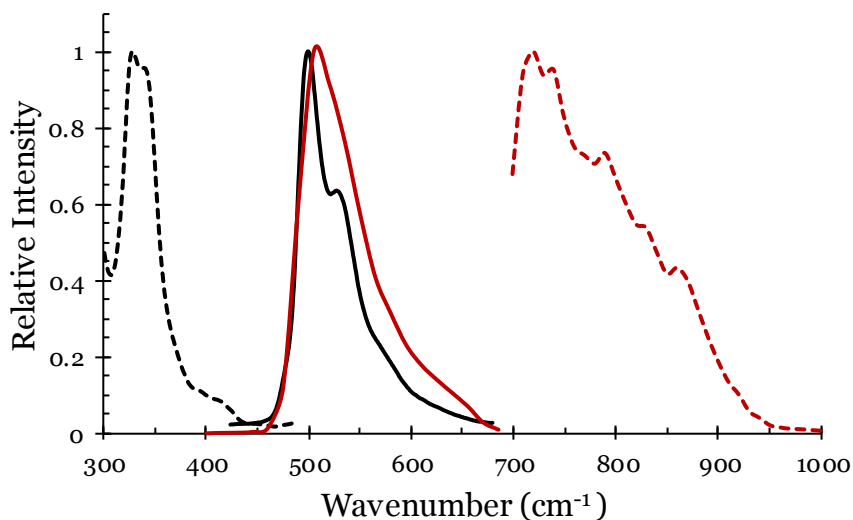


Figure 103. Normalized excitation (dotted line) and emission (solid line) spectra of **21** upon one photon (black) or two photon (red) excitation (350nm and 720 nm respectively), in aqueous solutions.

Compound **21** presents therefore the possibility to combine one and two photon excitation (OPE or TPE, respectively), opening a way to integrate multiple excitation channels to observe its luminescence.

Two-photon absorption (TPA) is defined as the electronic excitation of a molecule induced by a simultaneous absorption of pair of photons of the same or different energy. The dependence of the emission intensity on the laser power was measured. The quadratic dependence obtained confirmed the two-photonic nature of the observed phenomenon. The TPA activity is usually quantified

through two-photon absorption cross section. In this study, TPA cross-sections were determined by the two-photon-excited fluorescence (TPEF) method.²¹⁶ The TPEF technique measures the fluorescence induced by TPA by comparison to a reference compound. In this case, Rhodamine B with a known cross section (δ) value in MeOH was used. The TPA cross section for an aqueous solution of **21** was calculated following the equation:

$$\delta_{21} = \delta_R \frac{C_R \eta_R \Phi_R}{C_{21} \eta_{21} \Phi_{21}} \frac{F_{21}}{F_R}$$

Where C is the concentration, η the refractive index, Φ the quantum yield and F the integrated area under the TPEF spectrum.

TPA cross section thus calculated for **21** (δ_{21}) was of around 3.90 GM ($10^{-50} \text{ cm}^4 \text{ s molecules}^{-1} \text{ photon}^{-1}$) at 710 nm (Figure 104).

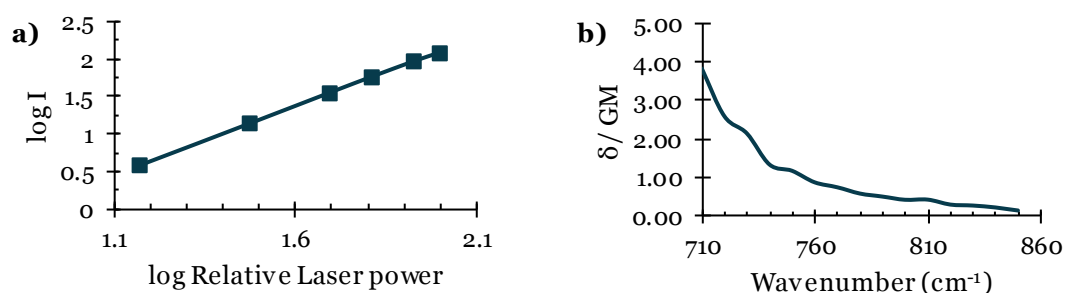


Figure 104. **a)** Dependence of emission on the Laser power (measured at $\lambda_{\text{exc}}=720 \text{ nm}$ and $\lambda_{\text{em}}=500 \text{ nm}$); **b)** TPA cross section values.

IV.4 Biological studies

To evaluate the use of **21** as a multichannel luminescent marker for biological samples, two *E. coli* and *P. subtilis* bacterial strains were employed as model targets. These studies were made in collaboration with Dr. Guadix and Dr. Perez-Pomares of the Animal Biology Department, University of Malaga.

IV.4.1 Studies with *E. coli* Bacteria (gram-negative)

The amino terminal groups of **21** provide an effective binder to bacterial surface, owing to their capacity for hydrogen bonds and electrostatic interaction.¹⁷⁵ Bacteria *E.coli* was incubated with a 10^{-4} M solution of compound **21** in PBS during 2 hours and a control was suspended in 5 mL of only PBS. After incubation both samples were centrifuged (5000g, 10 minutes) and washed twice in 10 mL of PBS. Finally, each bacterial sample was resuspended in 500 μ L of PBS. As can be seen in the optical micrographs (Figure 105), **21** effectively labelled both *E. coli* bacteria.

An intense green luminescence can be observed from the outer surface of the bacteria, confirming the adhesion of the complex to the bacterial wall. This characteristic emission can be observed under both OPE and TPE conditions. This is a key point when performing imaging experiments of biological samples, where is relevant to distinguish the intrinsic emission of the luminescent probe from sample autofluorescence and background noise.¹⁷⁶ In untreated bacteria, an extremely weak autofluorescence is observed under OPE. However, no autofluorescence is observed under TPE conditions (capture settings and image processing are identical).

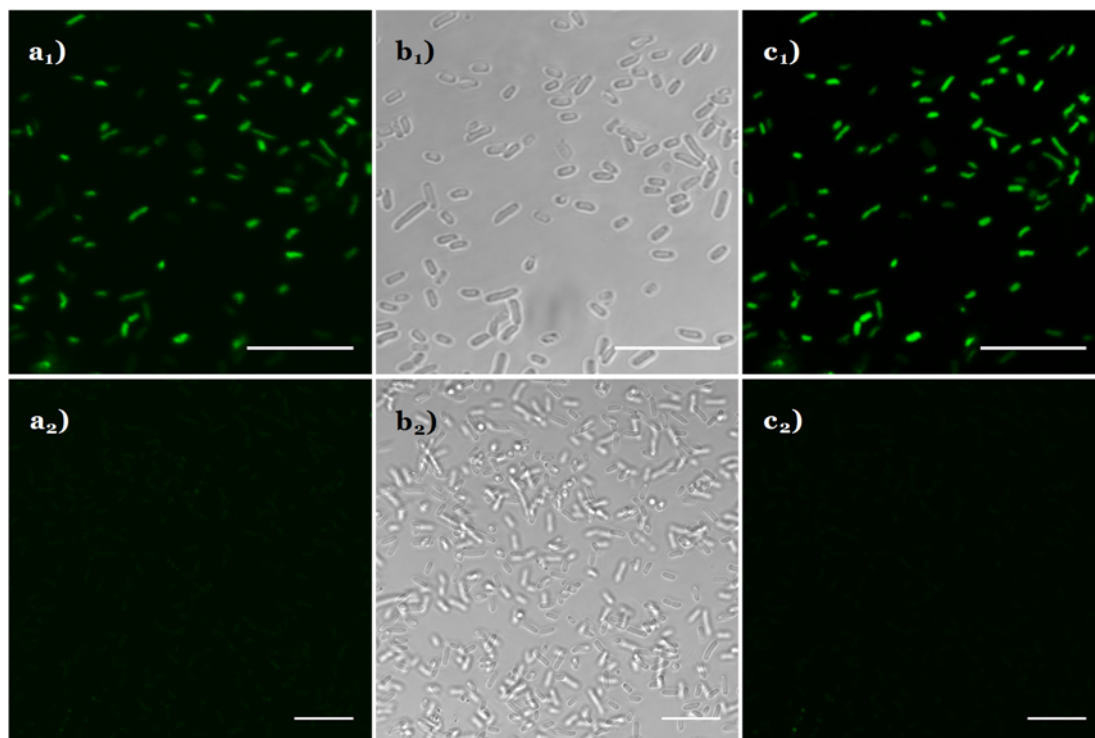


Figure 105. Confocal micrographs of *E. coli* incubated (2h) with (upper row) or without (lower row) compound **21**: **a)** recorded emission under one photon excitation ($\lambda_{\text{exc}} = 405$ nm; collected through 500-600 nm); **b)** bright field images; **c)** recorded emission under two photon excitation ($\lambda_{\text{exc}} = 720$ nm; collected through 500-550 nm). Scale bars: 5 μm

Moreover, the emission and excitation spectra of the stained bacteria resemble those of **21** in both OPE and TPE conditions (Figure 103, Figure 106). The longer excited state lifetime observed for stained bacteria (10 μs) also indicates the presence of the monomeric species and the protection of the Pt (II) core from quenching processes.

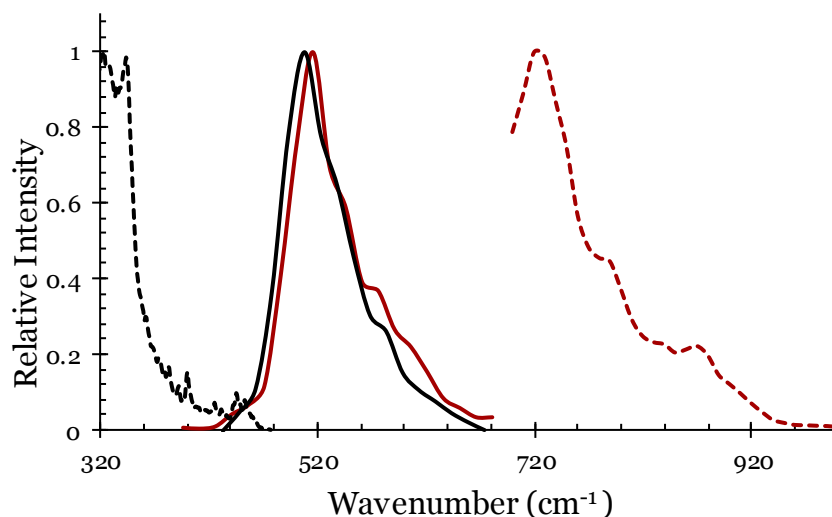


Figure 106. Normalized excitation (dotted line) and emission (solid line) spectra of *E. coli* cells incubated for 2 h with **21** upon one photon (black) or two photon (red) excitation (350nm and 720 nm respectively), in aqueous solutions.

TEM images of *E. coli* and *E. coli* incubated with **21** were also acquired, where EDX analysis confirms the presence of platinum (Figure 107). Although no measurable interaction between the metal centers is observed in solution, TEM images of incubated cells show high contrast clusters that are not observed in untreated bacteria (red arrow in Figure 107a). Such Pt-clusters provide a possibility to track the heavy atoms by means of electron microscopy.

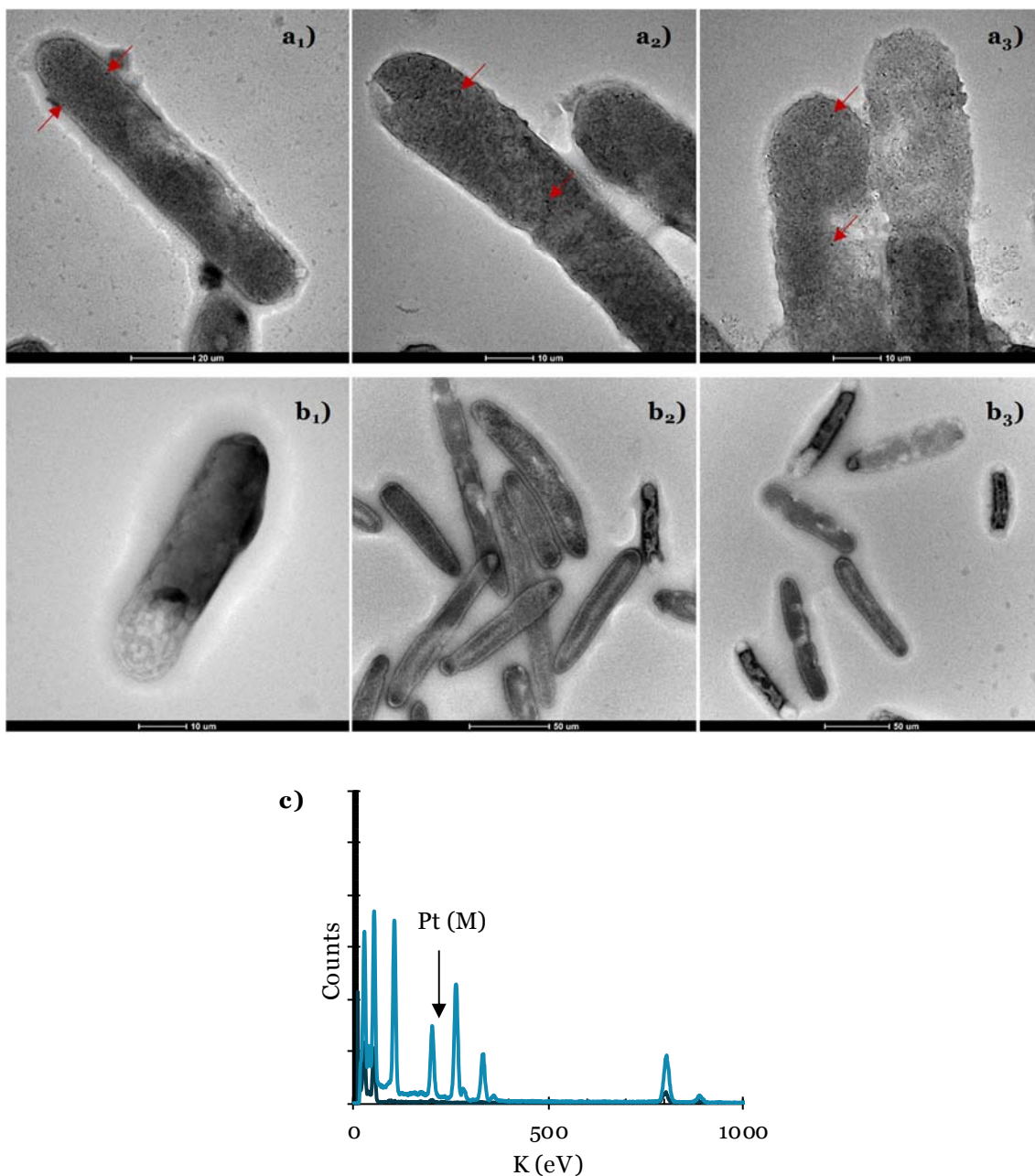


Figure 107. **a)** TEM images of incubated *E. coli* (arrows point to Pt clusters); **b)** TEM images of non-incubated *E. coli*; **c)** EDX spectra obtained from incubated *E. coli* (light blue) and non-incubated *E. coli* (dark blue).

IV.4.2 Studies with *P. subtilis* Bacteria (gram-positive)

Studies were also carried out using gram positive bacteria in order to confirm the adhesion of the compound **21** to the bacterial wall. The images taken under both OPE and TPE conditions show the successful marking of the *P.*

subtilis (Figure 108). No differences in the marking of both bacteria (*E. coli* and *P. subtilis*) were observed under these conditions.

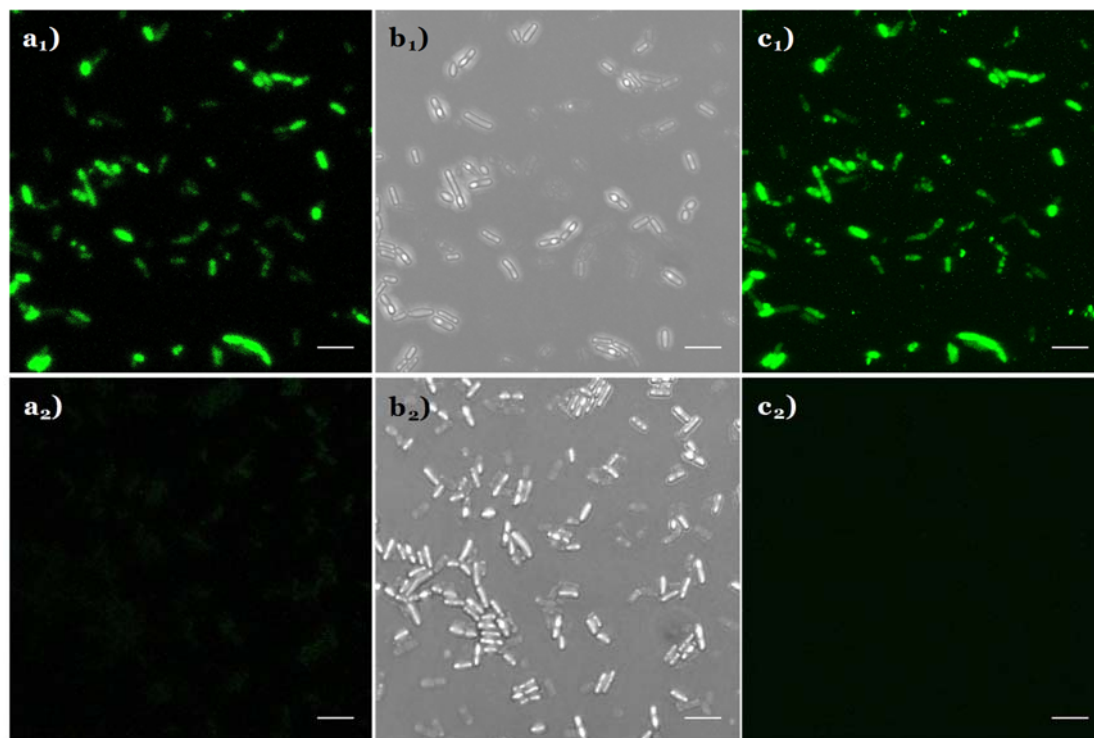


Figure 108. Confocal micrographs of *P. subtilis* incubated for 2 h with (upper row) or without (lower row) compound **21**. **a)** recorded emission under one photon excitation ($\lambda_{\text{exc}} = 405$ nm; collected through 500-600 nm); **b)** bright field images; **c)** recorded emission under two photon excitation ($\lambda_{\text{exc}} = 720$ nm; collected through 500-550 nm). Scale bars: 5 μm

IV.4.3 Bactericidal test

Bactericidal tests were carried out by Dr. Díaz-Martínez and Dr. Romero from the Microbiology Department, University of Malaga. The dynamics of bacterial growth was monitored in liquid LB medium originally inoculated with 4×10^6 *E. coli* and *P. subtilis* and incubated in the presence (10 or 100 μM) or absence of **21**. No significant *E. coli* growth delay was recorded with increasing **21** concentration from 10 to 100 μM . *P. subtilis* growth was significantly reduced at 100 μM of **21**. (Figure 109).

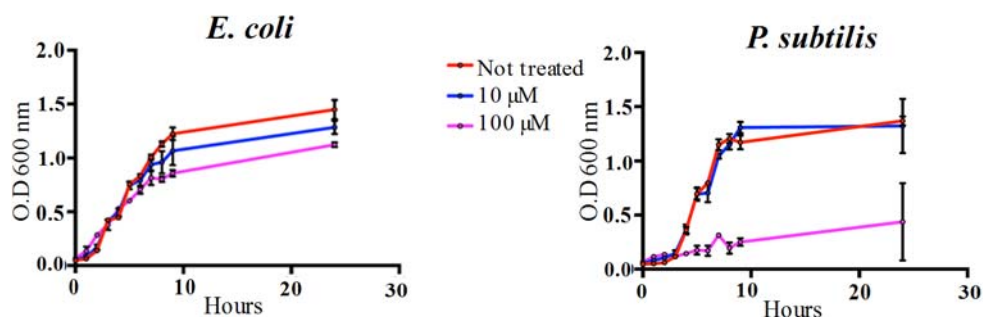


Figure 109. Bacterial growth of *E. coli* and *P. subtilis* when non-incubated (red) and incubated with a solution 10 μM (blue) or 100 μM (purple) of compound **21**.

By combining the characteristics of dendritic structures with the photophysical properties of Pt(II) complexes, an unique luminescent marker soluble in aqueous media was obtained. The dendritic moiety, with well-defined structure and three-dimensional geometry, possess the ability to encapsulate the emitting core and create a specific site-shielded nanoenvironment. In this way, the complex constitutes a triplet emitter whose photophysical properties are perfectly stable in biological media without the need of a carrier. The approach to exploit the luminescent properties of Pt(II) complexes in bioimaging has been demonstrated using both OPE and TPE conditions. Additionally, the array has proven to be traceable by electron microscopy and acting as a probe providing dual orthogonal readouts.²¹⁷

CHAPTER V

FUNCTIONALIZATION OF TITANIUM SURFACES

WITH RGD-DENDRITIC STRUCTURES

V.1 Introduction

Titanium is one of the most studied and used material in prosthetics due to its good biocompatibility, strong mechanical properties, high immunity to corrosion, complete inertness to body environment and ability, under favorable healing conditions, to form a structural and functional connection with bone.²¹⁸ The global dental implants and prosthetics market is worth billions of dollars each year. The facts that musculoskeletal disorders are one of the most widespread human health problems and that we are facing a globally aging population, are responsible for an increase in orthopedic research. In consequence, great efforts are being made in the development of new titanium implants that would improve the lifespan and lessen rejection rates of the biomaterials.

When a biomaterial is implanted in the human body, adsorption of water and proteins will take place. Afterwards, one of the following process can occur:²¹⁹

i) New bone cells begin to grow on the implant surface. Their proliferation and differentiation will lead to osseointegration. This is the most desired outcome when using implants.

ii) Inflammatory response by the human body to reject the implant.

iii) The formation of fibrous tissue on the material surface. With time, the implant becomes totally encapsulated by such fibrous tissue impeding osseointegration. It may be caused by the absorption of unspecific proteins in the surface that send unspecific signalling to the cellular environment.²²⁰

Great research efforts are being made to improve the biocompatibility of the titanium implants in which chemistry and topography play a crucial role. Titanium implants present a thin Ti-oxide surface. Modification of these surfaces has been traditionally carried out employing mechanical, physical and chemical techniques and can be grouped in two major categories: morphological or chemical modifications (Table 10).²²¹

Morphology	Physico-chemistry	Chemistry		
		Inorganic	Organic	Inorganic/Organic coatings
Micromorphology to improve	Adaptation of	Plasma oxidation	Adsorption	Compound coating from CPP
Adhesion	Surface energy	F-Treatment	Covalent coupling	with
Proliferation	Isoelectric point	CaP	Nanomechanical fixation	Collagen
Differentiation of cells	Ionic/electronic conductivity	nanocrystals	Self organisation principles	Chlorhexidine
		Calcium phosphate phases (CPP)	Drug delivery coating <i>e.g.</i> antibiotics/ growth factors	Chitosan
Mechanical interactions with surrounding tissue – interlocking		Termal		Growth factors
		Exposure to SBF ^a		
		ECAD ^b		
		Sol-gel		

Table 10. Classification of biofunctionalization methodology.²²¹ ^a SBF = simulated body fluid. ^b ECAD = electrochemically assisted deposition

Different studies show that surface roughness affects cell morphology and growth.²²² Osteoblasts, the cells responsible for the synthesis and mineralization of bone, tend to adhere to a rougher surface.²²³ In contrast, fibroblasts, whose proliferation along with collagen production are responsible for fibrotic tissue reactions to biomaterials implants,²²⁴ are demonstrated to prefer smoother surfaces.²²⁵ Topographical modifications techniques include polishing, blasting, etching, oxidation, and titanium plasma spraying.²²⁶ More recently, new

techniques like metal 3D-printing by laser or electron beam melting has opened the possibility of fabrication personalized implants from digital models while controlling the grade of porosity.^{227–230}

To favor osseointegration and diminish the risk of adverse tissue response, researchers have traditionally focused on coating implant surfaces with bioactive materials. The effects of a thin layer of hydroxyapatite (HA) in the surface of titanium on the formation of bond between the bone and the surface were first studied in the 80s.²³¹ Since then, numerous advances have been made in the field and new HA coatings that present advantages like antibacterial properties have been introduced.²³²

New methodologies like anodic plasma oxidation have made possible the obtention of a structured layer of titanium oxide and the incorporation of inorganic components like Ca, Mg or phosphates which have been demonstrated that have a positive effect on bond formation.²³³ Studies show that the presence of fluoride on implant surfaces improve osteoblastic differentiation²³⁴ and bone implant contact.²³⁵

Recent research has focused on the immobilization of biological functional molecules, specially peptides that are relevant in adhesion and growth processes, on the surface of these devices. Integrins are membrane proteins that interact with components of the extracellular matrix (ECM) leading to the formation of specialized adhesive structures, called focal adhesions, where signal molecules concentrate. Thus, there is a clear relation between integrin-mediated adhesion and cellular processes such as proliferation and differentiation which are controlled by signal transduction pathways.²³⁶

Among the group of peptide motifs that interact specifically with integrins, RGD (Arginine-glycine-aspartic acid) motifs have been widely studied. Early studies in the 80s already showed the importance of this peptide sequence in cell adhesion processes.^{237,238} The use of the small peptide motif RGD has several advantages over the use of whole proteins of ECM like easier manipulation and higher stability and selectivity.

Mesenchymal stem cells (MSCs) are multipotent cells that have the capacity of differentiate into multiple cell types including osteoblasts,

chondrocytes and other connective tissue cells (Figure 110). Since the late 80s, when their isolation was optimized, their application in tissue engineering has been widely studied.^{239,240} For example, the evaluation of bone formation using hyaluronic acid-based hydrogel containing MSCs has shown promising results when compared with similar scaffolds without MSCs²⁴¹ and the role and potential application of MSCs in bone fracture repair process has raised a special interest.²⁴²

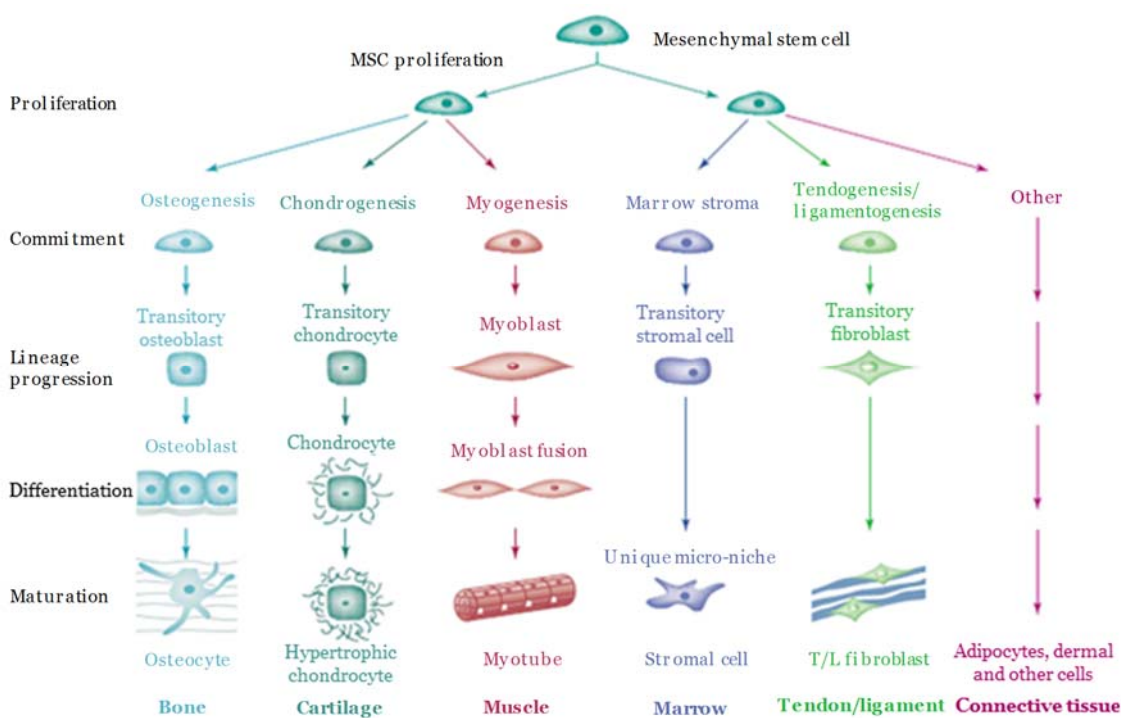


Figure 110. Differentiation of mesenchymal stem cells into different tissue cells.²³⁹ Reprinted with permission from Elsevier Science Ltd.

The peptide motif RGD can function as a promoter of MSCs adhesion and proliferation. Numerous studies have focused in the modification of implant surfaces with this motif in order to enhance osseointegration. The effects on MSCs attachment to HA disks of different concentrations of RGD have been studied.²⁴³ These studies demonstrate that higher concentrations of RGD stimulates attachment and spreading of MSCs and suggests potential applications in tissue regeneration. Numerous works have been published about the positive effects of RGD motifs on differentiation of MSCs when being part of different scaffolds such as PEG gels,²⁴⁴ poly(lactic-co-glycolic acid) (PLGA)

microspheres,²⁴⁵ polyurethanes-based materials²⁴⁶ or alginate-based porous materials.²⁴⁷ Recent work has demonstrated that the immobilization of RGD in titanium implants have shown promising results in bone formation and osseointegration.^{248,249}

Traditionally, the techniques used for the modification of biomaterial surfaces with RGD involved self assembled monolayers²⁵⁰ or the immobilization of RGD containing peptides on polymer surfaces.²⁵¹ The linking of such peptide to these surfaces can be achieved by adsorption or covalent methods, the latter being preferred since it provides more stable linkage and leads to better cell attachment. RGD motif has been linked to the surface through formation of amide bonds,²⁵² disulphide bonds²⁵³ or through thiol-containing RGD peptides that can be linked through Michael addition²⁵⁴ or react with maleimide functionalized surfaces.²⁵⁵

Recently, there has been an increasing interest on dendrimers as linkers between the biomaterial surfaces and biological active compounds. The possibility of modifying the nature and control the number of terminal groups of these dendritic molecules makes them a highly interesting tool. Previous studies have demonstrated that PAMAM dendrimer-RGD conjugates enhance delivery of drugs²⁵⁶ and can be used as delivery vectors.²⁵⁷

Our group has studied the effects of the orientation of the RGD motif presented by the dendrimer to the cell on the adhesion on MSCs to a polystyrene test surface. Two peptides containing the RGD motif (RGD-Cys and Cys-RGD) were attached to a maleimide-functionalized PAMAM dendrimer. The results confirm that orientation of the tripeptide influences cellular response, being RGD-Cys the optimal choice.¹²⁷ Additionally, our group reported the use of dendrimers as a powerful tool to tailor the local density of RGD and its effect on MSCs adhesion and early chondrogenic differentiation.^{128,258,259}

The objective of this work is to present a new bioactive surface based on the covalent immobilization of RGD modified dendrons on Ti substrates, using an organosilane as coupling agent to create a monolayer film. For that purpose, we have employed compound **12**, a dendron with a carboxylic acid as focal point and four terminal amino groups, that will make possible the immobilization of the tripeptide *via* thiol-maleimide *click* reaction. This dendron will provide an

excellent scaffold for bioactive molecules to be appropriately oriented and exposed to the media in the most efficacious arrangement for a specific and desired tissue response.

Titanium disks will be modified with 3-aminopropyltrimetoxysilane (APTMS) in order to provide the surface with amino groups that will react with the focal point of **12**. After the blockage of the free amino groups that hadn't react with **12**, deprotection of the terminal amino groups of the dendritic structure and their reaction with 3-(maleimido)propionic acid *N*-hydroxysuccinimide ester (**22**) will be carried out. The last step will involve the reaction between the maleimide group in the periphery of the dendron and the thiol group of RGD-Cys (Figure 111).

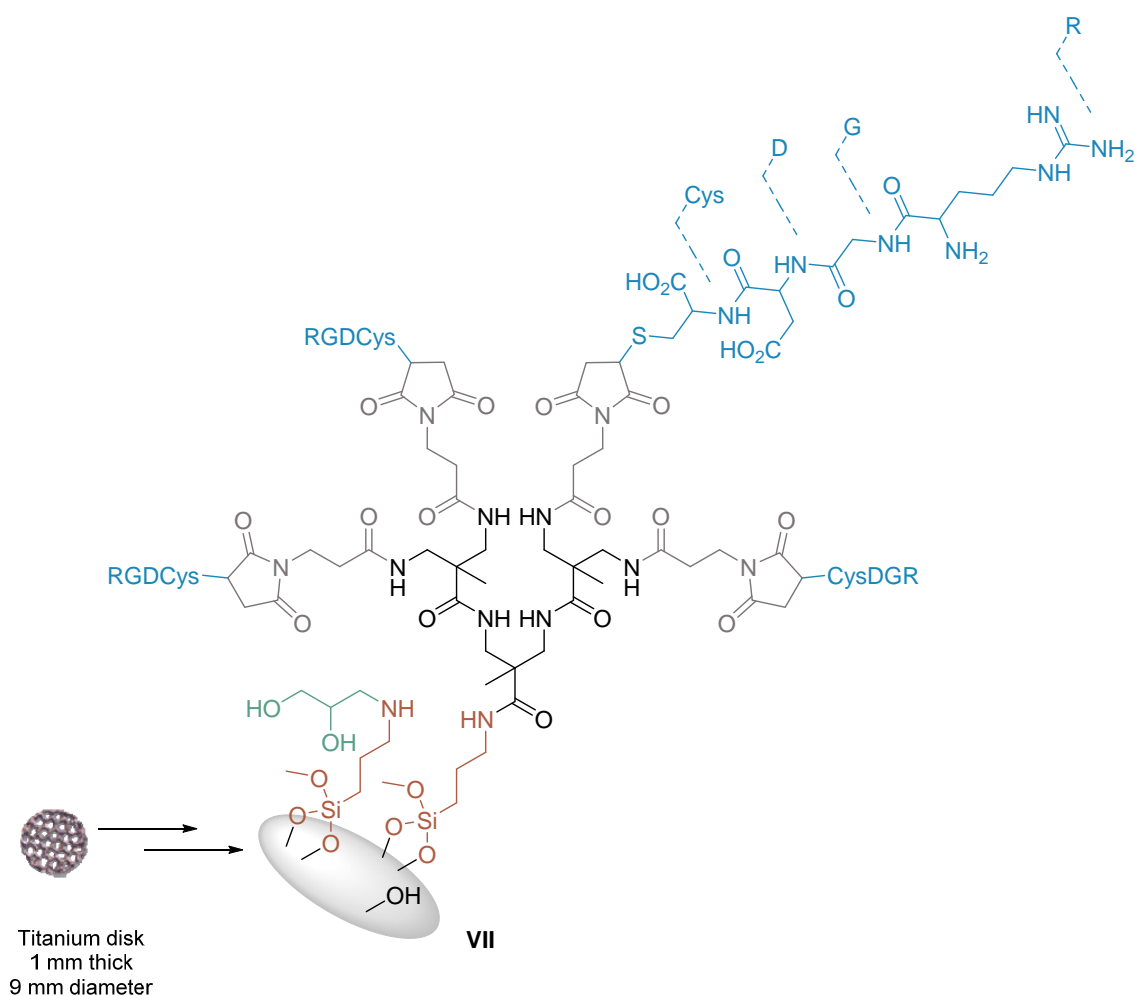


Figure 111. Covalent functionalization of titanium surfaces with RGD peptide.

V.2 Functionalization of the Titanium disks

Titanium disks (1 mm thick, 9 mm diameter) were provided by the group of Dr. Santos and Dr. Becerra from the Cellular Biology, Genetics and Physiology Department, University of Malaga. Initially, the titanium surfaces were treated with a mixture of sulfuric acid and hydrogen peroxide²⁶⁰ (Figure 112) in order to obtain a clean titanium oxide surface since normally the outer layer of titanium surfaces are composed of irregular oxide and can be impurified with other elements from the surroundings. This controlled oxidation provides a clean surface homogeneously covered by hydroxyl groups, which are indispensable for a chemical binding.

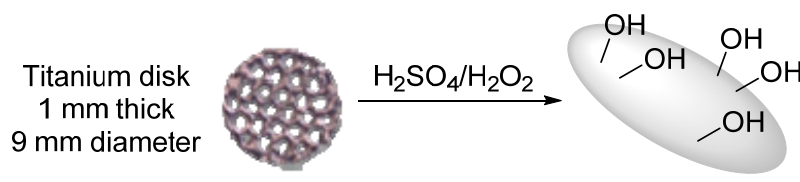


Figure 112. Oxidation treatment and representation of titanium disks.

Next, titanium disks were treated with a solution of APTMS in ethanol, so bonds are formed between silicon and the hydroxyl groups at the disk surface (**II**). The disks are thus functionalized with terminal amino groups that will react with the focal point of dendron **12** (Figure 113). Silanization is undoubtedly the most widely used approach to introduce organic functional groups on inorganic surfaces.²⁶¹ In fact, silane based strategies have been previously used to couple organic compounds to titanium implants.^{262,263}

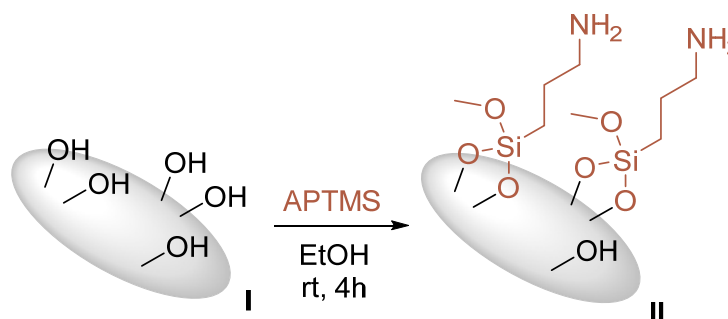


Figure 113. Synthesis of **II**.

Compound **12** was then covalently attached to the surface of the modified titanium disks (**II**). In order to form the amide bonds, the carboxylic acid group of dendron **12** was activated with CDI. The disks (**II**) were treated with a solution of the activated acid and after 16h, were washed with MeCN (Figure 114).

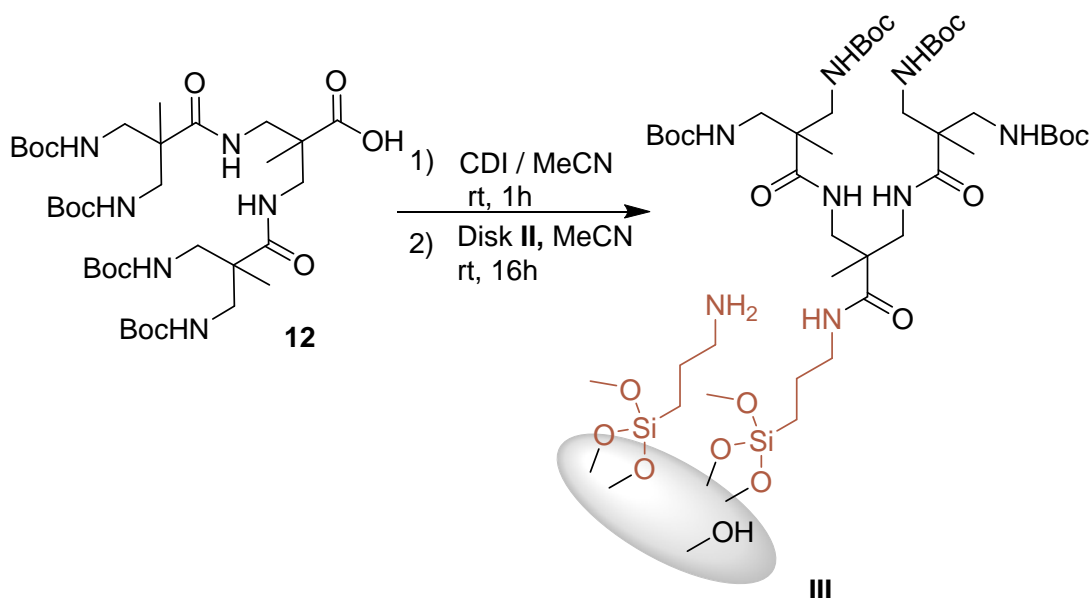


Figure 114. Synthesis of **III**.

These disks (**III**) were treated with glycidol in order to block the possible amino groups that hadn't reacted with **12**, obtaining disks **IV** (Figure 115). By blocking the free amino groups, side reaction are prevented and the surfaces are provided with a more neutral and hydrophilic character.²⁶⁴

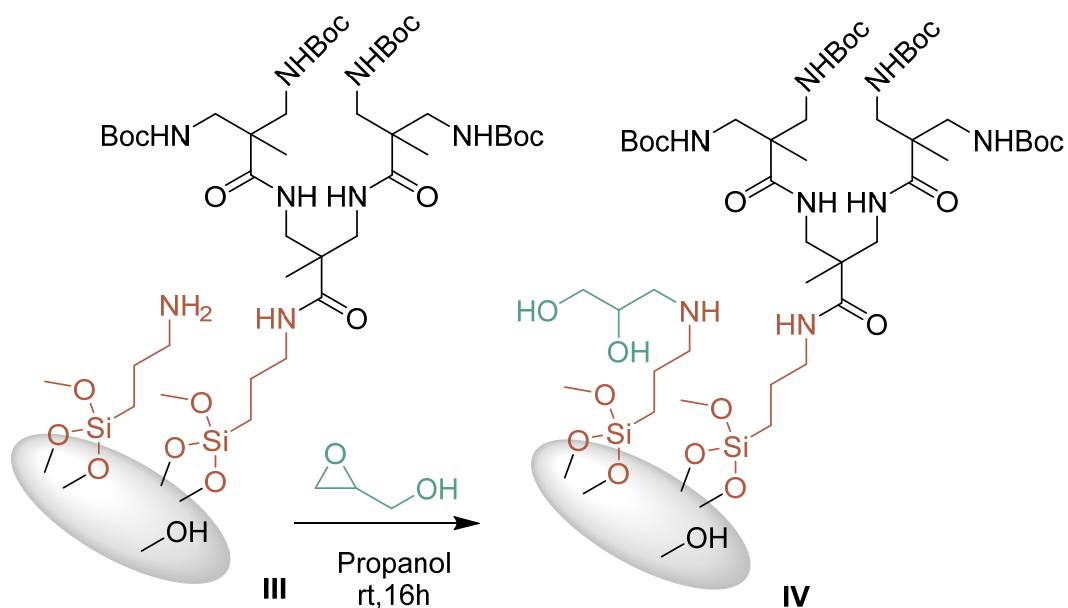


Figure 115. Synthesis of IV.

The final step was the deprotection of the amino groups of the dendron (V) in the presence of hydrochloric acid (Figure 116).

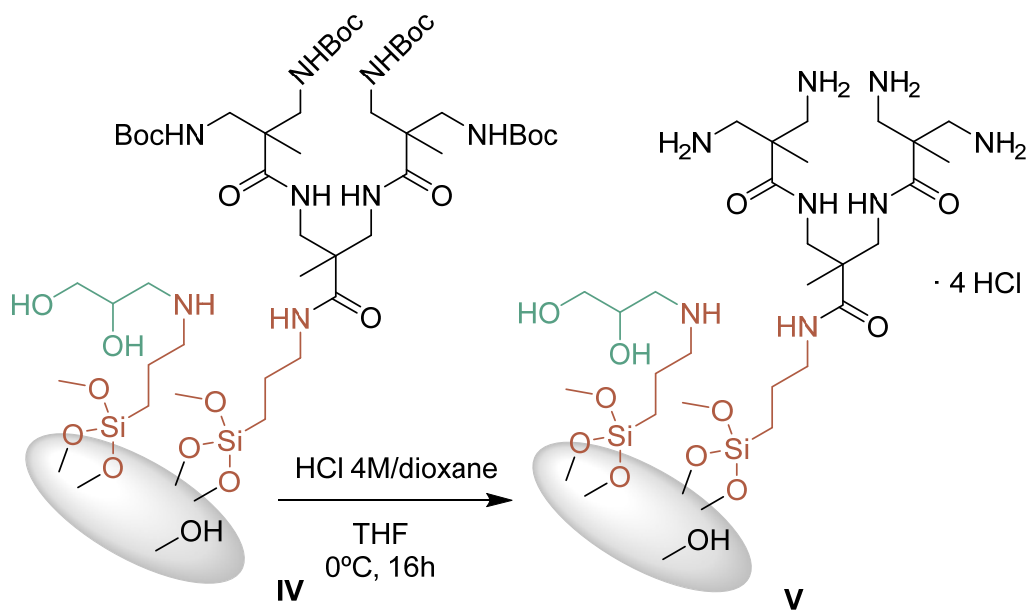


Figure 116. Synthesis of V.

V.3 Functionalization of the titanium disks with the cell recognition pattern RGD

The introduction of the RGD-Cys peptide was carried out using the terminal thiol group of the cysteine moiety. For that purpose, the amino groups of the dendrons coupled with the disks needed to be functionalized with a maleimide group. Michael's reaction is a nucleophilic addition of a nucleophile, or Michael donor, to an α,β -unsaturated carbonyl compound, or Michael acceptor. The maleimide group is a perfect Michael acceptor which can react with a variety of nucleophiles. In this particular case, the nucleophile is the terminal thiol group of the RGD-Cys tetrapeptide.

According to our research group experience,^{127,128} we chose to use a β -alanine derivative²⁶⁵ (**22**) which includes an ethylene spacer group and a carboxylic acid that will react with the amino terminal groups of the dendron. β -alanine was added to a solution of maleic anhydride in DMF and the mixture was left stirring at room temperature for two hours. Afterwards, it was introduced in an ice-cooled bath. NHS and DCC were added and the mixture was left stirring at room temperature for 16 hours (Figure 117). Urea by-product was removed by filtration. The product was obtained as a colorless solid (53% yield) after precipitation with cold water.

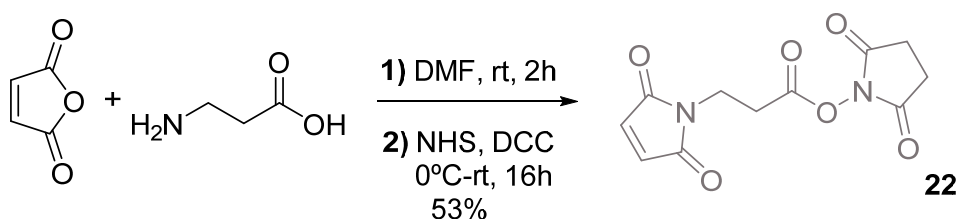


Figure 117. Synthesis of compound **22**.

The disks **V** were immersed in a solution of **22** and DIPEA in DMF and left in an orbital agitator for 16 hours. Finally, the Michael addition was carried out under argon atmosphere. A solution of RGD-Cys in PBS was added to the disks, **VI**, and were placed in an orbital agitator for two days (Figure 118).

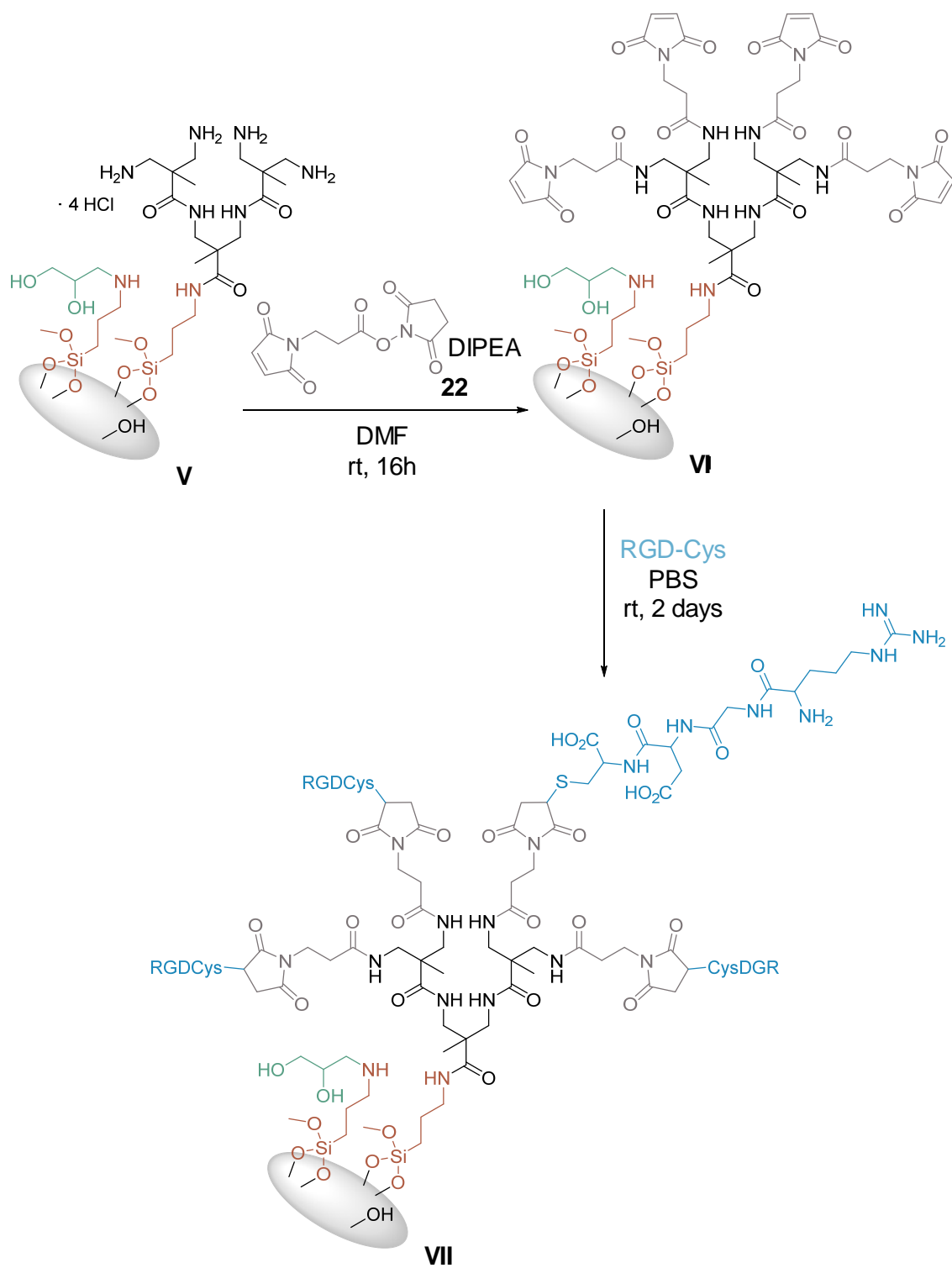


Figure 118. Synthesis of VII.

V.4. Monitorization of the derivatization process

The functionalization process has been followed *via* the ninhydrin test (since the derivatization alters the amount of free amino groups) and XPS measurements.

The number of amino groups introduced in the disk surface during each functionalization step can be estimated by running the ninhydrin test based on the reaction of free primary amino groups with ninhydrin to form Ruhemann's purple complex.¹²⁴ According to this test, the results are represented in Table 11.

Ti-disk	II	III	IV	V	VI
free NH ₂ ^a	+	-	-	+	-

Table 11. Amino groups present in Ti disk. a = Measurements were carried out in duplicate with half-disc.

We consider a positive value if absorbance is above 0.015 and a negative value if absorbance is below 0.007.

The introduction of amino groups when treating disks **I** with APTMS is confirmed by increase in the signal of the amino groups obtained in the test. The coupling of dendron **12** to the surface of the disks (**III**) is corroborated by the disappearance of a considerable number of amino groups. In contrast, the positive results for the tests performed on disks **V** confirms the deprotection reaction. Finally, the ninhydrin test results show that the number of free amino groups becomes almost insignificant when the maleimide is attached to the dendritic structure (**VI**).

Moreover, successful immobilization of the peptide on the titanium surface was corroborated by XPS. Chemical compositions of end-functionalized peptide and unmodified titanium surfaces are summarized in Table 12. As expected, the XPS-determined elemental composition of the **VI** titanium surface showed the presence of titanium, oxygen, nitrogen and carbon components. After

peptide functionalization (**VII**) the presence of sulfur was observed, which are consistent with the immobilization of the peptide on the surface.

Sample	Atomic concentration (at. %)					
	C 1s	O 1s	Ti 2p	N 1s	Si 2p	S 2p
VI	38.3	32.0	12.9	10.6	6.1	—
VII	29.2	37.7	13.5	8.2	7.2	4.2

Table 12. XPS results for samples **VI** and **VII**.

The C1s spectra of disks **VI** and **VII** show how the concentration of sp^2 carbon decreases when RGD-Cys is coupled to the maleimide group present in the dendritic structure (Figure 119), which is consistent with the reaction between the maleimide and the thiol group.

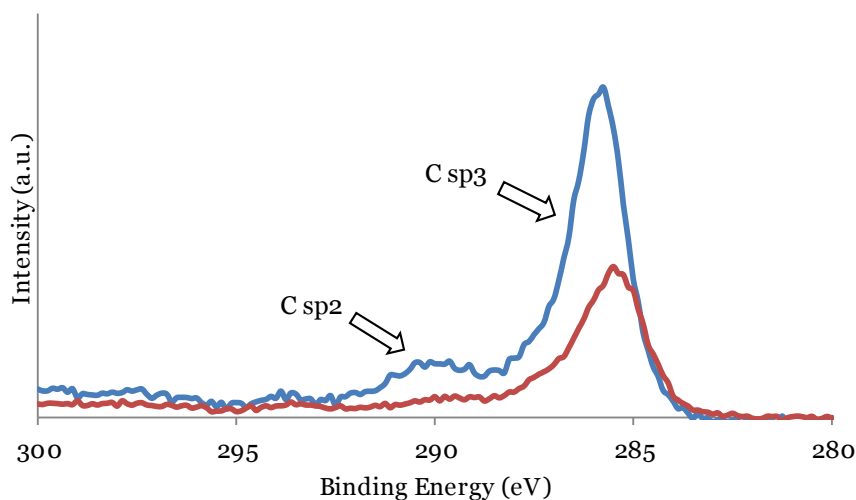


Figure 119. Carbon hybridization analysis by XPS of **VI** (blue line) and **VII** (red line).

The results from the ninhydrin tests as well as XPS studies confirm that the disks have been successfully functionalized with the RGD motif.

V.5 Assays of RGD-functionalized titanium surfaces with pre-osteoblastic cells

These assays were carried out in collaboration with the research group of Dr J. Becerra and Dr. Santos from the Cellular Biology, Genetics and Physiology Department, University of Malaga. In them, a number of around 50.000 cells were incubated in the presence of the titanium surfaces. Two different conditions were tested, a normal serum concentration (10%) and low serum concentration (2%). Moreover, a set of control cells were incubated in the same conditions but with **VI** titanium surfaces as controls.

Two parameters were studied in the assays: cell adhesion and proliferation. When studying cell adhesion (Figure 120), no major differences were appreciated between the functionalized disks and the controls. In both cases, better adhesion results were obtained when the concentration of serum was higher and in the rough side of the disks.

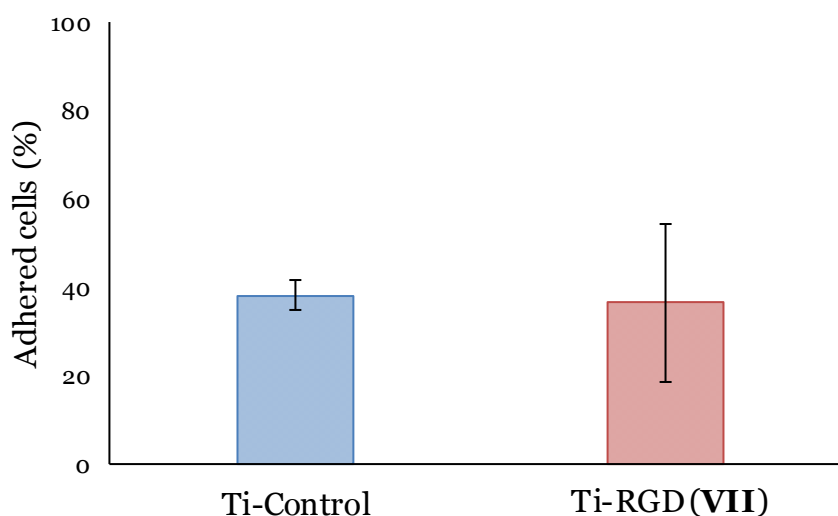


Figure 120. Cell adhesion studies with human fetal osteoblasts (5000 cells/disk) and a normal concentration of serum (10%) of Titanium control disks (**VI**) (blue) and **VII** (red).

In cell proliferation studies (Figure 121), however, a better effect of the dendron could be seen at long-term. It seems that although cell adhesion is not affected, proliferation improves. The plateau seen in the proliferation graphic in the case of the cells studied with **VII** points to the formation of tissue along the titanium surface, making a more favorable interphase.

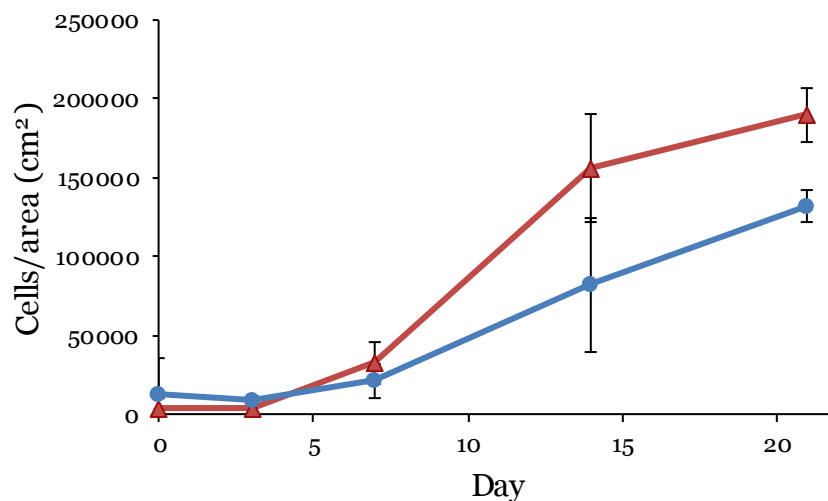


Figure 121. Cell proliferation studies with human fetal osteoblasts (5000 cells/disk) and a normal concentration of serum (10%) of Titanium control disks (VI) (blue) and VII (red).

Titanium surfaces have been successfully modified with RGD motif. A dendron has been synthesized to link covalently the peptide to the surfaces. The correct immobilization has been confirmed by ninhydrin test during the different functionalization steps and by the XPS results in the final step, which show the presence of sulfur, inexistent in the control disks, due to the presence of the peptide.

CHAPTER VI

CONCLUSIONS

1.- A new convergent synthetic route has been successfully developed using the orthogonal reactivity of *click* chemistry and peptide synthesis, especially protection/deprotection strategies of amino and carboxylic acid groups. Following this methodology, a family of dendrons and dendrimers can be successfully synthesized. The size and number of terminal groups in the final dendrimeric structures can be easily tailored in one step by means of choosing the proper dendron generation and multifunctional core. All compounds can be properly characterized using NMR techniques, mass spectroscopy and IR spectroscopy. Furthermore, a synthesis of a water-soluble fluorescent dendrimer with potential applications in bioimaging using both OPE and TPE conditions can be carried out.

2.- The synthesis of a dendritic water-soluble Pt(II) complex can be carried out. The resulting structure combines characteristics that makes it a unique luminescent probe in aqueous media. A complete characterization of the intermediate compounds can be carried out using NMR techniques, mass spectroscopy and IR spectroscopy. The photophysical properties of the final compound in aqueous solutions as well as its stability have been studied. The

studies of labelled bacteria using OPE and TPE conditions demonstrate its potential application in bioimaging. Additionally, the array has proven to be traceable by electron microscopy and acting as a probe providing dual orthogonal readouts.

3.- Titanium surfaces can be successfully modified with RGD motif. A new BAPAD dendron has been synthesized to link covalently the peptide to the surfaces. The correct immobilization has been confirmed by ninhydrin test during the different functionalization steps and by the XPS results in the final step, which show the presence of sulfur, inexistent in the control disks, due to the presence of the peptide.

CHAPTER VII

EXPERIMENTAL SECTION

VII.1 Reagents, solvents and analytical techniques

Chemicals were purchased from Sigma-Aldrich, Merck or Alfa Aesar and used without further purification unless otherwise indicated. Solvents were purchased from VWR and Panreac. H₂O was purified with a Mili-Q purification system from Millipore.

Unless otherwise stated, all reactions were performed in air. All reactions that needed dry conditions were carried out using standard techniques under an inert atmosphere of oxygen-free Argon or Nitrogen, unless otherwise stated.

TLC were performed using pre-coated aluminum chromate-plates Silica Gel 60 F254 Merck of 0.25 mm thick. Compounds were visualized by using UV light (254 nm) or stains to visualize the product using solutions of 0.04 % bromocresol green in ethaol, 1.5 % ninhydrin in ethanol, or a basic solution (20% w/w K₂CO₃ in water) of KMnO₄.

Purification by column chromatography were performed using Silica Gel 60 (particle size 0.040-0.063 mm), from Merck. Purifications by Size-Exclusion Chromatography have been carried out in Sephadex™ G-10 pre-packed columns (GE Healthcare Life Science), eluting by gravity.

^1H and ^{13}C NMR spectra were measured in the indicated deuterated solvent at 25°C on a Bruker Ascend 400 MHz spectrometer. Proton chemical shifts (δ) are reported with the solvent resonance peak employed as the internal standard (CDCl_3 δ 7.26, $\text{DMSO-}d_6$ δ 2.50, D_2O δ 4.79, $\text{MeOD-}d_4$ δ 3.31). Data are reported as follows: chemical shift, multiplicity, coupling constants (Hz) and integration. Carbon chemical shifts are reported in ppm with the solvent resonance as the internal standard (CDCl_3 δ 77.16, $\text{DMSO-}d_6$ δ 39.52, $\text{MeOD-}d_4$ δ 49.00). These abbreviations were used to indicate the multiplicities: s = singlet, d = doublet, t = triplet, q = quartet, dd = doublet of doublets, m = multiplet. These experiments were performed in the Andalusian Center for Nanomedicine and Biotechnology (BIONAND).

DOSY experiments were performed in BIONAND. The samples were prepared in deuterium oxide at a concentration between 0.5 and 2 mM (within the infinite dilution range for similar samples at 0.1–2.1 mM).¹⁵⁵ The experiments have been performed on a The Bruker Ascend™ 400 MHz spectrometer, equipped with a 5 mm BBFO^{PLUS} probe with ^2H “lock” channel and Z gradient. The spectrometer is also equipped with a control temperature unit prepared to work at temperatures ranging from 0 °C to +50 °C. Gradient strength was calibrated by measuring the diffusion rate of pure water of residual protons in D_2O . All experiments were conducted at 300 K. The samples were allowed to equilibrate for no fewer than 15 min. To determine the diffusion rates, a 2D sequence using double stimulated echo for convection compensation and LED using bipolar gradient pulses for diffusion was used. The Diffusion coefficients (D) were determined from the slope of the Stejskal-Tanner plot, which relates it to the signal intensity through the equation: $\ln(\frac{I}{I_0}) = -\gamma^2 \delta^2 G^2 (\Delta - \frac{\delta}{3}) D$, where I is the integral of the peak area at a given value of G, I_0 is the integral of the peak area at a G=0, G is the gradient field strength, γ is the gyromagnetic ratio, δ is the gradient duration and Δ is the time between the gradient pulses.¹⁵⁴ The diffusion coefficients determined were used to calculate the hydrodynamic radius via the Stokes-Einstein equation: $R_H = K_B T / 6\pi\eta D$, where K_B is the Boltzmann constant, T is the temperature and η is the viscosity of the solvent (1.0963 cP for D_2O viscosity).¹⁵⁵

The HRMS (Electrospray Ionization Time of Flight, ESI-TOF) mass spectra (MS) were performed on a High Resolution Mass Spectrometer Orbitrap, Q-Exactive (Thermo Fisher Scientific, Waltham, MA, USA), in either positive or negative ion mode. The experiments were carried out in Servicios Centrales de Investigación, University of Malaga.

Infrared (IR) spectra were recorded using a Jasco FT/IR-4100 spectrophotometer at ambient temperature in BIONAND.

XPS data was obtained from a Multilab System 2000 (Thermo Fisher) in Servicios Centrales de Investigación, University of Malaga.

Hydrogenation reactions were carried out under hydrogen atmosphere (50 bar) using a Mini-Reactor from Erie-Autoclave Engineers in BIONAND.

Luminescence measurements were performed in Servicios Centrales de Investigación, University of Malaga or Muenster, using an Edinburgh Instruments FLS920 spectrometer equipped with a 450W Xenon lamp (Xe900) as continuous excitation source for stationary state measurements and Picoquant PLS-450 and PLS-500 pulsed LED diodes as pulsed excitation source for time-resolved measurements. Phosphorescence measurements were performed using a detector system with a R928P photomultiplier-based delay generator. Lifetime analysis was also performed using the commercial FluoFit software. The quality of the fit was assessed by minimizing the reduced chi squared function (χ^2) and visual inspection of the weighted residuals and their autocorrelation. Luminescence lifetimes were also recorded in TCSPC mode by a PicoHarp 300 (minimum base resolution 4 ps) on a FluoTime300 spectrometer from PicoQuant equipped with a 300 W ozone-free Xe lamp (250-900nm), a 10 W Xe flash-lamp (250-900 nm, pulse width < 10 μ s) with repetition rates of 0.1 – 300 Hz, an excitation mono-chromator (Czerny-Turner 2.7 nm/mm dispersion, 1200 grooves/mm, blazed at 300 nm), diode lasers (pulse width < 80 ps) operated by a computer-controlled laser driver PDL-820 (repetition rate up to 80 MHz, burst mode for slow and weak decays), two emission mono-chromators (Czerny-Turner, selectable gratings blazed at 500 nm with 2.7 nm/mm dispersion and 1200 grooves/mm, or blazed at 1250 nm with 5.4 nm/mm dispersion and 600 grooves/mm), Glan-Thompson polarizers for excitation (Xe-lamps) and emission, a Peltier-thermostated sample holder from Quantum Northwest (-

40°C – 105°C), and two detectors, namely a PMA Hy-brid 40 (transit time spread FWHM < 120 ps, 300 – 720 nm) and a R5509-42 NIR-photomultiplier tube (transit time spread FWHM 1.5 ns, 300-1400 nm) with external cooling (-80°C) from Hamamatsu. UV-Visible absorption spectra were performed on a Cary 100 Bio UV-Visible Spectrophotometer in BIONAND.

Two Photon Excitation experiments were carried out in BIONAND. Excitation and emission scans were performed using a Leica SP5 MP confocal microscope equipped with Spectraphysics MaiTai HP pulse IR laser for multiphoton excitation and a HCX PL APO lambda blue 63x NA 1.40 oil immersion objective lens. For excitations scans, fluorescence was measured using an internal PMT detector with excitation varying from 700 nm to 1040 nm at 10 nm intervals. For emission scans, samples were excited and emissions measured using internal spectral PMT detectors as a 30 nm window moving from 400 to 700 nm in 15 nm intervals (20 measurements). TPA cross-sections were determined by the TPEF method.²¹⁶ It is assumed that the quantum efficiencies after two-photon excitation are the same as those after one-photon excitation. The TPA cross-sections (δ) were obtained by calibration against Rodamine B with a known δ value in MeOH solution. Then, the TPA cross-section δ values were calculated on the basis of the following expression: $\delta_S = \delta_R \frac{C_R \eta_R \phi_R F_S}{C_S \eta_S \phi_S F_R}$ where δ is the TPA cross-section, C and η are the concentration and refractive index of the sample solution, and F is the integrated area under the TPEF spectrum.

Luminescent Microscopy experiments with *E. coli* (Gram-negative) and *P. subtilis* (Gram-positive) bacteria were carried out in BIONAND. Both bacteria (*E. coli* and *P. subtilis*) were grown in 10 mL of LB Broth at 37°C in a rocking incubator (18 hours). Then, culture contents were split into four 15 mL vials, centrifuged (5000g, 5 minutes), and washed again in 5 mL PBS. After an additional centrifugation (5000g, 5 minutes), bacterial pellets were either resuspended in 3 mL PBS with the desired compound (10⁻⁴ M dilution) or resuspended in 3 mL PBS alone. A 2 h incubation step in a rocking incubator followed (37°C). Then, both samples were centrifuged (5000g, 5 minutes) and washed twice in 3 mL PBS. Finally, each bacterial sample was resuspended in 100

μL PBS. Bacterial cultures were analyzed using a Leica SP5 MP confocal microscope equipped with Spectraphysics MaiTai HP pulse IR laser for multiphoton excitation and a HCX PL APO lambda blue 63x NA 1.40 oil immersion objective lens was used. Brightfield and confocal images were acquired using 405 nm excitation with emissions detected with a spectral PMT detector set to 500-600 nm. Multiphoton images were acquired sequentially with excitation at 720 nm and detection between 500-550 nm with an external HyD non-descanned detector.

Bactericidal tests were carried out in the Microbiology Department, University of Malaga. To examine the bactericidal effect of the compounds on Gram-negative and Gram-positive bacteria, approximately $4 \cdot 10^6$ colony-forming units (CFU) of *E. coli* and *P. subtilis* were cultured on LB agar plates supplemented with 10 or 100 μM the desired compound. Compound free LB plates cultured under the same conditions were used as controls. The plates were incubated for 24 h at 37°C and the number of colonies was recorded. Counts on the three plates corresponding to a particular sample were averaged. To examine the bacterial growth rate as well as to determine the growth curve in the presence of the compound, *E. coli* and *P. subtilis* were grown in liquid LB medium supplemented with 10 or 100 μM. Growth rates and bacterial concentrations were determined by measuring optical density (OD) at 600 nm each 1 hour (OD of 0.1 corresponds to a concentration of 10^8 cells per cm³) in a FLUOstar Omega de BMG Labtech device.

Transmission Electron Microscopy (TEM) experiments were performed in BIONAND. TEM and EDXs measurements of bacteria were performed using a Thermo Fisher Tecnai G2 20 Twin microscope. For TEM measurements, a drop of a solution of bacteria in PBS was placed in a copper grid covered with a Formvar-Carbon film and was left to dry for 16 hours. No contrast agent was used for these samples. The voltage used was 120 Kv and the beam of electrons was between 6.94 and 8.80 uA. The exposure time for the images captions was of 1 second. In order to obtain EDX data, a magnification between 200 and 240 kX was used, focusing the beam on the center of the bacteria. The spectrum measurement was carried out in a way so death time (waiting time for the

acquisition between counts) was around 10-15%, with a total counting duration of 50 seconds.

VII.2 General Procedures

VII.2.1 General procedure for click reactions

Azido-compound (1 eq), alkyne (1.1 eq per azido group), copper (II) sulphate 5-hydrate (0.01 eq per azido group) and L (+)-ascorbic acid Sodium salt (0.1 eq per azido group) were dissolved in a tert-butanol/water 1:2 mixture. The mixture was stirred at room temperature for one week. Afterwards, the solvent was removed using rotatory evaporation. NH_3 aq. (50 mL) and dichloromethane (50 mL) were added and the phases were separated. The aqueous phase was extracted with CH_2Cl_2 (3×30 mL). The combined organic layers were washed with NH_3 aq./Brine 1:1 (3×80 mL). The organic layer was dried over MgSO_4 anh. and the solvent was removed by rotary evaporation. The product was purified by precipitation in n-hexane.

VII.2.2 General procedure for deprotection of amines

The compounds were dissolved in THF (10 mL) and the solution was cooled in an ice-water bath. HCl 4M in dioxane (10 mL) was added dropwise and the mixture was stirred overnight. Afterwards, the solvent was evaporated under vacuum. The compounds were purified by sephadex column.

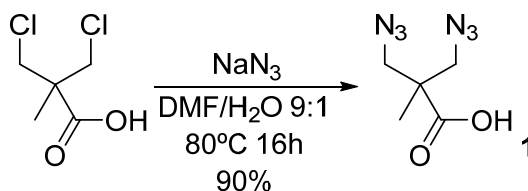
VII.2.3 Quantitation of Free Primary Amine Groups (Ninhydrin Test)

Ninhydrine test was performed following a previously described procedure.¹²⁴ The amine test solution consisted of ninhydrin (100 mg) dissolved in 95% EtOH (10 mL). The amine test was previously applied to 10 μL of a 2mM solution of butylamine in water, as a standard solution. The absorbance of the Ruhemann's purple complex at 576 nm in EtOH was measured: Abs (576 nm) =

0.264; $\epsilon = 26416 \text{ M}^{-1} \text{ cm}^{-1}$. Then, half a disk of functionalized titanium was suspended in a 2 mL aliquot of the ninhydrin test solution in a test tube and heated under reflux for 45 min, the resulting suspension then being allowed to cool. Next, the reaction volume was made to 5 mL with 95% EtOH and the solution absorption was measured at 570 nm, with the number of amine groups present per disk of titanium being calculated from ϵ .

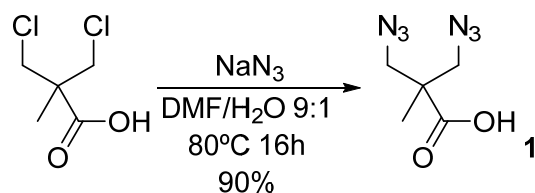
VII.3 Synthesis of new dendritic structures *via click chemistry*

Synthesis of 3,3'-diazidopivalic acid (**1**)



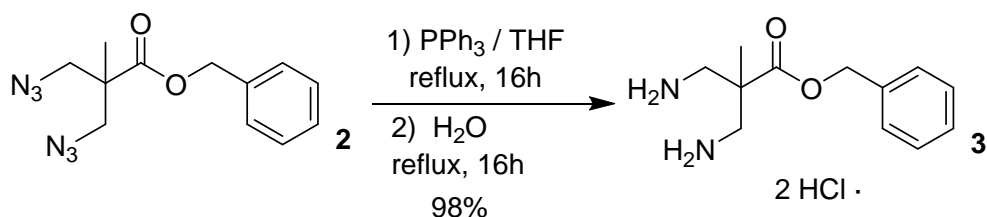
Sodium azide (7.50 g, 115 mmol, 4 eq) was added to a solution of 3,3'-dichloropivalic acid (5.00 g, 29 mmol, 1 eq) in DMF/ H_2O 9:1 (20 mL). The resulting solution was heated in a heat block at 80°C for 16 hours. The solvent was removed under vacuum and ethyl acetate (50 mL) was added to promote the precipitation of the remaining sodium azide. Then the mixture was filtered, and the solvent was removed under vacuum to obtain the product (4.80 g, 26.1 mmol, 90%) as a colorless oil. **^1H NMR** (400 MHz, CDCl_3) δ ppm: 3.63 (d, $J = 12.3$ Hz, 2 H, $\text{CH}_2\text{-N}_3$), 3.52 (d, $J = 12.3$ Hz, 2 H, $\text{CH}_2\text{-N}_3$), 1.27 (s, 3 H, CH_3). **^{13}C NMR** (100 MHz, CDCl_3) δ : 179.8 (CO), 54.6 ($\text{CH}_2\text{-N}_3$), 47.6 (C), 19.4 (CH_3). **HRMS** calcd. for $\text{C}_5\text{H}_7\text{N}_6\text{O}_2^-$ 183.0625 [$\text{M} - \text{H}$] $^-$, found 183.0626.

Synthesis of Benzyl-3,3'-diazidopivaloate (**2**)



To solution of **1** (5.00 g, 27 mmol, 1 eq) in DMF (20 mL) was added sodium carbonate (4.29 g, 40.5 mmol, 1.5 eq) and benzyl bromide (4.8 mL, 40.5 mmol, 1.5 eq). The mixture was stirred for 16 hours at room temperature. Then, hexane (100 mL) and water (50 mL) were added and the phases were separated. The organic layer was washed with water (3× 50mL), dried over MgSO_4 and the solvent was removed under vacuum. Purification was performed by silica gel column chromatography (hexane/ethyl acetate, 9:1 v/v) to obtain the product (6.67 g, 24.3 mmol, 90%) as a colorless oil. **^1H NMR** (400 MHz, CDCl_3) δ : 7.42 – 7.32 (m, 5 H, BnCH), 5.19 (s, 2 H, BnCH_2), 3.63 (d, $J = 12.2$ Hz, 2 H, $\text{CH}_2\text{-N}_3$), 3.52 (d, $J = 12.2$ Hz, 2 H, $\text{CH}_2\text{-N}_3$) 1.24 (s, 3 H, CH_3). **^{13}C NMR** (100 MHz, CDCl_3) δ : 173.1 (CO), 135.4 (Bnc), 128.8 (BnCH), 128.6 (BnCH), 128.3 (BnCH), 67.3 (BnCH_2), 54.9 ($\text{CH}_2\text{-N}_3$), 47.8 (C), 19.4 (CH_3). **HRMS** calcd. for $\text{C}_{12}\text{H}_{14}\text{N}_6\text{O}_2\text{Na}^+$ 297.1070 $[\text{M} + \text{Na}]^+$, found 297.1072.

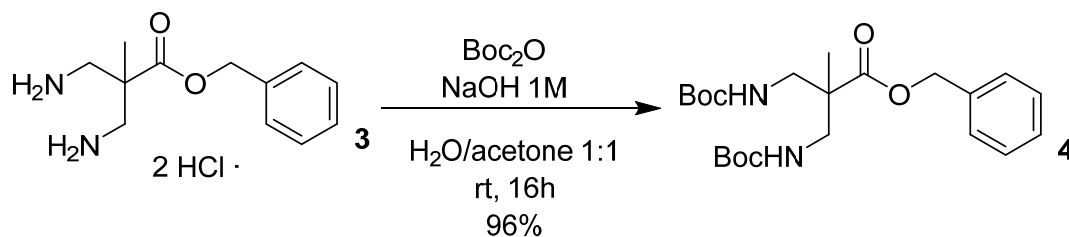
Synthesis of Benzyl-3,3'-diaminopivaloate (**3**)



Compound **2** (2 g, 7.30 mmol, 1eq) was dissolved in THF (20 mL) and placed in an ice bath. Triphenylphosphine (10.20 g, 38.69 mmol, 5.3 eq) was dissolved in THF (10 mL) and added dropwise to the previous solution. The mixture was left under reflux in a heat block for 16 hours. Afterwards, 1.5 mL of water were added, and the reaction was left under reflux for another day. Then, THF was removed under vacuum and the product was dissolved in HCl 1M (10 mL). The aqueous phase was washed with dichloromethane (5×30 mL). The aqueous layer was later removed under vacuum to obtain the desired compound (2.11 g, 7.15 mmol, 98%) as a colorless solid; **mp** 160–162 °C. **^1H NMR** (400 MHz,

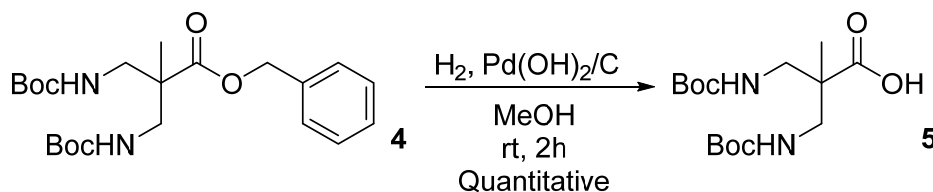
D₂O) δ : 7.56 - 7.43 (m, 5 H, BnCH), 5.35 (s, 2 H, BnCH₂), 3.45 (d, J = 13.7 Hz, 2 H, CH₂-NH₂), 3.29 (d, J = 13.7 Hz, 2 H, CH₂-NH₂), 1.49 (s, 3 H, CH₃). ¹³C NMR (100 MHz, MeOD-d₄) δ : 173.2 (CO), 136.3 (BnC), 129.63 (BnCH), 129.61 (BnCH), 129.59 (BnCH), 69.4 (BnCH₂), 45.0 (C), 44.34 (CH₂-NH₂), 19.4 (CH₃). HRMS calcd. for C₁₂H₁₉N₂O₂⁺ 223.1441 [M + H]⁺, found 223.1441.

Synthesis of Benzyl-3,3'-bis(*tert*-butoxycarbonyl)aminopivaloate (4)



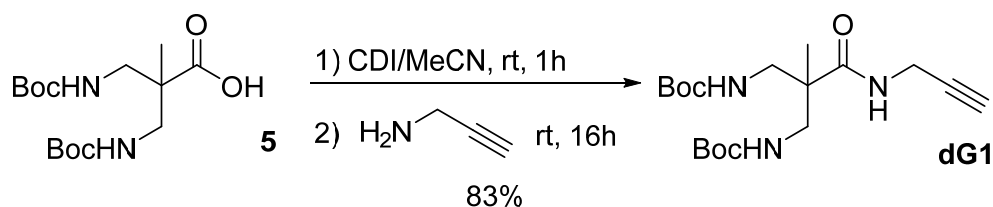
To an ice-cooled solution of **3** (2.07 g, 7.00 mmol, 1 eq) in H₂O/acetone 1:1 (20 mL), NaOH 1M was added dropwise until pH > 10 was achieved. Di-*tert*-butyl dicarbonate (3.05 g, 15.40 mmol, 2 eq) was then added and the reaction was stirred for 16 hours at room temperature. The product was extracted using dichloromethane (5 × 30 mL). The organic phase was dried with MgSO₄ and the solvent was removed under vacuum to obtain the product (2.84 g, 6.72 mmol, 96%) as a colorless oil. ¹H NMR (400 MHz, CDCl₃) δ : 7.39-7.30 (m, 5 H, BnCH), 5.14 (s, 2 H, BnCH₂), 3.48 (dd, J = 14.4, 8.6 Hz, 2 H, CH₂-NHBoc), 3.12 (dd, J = 14.4, 5.2 Hz, 2 H, CH₂-NHBoc), 1.43 (s, 18 H, BocCH₃), 1.14 (s, 3 H, CH₃). ¹³C NMR (100 MHz, CDCl₃) δ : 175.2 (CO), 156.7 (BocCO), 135.8 (BnC), 128.7 (BnCH), 128.4 (BnCH), 128.0 (BnCH), 79.4 (BocC), 66.7 (BnCH₂), 48.9 (CH₂-NHBoc), 43.5 (C), 28.4 (BocCH₃), 19.0 (CH₃). HRMS calcd. for C₂₂H₃₄N₂O₆Na⁺ 445.2309 [M + Na]⁺, found 445.2309.

Synthesis of 3,3'-bis(*tert*-butoxycarbonyl)aminopivalic acid (5)

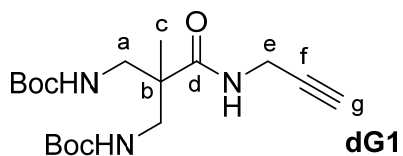


To a solution of **4** (400 mg, 0.95 mmol, 1eq) in methanol (10 mL), Pearlman's catalyst (100 mg, 0.71 mmol, 0.7eq) is added. After hydrogenation for two hours, the catalyst was removed by filtration through MeOH-pre-wetted Celite. The solvent was removed under vacuum to obtain the desired compound (309 mg, 0.93 mmol, 98%) as a colorless oil. **¹H NMR** (400 MHz, MeOD-*d*₄) δ : 3.25 (d, J = 14.2 Hz, 2 H, CH₂), 3.17 (d, J = 14.2 Hz, 2 H, CH₂), 1.43 (s, 18 H, BocCH₃) 1.07 (s, 3 H, CH₃). **¹³C NMR** (100 MHz, DMSO-*d*₆) δ : 180.0 (CO), 158.7 (BocCO), 80.2 (BocC), 46.7 (C), 45.5 (CH₂), 28.7 (BocCH₃), 19.6 (CH₃). **HRMS** calcd. for C₁₅H₂₈N₂O₆Na⁺ 355.1840 [M + Na]⁺, found 355.1838.

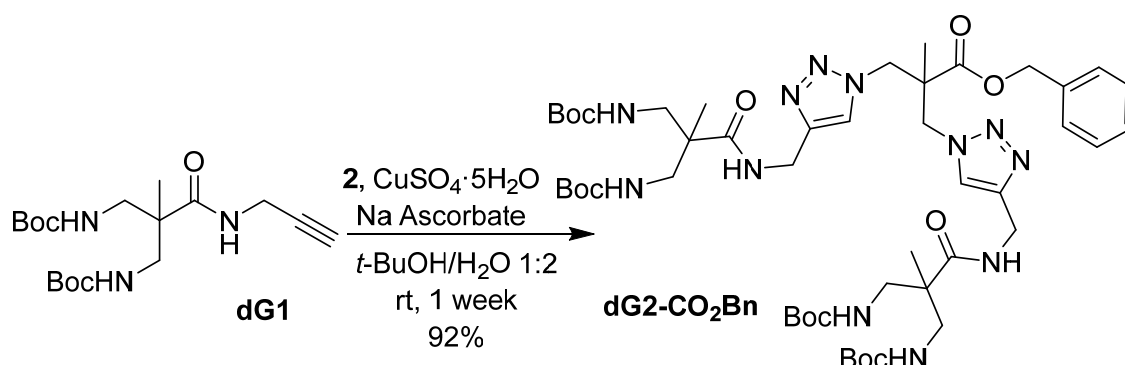
Synthesis of dG1



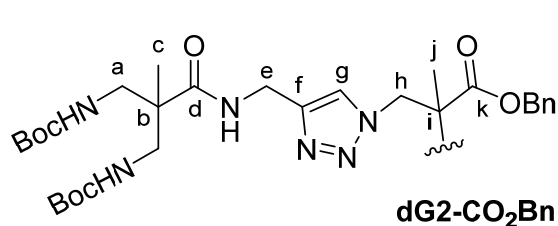
A solution of **5** (1.70 g, 5.11 mmol, 1 eq) in anhydrous acetonitrile (5 mL) was added to a solution of 1,1'-carbonyldiimidazole (CDI) (1.3 g, 7.66 mmol, 1.5 eq) in anhydrous acetonitrile (15 mL) and the mixture was stirred at room temperature for one hour. Afterwards, propargylamine (0.7 mL, 10.22 mmol, 2 eq) was added and the stirring mixture was left for 16 hours at room temperature. The solvent was removed under vacuum. The residue was dissolved in dichloromethane (50 mL) and washed with HCl 0.05M (3 × 50 mL). The combined organic phase was dried with MgSO₄, filtered and concentrated under reduced pressure to obtain the product (1.57 g, 4.24 mmol, 83 %) as a colorless solid; **mp** 70–71 °C. **¹H NMR** (400 MHz, DMSO-*d*₆) δ ppm: 3.80 (dd, J = 4.8, 2.1 Hz, 2 H, H_e), 3.14–3.01 (m, 5 H, H_a, H_g), 1.37 (s, 18 H, BocCH₃), 0.95 (s, 3 H, H_c). **¹³C NMR** (100 MHz, DMSO-*d*₆) δ ppm: 173.9 (C_d), 156.1 (BocCO), 81.3 (BocC), 78.0 (C_f), 72.7 (C_g), 47.6 (C_a), 44.3 (C_b), 28.4 (C_e), 28.2 (BocCH₃), 18.5 (C_c). **HRMS** calcd. for C₁₈H₃₁N₃O₅Na⁺ 392.2161 [M + Na]⁺, found 392.2164.



Synthesis of dG2-CO₂Bn



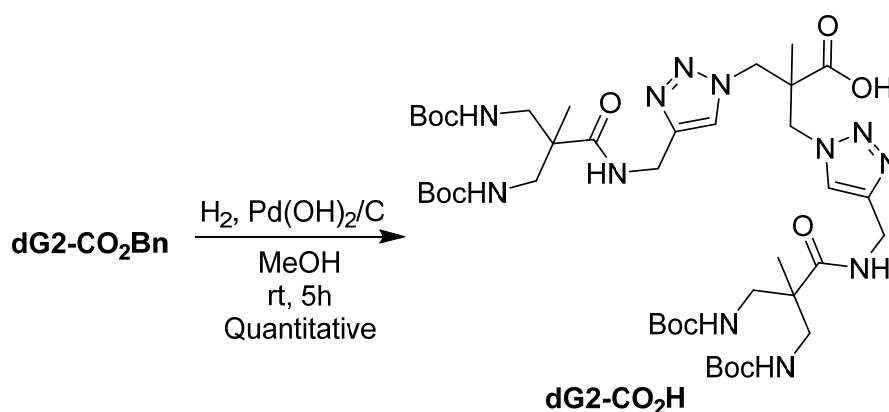
This compound was obtained from **2** (418 mg, 1.53 mmol, 1 eq), **dG1** (1.23 g, 3.37 mmol, 2.2 eq), copper (II) sulphate 5-hydrate (10 mg, 0.04 mmol, 0.02 eq) and L(+)-ascorbic acid sodium salt (32 mg, 0.16 mmol, 0.1 eq) in *tert*-butanol/water 1:2 (10 mL) to obtain the product (1.34 g, 1.32 mmol, 87%) as a colorless powder; **mp** 111–113 °C. **¹H NMR** (400 MHz, DMSO-*d*₆) δ ppm: 7.79 (s, 2 H, H_g), 7.40–7.32 (m, 5 H, BnCH), 5.09 (s, 2 H, BnCH₂), 4.72 (d, J = 14.2 Hz, 2 H,



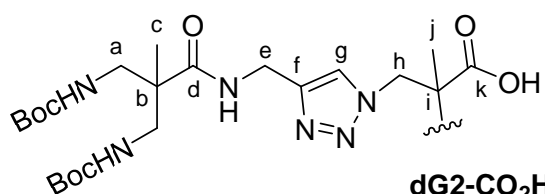
H_h), 4.59 (d, J = 14.1 Hz, 2 H, H_h), 4.27 (d, J = 4.8 Hz, 4 H, H_e), 3.16–3.04 (m, 8 H, H_a), 1.35 (s, 36 H, BocCH₃), 1.00 (s, 6 H, C_c), 0.96 (s, 3 H, H_j). **¹³C NMR** (100 MHz, DMSO-*d*₆) δ ppm: 174.1 (C_d),

171.8 (C_k), 156.1 (BocCO), 145.0 (C_f), 135.3 (BnCH), 128.4 (BnCH), 128.1 (BnCH), 128.0 (BnCH), 124.2 (C_g), 77.9 (BocC), 66.8 (BnCH₂), 53.4 (C_b), 48.3 (C_a, C_h), 47.6 (C_a, C_h), 44.4 (C_i), 34.6 (C_e), 28.1 (BocCH₃), 18.4 (C_c), 17.7 (C_j). **HRMS** calcd. for C₄₈H₇₇N₁₂O₁₂⁺ 1013.5784 [M + H]⁺, found 1013.5781.

Synthesis of dG2-CO₂H

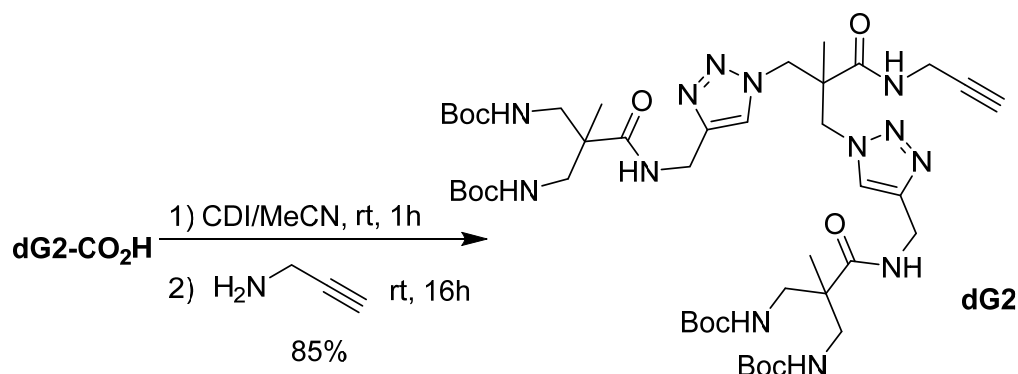


$\text{Pd}(\text{OH})_2$ (100 mg, 0.71 mmol, 0.3 eq) was added to a solution of **dG2-CO₂Bn** (1.76 g, 1.74 mmol, 1 eq) in MeOH (10 mL). Hydrogenation took place in a hydrogenation reactor at room temperature and 50 bar hydrogen pressure. After five hours, the catalyst was removed by filtration through MeOH-pre-wetted Celite. The solvent was removed under vacuum to obtain the product (1.61 g, 1.71 mmol, 98%) as a solid (compound decomposes above 210 °C). **¹H NMR** (400 MHz, DMSO-*d*₆) δ ppm: 7.92 (s, 2 H, H_g), 4.51 (d, J = 13.7 Hz, 2 H, H_h), 4.35 (d, J = 13.7 Hz, 2 H, H_h), 4.27 (s, 4 H, H_e), 3.16-3.04 (m, 8 H, H_a), 1.35 (s, 36 H, BocCH₃), 0.96 (s, 6 H, H_c), 0.81 (s, 3 H, H_j). **¹³C NMR** (100 MHz, DMSO-*d*₆) δ ppm: 174.2 (C_d), 174.1 (C_k), 156.2

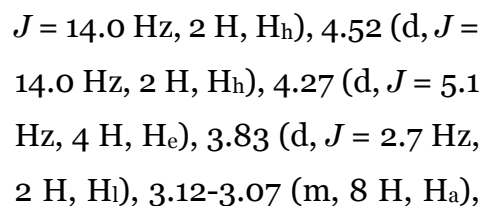
**dG2-CO₂H**

(BocCO), 144.6 (C_f), 124.0 (C_g), 77.9 (BocC), 54.3 (C_b), 48.5 (C_a, C_h), 47.7 (C_a, C_h), 44.4 (C_i), 34.6 (C_e), 28.1 (BocCH₃), 19.1 (C_c), 18.5 (C_j). **HRMS** calcd. for C₄₁H₇₀N₁₂O₁₂Na⁺ 945.5134 [M + Na]⁺, found: 945.5124.

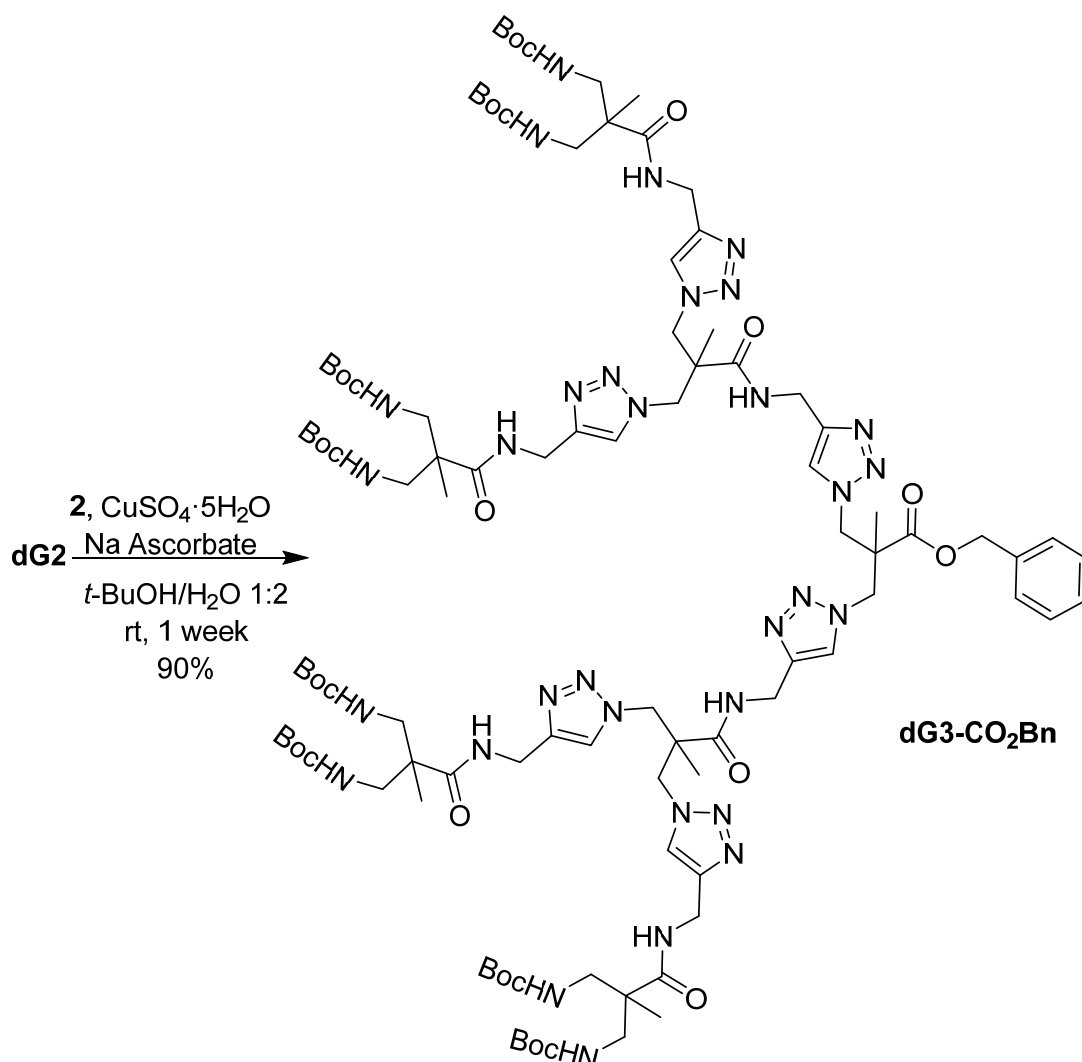
Synthesis of dG2



A solution of **dG2-CO₂H** (2.78 g, 3.02 mmol, 1 eq) in anhydrous acetonitrile (15 mL) was added to a solution of CDI (734 mg, 4.53 mmol, 1.5 eq) in anhydrous acetonitrile (45 mL). The mixture was stirred at room temperature for one hour. Afterwards, propargylamine (0.3 mL, 4.53 mmol, 1.5 eq) was added and the stirring mixture was left for 16 hours at room temperature. The solvent was removed under vacuum. The residue was dissolved in dichloromethane (50 mL) and washed with HCl 0.05M (5 × 50 mL). The combined organic phase was dried with MgSO₄, filtered and concentrated under reduced pressure to obtain the product (2.46 g, 2.57 mmol, 85 %) as a colorless solid (compound decomposes above 105 °C). **¹H NMR** (400 MHz, DMSO-*d*₆) δ ppm: 7.22 (s, 2 H, H_g), 4.66 (d,

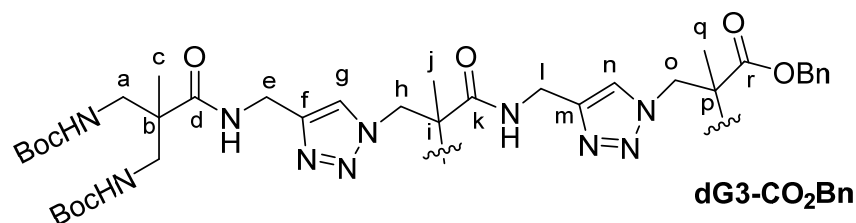


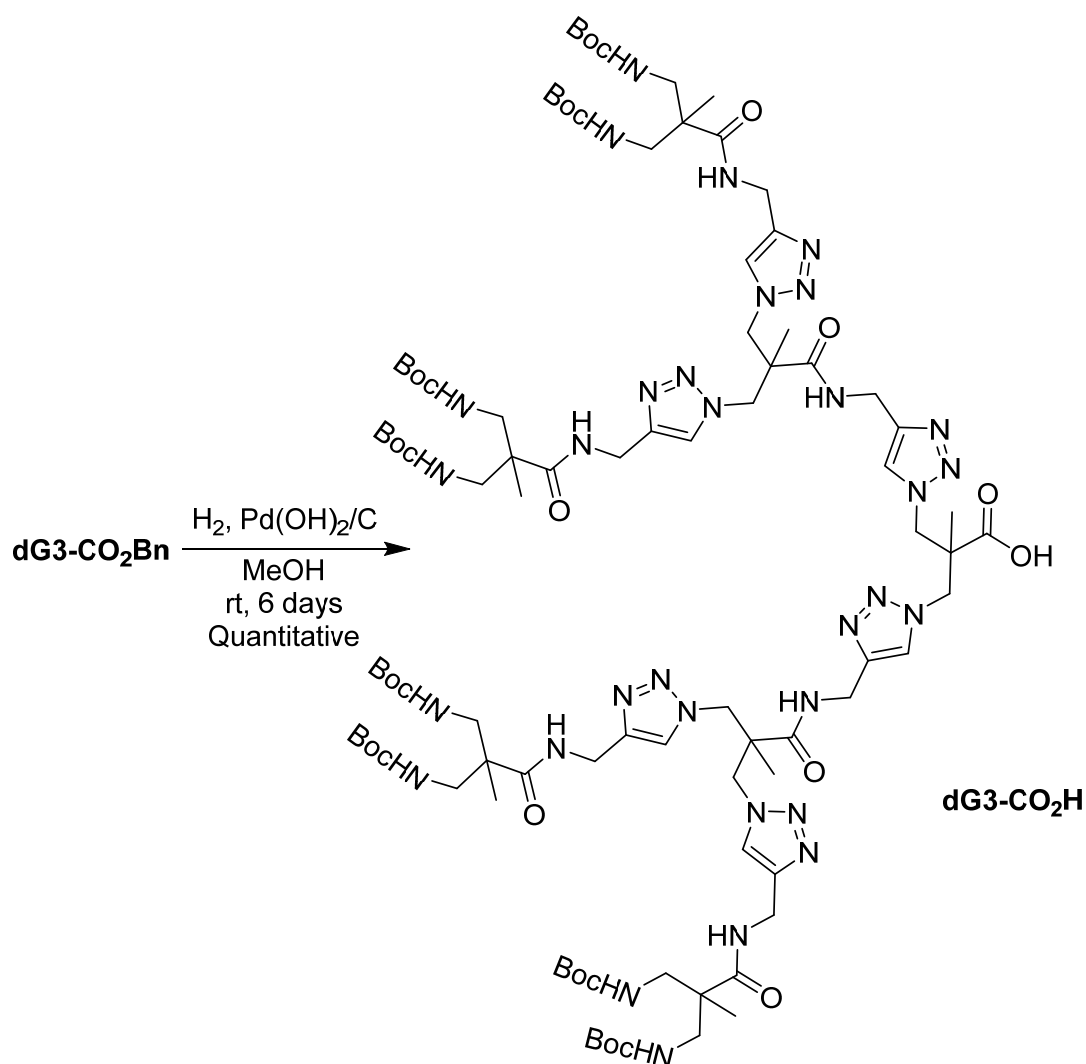
Synthesis of dG3-CO₂Bn



201

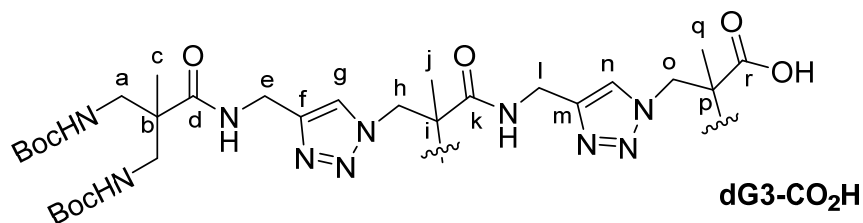
butanol/water 1:2 (27 mL) to obtain the desired product (2.31 g, 1.05 mmol, 90%) as a colorless solid (compound decomposes above 149 °C). **¹H NMR** (400 MHz, DMSO-*d*₆) δ ppm: 7.94-7.75 (m, 6 H, H_g, H_n), 7.36-7.32 (m, 5 H, Bn_{CCH}), 5.10 (s, 2 H, Bn_{CH2}), 4.80 (d, *J* = 14.3 Hz, 2 H, H_o), 4.65 (d, *J* = 14.3 Hz, 4 H, H_h), 4.51 (d, *J* = 13.8 Hz, 4 H, H_h), 4.44 (d, *J* = 13.8 Hz, 2 H, H_o), 4.31-4.18 (m, 12 H, H_e, H_f), 3.18-3.04 (m, 16 H, H_a), 1.35 (s, 72 H, Boc_{CCH3}), 0.96-0.93 (m, 21 H, H_c, H_j, H_q). **¹³C NMR** (100 MHz, DMSO-*d*₆) δ ppm: 174.2 (C_d), 171.8 (C_k, C_r), 171.4 (C_k, C_r), 156.1 (Boc_{CO}), 144.9 (C_f, C_m), 144.2 (C_f, C_m), 135.3 (Bn_C), 128.4 (Bn_{CH}), 128.1 (Bn_{CH}), 128.0 (Bn_{CH}), 126.4 (C_g, C_n), 124.0 (C_g, C_n), 78.0 (Boc_C), 66.8 (Bn_{CH2}), 53.8 (C_b, C_i), 53.5 (C_b, C_i), 48.4 (C_a, C_h, C_o), 47.9 (C_a, C_h, C_o), 47.6 (C_a, C_h, C_o), 44.4 (C_p), 34.8 (C_e, C_l), 34.6 (C_e, C_l), 28.1 (Boc_{CCH3}), 18.4 (C_c, C_j, C_q), 17.8 (C_c, C_j, C_q), 17.6 (C_c, C_j, C_q). **HRMS** calcd. for C₁₀₀H₁₆₀N₃₂O₂₄Na⁺ 2216.2181 [M + Na]⁺, found: 2216.2263.



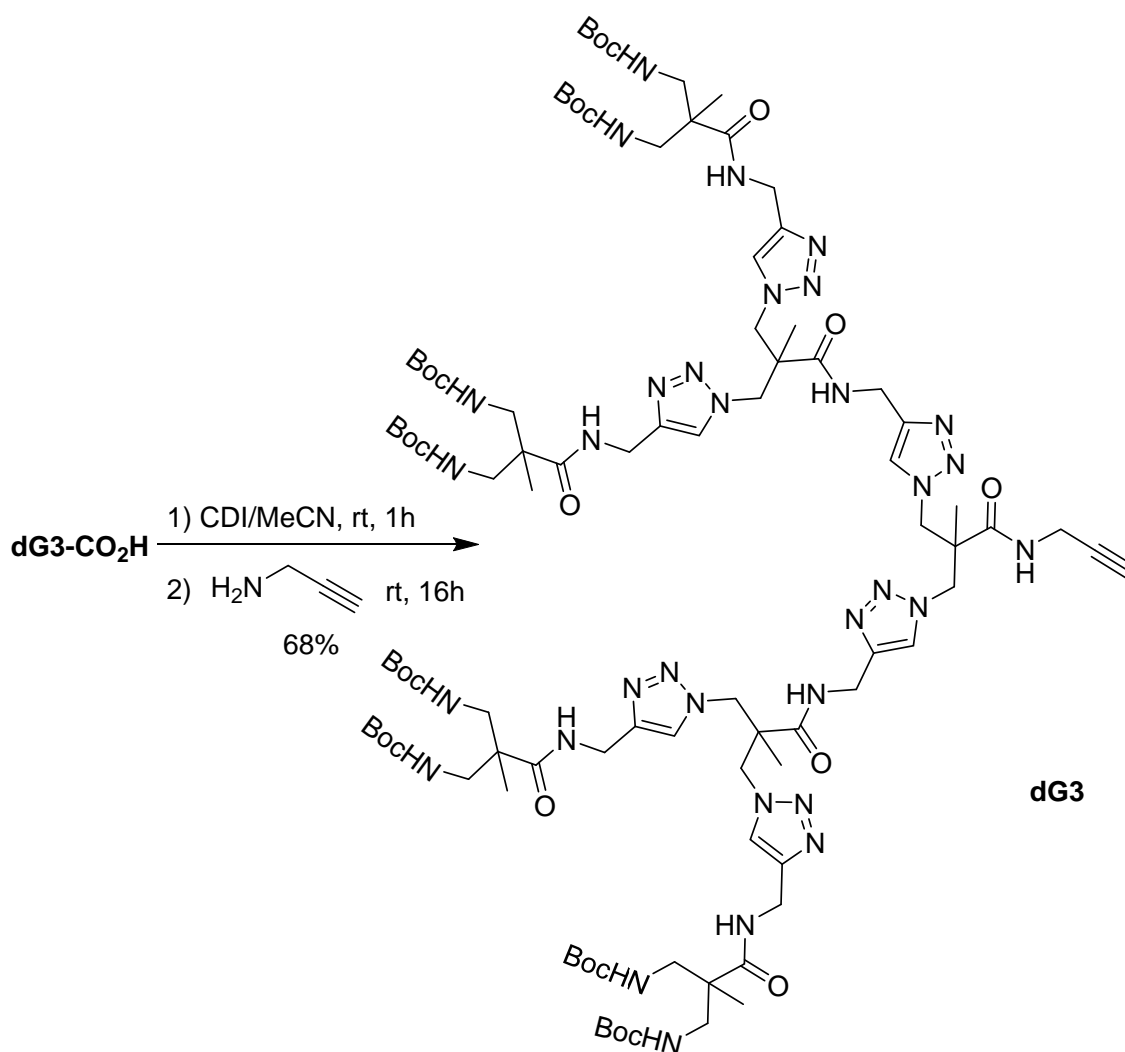
Synthesis of **dG3-CO₂H**

$\text{Pd}(\text{OH})_2$ (23 mg, 0.16 mmol, 0.3 eq) was added to a solution of **dG3-CO₂Bn** (1.18 g, 0.54 mmol, 1 eq) in MeOH (10 mL). After hydrogenating for 6 days, the catalyst was removed by filtration through MeOH -pre-wetted Celite. The solvent was removed under vacuum to obtain the product (966 mg, 0.46 mmol, 85%) as a solid (compound decomposes above 230 °C). **¹H NMR** (400 MHz, $\text{DMSO}-d_6$) δ ppm: 8.18-7.54 (m, 6 H, H_g , H_n), 4.72-4.44 (m, 12 H, H_h , H_o), 4.37-4.22 (m, 12 H, H_e , H_f), 3.16-2.96 (m, 16 H, H_a), 1.36 (s, 72 H, BocCH_3), 0.96 (s, 12 H, H_c), 0.95 (s, 6 H, H_j), 0.81 (s, 3 H, H_q). **¹³C NMR** (100 MHz, $\text{DMSO}-d_6$) δ ppm: 174.3 (C_d), 173.8 (C_k , C_r), 171.1 (C_k , C_r), 156.2 (BocCO), 145.0 (C_f , C_m), 144.5 (C_f , C_m), 123.9 (C_g , C_n), 123.9 (C_g , C_n), 77.9 (BocC), 54.7 (C_b , C_i), 53.9 (C_b , C_i), 48.7 (C_a , C_h , C_o), 47.6 (C_a , C_h , C_o), 47.5 (C_a , C_h , C_o), 44.4 (C_p), 34.6 (C_e , C_l), 34.5 (C_e , C_l),

28.1 (BocCH₃), 19.0 (C_c, C_j, C_q), 18.5 (C_c, C_j, C_q), 17.6 (C_c, C_j, C_q). **HRMS** calcd. for C₉₃H₁₅₃N₃₂O₂₄⁻ 2102.1735 [M - H]⁻, found: 2102.1636.

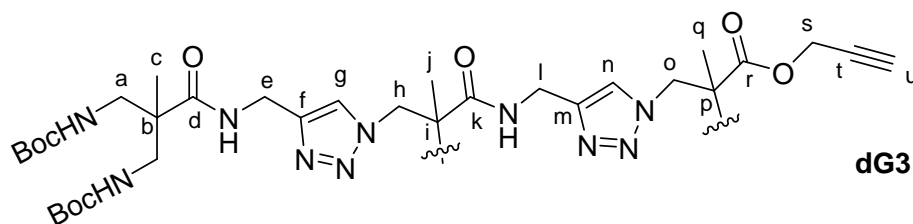


Synthesis of dG3

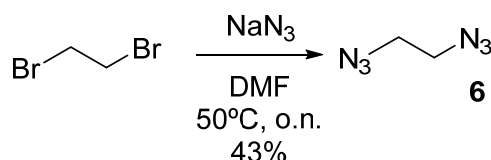


A solution of **dG3-CO₂H** (1.10 g, 0.52 mmol, 1 eq) in anhydrous acetonitrile (10 mL) was added to a solution of CDI (126 mg, 0.78 mmol, 1.5 eq) in anhydrous acetonitrile (10 mL) and the mixture was stirred at room temperature for one hour. Afterwards, propargylamine (52 μ L, 0.78 mmol, 1.5 eq) was added and the stirring mixture was left overnight at room temperature. The

solvent was removed under vacuum and the residue was dissolved in dichloromethane (30 mL) and washed with HCl 0.05M ($5 \times 30\text{mL}$). The combined organic phases were dried with MgSO_4 anhyd., filtered and concentrated under reduced pressure to obtain the product (723 mg, 0.34 mmol, 65 %) as a colorless solid (compound decomposes above 146°C). **^1H NMR** (400 MHz, $\text{DMSO-}d_6$) δ ppm: 7.93-7.54 (m, 6 H, H_g, H_n), 4.71-4.53 (m, 12 H, H_h, H_o), 4.39-4.15 (m, 12 H, H_e, H_f), 3.83 (s, 2 H, H_s), 3.20-2.95 (m, 16 H, H_a), 1.74 (s, 1 H, H_u), 1.35 (s, 72 H, BocCH_3), 0.96-0.93 (m, 21 H, $\text{H}_c, \text{H}_j, \text{H}_q$). **^{13}C NMR** (100 MHz, $\text{DMSO-}d_6$) δ ppm: 174.2 (C_d), 171.5 (C_k, C_r), 171.4 (C_k, C_r), 156.2 (BocCO), 144.9 (C_f, C_m), 144.2 (C_f, C_m), 124.2 (C_g, C_n), 124.0 (C_g, C_n), 78.2 (C_t), 78.0 (BocC), 73.1 (C_u), 53.92 (C_b, C_i), 53.88 (C_b, C_i), 48.0 ($\text{C}_a, \text{C}_h, \text{C}_o$), 47.9 ($\text{C}_a, \text{C}_h, \text{C}_o$), 47.6 ($\text{C}_a, \text{C}_h, \text{C}_o$), 44.4 (C_p), 35.9 (C_e, C_l), 34.6 (C_e, C_l), 28.6 (C_s), 28.2 (BocCH_3), 18.5 ($\text{C}_c, \text{C}_j, \text{C}_q$), 17.6 ($\text{C}_c, \text{C}_j, \text{C}_q$), 17.4 ($\text{C}_c, \text{C}_j, \text{C}_q$). **HRMS** calcd. for $\text{C}_{96}\text{H}_{159}\text{N}_{33}\text{O}_{23}^{2+}$ 2142.2287 [$\text{M} + 2\text{H}$] $^{2+}$, found: 1071.1137.

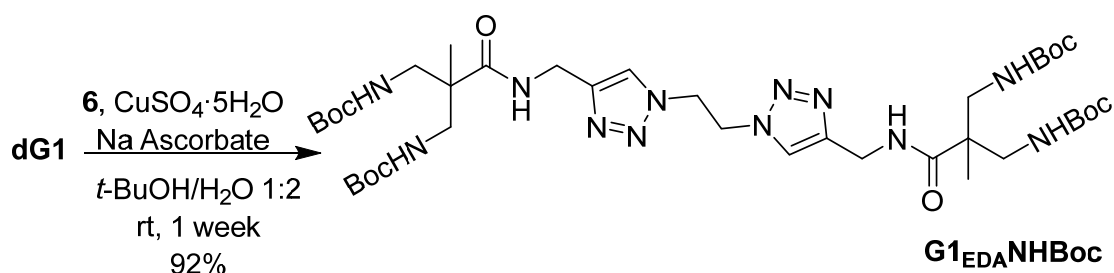


Synthesis of 1,2-diazidoethane (**6**)



Compound **6** was synthesized as described in literature.¹⁴¹ 3-Bromopropylamine hydrobromide (5 g, 22.84 mmol, 1 eq) was dissolved in water (10mL) and sodium azide was added (4.45 g, 68.52 mmol, 3 eq). The reaction was stirred during three days at 80°C . The mixture was cooled in an ice-water bath and ether was added (20mL). KOH was added until basic pH was attained. The organic layer was separated, and the aqueous phase was extracted with ether ($3 \times 20\text{ mL}$). The combined organic layer was dried with MgSO_4 and concentrated to obtain **6** as a colorless oil (1.3 g, 11.42mmol, 50%). **^1H NMR** (400 MHz, CDCl_3) δ ppm: 3.46 (s, 4 H, $\text{CH}_2\text{-N}_3$). **^{13}C NMR** (100 MHz, CDCl_3) δ ppm: 50.7 ($\text{CH}_2\text{-N}_3$).

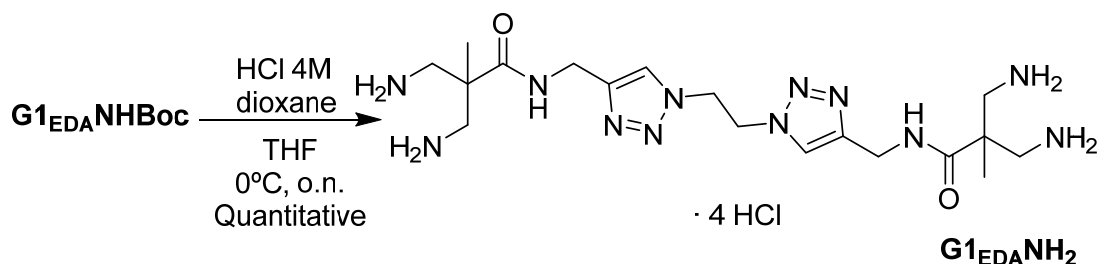
Synthesis of **G1_{EDA}NHBoc**



dG1 (500 mg, 1.36 mmol, 2.2 eq), **6** (69 mg, 0.62 mmol, 1 eq), copper (II) sulphate 5-hydrate (3 mg, 0.01 mmol, 0.02 eq) and L(+)-ascorbic acid sodium salt (12 mg, 0.06 mmol, 0.1 eq) in *tert*-butanol/water 1:2 (18 mL) to obtain the product (485 mg, 0.57 mmol, 92 %) as a colorless oil. **¹H NMR** (400 MHz,

DMSO-*d*₆) δ ppm: 7.76 (s, 2 H, H_g), 4.82 (s, 4 H, EDACH₂), 4.24 (d, $J = 5.2$ Hz, 4 H, H_e), 3.18–2.98 (m, 8 H, H_a), 1.36 (s, 36 H, BocCH₃), 0.96 (s, 6 H, H_c). **¹³C NMR** (100 MHz, DMSO-*d*₆) δ ppm: 174.1 (C_d), 156.1 (BocCO), 145.3 (C_f), 122.9 (C_g), 78.0 (BocC), 48.9 (EDACH₂), 47.6 (C_b), 44.4 (C_a), 34.6 (C_e), 28.1 (BocCH₃), 18.4 (C_c). **HRMS** calcd. for C₃₈H₆₆N₁₂O₁₀Na⁺ 873.4923 [M + Na]⁺, found: 873.4921.

Synthesis of **G1_{EDA}NH₂**

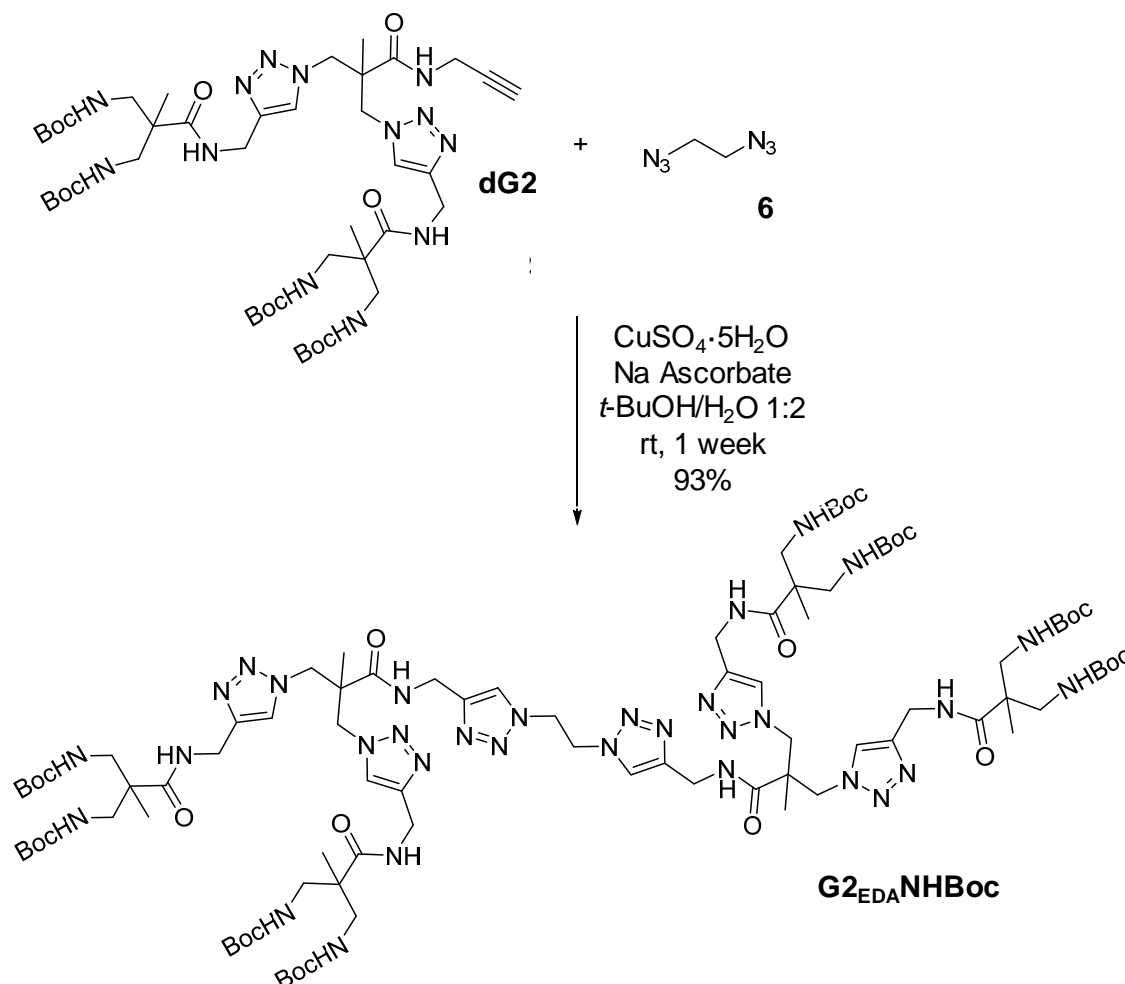


This compound was obtained from **G1_{EDA}NHBoc** (450 mg, 0.53 mmol) to obtain the desired product (309 mg, 0.52 mmol, 98%) as a colorless solid. **¹H NMR** (400 MHz, D₂O) δ ppm: 7.85 (s, 2 H, H_g),

4.94 (s, 4 H, EDACH₂), 4.49 (s, 4 H, H_e), 3.34 (d, $J = 13.5$ Hz, 4 H, H_a), 3.15 (d, $J = 13.5$ Hz, 4 H, H_a), 1.42 (s, 6 H, H_c). **¹³C NMR** (100 MHz, D₂O) δ ppm: 174.1 (C_d), 156.1 (BocCO), 145.3 (C_f), 122.9 (C_g), 78.0 (BocC), 48.9 (EDACH₂), 47.6 (C_b), 44.4 (C_a), 34.6 (C_e), 28.1 (BocCH₃), 18.4 (C_c). **HRMS** calcd. for C₃₈H₆₆N₁₂O₁₀Na⁺ 873.4923 [M + Na]⁺, found: 873.4921.

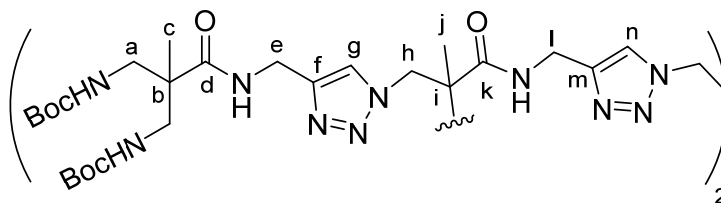
δ ppm: 173.1 (C_d), 143.7 (C_f), 123.2 (C_g), 49.2 (EDA_{CH_2}), 44.2 (C_a), 43.3 (C_b), 33.8 (C_e), 16.6 (C_c).

Synthesis of $G2_{EDA}NH\text{Boc}$

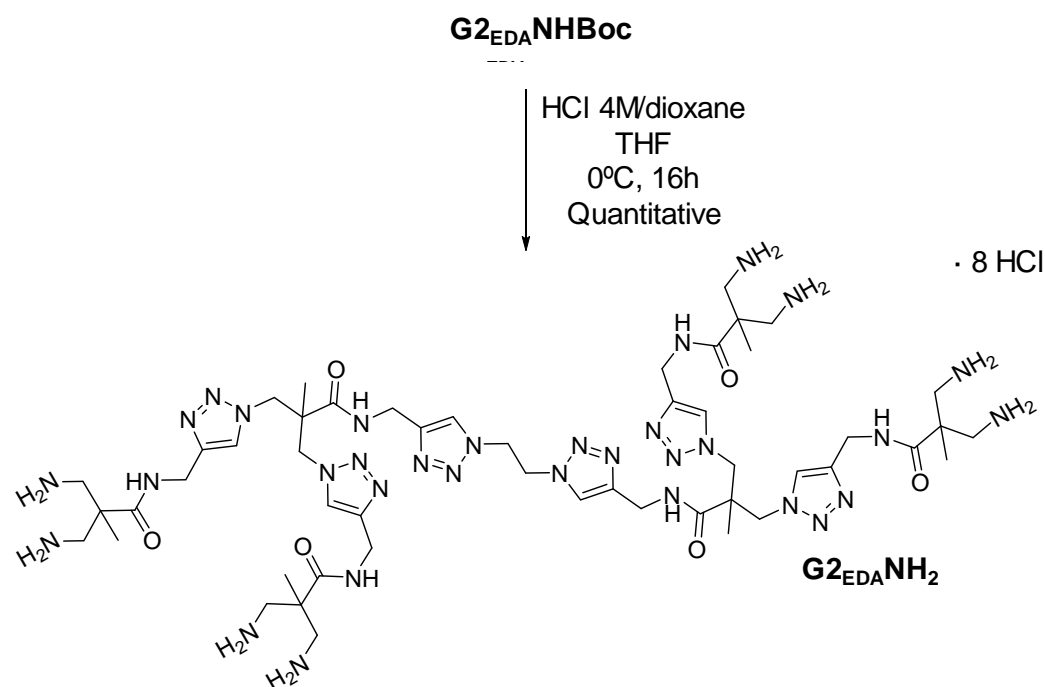


dG2 (1.09 g, 1.14 mmol, 2.2 eq), **6** (58 mg, 0.52 mmol, 1 eq), copper (II) sulphate 5-hydrate (3 mg, 0.01 mmol, 0.02 eq) and L(+)-ascorbic acid sodium salt (10 mg, 0.06 mmol, 0.1 eq) in *tert*-butanol/water 1:2 (18 mL) to obtain the product (845 mg, 0.42 mmol, 80 %) as a colorless solid (compound decomposes above 140 °C). 1H NMR (400 MHz, $DMSO-d_6$) δ ppm: 8.55-7.72 (m, 6 H, H_g , H_n), 4.90 (d, $J = 14.7$ Hz, 4 H, EDA_{CH_2}), 4.66 (d, $J = 14.0$ Hz, 4 H, H_h), 4.51 (d, $J = 14.0$ Hz, 4 H, H_h), 4.30-4.14 (m, 12 H, H_e , H_l), 3.24-3.00 (m, 16 H, H_a), 1.35 (s, 72 H, $BocCH_3$), 0.96 (s, 12 H, H_c), 0.93 (s, 6 H, H_j). ^{13}C NMR (100 MHz, $DMSO-d_6$) δ ppm: 174.1 (C_d), 171.4 (C_k), 156.1 ($BocCO$), 144.9 (C_f , C_m), 144.6 (C_f , C_m), 124.0 (C_g ,

C_n), 123.4 (C_g, C_n), 78.0 (Boc_c), 53.8 (C_h), 49.0 (EDACH₂), 47.9 (C_b, C_i), 47.6 (C_b, C_i), 44.4 (C_a), 34.8 (C_e, C_l), 34.6 (C_e, C_l), 28.1 (BocCH₃), 18.4 (C_c), 17.5 (C_j).

**G2_{EDA}NHBoc**

Synthesis of G2_{EDA}NH₂

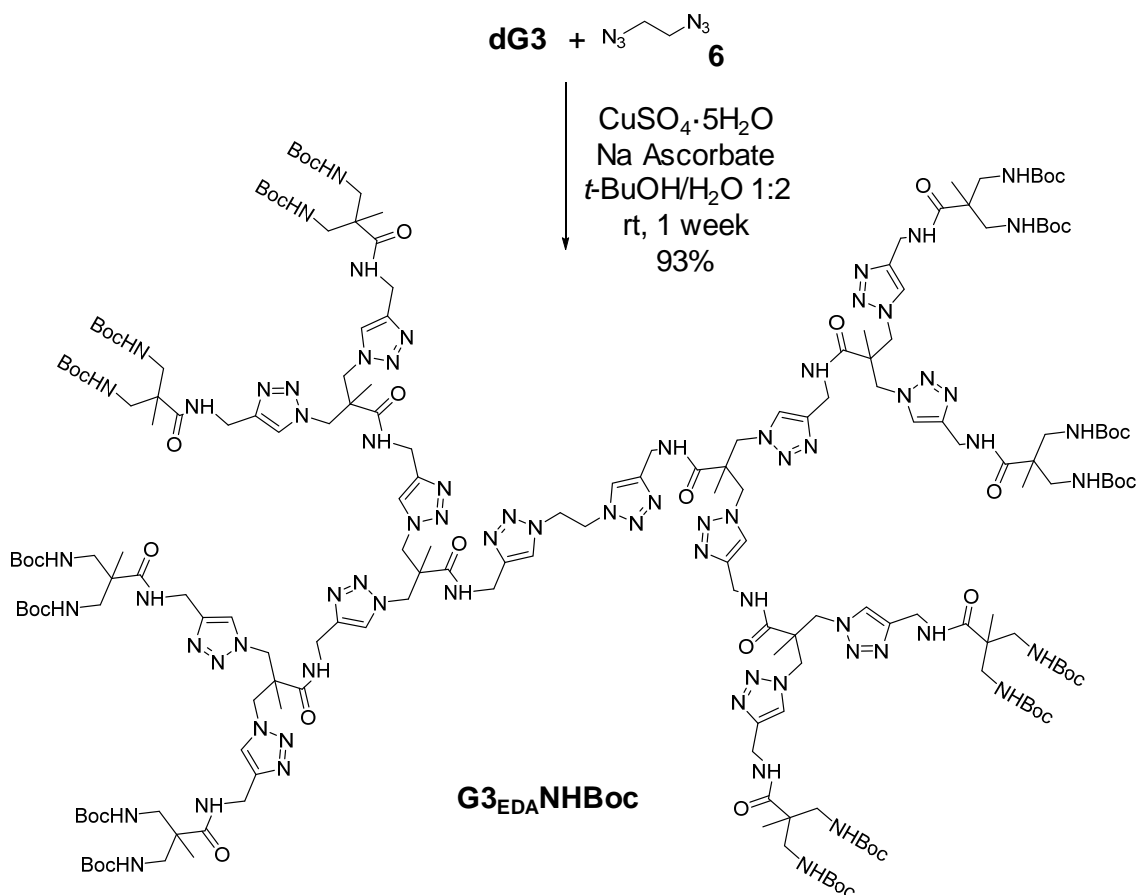


This compound was obtained from **G2_{EDA}NHBoc** (400 mg, 0.20 mmol) to obtain the product (299 mg, 0.20 mmol, 98 %) as a colorless solid. ¹H NMR

(400 MHz, D₂O) δ ppm: 7.78-7.66 (m, 6 H, H_g, H_n), 5.02 (s, 4 H, EDACH₂), 4.58-4.43 (m, 12 H, H_e, H_l), 4.31 (s, 8 H, H_h), 3.33 (d, *J* = 13.3 Hz, 8 H, H_a), 3.15 (d, *J* = 13.3 Hz, 8 H, H_a), 1.41 (s, 12 H, H_c), 1.13 (s, 6 H, H_j). ¹³C NMR

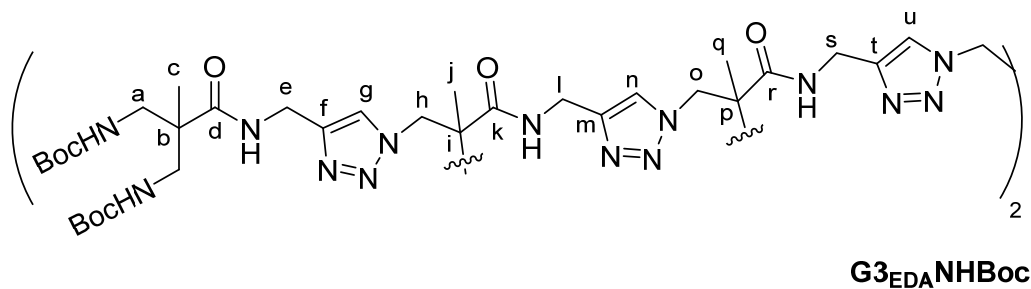
(100 MHz, D₂O) δ ppm: 173.2 (C_d), 172.4 (C_k), 143.6 (C_f, C_m), 143.1 (C_f, C_m), 124.2 (C_g, C_n), 123.8 (C_g, C_n), 54.1 (C_h), 49.2 (EDACH₂), 48 (C_b, C_i), 47.9 (C_b, C_i), 44.3 (C_a), 34.0 (C_e, C_l), 33.8 (C_e, C_l), 16.7 (C_c), 15.8 (C_j).

Synthesis of G₃EDANH₂Boc

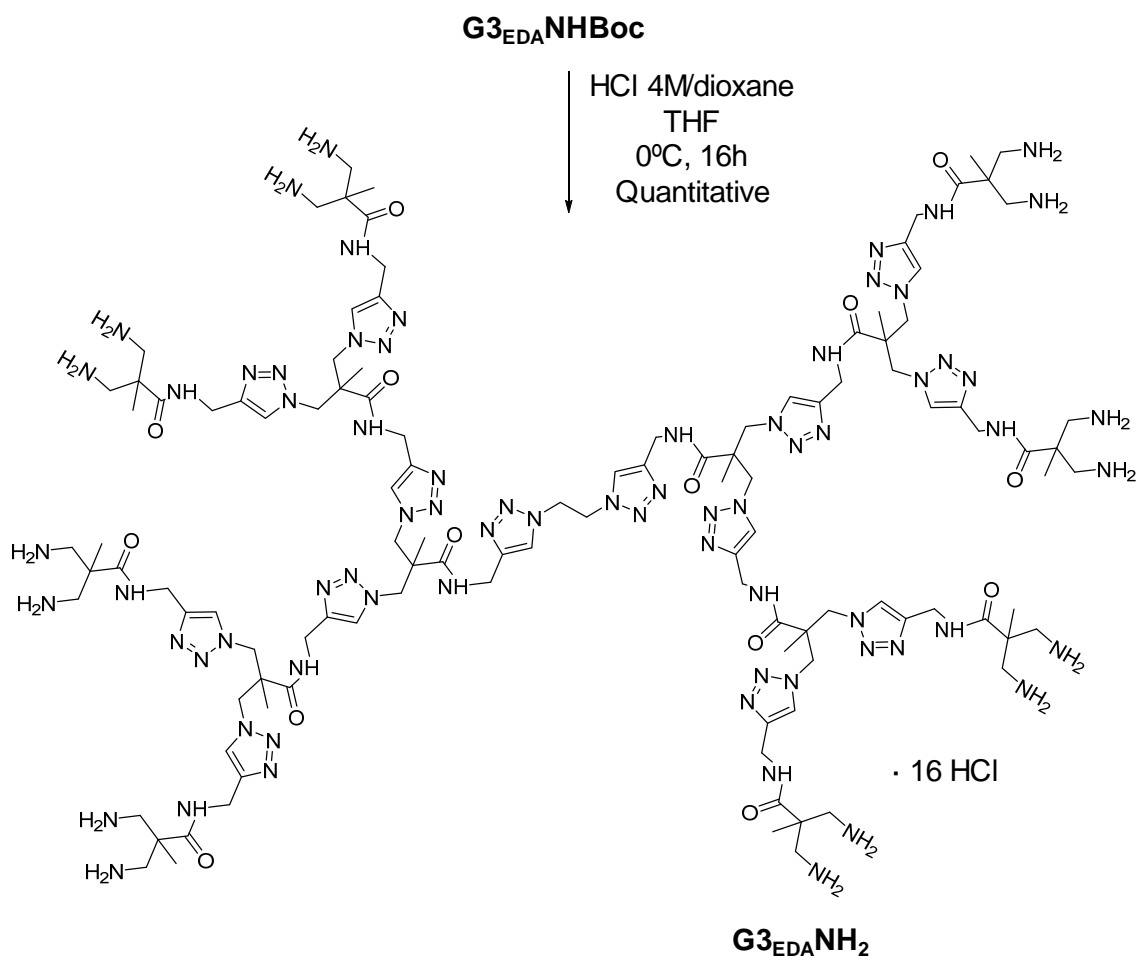


This compound was obtained from **dG3** (179 mg, 0.084 mmol, 2.2 eq), **6** (4 mg, 0.04 mmol, 1 eq), copper (II) sulphate 5-hydrate (0.2 mg, 0.001 mmol, 0.02 eq) and L(+)-ascorbic acid sodium salt (2 mg, 0.01 mmol, 0.1 eq) in *tert*-butanol/water 1:2 (6 mL) to obtain the desired product (163 mg, 0.04 mmol, 93 %) as a colorless solid (compound decomposes above 145 °C). ¹H NMR (400 MHz, DMSO-*d*₆) δ ppm: 7.97-7.77 (m, 14 H, H_g, H_n, H_u), 4.90 (s, 4 H, EDACH₂), 4.68-4.57 (m, 24 H, H_h, H_o), 4.43-4.16 (m, 28 H, H_e, H_l, H_s), 3.22-2.98 (m, 32 H, H_a), 1.34 (s, 144 H, BocCH₃), 1.08-0.88 (m, 42 H, H_c, H_j, H_q). ¹³C NMR (100 MHz, DMSO-*d*₆) δ ppm: 174.2 (C_d), 171.48 (C_k, C_r), 171.49 (C_k, C_r), 156.2 (BocCO), 145.1 (C_f, C_m, C_t), 145.0 (C_f, C_m, C_t), 144.9 (C_f, C_m, C_t), 124.2 (C_g, C_n, C_u), 124.1 (C_g, C_n, C_u), 124.0 (C_g, C_n, C_u), 78.0 (BocC), 53.8 (C_b, C_i), 51.4 (C_b, C_i), 48.4 (EDACH₂), 47.9 (C_a, C_h, C_o), 47.7 (C_a, C_h, C_o), 47.4 (C_a, C_h, C_o), 44.4 (C_p), 34.6 (C_e, C_i, C_s), 34.59 (C_e,

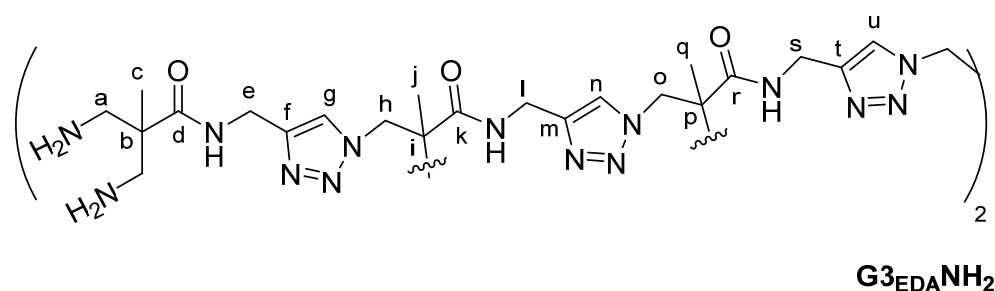
C_l, C_s), 34.57 (C_e, C_l, C_s), 28.1 (BocCH₃), 18.5 (C_c, C_j, C_q), 17.7 (C_c, C_j, C_q), 17.6 (C_c, C_j, C_q).



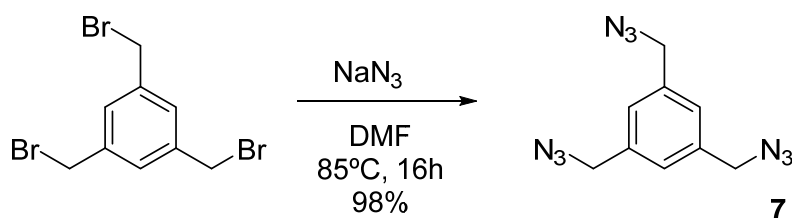
Synthesis of G3_{EDA}NH₂



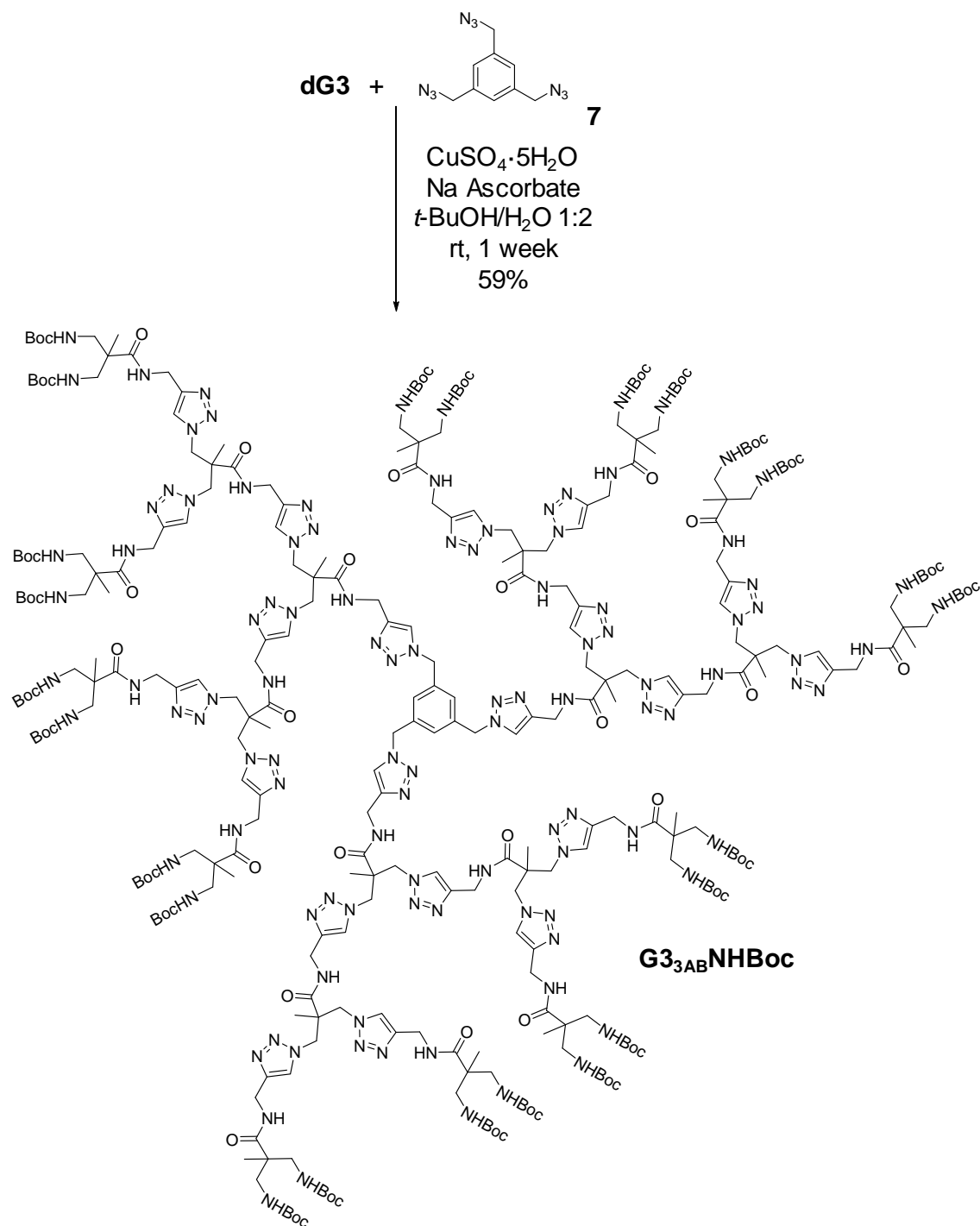
This compound was obtained from **G3_{EDA}NHBoc** (109 mg, 0.025 mmol) to obtain the product (82 mg, 0.025, 98 %) as a colorless solid. **¹H NMR** (400 MHz, D₂O) δ ppm: 8.04-7.62 (m, 14 H, H_g, H_n, H_u), 5.01 (s, 4 H, EDA_{CH2}), 4.66-4.20 (m, 44 H, H_e, H_h, H_l, H_s), 3.85-3.56 (m, 8 H, H_o), 3.44-3.09 (m, 32 H, H_a), 1.45 (s, 24 H, H_c), 1.16 (s, 12 H, H_j), 1.00 (s, 6 H, H_q). **¹³C NMR** (100 MHz, D₂O) δ ppm: 174.0 (C_d), 173.0 (C_k, C_r), 172.4 (C_k, C_r), 143.2 (C_f, C_m, C_t), 143.1 (C_f, C_m, C_t), 143.0 (C_f, C_m, C_t), 123.93 (C_g, C_n, C_u), 123.90 (C_g, C_n, C_u), 123.88 (C_g, C_n, C_u), 54.7 (C_h, C_o), 54.2 (C_h, C_o), 49.2 (EDA_{CH2}), 48.1 (C_a, C_b, C_i, C_p), 44.2 (C_a, C_b, C_i, C_p), 44.0 (C_a, C_b, C_i, C_p), 43.2 (C_a, C_b, C_i, C_p), 34.0 (C_e, C_l, C_s), 33.83 (C_e, C_l, C_s), 33.77 (C_e, C_l, C_s), 16.5 (C_c, C_j, C_q), 16.4 (C_c, C_j, C_q), 15.9 (C_c, C_j, C_q).



Synthesis of 1,3,5-tris(azidomethyl)benzene (**7**)

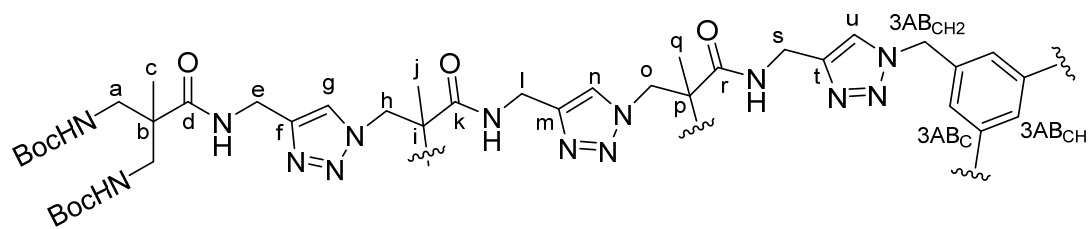


Compound **7** was synthesized as described.¹⁴² 1,3,5-tris(bromomethyl)benzene (1 g, 2.8 mmol, 1 eq.) was dissolved in DMF (5 mL) and sodium azide (2.7 g, 42 mmol, 15 eq) was added. The reaction mixture was stirred for at 85°C for 16 hours. After cooling, water (50 mL) was added and the mixture was extracted with CH₂Cl₂ (5 x 30 mL). The combined organic phases were dried (MgSO₄), filtered and concentrated to provide compound **7** as a colorless oil in (666 mg, 2.7 mmol, 98%). **¹H NMR** (400 MHz, CDCl₃) δ ppm: 7.25 (s, 3 H, CH), 4.40 (s, 6H, CH₂-N₃).

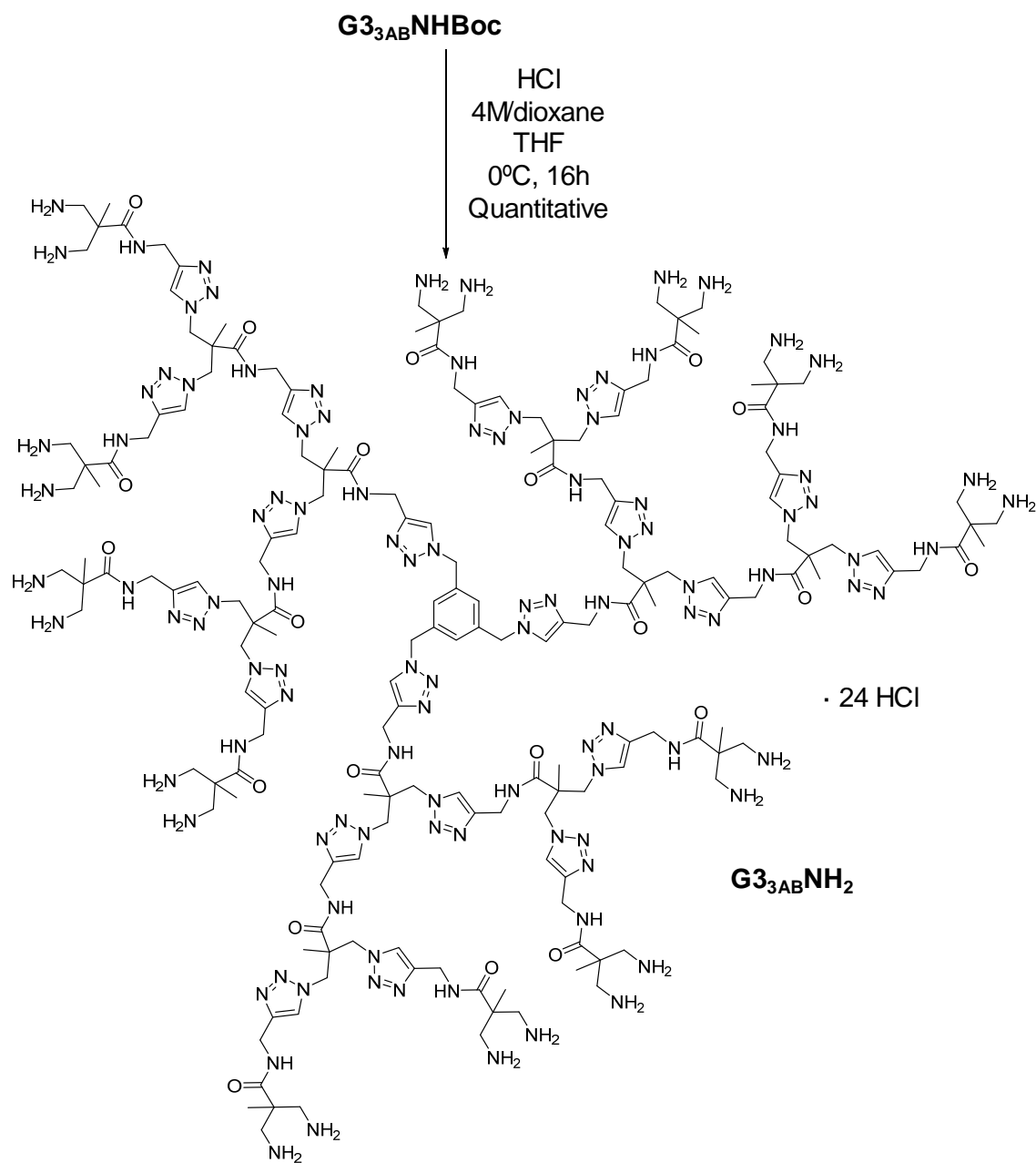
Synthesis of **G3_{3AB}NHBoc**

This compound was obtained from **dG3** (179 mg, 0.084 mmol, 3.3 eq), **7** (6 mg, 0.025 mmol, 1 eq), copper (II) sulphate 5-hydrate (0.2 mg, 0.001 mmol, 0.03 eq) and L(+)-ascorbic acid sodium salt (3 mg, 0.01 mmol, 0.3 eq) in *tert*-butanol/water 1:2 (6 mL) to obtain the product (98 mg, 0.015 mmol, 59 %) as a colorless solid (compound decomposes above 140 °C). ^1H NMR (400 MHz, DMSO-*d*₆) δ ppm: 7.97-7.77 (m, 24 H, H_g, H_n, H_u, 3ABCH), 5.63-5.56 (m, 6 H,

3AB_{CH2}), 4.77-4.45 (m, 36 H, H_h, H_o), 4.39-4.14 (m, 42H, H_e, H_l, H_s), 3.22-2.93 (m, 48 H, H_a), 1.34 (s, 216 H, BocCH₃), 1.06-0.88 (m, 54 H, H_c, H_j, H_q). ¹³C NMR (100 MHz, DMSO-*d*₆) δ ppm: 174.2 (C_d), 172.4 (C_k, C_r), 171.4 (C_k, C_r), 156.2 (BocCO), 145.1 (C_f, C_m, C_t), 144.9 (C_f, C_m, C_t), 144.6 (C_f, C_m, C_t), 137.1 (3AB_C), 131.5 (3AB_{CH}), 128.7 (3AB_{CH}), 127.5 (3AB_{CH}), 124.04 (C_g, C_n, C_u), 123.95 (C_g, C_n, C_u), 123.4 (C_g, C_n, C_u), 78.0 (BocC), 53.8 (C_h, C_o), 53.1 (C_h, C_o), 52.4 (3AB_{CH2}), 47.9 (C_b, C_i, C_p), 47.6 (C_b, C_i, C_p), 47.3 (C_b, C_i, C_p), 44.4 (C_a), 35.9 (C_e, C_l, C_s), 34.9 (C_e, C_l, C_s), 34.6 (C_e, C_l, C_s), 28.1 (BocCH₃), 18.5 (C_c, C_j, C_q), 18.0 (C_c, C_j, C_q), 17.7 (C_c, C_j, C_q).

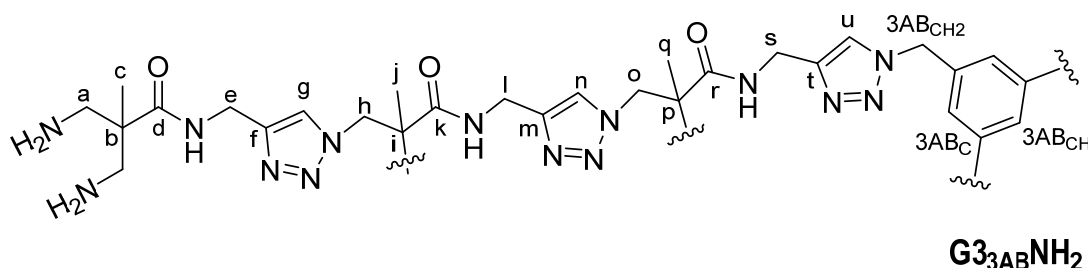


G3_{3AB}NHBoc

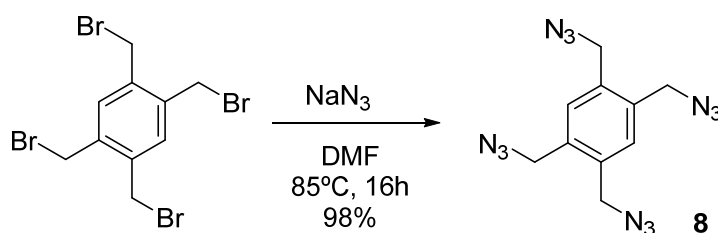
Synthesis of **G3_{3AB}NH₂**

This compound was obtained from **G3_{3AB}NHBoc** (50 mg, 0.008mmol) to obtain the product (40 mg, 0.008 mmol, 98%) as a colorless solid in a quantitative way. ¹H NMR (400 MHz, D₂O) δ ppm: 8.10-7.62 (m, 21 H, H_g, H_n, H_u), 7.26 (s, 3 H, 3ABCH), 5.65 (m, 6 H, 3ABCH₂), 4.67-4.18 (m, 66 H, H_e, H_h, H_i, H_s), 3.71-3.52 (m, 6H, H_o), 3.47 (d, *J* = 13.5 Hz, 24 H, H_a), 3.23 (d, *J* = 13.5 Hz, 24 H, H_a), 3.14-2.93 (m, 6 H, H_o), 1.50 (s, 36 H, H_c), 1.16 (s, 18 H, H_j) 1.01 (s, 9 H, H_q). ¹³C NMR (100 MHz, D₂O) δ ppm: 172.3 (C_d), 172.1 (C_k, C_r), 170.3 (C_k, C_r), 143.0 (C_f, C_m, C_t), 142.9 (C_f, C_m, C_t), 142.8 (C_f, C_m, C_t), 124.3 (C_g, C_n, C_u), 124.2 (C_g,

C_n, C_u), 124.1 (C_g, C_n, C_u), 54.2 (C_h), 52.5 ($3AB_{CH_2}$), 48.1 (C_b, C_i, C_p), 48.0 (C_b, C_i, C_p), 47.8 (C_b, C_i, C_p), 43.6 (C_a, C_o), 42.7 (C_a, C_o), 34.0 (C_e, C_l, C_s), 33.9 (C_e, C_l, C_s), 33.8 (C_e, C_l, C_s), 16.3 (C_c, C_j, C_q), 15.9 (C_c, C_j, C_q), 15.8 (C_c, C_j, C_q).

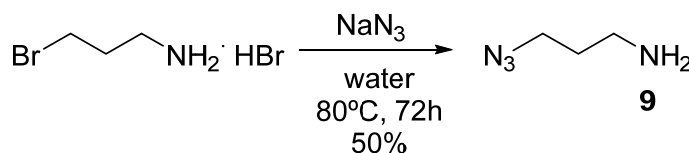


Synthesis of 1,2,4,5-tetrakis(azidomethyl)benzene (**8**)



Sodium azide (1.50 g, 22.23 mmol, 20 eq) was added to a solution of 1,2,4,5-tetrakis(bromomethyl)benzene (500 mg, 1.11 mmol, 1 eq) in DMF (3 mL). The resulting solution was heated in a heat block at 85°C for 16 hours. Water (50 mL) and dichloromethane (30 mL) were added and the phases separated. The aqueous phase was extracted with CH_2Cl_2 (2 \times 30 mL). The combined organic layers were dried over MgSO_4 and the solvent was removed by rotary evaporation to obtain the product (303 mg, 1.02 mmol, 92%) as a colorless oil. $^1\text{H NMR}$ (400 MHz, CDCl_3) δ ppm: 7.39 (s, 2H, CH), 4.46 (s, 8H, $\text{CH}_2\text{-N}_3$).

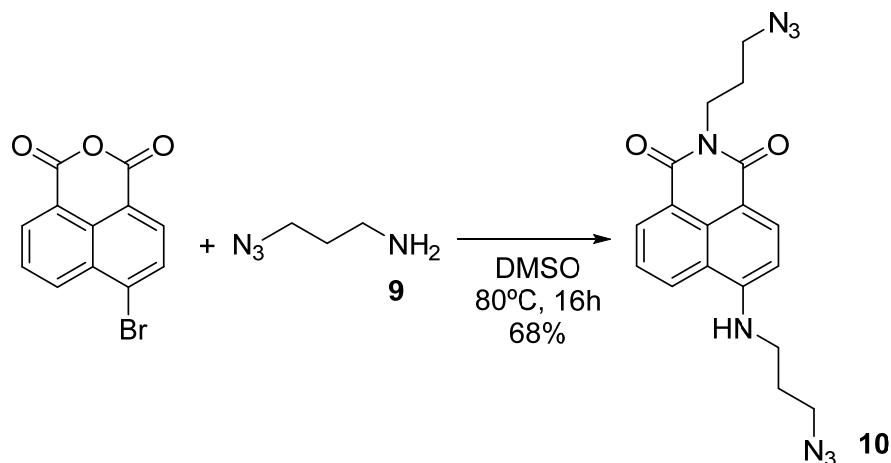
Synthesis of 3-azidopropylamine (**9**)



3-Bromopropylamine hydrobromide (5.00 g, 22.84 mmol, 1 eq) was dissolved in water (10 mL) and sodium azide was added (4.45 g, 68.52 mmol, 3 eq). The reaction was stirred during three days at 80°C in a heat block. The mixture was cooled in an ice-water bath and ether was added (20 mL). Potassium hydroxide was added until basic pH was attained. The organic layer was separated, and the aqueous phase was extracted with ether (3 \times 20 mL). The

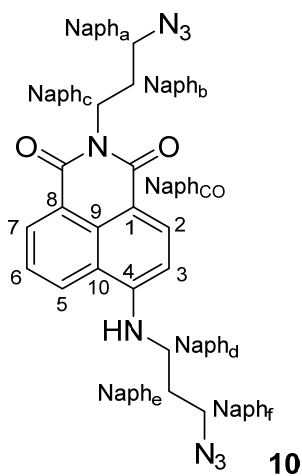
combined organic layers were dried with MgSO_4 and concentrated to obtain the product (1.14 g, 11.42 mmol, 50 %) as a colorless oil. ^1H NMR (400 MHz, D_2O) δ ppm: 3.67 (t, $J = 7.5$ Hz, 2 H, $\text{CH}_2\text{-NH}_2$), 3.24 (t, $J = 6.8$ Hz, 2 H, $\text{CH}_2\text{-N}_3$), 2.11 (m, 2 H, $\text{CH}_2\text{-CH}_2\text{-CH}_2$).

Synthesis of *N*-(2-azidopropyl)-4-((2-azidopropyl)amino)-1,8-naphthalimide (**10**)



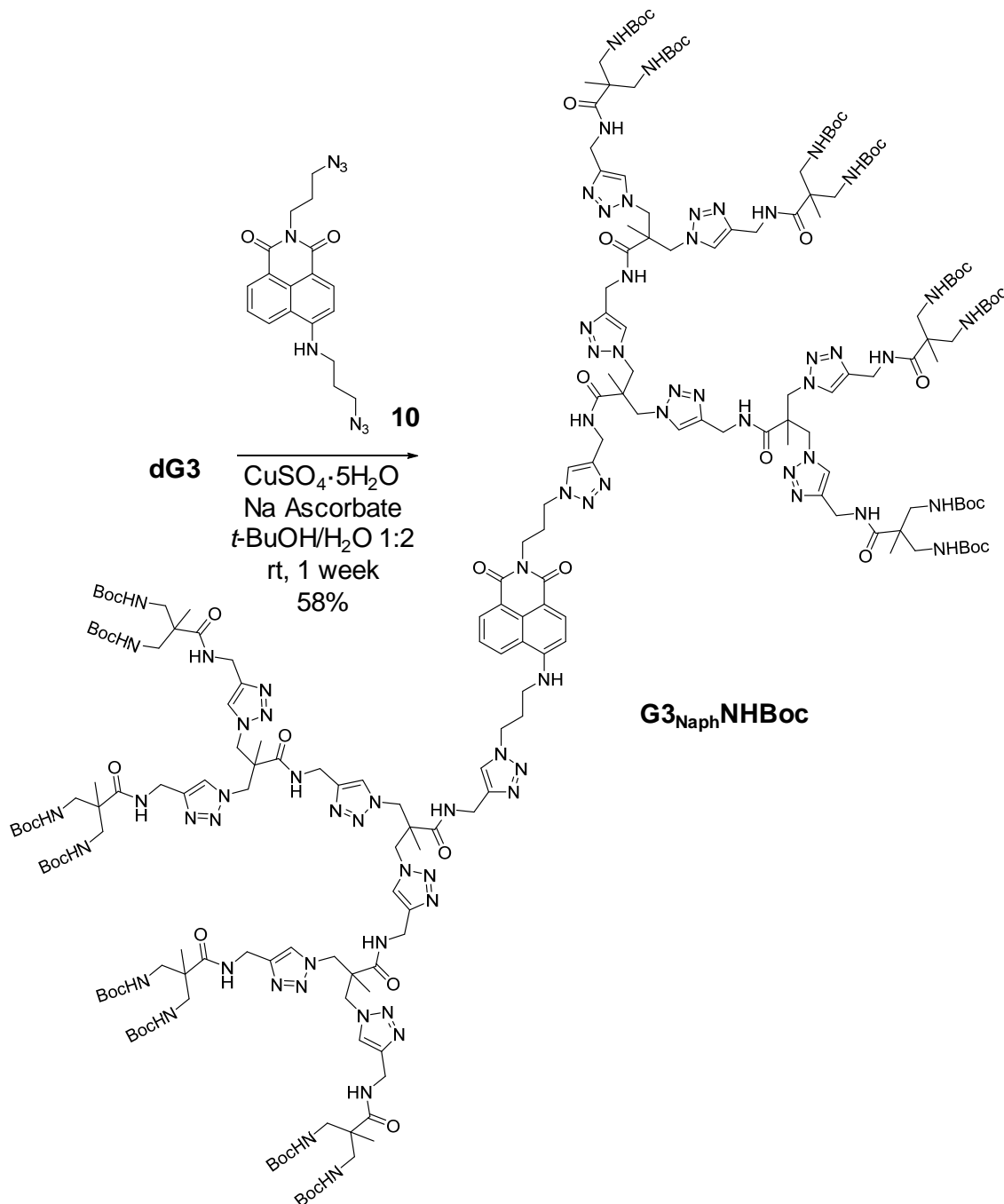
A solution of 4-bromo-1,8-naphthalic anhydride (500 mg, 1.80 mmol, 1 eq) and **9** (2.7 g, 27 mmol, 15 eq) in DMSO (2.5 mL) was heated in a heat block at 80°C for 16 hours. Then, dichloromethane was added (50 mL) and the mixture was washed with HCl (3×30 mL). The organic layer was dried using MgSO_4 and was concentrated. Purification was performed by silica gel column chromatography (dichloromethane:methanol, 99:1 v/v) to obtain the product (4.23 g, 1.22 mmol, 68 %) as a yellow solid (compound decomposes above 171 °C).

^1H NMR (400 MHz, CDCl_3) δ ppm: 8.57 (d, $J = 7.3$ Hz, 1 H, H_8), 8.45 (d, $J = 8.4$ Hz, 1 H, H_3), 8.09 (d, $J = 8.1$ Hz, 1 H, H_6), 7.62 (t, $J = 8.1$ Hz, 1 H, H_7), 6.71 (d, $J = 8.5$ Hz, 1 H, H_4), 4.25 (t, $J = 7$ Hz, 2 H, Naph_a), 3.69-3.49 (m, 4 H, Naph_e , Naph_c), 3.41 (t, $J = 7$ Hz, 2 H, Naph_g), 2.18-1.93 (m, 4 H, Naph_b , Naph_f). ^{13}C NMR (100 MHz, CDCl_3) δ ppm: 164.8 (Naph_{CO}), 164.2 (Naph_{CO}), 149.4 (C_4), 134.6 (C_2), 131.4 (C_7), 129.9 (C_9), 126.1 (C_5), 125.1 (C_6), 123.1 (C_1 , C_8), 120.5 (C_1 , C_8), 110.6 (C_{10}), 104.4 (C_3), 49.9 (Naph_a , Naph_f), 49.6 (Naph_a , Naph_f), 41.8 (Naph_d), 37.7 (Naph_c), 28.0 (Naph_b , Naph_e).



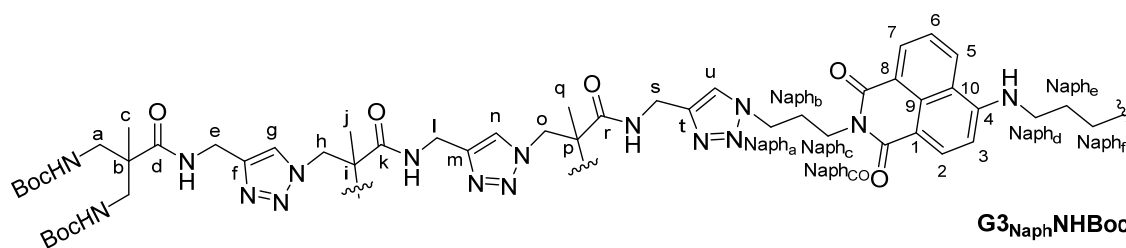
27.9 (Naph_b, Naph_e). **HRMS** calcd. for C₁₈H₁₉N₈O₂⁻ 379.1631 [M + H]⁺, found: 379.1625.

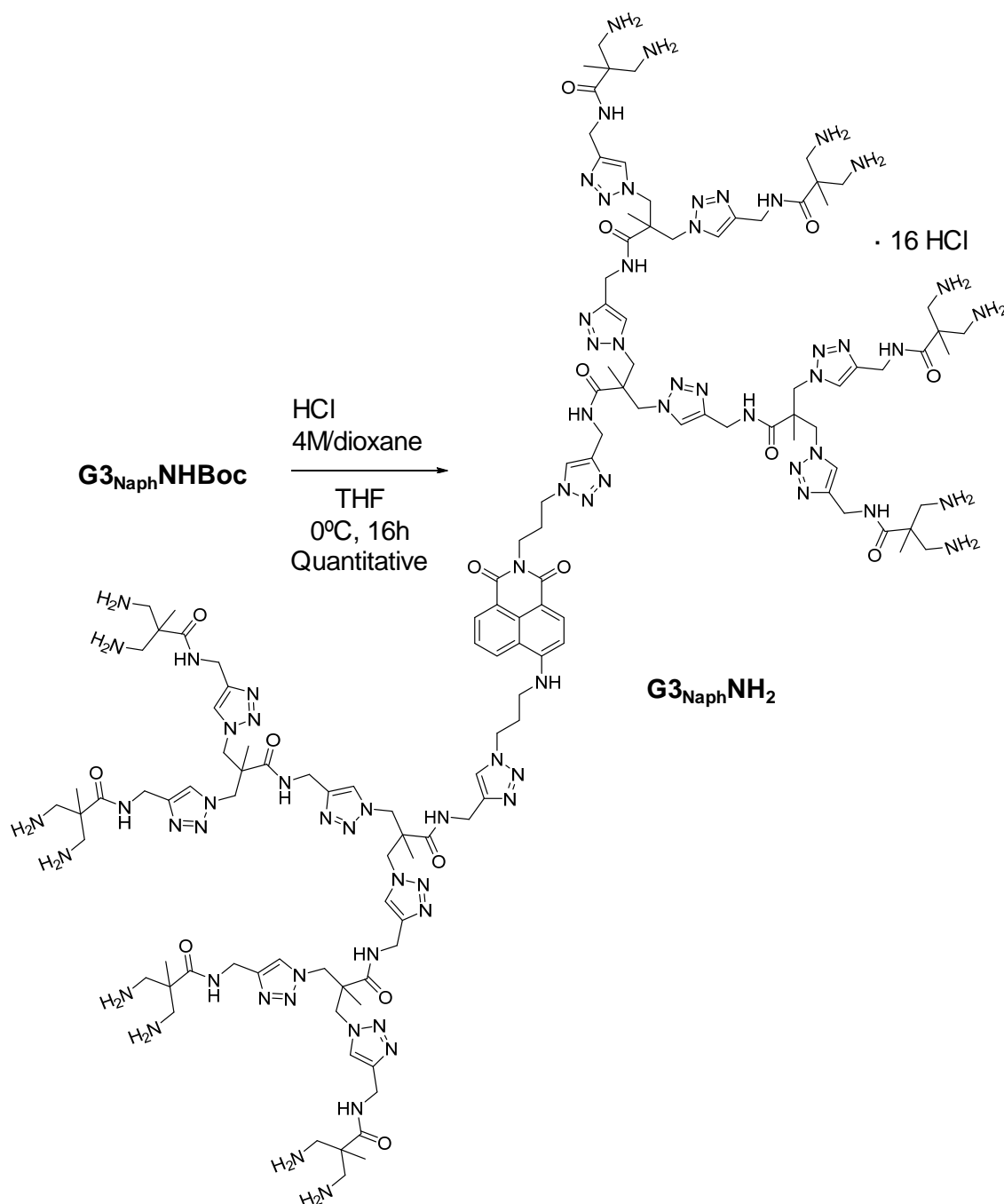
Synthesis of G₃NaphNHBoc



This compound was obtained from **dG3** (179 mg, 0.084 mmol, 2.2 eq), **10** (14 mg, 0.04 mmol, 1 eq), copper (II) sulphate 5-hydrate (0.2 mg, 0.001 mmol, 0.02 eq) and L(+)-ascorbic acid sodium salt (2 mg, 0.01 mmol, 0.1 eq) in tert-butanol/water 1:2 (6 mL) to obtain the product (107 mg, 0.02 mmol, 58 %) as a yellow solid (compound decomposes above 126 °C). **¹H NMR** (400 MHz, DMSO-

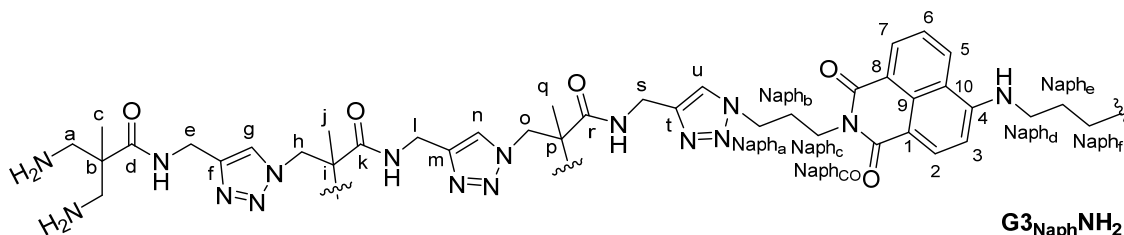
d_6) δ ppm: 8.14-7.59 (m, 19 H, H_g, H_n, H_u, H₃, H₄, H₆, H₇, H₈), 4.77-4.04 (m, 56 H, H_e, H_h, H_i, H_o, H_s, Naph_a, Naph_f), 3.52 (s, 2H, Naph_c), 3.21-2.94 (m, 34 H, H_a, Naph_d), 2.34-2.15 (m, 2 H, Naph_b), 2.01-1.83 (m, 2 H, Naph_e) 1.35 (s, 144 H, BocCH₃), 1.08-0.88 (m, 42 H, H_c, H_j, H_q). ^{13}C NMR (100 MHz, DMSO- d_6) δ ppm: 174.2 (C_d), 172.4 (C_k, C_r), 171.5 (C_k, C_r), 163.9 (Naph_{co}), 163.1 (Naph_{co}), 156.2 (BocCO), 150.7 (C₄), 145.1 (C_f, C_m, C_t), 145.0 (C_f, C_m, C_t), 144.9 (C_f, C_m, C_t), 134.3 (C₂), 130.8 (C₇), 129.5 (C₉), 129.0 (C_g, C_n, C_u), 128.9 (C_g, C_n, C_u), 128.3 (C_g, C_n, C_u), 124.3 (C₅), 124.0 (C₆), 121.9 (C₁, C₈), 120.3 (C₁, C₈), 107.9 (C₁₀), 103.8 (C₃), 78.0 (BocC), 53.9 (C_h, C_o), 53.5 (C_h, C_o), 48.9 (Naph_a, Naph_f), 48.6 (Naph_a, Naph_f), 48.4 (C_b, C_i, C_p), 48.0 (C_b, C_i, C_p), 47.7 (C_b, C_i, C_p), 44.4 (C_a), 37.0 (Naph_d), 35.6 (Naph_c), 34.9 (C_e, C_l, C_s), 34.6 (C_e, C_l, C_s), 34.6 (C_e, C_l, C_s), 28.2 (BocCH₃), 27.2 (Naph_b, Naph_e), 27.2 (Naph_b, Naph_e), 18.5 (C_c, C_j, C_q), 17.7 (C_c, C_j, C_q), 17.6 (C_c, C_j, C_q).



Synthesis of **G3_{Naph}NH₂**

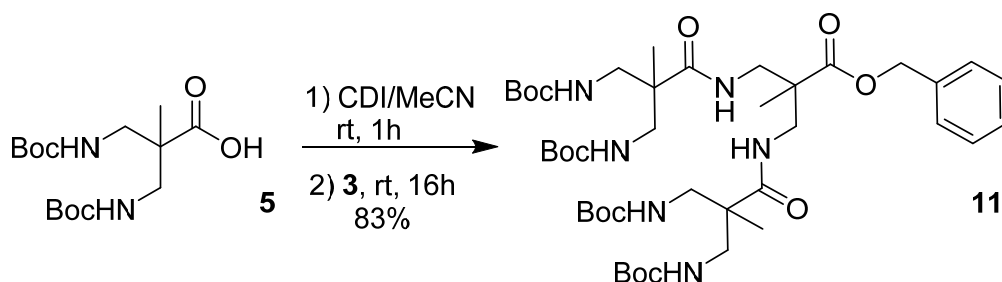
This compound was obtained from **G3_{Naph}NHBoc** (67 mg, 0.014mmol) to obtain the product (50 mg, 0.014 mmol, 98 %) as a yellow solid. **¹H NMR** (400 MHz, D₂O) δ ppm: 8.05-7.62 (m, 19 H, H_g, H_n, H_u, H₃, H₄, H₆, H₇, H₈), 4.65-4.23 (m, 44 H, H_e, H_h, H_l, H_s), 3.75 (d, J = 13.6 Hz, 4 H, H_o), 3.66 (d, J = 11.6 Hz, 4 H, H_o), 3.60-3.49 (m, 6 H, Naph_a, Naph_c, Naph_f), 3.41 (d, J = 13.2 Hz, 16 H, H_a), 3.20 (d, J = 10.1 Hz, 16 H, H_a), 3.11-2.89 (m, 6 H, Naph_b, Naph_d, Naph_e), 1.46 (s, 24 H, H_c), 1.16 (s, 12 H, H_j), 1.00 (s, 6H, H_q). **¹³C NMR** (100 MHz, D₂O) δ ppm:

172.64 (C_d), 172.57 (C_k, C_r), 172.3 (C_k, C_r), 143.02 (C_f, C_m, C_t), 143.05 (C_f, C_m, C_t), 143.11 (C_f, C_m, C_t), 124.7 (C_g, C_n, C_u, C₅, C₆), 124.5 (C_g, C_n, C_u, C₅, C₆), 124.2 (C_g, C_n, C_u, C₅, C₆), 124.1 (C_g, C_n, C_u, C₅, C₆), 123.9 (C_g, C_n, C_u, C₅, C₆), 54.7 (C_h), 54.2 (Naph_a, Naph_f), 53.3 (Naph_a, Naph_f), 48.1 (C_b, C_i, C_p), 48.0 (C_b, C_i, C_p), 43.8 (C_b, C_i, C_p), 42.97 (C_a, C_o), 42.91 (C_a, C_o), 34.0 (C_e, C_l, C_s), 33.9 (C_e, C_l, C_s), 33.8 (C_e, C_l, C_s), 17.0 (C_c, C_j, C_q), 16.5 (C_c, C_j, C_q), 15.9 (C_c, C_j, C_q). UV (H₂O): λ_{max} nm (ϵ , cm⁻¹ M⁻¹): 190 (91974), 259 (4709), 284 (4125), 447 (3209).

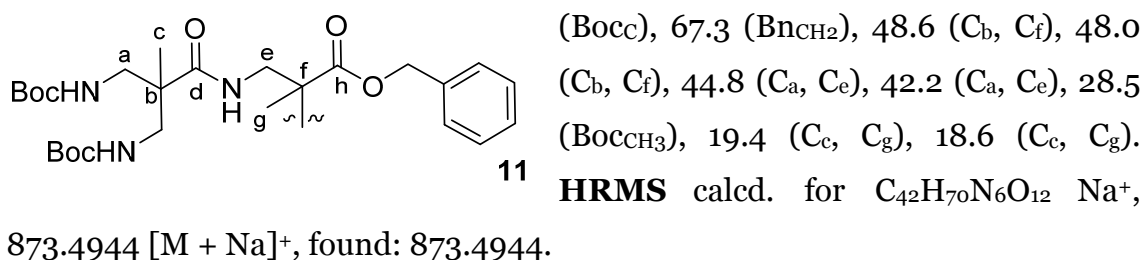


VII.4 Synthesis of platinum-doped dendritic structure

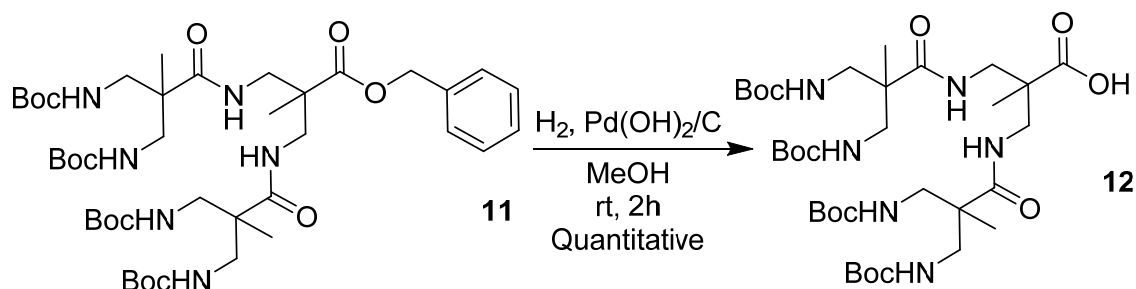
Synthesis of compound 11



A solution of **5** (644 mg, 1.94 mmol, 2 eq) in anhydrous acetonitrile (3 mL) was added to a solution of CDI (315 mg, 1.94 mmol, 2 eq) in anhydrous acetonitrile (3 mL) and the mixture was stirred at room temperature for one hour. Afterwards, a solution of **3** (215 mg, 0.96 mmol, 1 eq) was added and the stirring mixture was left for 16 hours at room temperature. The solvent was removed under vacuum and the residue was dissolved in dichloromethane (40 mL) and washed with HCl 0.05M (3 × 30 mL). The combined organic phase was dried with MgSO₄, filtered and concentrated under reduced pressure to obtain the product (678 mg, 0.78 mmol, 83%) as a colorless solid. ¹H NMR (400 MHz, CDCl₃, δ): 7.40–7.29 (m, 5 H, Bn_{CH}), 5.14 (s, 2 H, Bn_{CH2}), 3.51–3.06 (m, 12 H, H_a, H_e), 1.42 (s, 36 H, BocCH₃), 1.17–1.05 (m, 9 H, H_c, H_g). ¹³C NMR (100 MHz, CDCl₃, δ): 174.9 (C_h), 157.2 (BocCO), 130.1 (Bn_c), 128.8 (Bn_{CH}), 128.6 (Bn_{CH}), 128.5 (Bn_{CH}), 79.6

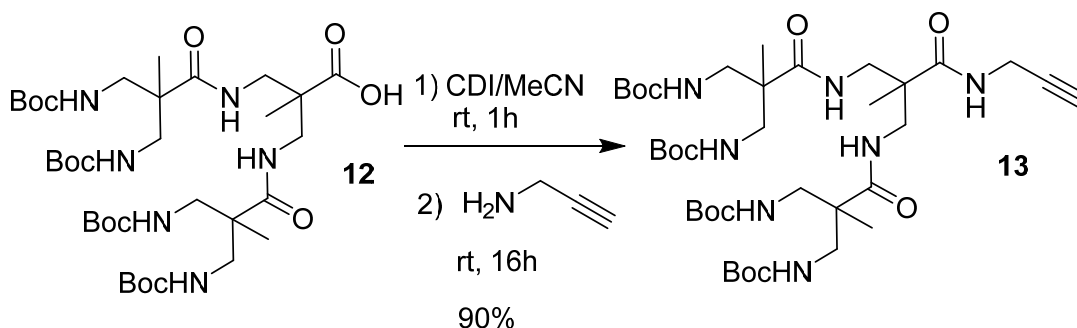


Synthesis of compound 12



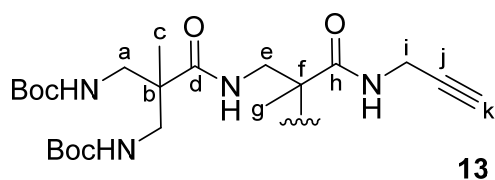
To a solution of **11** (515 mg, 0.61 mmol) in methanol (10 mL), Pearlman's catalyst (60 mg, 0.44 mmol) is added. After hydrogenation for two hours, the catalyst was removed by filtration through MeOH-pre-wetted celite. The solvent was removed under vacuum to obtain **12** (460 mg, 98%) as a colorless solid. **¹H NMR** (400 MHz, MeOD-*d*₄, δ): 3.48-3.20 (m, 12 H, H_a, H_e), 1.44 (s, 36 H, BocCH₃) 1.18-1.03 (m, 9 H, H_c, H_g). **¹³C NMR** (100 MHz, MeOD-*d*₄, δ): 177.5 (C_d, C_h), 158.7 (BocCO), 80.3 (BocC), 49.8 (C_b, C_f), 46.0 (C_a, C_e), 45.3 (C_a, C_e), 43.7 (C_b, C_f), 28.8 (BocCH₃), 20.3 (C_c, C_g), 19.5 (C_c, C_g). **HRMS** calcd. for C₃₅H₆₄N₆O₁₂Na⁺, 783.4474 [M + Na]⁺, found: 783.4481.

Synthesis of compound 13



Compound **12** (402 mg, 0.53 mmol, 1 eq) was dissolved in anhydrous acetonitrile (3 mL). Afterwards, a solution of CDI (97 mg, 0.6 mmol, 1.1 eq) in anhydrous acetonitrile (3 mL) was added and the mixture was stirred at room

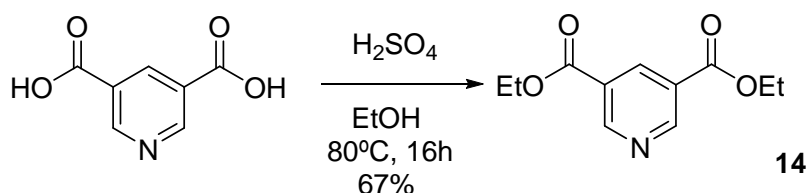
temperature for one hour. Propargylamine (40 μ L, 0.6 mmol, 1.1 eq) was then added and the stirring mixture was left for 16 hours at room temperature. The solvent was removed under vacuum and the residue was dissolved in dichloromethane (40 mL) and washed with HCl 0.05M (3 \times 30 mL). The organic phase was dried over MgSO₄, filtered and concentrated under reduced pressure to obtain the product (381 mg, 0.48 mmol, 90%) as a colorless solid. **¹H NMR** (400 MHz, DMSO-*d*₆) δ : 3.85-3.75 (m, 2 H, H_i), 3.23-2.84 (m, 13 H, H_a, H_e, H_k),



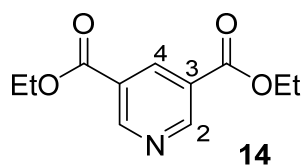
1.36 (s, 36 H, BocCH₃), 1.07-0.91 (m, 9 H, H_c, H_g). **¹³C NMR** (100 MHz, DMSO-*d*₆) δ ppm: 180.8 (C_d, C_h), 156.1 (BocCO), 77.9 (BocC), 77.51 (C_j), 72.8 (C_k), 47.9 (C_b, C_f), 46.7 (C_b, C_f), 44.6 (C_a, C_e), 42.3 (C_a, C_e), 28.2 (C_i), 28.1 (BocCH₃), 19.1 (C_c, C_g), 18.4 (C_c, C_g).

HRMS calcd. for C₃₈H₆₈N₇O₁₁⁺ 798.4971 [M + H]⁺, found 798.4970.

Synthesis of 3,5-bis(ethoxycarbonyl)pyridine (**14**)

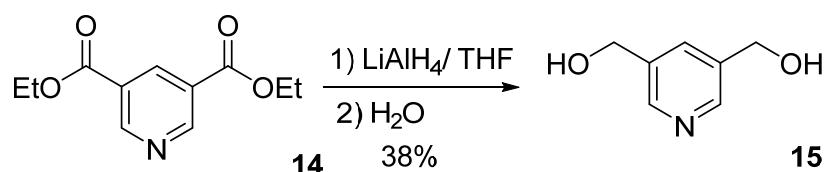


Compound **14** was synthesized as described.²¹³ Concentrated sulfuric acid (24 mL, 96%) was introduced dropwise into a solution of 3,5-Pyridine Dicarboxylic Acid (12g, 72 mmol) in 150 mL absolute ethanol. After 16h reflux, ethanol was evaporated under vacuum. 60 mL of ice water was poured into reaction mixture, which was then neutralized with Na₂CO₃ 1M (35 mL) until pH=10. The aqueous phase was extracted with diethyl ether (5 \times 80 mL). The organic phases were mixed, concentrated, and dried with anhydrous MgSO₄. After removal of diethyl ether and drying under vacuum, **14** was obtained as a yellow oil (10.8 g, 48.2 mmol, 67%). **¹H NMR** (400 MHz, DMSO-*d*₆) δ : 9.36 (d,

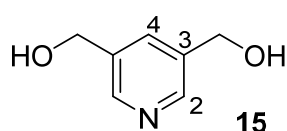


$J = 2.1$ Hz, 2 H, H₂), 8.86 (t, $J = 2.1$ Hz, 1 H, H₄), 4.45 (q, $J = 7.1$ Hz, 4 H, CH₂-CH₃), 1.43 (t, $J = 7.1$ Hz, 6 H, CH₂-CH₃).

Synthesis of 3,5-bis(hydroxymethyl)pyridine (**15**)

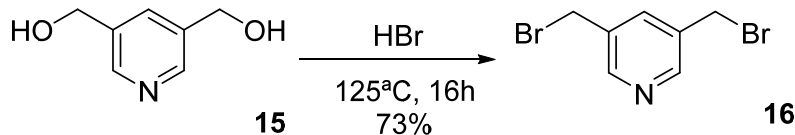


Compound **15** was synthesized as described.²¹³ A solution of **14** (4 g, 18 mmol, 1 eq) in THF (20 mL) was added dropwise under vigorous stirring to a suspension of LiAlH₄ (2.3 g, 59 mmol, 3.3 eq) in THF (100 mL) under a nitrogen stream. Afterwards, 30 mL of water was slowly added in order to hydrolyze LiAlH₄ excess. The white pastry precipitate was filtered, and the filtrate was evaporated under vacuum. **15** was purified by column chromatography with dichloromethane/methanol (9:1) to obtain the product as a colorless oil (960 mg,

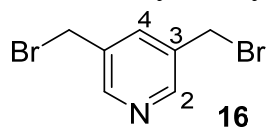


6.9 mmol, 38%). ¹H NMR (400 MHz, DMSO-*d*₆) δ: 8.38 (d, *J* = 1.8 Hz, 2 H, H₂), 7.68-7.64 (m, 1 H, H₄), 4.53 (d, *J* = 5.7 Hz, 4 H, CH₂-OH).

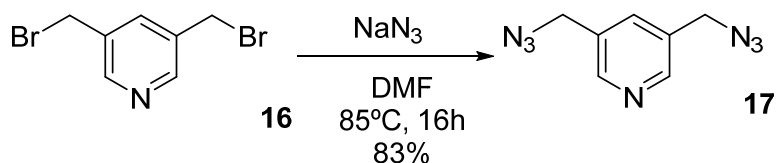
Synthesis of 3,5-bis(bromomethyl)pyridine (**16**)



Compound **16** was synthesized as described.²¹³ Compound **15** (960 mg, 6.90 mmol) was added in 10 mL of 60% aqueous HBr. The mixture was heated at 125 °C for 16 hours and then cooled to room temperature. The resulting residue was dissolved in H₂O (50 mL) to give a yellow solution. To this solution was added Na₂CO₃ to pH 8. The resulting aqueous solution was extracted with CH₂Cl₂ (4 x 50 mL), and the combined organic layers were dried over MgSO₄. The solvent was removed by rotary evaporation to obtain **16** as an oil (1.3 g, 5.0 mmol, 73%). ¹H



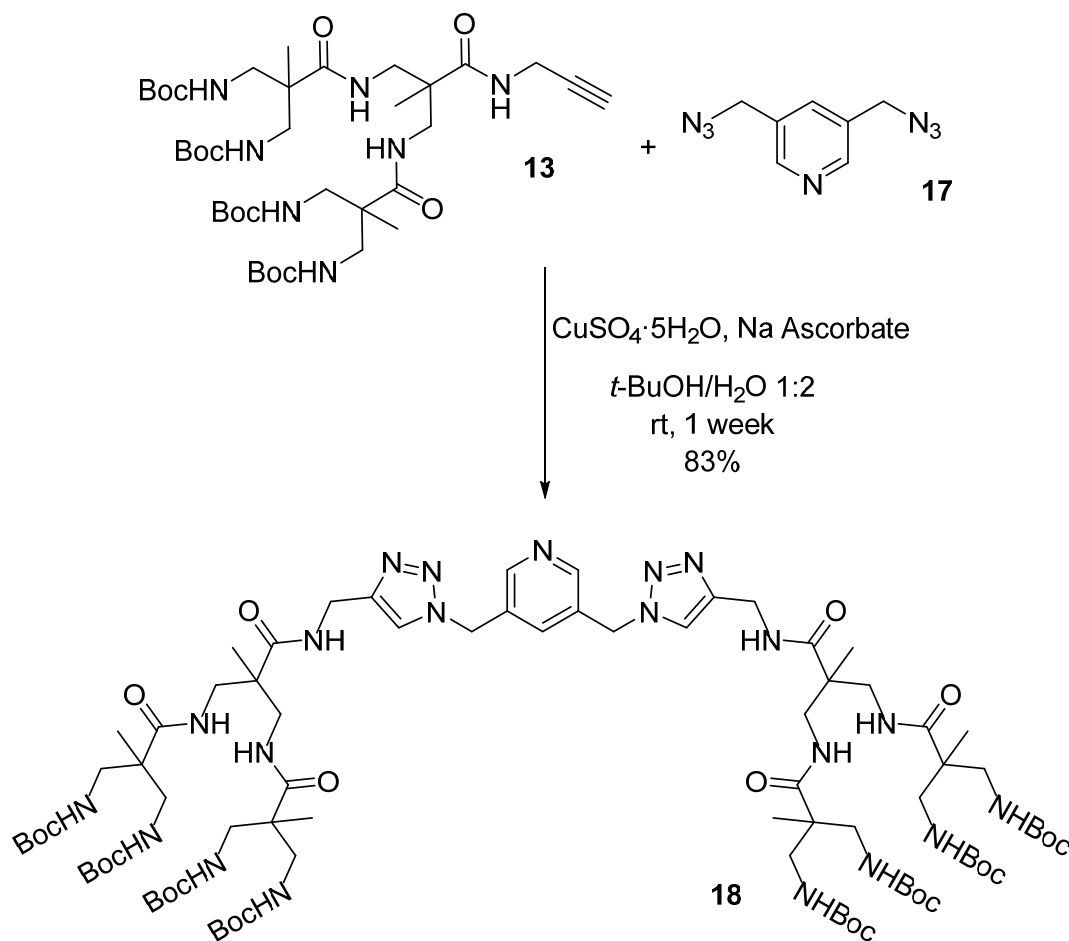
NMR (400 MHz, CDCl₃) δ: 8.54 (d, *J* = 1.8 Hz, 2 H, H₂), 7.76-7.74 (m, 1 H, H₄), 4.45 (s, 4 H, CH₂-Br).

Synthesis of 3,5-bis(azidomethyl)pyridine (**17**)

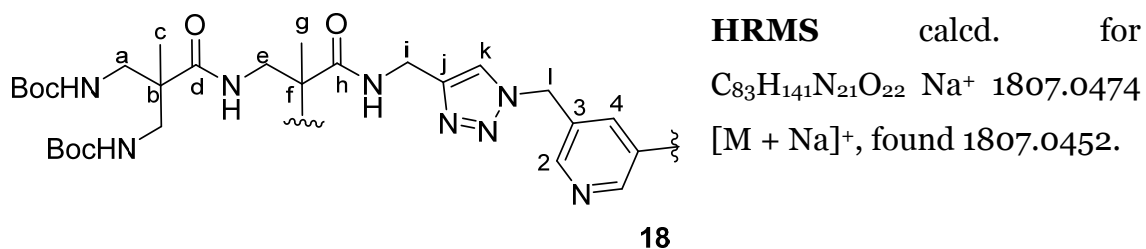
Sodium Azide (429 mg, 6.6 mmol, 5 eq) was added to a solution of **16** (343 mg, 1.3 mmol, 1 eq) in DMF (5 mL). The mixture was heated at 85°C for 16 hours and then cooled to room temperature. H₂O (80 mL) was added and the resulting aqueous solution was extracted with CH₂Cl₂ (5 x 25 mL). The combined organic layers were dried over MgSO₄. The solvent was removed by rotary evaporation to obtain **17** (145 mg, 0.77 mmol, 58%) as a brown oil. **¹H NMR** (400 MHz, CDCl₃)

17 δ: 8.56 (d, *J* = 1.9 Hz, 2 H, H₂), 7.67-7.63 (m, 1 H, H₄), 4.44 (s, 4 H, CH₂). **¹³C NMR** (100 MHz, CDCl₃) δ: 149.3 (C₂), 135.4 (C₄), 131.6 (C₃), 52.0 (CH₂). **HRMS** calcd. for C₇H₈N₇⁺ 190.0836 [M + H]⁺, found 190.0836.

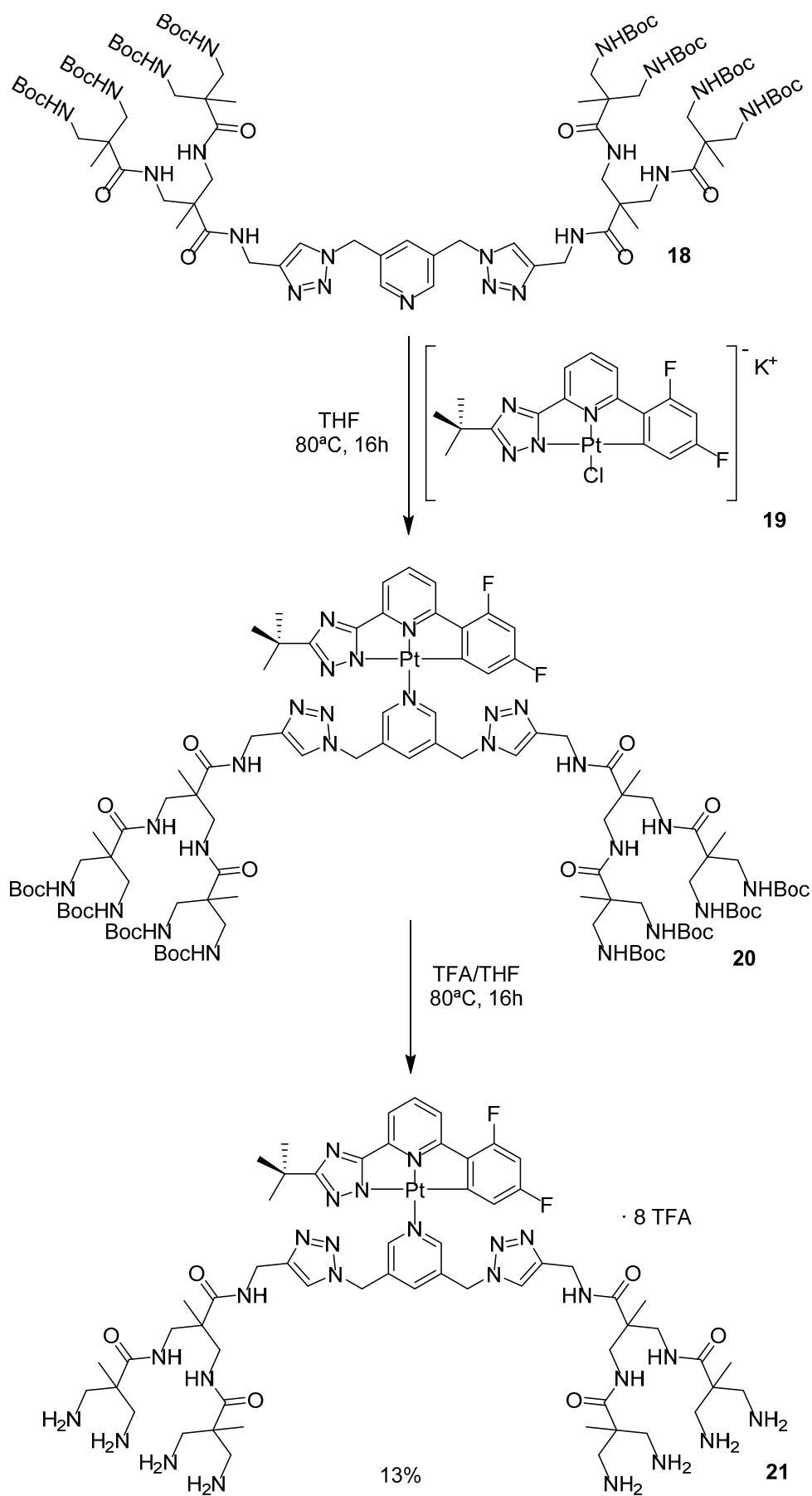
Synthesis of compound 18



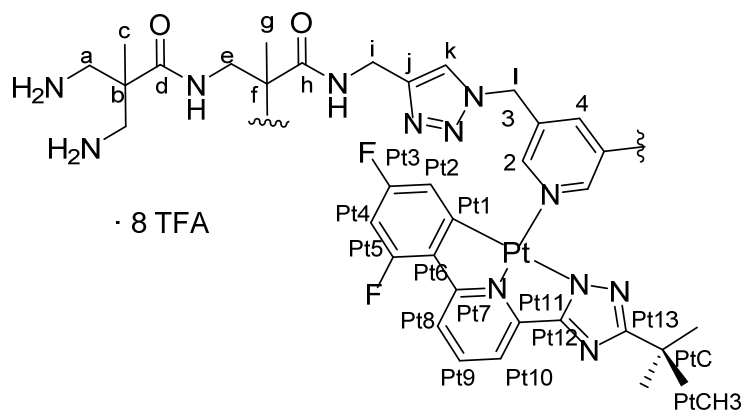
This compound was obtained from **17** (30 mg, 0.16 mmol, 1 eq), **13** (250 mg, 0.31 mmol, 2 eq), copper (II) sulphate 5-hydrate (4 mg, 0.016 mmol, 0.02 eq) and L(+)-ascorbic acid sodium salt (13 mg, 0.064 mmol, 0.1 eq) in *tert*-butanol/water 1:2 (9 mL) to obtain the desired product (234 mg, 0.13 mmol, 83%) as a colorless solid. **¹H NMR** (400 MHz, DMSO-*d*₆) δ : 8.54 - 7.97 (m, 5 H, H_k, H₂, H₄), 5.61 (s, 4 H, H_l), 4.33-4.25 (m, 4 H, H_i), 3.61-3.45 (m, 4 H, H_e), 3.20 - 2.83 (m, 20 H, H_a, H_e), 1.35 (s, 72 H, BocCH₃), 1.09-0.91 (m, 18 H, H_c, H_g). **¹³C NMR** (100 MHz, DMSO-*d*₆) δ : 174.8 (C_d, C_h), 174.6 (C_d, C_h), 156.1 (BocCO), 149.0 (C_k), 145.5 (C₃), 135.6 (C₂, C₄), 131.7 (C_j), 123.1 (C₂, C₄), 77.9 (BocC), 50.0 (C_i), 47.9 (C_b), 46.7 (C_f), 44.6 (C_a), 42.4 (C_e), 34.8 (C_i), 28.1 (BocCH₃), 19.2 (C_c, C_g), 18.5 (C_c, C_g).



Synthesis of compound 21

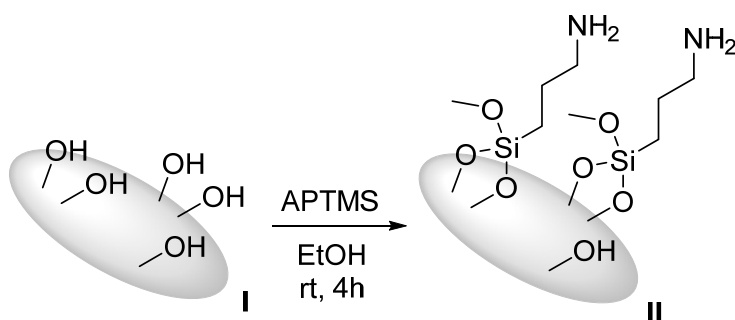


Compound **18** (50 mg, 0.028 mmol) and **19**²⁰² (16 mg, 0.028 mmol) were dissolved in THF (10 mL) and heated at reflux for 16 hours. The solvent was removed under vacuum and the residue was dissolved in ethyl acetate (30 mL) and washed with water (3 × 30 mL). The organic phase was dried over MgSO₄ and the solvent was removed. The obtained compound was dissolved in dry THF (5 mL) and the solution was cooled in an ice-water bath. TFA (2 mL) was added dropwise and the mixture was stirred for 16 hours. Afterwards, the solvent was evaporated under vacuum. The residue was dissolved in ethyl acetate (10 mL) and extracted with water (3 × 10 mL). The aqueous phase was lyophilized, and the remains were purified by sephadex column to obtain **21** as ammonium salt (9 mg, 13%). **¹H NMR** (600 MHz, D₂O) δ : 9.00-7.68 (m, 10 H, H_k, H₂, H₄, Pt_{Ar}), 5.69 (s, 4 H, H_l), 4.44 (s, 4 H, H_i), 3.80-2.95 (m, 24 H, H_a, H_e), 1.65-0.99 (m, 27 H, H_c, H_g, Pt_{CH3}). **¹³C NMR** (100 MHz, D₂O) δ : 175.3 (C_d, C_h), 172.4 (C_d, C_h), 162.3 (Pt₃, Pt₅), 161.9 (Pt₃, Pt₅), 150.1 (Pt₇, Pt₁₁), 148.4 (C_k, Pt₉, Pt₁₂, Pt₁₃), 147.4 (C_k, Pt₉, Pt₁₂, Pt₁₃), 144.04 (C₃, Pt₉, Pt₁₂, Pt₁₃), 143.97 (C₃, Pt₉, Pt₁₂, Pt₁₃), 136.1 (C₂, C₄), 130.8 (C_j), 123.57 (C₂, C₄, Pt₁, Pt₆, Pt₈, Pt₁₀), 123.55 (C₂, C₄, Pt₁, Pt₆, Pt₈, Pt₁₀), 119.9 (Pt₁, Pt₆, Pt₈, Pt₁₀), 117.0 (Pt₁, Pt₆, Pt₈, Pt₁₀), 114.1 (Pt₁, Pt₆, Pt₈, Pt₁₀), 111.2 (Pt₂), 107.9 (Pt₄), 50.1 (C_l), 43.6 (C_a, C_b, C_e, C_f, Pt_C), 43.4 (C_a, C_b, C_e, C_f, Pt_C), 43.3 (C_a, C_b, C_e, C_f, Pt_C), 42.8 (C_a, C_b, C_e, C_f, Pt_C), 42.7 (C_a, C_b, C_e, C_f, Pt_C), 33.8 (C_i), 28.3 (Pt_{CH3}), 16.8 (C_c, C_g), 16.4 (C_c, C_g). **UV** (H₂O): λ_{max} nm (ϵ , cm⁻¹M⁻¹): 247 (10363), 320 (3246).



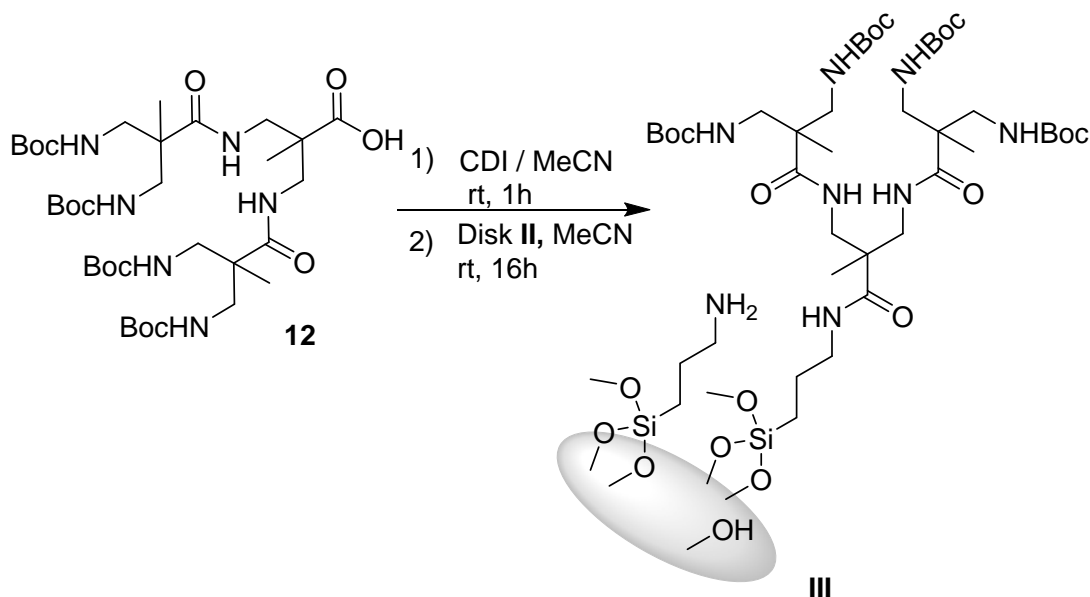
VII.5 Functionalization of titanium surfaces

Preparation of Ti-disk (II)



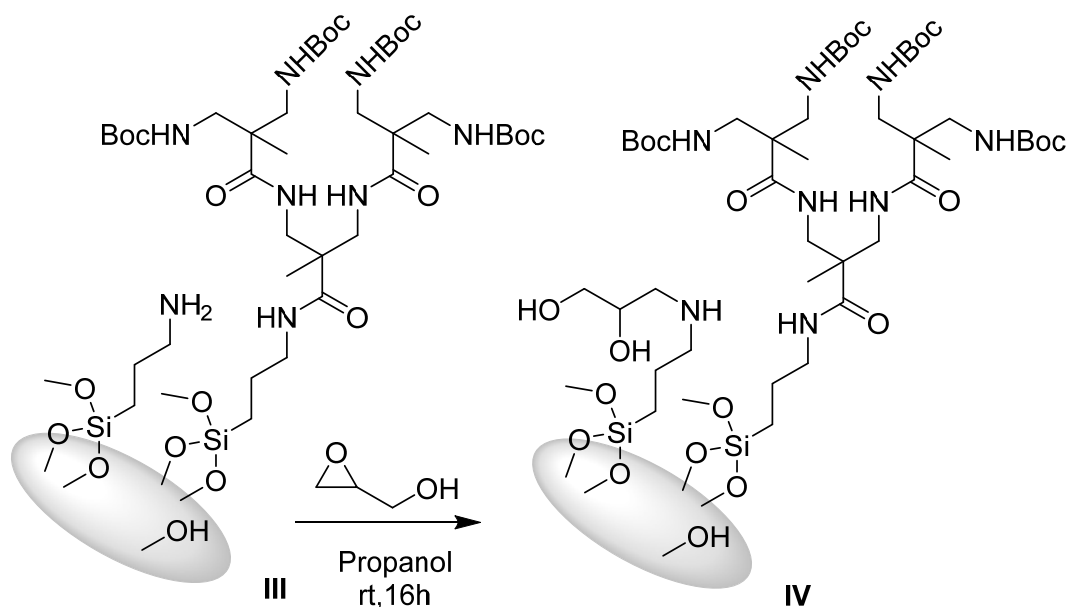
The disks were immersed in a solution of (3-Aminopropyl)trimethoxysilane in ethanol 1:3 v/v (100 mL) and were placed in an orbital agitator for four hours. Afterwards, the disks were washed with ethanol.

Preparation of Ti-disk (III)



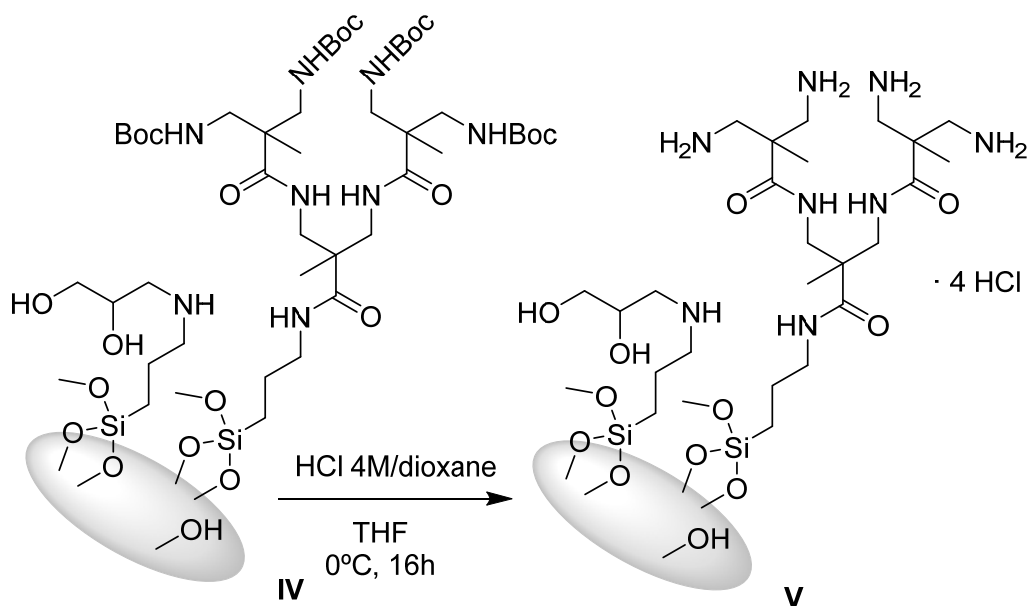
A solution of **12** (30 mg, 0.04 mmol, 1 eq) in anhydrous acetonitrile (2 mL) was added to a solution of CDI (7 mg, 0.04 mmol, 1 eq) in anhydrous acetonitrile (2 mL) and the mixture was stirred at room temperature for one hour. The disks (**II**) were immersed in anhydrous acetonitrile and the mixture was added. They were placed in an orbital agitator for 16 hours. Afterwards, they were washed with ethanol.

Preparation of Ti-disk (IV)



The disks (**III**) were immersed in a solution of glycidol (5 μ L, 6.5×10^{-2} mmol, 1000 eq) in 2-propanol (60 mL) and placed in an orbital agitator for 16 hours. Afterwards the disks were washed with 2-propanol and dichloromethane.

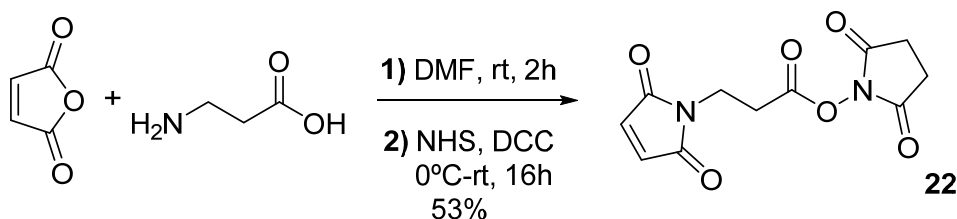
Preparation of Ti-disk (V)



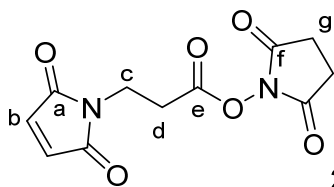
The disks (**IV**) were immersed in a solution of hydrochloric acid 4 M in dioxane/THF 1:1 (20 mL) and were placed in an orbital agitator for two hours under nitrogen atmosphere. Afterwards, they were washed with THF and

immersed in a solution of sodium hydroxide 10% for one hour. The disks were washed with acetone.

Synthesis of 3-maleimidopropionic acid *N*-hydroxysuccinimide ester (**22**)

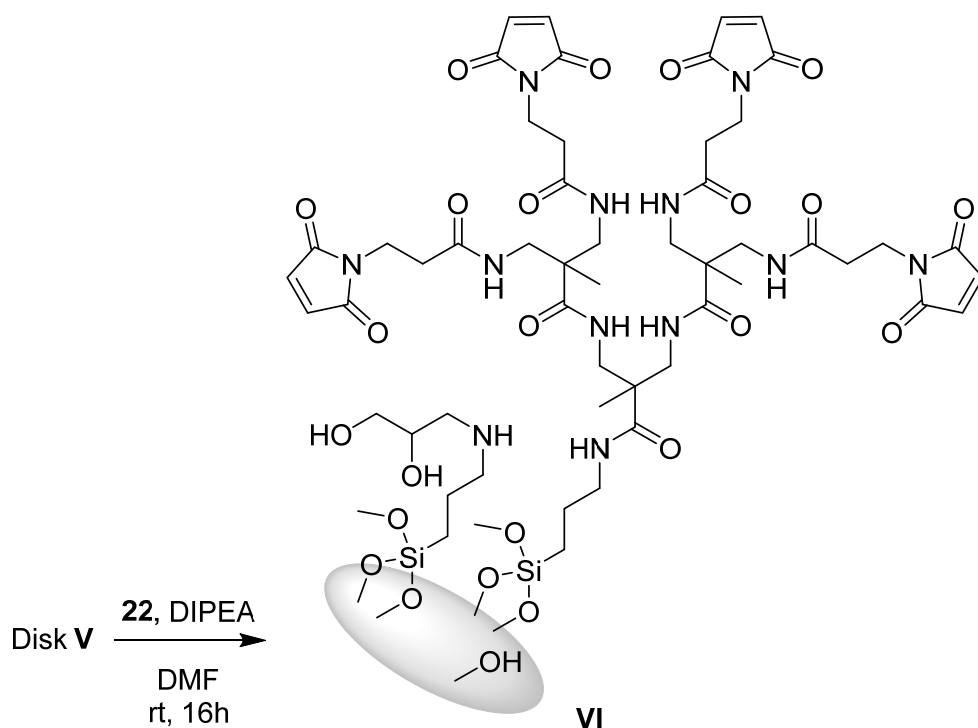


Compound **22** was synthesized as described.²⁶⁵ β -alanine (2.0 g, 22.4 mmol, 1 eq) was added to a solution of maleic anhydride (2.2 g, 22.4 mmol, 1 eq) in DMF (25 mL) and the mixture was left stirring at room temperature for two hours. Afterwards, it was introduced in an ice-cooled bath. NHS (3.2 g, 27.5 mmol, 1.2 eq) and DCC (9.5 g, 46.2 mmol, 2 eq) were added and the mixture was left stirring at room temperature for 16 hours. Urea by-product was removed by filtration. Compound **22** was obtained as a colorless solid (3.2 g, 11.9 mmol, 53%) after precipitation with cold water. ¹H NMR (400 MHz, DMSO-*d*₆) δ ppm: 7.04



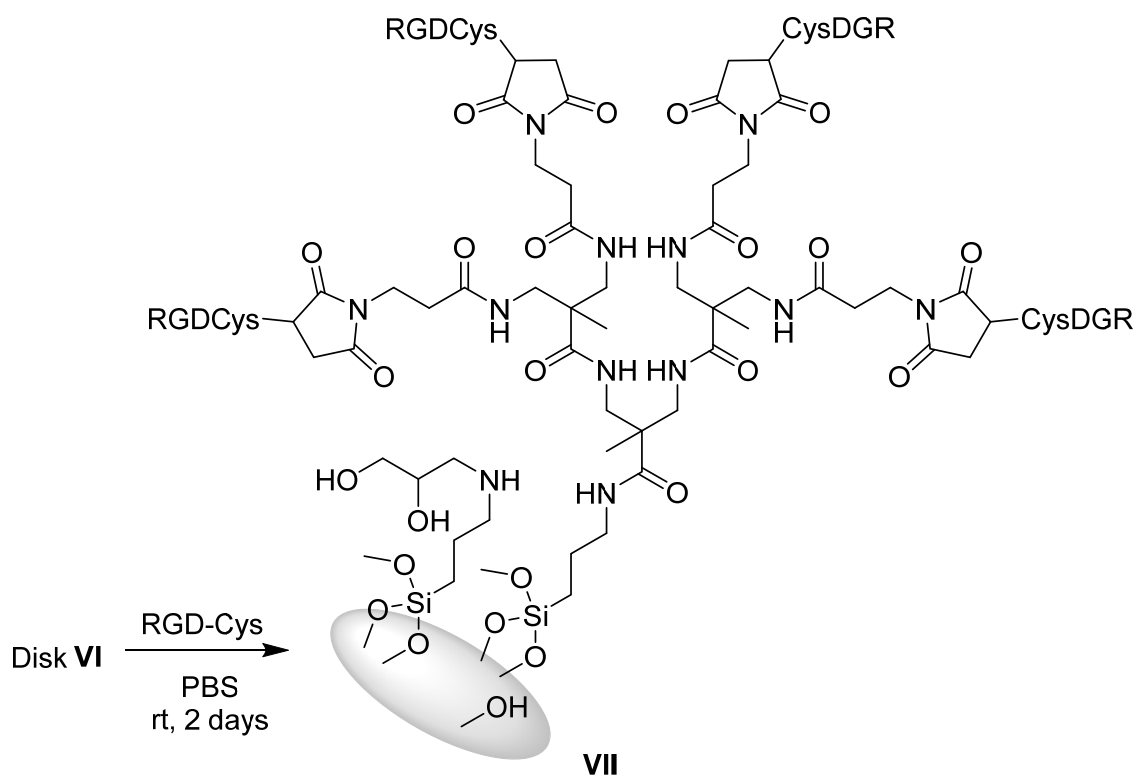
(s, 2 H, H_b), 3.74 (t, *J* = 6.9 Hz, 2H, H_c), 3.04 (t, *J* = 6.9 Hz, 2 H, H_d), 2.79 (s, 4 H, H_g). ¹³C NMR (100 MHz, DMSO-*d*₆, δ): 170.5 (C_a), 169.9 (C_f), 166.7 (C_e), 134.7 (C_b), 32.7 (C_c), 29.0 (C_d), 25.4 (C_g).

Preparation of Ti-disk (VI)



The disks were immersed (**V**) in an ice-cooled solution of *N,N*-Diisopropylethylamine (DIPEA) (3 mL, 1000 eq) in DMF (60 mL). A solution of **22** (50 mg, 1000 eq) in DMF (3 mL) was added and the disks were placed in an orbital agitator for 16 hours. The disks were washed with DMF and acetone. **XPS** analysis (%): C 1s (38.32), O 1s (32.03), Ti 2p (12.94), N 1s (10.64, Si 2p (6.08).

Preparation of Ti-disk (VII)



A solution of RGD-Cys (2 mg, 4.4 eq) in PBS (10 mL) was added to the disks (VI). They were placed in an orbital agitator for two days under argon atmosphere. Afterwards, the discs were washed with PBS, water and acetone. **XPS** analysis (%): C 1s (29.21), O 1s (37.72), Ti 2p (13.45), N 1s (8.22), Si 2p (7.23), S 2p (4.17).

CHAPTER VIII

REFERENCES

VIII. References

- (1) Mandelbrot, B. B. *The Fractal Geometry of Nature*.; W. H. Freeman and Company, Ed.; San Francisco, 1982.
- (2) Vögtle, F.; Richardt, G.; Werner, N. *Dendrimer Chemistry*; 2009.
- (3) Caminade, A.; Yan, D.; Smith, D. K. Dendrimers and Hyperbranched Polymers. *Chem. Soc. Rev.* **2015**, *44*, 3870–3873.
- (4) Cardona, C. M.; Kaifer, A. E. Asymmetric Redox-Active Dendrimers Containing a Ferrocene Subunit. Preparation, Characterization, and Electrochemistry [5]. *J. Am. Chem. Soc.* **1998**, *120* (16), 4023–4024.
- (5) Astruc, D.; Boisselier, E.; Ornelas, C. Dendrimers Designed for Functions: From Physical, Photophysical, and Supramolecular Properties to Applications in Sensing, Catalysis, Molecular Electronics, Photonics, and Nanomedicine. *Chem. Rev.* **2010**, *110* (4), 1857–1959.
- (6) Tomalia, D. A.; Baker, H.; Dewald, J.; Hall, M.; Kallos, G.; Martin, S.; Roeck, J.; Ryder, J.; Smith, P. A New Class of Polymers: Starburst-Dendritic Macromolecules. *Polymer Journal*. 1985, pp 117–132.
- (7) Miller, T. M.; Neenan, T. X. Convergent Synthesis of Monodisperse Dendrimers Based upon 1,3,5-Trisubstituted Benzenes. *Chem. Mater.* **1990**, *2* (4), 346–349.
- (8) Hu, Q. S.; Pugh, V.; Sabat, M.; Pu, L. Structurally Rigid and Optically Active Dendrimers. *J. Org. Chem.* **1999**, *64* (20), 7528–7536.
- (9) Gennes, P. G. De; Hervet, H. Statistics of “Starburst” Polymers. *J. Phys. Lettres* **1983**, *44* (9), 351–360.
- (10) Flory, P. J. Molecular Size Distribution in Three Dimensional Polymers. I. Gelation. *J. Am. Chem. Soc.* **1941**, *63*, 3083–3090.
- (11) Flory, P. J. Molecular Size Distribution in Three Dimensional Polymers. II. Trifunctional Branching Units. *J. Am. Chem. Soc.* **1941**, *63*, 3091–3096.
- (12) Flory, P. J. Molecular Size Distribution in Three Dimensional Polymers. III. Tetrafunctional Branching Units. *J. Am. Chem. Soc.* **1941**, *63*, 3096–3100.
- (13) Stockmayer, W. H. Theory of Molecular Size Distribution and Gel Formation in Branched-Chain Polymers. *J. Chem. Phys.* **1943**, *11*, 45.
- (14) Stockmayer, W. H. Theory of Molecular Size Distribution and Gel Formation in Branched Polymers II. General Cross Linkings. *J. Chem. Phys.* **1944**, *12*, 125.
- (15) Buhleier, E.; Wehner, W.; Vögtle, F. “Cascade”- and “Nonskid-Chain-like” Syntheses of

Molecular Cavity Topologies. *Synthesis (Stuttg)*. **1978**, 2, 155–158.

- (16) Mühlaupt, C.; Wörner, R. Polynitril- Und Polyaminfunktionalisierte Poly(Trimethylenimin)-Dendrimere. *Angew. Chemie* **1993**, 105 (9), 1367–1370.
- (17) De Brabander-Van Den Berg, E. M. M.; Meijer, E. W. Poly(Propylenimin)-Dendrimere: Synthese in Größerem Maßstab Durch Heterogen Katalysierte Hydrierungen. *Angew. Chemie* **1993**, 105 (9), 1370–1372.
- (18) Denkwalter, R. G.; Kolc, J.; Lukasavage, W. J. Macromolecular Highly Branched Homogeneous Compound Based on Lysine Units. US 4289872, 1981.
- (19) Tomalia, D. A.; Baker, H.; Dewald, J.; Hall, M.; Kallos, G.; Martin, S.; Roeck, J.; Ryder, J.; Smith, P. Dendritic Macromolecules: Synthesis of Starburst Dendrimers. *Macromolecules* **1986**, 19 (9), 2466–2468.
- (20) Newkome, G. R.; Yao, Z.; Baker, G. R.; Gupta, V. K. Micelles. Part 1. Cascade Molecules: A New Approach to Micelles. A [27]-Arborol. *J. Org. Chem.* **1985**, 50 (11), 2003–2004.
- (21) Tomalia, D. A.; Naylor, A. M.; Goddard III, W. A. Starburst Dendrimers: Molecular-Level Control of Size, Shape, Surface Chemistry, Topology, and Flexibility from Atoms to Macroscopic Matter. *Angew. Chemie Int. Ed. English* **1990**, 29 (2), 138–175.
- (22) Hawker, C. J.; Frechet, J. M. J. Preparation of Polymers with Controlled Molecular Architecture. A New Convergent Approach to Dendritic Macromolecules. *J. Am. Chem. Soc.* **1990**, 112 (21), 7638–7647.
- (23) Xu, Z.; Moore, J. S. Synthesis and Characterization of a High Molecular Weight Stiff Dendrimer. *Angew. Chemie Int. Ed. English* **1993**, 32 (2), 246–248.
- (24) Percec, V.; Heck, J.; Tomazos, D.; Falkenberg, F.; Helen, B.; Ungar, G. Self-Assembly of Taper-Shaped Monoesters of Oligo(Ethylene Oxide) with 3,4,5-Tris(p-Dodecyloxybenzyloxy)Benzoic Acid and of Their Polymethacrylates into Tubular Supramolecular Architectures Displaying a Columnar Mesophase. *J. Chem. Soc. Perkin Trans. 1* **1993**, No. 22, 2799–2811.
- (25) Zimmerman, S. C.; Zeng, F.; Reichert, D. E.; Kolotuchin, S. V. Self-Assembling Dendrimers. *Science (80-.)*. **1996**, 271, 1095–1098.
- (26) Uchida, H.; Kabe, Y.; Yoshino, K.; Kawamata, A.; Kabe, Y.; Tsumuraya, T.; Masamune, S. General Strategy for the Systematic Synthesis of Oligosiloxanes. Silicone Dendrimers. *J. Am. Chem. Soc.* **1990**, 112 (19), 7077–7079.
- (27) Launay, N.; Caminade, A. -M; Lahana, R.; Majoral, J. -P. A General Synthetic Strategy for Neutral Phosphorus-Containing Dendrimers. *Angew. Chemie Int. Ed. English* **1994**, 33 (15–16), 1589–1592.
- (28) Tomalia, D. A.; Christensen, J. B.; Boas, U. *Dendrimers, Dendrons, and Dendritic*

- Polymers: Discovery, Applications, and the Future*, 1 edition.; Cambridge University Press, 2012.
- (29) Tomalia, D. A. Dendrons/Dendrimers: Quantized, Nano-Element like Building Blocks for Soft-Soft and Soft-Hard Nano-Compound Synthesis. *Soft Matter* **2010**, 6 (3), 456–474.
 - (30) Percec, V.; Dulcey, A. E.; Balagurusamy, V. S.; Miura, Y.; Smidrkal, J.; Peterca, M.; Nummelin, S.; Edlund, U.; Hudson, S. D.; Heiney, P. A.; et al. Self-Assembly of Amphiphilic Dendritic Dipeptides into Helical Pores. *Nature* **2004**, 430, 764–768.
 - (31) Ruiz-Sanchez, A. J.; Mesa-Antunez, P.; Barbero, N.; Collado, D.; Vida, Y.; Najera, F.; Perez-Inestrosa, E. Synthesis of All-Aliphatic Polyamide Dendrimers Based on a 3,3'-Diaminopivalic Acid Scaffold. *Polym. Chem.* **2015**, 6 (16), 3031–3038.
 - (32) Newkome, G. R.; Shreiner, C. D. Poly (Amidoamine), Polypropylenimine , and Related Dendrimers and Dendrons Possessing Different 1 → 2 Branching Motifs : An Overview of the Divergent Procedures. *Polymer (Guildf)*. **2008**, 49 (1), 1–173.
 - (33) Rosen, B. M.; Wilson, C. J.; Wilson, D. A.; Peterca, M.; Imam, M. R.; Percec, V. Dendron-Mediated Self-Assembly, Disassembly, and Self-Organization of Complex Systems. *Chem. Rev.* **2009**, 109 (11), 6275–6540.
 - (34) Mintzer, M. A.; Grinstaff, M. W. Biomedical Applications of Dendrimers: A Tutorial. *Chem. Soc. Rev.* **2011**, 40, 173–190.
 - (35) Jishkariani, D.; Macdermaid, C. M.; Timsina, Y. N.; Grama, S.; Gillani, S. S. Self-Interrupted Synthesis of Sterically Hindered Aliphatic Polyamide Dendrimers. *Proc. Natl. Acad. Sci. U. S. A.* **2017**, 114, E2275–E2284.
 - (36) *Dendrimers and Other Dendritic Polymers*, 1st ed.; Frechet, J. M. J., Tomalia, D. A., Eds.; John Wiley & Sons, Ltd, 2001; Vol. 1.
 - (37) Carlmark, A.; Hawker, C.; Malkoch, M.; Hawker, C. New Methodologies in the Construction of Dendritic Materials. *Chem. Soc. Rev.* **2009**, 38, 352–362.
 - (38) Grayson, S. M.; Frechet, J. M. J. Convergent Dendrons and Dendrimers : From Synthesis to Applications. *Chem. Rev.* **2001**, 101 (12), 3819–3867.
 - (39) Wooley, K. L.; Hawker, C. J.; Frechet, J. M. J. A "Branched-Monomer Approach" for the Rapid Synthesis of Dendimers. *Angew. Chemie Int. Ed. English* **1994**, 33 (1), 82–85.
 - (40) Ihre, H.; Hult, A.; Frechet, J. M. J.; Gitsov, I. Double-Stage Convergent Approach for the Synthesis of Functionalized Dendritic Aliphatic Polyesters Based on 2,2-Bis(Hydroxymethyl)Propionic Acid. *Macromolecules* **1998**, 31 (13), 4061–4068.
 - (41) Kawaguchi, T.; Walker, K. L.; Wilkins, C. L.; Moore, J. S. Double Exponential Dendrimer Growth. *J. Am. Chem. Soc.* **1995**, 117, 2159–2165.

- (42) Ihre, H.; Hult, A.; Soderlind, E. Synthesis, Characterization, and ^1H NMR Self-Diffusion Studies of Dendritic Aliphatic Polyesters Based on 2,2-Bis(Hydroxymethyl)Propionic Acid and 1,1,1-Tris(Hydroxyphenyl)Ethane. *J. Am. Chem. Soc.* **1996**, *118* (15), 6388–6395.
- (43) Wooley, K. L.; Hawker, C. J.; Fréchet, J. M. J. Polymers with Controlled Molecular Architecture: Control of Surface Function- Ality in the Synthesis of Dendritic Hyperbranched Macromolecules Using the Convergent Approach. *J. Chem. Soc. Perkin Trans. 1* **1991**, *74* (5), 1059–1076.
- (44) Hawker, C. J.; Fréchet, J. M. J. Unusual Macromolecula Architectures: The Convergent Growth Approach to Der Dritic Polyesters and Novel Block Copolymers. *J. Am. Chem. Soc.* **1992**, *114* (22), 8405–8413.
- (45) Wooley, K. L.; Hawker, C. J.; Fréchet, J. M. J. Unsymmetrical Three-Dimensional Macromolecules: Preparation and Characterization of Strongly Dipolar Dendritic Macromolecules. *J. Am. Chem. Soc.* **1993**, *115* (24), 11496–11505.
- (46) Maraval, V.; Laurent, R.; Donnadiou, B.; Mauzac, M.; Caminade, A.; Majoral, J. Rapid Synthesis of Phosphorus-Containing Dendrimers with Controlled Molecular Architectures: First Example of Surface-Block , Layer-Block , and Segment-Block Dendrimers Issued from the Same Dendron. *J. Am. Chem. Soc.* **2000**, *122* (11), 2499–2511.
- (47) Caminade, A.-M.; Laurent, R.; Delavaux-Nicot, B.; Majoral, J.-P. “Janus” Dendrimers: Syntheses and Properties. *New J. Chem.* **2012**, *36* (2), 217–226.
- (48) Crespo, L.; Sanclimens, G.; Pons, M.; Giralt, E.; Royo, M.; Albericio, F. Peptide and Amide Bond-Containing Dendrimers. *Chem. Rev.* **2005**, *105* (5), 1663–1681.
- (49) *Peptides Synthesis, Structures, and Applications*; Gutte, B., Ed.; Academic Press: San Diego, 1995.
- (50) Carpino, L. A. Oxidative Reactions of Hydrazines. II. Isophthalimides. New Protective Groups on Nitrogen. *J. Am. Chem. Soc.* **1957**, *79* (1), 98–101.
- (51) McKay, F. C.; Albertson, N. F. New Amine-Masking Groups for Peptide Synthesis. *J. Am. Chem. Soc.* **1957**, *79* (17), 4686–4690.
- (52) Greene, T. W.; Wuts, P. G. M. *Protective Groups in Organic Synthesis*, 3rd ed.; John Wiley & Sons, Ltd: New York, 1999.
- (53) Bocchi, V.; Casnati, G.; Dossena, A.; Marchelli, R. Esterification of Amino Acids and Dipeptides under Mild Conditions; Part I: Via Phase Transfer Catalysis. *Synthesis (Stuttg.)*. **1979**, *12*, 957–961.
- (54) Fischer, E.; Fourneau, E. Ueber Einige Derivate Des Glykocolls. *Berichte der Dtsch. Chem. Gesellschaft* **1901**, *34* (2), 2868–2877.

- (55) Sheehan, J. C.; Hess, G. P. A New Method Of Forming Peptide Bonds. *J. Am. Chem. Soc.* **1955**, *77* (4), 1067–1068.
- (56) *The Peptides. Analysis, Synthesis, Biology.*; Gross, E., Meienhofer, J., Eds.; Academic Press: New York, 1979; Vol. 1. Major M.
- (57) Paul, R.; Anderson, G. W.; Anderson, G. W. New Peptide Forming Reagent. *J. Am. Chem. Soc.* **1960**, *82* (1), 4596–4600.
- (58) Montalbetti, C. A. G. N.; Falque, V. Amide Bond Formation and Peptide Coupling. *Tetrahedron* **2005**, *61* (46), 10827–10852.
- (59) Kolb, H. C.; Finn, M. G.; Sharpless, K. B. Click Chemistry: Diverse Chemical Function from a Few Good Reactions. *Angew. Chemie - Int. Ed.* **2001**, *40* (11), 2004–2021.
- (60) Huisgen, R. 1,3-Dipolar Cycloadditions. *Proc. Chem. Soc.* **1961**, *0*, 357–369.
- (61) Rostovtsev, V. V; Green, L. G.; Fokin, V. V; Sharpless, K. B. A Stepwise Huisgen Cycloaddition Process: Copper (I) -Catalyzed Regioselective “Ligation” of Azides and Terminal Alkynes. *Angew. Chemie Int. Ed.* **2002**, *41* (14), 2596–2599.
- (62) Tornøe, C. W.; Christensen, C.; Meldal, M. Peptidotriazoles on Solid Phase: [1,2,3]-Triazoles by Regiospecific Copper(I)-Catalyzed 1,3-Dipolar Cycloadditions of Terminal Alkynes to Azides. *J. Org. Chem.* **2002**, *67* (9), 3057–3064.
- (63) Arseneault, M.; Wafer, C.; Morin, J. Recent Advances in Click Chemistry Applied to Dendrimer Synthesis. **2015**, 9263–9294.
- (64) Brewer, G. J. Copper Toxicity in the General Population. *Clin. Neurophysiol.* **2009**, *121* (4), 459–460.
- (65) Haridas, V.; Sharma, Y. K.; Sahu, S.; Verma, R. P.; Sadanandan, S.; Kacheshwar, B. G. Designer Peptide Dendrimers Using Click Reaction. *Tetrahedron* **2011**, *67* (10), 1873–1884.
- (66) *Nanotechnology in Catalysis 3*, 1st ed.; Shou, B., Han, S., Raja, R., Somorjai, G. A., Eds.; Springer-Verlag: New York, 2007.
- (67) Fedeli, E.; Lancelot, A.; Serrano, L.; Calvo, P. Self-Assembling Amphiphilic Janus Dendrimers: Mesomorphic Properties and Aggregation in Water. *New J. Chem.* **2015**, *39* (3), 1960–1967.
- (68) Kecsk, A.; Tosh, D. K.; Wei, Q.; Gao, Z.; Jacobson, K. A. GPCR Ligand Dendrimer (GLiDe) Conjugates: Adenosine Receptor Interactions of a Series of Multivalent Xanthine Antagonists. *Bioconjug. Chem.* **2011**, *22* (6), 1115–1127.
- (69) Berg, R.; Straub, B. F. Advancements in the Mechanistic Understanding of the Copper-Catalyzed Azide – Alkyne Cycloaddition. *Beilstein J. Org. Chem.* **2013**, *9*, 2715–2750.

- (70) Gordon, C. G.; Mackey, J. L.; Jewett, J. C.; Sletten, E. M.; Houk, K. N.; Bertozzi, C. R. Reactivity of Biarylazacyclooctynones in Copper-Free Click Chemistry. *J. Am. Chem. Soc.* **2012**, *134* (22), 9199–9208.
- (71) Gonzaga, F.; Sadowski, L. P.; Rambarran, T.; Grande, J.; Adronov, A.; Brook, M. A. Highly Efficient Divergent Synthesis of Dendrimers via Metal-Free “ Click ” Chemistry. **2013**, 1272–1277.
- (72) Lowe, A. B. Thiol-Ene “ Click ” Reactions and Recent Applications in Polymer and Materials Synthesis. *Polym. Chem.* **2010**, *1* (1), 17–36.
- (73) Hoogenboom, R. Thiol – Yne Chemistry : A Powerful Tool for Creating Highly Functional Materials. *Angew. Chemie Int. Ed. English* **2010**, *49* (20), 3415–3417.
- (74) Wu, P.; Feldman, A. K.; Nugent, A. K.; Hawker, C. J.; Scheel, A.; Voit, B.; Pyun, J.; Fr chet, J. M. J.; Sharpless, K. B.; Fokin, V. V. Efficiency and Fidelity in a Click-Chemistry Route to Triazole Dendrimers by the Copper(i)- Catalyzed Ligation of Azides and Alkynes. *Angew. Chemie - Int. Ed.* **2004**, *43*, 3928–3932.
- (75) Nguyen, T.; Baumgarten, M.; Rouhanipour, A.; Joachim, H.; Lieberwirth, I. Extending the Limits of Precision Polymer Synthesis: Giant Polyphenylene Dendrimers in the Megadalton Mass Range Approaching Structural Perfection. *J. Am. Chem. Soc.* **2013**, *135* (11), 4183–4186.
- (76) Dendrons, A.; Lamanna, G.; Smulski, C. R.; Chekkat, N.; Estieu-gionnet, K.; Guichard, G.; Fournel, S.; Bianco, A. Multimerization of an Apoptogenic TRAIL-Mimicking Peptide by Using. *Chem. A Eur. J.* **2013**, *19* (5), 1762–1768.
- (77) Liu, H.; T rring, T.; Dong, M.; Rosen, C. B.; Besenbacher, F.; Gothelf, K. V. DNA-Templated Covalent Coupling of G4 PAMAM Dendrimers. *J. Org. Chem.* **2010**, *132* (51), 18054–18056.
- (78) Wu, P.; Malkoch, M.; Hunt, J. N.; Vestberg, R.; Kaltgrad, E.; Finn, M. G.; Fokin, V. V.; Barry, K.; Hawker, C. J. Multivalent , Bifunctional Dendrimers Prepared by Click Chemistry. *Chem. Commun.* **2005**, 5775–5777.
- (79) Han, S. C.; Kwak, S. H.; Jin, S.; Lee, J. W. Synthesis of Unsymmetrical Fr chet-Type Dendrimers via Double Click Chemistry. *Bull. Korean Chem. Soc.* **2012**, *33* (4), 1393–1396.
- (80) Bao, G.; Tanaka, K.; Ikenaka, K.; Fukase, K. Bioorganic & Medicinal Chemistry Motif of N -Glycan. *Bioorg. Med. Chem.* **2010**, *18* (11), 3760–3766.
- (81) Sharma, R.; Kottari, N.; Chabre, Y. M.; Abbassi, L.; Shiao, T. C.; Rene, R. A Highly Versatile Convergent / Divergent “ Onion Peel ” Synthetic Strategy toward Potent Multivalent. *Chem. Commun.* **2014**, *50*, 13300–13303.

- (82) Lee, C. C.; MacKay, J. A.; Fréchet, J. M. J.; Szoka, F. C. Designing Dendrimers for Biological Applications. *Nat. Biotechnol.* **2005**, *23* (12), 1517–1526.
- (83) Svenson, S.; Tomalia, D. A. Dendrimers in Biomedical Applications - Reflections on the Field. *Adv. Drug Deliv. Rev.* **2005**, *57* (15), 2106–2129.
- (84) Dandliker, P. J.; Diederich, F.; Gross, M.; Knobler, C. B.; Louati, A.; Sanford, E. M. Dendritic Porphyrins: Modulating Redox Potentials of Electroactive Chromophores with Pendant Multifunctionality. *Angew. Chemie Int. Ed. English* **1994**, *33* (17), 1739–1742.
- (85) Jansen, J.; De Brabander-van den Berg, E. M. M.; Meijer, E. W. Encapsulation of Guest Molecules into a Dendritic Box. *Synthesis (Stuttg.)*. **1994**, *266* (November), 1226–1229.
- (86) Watkins, D. M.; Sayed-Sweet, Y.; Klimash, J. W.; Turro, N. J.; Tomalia, D. A. Dendrimers with Hydrophobic Cores and the Formation of Supramolecular Dendrimer–Surfactant Assemblies. *Langmuir* **1997**, *13* (12), 3136–3141.
- (87) Bosman, A. W.; Janssen, H. M.; Meijer, E. W. About Dendrimers: Structure, Physical Properties, and Applications. *Chem. Rev.* **1999**, *99* (7), 1665–1688.
- (88) Lee, J.; Ford, W. T.; Moore, J. A.; Li, Y. Reactivity of Organic Anions Promoted by a Quaternary Ammonium Ion Dendrimer. *Macromolecules* **1994**, *27* (16), 4632–4634.
- (89) Brunner, H. Dendrzymes: Expanded Ligands for Enantioselective Catalysis. *J. Organomet. Chem.* **1995**, *500*, 39–46.
- (90) Deraedt, C.; Pinaud, N.; Astruc, D. Catalysis of “Click” Chemistry in Water. *J. Am. Chem. Soc.* **2014**, *136* (34), 12092–12098.
- (91) Fujita, K.; Hattori, H. Suzuki–Miyaura Reaction Catalyzed by a Dendritic Phosphine–Palladium Complex. *Tetrahedron* **2016**, *72* (11), 1485–1492.
- (92) Peng, M.; Chen, Y.; Tan, R.; Zhenga, W.; Yin, D. A Highly Efficient and Recyclable Catalyst–Dendrimer Supported Chiral Salen Mn(III) Complex for Asymmetric Epoxidation. *RSC Adv.* **2013**, *3* (43), 20684–20692.
- (93) Hecht, S.; Frechet, J. M. J. Dendritic Encapsulation of Function: Applying Nature’s Site Isolation Principle from Biomimetics to Materials Science. *Angew. Chemie - Int. Ed.* **2001**, *40* (1), 74–91.
- (94) Goodson, T. G. Optical Excitations in Organic Dendrimers Investigated by Time-Resolved and Nonlinear Optical Spectroscopy. *Acc. Chem. Res.* **2005**, *38* (2), 99–107.
- (95) Katsuma, B. K.; Shirota, Y. A Novel Class of p -Electron Dendrimers for Thermally and Morphologically Stable Amorphous Molecular Materials. *Adv. Mater.* **1998**, *45* (3), 223–226.
- (96) Furuta, P.; Brooks, J.; Thompson, M. E.; Fre, J. M. J.; Science, M.; Di, V.; Berkeley, L.

Simultaneous Light Emission from a Mixture of Dendrimer Encapsulated Chromophores : A Model for Single-Layer Multichromophoric Organic Light-Emitting Diodes. *J. Am. Chem. Soc.* **2003**, *125* (43), 13165–13172.

- (97) Lo, B. S.; Richards, G. J.; Markham, J. P. J.; Namdas, E. B.; Sharma, S.; Burn, P. L.; Samuel, I. D. W. A Light-Blue Phosphorescent Dendrimer for Efficient Solution-Processed Light-Emitting Diodes. *Adv. Funct. Mater.* **2005**, *15* (9), 1451–1458.
- (98) Lo, B. S.; Anthopoulos, T. D.; Namdas, E. B.; Burn, P. L.; Samuel, I. D. W. Encapsulated Cores : Host-Free Organic Light-Emitting Diodes Based on Solution-Processible Electrophosphorescent Dendrimers **. *Adv. Mater.* **2005**, *17* (16), 1945–1948.
- (99) Liang, B. B.; Wang, L.; Xu, Y.; Shi, H.; Cao, Y. High-Efficiency Red Phosphorescent Iridium Dendrimers with Charge-Transporting Dendrons : Synthesis and Electroluminescent Properties. *Adv. Funct. Mater.* **2007**, *17* (17), 3580–3589.
- (100) Abd-El-Aziz, A. S.; Agatemor, C. Emerging Opportunities in the Biomedical Applications of Dendrimers. *J. Inorg. Organomet. Polym. Mater.* **2018**, *28* (2), 369–382.
- (101) Mammen, M.; Choi, S.-K.; Whitesides, G. M. Polyvalent Interactions in Biological Systems: Implications for Design and Use of Multivalent Ligands and Inhibitors. *Angew. Chemie Int. Ed.* **1998**, *37* (20), 2754–2794.
- (102) Tang, M. X.; Redemann, C. T.; Szoka Jr., F. C. In Vitro Gene Delivery by Degraded Polyamidoamine Dendrimers. *Bioconjug Chem* **1996**, *7* (6), 703–714.
- (103) Grinstaff, M. W. Biodendrimers: New Polymeric Biomaterials for Tissue Engineering. *Chemistry (Easton)*. **2002**, *8* (13), 2839–2846.
- (104) Hed, Y.; Oberg, K.; Berg, S.; Nordberg, A.; Holst, V.; Malkoch, M. Multipurpose Heterofunctional Dendritic Scaffolds as Crosslinkers towards Functional Soft Hydrogels and Implant Adhesives in Bone Fracture Applications. *J. Mater. Chem. B* **2013**, *1*, 6015–6019.
- (105) Amir, R. J.; Pessah, N.; Shamis, M.; Shabat, D. Self-Immolative Dendrimers. *Angew. Chemie - Int. Ed.* **2003**, *42* (37), 4494–4499.
- (106) Duncan, R.; Izzo, L. Dendrimer Biocompatibility and Toxicity. *Adv. Drug Deliv. Rev.* **2005**, *57* (15), 2215–2237.
- (107) Malik, N.; Wiwattanapatapee, R.; Klopsch, R.; Lorenz, K.; Frey, H. Dendrimers : Relationship between Structure and Biocompatibility in Vitro , and Preliminary Studies on the Biodistribution of 125 I-Labelled Polyamidoamine Dendrimers in Vivo. *J. Control. Release* **2000**, *65* (1–2), 133–148.
- (108) Gingras, M.; Raimundo, J. M.; Chabre, Y. M. Cleavable Dendrimers. *Angew. Chemie - Int. Ed.* **2007**, *46* (7), 1010–1017.

- (109) Wong, P. T.; Tang, S.; Mukherjee, J.; Tang, K.; Gam, K.; Isham, D.; Murat, C.; Sun, R.; Baker, J. R.; Choi, S. K. Light-Controlled Active Release of Photocaged Ciprofloxacin for Lipopolysaccharide-Targeted Drug Delivery Using Dendrimer Conjugates. *Chem. Commun.* **2016**, 52 (68), 10357–10360.
- (110) Zhang, F.; Nance, E.; Alnasser, Y.; Kannan, R.; Kannan, S. Microglial Migration and Interactions with Dendrimer Nanoparticles Are Altered in the Presence of Neuroinflammation. *J. Neuroinflammation* **2016**, 13 (65), 1–11.
- (111) Malik, N.; Evagorou, E. G.; Duncan, R. Dendrimer-Platinate: A Novel Approach to Cancer Chemotherapy. *Anticancer. Drugs* **1999**, 10, 767–776.
- (112) Bai, S.; Thomas, C.; Ahsan, F. Dendrimers as a Carrier for Pulmonary Delivery of Enoxaparin, a Low-Molecular Weight Heparin. *J. Pharm. Sci.* **2007**, 96 (8), 2090–2106.
- (113) Tai, L.; Liu, C.; Jiang, K.; Chen, X.; Feng, L.; Pan, W.; Wei, G.; Lu, W. A Novel Penetratin-Modified Complex for Noninvasive Intraocular Delivery of Antisense Oligonucleotides. *Int. J. Pharm.* **2017**, 529 (1–2), 347–356.
- (114) Gungor, S.; Rezigue, M. Nanocarriers Mediated Topical Drug Delivery for Psoriasis Treatment. *Curr. Drug Metab.* **2017**, 18 (5), 454–468.
- (115) Haensler, J.; Francisco, S. Polyamidoamine Cascade Polymers Mediate Efficient Transfection of Cells in Culture+. *Bioconjug. Chem.* **1993**, 4 (5), 372–379.
- (116) *Polymers and Nanomaterials for Gene Therapy*; Narain, R., Ed.; Elsevier: Cambridge, 2016.
- (117) Wiener, E. C.; Brechbiel, M. W.; Brothers, H.; Magin, R. L.; Gansow, O. A.; Tomalia, D. A.; Lauterbur, P. C. Dendrimer-Based Metal Chelates: A New Class of Magnetic Resonance Imaging Contrast Agents. *Magn. Reson. Med.* **1994**, 31 (1), 1–8.
- (118) Kim, Y.; Kim, S. H.; Tanyeri, M.; Katzenellenbogen, J. A.; Schroeder, C. M. Dendrimer Probes for Enhanced Photostability and Localization in Fluorescence Imaging. *Biophys. J.* **2013**, 104 (7), 1566–1575.
- (119) Barman, S. R.; Nain, A.; Jain, S.; Punjabi, N.; Mukherji, S.; Satija, J. Dendrimer as a Multifunctional Capping Agent for Metal Nanoparticles for Use in Bioimaging, Drug Delivery and Sensor Applications. *J. Mater. Chem. B* **2018**, 6 (16), 2368–2384.
- (120) Tam, J. P. Synthetic Peptide Vaccine Design: Synthesis and Properties of a High-Density Multiple Antigenic Peptide System. *Proc. Natl. Acad. Sci.* **1988**, 85 (August), 5409–5413.
- (121) Sánchez-Sancho, F.; Pérez-Inestrosa, E.; Suau, R.; Mayorga, C.; Torres, M. J.; Blanca, M. Dendrimers as Carrier Protein Mimetics for IgE Antibody Recognition. Synthesis and Characterization of Densely Penicilloylated Dendrimers. *Bioconjug. Chem.* **2002**, 13 (3), 647–653.

- (122) Montañez, M. I.; Najera, F.; Mayorga, C.; Ruiz-Sanchez, A. J.; Vida, Y.; Collado, D.; Blanca, M.; Torres, M. J.; Perez-Inestrosa, E. Recognition of Multiepitope Dendrimeric Antigens by Human Immunoglobulin E. *Nanomedicine Nanotechnology, Biol. Med.* **2015**, *11* (3), 579–588.
- (123) Molina, N.; Martin-Serrano, A.; Fernandez, T. D.; Tesfaye, A.; Najera, F.; Torres, M. J.; Mayorga, C.; Vida, Y.; Montañez, M. I.; Perez-Inestrosa, E. Dendrimeric Antigens for Drug Allergy Diagnosis: A New Approach for Basophil Activation Tests. *Molecules* **2018**, *23* (5), 997.
- (124) Montañez, M. I.; Perez-Inestrosa, E.; Suau, R.; Mayorga, C.; Torres, M. J.; Blanca, M. Dendrimerized Cellulose as a Scaffold for Artificial Antigens with Applications in Drug Allergy Diagnosis. *Biomacromolecules* **2008**, *9* (5), 1461–1466.
- (125) Ruiz-Sanchez, A. J.; Montanez, M. I.; Mayorga, C.; Torres, M. J.; Kehr, N. S.; Vida, Y.; Collado, D.; Najera, F.; De Cola, L.; Perez-Inestrosa, E. Dendrimer-Modified Solid Supports: Nanostructured Materials with Potential Drug Allergy Diagnostic Applications. *Curr. Med. Chem.* **2012**, *19* (29), 4942–4954.
- (126) Vida, Y.; Montañez, M. I.; Collado, D.; Najera, F.; Ariza, A.; Blanca, M.; Torres, M. J.; Mayorga, C.; Perez-Inestrosa, E. Dendrimeric Antigen-Silica Particle Composites: An Innovative Approach for IgE Quantification. *J. Mater. Chem. B* **2013**, *1* (24), 3044–3050.
- (127) Vida, Y.; Collado, D.; Najera, F.; Claros, S.; Becerra, J.; Andrades, J. A.; Perez-Inestrosa, E. Dendrimer Surface Orientation of the RGD Peptide Affects Mesenchymal Stem Cell Adhesion. *RSC Adv.* **2016**, *6* (55), 49839–49844.
- (128) Lagunas, A.; Tsintzou, I.; Vida, Y.; Collado, D.; Pérez-inestrosa, E.; Pereira, C. R.; Magalhaes, J.; Andrades, J. A.; Samitier, J. Tailoring RGD Local Surface Density at the Nanoscale toward Adult Stem Cell Chondrogenic Commitment. *Nano Researc* **2016**, *10* (6), 1959–1971.
- (129) Ruiz-Sanchez, A. J.; Mesa-Antunez, P.; Barbero, N.; Collado, D.; Vida, Y.; Najera, F.; Perez-Inestrosa, E. Synthesis of All-Aliphatic Polyamide Dendrimers Based on a 3,3'-Diaminopivalic Acid Scaffold. *Polym. Chem.* **2015**, *6* (16), 3031–3038.
- (130) Soler, M.; Mesa-Antunez, P.; Estevez, M. C.; Ruiz-Sanchez, A. J.; Otte, M. A.; Sepulveda, B.; Collado, D.; Mayorga, C.; Torres, M. J.; Perez-Inestrosa, E.; et al. Highly Sensitive Dendrimer-Based Nanoplasmonic Biosensor for Drug Allergy Diagnosis. *Biosens. Bioelectron.* **2015**, *66*, 115–123.
- (131) Mesa-Antunez, P.; Collado, D.; Vida, Y.; Najera, F.; Fernandez, T.; Torres, M. J.; Perez-Inestrosa, E. Fluorescent BAPAD Dendrimeric Antigens Are Efficiently Internalized by Human Dendritic Cells. *Polymers (Basel)*. **2016**, *8* (4), 1–17.
- (132) Denkewalter, R. G.; Kolc, J. F.; Lukasavage, W. J.; Stroup, K. E.; Stewart, R. C.; Doernberg,

- A. M. Macromolecular Highly Branched Homogeneous Compound. United States Patent, 4,410,688, 1983.
- (133) Stenström, P.; Hjorth, E.; Zhang, Y.; Andrén, O. C. J.; Guette-Marquet, S.; Schultzberg, M.; Malkoch, M. Synthesis and in Vitro Evaluation of Monodisperse Amino-Functional Polyester Dendrimers with Rapid Degradability and Antibacterial Properties. *Biomacromolecules* **2017**, *18* (12), 4323–4330.
- (134) Falkovich, S.; Markelov, D.; Neelov, I.; Darinskii, A.; Falkovich, S.; Markelov, D.; Neelov, I.; Darinskii, A. Are Structural Properties of Dendrimers Sensitive to the Symmetry of Branching? Computer Simulation of Lysine Dendrimers Are Structural Properties of Dendrimers Sensitive to the Symmetry of Branching? Computer Simulation of Lysine Dendrimers. *J. Chem. Phys.* **2013**, *139*, 064903.
- (135) Lloyd, J. R.; Jayasekara, P. S.; Jacobson, K. A. Characterization of Polyamidoamino (PAMAM) Dendrimers Using in-Line Reversed Phase LC Electrospray Ionization Mass Spectrometry. *Anal. Methods* **2016**, *8* (2), 263–269.
- (136) Holman, R. W. Strategic Applications of Named Reactions in Organic Synthesis: Background and Detailed Mechanisms (Kürti, László; Czakó, Barbara). In *Journal of Chemical Education*; 2005; Vol. 82, p 1780.
- (137) Pearlman, W. M. Noble Metal Hydroxides on Carbon Nonpyrophoric Dry Catalysts. *Tetrahedron Lett.* **1967**, *8* (17), 1663–1664.
- (138) Chemistry, O.; Synthesis, O. *PART I Introduction and Background*; 2002.
- (139) Wang, Z. Pearlman's Catalyst. In *Comprehensive Organic Name Reactions and Reagents*; American Cancer Society, 2010; pp 2143–2146.
- (140) Chan, T. R.; Hilgraf, R.; Sharpless, K. B.; Fokin, V. V. Polytriazoles as Copper(I)-Stabilizing Ligands in Catalysis. *Org. Lett.* **2004**, *6* (17), 2853–2855.
- (141) Blumenstein, J. J.; Michejda, C. J. Bistriazenes: Multifunctional Alkylating Agents. *Tetrahedron Lett.* **1991**, *32* (2), 183–186.
- (142) Mancuso, L.; Knobloch, T.; Buchholz, J.; Hartwig, J.; Mçller, L.; Seidel, K.; Collisi, W.; Sasse, F.; Kirschning, A. Preparation of Thermocleavable Conjugates Based on Ansamitocin and Superparamagnetic Nanostructured Particles by a Chemobiosynthetic Approach. *Chem. - An Eur. J.* **2014**, *20* (52), 17541–17551.
- (143) Appukkuttan, P.; Van Der Eycken, E. Recent Developments in Microwave-Assisted, Transition-Metal-Catalysed C-C and C-N Bond-Forming Reactions. *European J. Org. Chem.* **2008**, No. 7, 1133–1155.
- (144) Barge, A.; Tagliapietra, S.; Binello, A.; Cravotto, G. Click Chemistry Under Microwave or Ultrasound Irradiation. *Curr. Org. Chem.* **2010**, *15* (2), 189–203.

- (145) Grabchev, I.; Staneva, D.; Betcheva, R. Fluorescent Dendrimers As Sensors for Biologically Important Metal Cations. *Curr. Med. Chem.* **2012**, *19* (29), 4976–4983.
- (146) Caminade, A. Luminiscent Dendrimers. In *Dendrimers: Towards Catalytic, Material and Biomedical Uses*; John Wiley & Sons, Ltd, 2011; pp 67–98.
- (147) Amaral, S. P.; Tawara, M. H.; Fernandez-Villamarin, M.; Borrajo, E.; Martínez-costas, J.; Vidal, A.; Riguera, R.; Fernandez-megia, E. Tuning the Size of Nanoassemblies: A Hierarchical Transfer of Information from Dendrimers to Polyion Complexes. *Angew. Chemie Int. Ed.* **2018**, *57*, 5273–5277.
- (148) Lee, J. A. E. W.; Kim, H. E. E. J. O. O.; Han, S. C.; Kim, J. I. H.; Jin, S. Designing Poly (Amido Amine) Dendrimers Containing Core Diversities by Click Chemistry of the Propargyl Focal Point Poly (Amido Amine) Dendrons. *J. Poly. Sci., Part A Polym. Chem.* **2008**, *46*, 1083–1097.
- (149) Zhang, C.; Tomalia, D. A. Characterization of Dendritic Polymers Gel Electrophoretic Characterization of Dendritic Polymers. In *Dendrimers and other Dendritic Polymers*; John Wiley & Sons, Ltd: Chichester, U.k., 2003; pp 237–253.
- (150) Xiao, T.; Cao, X.; Shi, X. Analytical Methods Probing the Molecular Weight of Poly (Amidoamine) Dendrimers and Derivatives Using SDS-PAGE. *Anal. Methods* **2011**, *3*, 2348–2353.
- (151) Bakkour, Y.; Darcos, V.; Li, S.; Coudane, J. Diffusion Ordered Spectroscopy (DOSY) as a Powerful Tool for Amphiphilic Block Copolymer Characterization and for Critical Micelle Concentration (CMC) Determination. *Polym. Chem.* **2012**, *3* (8), 2006–2010.
- (152) Bailie, W. E.; Malveau, C.; Zhu, X. X.; Kim, Y. H.; Ford, W. T. Self-Diffusion of Hydrophilic Poly(Propyleneimine) Dendrimers in Poly(Vinyl Alcohol) Solutions and Gels by Pulsed Field Gradient NMR Spectroscopy. *Macromolecules* **2003**, *36* (3), 839–847.
- (153) Fritzinger, B.; Scheler, U. Scaling Behaviour of PAMAM Dendrimers Determined by Diffusion NMR. *Macromol. Chem. Phys.* **2005**, *206*, 1288–1291.
- (154) van Dongen, M. A.; Orr, B. G.; Banaszak Holl, M. M. Diffusion NMR Study of Generation-Five PAMAM Dendrimer Materials. *J. Phys. Chem. B* **2014**, *118* (25), 7195–7202.
- (155) Jiménez, V. A.; Gavín, J. A.; Alderete, J. B. Scaling Trend in Diffusion Coefficients of Low Generation Go-G3 PAMAM Dendrimers in Aqueous Solution at High and Neutral PH. *Struct. Chem.* **2012**, *23* (1), 123–128.
- (156) Marion, A.; Góra, J.; Kracker, O.; Fröhr, T.; Latajka, R.; Sewald, N.; Antes, I. Amber-Compatible Parametrization Procedure for Peptide-like Compounds: Application to 1,4- and 1,5-Substituted Triazole-Based Peptidomimetics. *J. Chem. Inf. Model.* **2018**, *58* (1), 90–110.

- (157) Wang, J.; Wolf, R. M.; Caldwell, J. W.; Kollman, P. A.; Case, D. A. Development and Testing of a General Amber Force Field. *J. Comput. Chem.* **2004**, *25* (9), 1157–1174.
- (158) M. J. Frisch, G. W. Trucks, H. B. Schlegel, G. E. Scuseria, M. A. Robb, J. R. Cheeseman, G. Scalmani, V. Barone, G. A. Petersson, H. Nakatsuji, X. Li, M. Caricato, A. Marenich, J. Bloino, B. G. Janesko, R. Gomperts, B. Mennucci, H. P. Hratchian, J. V. Ort, and D. J. F. Gaussian 09, Revision A.02. Gaussian, Inc., Wallingford CT 2016.
- (159) Tomasi, J.; Mennucci, B.; Cammi, R. Quantum Mechanical Continuum Solvation Models. *Chem. Rev.* **2005**, *105* (8), 2999–3094.
- (160) Bayly, C. I.; Cieplak, P.; Cornell, W.; Kollman, P. A. A Well-Behaved Electrostatic Potential Based Method Using Charge Restraints for Deriving Atomic Charges: The RESP Model. *J. Phys. Chem.* **1993**, *97* (40), 10269–10280.
- (161) D. A. Case, T. A. Darden, T. E. Cheatham, III, C. L. Simmerling, J. Wang, R. E. Duke, R. Luo, R. C. Walker, W. Zhang, K. M. Merz, B. P. Roberts, S. Hayik, A. E. Roitberg, G. Seabra, J. M. Swails, I. Kolossváry, K. F. Wong, F. Paesani, J. Vanicek, R. M. Wo, A. K. and P. A. K. AMBER 12, University of California, San Francisco. 2012.
- (162) Maingi, V.; Jain, V.; Bharatam, P. V.; Maiti, P. K. Dendrimer Building Toolkit: Model Building and Characterization of Various Dendrimer Architectures. *J. Comput. Chem.* **2012**, *33* (25), 1997–2011.
- (163) Jorgensen, W. L.; Chandrasekhar, J.; Madura, J. D.; Impey, R. W.; Klein, M. L. Comparison of Simple Potential Functions for Simulating Liquid Water. *J. Chem. Phys.* **1983**, *79* (2), 926–935.
- (164) Verlet, L. Computer “Experiments” on Classical Fluids. I. Thermodynamical Properties of Lennard-Jones Molecules. *Phys. Rev.* **1967**, *159* (1), 98–103.
- (165) Ryckaert, J.-P.; Ciccotti, G.; Berendsen, H. J. . Numerical Integration of the Cartesian Equations of Motion of a System with Constraints: Molecular Dynamics of n-Alkanes. *J. Comput. Phys.* **1977**, *23* (3), 327–341.
- (166) Berendsen, H. J. C.; Postma, J. P. M.; van Gunsteren, W. F.; DiNola, A.; Haak, J. R. Molecular Dynamics with Coupling to an External Bath. *J. Chem. Phys.* **1984**, *81* (8), 3684–3690.
- (167) Darden, T.; York, D.; Pedersen, L. Particle Mesh Ewald: An $N \cdot \log(N)$ Method for Ewald Sums in Large Systems. *J. Chem. Phys.* **1993**, *98* (12), 10089–10092.
- (168) Humphrey, W.; Dalke, A.; Schulten, K. VMD: Visual Molecular Dynamics. *J. Mol. Graph.* **1996**, *14* (1), 33–38.
- (169) Maiti, P. K.; Tahir, C.; Wang, G.; Goddard, W. A. Structure of PAMAM Dendrimers : Generations 1 through 11. *Macromolecules* **2004**, *37*, 6236–6254.

- (170) Gupta, S.; Biswas, P. Effect of PH on Size and Internal Structure of Poly (Propylene Imine) Dendrimers : A Molecular Dynamics Simulation Study. *J. Phys. Chem. B* **2018**, *122*, 9250–9263.
- (171) Kucheryavy, P.; Li, G.; Vyas, S.; Hadad, C.; Glusac, K. D. Electronic Properties of 4-Substituted Naphthalimides. *J. Phys. Chem. A* **2009**, *113* (23), 6453–6461.
- (172) Grabchev, I.; Konstantinova, T. Synthesis of Some Polymerisable 1,8-Naphthalimide Derivatives for Use as Fluorescent Brighteners. *Dye. Pigment.* **1997**, *33* (3), 197–203.
- (173) Alexiou, M. S.; Tychopoulos, V.; Ghorbanian, S.; Tyman, J. H. P.; Brown, R. G.; Brittain, P. The UV-Visible Absorption and Fluorescence of Some Substituted 1,8-Naphthalimides and Naphthalic Anhydrides. *J. Chem. Soc. Perkin Trans.* **1990**, *2* (5), 837–842.
- (174) Collado, D.; Remón, P.; Vida, Y.; Najera, F.; Sen, P.; Pischel, U.; Perez-inestrosa, E. Energy Transfer in Aminonaphthalimide-Boron-Dipyrromethene (BODIPY) Dyads upon One- and Two-Photon Excitation : Applications for Cellular Imaging. *Chem. Asian J.* **2014**, *9*, 797–804.
- (175) Strassert, C. A.; Otter, M.; Albuquerque, R. Q.; Höne, A.; Vida, Y.; Maier, B.; De Cola, L. Photoactive Hybrid Nanomaterial for Targeting, Labeling, and Killing Antibiotic-Resistant Bacteria. *Angew. Chemie Int. Ed.* **2009**, *48* (42), 7928–7931.
- (176) Levenson, R. M.; Lynch, D. T.; Kobayashi, H.; Backer, J. M.; Backer, M. V. Multiplexing with Multispectral Imaging: From Mice to Microscopy. *ILAR J.* **2008**, *49*, 78–88.
- (177) Molina, N.; Nájera, F.; Guadix, J. A.; Perez-Pomares, J. M.; Vida, Y.; Perez-Inestrosa, E. Synthesis of Amino Terminal Clicked Dendrimers. Approaches to the Application as a Biomarker. *J. Org. Chem.* **2019**, *84* (16), 10197–10208.
- (178) Williams, J. A. G. Photochemistry and Photophysics of Coordination Compounds : Platinum. *Top. Curr. Chem.* **2007**, *281*, 205–268.
- (179) Baggaley, E.; Weinstein, J. A.; Williams, J. A. G. Lighting the Way to See inside the Live Cell with Luminescent Transition Metal Complexes. *Coord. Chem. Rev.* **2012**, *256* (15–16), 1762–1785.
- (180) Yang, B. X.; Wang, Z.; Madakuni, S.; Li, J.; Jabbour, G. E. Efficient Blue- and White-Emitting Electrophosphorescent Devices Based on Platinum (II) [1,3-Difluoro-4,6-Di(2-Pyridinyl)Benzene] Chloride. *Adv. Mater.* **2008**, *20*, 2405–2409.
- (181) Sotoyama, W.; Satoh, T.; Sawatari, N.; Inoue, H.; Sotoyama, W.; Satoh, T.; Sawatari, N.; Inoue, H. Efficient Organic Light-Emitting Diodes with Phosphorescent Platinum Complexes Containing N⁺C⁺N⁻-Coordinating Tridentate Ligand Efficient Organic Light-Emitting Diodes with Phosphorescent Platinum Complexes Containing N⁺C⁺N⁻-Coordinating Tridentate Ligand. *Appl. Phys. Lett.* **2005**, *86*, 153505.

- (182) Turner, E.; Bakken, N.; Li, J. Cyclometalated Platinum Complexes with Luminescent Quantum Yields Approaching 100%. *Inorg. Chem.* **2013**, *52*, 7344–7351.
- (183) Graham, K. R.; Yang, Y.; Sommer, J. R.; Shelton, A. H.; Schanze, K. S.; Xue, J.; Reynolds, J. R. Extended Conjugation Platinum(II) Porphyrins for Use in Near-Infrared Emitting Organic Light Emitting Diodes. *Chem. Mater.* **2011**, *23*, 5305–5312.
- (184) Baggaley, E.; Sazanovich, I. V.; Williams, J. A. G.; Haycock, J. W.; Botchway, S. W.; Weinstein, J. A. Two-Photon Phosphorescence Lifetime Imaging of Cells and Tissues Using a Long-Lived Cyclometallated Npyridyl⁴Cphenyl⁴Npyridyl Pt(II) Complex. *RSC Adv.* **2014**, *4*, 35003–35008.
- (185) Zhao, Q.; Li, F.; Huang, C. Phosphorescent Chemosensors Based on Heavy-Metal Complexes. *Chem. Soc. Rev.* **2010**, *39*, 3007–3030.
- (186) Fleischauer, P. D.; Adamson, A. W.; Sartori, G. Excited States of Metal Complexes and Their Reactions. *Inorg. Chem.* **1972**, *17*, 1–56.
- (187) Allampally, N. K.; Strassert, C. A.; Cola, L. De. Controlling the Assembly of Luminescent Pt(II) Complexes. *Polym. Prepr.* **2011**, *52* (2), 888–889.
- (188) Mydlak, M.; Mauro, M.; Polo, F.; Felicetti, M.; Leonhardt, J.; Diener, G.; De Cola, L.; Strassert, C. A. Controlling Aggregation in Highly Emissive Pt(II) Complexes Bearing Tridentate Dianionic N⁴N⁴N Ligands. Synthesis, Photophysics, and Electroluminescence. *Chem. Mater.* **2011**, *23* (16), 3659–3667.
- (189) Zhao, J.; Feng, Z.; Zhong, D.; Yang, X.; Wu, Y.; Zhou, G.; Wu, Z. Cyclometalated Platinum Complexes with Aggregation-Induced Phosphorescence Emission Behavior and Highly Efficient Electroluminescent Ability. *Chem. Mater.* **2018**, *30*, 929–946.
- (190) Cheng, H.; Yeung, M. C.; Yam, V. W. Molecular Engineering of Platinum(II) Terpyridine Complexes with Tetraphenylethylene-Modified Alkynyl Ligands: Supramolecular Assembly via Pt...Pt and/or $\pi-\pi$ Stacking Interactions and the Formation of Various Superstructures. *ACS Appl. Mater. Interfaces* **2017**, *9* (41), 36220–36228.
- (191) Pasha, S. S.; Alam, P.; Sarmah, A.; Roy, R. K.; Laskar, I. R. Encapsulation of Multi-Stimuli AIE Active Platinum(II) Complex: A Facile and Dry Approach for Luminescent Mesoporous Silica. *RSC Adv.* **2016**, *6* (90), 87791–87795.
- (192) Kui, S. C. F.; Chow, P. K.; So, G.; Tong, M.; Lai, S.; Cheng, G.; Kwok, C.; Low, K.; Ko, M. Y.; Che, C. Robust Phosphorescent Platinum (II) Complexes Containing Tetradentate O⁴N⁴C⁴N Ligands: Excimeric Excited State and Application in Organic White-Light-Emitting Diodes. *Chem. A Eur. J.* **2013**, *19*, 69–73.
- (193) Tan, G.; Chen, S.; Siu, C.; Langlois, A.; Qiu, Y.; Fan, H.; Ho, C.-L.; Harvey, P. D.; Lo, Y. H.; Liu, L.; et al. Platinum(II) Cyclometallates Featuring Broad Emission Bands and Their Applications in Color-tunable OLEDs and High Color-Rendering WOLEDs. *J. Mater. Chem.*

C **2016**, *4*, 6016–6026.

- (194) Cebrián, C.; Mauro, M. Recent Advances in Phosphorescent Platinum Complexes for Organic Light-Emitting Diodes. *Beilstein J. Org. Chem.* **2018**, *14*, 1459–1481.
- (195) Kozhevnikov, V. N.; Donnio, B.; Bruce, D. W. Phosphorescent, Terdentate, Liquid-Crystalline Complexes of Platinum(II): Stimulus-Dependent Emission. *Angew. Chemie Int. Ed.* **2008**, *47*, 6286–6289.
- (196) Santoro, A.; Whitwood, A. C.; Williams, J. A. G.; Kozhevnikov, V. N.; Bruce, D. W. Synthesis, Mesomorphism and Luminescent Properties of Calamitic 2-Phenylpyridines and Their Complexes with Platinum (II). *Chem. Mater.* **2009**, *21*, 3871–3882.
- (197) Krikorian, M.; Liu, S.; Swager, T. M. Columnar Liquid Crystallinity and Mechanochromism in Cationic Platinum(II) Complexes. *J. Org. Chem.* **2014**, *136*, 2952–2955.
- (198) Tam, A. Y.; Wong, K. M.; Wang, G.; Yam, V. W. Luminescent Metallogels of Platinum(II) Terpyridyl Complexes: Interplay of Metal-Metal, π - π and Hydrophobic–Hydrophobic Interactions on Gel Formation. *Chem. Commun.* **2007**, *20*, 2028–2030.
- (199) Strassert, C. A.; Chien, C.; Lopez, M. D. G.; Kourkoulos, D.; Hertel, D.; Meerholz, K.; Cola, L. De. Switching On Luminescence by the Self-Assembly of a Platinum(II) Complex into Gelating Nanofibers and Electroluminescent Films. *Angew. Chemie Int. Ed.* **2011**, *50*, 946–950.
- (200) Ma, B.; Djurovich, P. I.; Thompson, M. E. Excimer and Electron Transfer Quenching Studies of a Cyclometalated Platinum Complex. *Coord. Chem. Rev.* **2005**, *249*, 1501–1510.
- (201) Lo, K. K. Luminescent Rhenium (I) and Iridium (III) Polypyridine Complexes as Biological Probes, Imaging Reagents, and Photocytotoxic Agents. *Acc. Chem. Res.* **2015**, *48*, 2985–2995.
- (202) Sanning, J.; Stegemann, L.; Ewen, P. R.; Schwermann, C.; Daniliuc, C. G.; Zhang, D.; Lin, N.; Duan, L.; Wegner, D.; Doltsinis, N. L.; et al. Colour-Tunable Asymmetric Cyclometalated Pt(II) Complexes and STM-Assisted Stability Assessment of Ancillary Ligands for OLEDs. *J. Mater. Chem. C* **2016**, *4*, 2560–2565.
- (203) Delcanale, P.; Galstyan, A.; Daniliuc, C. G.; Grecco, H. E.; Abbruzzetti, S.; Faust, A.; Viappiani, C.; Strassert, C. A. Oxygen-Insensitive Aggregates of Pt(II) Complexes as Phosphorescent Labels of Proteins with Luminescence Lifetime- Based Readouts. *ACS Appl. Mater. Interfaces* **2018**, *10*, 24361–24369.
- (204) Proetto, M. T.; Sanning, J.; Peterlechner, M.; Thunemann, M.; Stegemann, L.; Sadegh, S.; Devor, A.; Gianneschi, C.; Strassert, C. A. Phosphorescent Pt (II) Complexes Spatially Arrayed in Micellar Polymeric Nanoparticles Providing Dual Readout for Multimodal Imaging. *Chem. Commun.* **2019**, *55*, 501–504.

- (205) Thorp-greenwood, F. L.; Balasingham, R. G.; Coogan, M. P. Organometallic Complexes of Transition Metals in Luminescent Cell Imaging Applications. *J. Organomet. Chem.* **2012**, *714*, 12–21.
- (206) Allampally, N. K.; Bredol, M.; Strassert, C. A.; Cola, L. De. Highly Phosphorescent Supramolecular Hydrogels Based on Platinum Emitters. *Chem. - A Eur. J.* **2014**, *20* (51), 16863–16868.
- (207) Galstyan, A.; Naziruddin, A. R.; Cebrián, C.; Iordache, A.; Daniliuc, C. G.; Cola, L. De; Strassert, C. A. Correlating the Structural and Photophysical Features of Pincer Luminophores and Monodentate Ancillary Ligands in Pt II Phosphors Anzhela Galstyan , [a] Abbas Raja Naziruddin , [A]. *Eur. J. Inorg. Chem.* **2015**, 5822–5831.
- (208) Sanning, J.; Ewen, P. R.; Stegemann, L.; Schmidt, J.; Daniliuc, C. G.; Koch, T.; Doltsinis, N. L.; Wegner, D.; Strassert, C. A. Scanning-Tunneling-Spectroscopy-Directed Design of Tailored Deep- Blue Emitters. *Angew. Chemie Int. Ed.* **2014**, *53*, 1–6.
- (209) Vestberg, R.; Westlund, R.; Eriksson, A.; Lopes, C.; Carlsson, M.; Eliasson, B.; Glimsdal, E.; Lindgren, M.; Malmstro, E. Dendron Decorated Platinum (II) Acetylides for Optical Power Limiting. *Macromoles* **2006**, *39*, 2238–2246.
- (210) Lindgren, M.; Minaev, B.; Glimsdal, E.; Vestberg, R.; Westlund, R.; Malmstro, E. Electronic States and Phosphorescence of Dendron Functionalized Platinum (II) Acetylides. *J. Lumin.* **2007**, *124*, 302–310.
- (211) Li, H.; Yuan, W.; Wang, X.; Zhan, H.; Xie, Z.; Cheng, Y. Enhancement of Luminescence Performance from the Alteration of Stacking Patterns of Pt (II). *J. Mater. Chem. C* **2015**, *3*, 2744–2750.
- (212) Mydlak, M.; Mauro, M.; Polo, F.; Felicetti, M.; Leonhardt, J.; Diener, G.; Cola, L. De; Strassert, C. A. Controlling Aggregation in Highly Emissive P (II) Complexes Bearing Tridentate Dianionic N₃N₃N₃ Ligands . Synthesis , Photophysics , and Electroluminescence. *Chem. Mater.* **2011**, *23*, 3659–3667.
- (213) Monmoton, S.; Lefebvre, H.; Costa-Torero, F.; Fradet, A. Hyperbranched Poly[Bis(Alkylene)Pyridinium]S. *Macromol. Chem. Phys.* **2008**, *209* (23), 2382–2389.
- (214) Xue, F.; Fang, J.; Delker, S. L.; Li, H.; Martásek, P.; Roman, L. J.; Poulos, T. L.; Silverman, R. B. Symmetric Double-Headed Aminopyridines, a Novel Strategy for Potent and Membrane-Permeable Inhibitors of Neuronal Nitric Oxide Synthase. *J. Med. Chem.* **2011**, *54* (7), 2039–2048.
- (215) Sommerfeld, N. S.; Hejl, M.; Klose, M. H. M.; Schreiber-Brynzak, E.; Bileck, A.; Meier, S. M.; Gerner, C.; Jakupc, M. A.; Galanski, M.; Keppler, B. K. Low-Generation Polyamidoamine Dendrimers as Drug Carriers for Platinum(IV) Complexes. *Eur. J. Inorg. Chem.* **2017**, No. 12, 1713–1720.

- (216) Terenziani, B. F.; Katan, C.; Badaeva, E.; Tretiak, S.; Blanchard-desce, M. Enhanced Two-Photon Absorption of Organic Chromophores: Theoretical and Experimental Assessments. *Adv. Mater.* **2008**, *20* (24), 4641–4678.
- (217) Molina, N.; Cnudde, M.; Guadix, J. A.; Perez-pomares, J. M.; Strassert, C. A.; Vida, Y.; Perez-inestrosa, E. Platinum-Doped Dendritic Structure as a Phosphorescent Label for Bacteria in Two-Photon Excitation Microscopy. *ACS Omega* **2019**, *4*, 13027–13033.
- (218) Ingrassia, D.; Sladkova, M.; Palmer, M.; Xia, W.; Engqvist, H.; de Peppo, G. M. Stem Cell-Mediated Functionalization of Titanium Implants. *J. Mater. Sci. Mater. Med.* **2017**, *28* (9).
- (219) Geetha, M.; Singh, A. K.; Asokamani, R.; Gogia, A. K. Ti Based Biomaterials , the Ultimate Choice for Orthopaedic Implants – A Review. *Prog. Mater. Sci.* **2009**, *54* (3), 397–425.
- (220) Navarro, M.; Michiardi, A.; Castaño, O.; Planell, J. A.; Interface, J. R. S.; Navarro, M.; Michiardi, A.; Castan, O. Biomaterials in Orthopaedics Biomaterials in Orthopaedics. *J. R. Soc. Interface* **2008**, *5*, 1137–1158.
- (221) Schliephake, H.; Scharnweber, D. Chemical and Biological Functionalization of Titanium for Dental Implants. *J. Mater. Chem.* **2008**, *18*, 2404–2414.
- (222) Bovan, B. D.; Hummert, T. W.; Dean, D. D.; Schwartz, Z. Role of Material Surfaces in Regulating Bone and Cartilage Cell Response. **1996**, *17* (2), 137–146.
- (223) Webster, T. J.; Ergun, C.; Doremus, R. H.; Siegel, R. W.; Bizios, R.; Al, W. E. T. Specific Proteins Mediate Enhanced Osteoblast Adhesion on Nanophase Ceramics. *J. Biomed. Mater. Res.* **2000**, *51* (3), 475–483.
- (224) Wynn, T. A. Cellular and Molecular Mechanisms of Fibrosis. *J. Pathol.* **2008**, *214*, 199–210.
- (225) Larsson, C.; Thomsen, P.; Lausmaa, J.; Rodahl, M.; Kasemo, B.; Ericson, L. E. Bone Response to Surface Modified Titaniumimplants : Studies on Electropolished Implants with Different Oxide Thicknesses and Morphology. *Biomaterials* **1994**, *15* (13), 1062–1074.
- (226) Chakravorty, N.; Jaiprakash, A.; Ivanovski, S.; Xiao, Y. Implant Surface Modifications and Osseointegration. In *Biomaterials for Implants and Scaffolds*; Springer: Berlin, 2017; pp 107–131.
- (227) Yang, F.; Chen, C.; Zhou, Q.; Gong, Y.; Li, R.; Li, C.; Klämpfl, F.; Freund, S.; Wu, X.; Sun, Y.; et al. Laser Beam Melting 3D Printing of Ti6Al4V Based Porous Structured Dental Implants: Fabrication, Biocompatibility Analysis and Photoelastic Study. *Sci. Rep.* **2017**, *7* (February), 1–12.
- (228) Arabnejad, S.; Johnston, B.; Tanzer, M.; Pasini, D. Fully Porous 3D Printed Titanium

- Femoral Stem to Reduce Stress-Shielding Following Total Hip Arthroplasty. *J. Orthop. Res.* **2017**, *35* (8), 1774–1783.
- (229) Goriainov, V.; McEwan, J. K.; Oreffo, R. O.; Dunlop, D. G. Application of 3D-Printed Patient-Specific Skeletal Implants Augmented with Autologous Skeletal Stem Cells. *Regen. Med.* **2018**, *13* (3), 283–294.
- (230) Sing, S. L.; An, J.; Yeong, W. Y.; Wiria, F. E. Laser and Electron-Beam Powder-Bed Additive Manufacturing of Metallic Implants: A Review on Processes, Materials and Designs. *J. Orthop. Res.* **2016**, *34* (3), 369–385.
- (231) de Groot, K.; Geesink, R.; Klein, C. P. A. T.; Serekian, P. Plasma-Sprayed Coatings of Hydroxylapatite. *J. Biomed. Mater. Res.* **1987**, *21*, 1375–1381.
- (232) Zhao, L.; Chu, P. K.; Zhang, Y.; Wu, Z. Review Antibacterial Coatings on Titanium Implants. *J. Biomed. Mater. Res. Part B Appl. Biomater.* **2009**, *91* (1), 470–480.
- (233) Sul, Y. T.; Byon, E. S.; Jeong, Y. Biomechanical Measurements of Calcium-Incorporated Oxidized Implants in Rabbit Bone: Effect of Calcium Surface Chemistry of a Novel Implant. *Clin. Implant Dent. Relat. Res.* **2004**, *6* (2), 101–110.
- (234) Cooper, L. F.; Zhou, Y.; Takebe, J.; Guo, J.; Abron, A.; Holmén, A.; Ellingsen, J. E. Fluoride Modification Effects on Osteoblast Behavior and Bone Formation at TiO₂ Grit-Blasted c.p. Titanium Endosseous Implants. *Biomaterials* **2006**, *27* (6), 926–936.
- (235) Berglundh, T.; Abrahamsson, I.; Albouy, J. P.; Lindhe, J. Bone Healing at Implants with a Fluoride-Modified Surface: An Experimental Study in Dogs. *Clin. Oral Implants Res.* **2007**, *18* (2), 147–152.
- (236) Van der Flier, A.; Sonnenberg, A. Function and Interactions of Integrins. *Cell Tissue Res.* **2001**, *305* (3), 285–298.
- (237) Ruoslahti, E.; Pierschbacher, M. D. Arg-Gly-Asp: A Versatile Cell Recognition Signal. *Cell* **1986**, *44*, 517–518.
- (238) Pierschbacher, M. D.; Ruoslahti, E. Cell Attachment Activity of Fibronectin Can Be Duplicated by Small Synthetic Fragments of the Molecule. *Nature* **1984**, *309* (3), 30–33.
- (239) Caplan, A. I.; Bruder, S. P. Mesenchymal Stem Cells: Building Blocks for Molecular Medicine in the 21st Century. *Trends Mol. Med.* **2001**, *7* (6), 259–264.
- (240) Chamberlain, G.; Fox, J.; Ashton, B.; Middleton, J. Concise Review : Mesenchymal Stem Cells : Their Phenotype, Differentiation Capacity, Immunological Feature , and Potential for Homing. *Stem Cells* **2007**, *25*, 2739–2749.
- (241) Kim, J.; Sook, I.; Hyung, T.; Back, K.; Jung, S.; Tae, G.; Noh, I.; Hoon, S.; Park, Y.; Sun, K. Bone Regeneration Using Hyaluronic Acid-Based Hydrogel with Bone Morphogenic Protein-2 and Human Mesenchymal Stem Cells. *Biomaterials* **2007**, *28*, 1830–1837.

- (242) Granero-Moltó, F.; Weis, J. A.; Miga, M. I.; Landis, B.; Myers, T. J.; O'Rear, L.; Longobardi, L.; Jansen, E. D.; Mortlock, D. P.; Spagnoli, A. Regenerative Effects of Transplanted Mesenchymal Stem Cells in Fracture Healing. *Stem Cells* **2009**, *27*, 1887–1898.
- (243) Sawyer, A. A.; Hennessy, K. M.; Bellis, S. L. Regulation of Mesenchymal Stem Cell Attachment and Spreading on Hydroxyapatite by RGD Peptides and Adsorbed Serum Proteins. *Biomaterials* **2005**, *26*, 1467–1475.
- (244) Salinas, C. N.; Anseth, K. S. The Enhancement of Chondrogenic Differentiation of Human Mesenchymal Stem Cells by Enzymatically Regulated RGD Functionalities. *Biomaterials* **2008**, *29* (15), 2370–2377.
- (245) Park, J. S.; Yang, H. N.; Jeon, S. Y.; Woo, D. G.; Na, K.; Park, K. H. Osteogenic Differentiation of Human Mesenchymal Stem Cells Using RGD-Modified BMP-2 Coated Microspheres. *Biomaterials* **2010**, *31* (24), 6239–6248.
- (246) Tahlawi, A.; Klontzas, M. E.; Allenby, M. C.; Morais, J. C. F.; Panoskaltsis, N.; Mantalaris, A. RGD-Functionalized Polyurethane Scaffolds Promote Umbilical Cord Blood Mesenchymal Stem Cell Expansion and Osteogenic Differentiation. *J. Tissue Eng. Regen. Med.* **2019**, *13* (2), 232–243.
- (247) Re'em, T.; Tsur-Gang, O.; Cohen, S. The Effect of Immobilized RGD Peptide in Macroporous Alginate Scaffolds on TGFβ1-Induced Chondrogenesis of Human Mesenchymal Stem Cells. *Biomaterials* **2010**, *31* (26), 6746–6755.
- (248) Zhang, Q.; Wang, J.; Cheng, B. Effect of MinTBP-1-RGD/Titanium Implant on Osseointegration in Rats. *Mater. Lett.* **2018**, *228*, 424–426.
- (249) Chen, J.; Bly, R. A.; Saad, M. M.; Alkhodary, M. A.; El-Backly, R. M.; Cohen, D. J.; Kattamis, N.; Fatta, M. M.; Moore, W. A.; Arnold, C. B.; et al. In-Vivo Study of Adhesion and Bone Growth around Implanted Laser Groove/RGD-Functionalized Ti-6Al-4V Pins in Rabbit Femurs. *Mater. Sci. Eng. C* **2011**, *31* (5), 826–832.
- (250) Roberts, C.; Chen, C. S.; Mrksich, M.; Martichonok, V.; Ingber, D. E.; Whitesides, G. M. Using Mixed Self-Assembled Monolayers Presenting RGD and (EG)3OH Groups To Characterize Long-Term Attachment of Bovine Capillary Endothelial Cells to Surfaces. *J. Am. Chem. Soc.* **1998**, *120*, 6548–6555.
- (251) Hersel, U.; Dahmen, C.; Kessler, H. RGD Modified Polymers: Biomaterials for Stimulated Cell Adhesion and Beyond. *Biomaterials* **2003**, *24* (24), 4385–4415.
- (252) Quirk, R. A.; Chan, W. C.; Davies, M. C.; Tendler, S. J. B.; Shakeshe, K. M. Poly (L-Lysine)-GRGDS as a Biomimetic Surface Modifier for Poly(Lactic Acid). *Biomaterials* **2001**, *22*, 865–872.
- (253) Neff, J. A.; Caldwell, K. D.; Tresco, P. A. A Novel Method for Surface Modification to Promote Cell Attachment to Hydrophobic Substrates. *J. Biomed. Mater. Res.* **1998**, *40*,

- 511–519.
- (254) Elbert, D. L.; Hubbell, J. A. Conjugate Addition Reactions Combined with Free-Radical Cross-Linking for the Design of Materials for Tissue Engineering. *Biomacromolecules* **2001**, *2*, 430–441.
 - (255) Stile, R. A.; Healy, K. E. Thermo-Responsive Peptide-Modified Hydrogels for Tissue Regeneration. *Biomacromolecules* **2001**, *2*, 185–194.
 - (256) He, X.; Alves, C. S.; Oliveira, N.; Rodrigues, J.; Zhu, J.; Bánya, I.; Tomás, H.; Shi, X. Colloids and Surfaces B : Biointerfaces RGD Peptide-Modified Multifunctional Dendrimer Platform for Drug Encapsulation and Targeted Inhibition of Cancer Cells. *Colloids Surfaces B Biointerfaces* **2015**, *125*, 82–89.
 - (257) Pandita, D.; Santos, L.; Pe, A. P.; Toma, H. Gene Delivery into Mesenchymal Stem Cells : A Biomimetic Approach Using RGD Nanoclusters Based on Poly (Amidoamine) Dendrimers. *Biomacromolecules* **2011**, *12*, 472–481.
 - (258) Lagunas, A.; Castaño, A. G.; Artés, J. M.; Vida, Y.; Collado, D.; Gorostiza, P.; Claros, S.; Andrades, J. A.; Samitier, J. Large-Scale Dendrimer-Based Uneven Nanopatterns for the Study of Local Arginine – Glycine – Aspartic Acid (RGD) Density Effects on Cell Adhesion. *Nano Reseach* **2014**, *7* (3), 399–409.
 - (259) Casanellas, I.; Lagunas, A.; Tsintzou, I.; Vida, Y.; Collado, D.; Pérez-inestrosa, E.; Rodríguez-pereira, C.; Andrades, J. A.; Becerra, J. Dendrimer-Based Uneven Nanopatterns to Locally Control Surface Adhesiveness : A Method to Direct Chondrogenic Differentiation. *J. Vis. Exp.* **2018**, *131*, e5634.
 - (260) Nanci, A.; Wuest, J. D.; Brunet, P.; Sharma, V.; Zalzal, S.; Mckee, M. D. Chemical Modification of Titanium Surfaces for Covalent Attachment of Biological Molecules. *J. Biomed. Mater. Res.* **1998**, *40* (2), 324–335.
 - (261) Zhu, M.; Lerum, M. Z.; Chen, W. How To Prepare Reproducible, Homogeneous, and Hydrolytically Stable Aminosilane-Derived Layers on Silica. *Langmuir* **2012**, *28* (1), 416–423.
 - (262) Rocas, P.; Hoyos-Nogués, M.; Rocas, J.; Manero, J. M.; Gil, J.; Albericio, F.; Mas-Moruno, C. Installing Multifunctionality on Titanium with RGD-Decorated Polyurethane-Polyurea Roxithromycin Loaded Nanoparticles: Toward New Osseointegrative Therapies. *Adv. Healthc. Mater.* **2015**, *4* (13), 1956–1960.
 - (263) Córdoba, A.; Satué, M.; Gómez-Florit, M.; Hierro-Oliva, M.; Petzold, C.; Lyngstadaas, S. P.; González-Martín, M. L.; Monjo, M.; Ramis, J. M. Flavonoid-Modified Surfaces: Multifunctional Bioactive Biomaterials with Osteopromotive, Anti-Inflammatory, and Anti-Fibrotic Potential. *Adv. Healthc. Mater.* **2015**, *4* (4), 540–549.
 - (264) Thevenot, P.; Hu, W.; Tang, L. Surface Chemistry Influences Implant Biocompatibility.

Curr. Top. Med. Chem. **2008**, 8 (4), 270–280.

- (265) Song, H. Y.; Ngai, M. H.; Song, Z. Y.; Macary, P. A.; Lear, M. J. Practical Synthesis of Maleimides and Coumarin-Linked Probes for Protein and Antibody Labelling via Reduction of Native Disulfides. *Org. Biomol. Chem.* **2009**, 7 (17), 3400–3406.
- (266) Allampally, N. K.; Strassert, C. A.; De Cola, L. Luminescent Gels by Self-Assembling Platinum Complexes. *Dalt. Trans.* **2012**, 41 (42), 13132–13137.

APPENDIX

SPECTRA

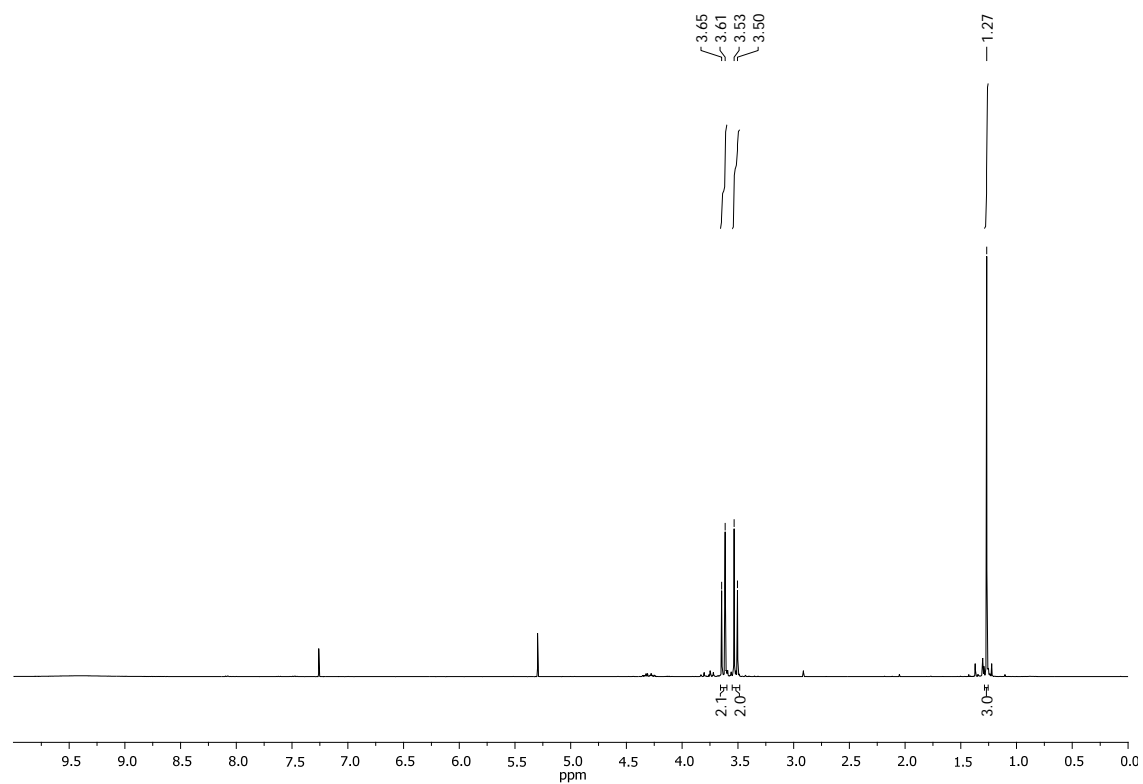


Figure 122. ¹H spectrum of 3,3'-diazidopivalic acid (1) in CDCl₃.

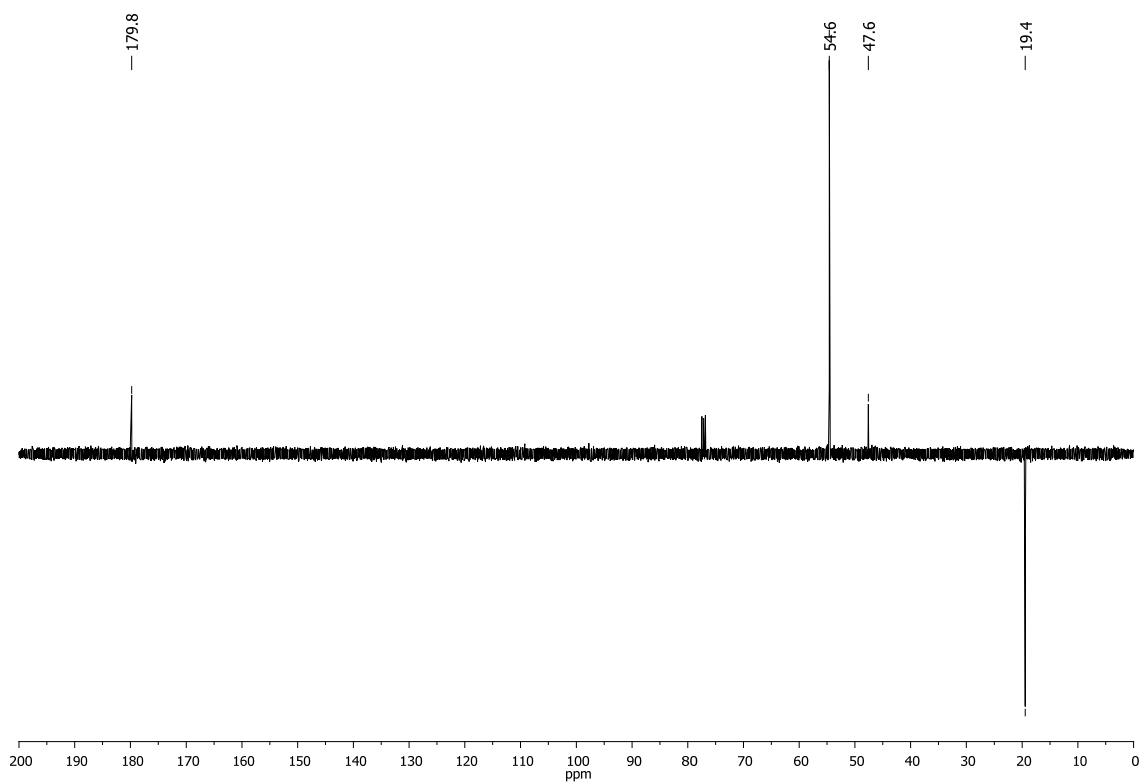


Figure 123. ¹³C (SEFT) spectrum of 3,3'-diazidopivalic acid (1) in CDCl₃.

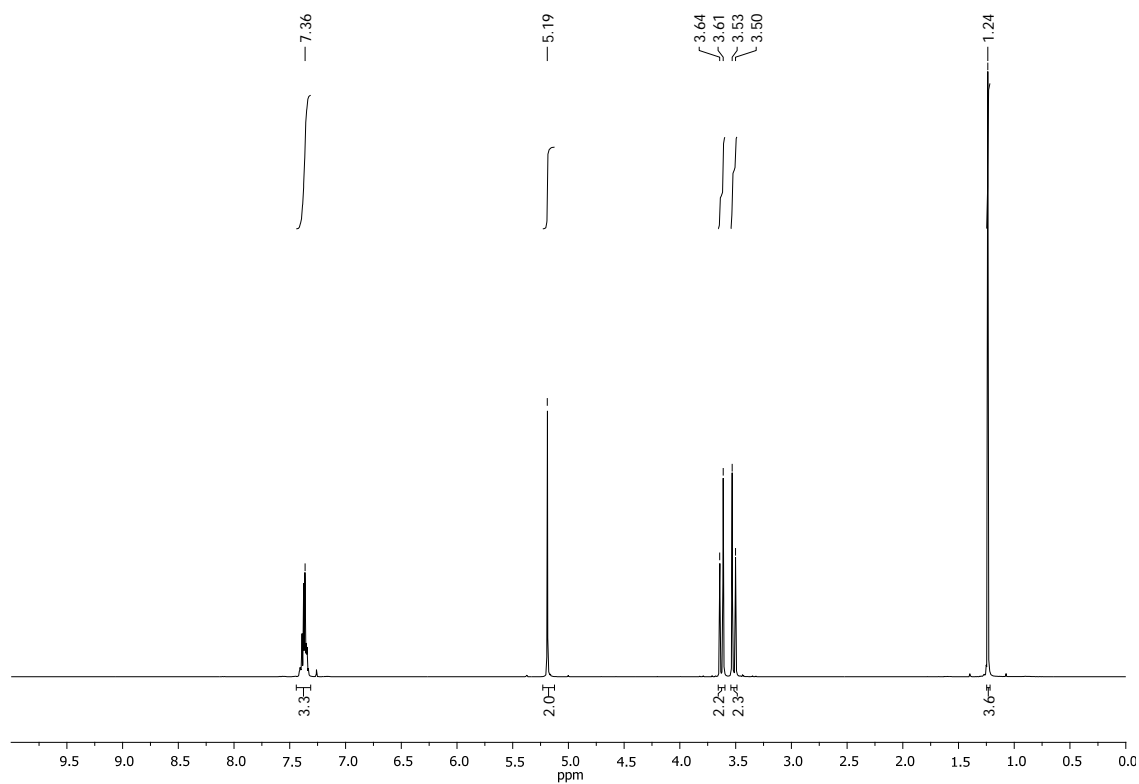


Figure 124. ¹H spectrum of **benzyl-3,3'-diazidopivaloate (2)** in CDCl₃.

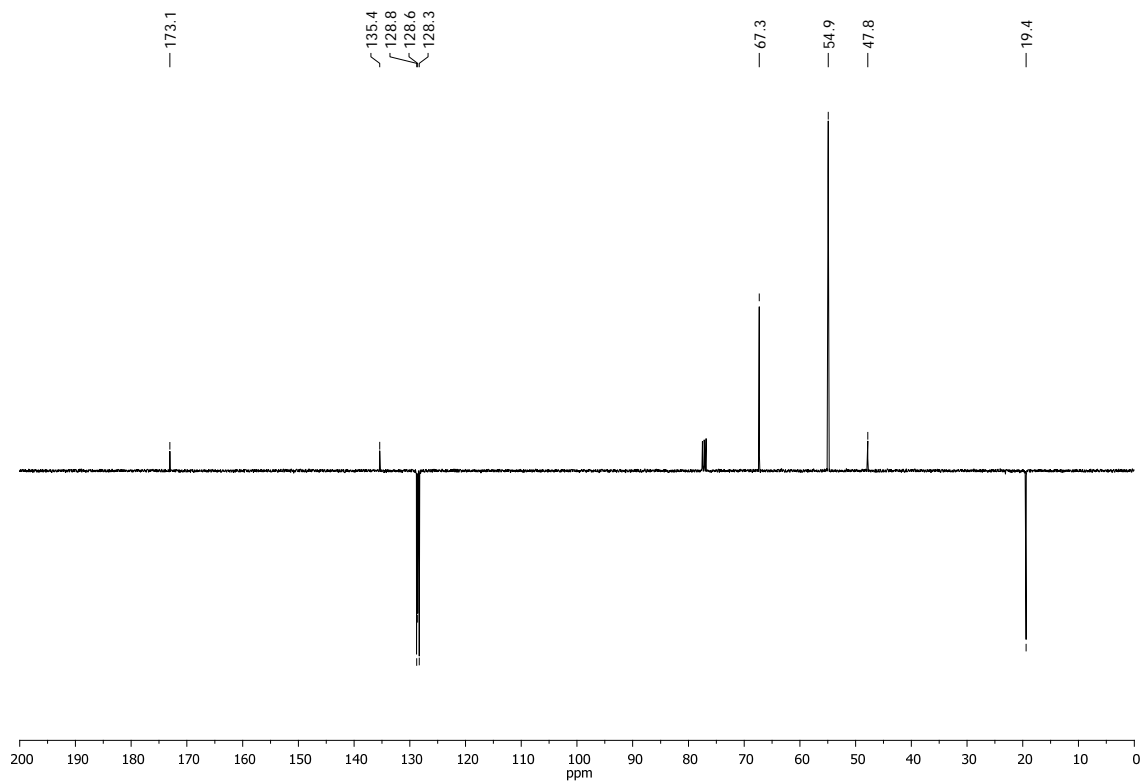


Figure 125. ¹³C (SEFT) spectrum of **benzyl-3,3'-diazidopivaloate (2)** in CDCl₃.

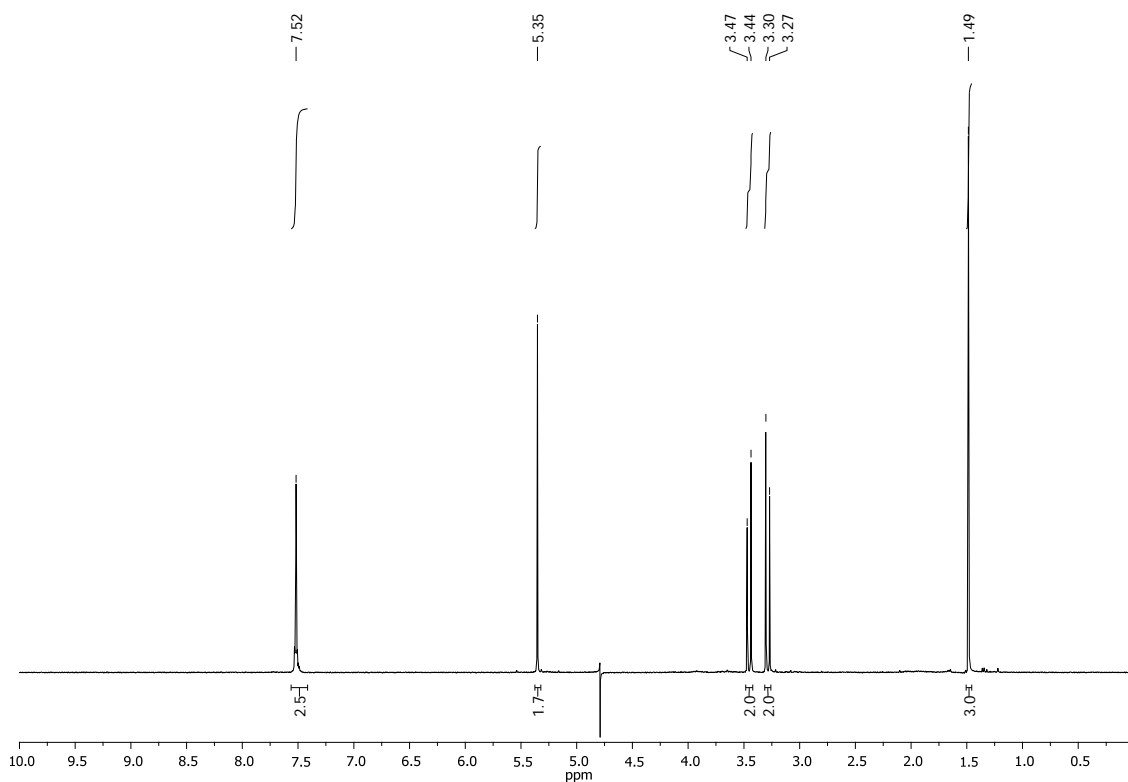


Figure 126. ¹H spectrum of benzyl-3,3'-diaminopivaloate (3) in D₂O.

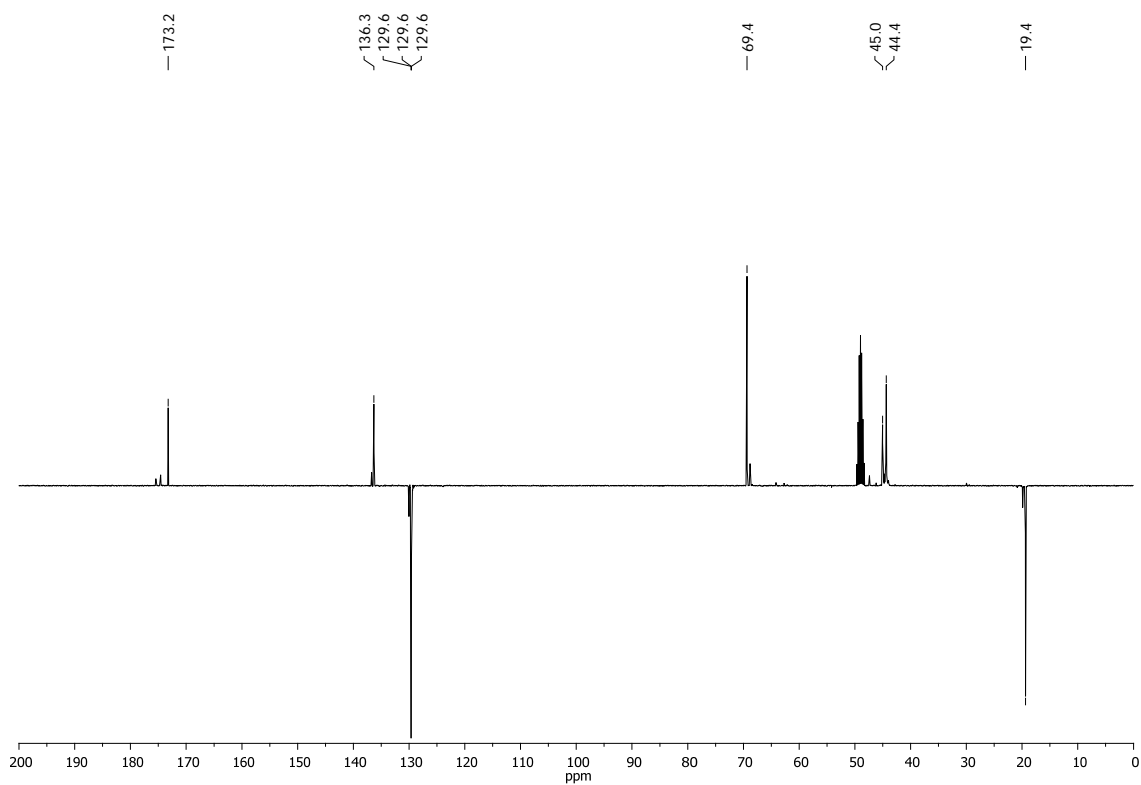


Figure 127. ¹³C (SEFT) spectrum of benzyl-3,3'-diaminopivaloate (3) in D₂O.

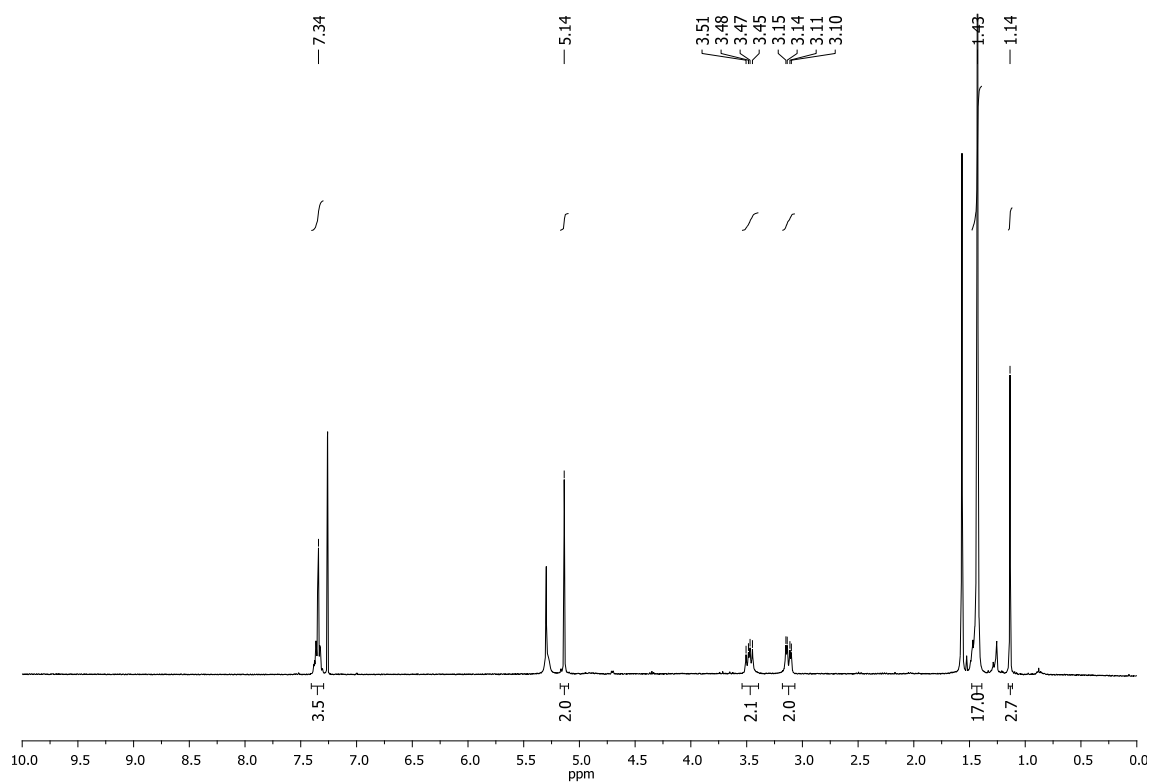


Figure 128. ¹H spectrum of benzyl-3,3'-bis(tert-butoxycarbonyl)aminopivaloate (**4**) in CDCl₃.

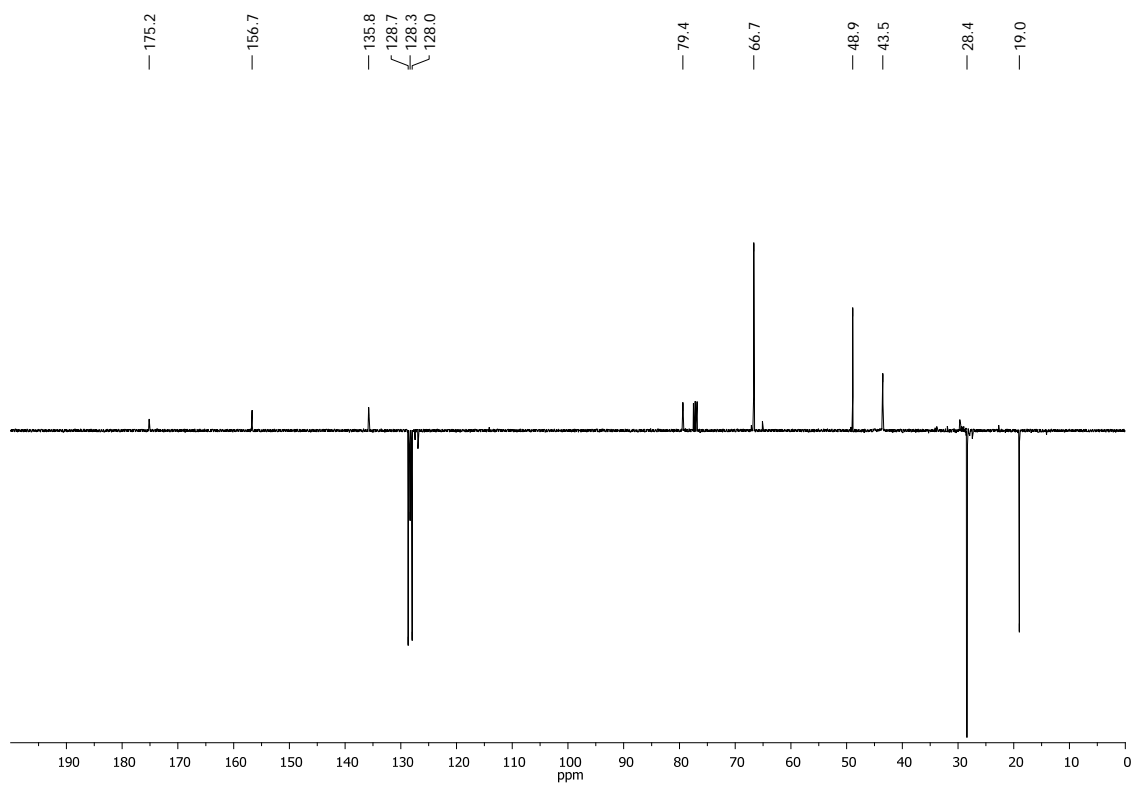


Figure 129. ¹³C (SEFT) spectrum of benzyl-3,3'-bis(tert-butoxycarbonyl)aminopivaloate (**4**) in CDCl₃.

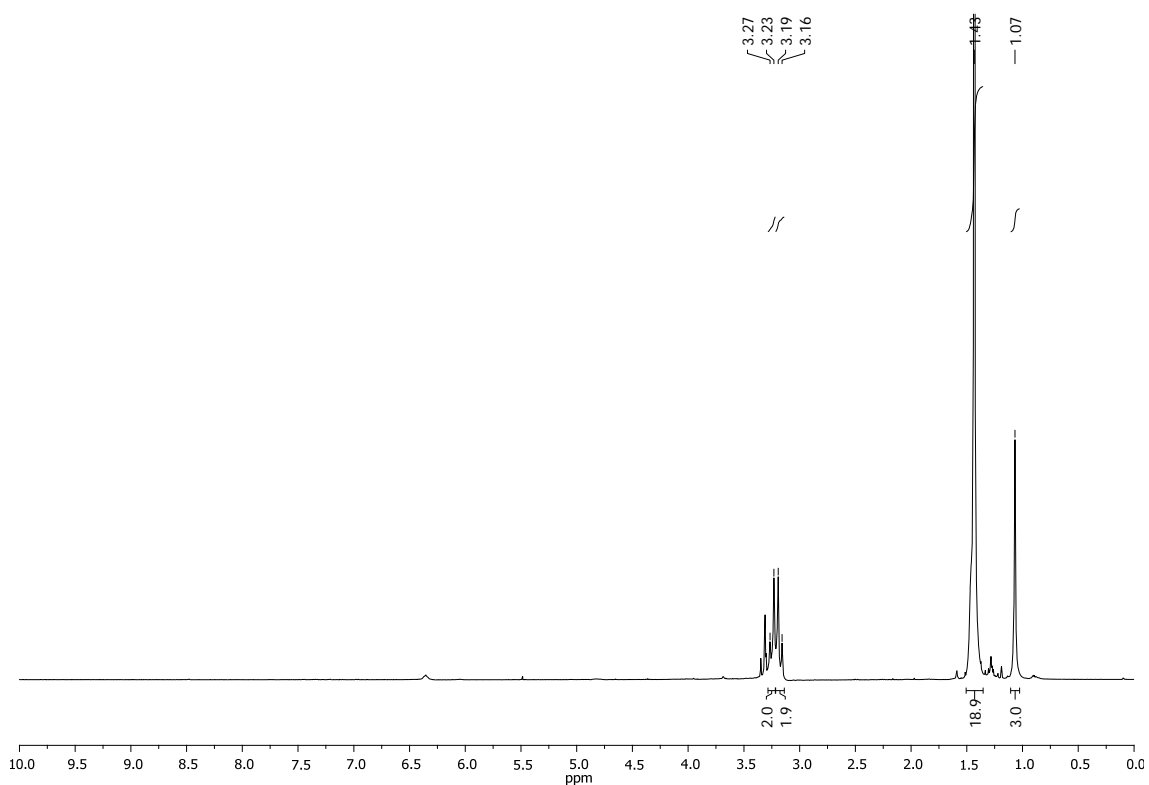


Figure 130. ¹H spectrum of **3,3'-bis(*tert*-butoxycarbonyl)aminopivalic acid (5)** in MeOD-*d*₄.

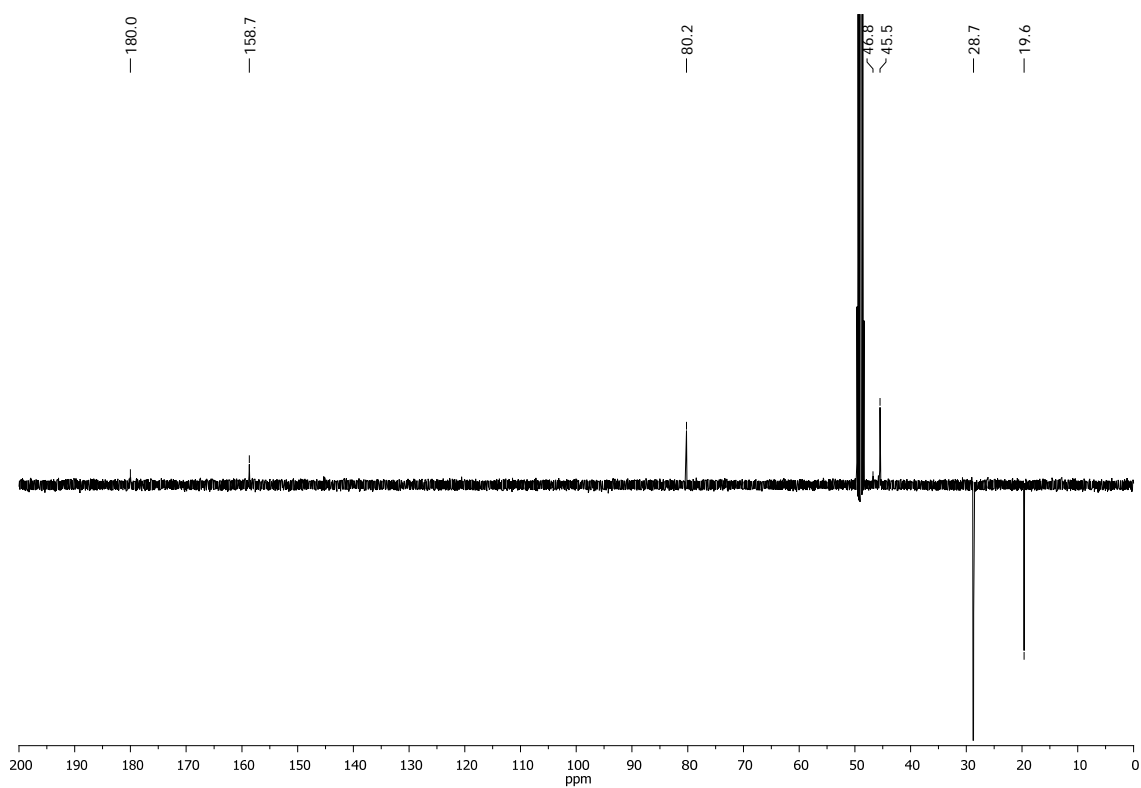


Figure 131. ¹³C (SEFT) spectrum of **3,3'-bis(*tert*-butoxycarbonyl)aminopivalic acid (5)** in MeOD-*d*₄.

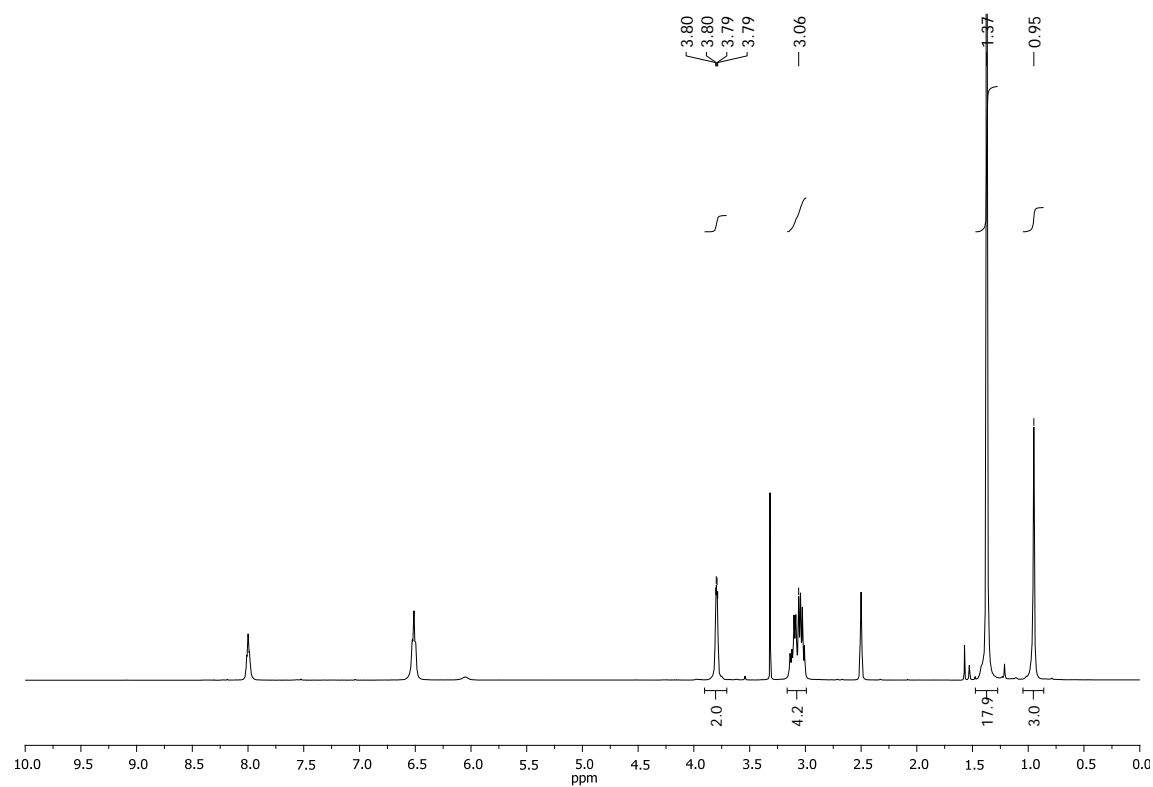


Figure 132. ¹H spectrum of **dG1** in DMSO-*d*₆.

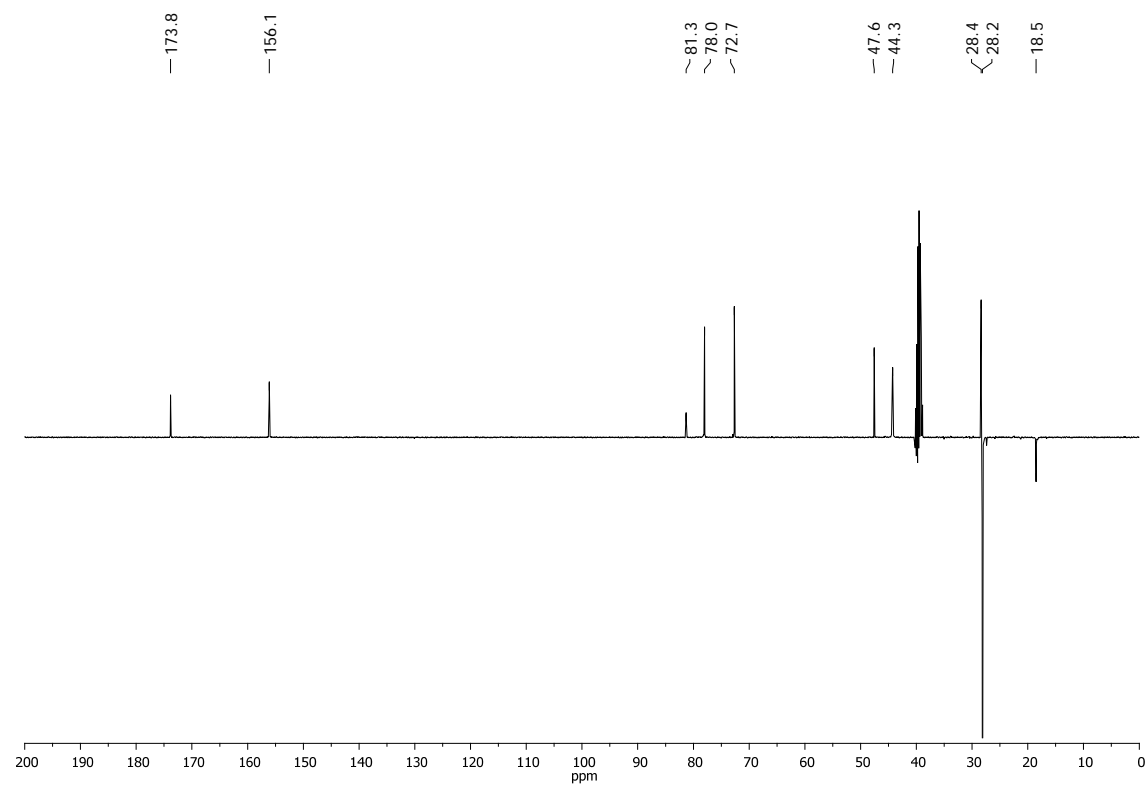


Figure 133. ¹³C (SEFT) spectrum of **dG1** in DMSO-*d*₆.

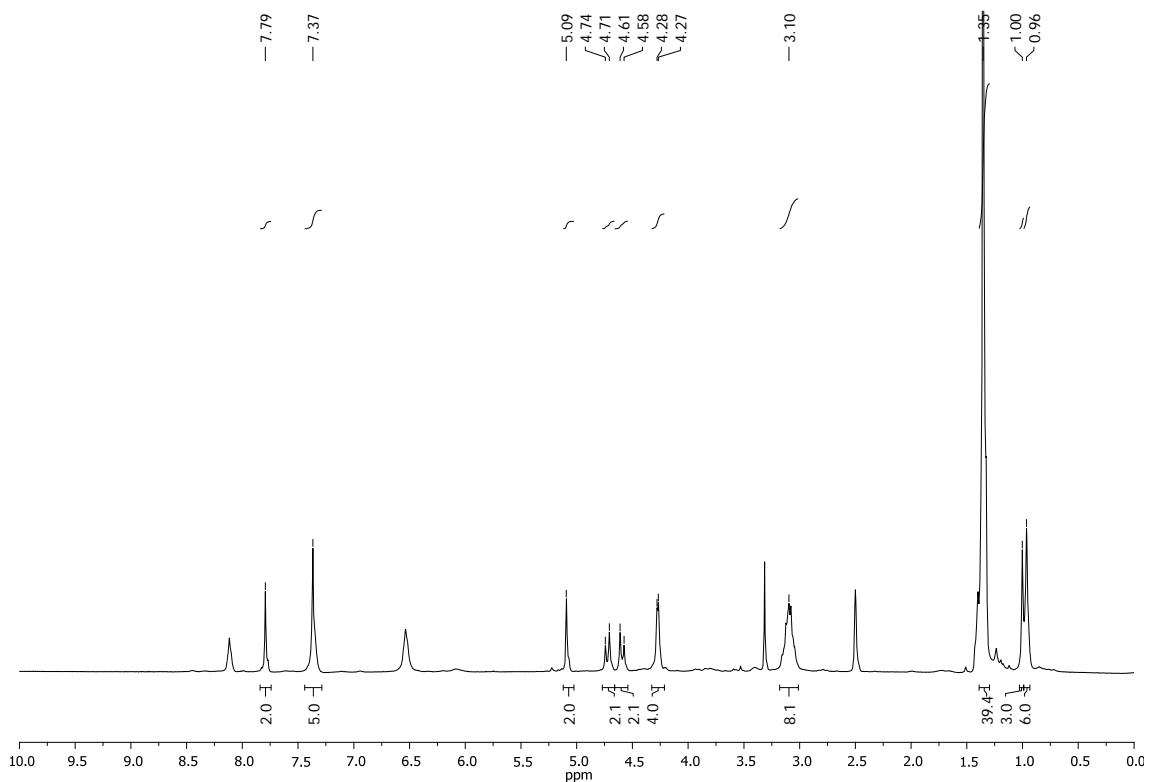


Figure 134. ¹H spectrum of **dG2-CO₂Bn** in DMSO-*d*₆.

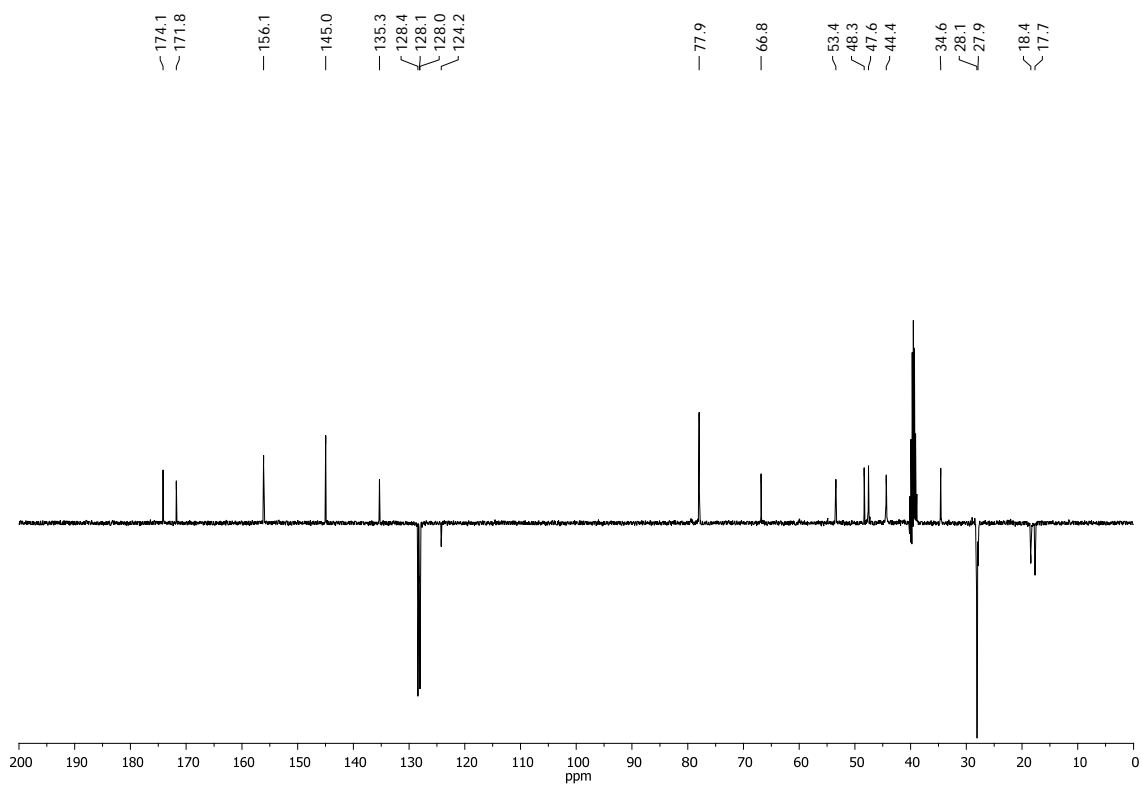


Figure 135. ¹³C (SEFT) spectrum of **dG2-CO₂Bn** in DMSO-*d*₆.

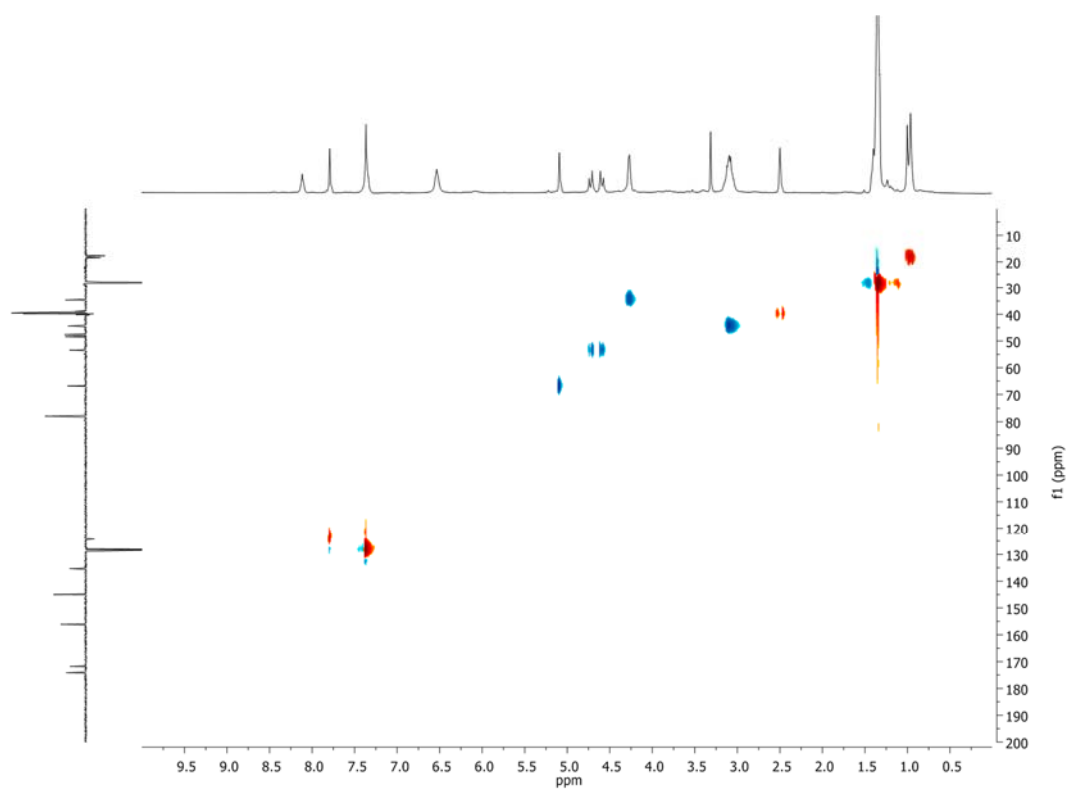


Figure 136. HSCQ spectrum of **dG2-CO₂Bn** in DMSO-*d*₆.

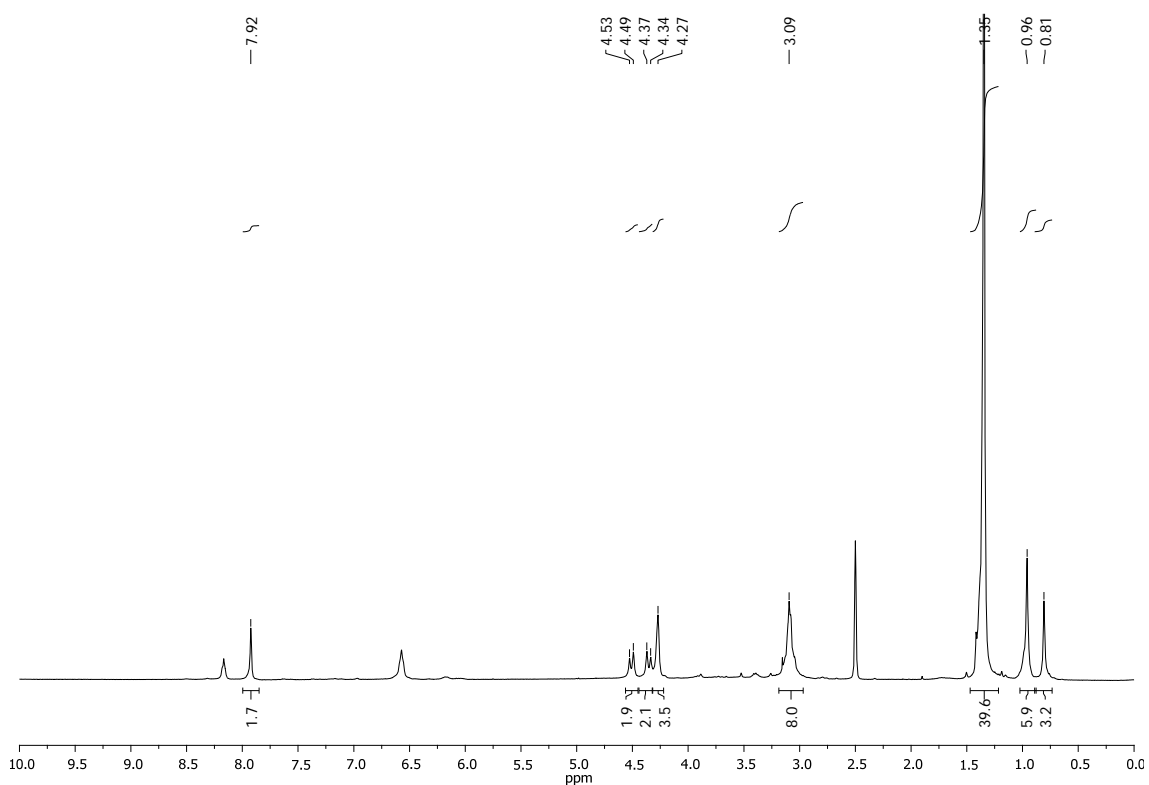


Figure 137. ¹H spectrum of dG2-CO₂H in DMSO-*d*₆.

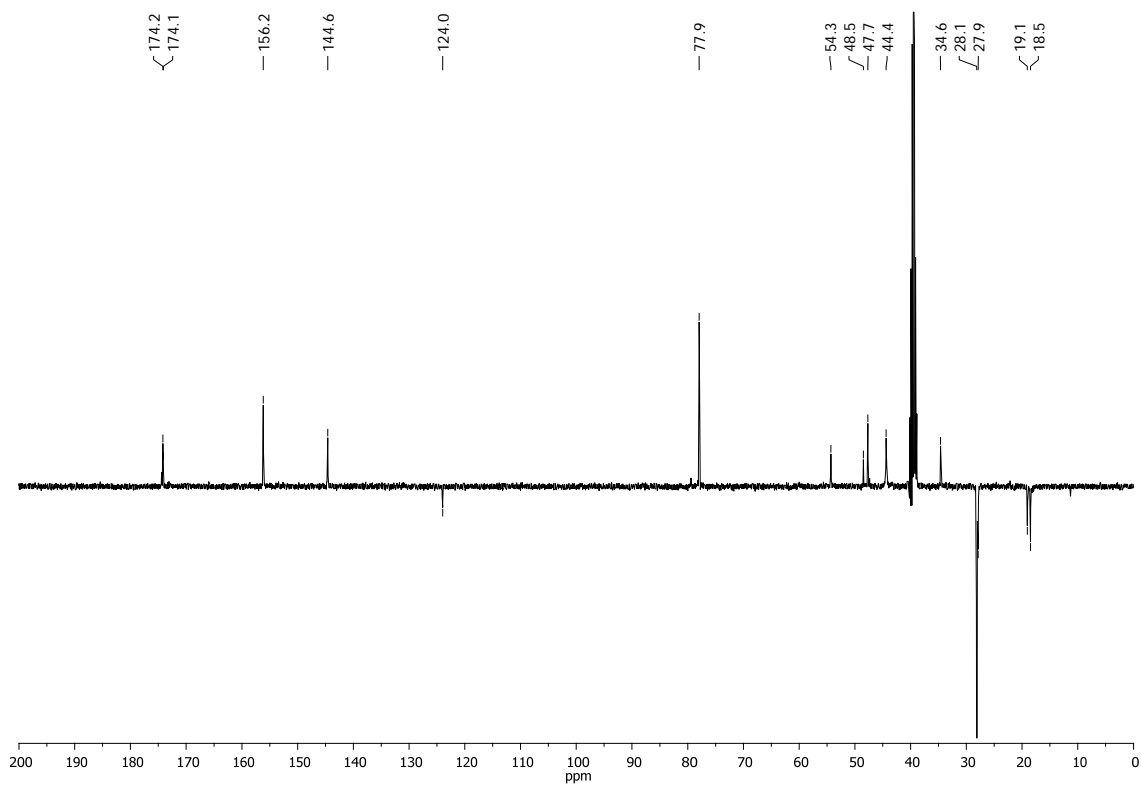


Figure 138. ¹³C (SEFT) spectrum of dG2-CO₂H in DMSO-*d*₆.

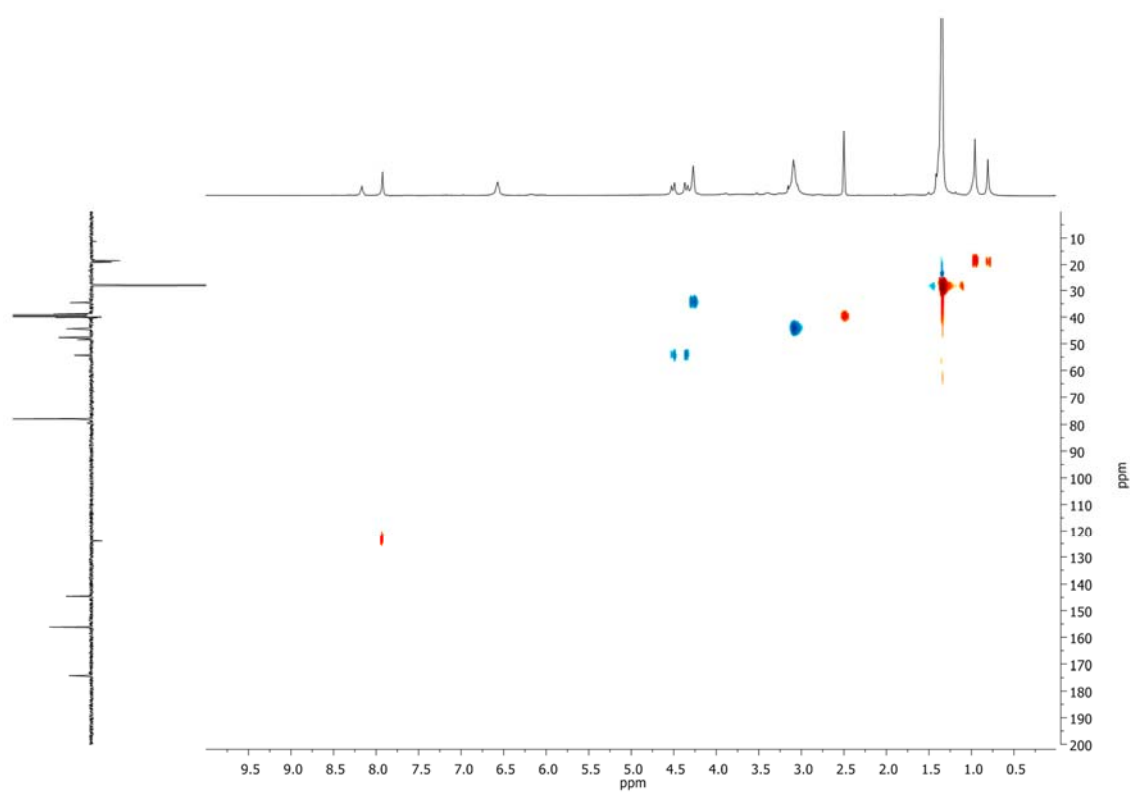


Figure 139. HSQC spectrum of **dG2-CO₂H** in DMSO-*d*₆.

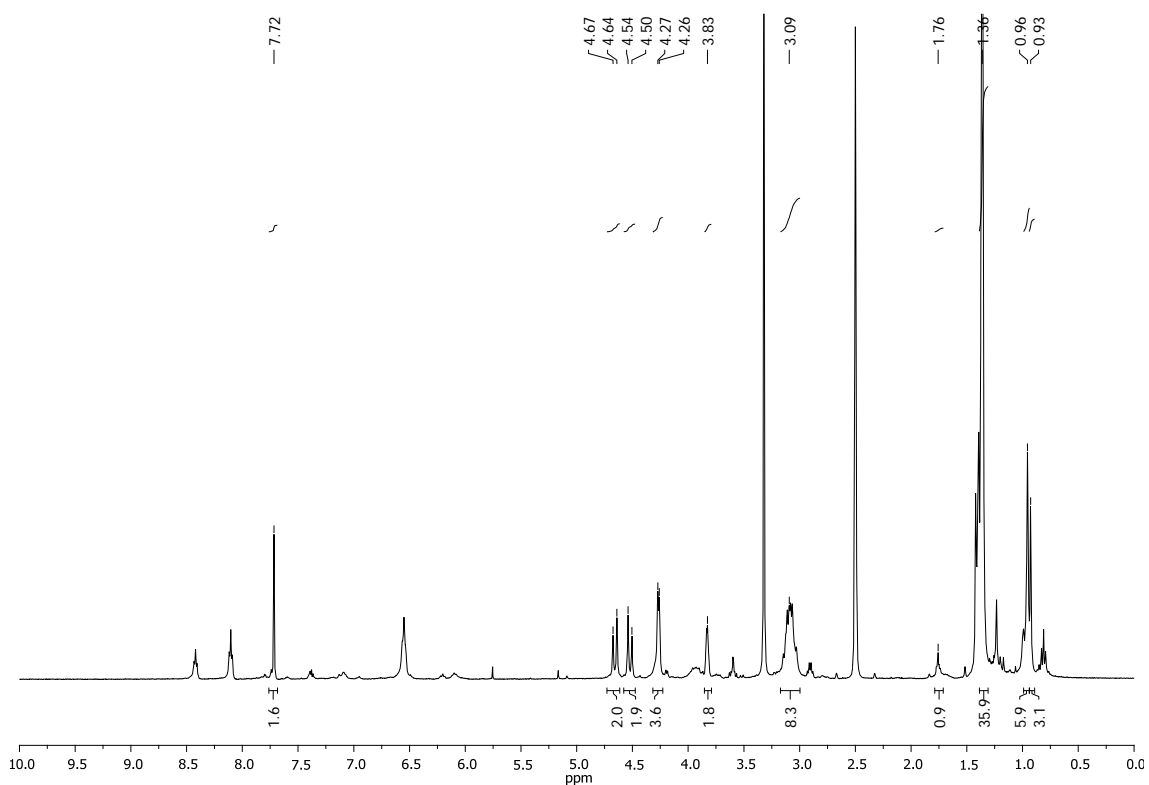


Figure 140. ¹H spectrum of **dG2** in DMSO-*d*₆.

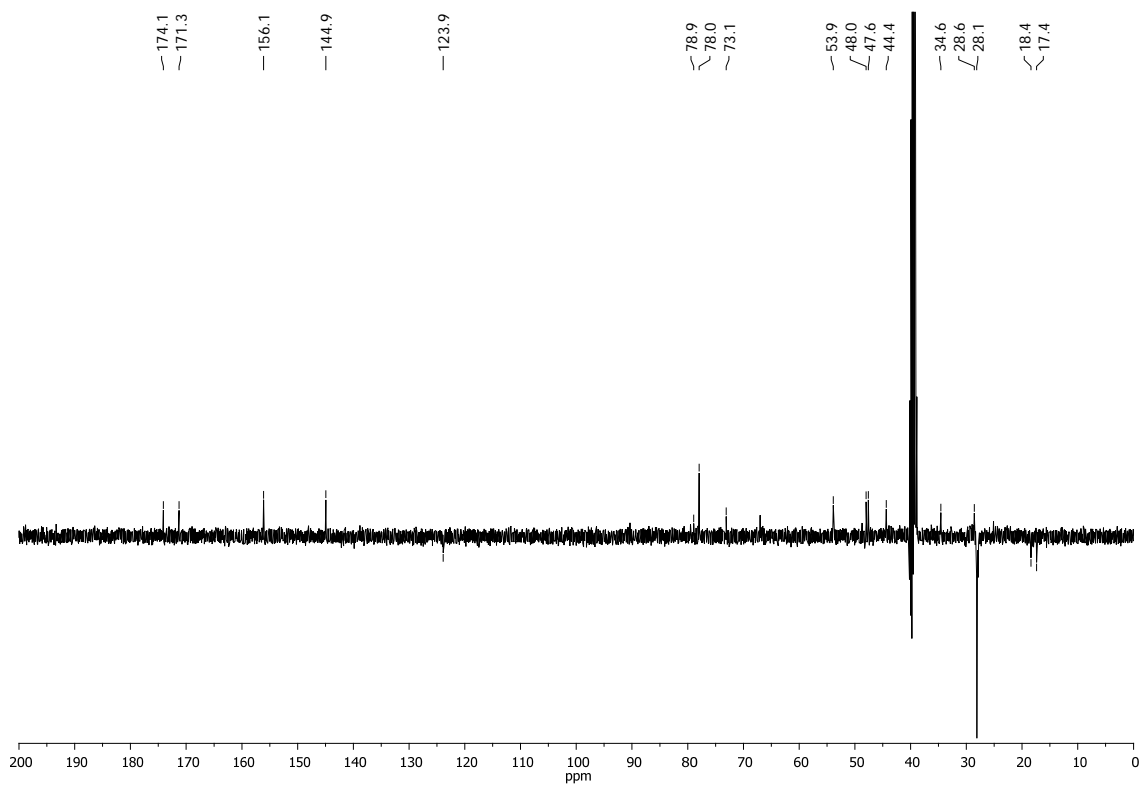


Figure 141. ¹³C (SEFT) spectrum of **dG2** in DMSO-*d*₆.

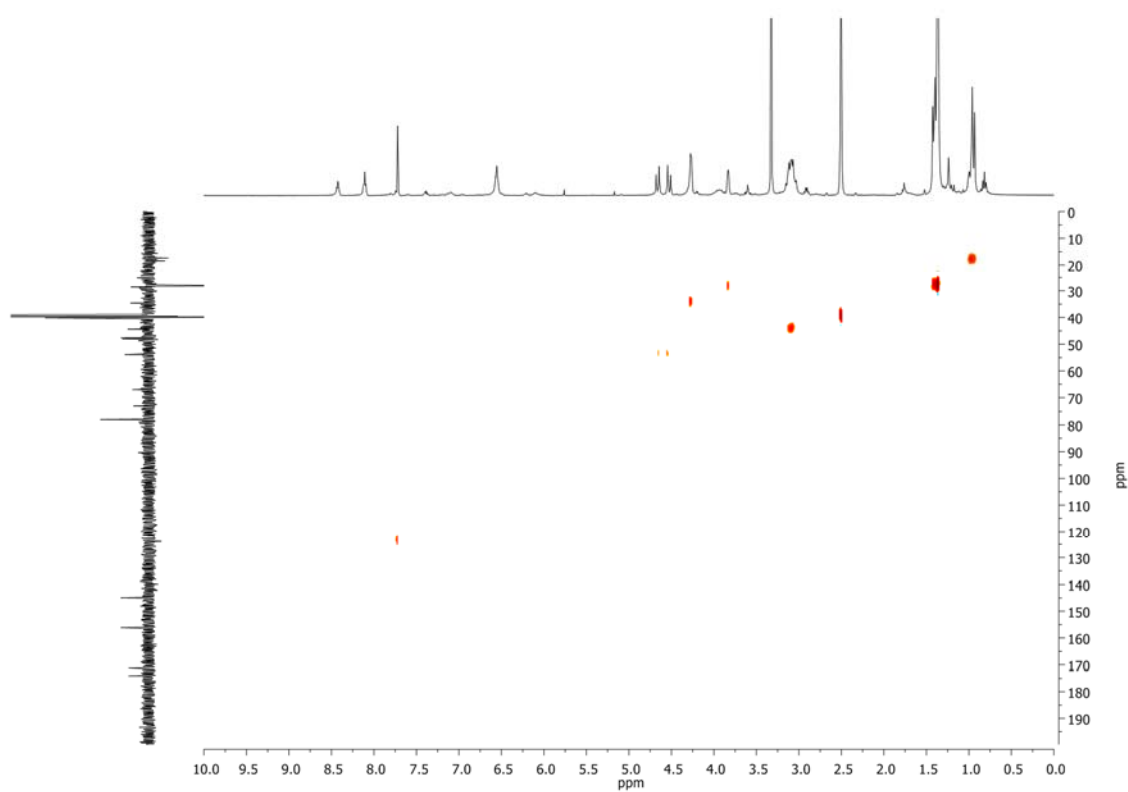


Figure 142. HSQC spectrum of **dG2** in $\text{DMSO-}d_6$.

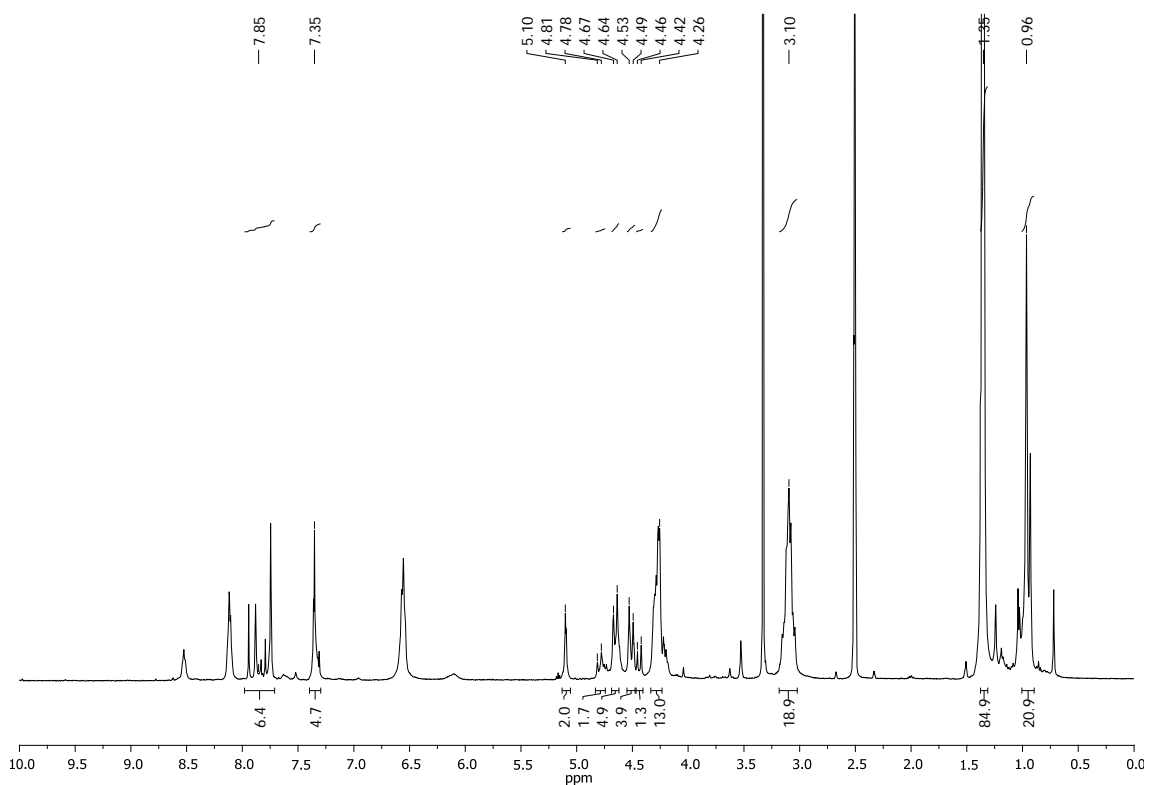


Figure 143. ¹H spectrum of **dG3-CO₂Bn** in DMSO-*d*₆.

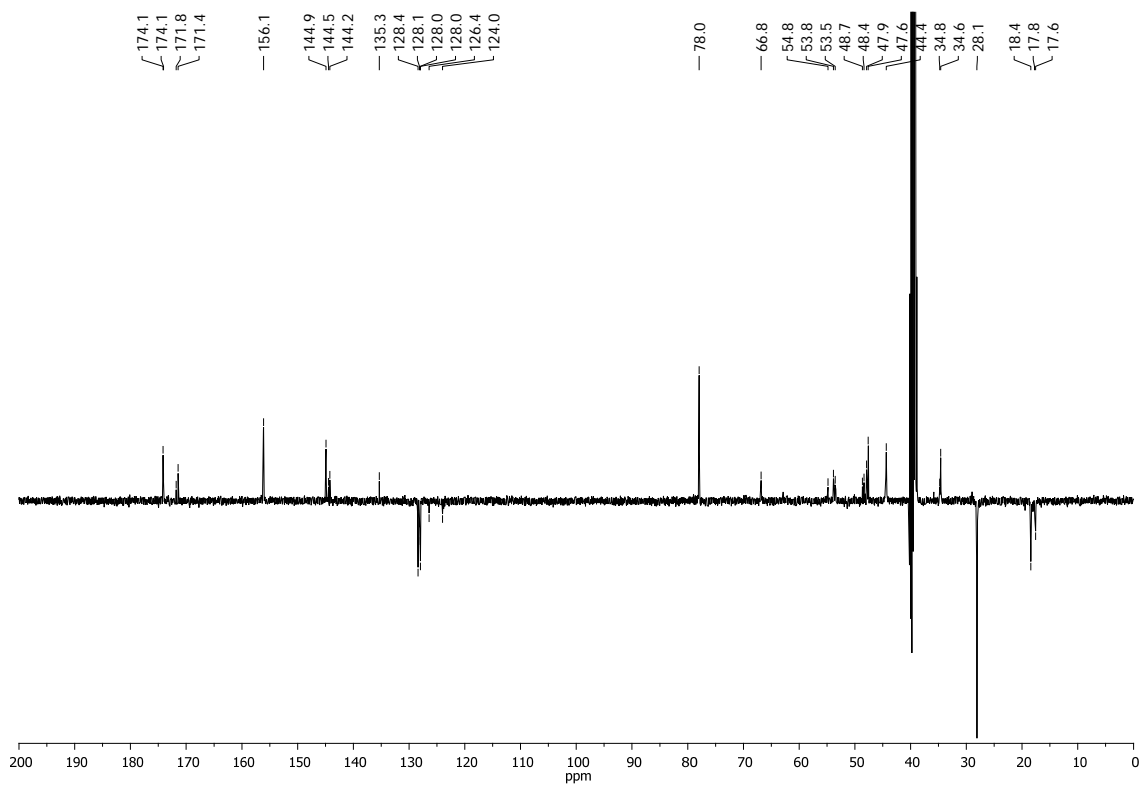


Figure 144. ¹³C (SEFT) spectrum of **dG3-CO₂Bn** in DMSO-*d*₆.

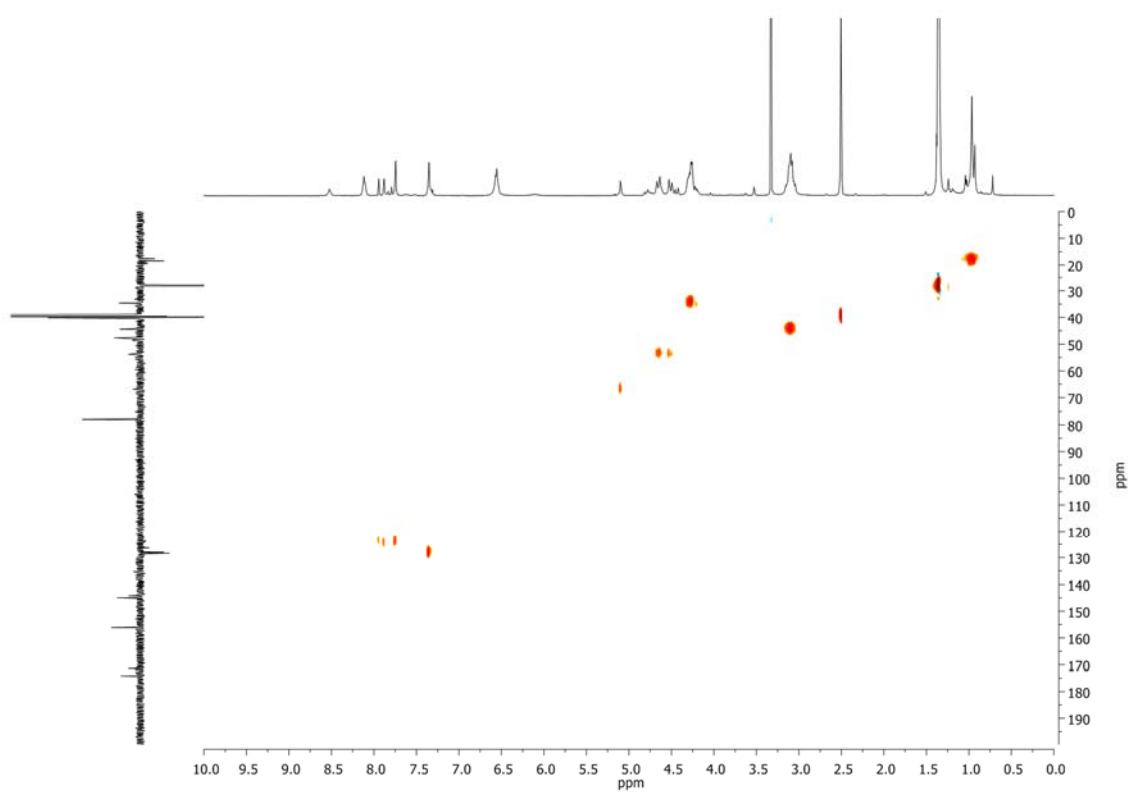


Figure 145. HSQC spectrum of **dG3-CO₂Bn** in DMSO-*d*₆.

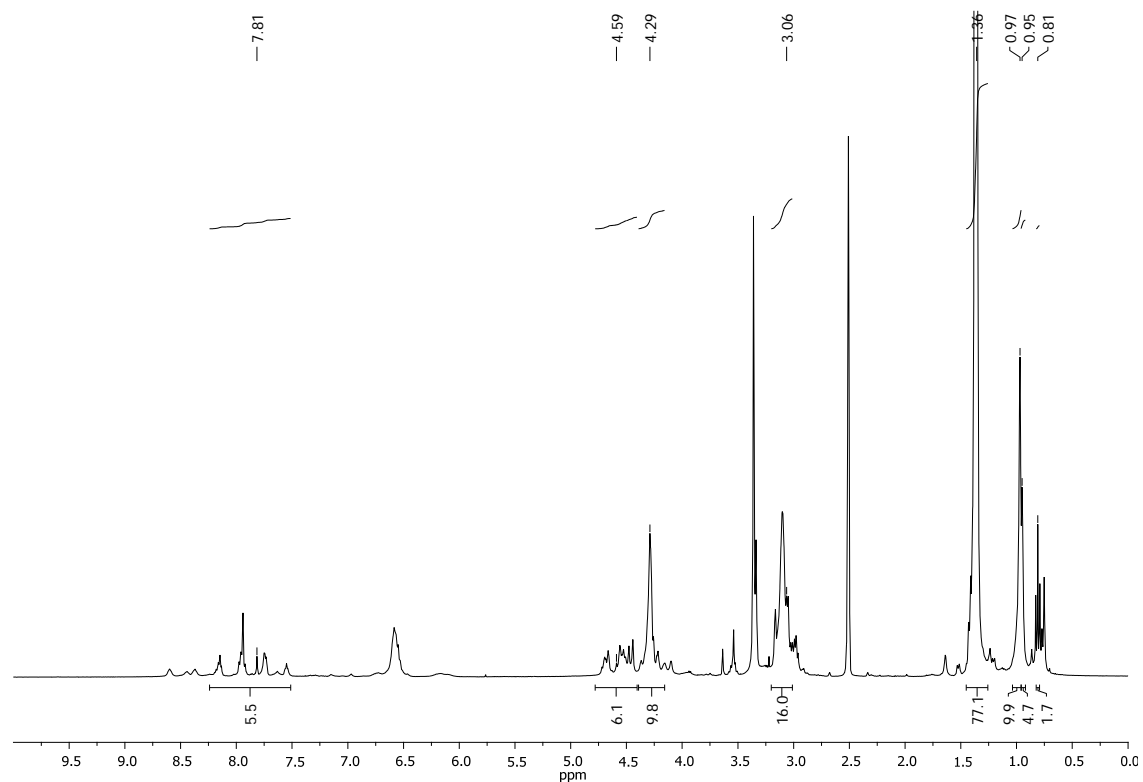


Figure 146. ¹H spectrum of dG3-CO₂H in DMSO-*d*₆.

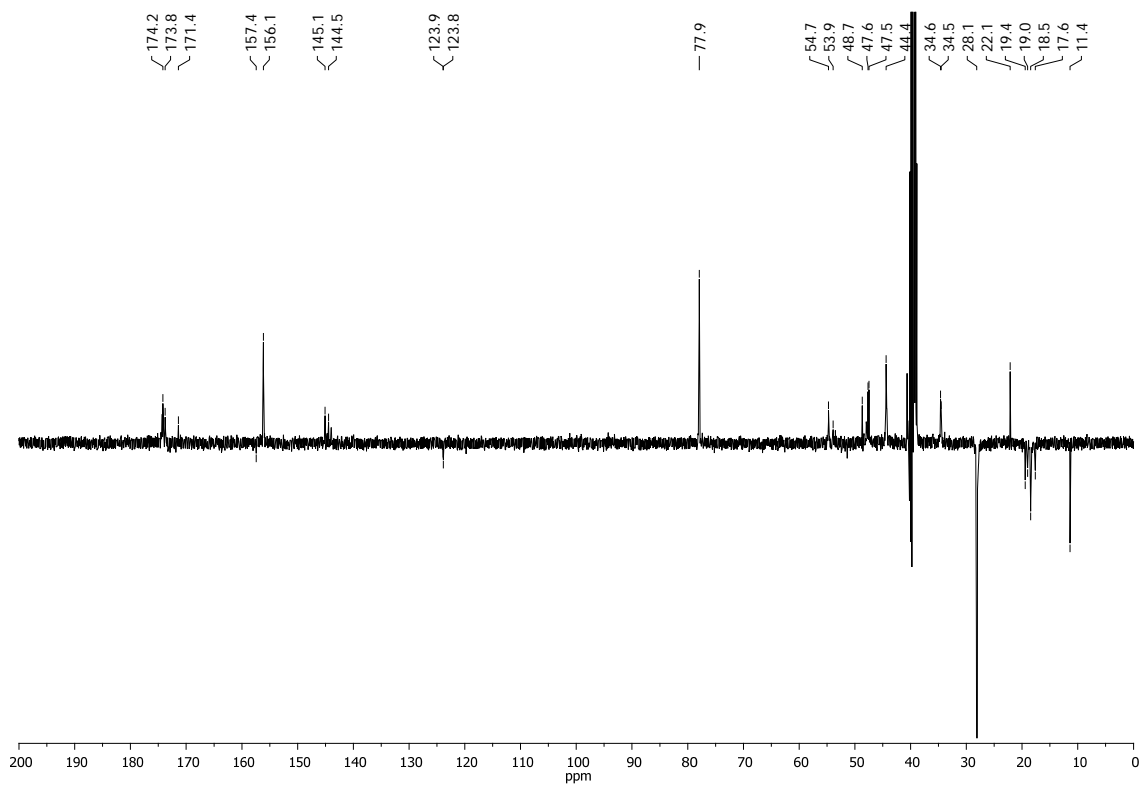


Figure 147. ¹³C (SEFT) spectrum of dG3-CO₂H in DMSO-*d*₆.

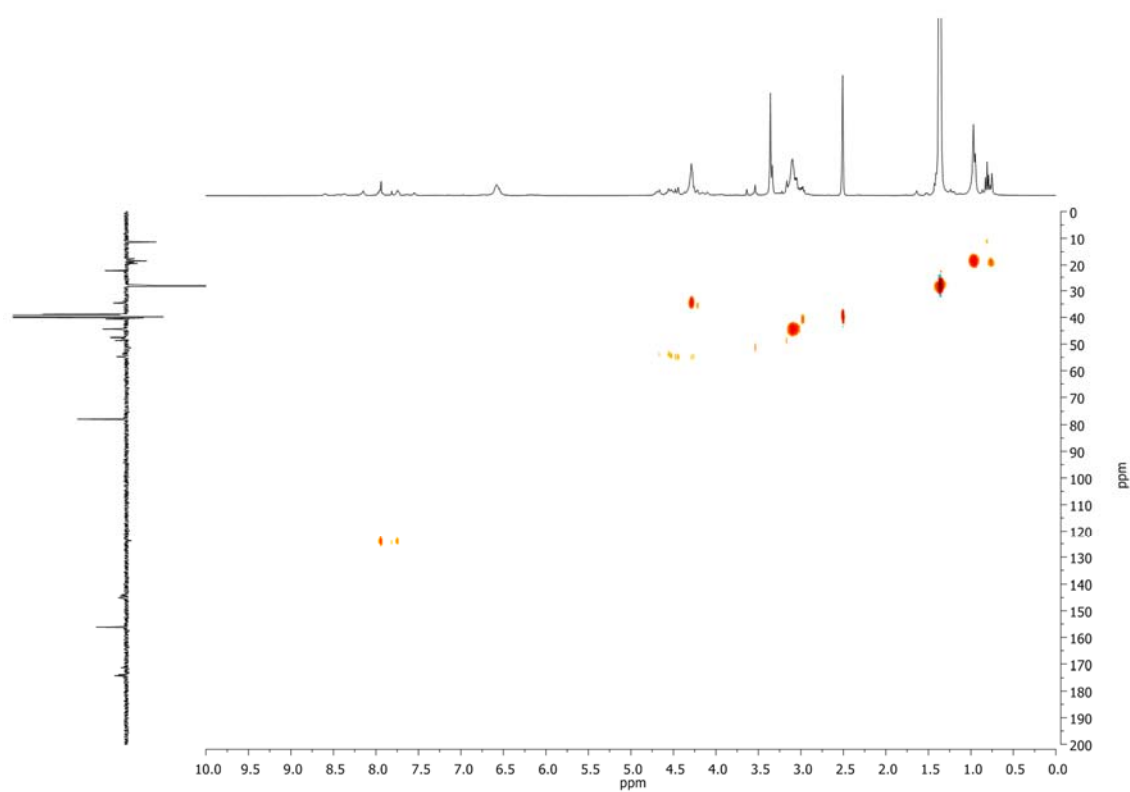


Figure 148. HSQC spectrum of **dG3-CO₂H** in DMSO-*d*₆.

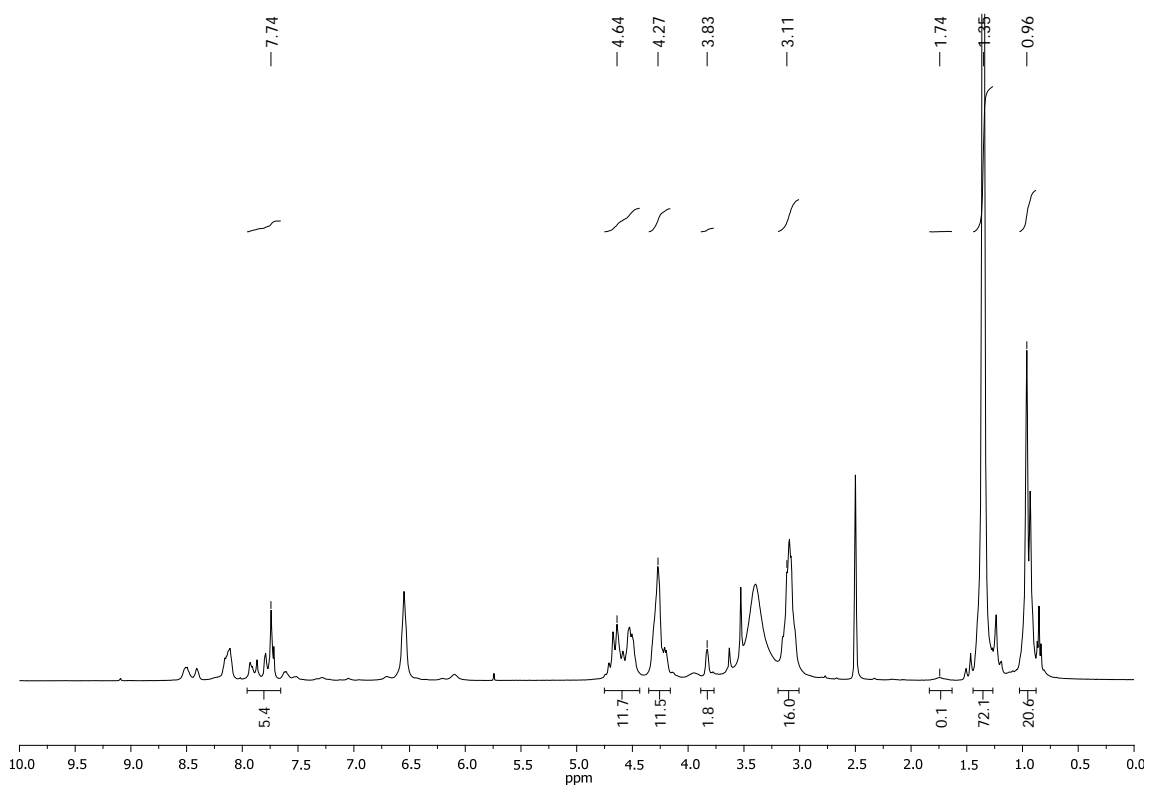


Figure 149. ¹H spectrum of **dG3** in DMSO-*d*₆.

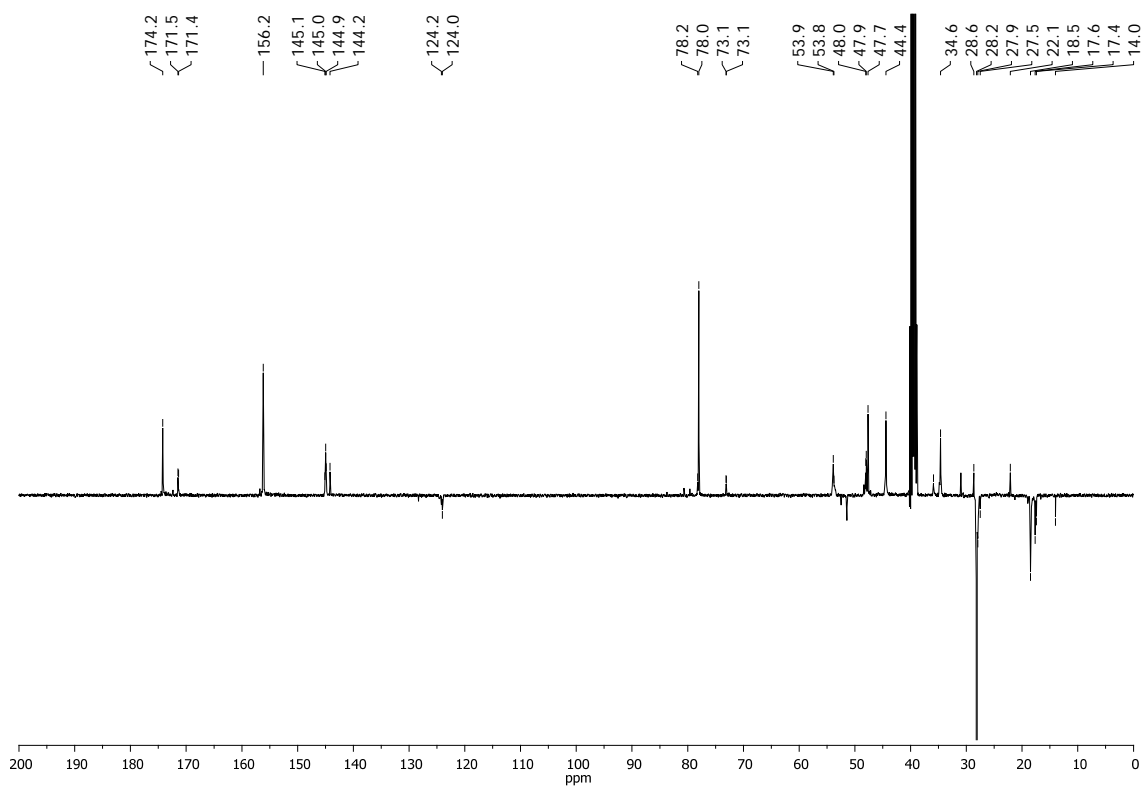


Figure 150. ¹³C (SEFT) spectrum of **dG3** in DMSO-*d*₆.

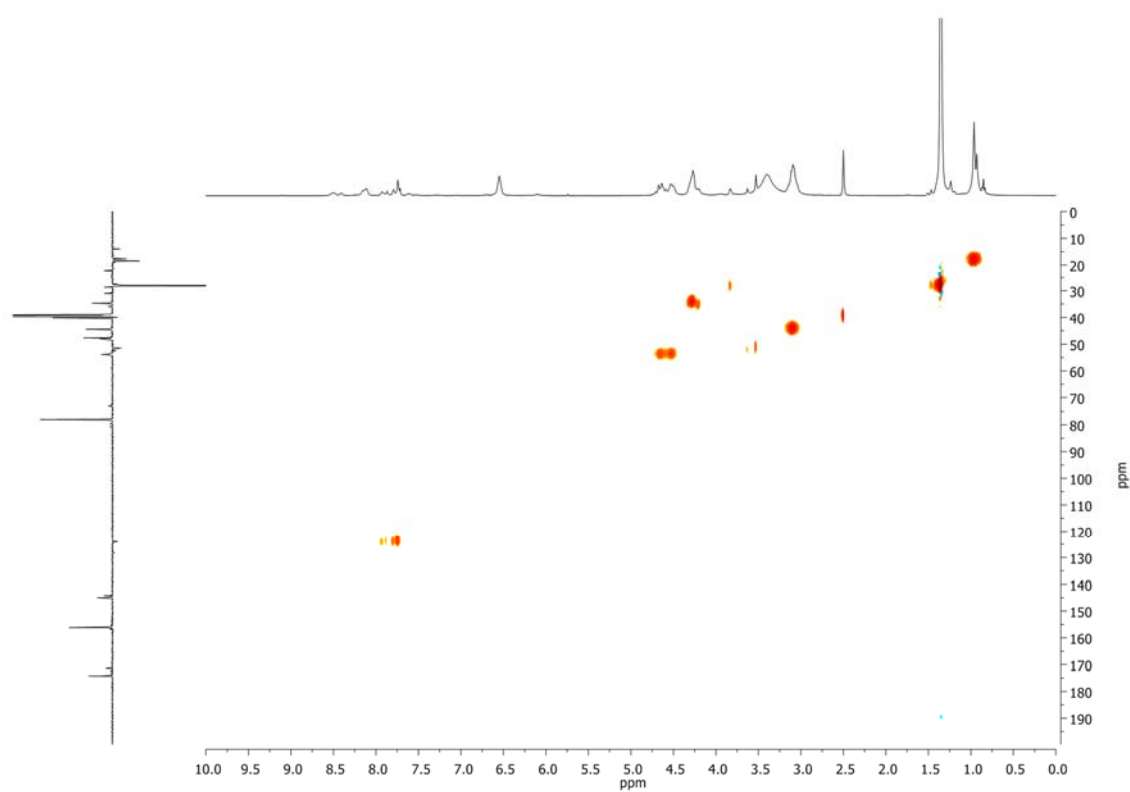


Figure 151. HSQC spectrum of **dG3** in $\text{DMSO-}d_6$.

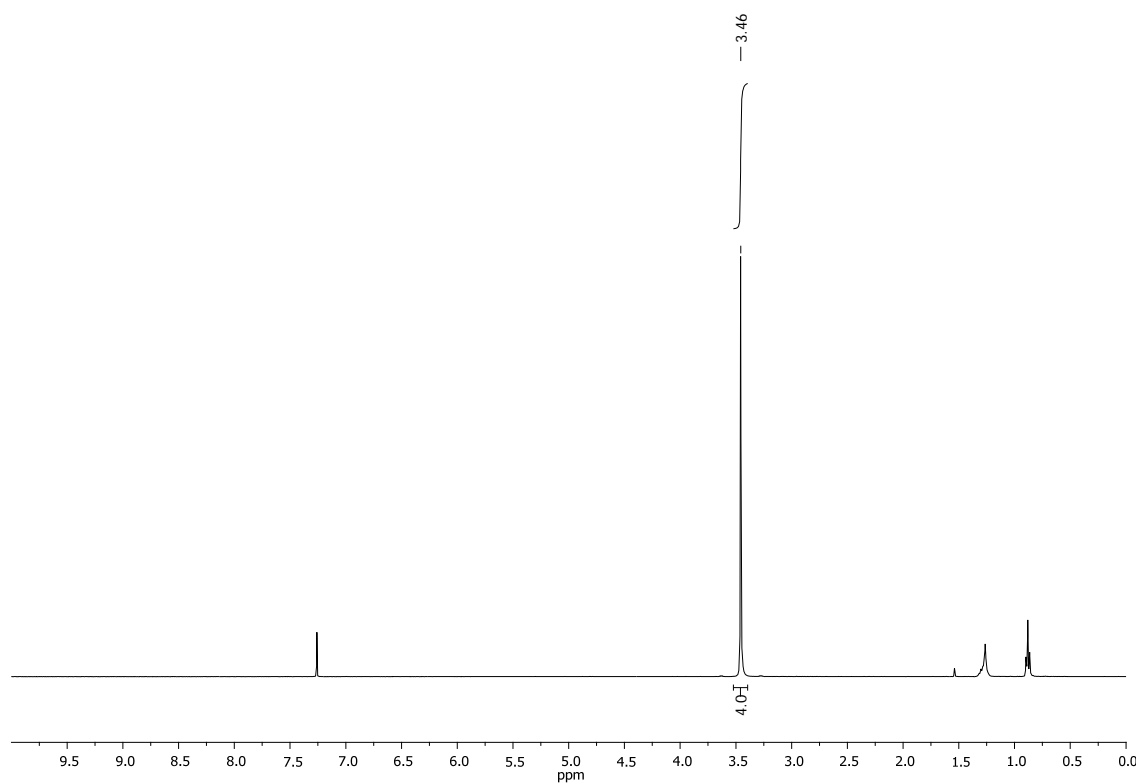


Figure 152. ^1H spectrum of **1,2-diazidoethane (6)** in CDCl_3 .

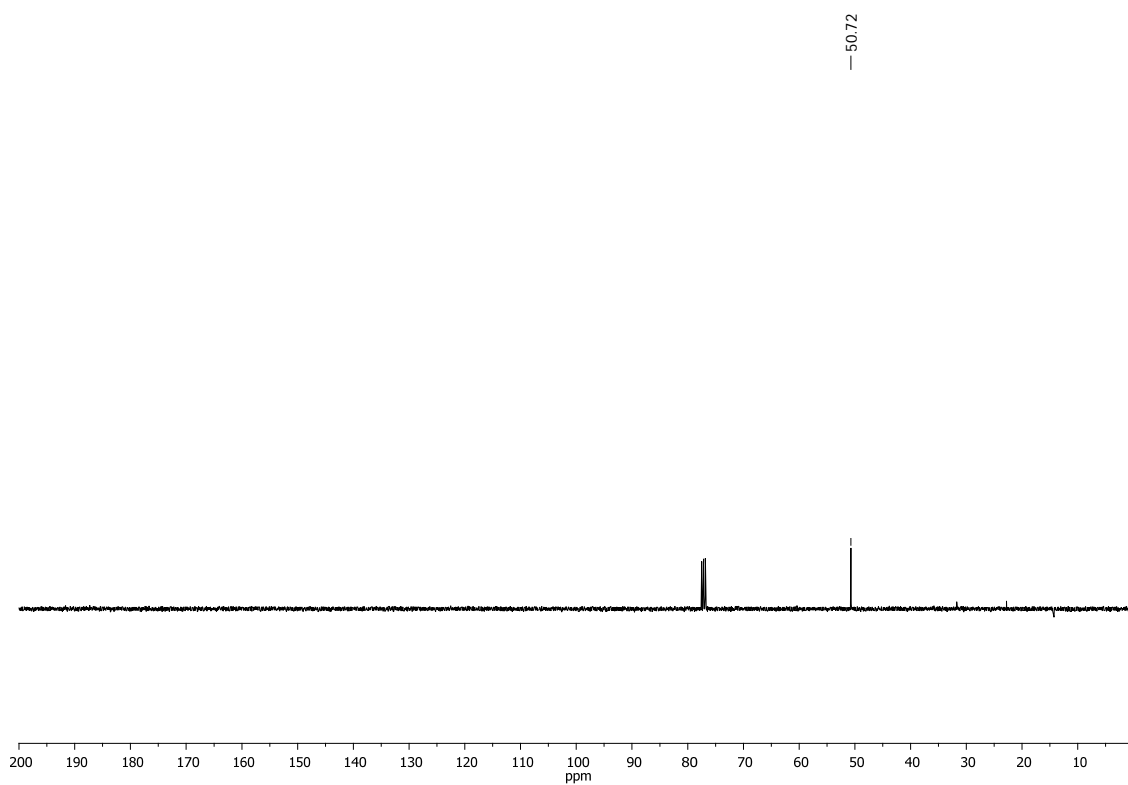


Figure 153. ^{13}C (SEFT) spectrum of **1,2-diazidoethane (6)** in CDCl_3 .

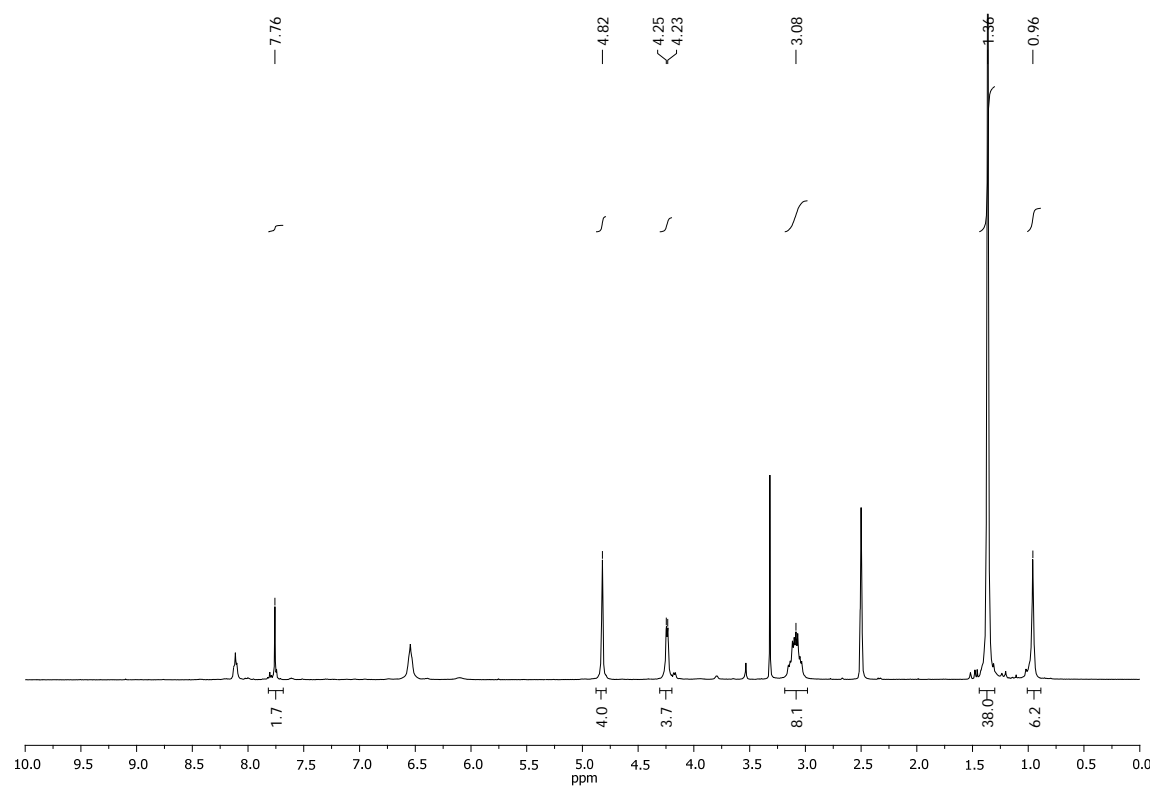


Figure 154. ¹H spectrum of **G1EDANHoc** in DMSO-*d*₆.

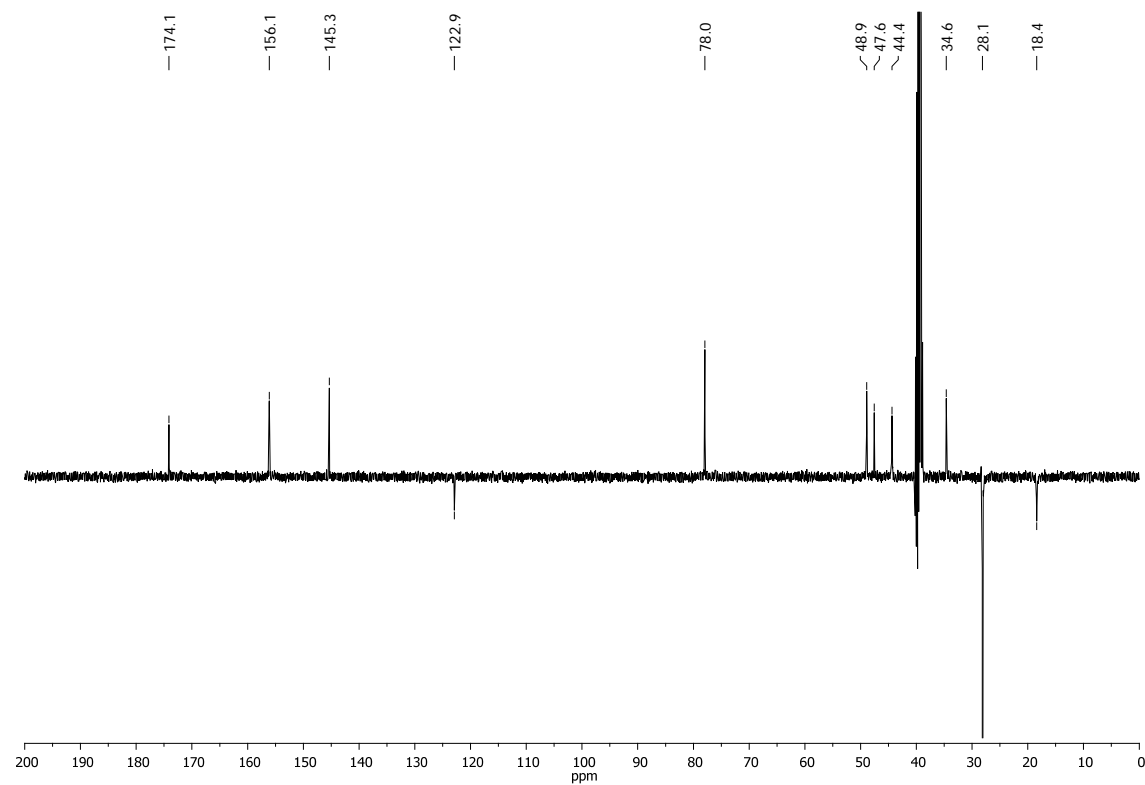


Figure 155. ¹³C (SEFT) spectrum of **G1EDANHoc** in DMSO-*d*₆.

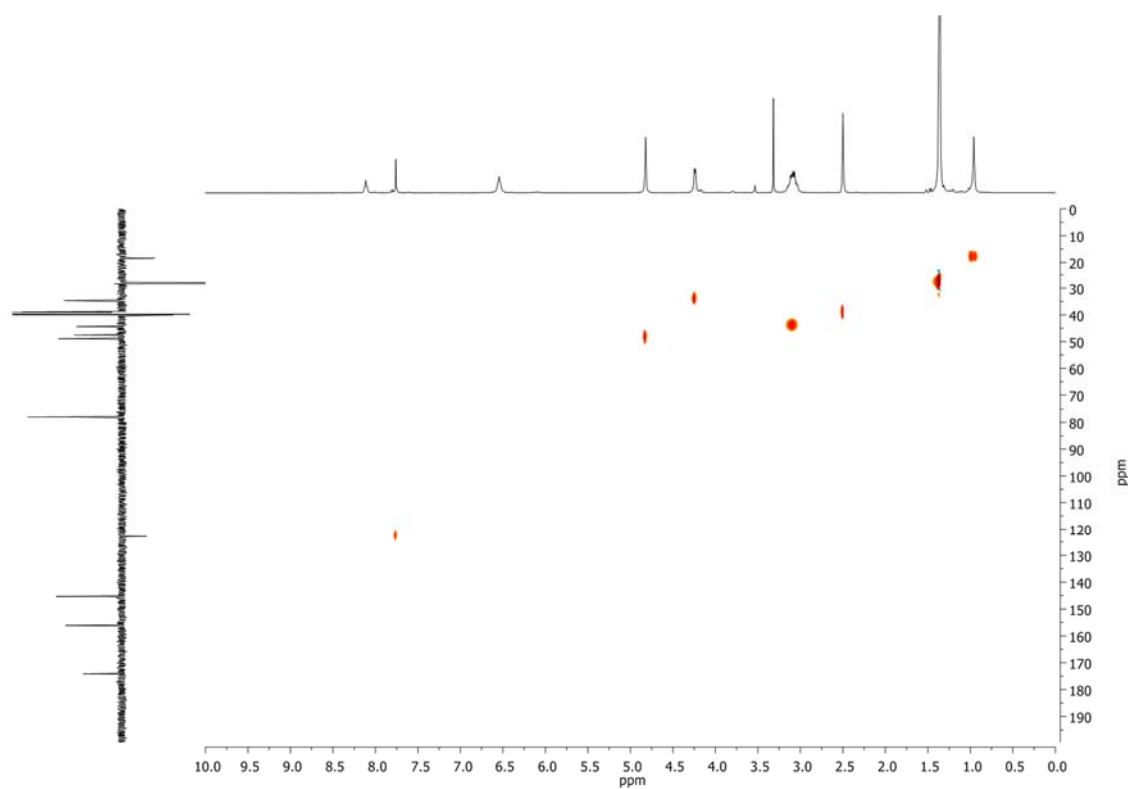


Figure 156. HSQC spectrum of **G1_{EDA}NHBoc** in $\text{DMSO-}d_6$.

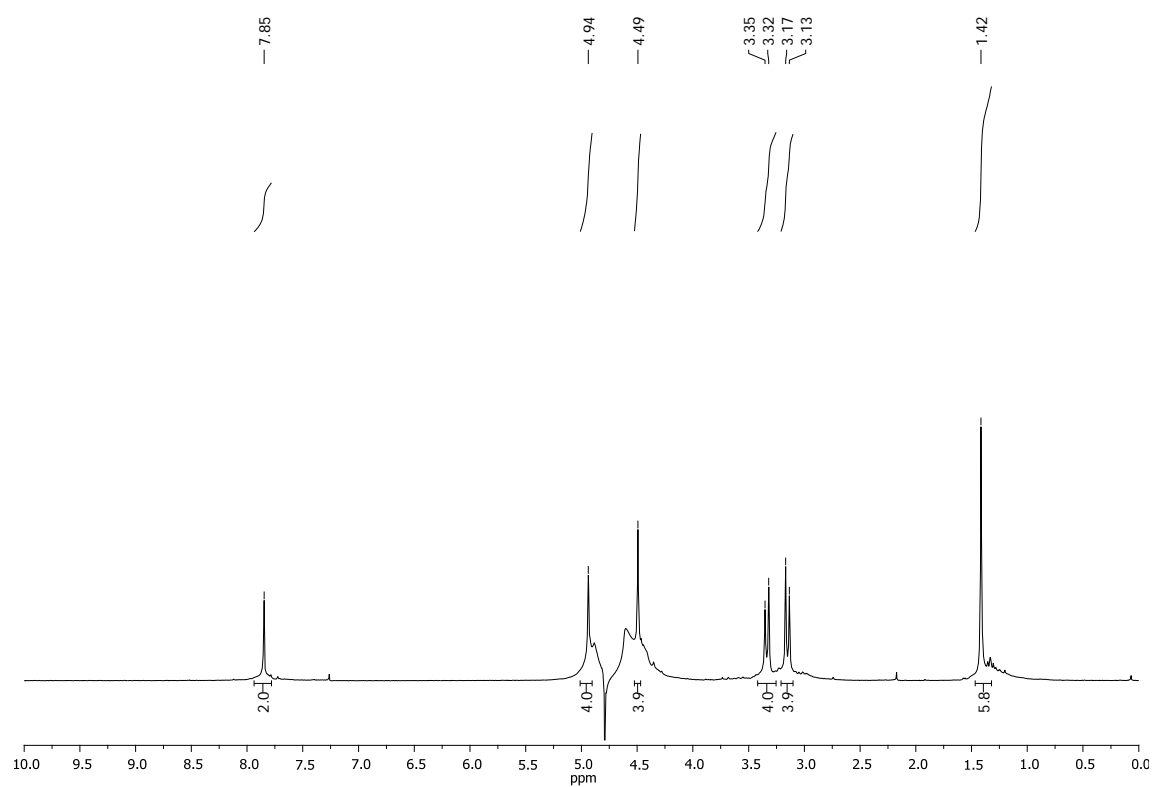


Figure 157. ¹H spectrum of **G1EDANH₂** in D₂O.

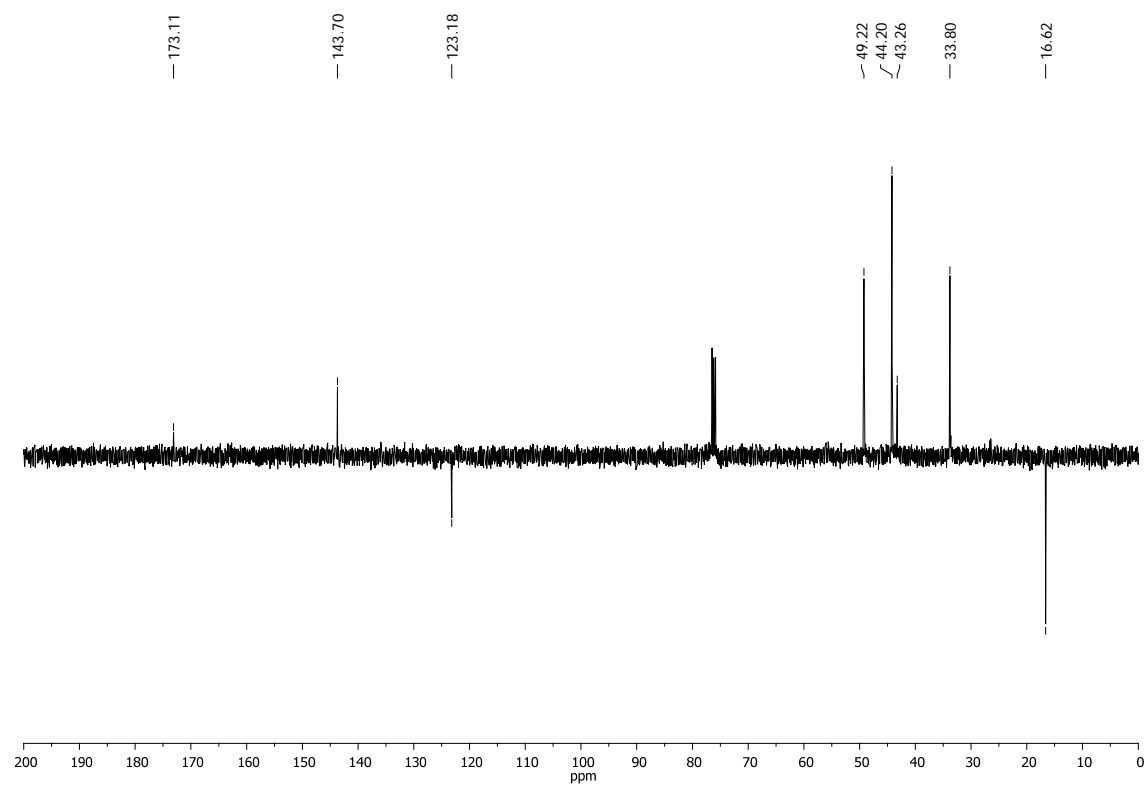


Figure 158. ¹³C (SEFT) spectrum of **G1EDANH₂** in D₂O.

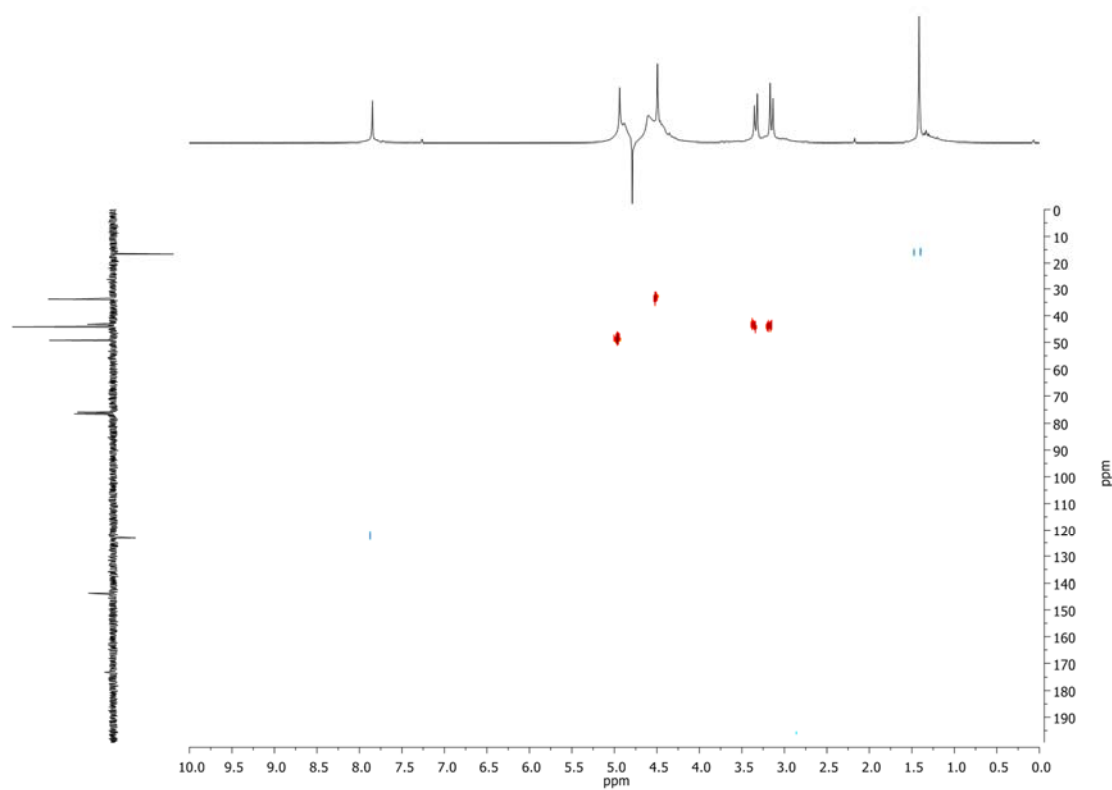


Figure 159. HSQC spectrum of **G1EDANH₂** in D₂O.

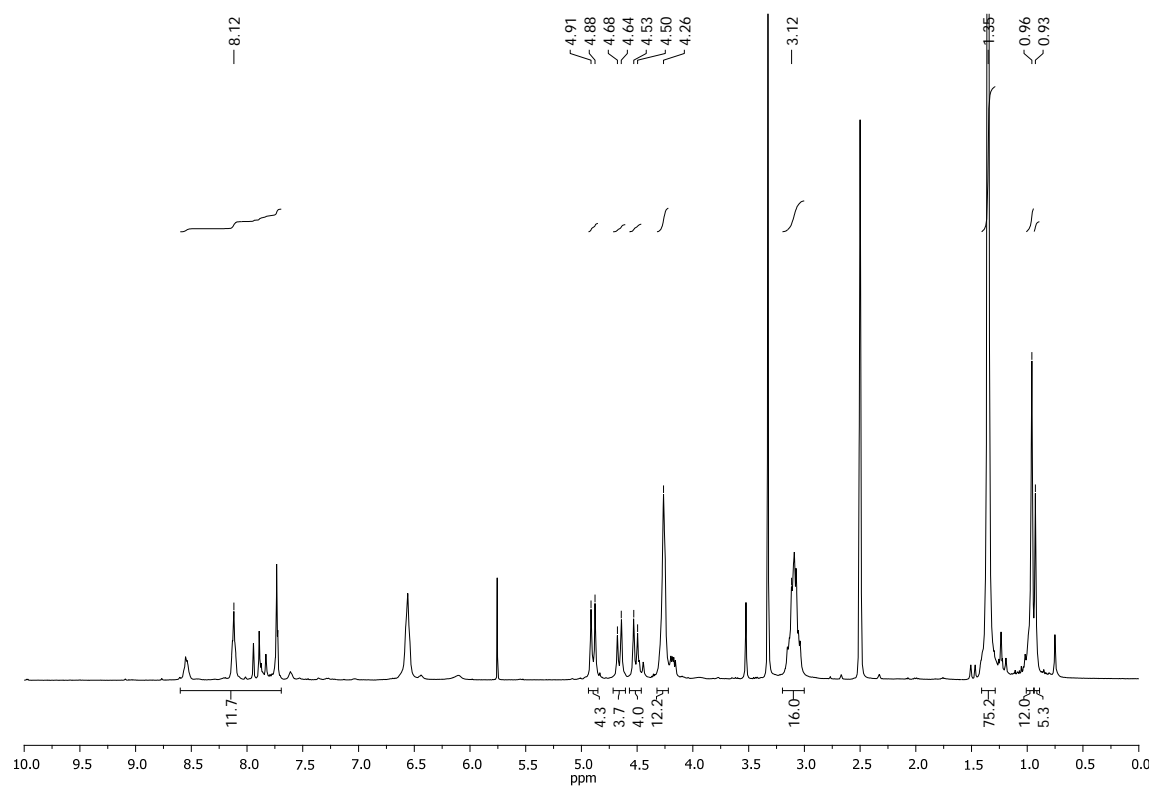


Figure 160. ¹H spectrum of **G2EDANH Boc** in DMSO-*d*₆.

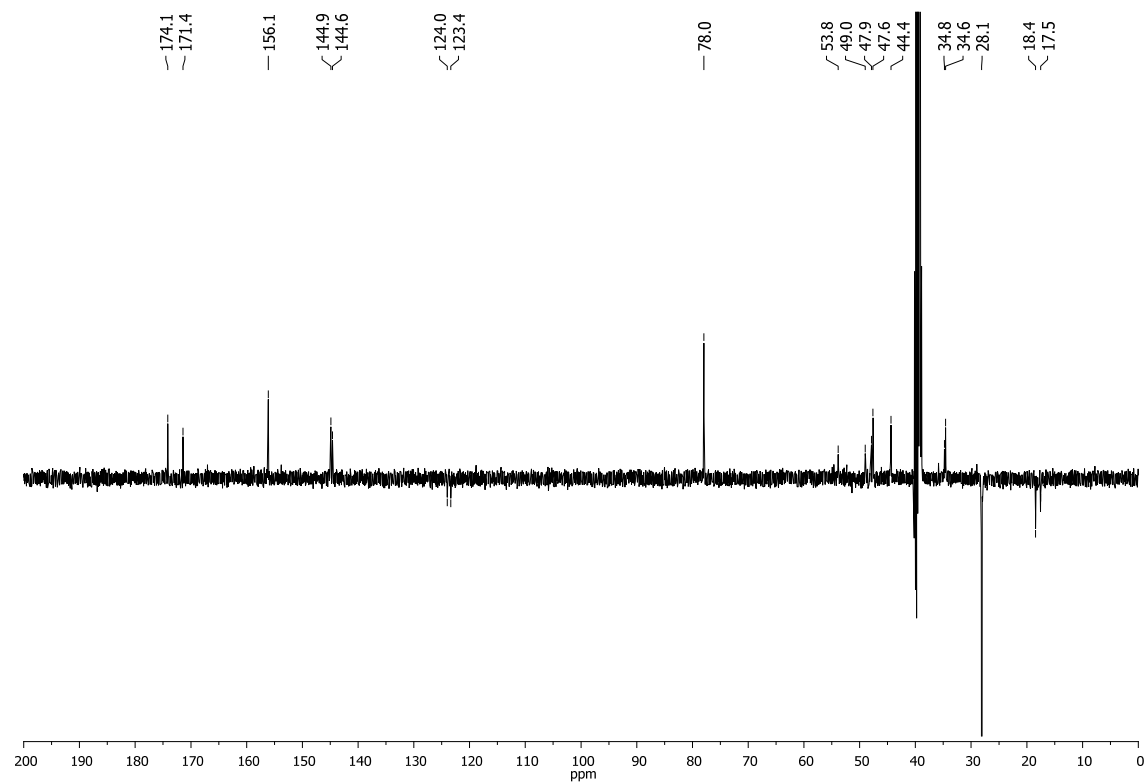


Figure 161. ¹³C (SEFT) spectrum of **G2EDANH Boc** in DMSO-*d*₆.

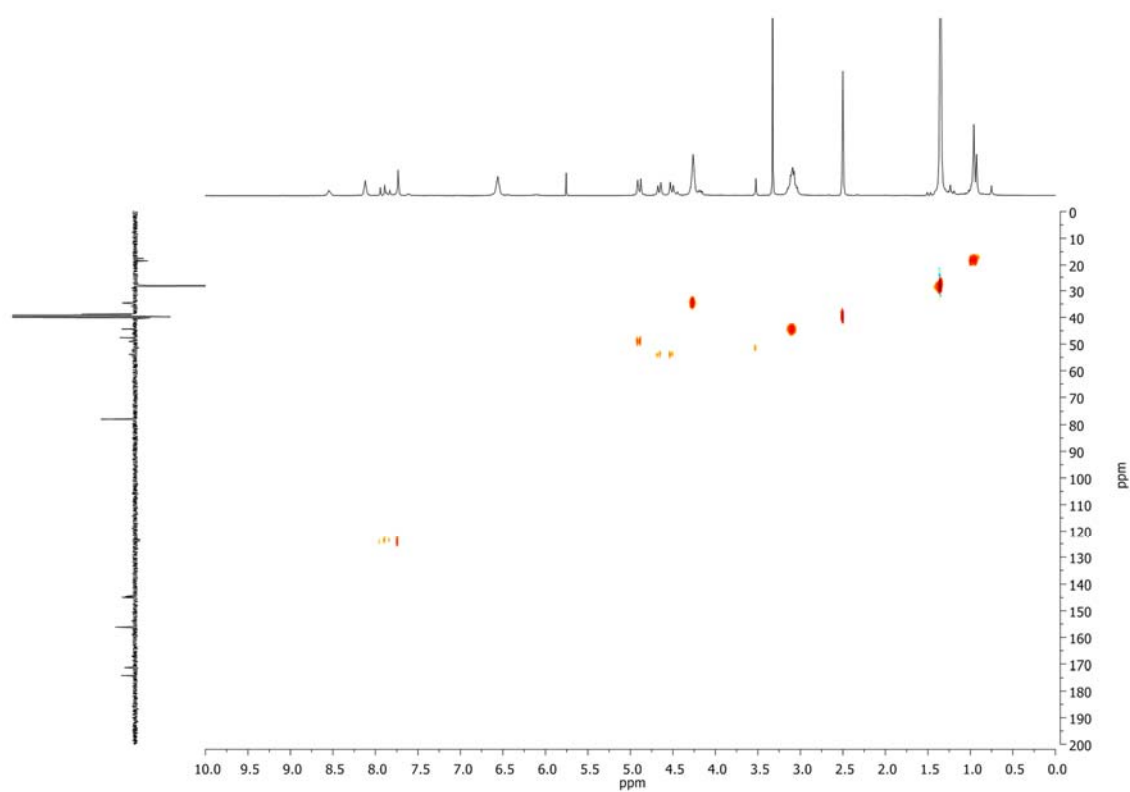


Figure 162. HSQC spectrum of **G2EDANHoc** in DMSO-*d*₆.

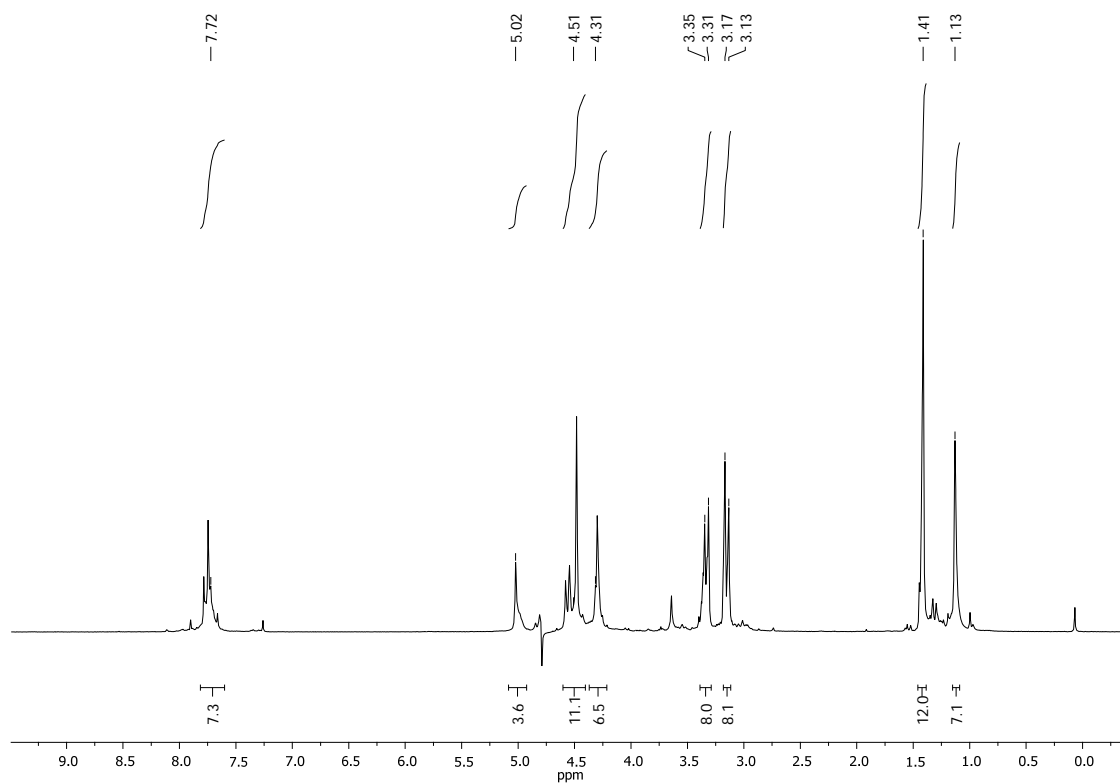


Figure 163. ¹H spectrum of **G2EDANH2** in D₂O.

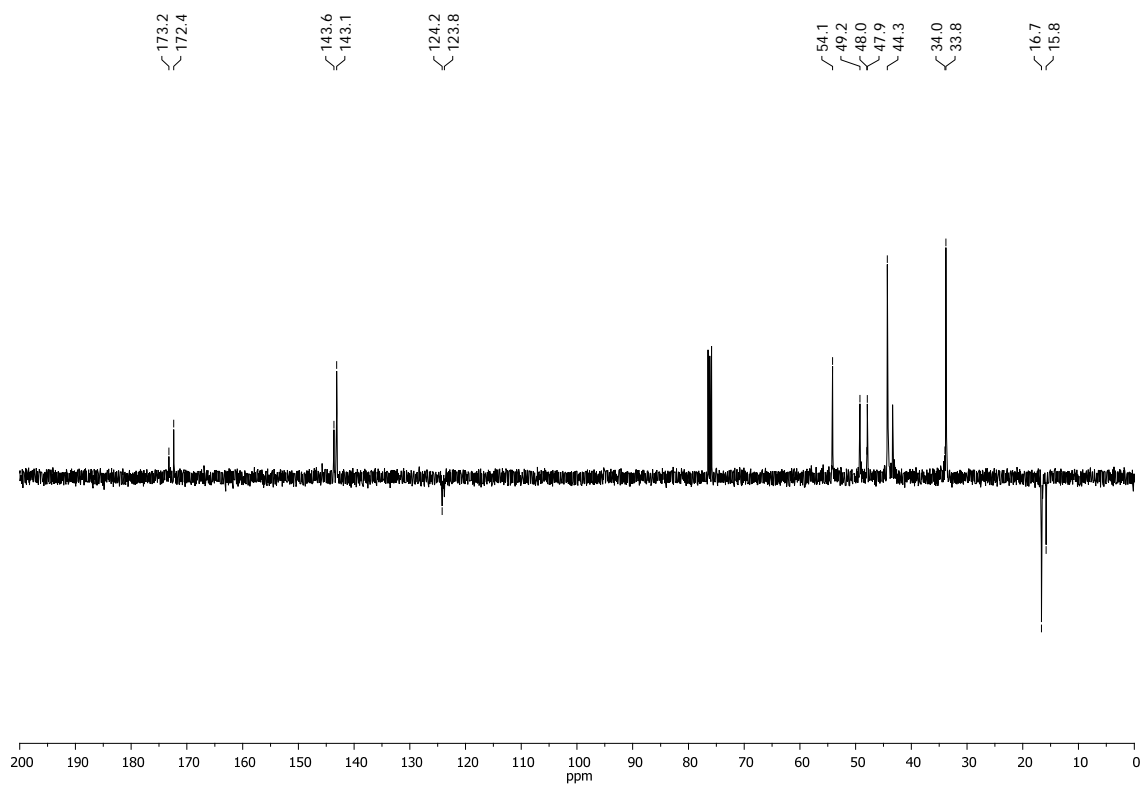


Figure 164. ¹³C (SEFT) spectrum of **G2EDANH2** in D₂O.

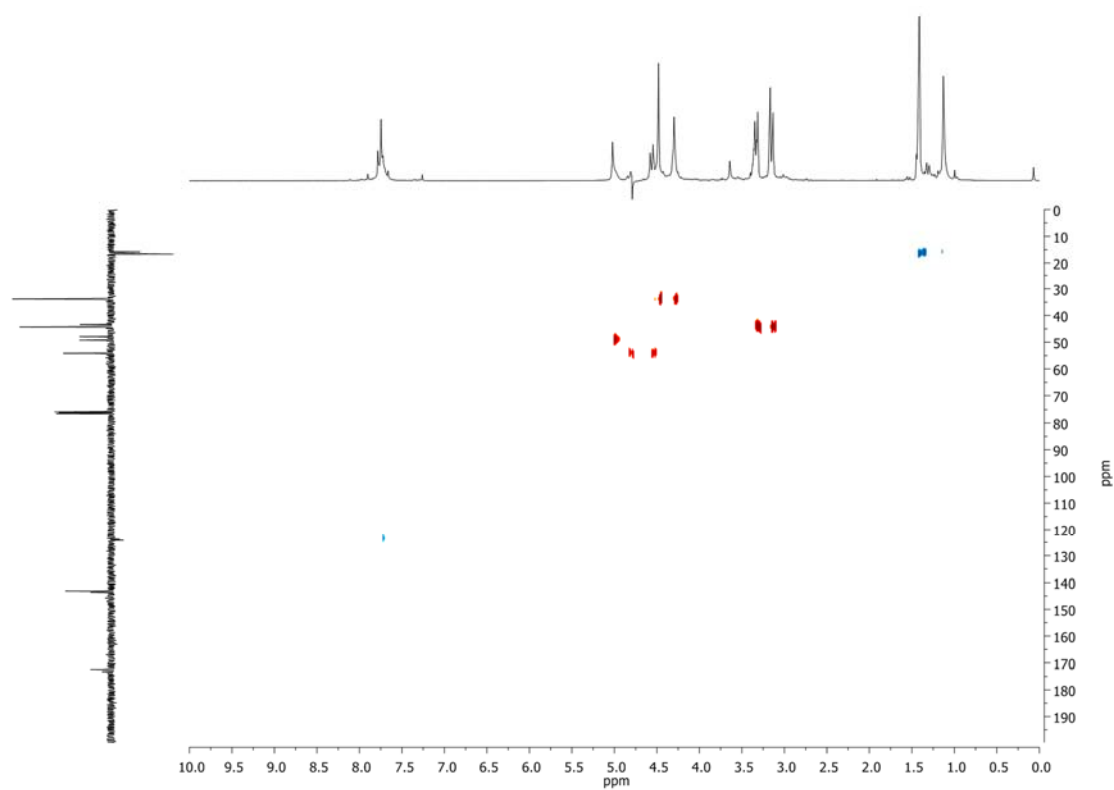


Figure 165. HSQC spectrum of **G2EDANH2** in D₂O.

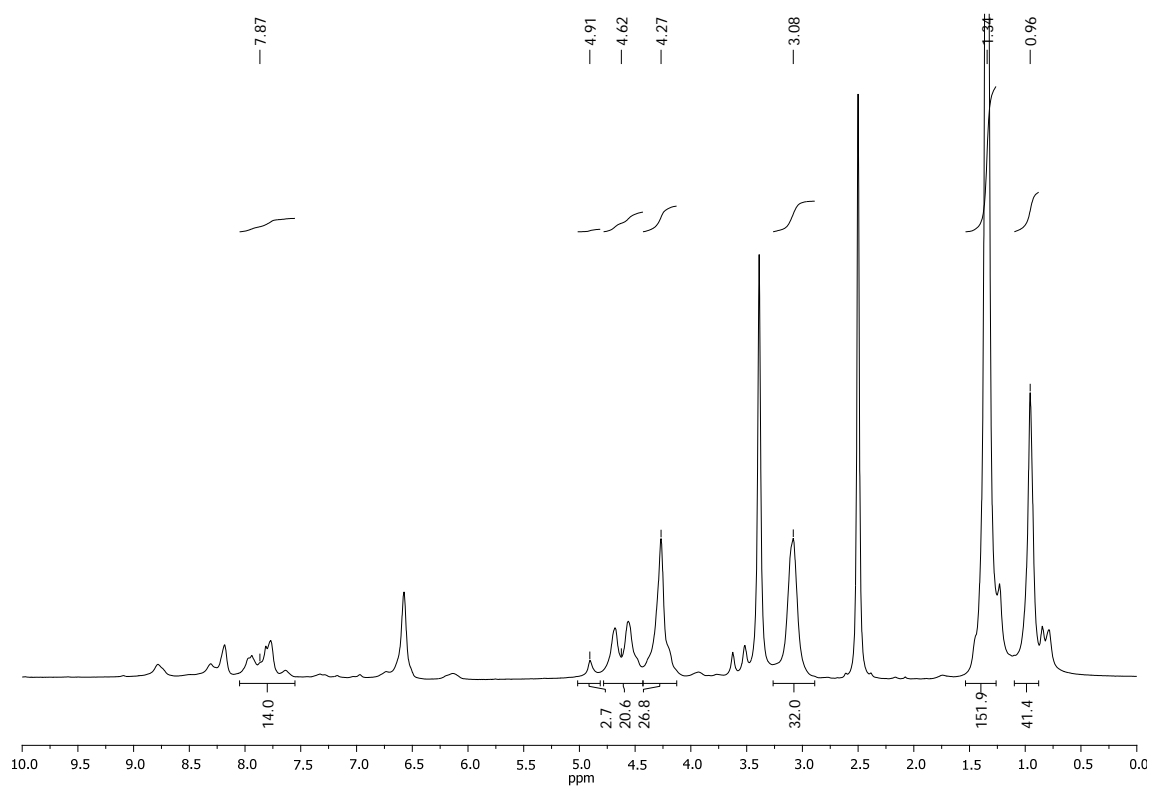


Figure 166. ^1H spectrum of **G3EDANH Boc** in $\text{DMSO-}d_6$.

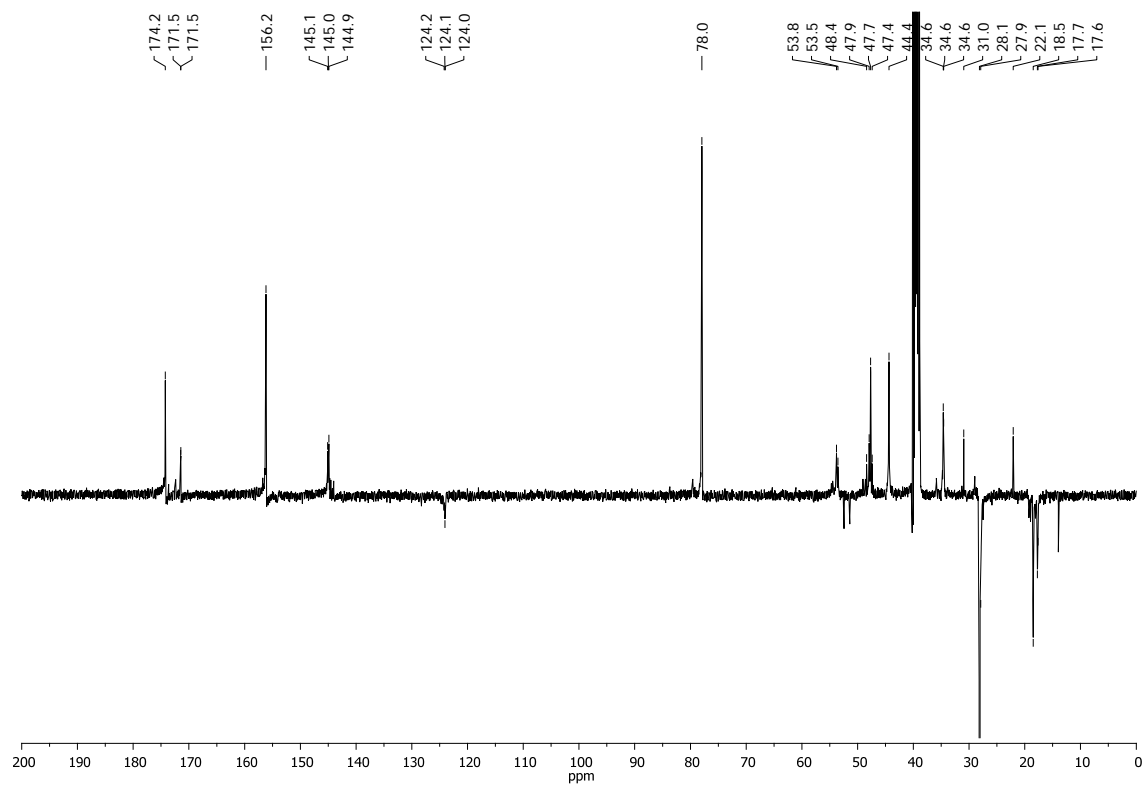


Figure 167. ^{13}C (SEFT) spectrum of **G3EDANH Boc** in $\text{DMSO-}d_6$.

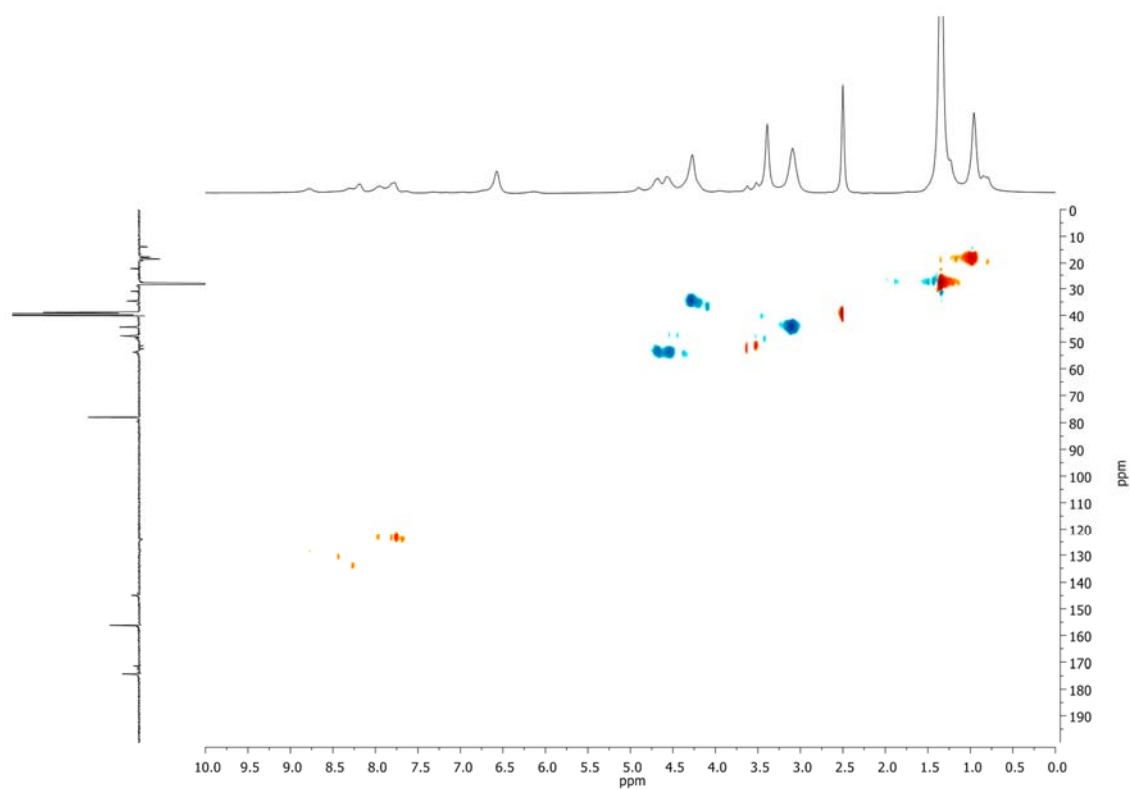


Figure 168. HSQC spectrum of **G3_{ED}ANH Boc** in DMSO-*d*₆.

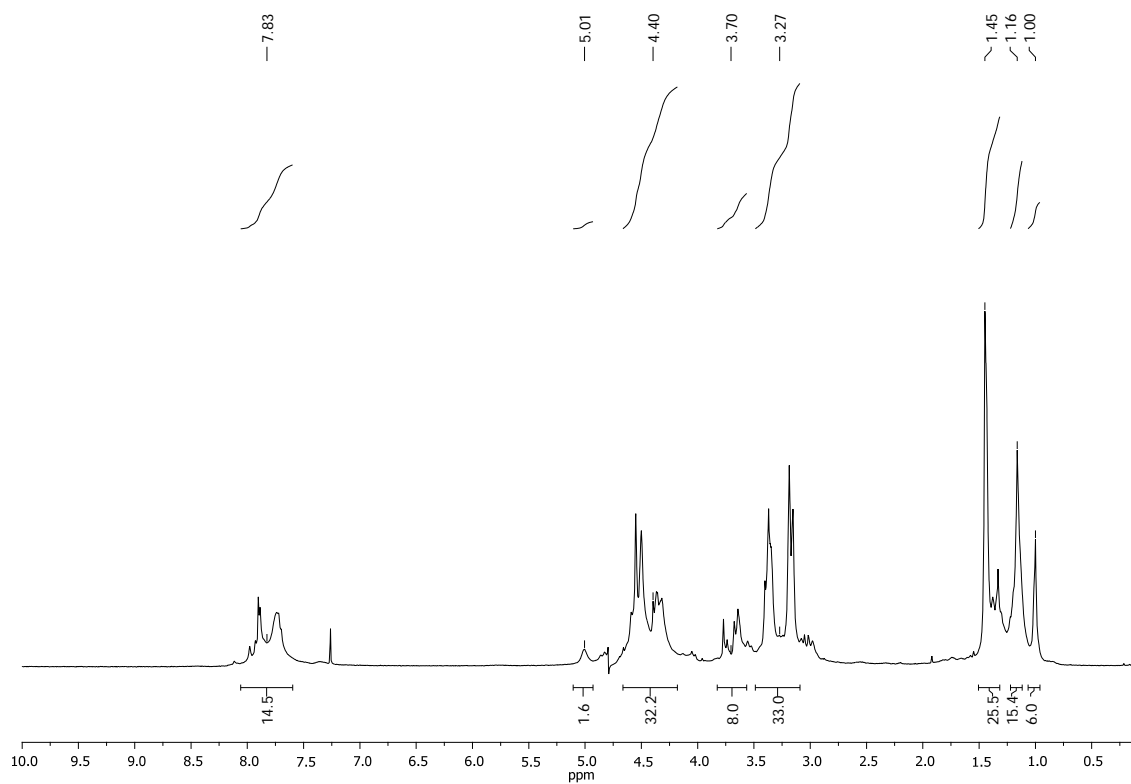


Figure 169. ^1H spectrum of G3EDANH_2 in D_2O .

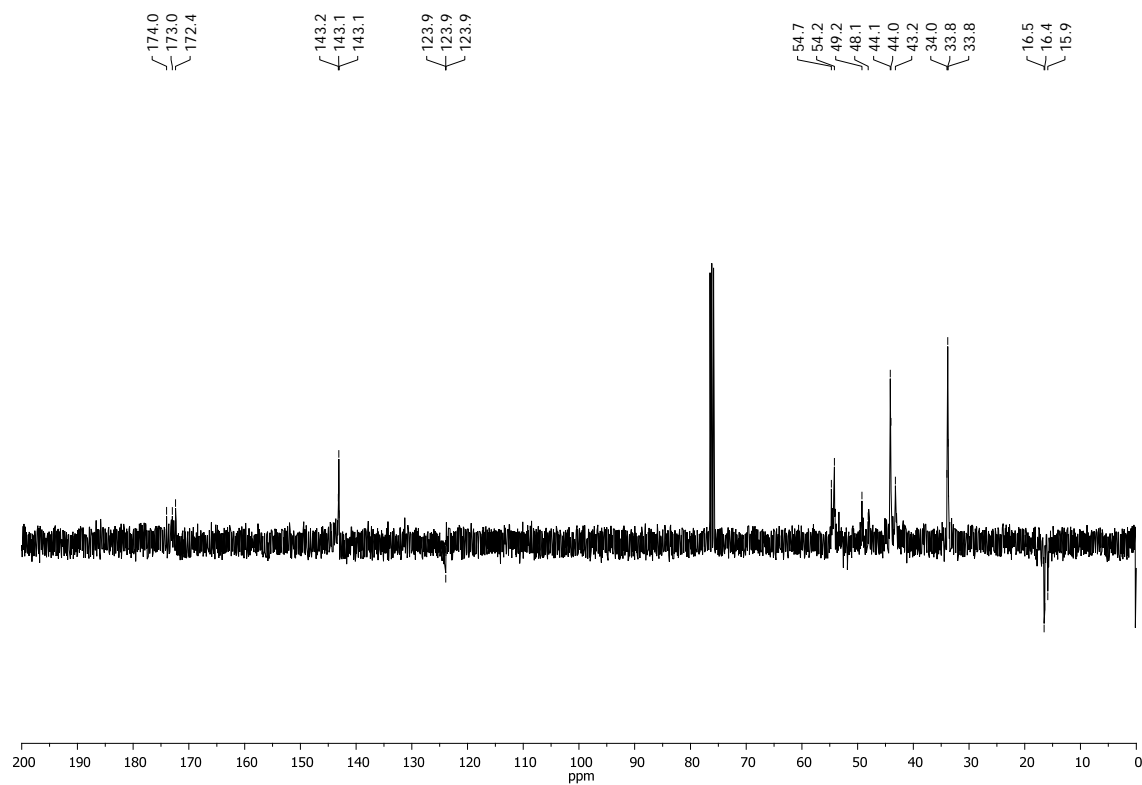


Figure 170. ^{13}C (SEFT) spectrum of G3EDANH_2 in D_2O .

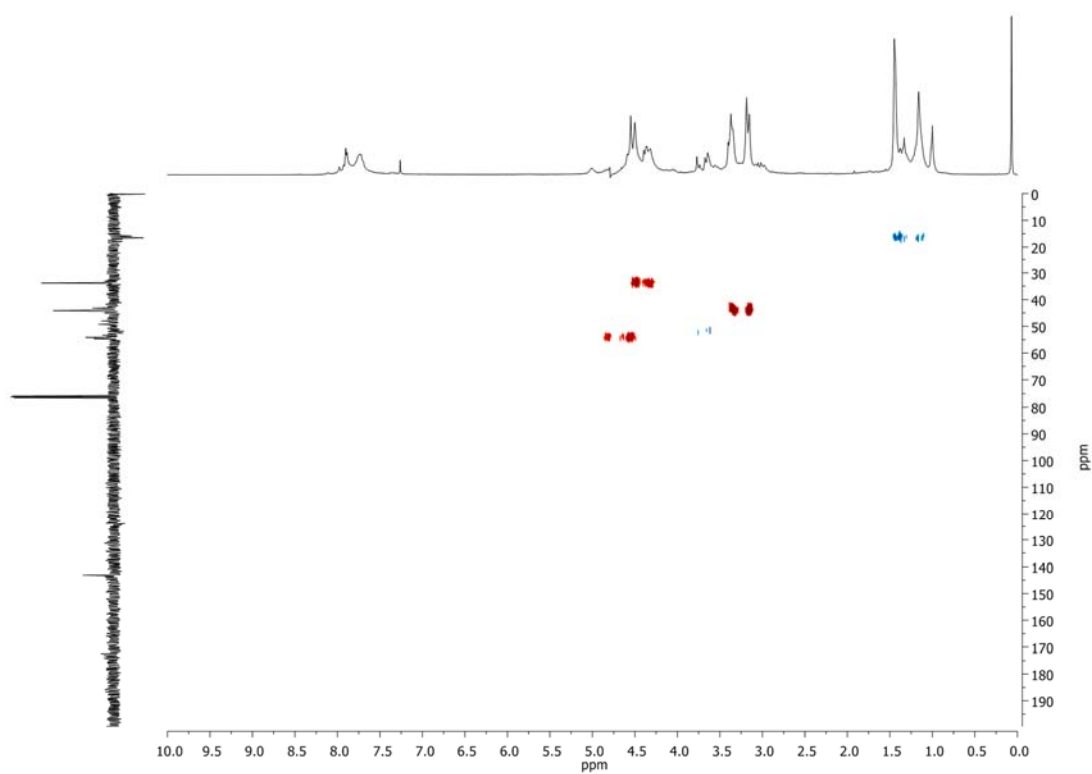


Figure 171. HSQC spectrum of G3EDANH_2 in D_2O .

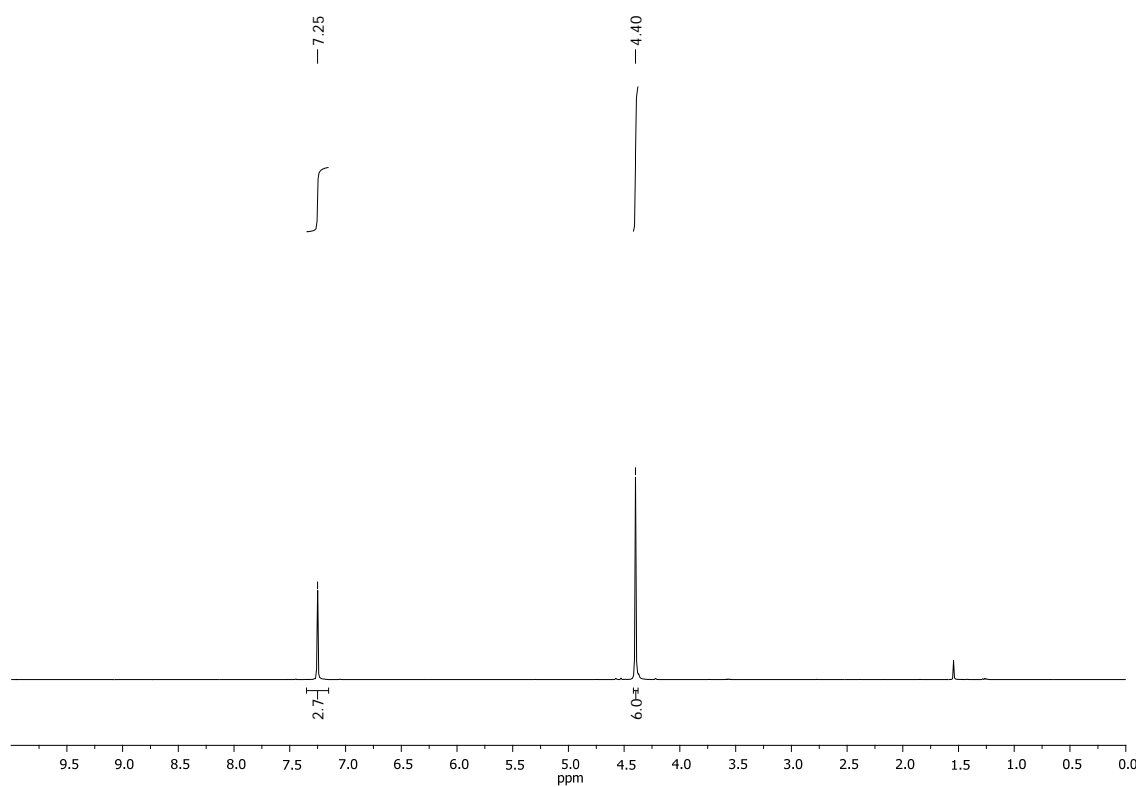


Figure 172. ^1H spectrum of **1,3,5-tris(azidomethyl)benzene (7)** in CDCl_3 .

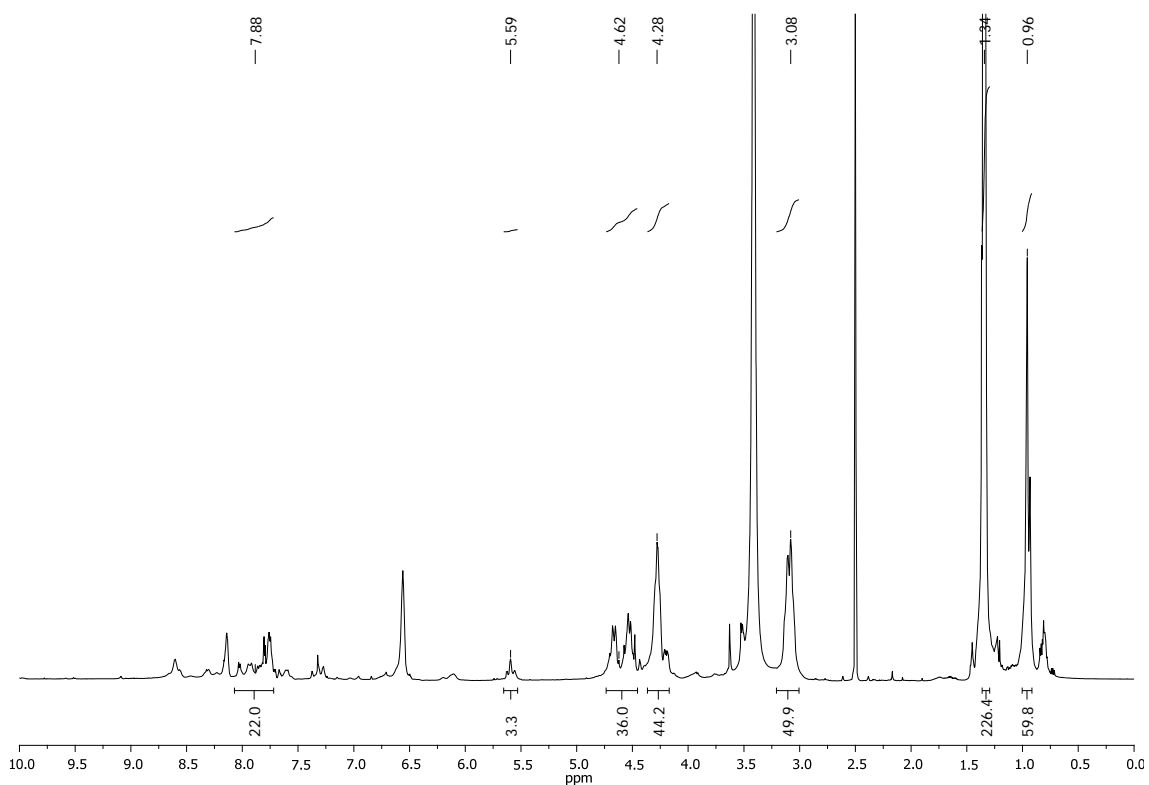


Figure 173. ¹H spectrum of **G3_{3AB}NHBoc** in DMSO-*d*₆.

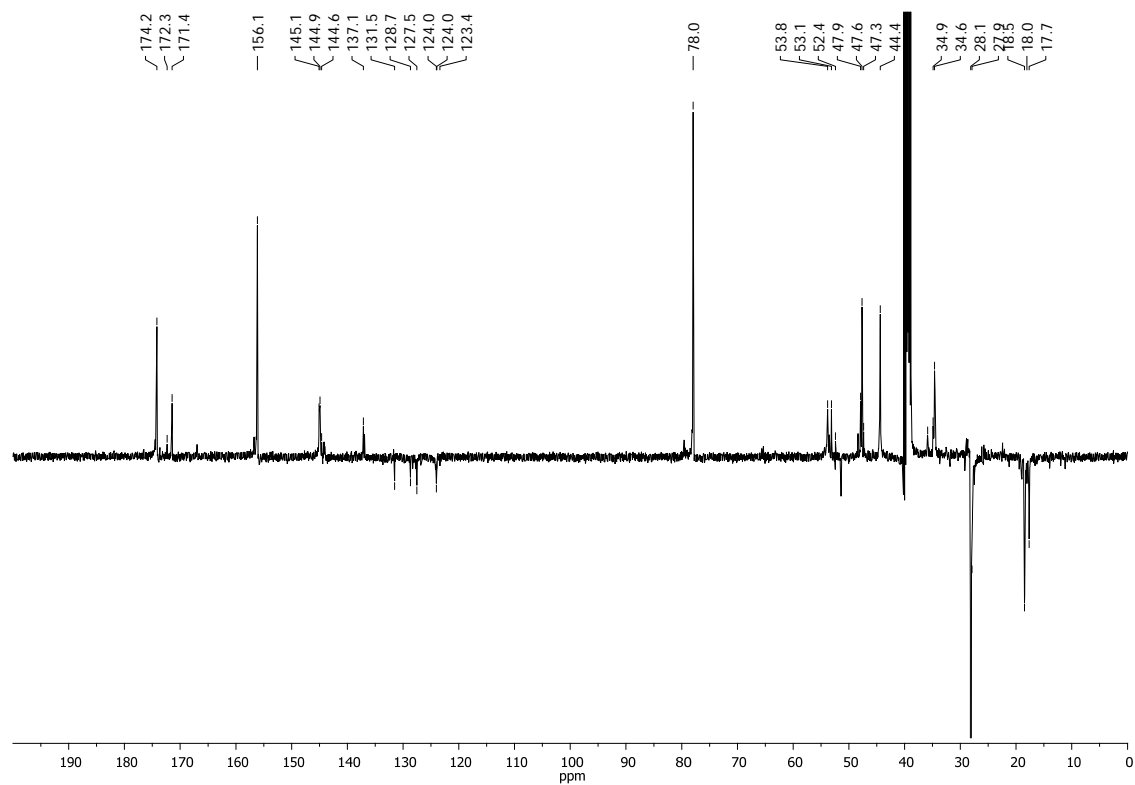


Figure 174. ¹³C (SEFT) spectrum of **G3_{3AB}NHBoc** in DMSO-*d*₆.

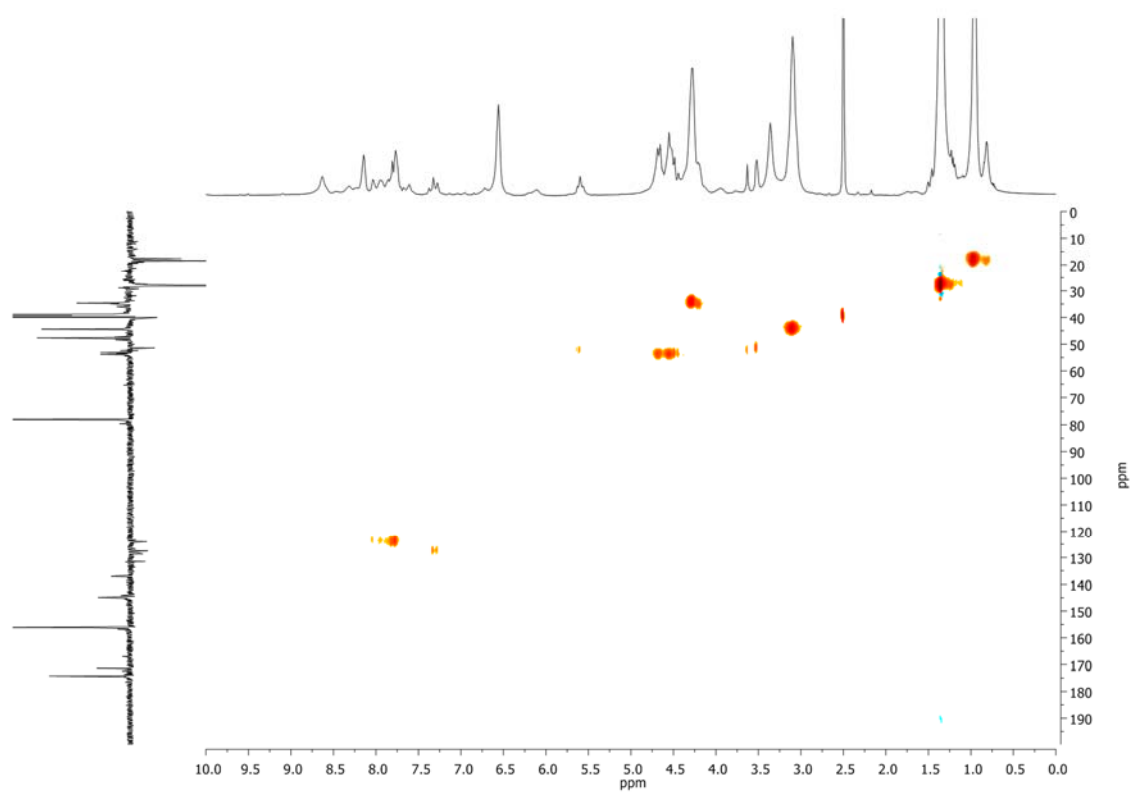


Figure 175. HSQC spectrum of **G3_{3AB}NHBoc** in DMSO-*d*₆.

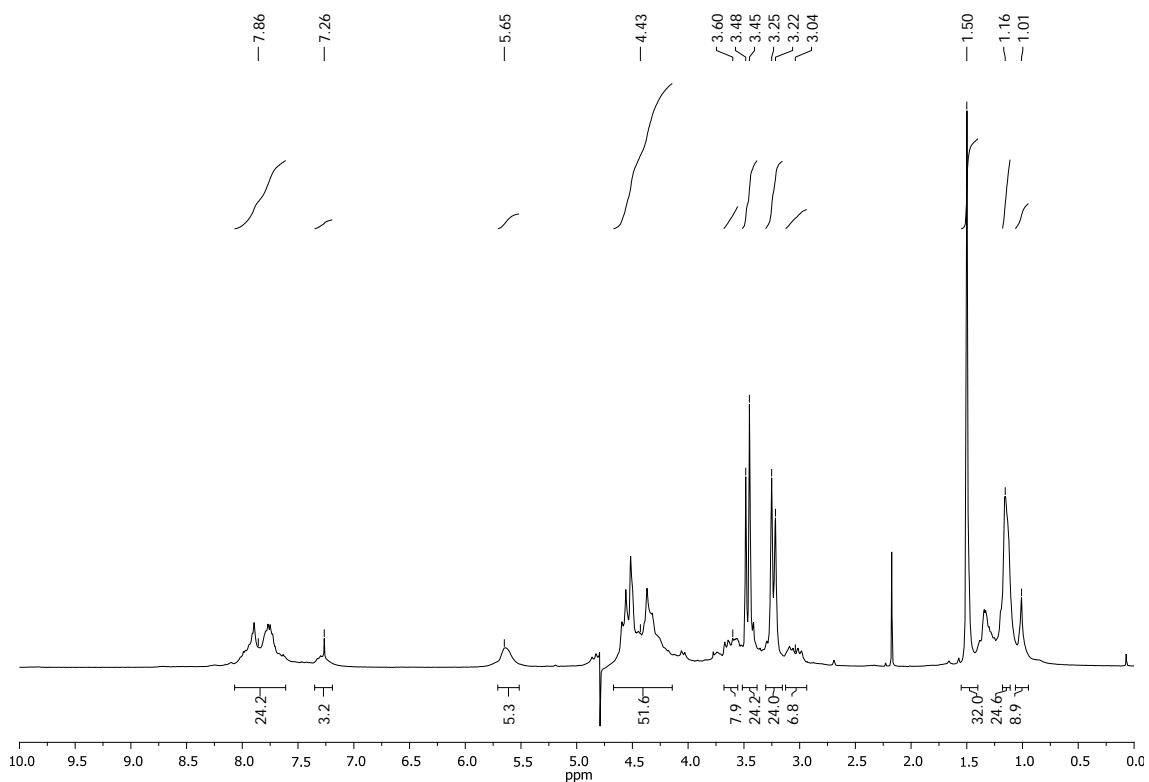


Figure 176. ¹H spectrum of **G**₃₃ABNH₂ in D₂O.

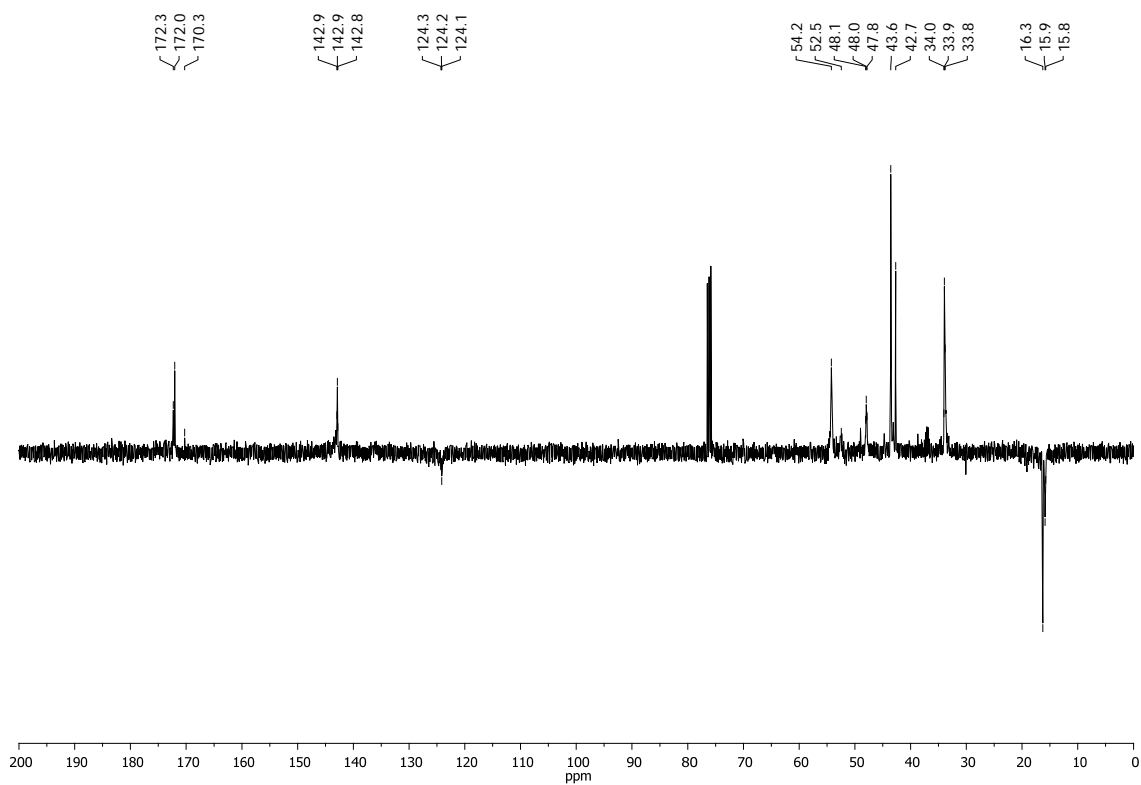


Figure 177. ¹³C (SEFT) spectrum of **G**₃₃ABNH₂ in D₂O.

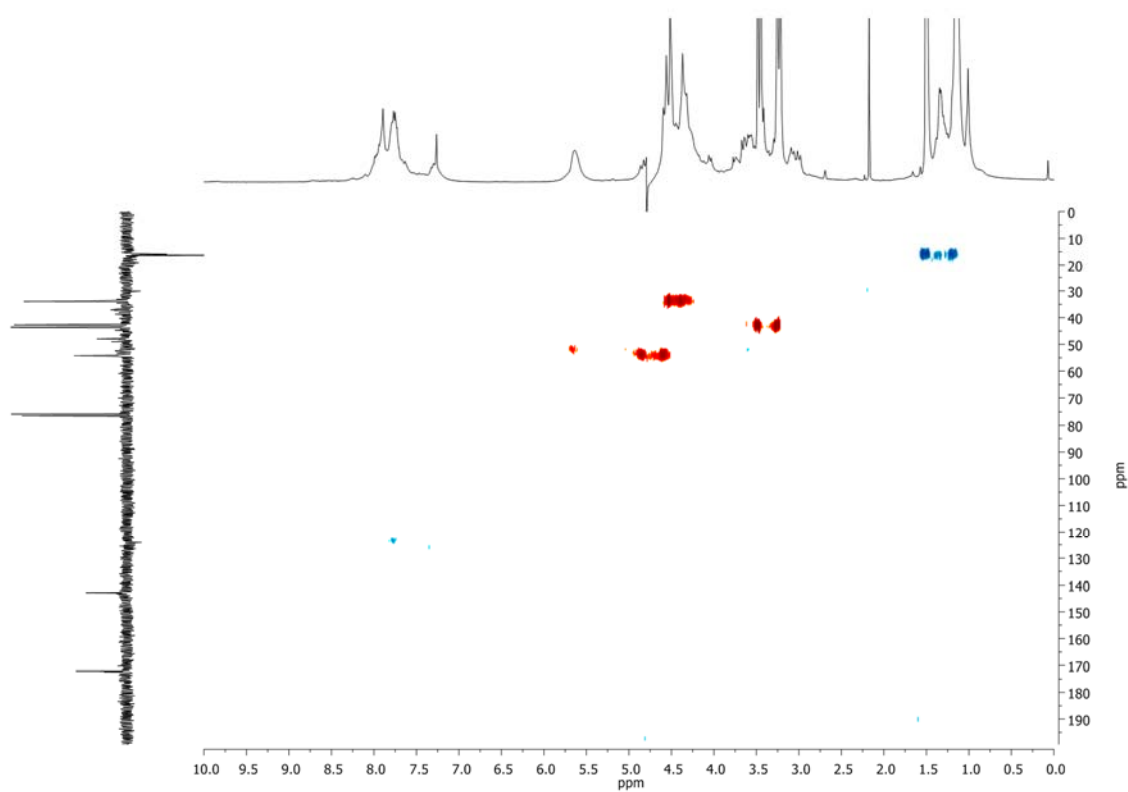


Figure 178. HSQC spectrum of **G3_{3AB}NH₂** in D₂O.

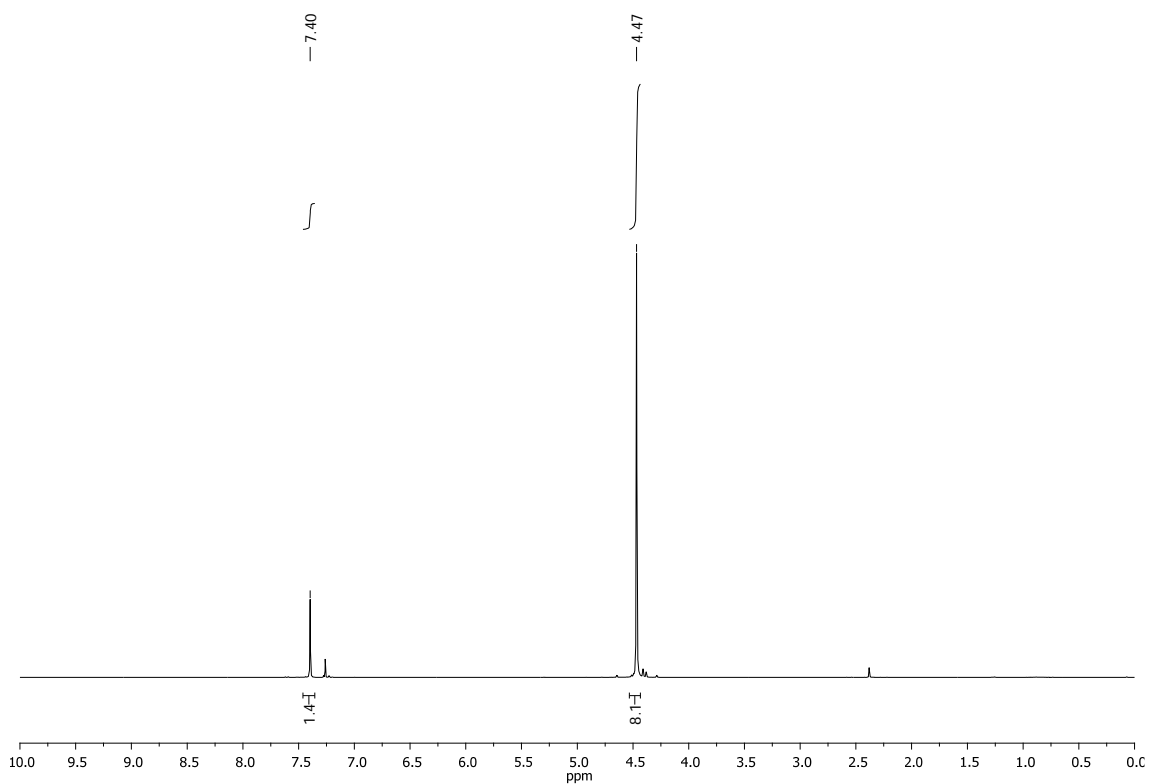


Figure 179. ¹H spectrum of 1,2,4,5-tetrakis(azidomethyl)benzene (**8**) in CDCl₃.

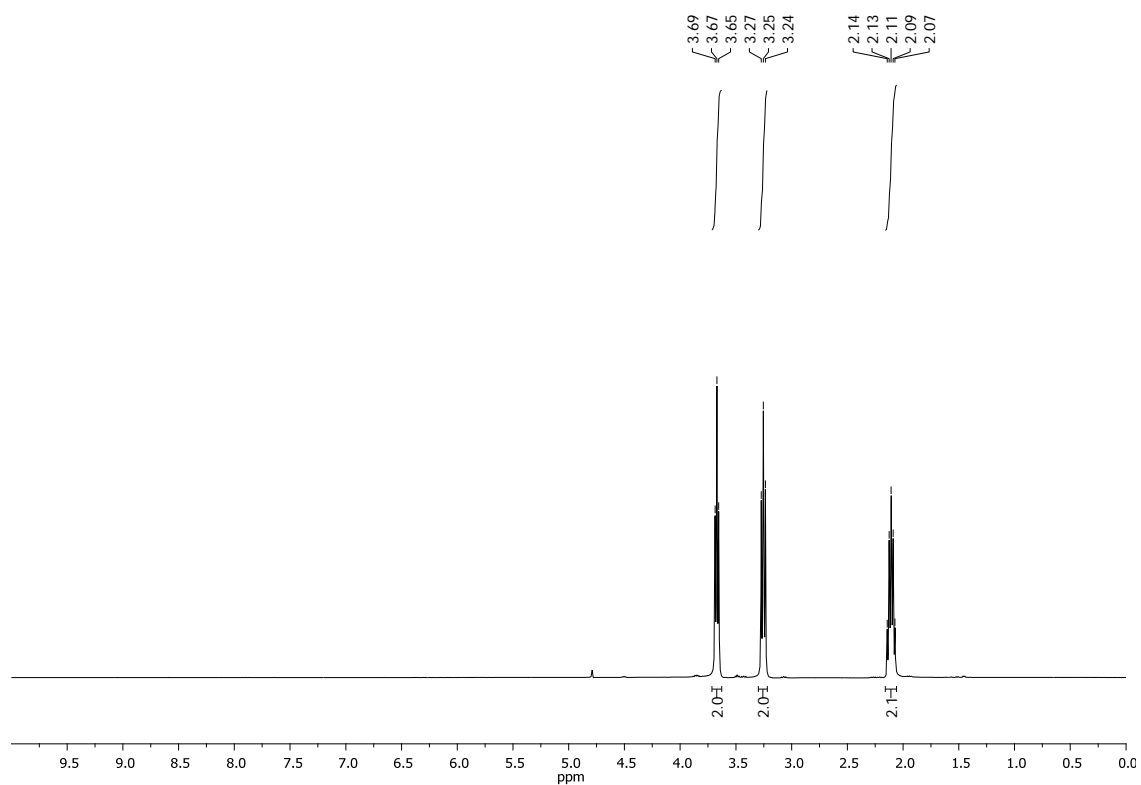


Figure 180. ¹H spectrum of 3-azidopropylamine (**9**) in D₂O.

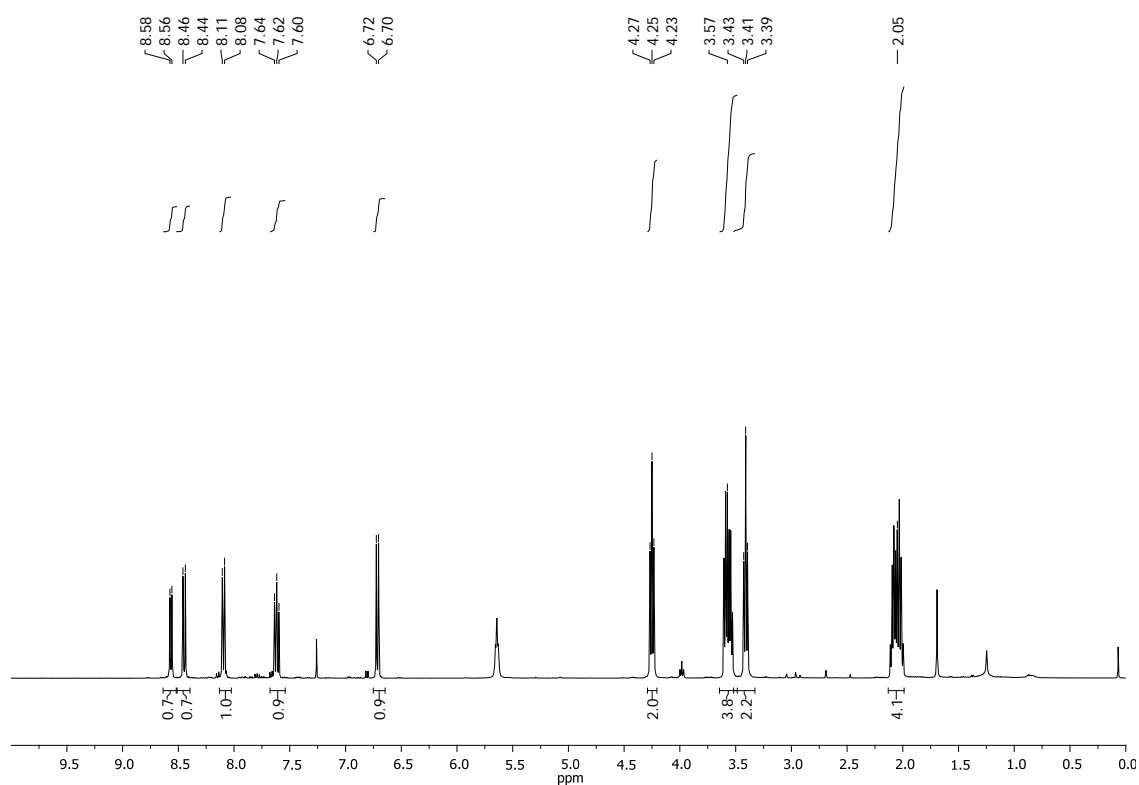


Figure 181. ¹H spectrum of *N*-(2-azidopropyl)-4-((2-azidopropyl)amino)-1,8-naphthalimide (**10**) in CDCl₃.

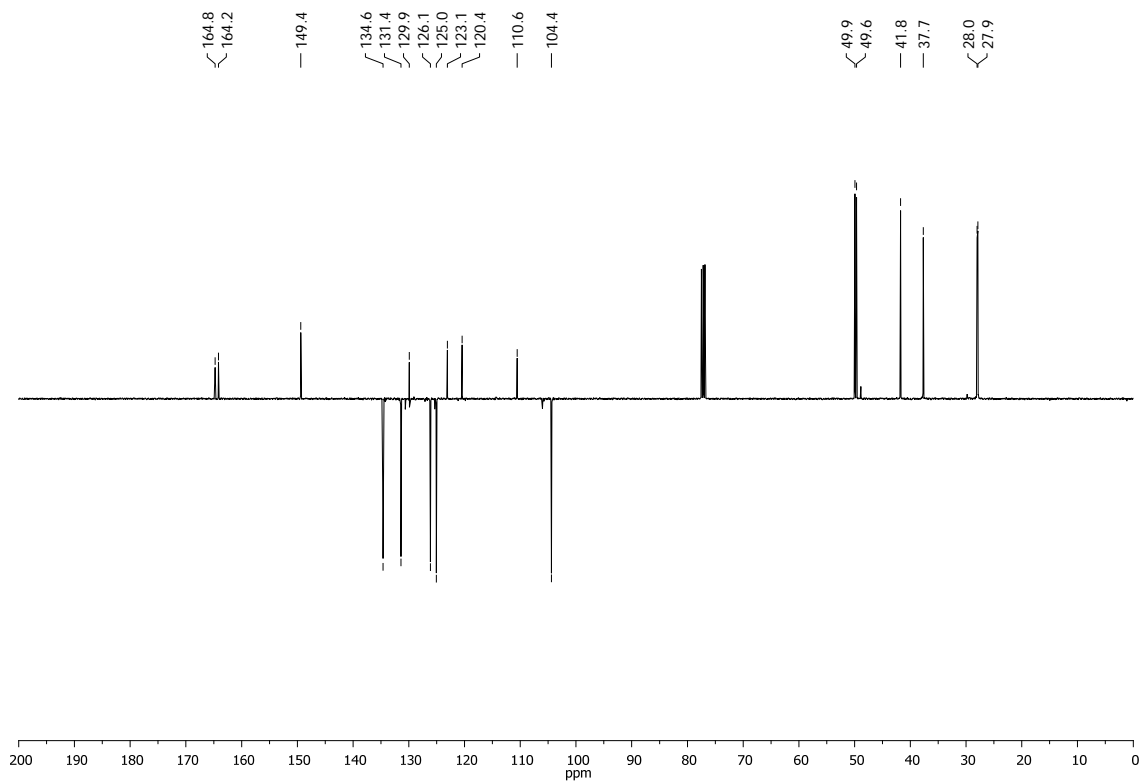


Figure 182. ¹³C (SEFT) spectrum of *N*-(2-azidopropyl)-4-((2-azidopropyl)amino)-1,8-naphthalimide (**10**) in CDCl₃.

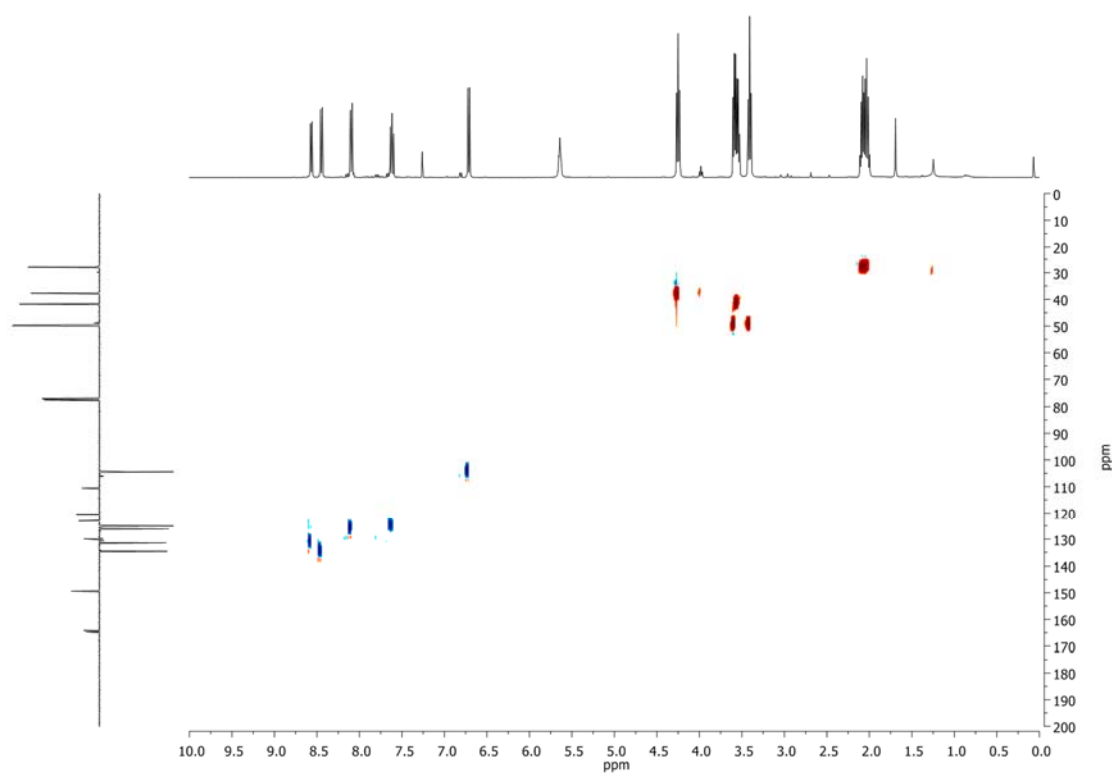


Figure 183. HSQC spectrum of *N*-(2-azidopropyl)-4-((2-azidopropyl)amino)-1,8-naphthalimide (**10**) in CDCl₃.

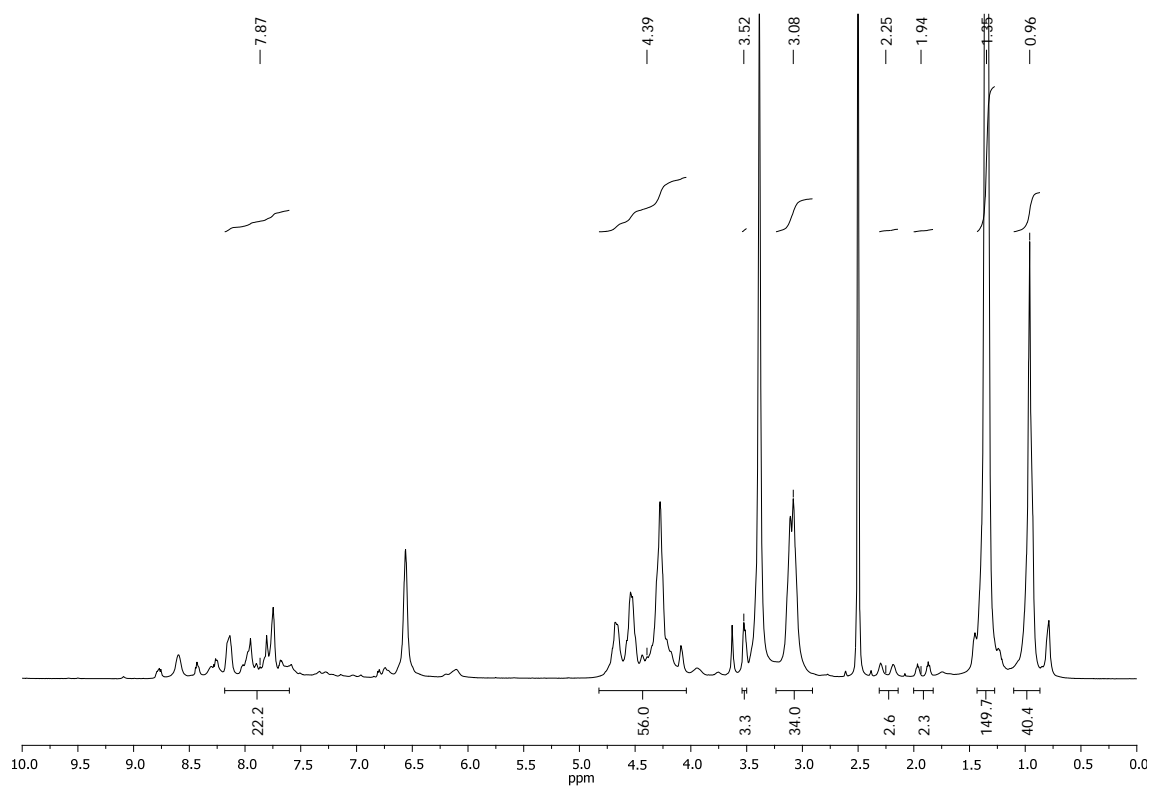


Figure 184. ¹H spectrum of **G3_{Naph}NHBoc** in DMSO-*d*₆.

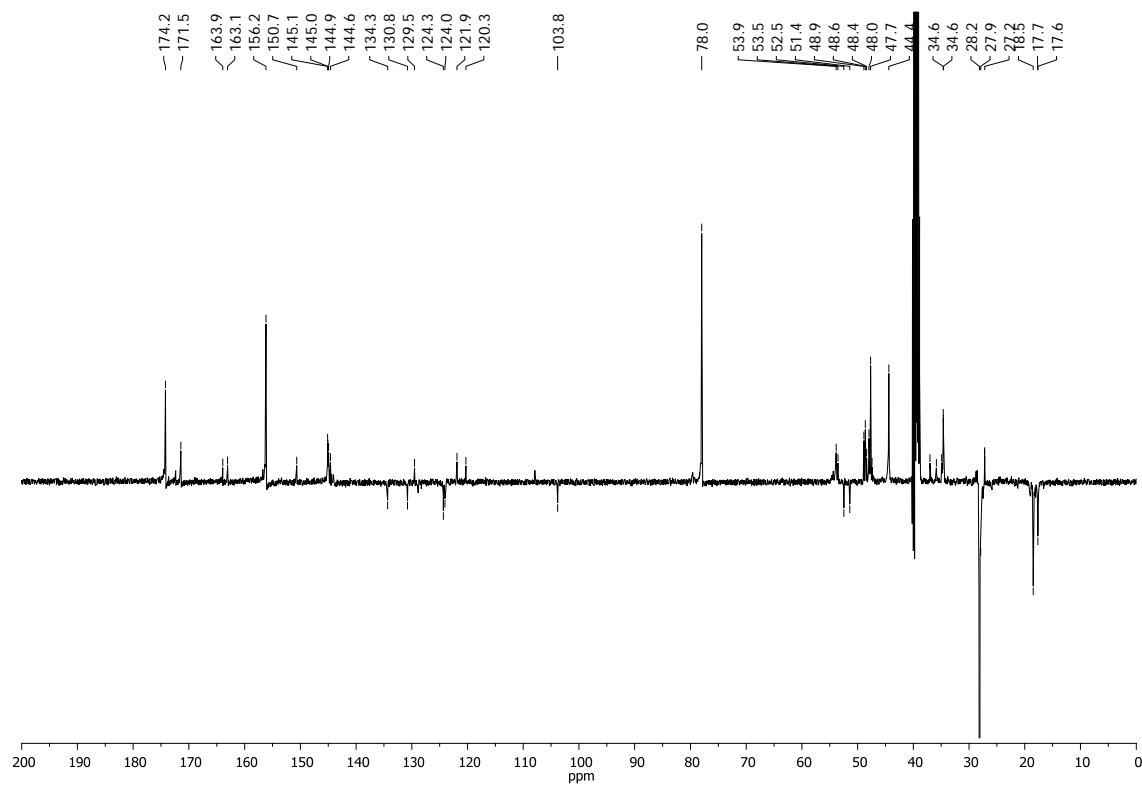


Figure 185. ¹³C (SEFT) spectrum of **G3_{Naph}NHBoc** in DMSO-*d*₆.

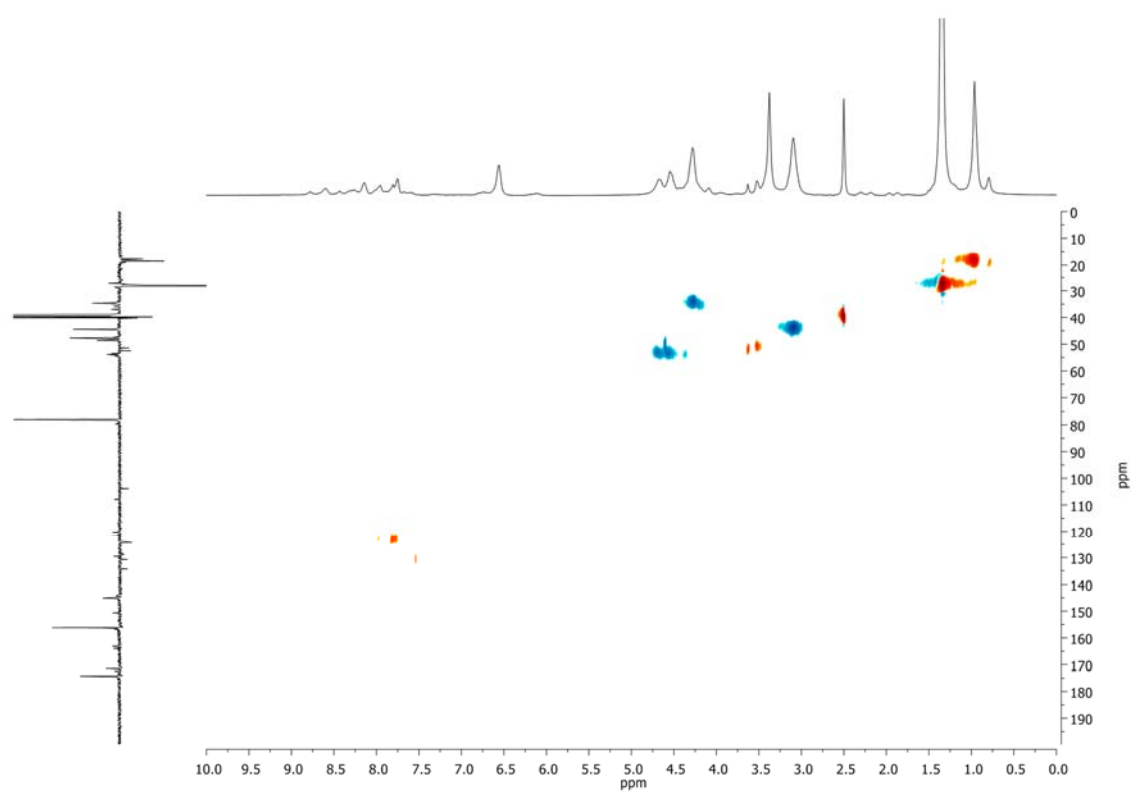


Figure 186. HSQC spectrum of **G3_{Naph}NHBoc** in DMSO-*d*₆.

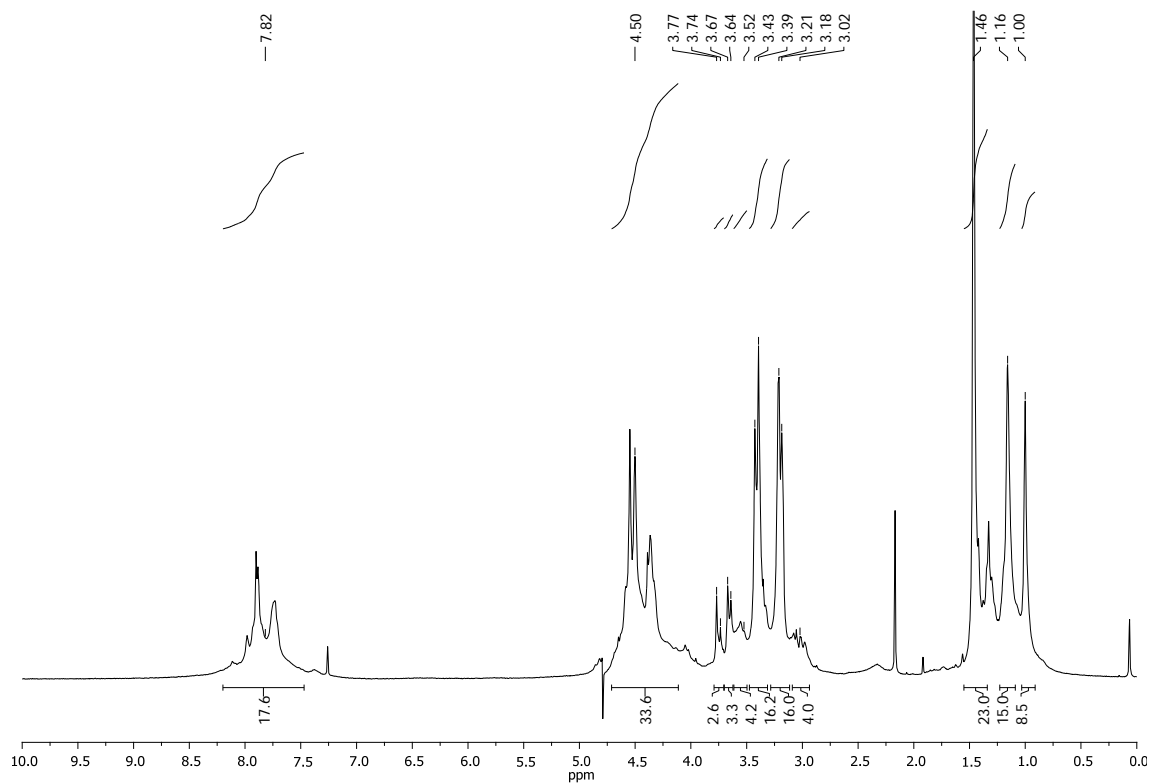


Figure 187. ¹H spectrum of **G3NaphNH₂** in D₂O.

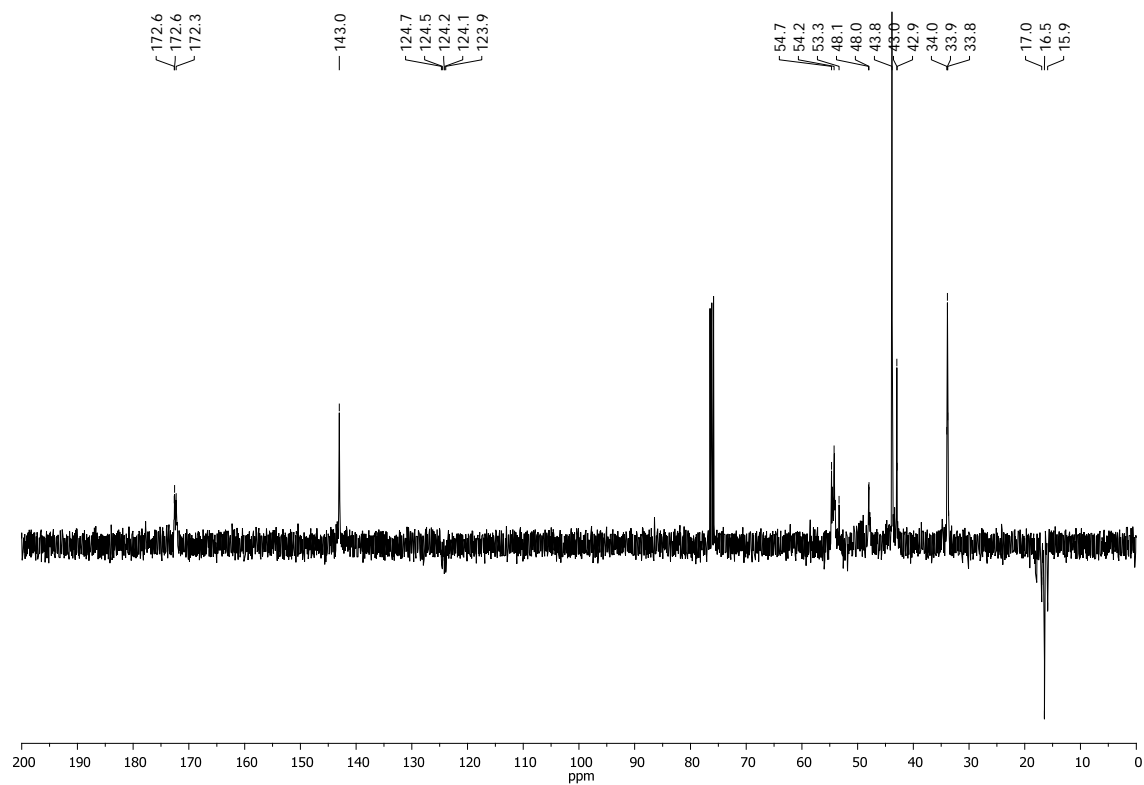


Figure 188. ¹³C (SEFT) spectrum of **G3NaphNH₂** in D₂O.

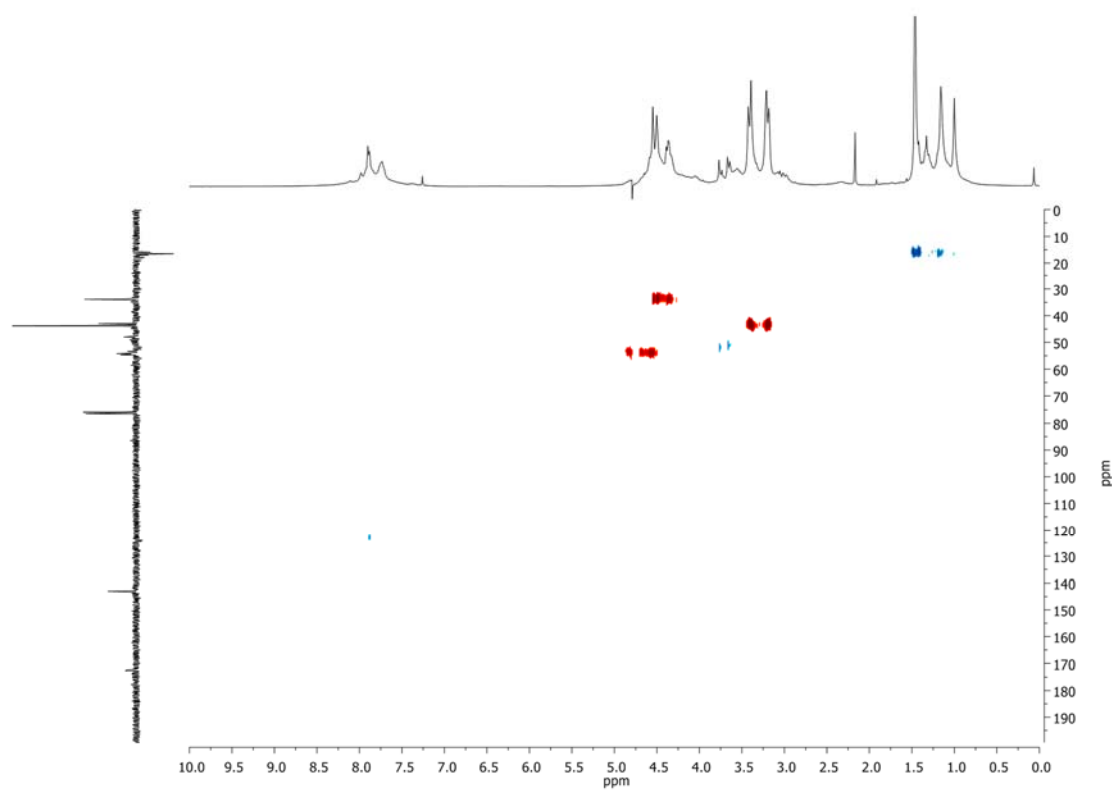


Figure 189. HSQC spectrum of **G3_{Naph}NH₂** in D₂O.

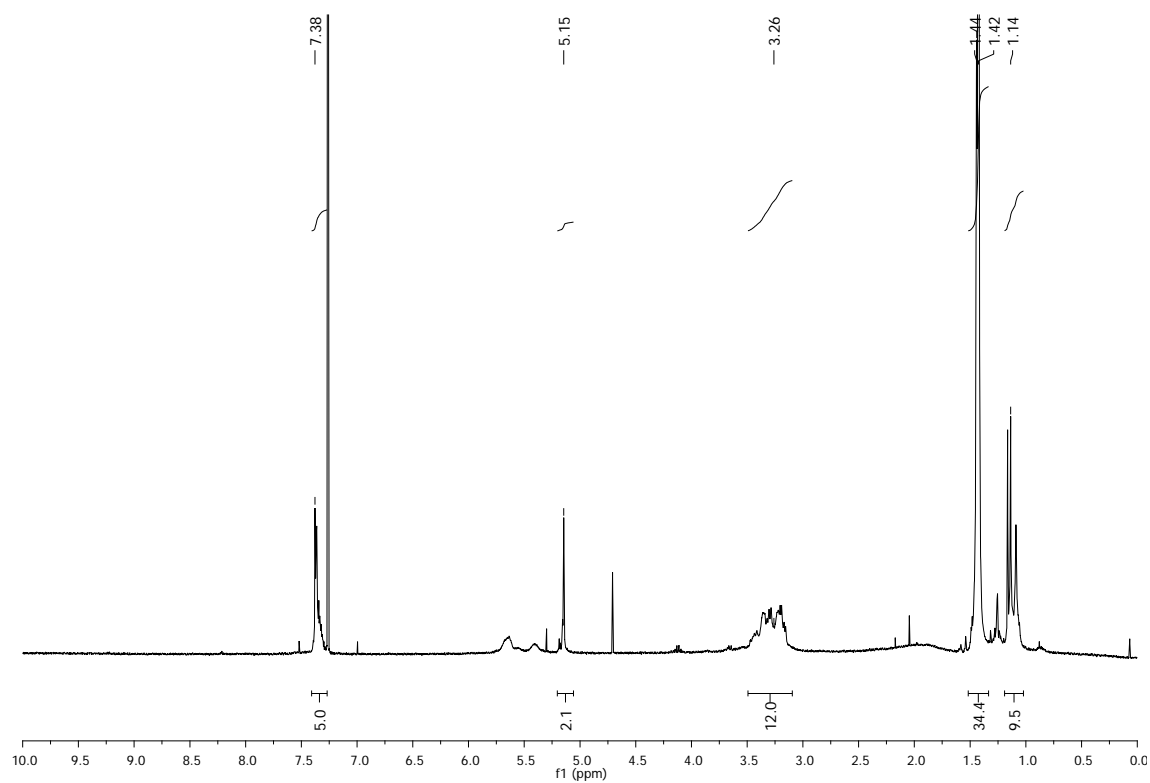


Figure 190. ¹H spectrum of **11** in CDCl₃.

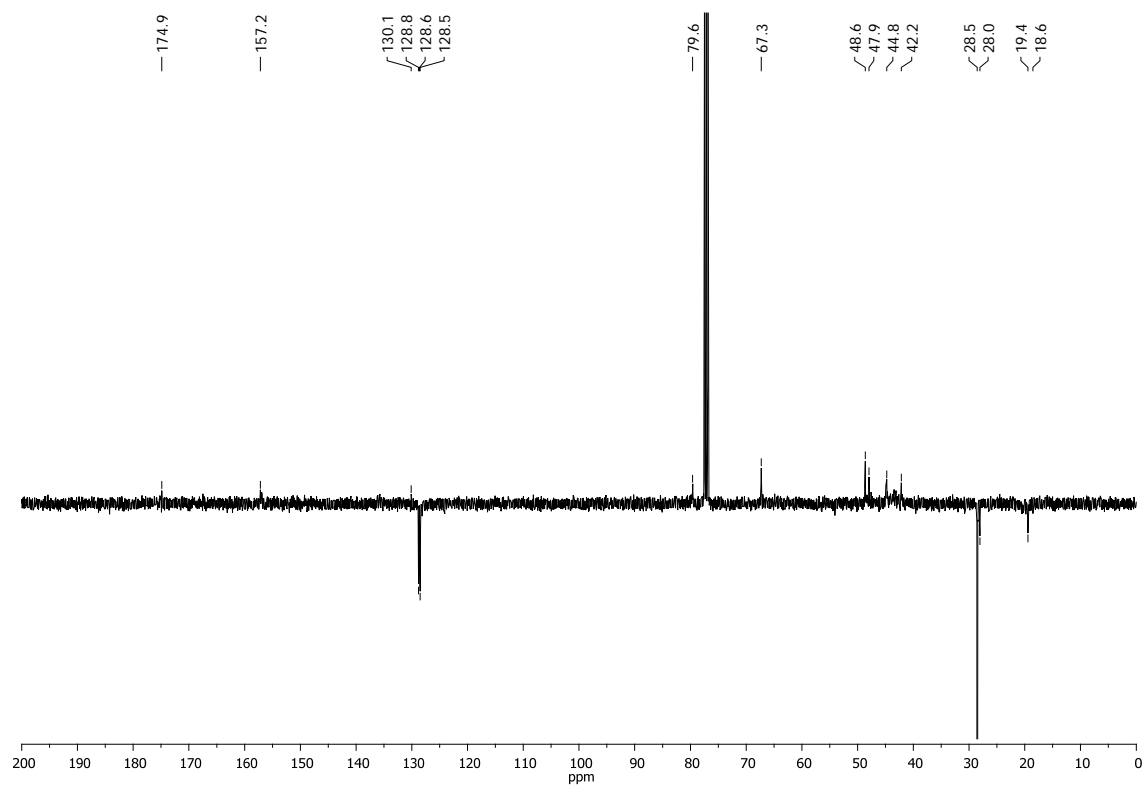


Figure 191. ¹³C (SEFT) spectrum of **11** in CDCl₃.

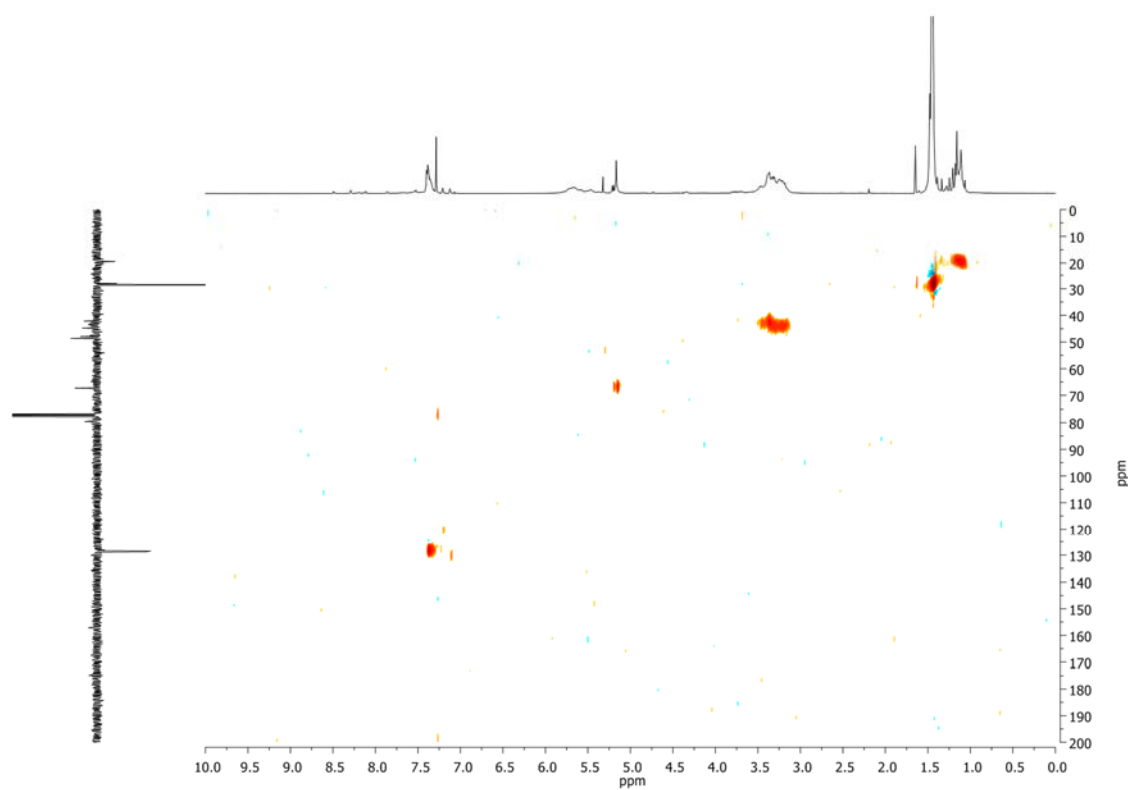


Figure 192. HSQC spectrum of **11** in CDCl_3 .

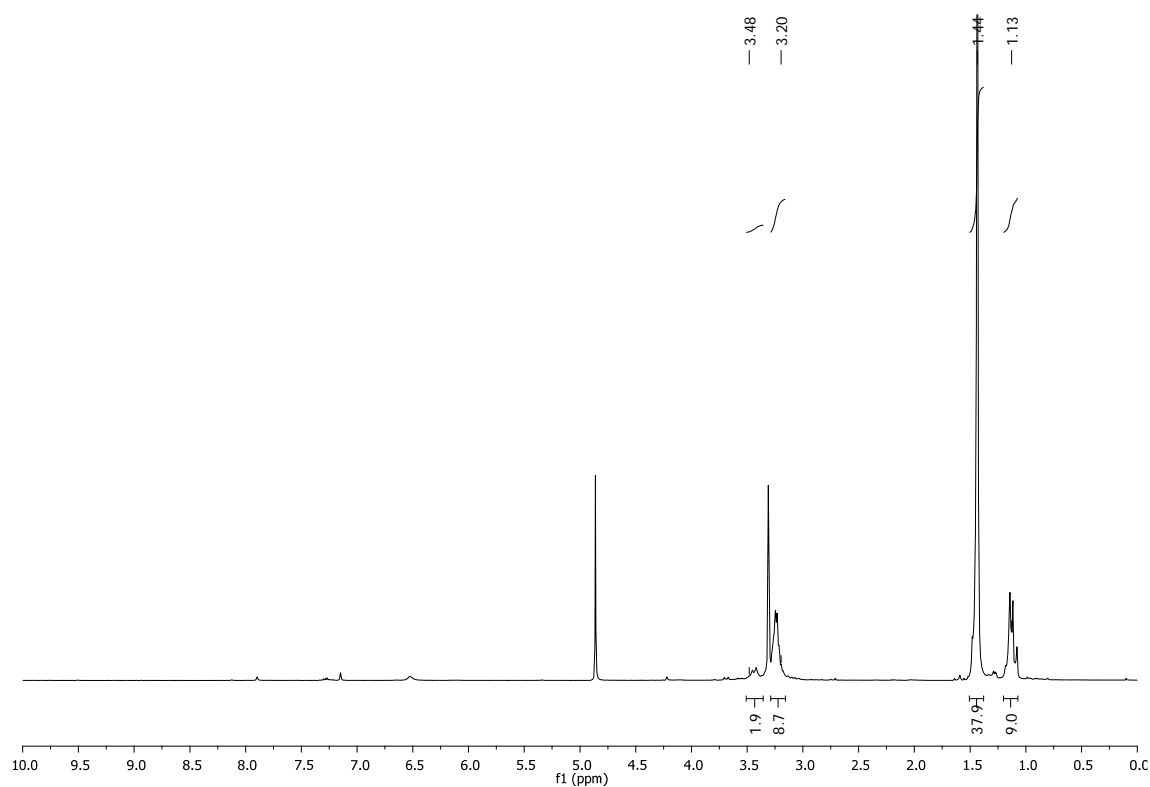


Figure 193. ¹H spectrum of **12** in MeOD-*d*₄.

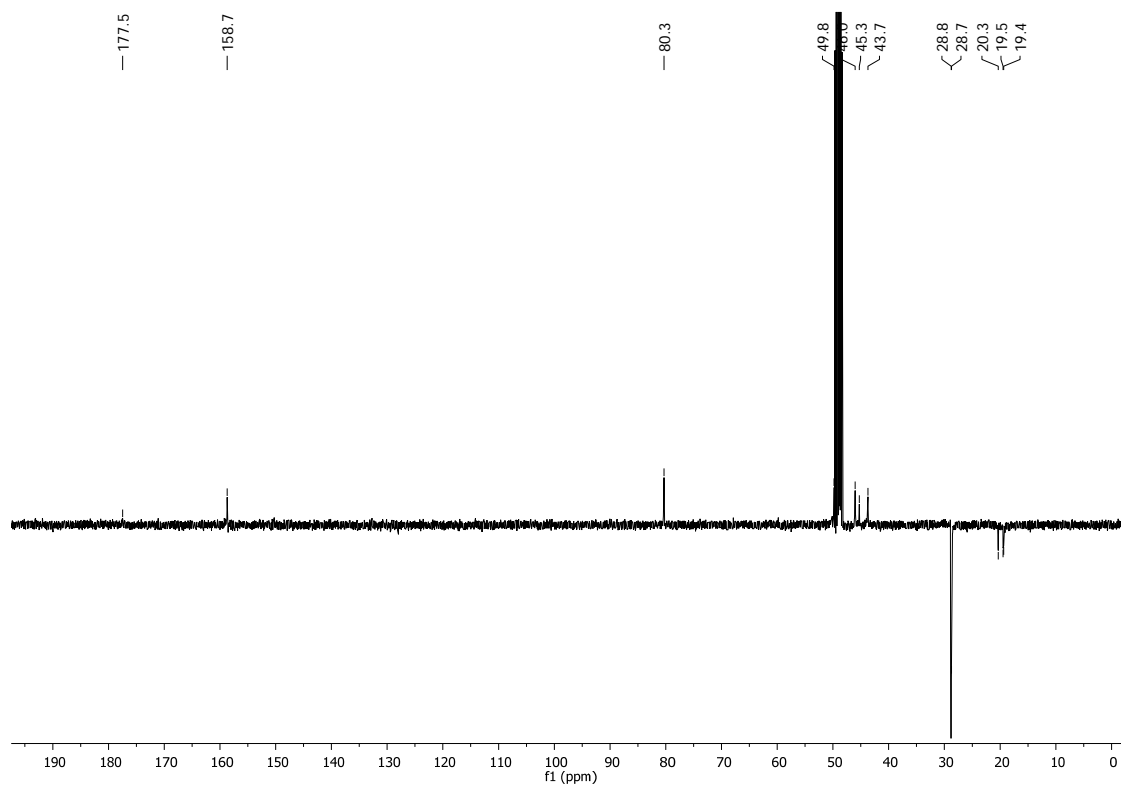


Figure 194. ¹³C (SEFT) spectrum of **12** in MeOD-*d*₄.

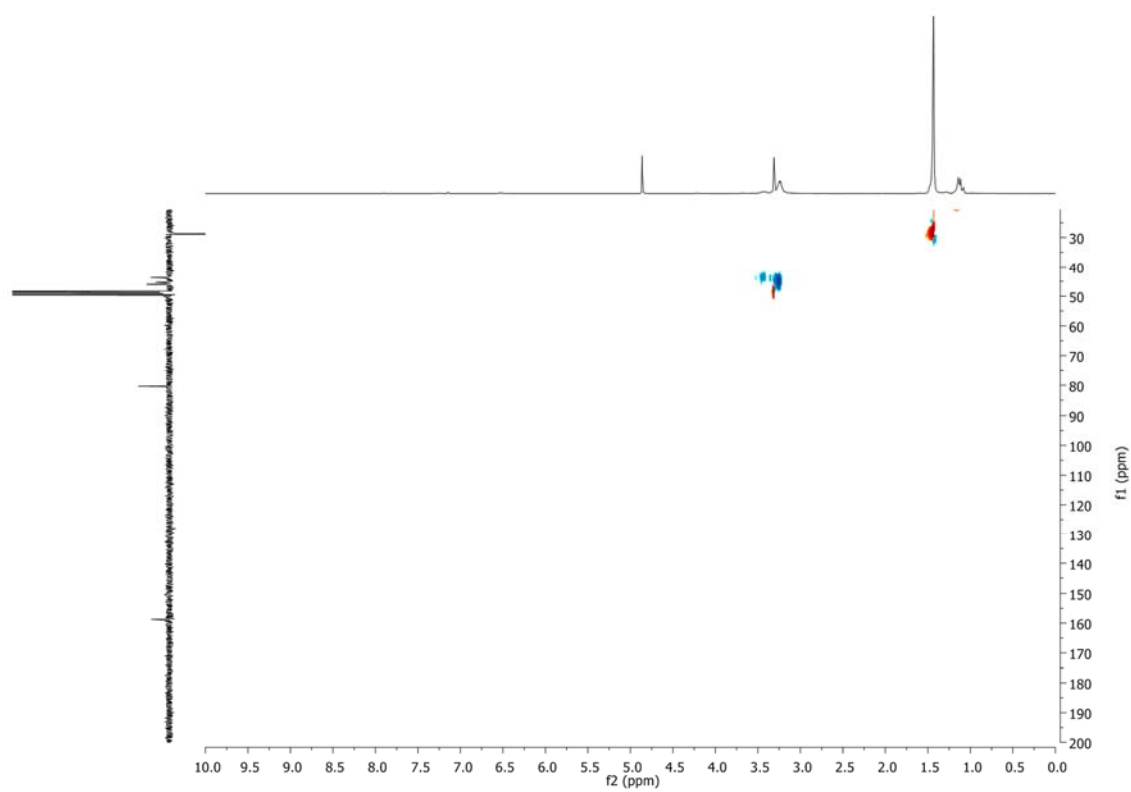


Figure 195. HSQC spectrum of **12** in MeOD- d_4 .

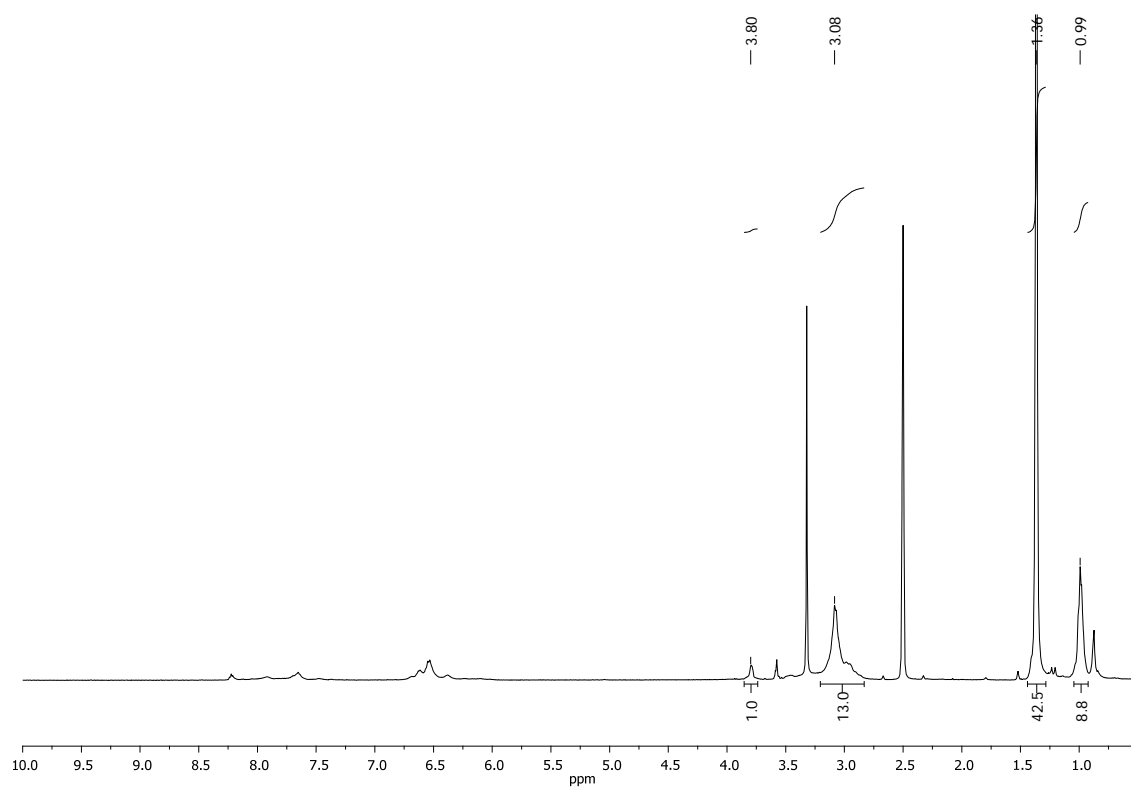


Figure 196. ¹H spectrum of **13** in DMSO-*d*₆.

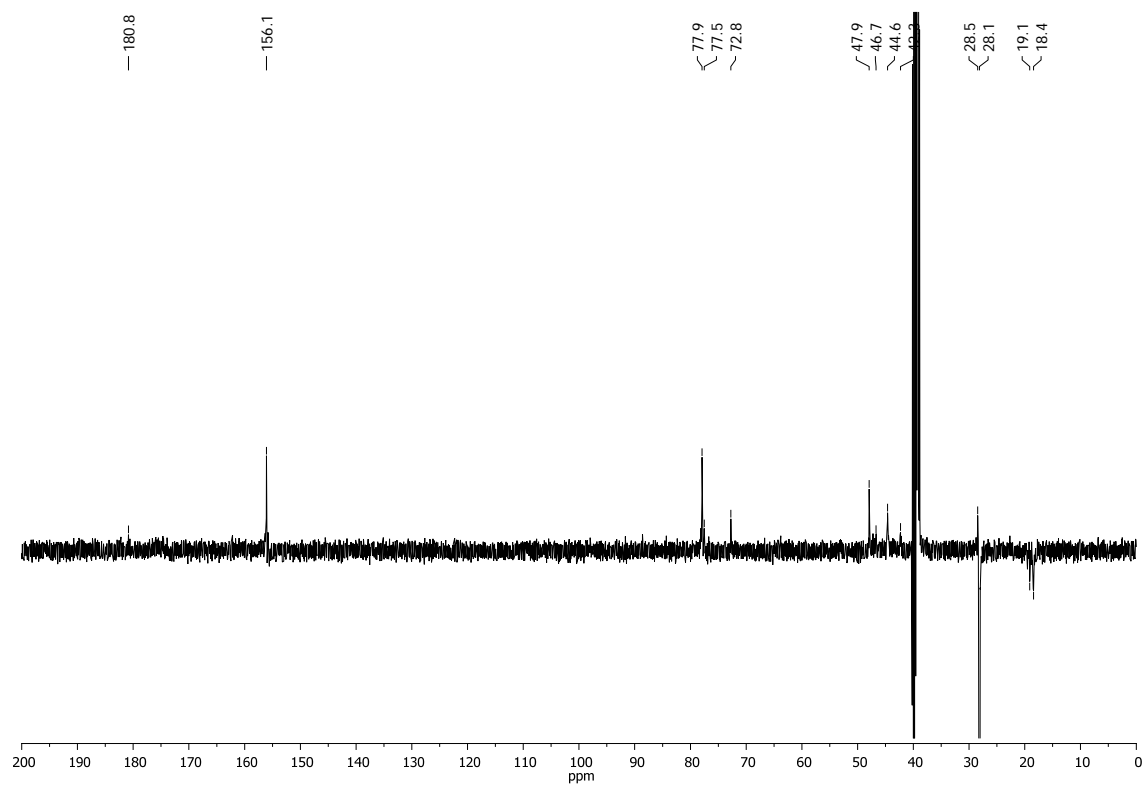


Figure 197. ¹³C (SEFT) spectrum of **13** in DMSO-*d*₆.

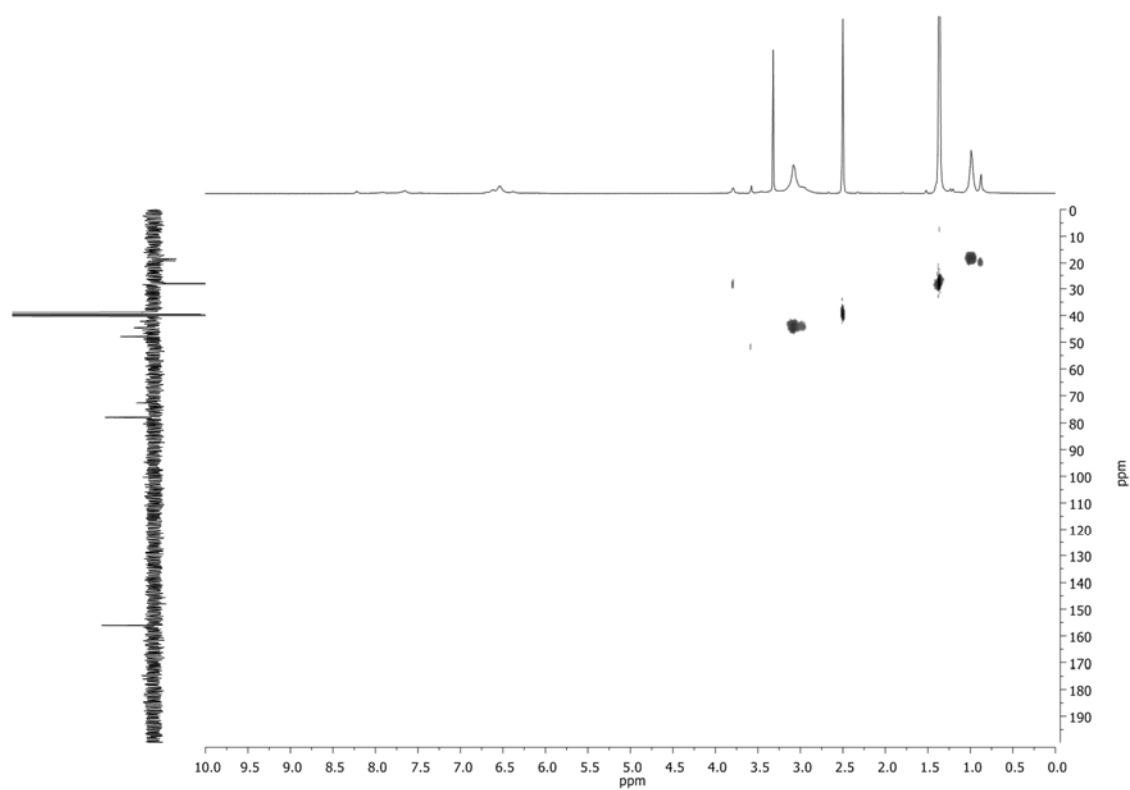


Figure 198. HSQC spectrum of **13** in $\text{DMSO}-d_6$.

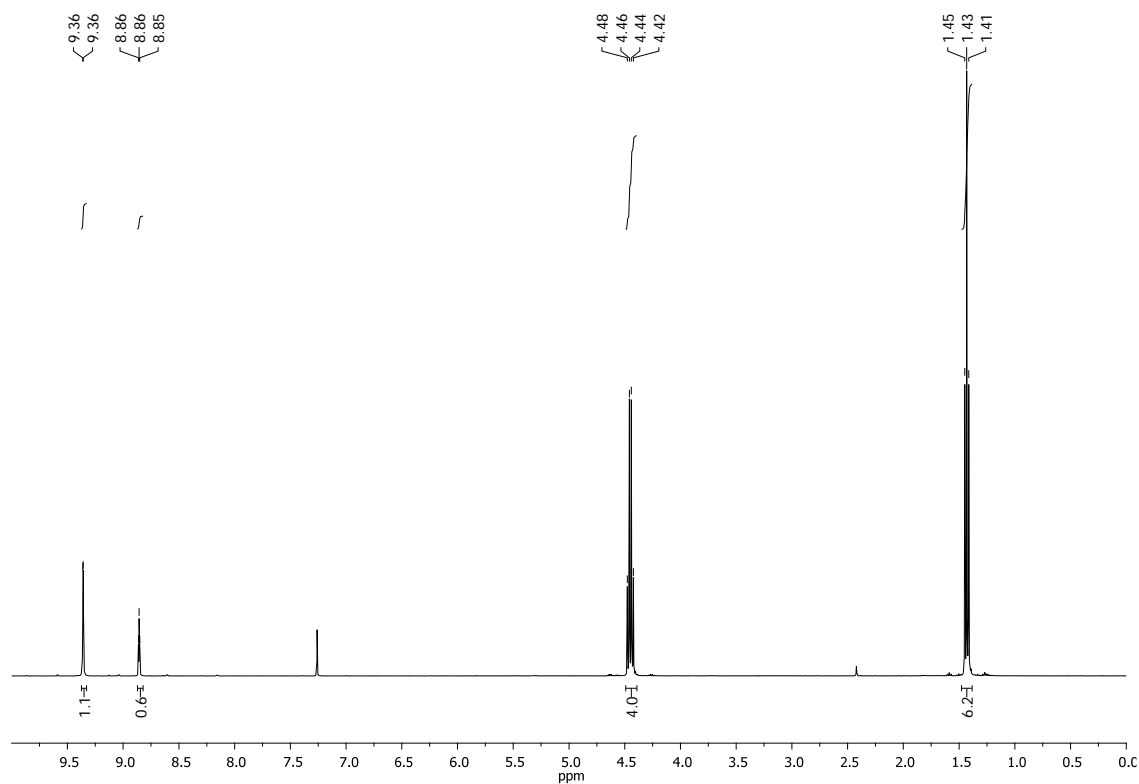


Figure 199. ¹H spectrum of 3,5-bis(ethoxycarbonyl)pyridine (14) in CDCl₃.

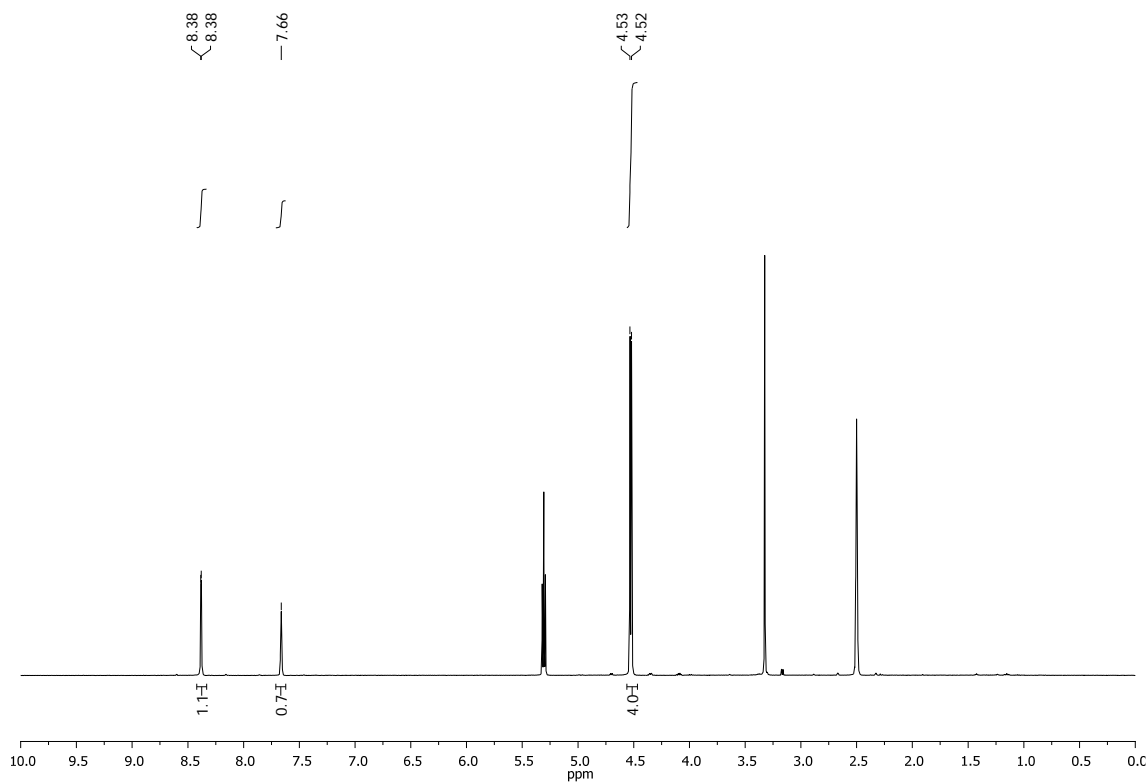


Figure 200. ¹H spectrum of 3,5-bis(hydroxymethyl)pyridine (15) in DMSO-*d*₆.

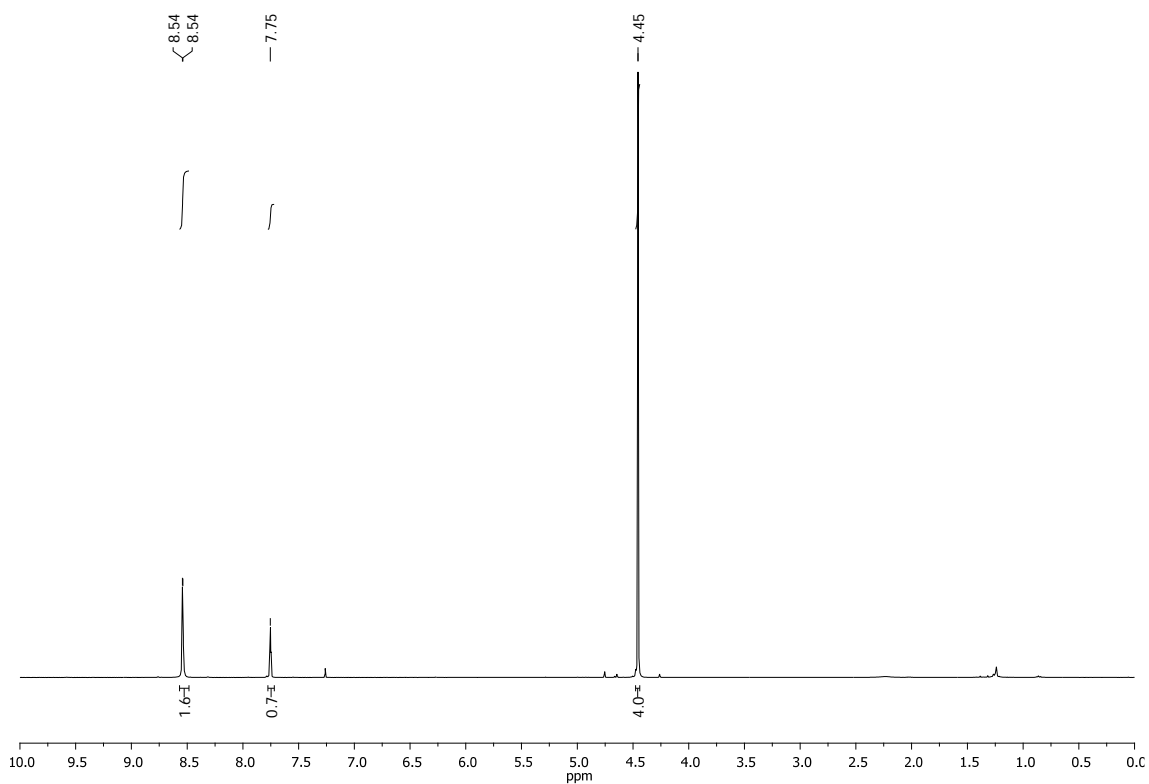


Figure 201. ^1H spectrum of **3,5-bis(bromomethyl)pyridine (16)** in CDCl_3 .

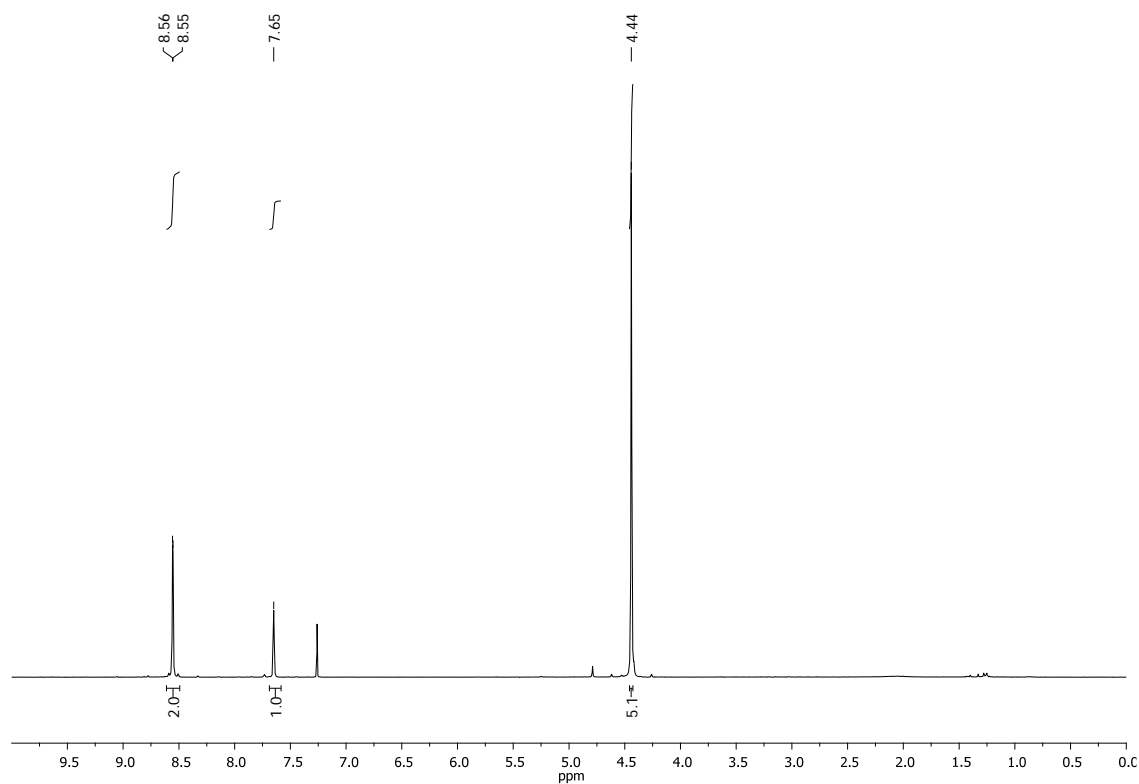


Figure 202. ¹H spectrum of 3,5-bis(azidomethyl)pyridine (17) in CDCl₃.

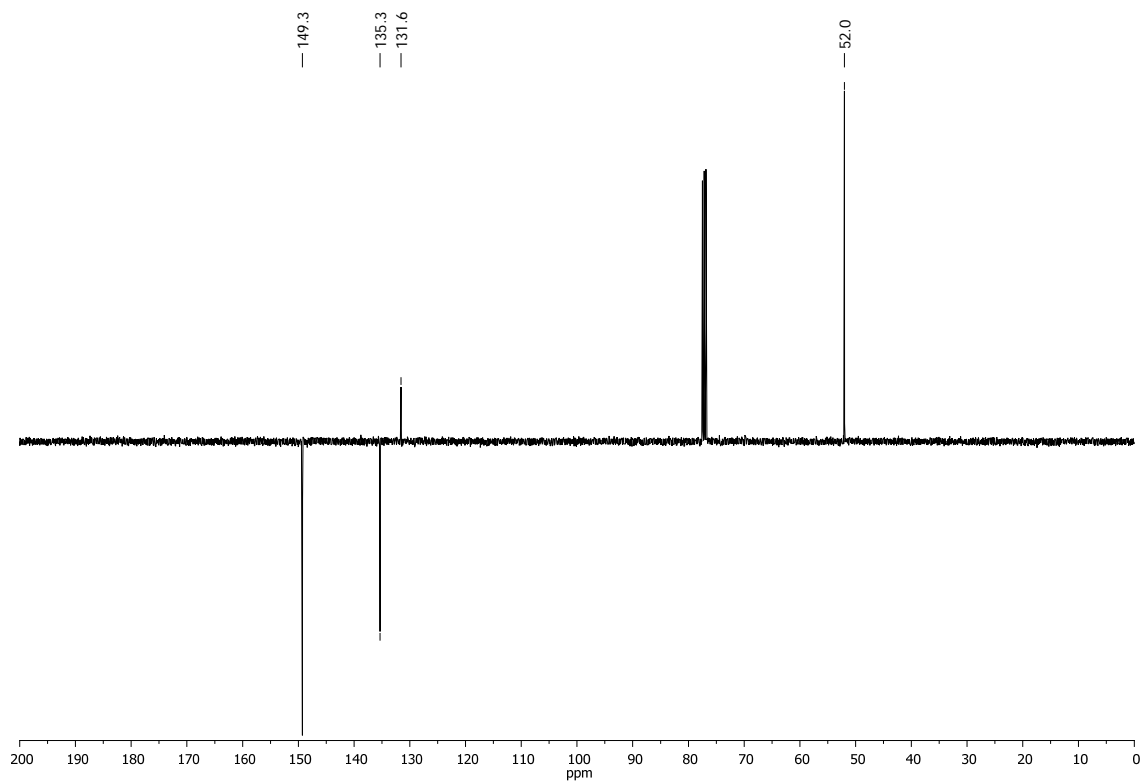


Figure 203. ¹³C (SEFT) spectrum of 3,5-bis(azidomethyl)pyridine (17) in CDCl₃.

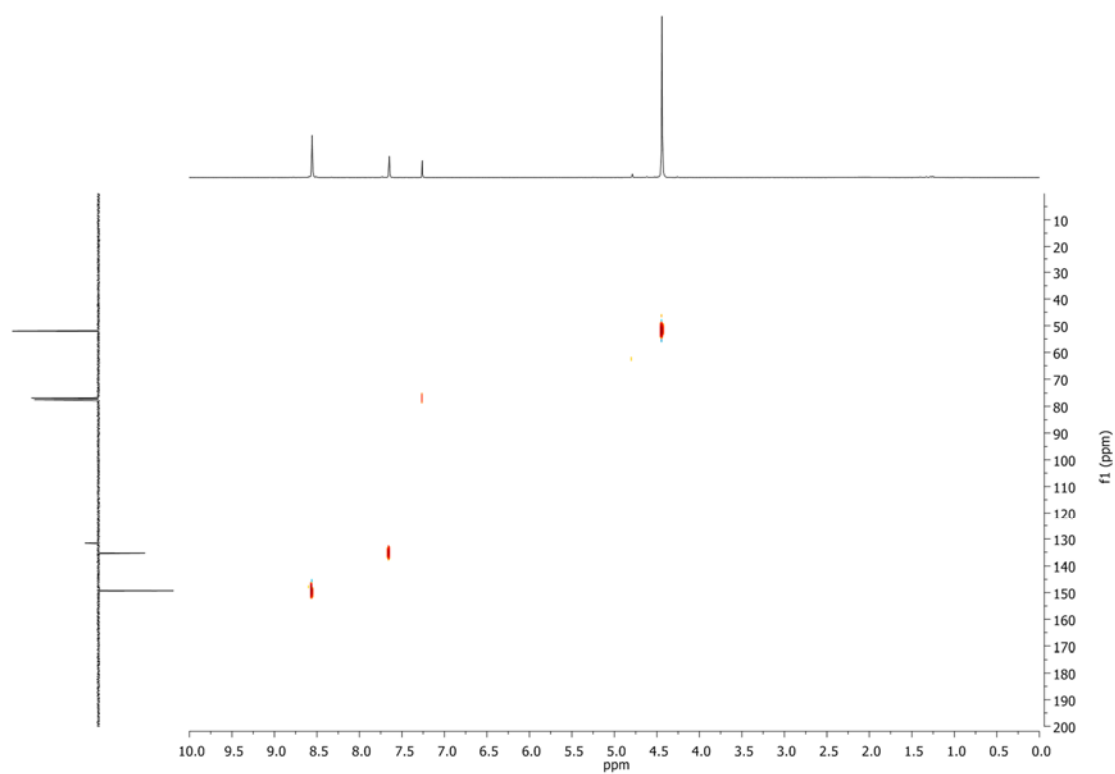


Figure 204. HSQC spectrum of **3,5-bis(azidomethyl)pyridine (17)** in CDCl₃.

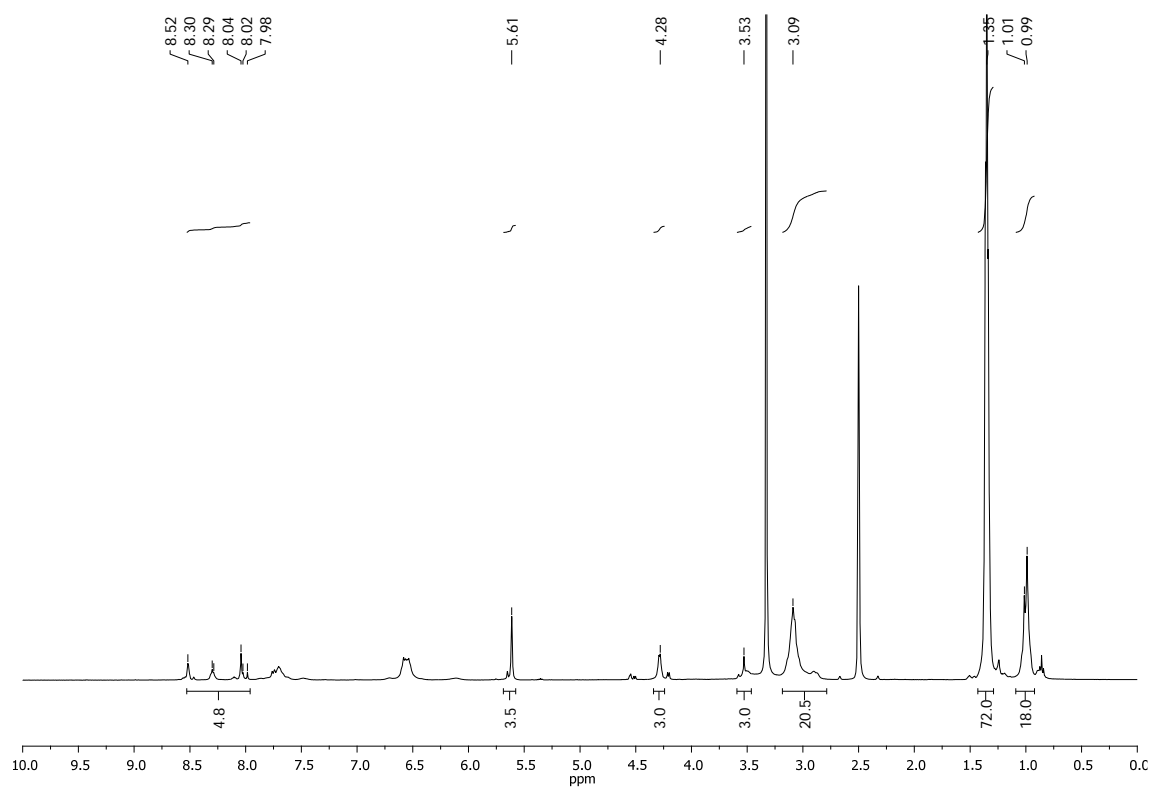


Figure 205. ¹H spectrum of **18** in DMSO-*d*₆.

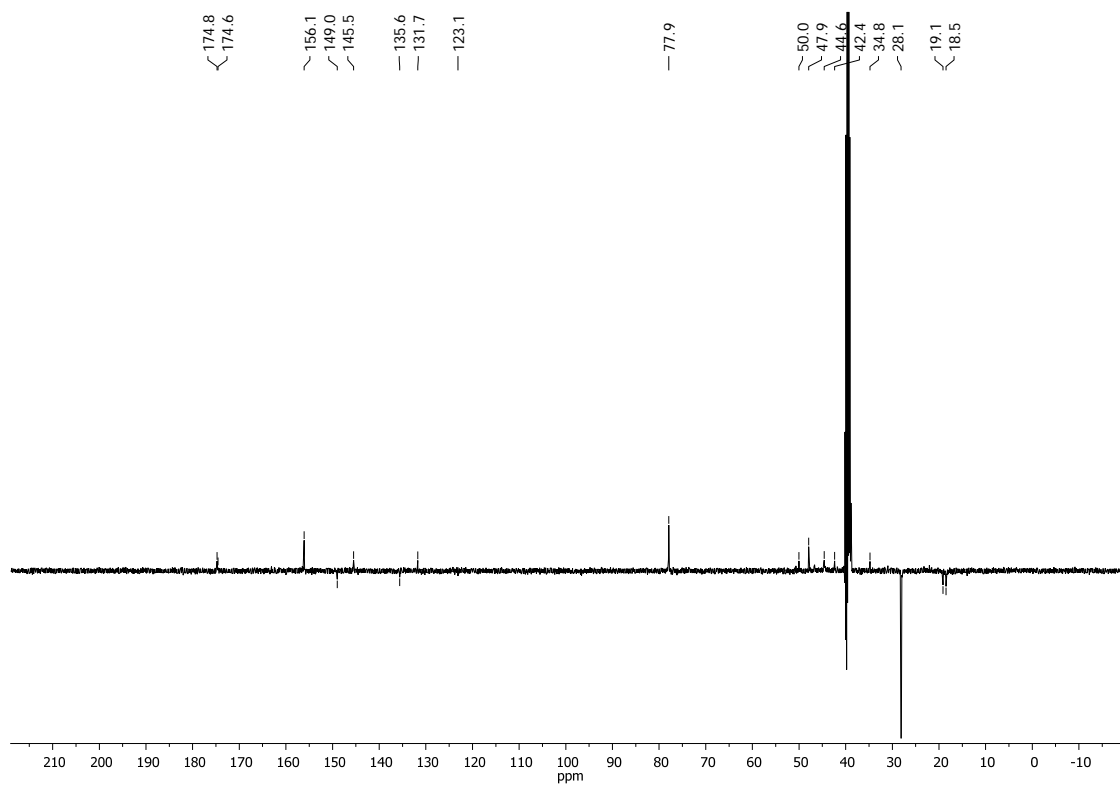


Figure 206. ¹³C (SEFT) spectrum of **18** in DMSO-*d*₆.

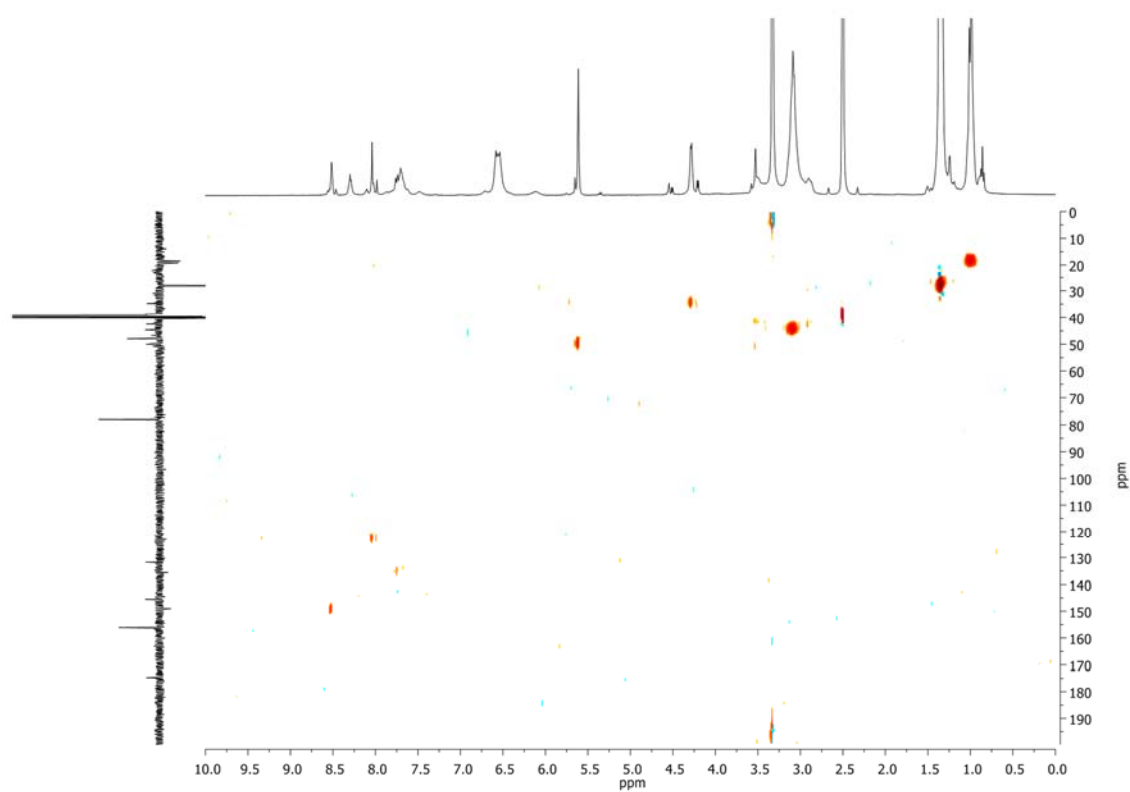


Figure 207. HSQC spectrum of **18** in DMSO-*d*₆.

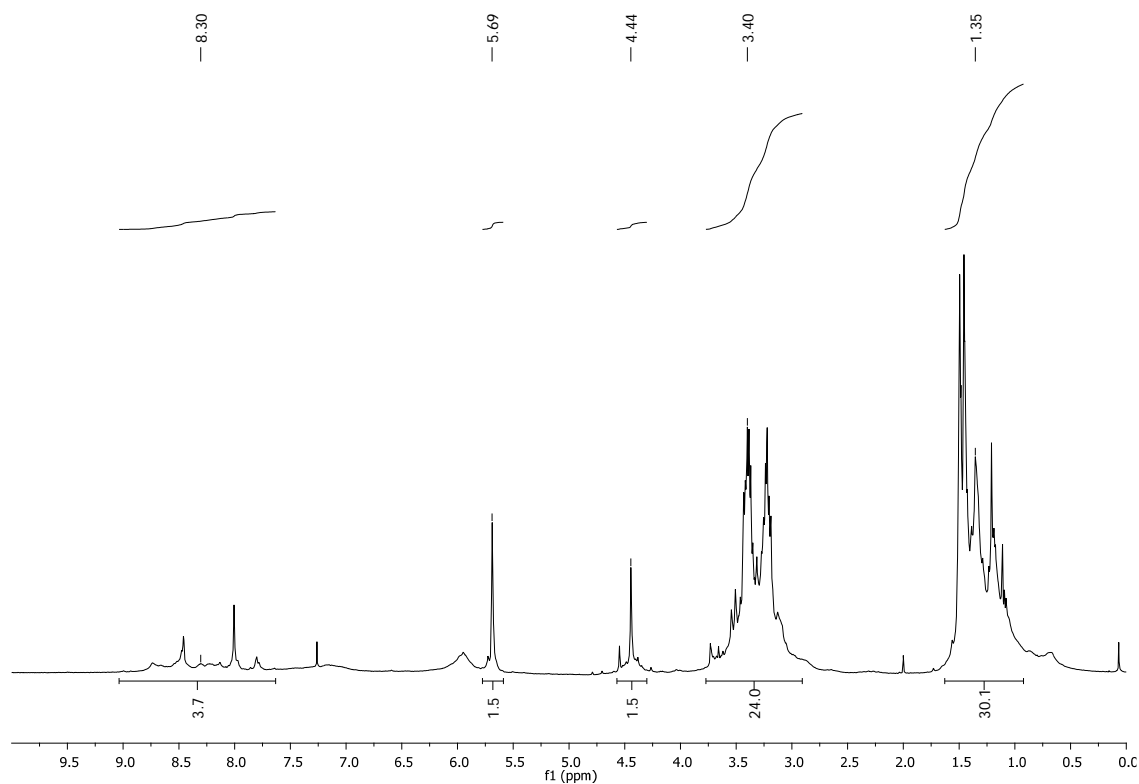


Figure 208. ¹H spectrum of **21** in D₂O.

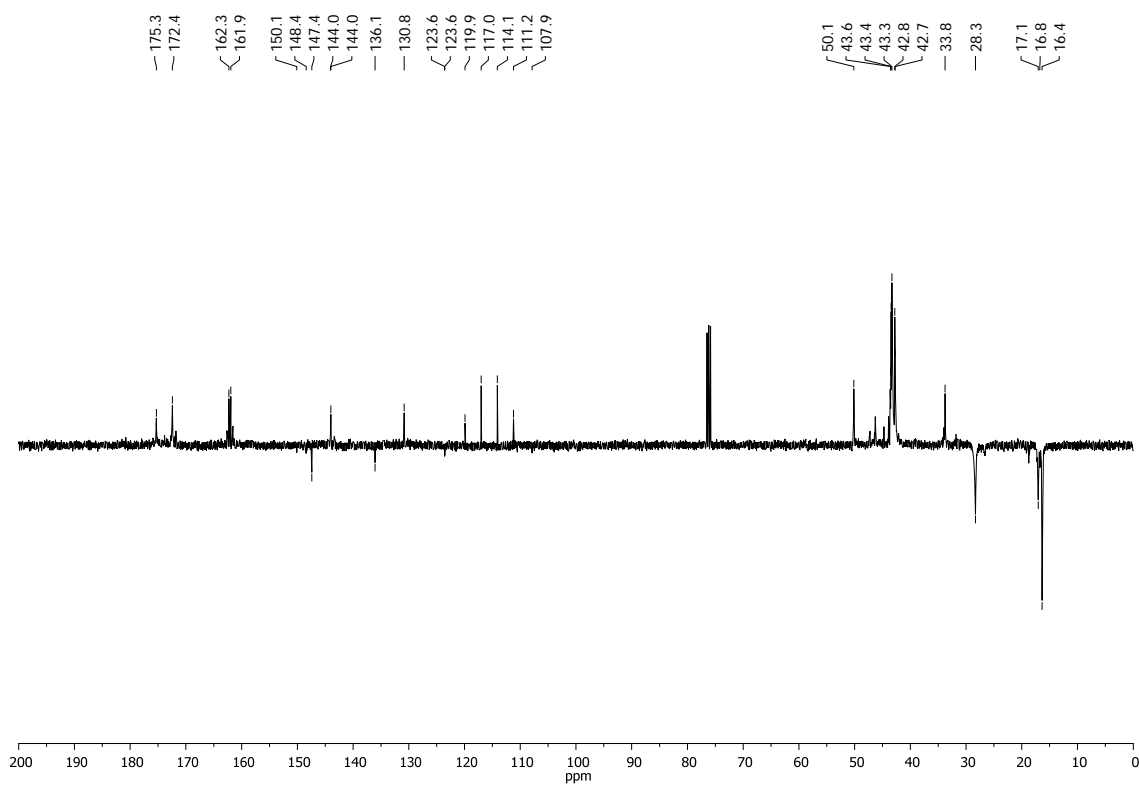


Figure 209. ¹³C (SEFT) spectrum of **21** in D₂O.

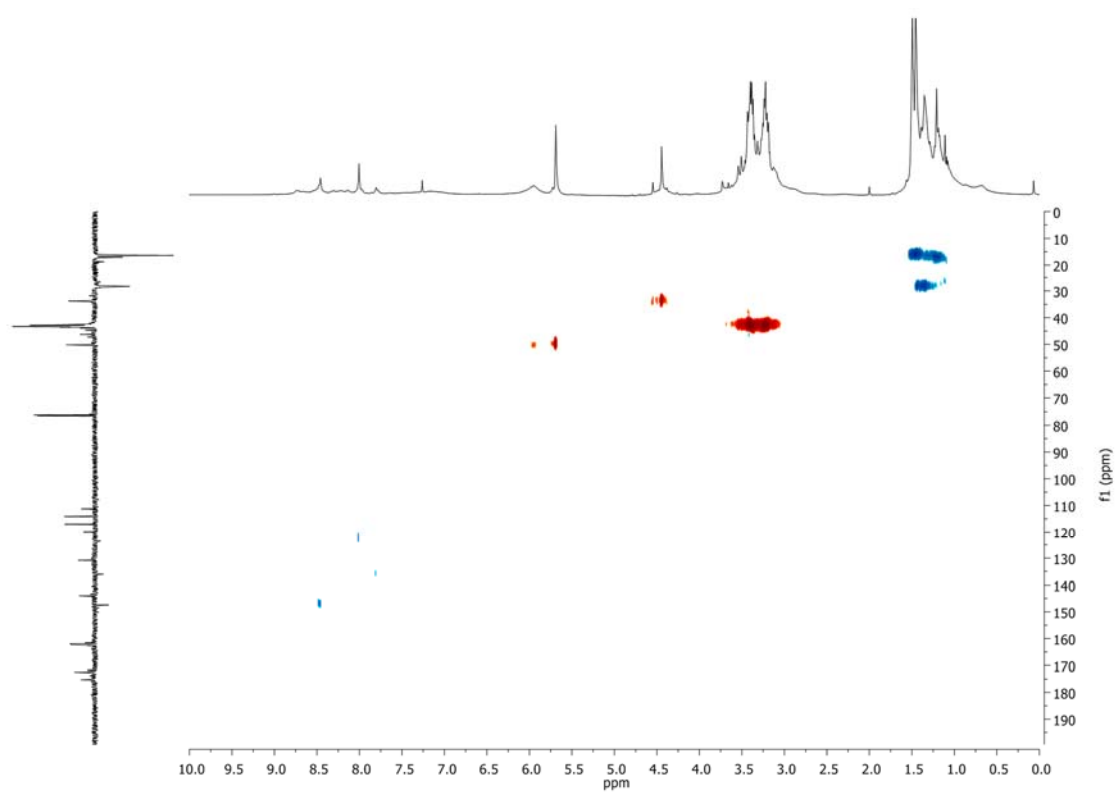


Figure 210. HSQC spectrum of **21** in D₂O.

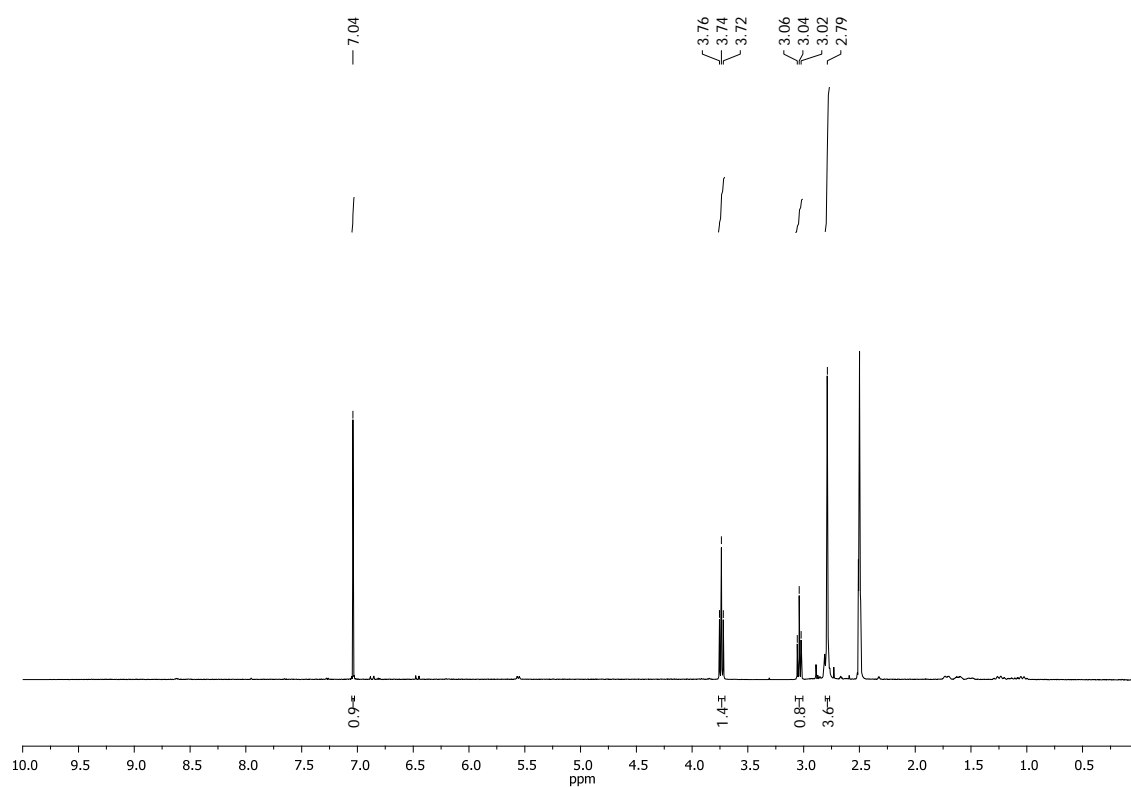


Figure 211. ¹H spectrum of *N*-hydroxysuccinimide ester (**22**) in DMSO-*d*₆.

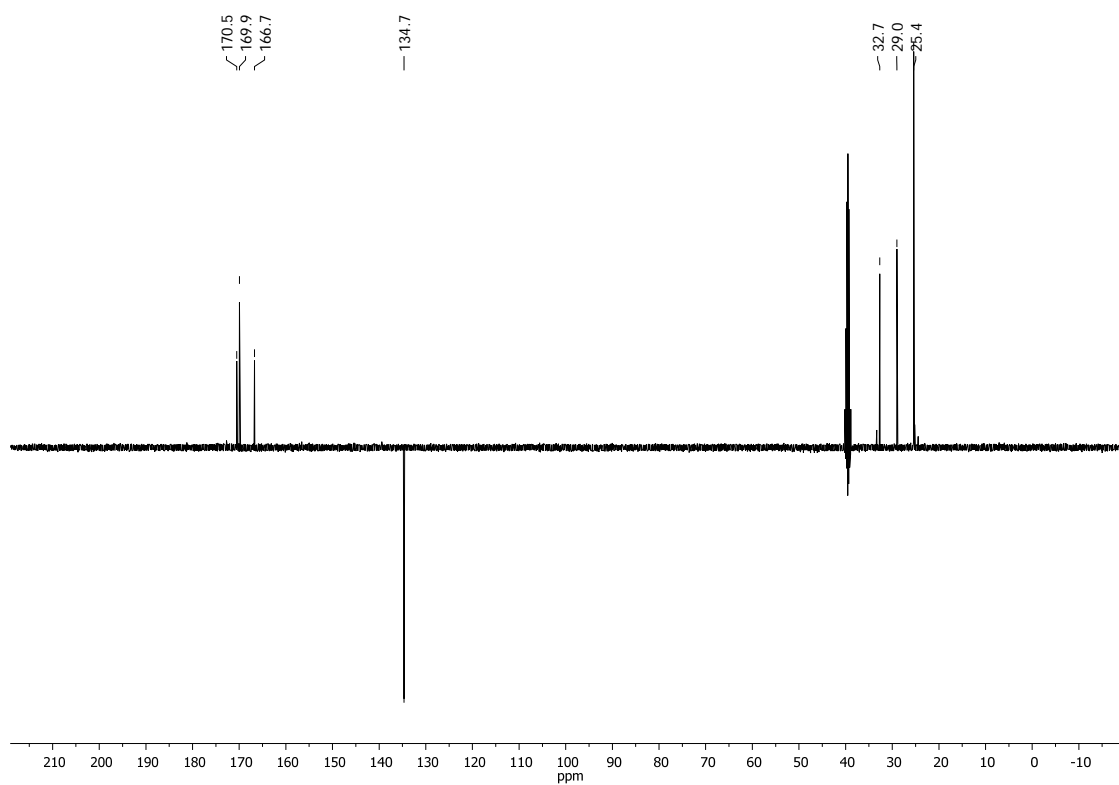


Figure 212. ¹³C (SEFT) spectrum of *N*-hydroxysuccinimide ester (**22**) in DMSO-*d*₆.

DOSY spectra

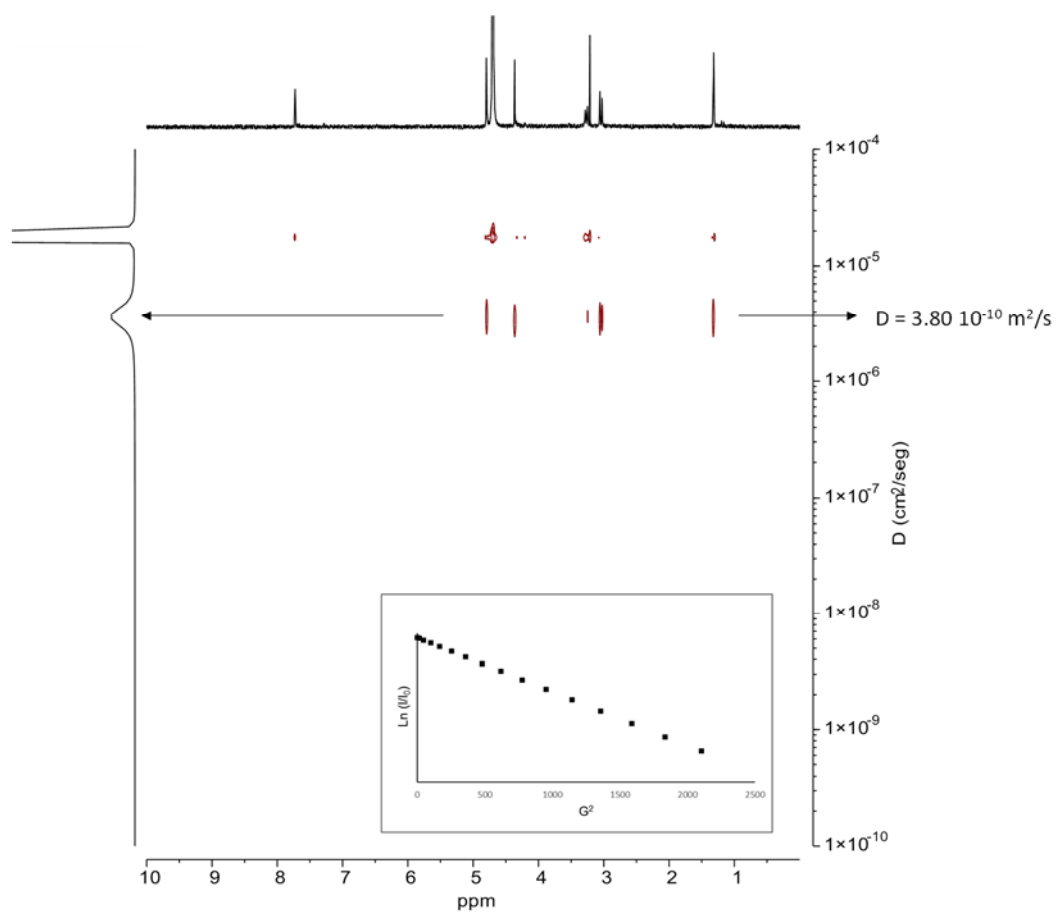


Figure 213. DOSY NMR experiment of $G1EDANH_2$ in D_2O . Inset, Stejskal-Tanner plot.

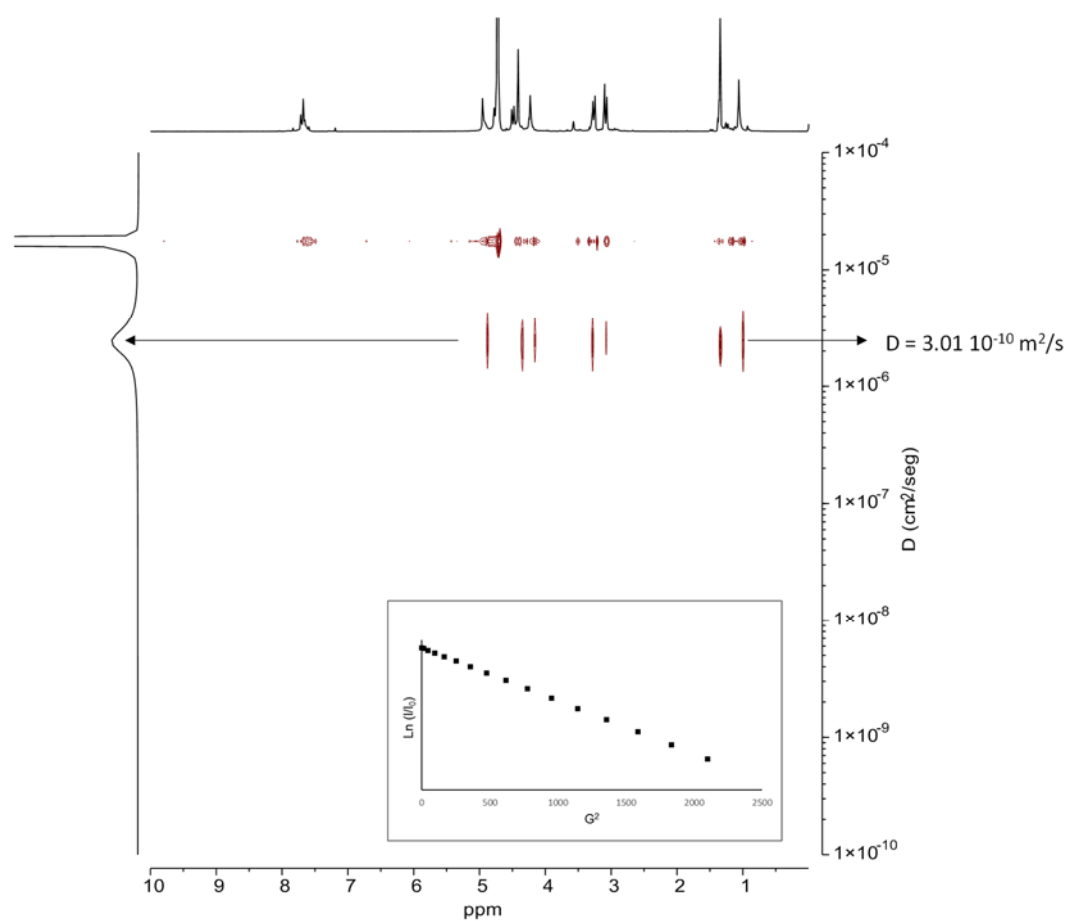


Figure 214. DOSY NMR experiment of $G2_{EDANH2}$ in D_2O . Inset, Stejskal-Tanner plot.

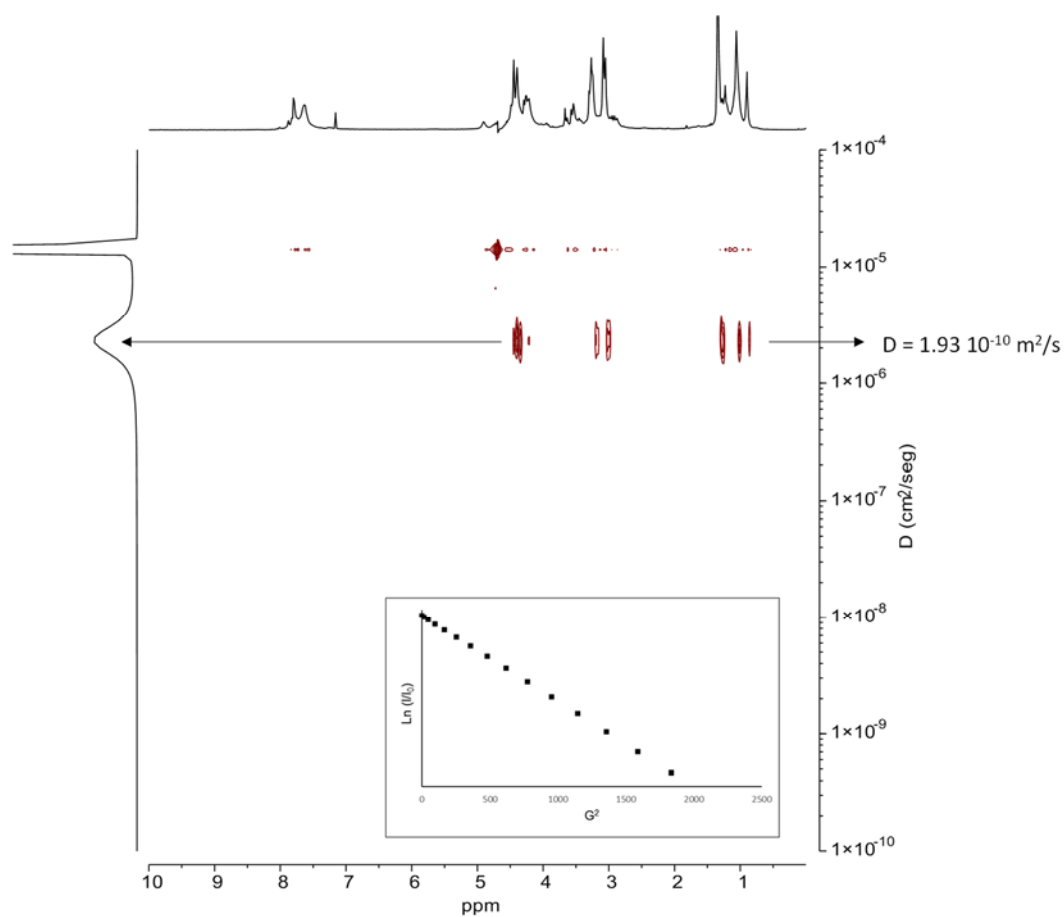


Figure 215. DOSY NMR experiment of $G3_{EDANH_2}$ in D_2O . Inset, Stejskal-Tanner plot.

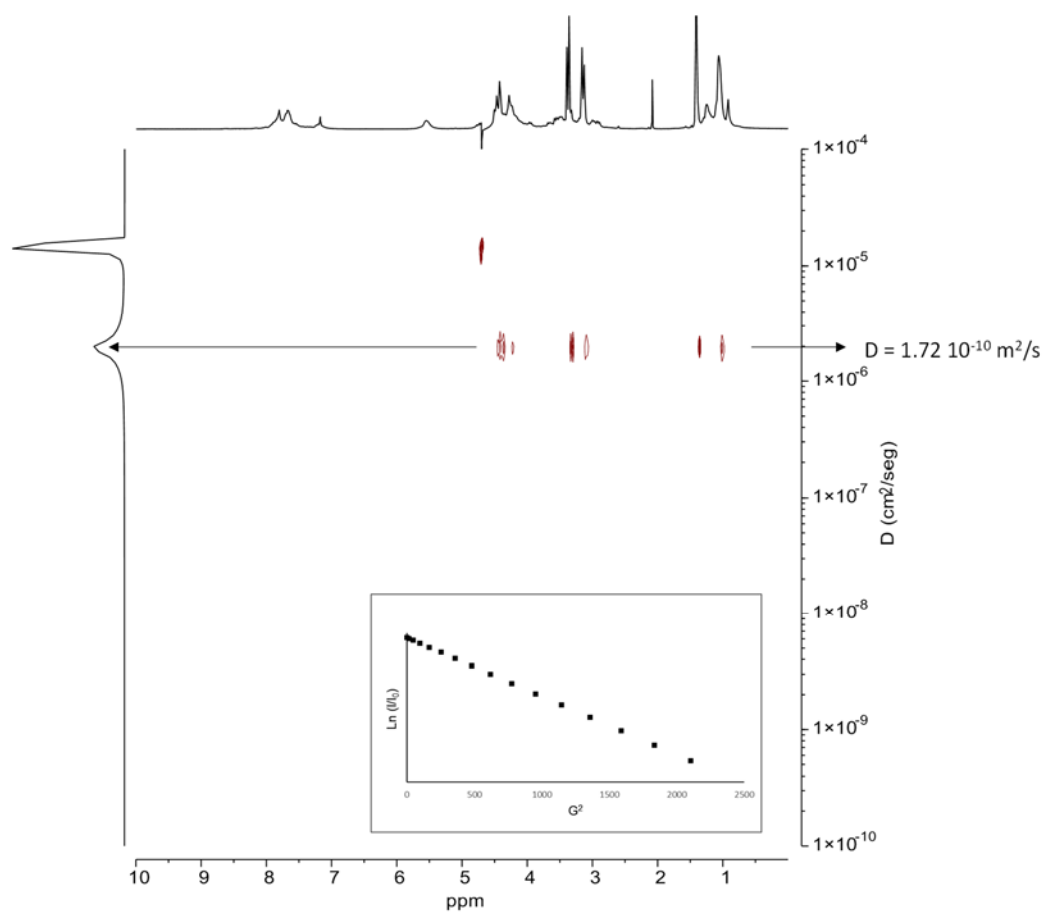


Figure 216. DOSY NMR experiment of $\text{G}_{33}\text{ABNH}_2$ in D_2O . Inset, Stejskal-Tanner plot.

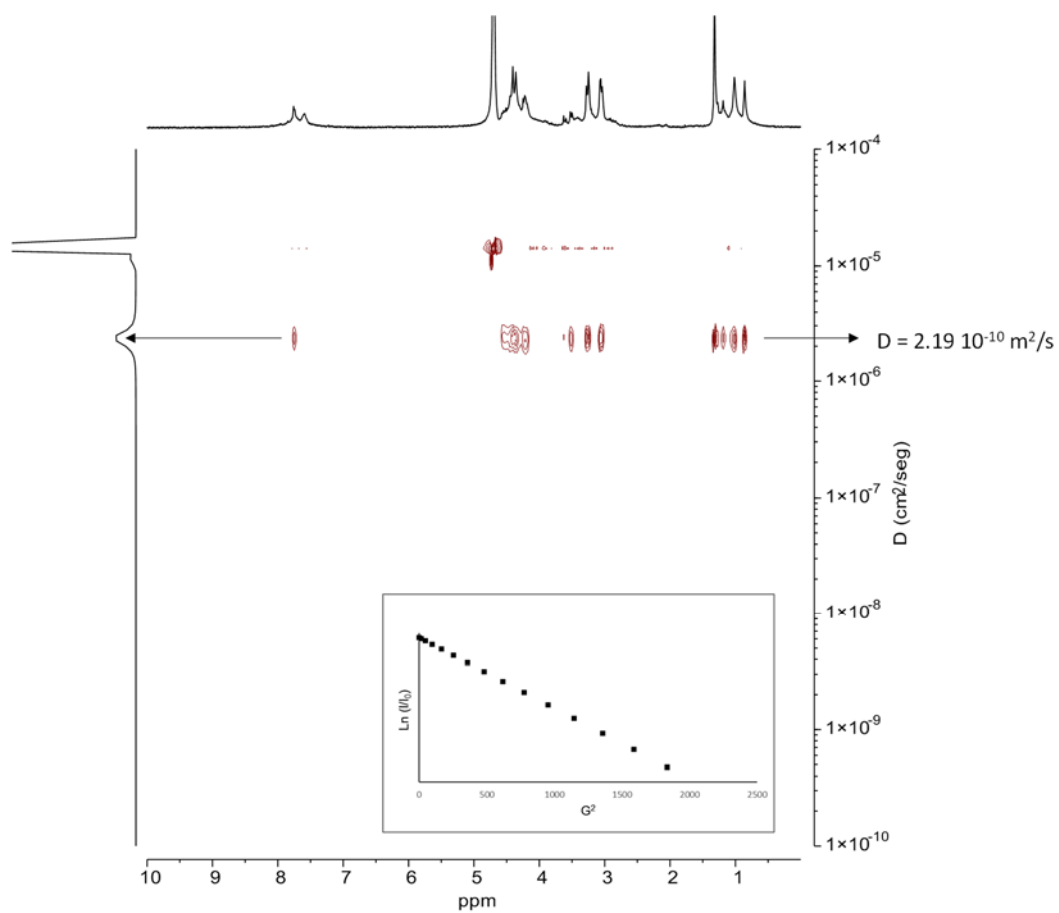


Figure 217. DOSY NMR experiment of $\text{G3}_{\text{Naph}}\text{NH}_2$ in D_2O . Inset, Stejskal-Tanner plot.

RESUMEN

Introducción

La palabra “dendrúmero” proviene de las palabras griegas δένδρον (dendrón) que significa “árbol” y μέρος (méros) que puede traducirse como “parte”. El término hace referencia a la geometría de estas moléculas, que simulan las ramas de un árbol.

Los dendrímeros pueden definirse como moléculas poliméricas con estructuras regulares y ramificadas que generalmente poseen propiedades características de compuestos monodispersos.² La principal diferencia con otros polímeros ramificados reside en su síntesis controlada, basada en una metodología iterativa, y que da como resultado estructuras libres de defectos, mientras que la síntesis de polímeros suele ocurrir en un único paso de polimerización.³

La estructura de los dendrímeros se compone de: un núcleo central multifuncional, una estructura interior dendrítica (las ramificaciones), y una superficie exterior con grupos funcionales terminales. Cada paso de crecimiento representa una nueva generación del dendrúmero y las estructuras ramificadas que forman segmentos unidos a la unidad central se denominan dendrones (Figura 1).

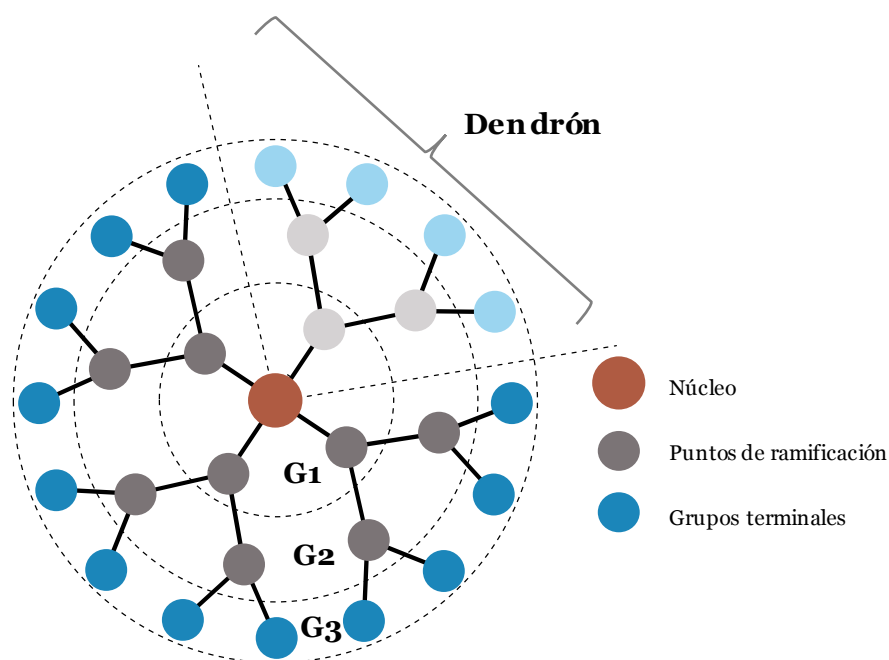


Figura 1. Estructura esquemática de un dendrímero.

La unidad central puede ser un átomo o una molécula y el número de ramas que se pueden unir a ella influirá en la multiplicidad y el tamaño de la estructura final. Otros parámetros, como la flexibilidad y la rigidez, están condicionados por las unidades de ramificación y los grupos terminales. El número de estos grupos terminales viene determinado por la generación del dendrímero y por el número de grupos reactivos del núcleo y los puntos de ramificación. Mediante la selección de los grupos funcionales adecuados en la superficie del dendrímero, se pueden modificar propiedades como la estabilidad, solubilidad o viscosidad.

A partir de cierta generación, sin embargo, el hecho de que no haya más espacio para nuevos grupos terminales implica la aparición de defectos en la estructura, al estar las reacciones de crecimiento condicionadas por impedimento estérico. Esto dará lugar a defectos estructurales y moléculas polidispersas.⁹

Históricamente, el interés en polímeros tridimensionales altamente ramificados se remonta a las teorías de Flory^{9,10,11} y Stockmayer.^{13,14} Sin embargo, fue Vögtle¹⁵ quien en 1978 publicó la primera síntesis mediante pasos de crecimiento reiterativos de un compuesto ramificado potencialmente infinito.

En 1985 Tomalia describió la síntesis de los dendrímeros PAMAM^{6,19} en los que los enlaces amida presentes en su estructura les confieren solubilidad en disolventes polares como diclorometano y alcoholes de cadena corta y hacen que estas estructuras sean estables a la hidrólisis (Figura 2). Ese mismo año, Newkome²⁰ publicó la síntesis divergente de sistemas arborol (del latín *arbor* que significa “árbol”).

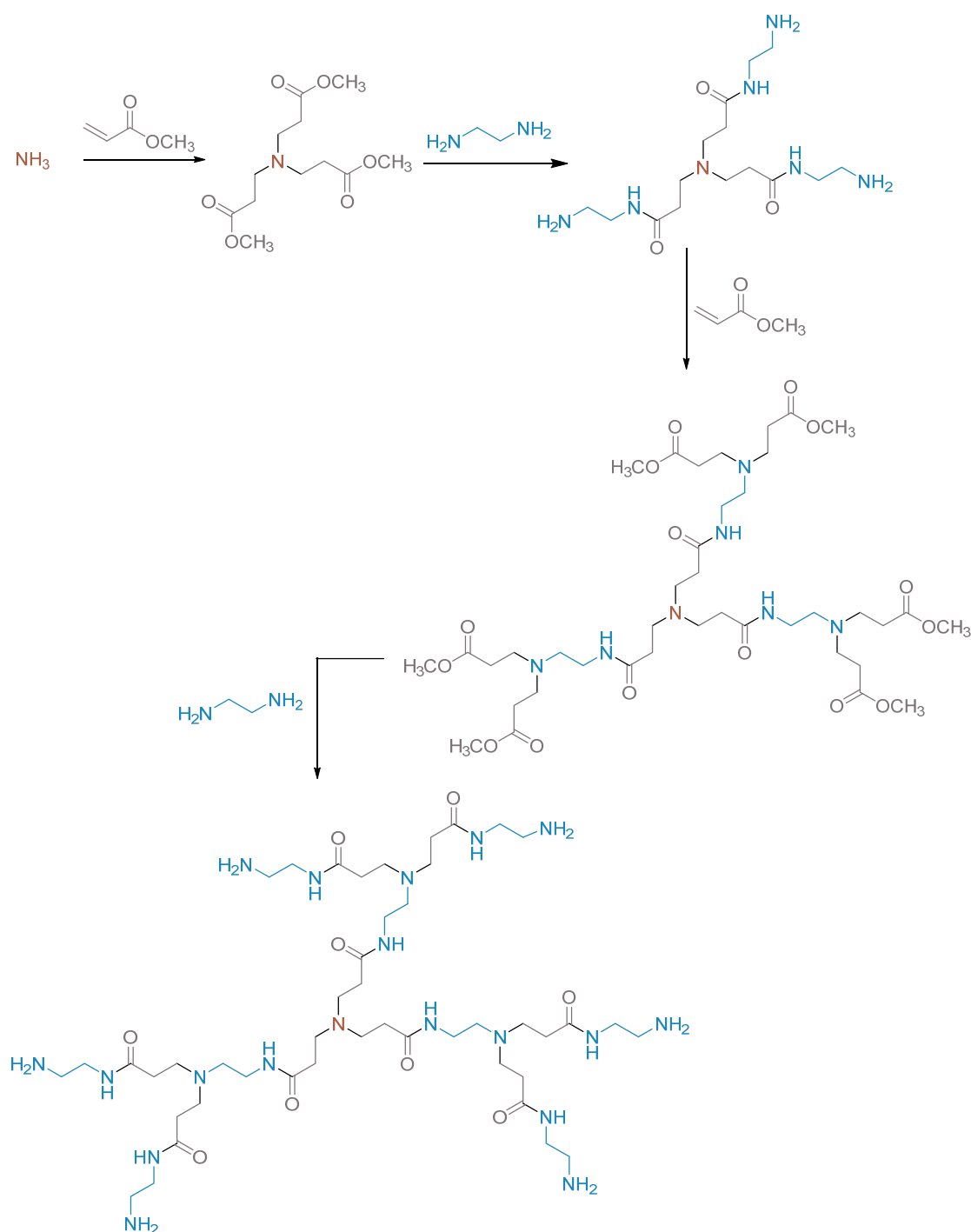


Figura 2. Síntesis de dendrímeros PAMAM.

A principio de los años noventa, la publicación de Tomalia “Starburst dendrimers: molecular-level control size, shape, surface chemistry, topology and flexibility from atoms to macroscopic matter” popularizó los conceptos básicos de la química de dendrímeros.²¹ En ese mismo año, Fréchet y Hawker publicaron su “síntesis convergente”²² que ampliaría el campo de la síntesis de dendrímeros. En esta década, también cabe destacar el crecimiento convergente de doble etapa,²³ las nuevas metodologías sintéticas basadas en autoensamblaje supramolecular^{24,25} y la síntesis de nuevos dendrímeros con diferentes heteroátomos en su estructura.^{26, 27}

Además, en los últimos 20 años se han llevado a cabo numerosos avances en este campo, entre los que destacan el desarrollo de nuevas estrategias sintéticas basadas en química *click*, la hibridación de arquitecturas dendriméricas con nano-bloques inorgánicos²⁹ y la síntesis de dendrones anfífilicos,³⁰ que han abierto un nuevo campo de síntesis de dendrímeros tipo *Janus* (dendrímeros formados por al menos dos porciones dendriméricas y que poseen diferentes funcionalizaciones terminales).

Nuestro grupo publicó en 2015 la síntesis de una nueva familia de dendrímeros de poliamida a los que nombró BAPAD (del inglés *Bis-Aminoalkyl-PolyAmide-Dendrimers*)³¹ cuyas estructuras están basadas en el uso del ácido 3,3'-diazidopiválico como monómero. Su síntesis consiste en la reducción de los grupos azido a grupos amino, a la que sigue un paso de crecimiento que conlleva la condensación de estas aminas con dos unidades de monómero, mediante la formación de enlaces amida (Figura 3).

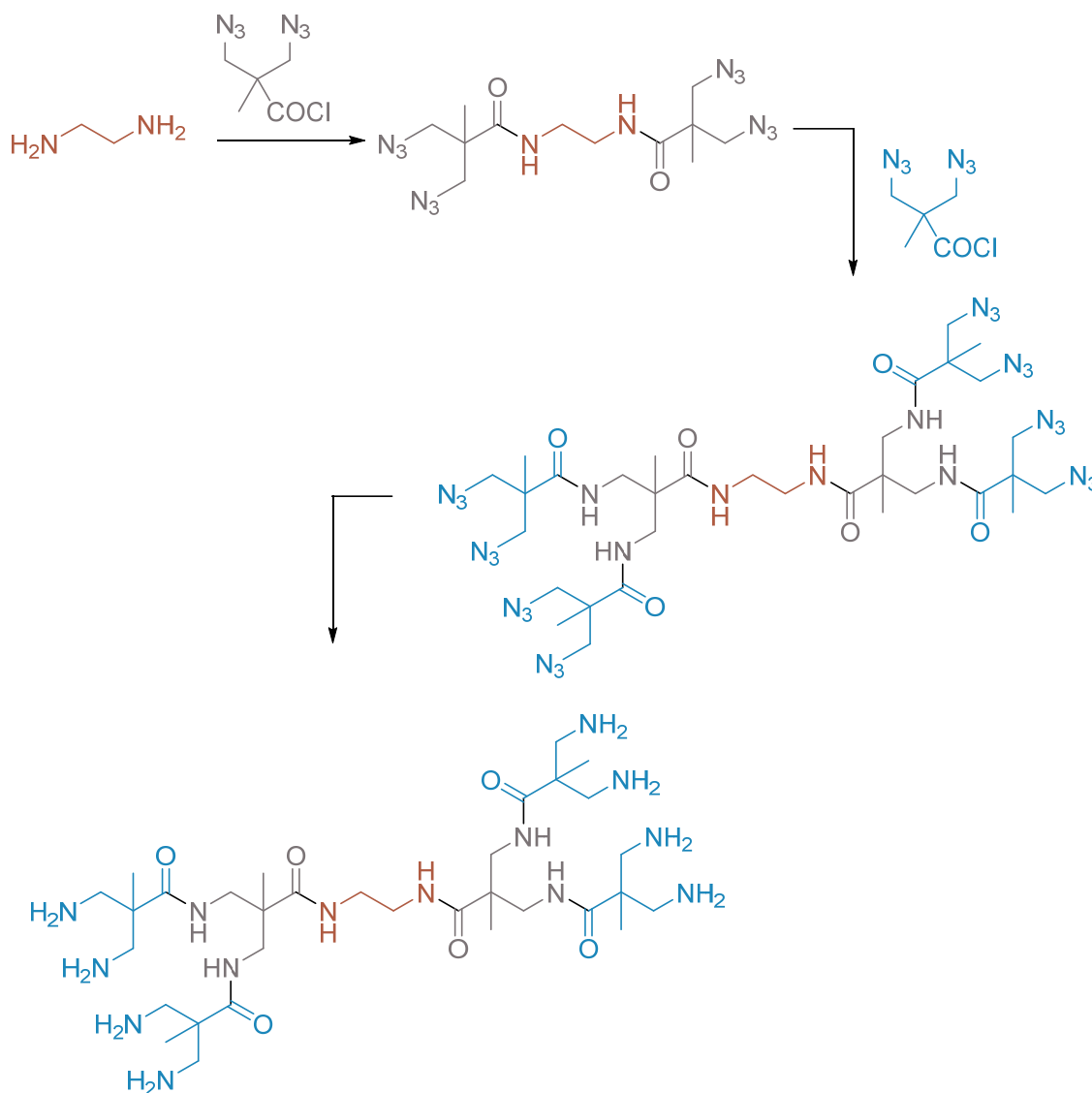


Figura 3. Síntesis de dendrímeros BAPAD.

Tradicionalmente, las metodologías para la síntesis estructuras dendríticas han sido dos: divergente y convergente.

Mediante el método divergente, el dendrímero se construye desde el núcleo hacia el exterior, gracias a la adición consecutiva de monómeros. Los monómeros más usados son del tipo AB_n ($n \geq 2$), donde A y B son dos grupos funcionales diferentes. El monómero más usado es de tipo AB_2 , en el que el grupo funcional B es un grupo no reactivo, o si lo es, se encuentra protegido para asegurar el crecimiento controlado mediante la reacción de los grupos reactivos

A del monómero. Esta estrategia es la usada en las primeras publicaciones de la síntesis de dendrímeros tipo PPI¹⁵ o PAMAM.⁶ Las primeras rutas sintéticas comerciales de estructuras dendriméricas siguieron este modelo, demostrando buenos resultados a gran escala. Sin embargo, conforme aumenta la generación, también lo hace el número de enlaces que necesitan formarse en una única reacción lo que da lugar a la aparición de defectos en las estructuras.¹⁹ Además, para forzar el crecimiento completo del dendrímero se necesita un exceso de monómero, lo que no sólo aumenta los costes de producción sino que puede dificultar los procesos de purificación.

En la metodología convergente, usada por primera vez en 1990,²² la síntesis comienza desde los grupos terminales, es decir, el dendrímero se construye desde la periferia hacia el interior. En este caso, el monómero tipo AB_n está formado por un número n de grupos B reactivos mientras que el grupo funcional A es un grupo no reactivo, o si lo es, se encuentra protegido. Las consecutivas reacciones de crecimiento dan lugar a dendrones cada vez más grandes con un único grupo reactivo como punto focal. El dendrímero correspondiente se construye mediante la unión de estos dendrones a través de su punto focal con la unidad central.

Con el objetivo de minimizar el número de pasos para obtener mayores generaciones, se han desarrollado nuevas metodologías que combinan estos dos modelos sintéticos:

- El método del hipermonómero³⁹ consiste en el uso de monómeros con más grupos funcionales que el tradicional AB₂, normalmente del tipo AB₃, AB₄ o AB₈.

- A través del método convergente de doble etapa⁴⁰ los puntos focales de dendrones se hacen reaccionar con un dendrímero de baja generación, que ha podido ser sintetizado de forma divergente o convergente.

- El método doble exponencial^{41,42} se basa en la síntesis de dendrones de baja generación con ambos grupos A y B protegidos. Tras la desprotección selectiva de uno de los grupos, estos dendrones reaccionan consigo mismo para dar lugar a generaciones mayores de dendrones totalmente protegidos. La etapa

final consiste en la desprotección del punto focal, el acoplamiento con un núcleo y la desprotección de los grupos terminales.

Debido a que un gran número de dendrímeros se basan en enlaces amida, un conocimiento de la química de péptido puede resultar de gran utilidad. La síntesis de péptidos está basada en la combinación y manipulación adecuada de grupos protectores, así como en la elección de agentes de acoplamiento eficientes para la formación controlada de los enlaces amida.⁴⁸ A continuación se muestran los métodos sintéticos más relevantes en la síntesis de los dendrímeros presentados en este trabajo.

1) Estrategias de protección/desprotección de grupos aminos: el grupo *tert*-butiloxicarbonilo (Boc) es un grupo protector de aminas resistente a la hidrogenación y a medios básicos fuertes. La desprotección se puede llevar a cabo en condiciones ácidas usando ácido trifluoroacético o ácido clorhídrico.

2) Estrategias de protección/desprotección de ácido carboxílicos: se puede llevar a cabo mediante la formación de un éster bencílico usando Cs_2CO_3 como base y bromuro de bencilo.⁵³ Este grupo funcional es estable en condiciones ácidas y la desprotección puede darse mediante hidrogenólisis usando un catalizador de paladio.

3) Reacciones de formación de amidas: Para un óptimo acoplamiento es necesario la activación del grupo amino o el grupo carboxílico, siendo esta última la más común. A continuación, se detallan algunos de los métodos más usados en la activación de grupos carboxílicos:

3.1) Formación de haluros de ácido.

3.2) Uso de carbodiimidas. Entre este grupo cabe destacar el uso de Diciclohexilcarbodiimida (DCC), diisopropilcarbodiimida (DIC) o 1-etil-3-(3-dimetilaminopropil)carbodiimida (EDCI).

3.3) Formación de acilimidazoles, siendo uno de los agentes más usado el carbonil diimidazol (CDI).

Por otro lado, en los últimos años se ha producido un creciente interés en el uso de la denominada química *click* para la síntesis de estructuras dendríticas, ya que puede llegar a tener rendimientos del 99% y presenta una buena ortogonalidad. La reacción *click* más usada es la cicloadición azido-alquino asistida por cobre (CuAAC), basada en la cicloadición [2+3] de Huisgen.⁶⁰ La presencia de Cu(I) juega un papel crucial ya que previene la formación del 1,5-triazol, haciendo que la reacción sea estereoselectiva y permitiendo que se lleve a cabo a temperatura ambiente.

En cuanto a las aplicaciones de este tipo de compuestos, un gran número de aplicaciones de dendrímeros están basadas en su multivalencia. Además, su estructura interna puede usarse para la encapsulación de moléculas que sean incompatibles con el medio exterior.⁸² Un cambio en las condiciones del medio (polaridad, pH...) puede producir un cambio en la conformación del dendrímero, lo que daría lugar a una diferencia en la forma y la densidad. Es por ello que numerosos estudios se han centrado en las propiedades de encapsulación y liberación de los dendrímeros para su potencial uso en la administración de medicamentos.⁸³

Su baja polidispersidad, el hecho de que el tamaño y forma de dendrímeros de alta generación simula los de proteínas y el gran número de sitios de unión en su periferia, hacen que resulten de interés en farmacoquímica, ya que pueden actuar como plataformas multifuncionales.¹⁰¹ Sin embargo, sus aplicaciones en el área de la biomedicina vienen limitadas por factores como la toxicidad y la facilidad de ser eliminados del sistema.

En el ámbito de inmunoensayos, nuestro grupo desarrolló nuevos materiales para el estudio de respuestas inmunológicas adversas a fármacos. Para ello se llevó a cabo la funcionalización de discos de celulosa¹²⁴ y nanopartículas de sílica¹²⁶ con dendrímeros PAMAM funcionalizados con antibióticos β -lactámicos. En ambos casos se demostró la reproducibilidad y el reconocimiento de las correspondientes IgEs.

Nuestro grupo también ha llevado a cabo la síntesis y el estudio de dendrímeros que potencialmente puedan emular proteínas y su papel en procesos

alérgicos.^{121–123} Con este objetivo, el grupo llevó a cabo la síntesis optimizada de dendrímeros basados en la unidad ácido 3,3'-diazidopiválico.¹²⁹ Siguiendo esta metodología, también se sintetizaron dendrones con un grupo tiol como punto focal. Estos dendrones fueron funcionalizados con grupos amoxiciloilos (AXO) y usados en diferentes proyectos.^{130,131}

Debido a los resultados alentadores, en este trabajo nos hemos centrado en la síntesis de nuevas estructuras dendríticas mediante el diseño de una ruta sintética versátil que permita la modificación del número de grupos terminales, así como la incorporación de ciertas funcionalidades al incluir las unidades centrales adecuadas.

Síntesis de Dendrímeros amino terminales mediante química *click*

Una de las líneas en las que se centra el grupo al que pertenezco, en colaboración con grupos médicos del Hospital Regional Universitario de Málaga, es el estudio de dendrímeros como emuladores de proteínas y su papel en procesos alérgicos. Otra de las líneas, en colaboración con grupos de investigación de la Universidad de Málaga y del CIBER BBN, es el uso de dendrímeros en regeneración tisular. Para ambas aplicaciones es necesaria la síntesis de dendrímeros estables, solubles en medios acuosos y que posean grupos aminos terminales que puedan ser funcionalizados.

La estrategia divergente se ha usado con éxito en la síntesis de dendrímeros PAMAM⁶ o PPI,¹⁵ sin embargo, mientras más altas sean las generaciones, mayor será la proporción de dendrímeros con defectos estructurales. En el caso de dendrímeros BAPAD sintetizados por nuestro grupo, solo es posible la síntesis sin defectos estructurales hasta tercera generación, con un total de 16 grupos amino en su superficie.^{35,129}

En cambio, la metodología convergente solo requiere de un limitado número de sitios reactivos en cada paso de crecimiento, pero puede presentar problemas en los pasos finales de acoplamiento si los dendrones sintetizados son muy voluminosos.

En este trabajo se ha llevado a cabo la síntesis, mediante una metodología convergente, de unas nuevas estructuras dendriméricas, solubles en agua, y con grupos amino terminales.

Para ello se ha hecho uso de la reactividad ortogonal de la química de péptidos y las reacciones *click*. Se ha empleado 3,3'-diazidopivaloato de bencilo (**2**) como monómero, que reaccionará a través de los grupos azidas mientras el grupo ácido carboxílico se mantiene protegido. A partir de esta estructura, también se sintetiza el dendrón de primera generación (**dG1**), que tiene un grupo acetileno terminal (que reaccionará con los grupos azido del compuesto **2**) y dos grupos aminos adecuadamente protegidos (Figura 4).

La reacción *click* entre **dG1** y el monómero **2** da lugar a una nueva estructura dendrítica con un punto focal protegido y, en este caso, cuatro grupos amino protegidos. Los sucesivos pasos de desprotección, reacción con propargilamina y acoplamiento *click* dan como resultado dendrones de generaciones más altas, **dG2** y **dG3** (Figura 4).

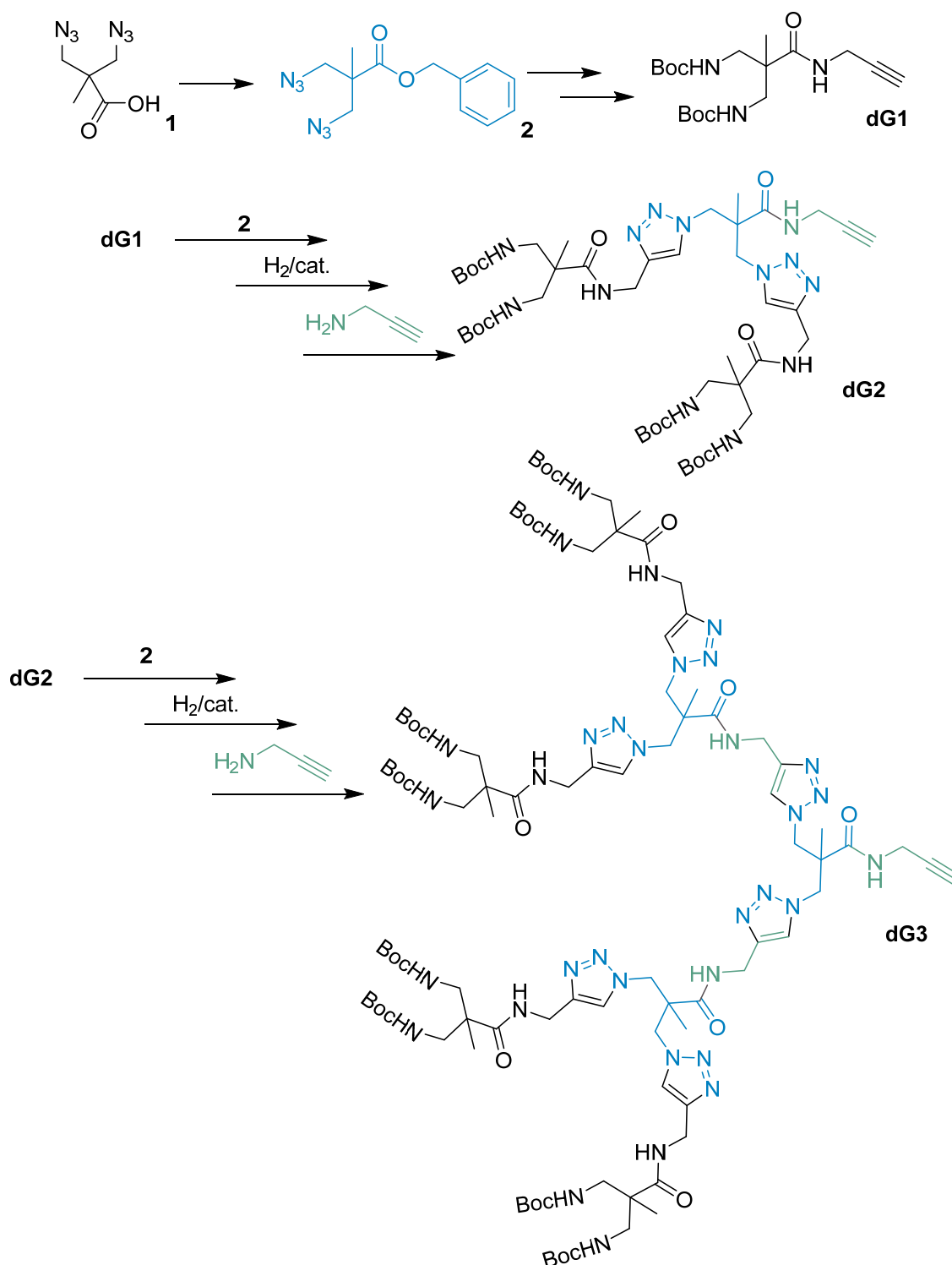


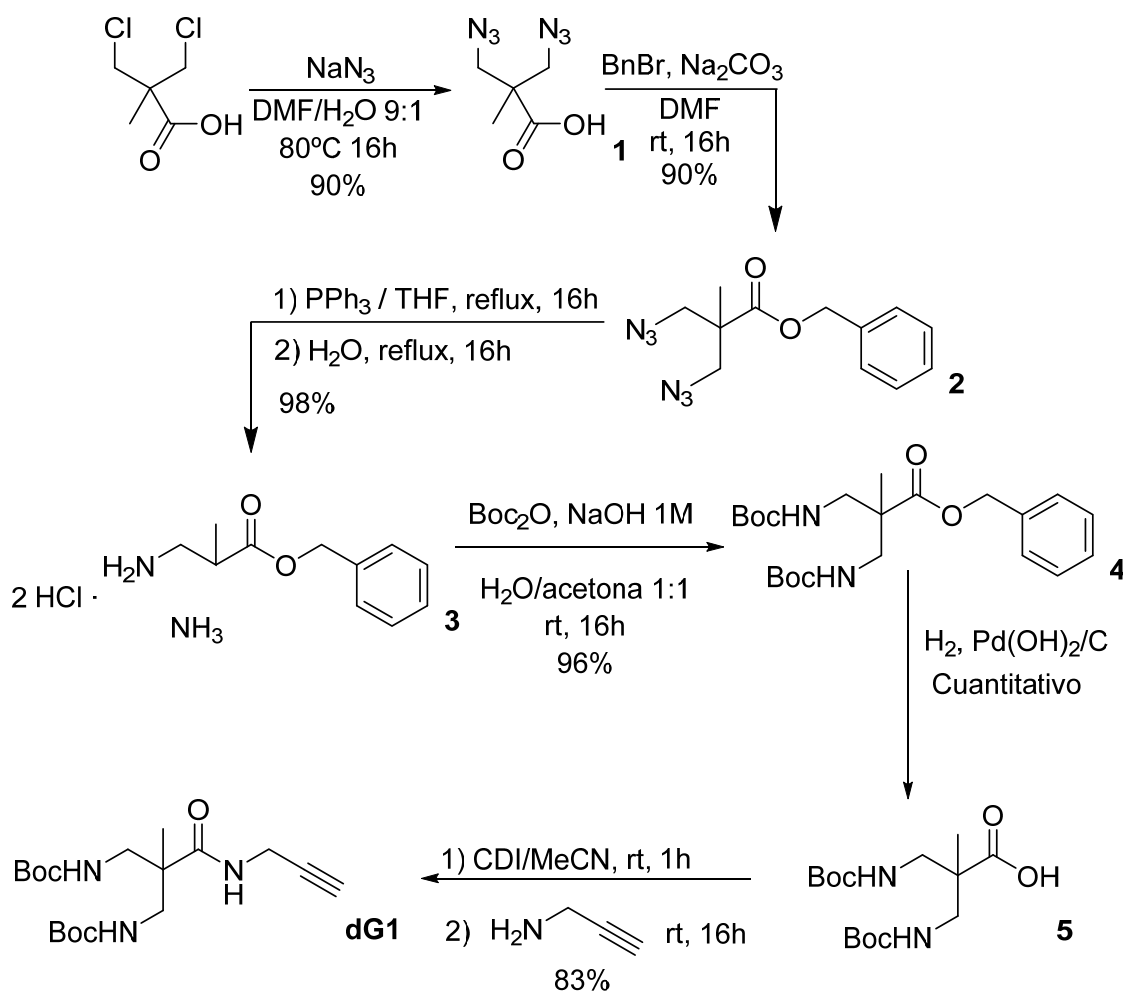
Figura 4. Síntesis esquemática de los dendrones **dG1**, **dG2** y **dG3**.

Siguiendo el método convergente, se pueden sintetizar dendrímeros gracias a las reacciones tipo *click* entre los dendrones y un núcleo central funcionalizado con grupos azida. En este trabajo, se ha realizado la síntesis de

una familia de tres generaciones de dendrímeros con etilendiamina como núcleo (**G1**_{EDANH₂}, **G2**_{EDANH₂} y **G3**_{EDANH₂}), un grupo de dendrímeros sintetizados a partir del dendrón de tercera generación y un núcleo trifuncionalizado (**G3**_{3ABNH₂}) y un dendrímero con un núcleo luminiscente (**G3**_{NaphNH₂}).

El objetivo de este apartado es el desarrollo de una metodología versátil de síntesis de dendrímeros usando química *click* entre grupos azido y amino y en donde se pueda modificar fácilmente el número de grupos terminales mediante el uso de diferentes generaciones de dendrones o diferentes núcleos multifuncionales. A continuación, se detalla con más precisión los principales pasos sintéticos de esta metodología.

La primera reacción se basa en la sustitución de los grupos cloro del ácido 3,3'-dicloropiválico por grupos azidas y se lleva a cabo empleando NaN₃, dando como resultado el ácido 3,3'-diazidopiválico (**1**), con buenos rendimientos. El compuesto **2** se obtuvo protegiendo el grupo carboxílico mediante la formación de un éster bencílico usando bromuro de bencilo y Cs₂CO₃ como base. Tras reducción de los grupos azido a amino (**3**), protección de los mismos (**4**) e hidrólisis del éster (**5**), se llevó a cabo el acoplamiento con propargilamina mediante la formación de un enlace amida, obteniendo dendrón de primera generación **dG1** con excelentes rendimientos (Figura 5).

Figura 5. Síntesis de **dG1**.

Para la obtención del dendrón de segunda generación, primero se llevó a cabo la reacción tipo *click* entre los compuestos **dG1** y **2** para obtener **dG2-Co₂Bn**. Los mejores resultados se obtuvieron cuando la reacción se llevó a cabo empleando como disolvente una mezcla de H₂O:tBuOH, en presencia de Cu₂SO₄·5H₂O y ascorbato sódico, y en ausencia de otro catalizador. El crecimiento total del dendrón viene confirmado por los experimentos de espectroscopía de infrarrojo, en donde se puede apreciar la desaparición de la señal correspondiente a los grupos azido (a 2095 cm⁻¹) del compuesto **2**. A continuación, se prosiguió con la hidrólisis del éster (**dG2-CO₂H**) y formación de la amida correspondiente (empleando propargilamina) para obtener **dG2** (Figura 6).

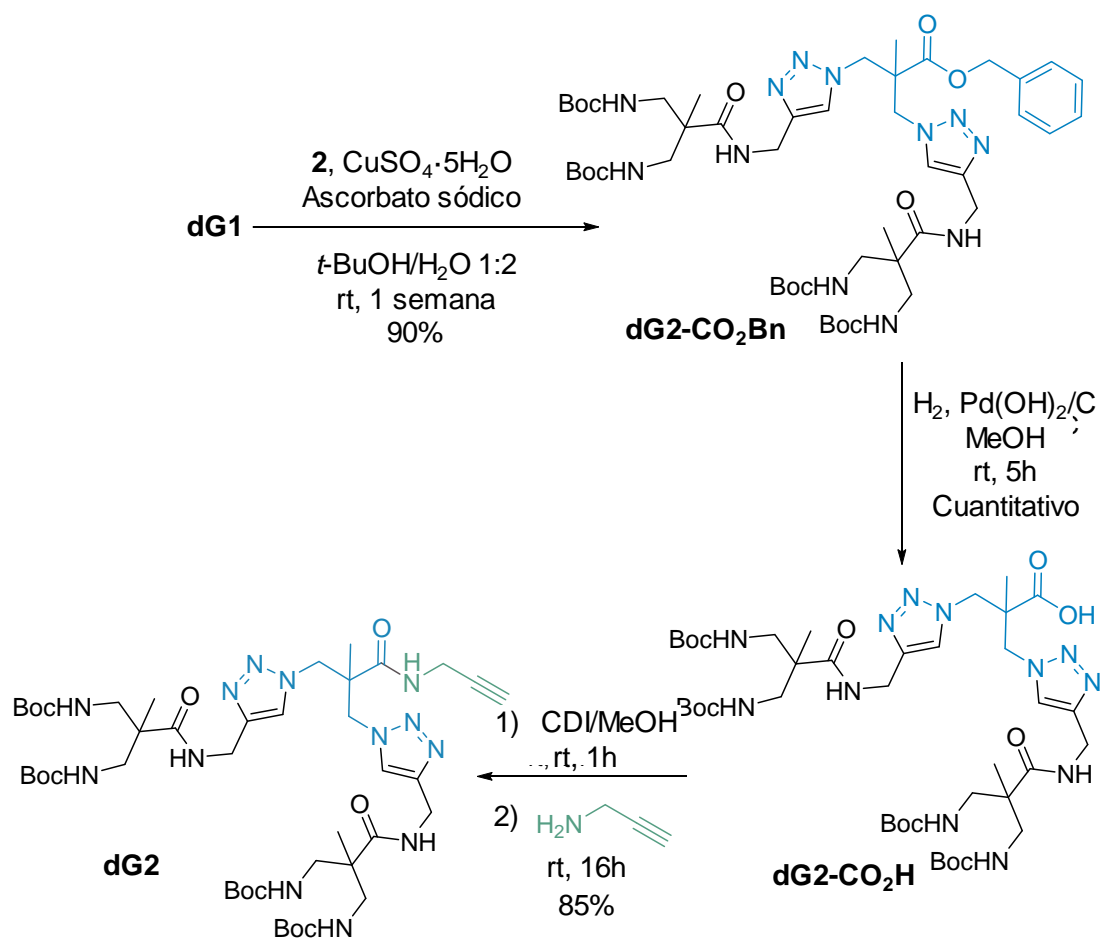
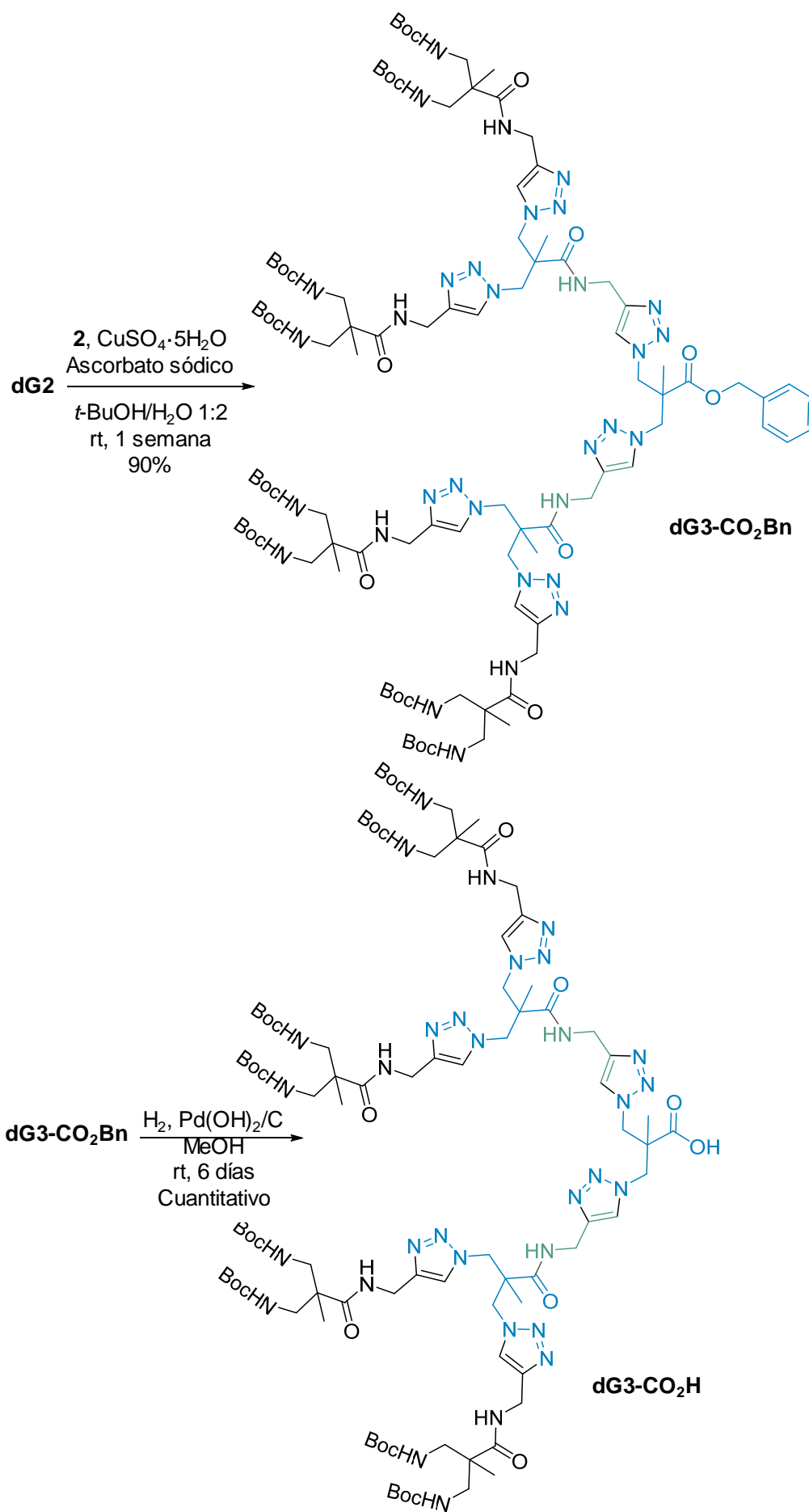


Figura 6. Síntesis de **dG2**.

Siguiendo la misma estrategia sintética formada por pasos de crecimiento, desprotección del grupo carboxílico y reacción con propargilamina, se consiguió la síntesis del dendrón de tercera generación **dG3** (Figura 7).



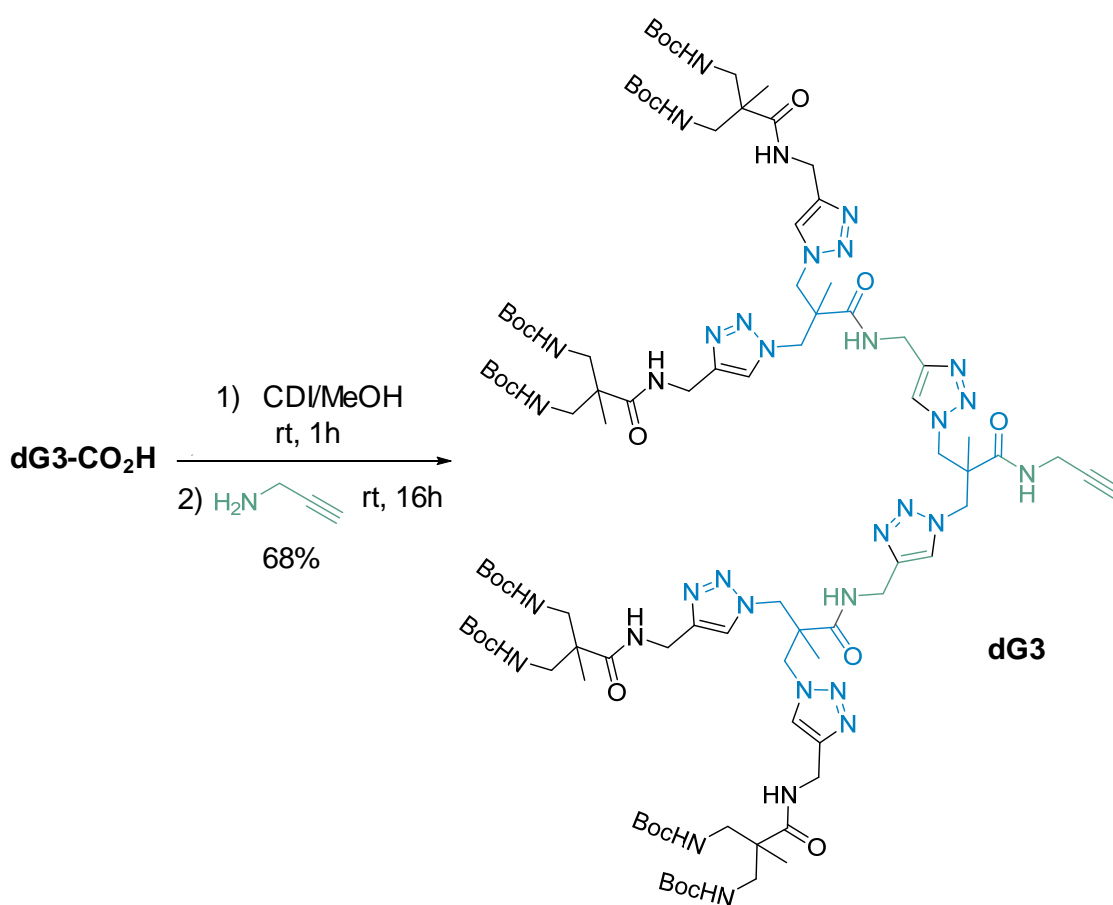


Figura 7. Síntesis de **dG3**.

Tras la obtención de las tres generaciones de dendrones, se procedió la síntesis de una familia de dendrímeros usando 1,2-diazidoetano (**6**). Los dendrímeros se obtuvieron tras hacer reacciones los dendrones de diferentes generaciones (**dG1**, **dG2**, **dG3**) con **6** y la desprotección de los grupos aminos para obtener las estructuras finales, **G1_{EDANH₂}**, **G2_{EDANH₂}** y **G3_{EDANH₂}** respectivamente (Figura 8).



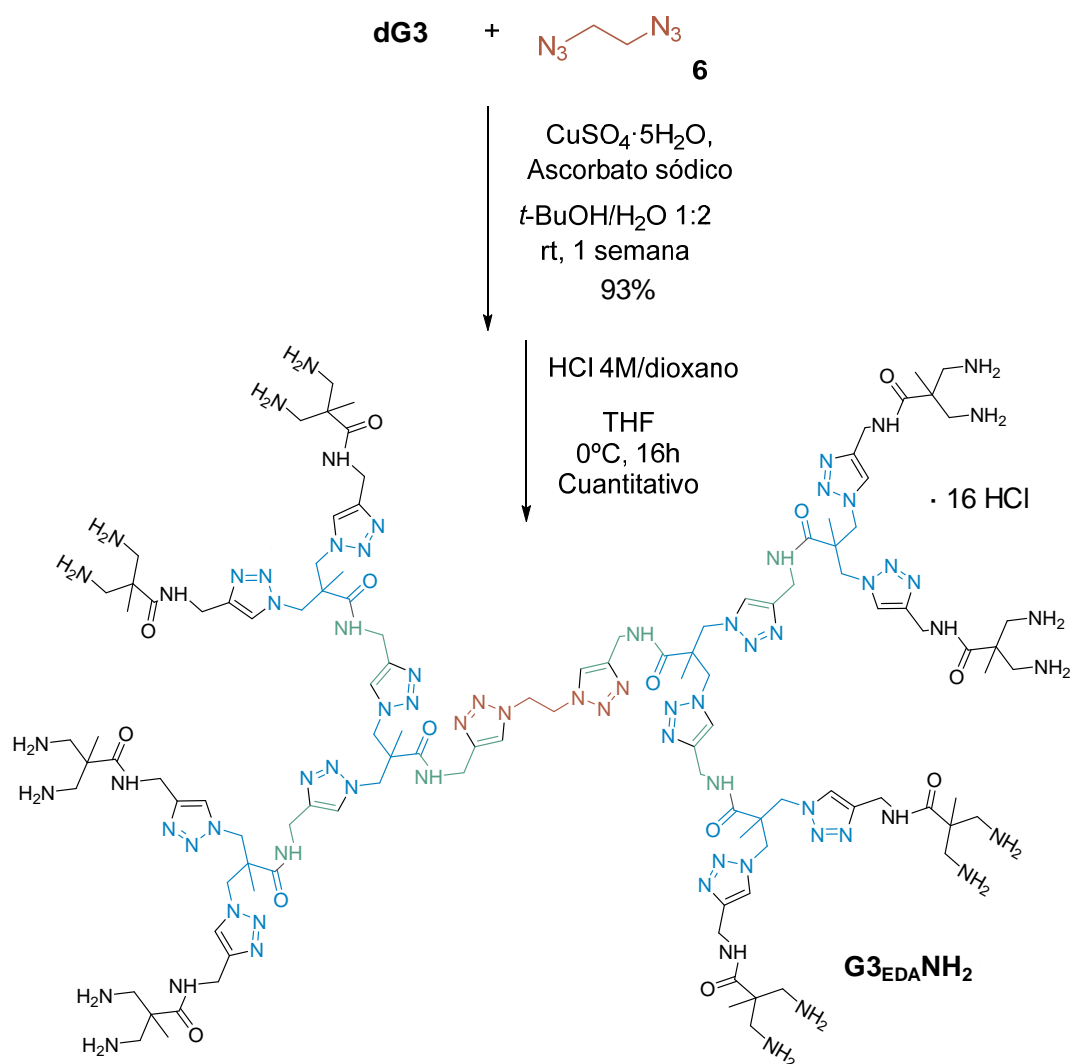


Figura 8. Síntesis de **G1_{EDA}NH₂**, **G2_{EDA}NH₂** y **G3_{EDA}NH₂**.

Siguiendo esta metodología se sintetizó un dendrímero con 24 grupos amino terminales (**G3_{3AB}NH₂**) mediante la reacción *click* entre **dG3** y 1,3,5-tris(azidometil)benceno (**7**) (Figura 9).

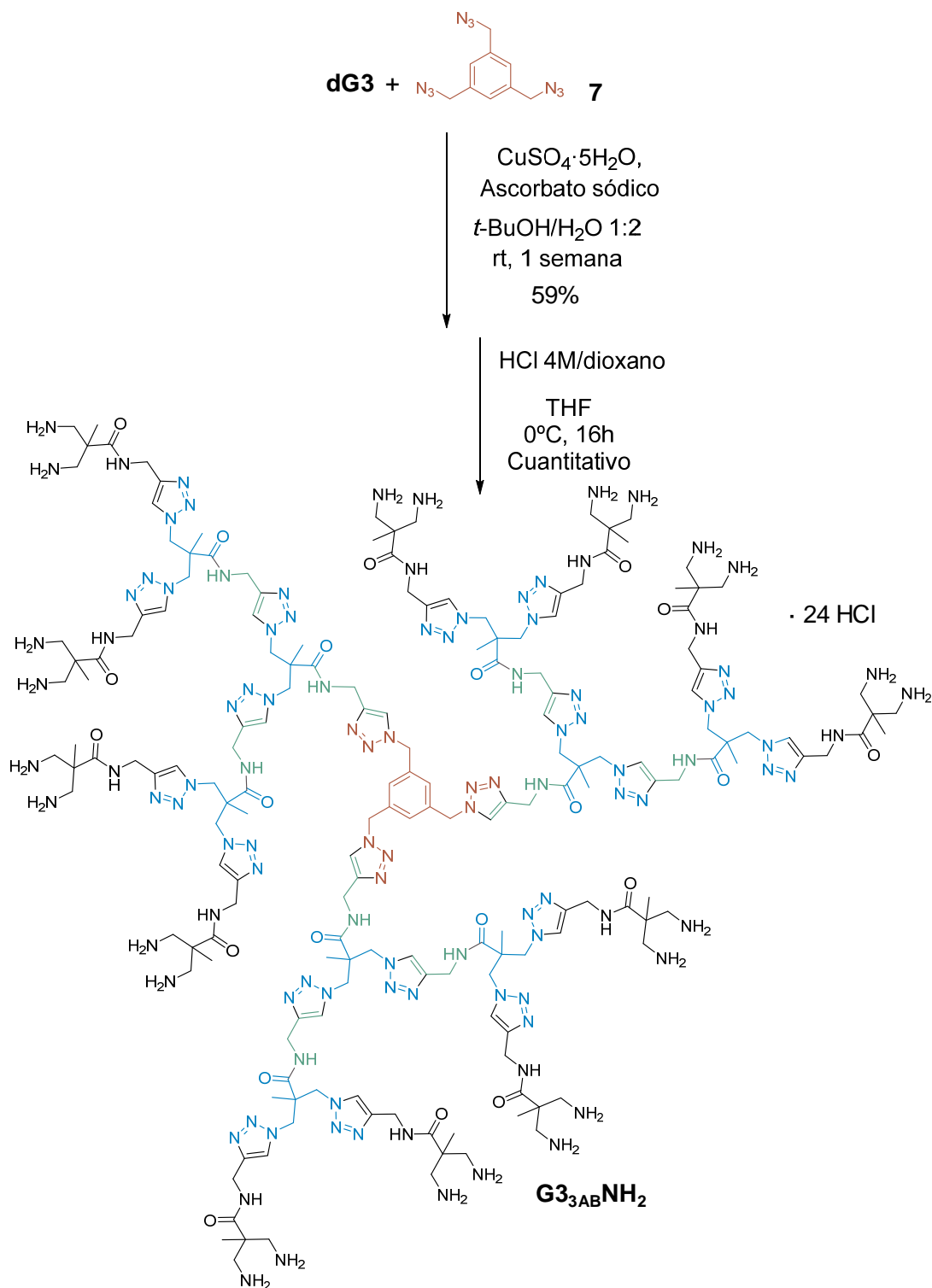


Figura 9. Síntesis de **G3_{3AB}NH₂**.

Por último, se llevó a cabo la síntesis de una dendrímero fluorescente. Para ello, se diseñó una unidad central basada en una estructura de naftalimida y funcionalizada con dos grupos azido (**10**). Tras el acoplamiento de esta unidad con **dG3** y la posterior desprotección de los grupos amino, se obtuvo con éxito el compuesto deseado **G3_{Naph}NH₂** (Figura 10).

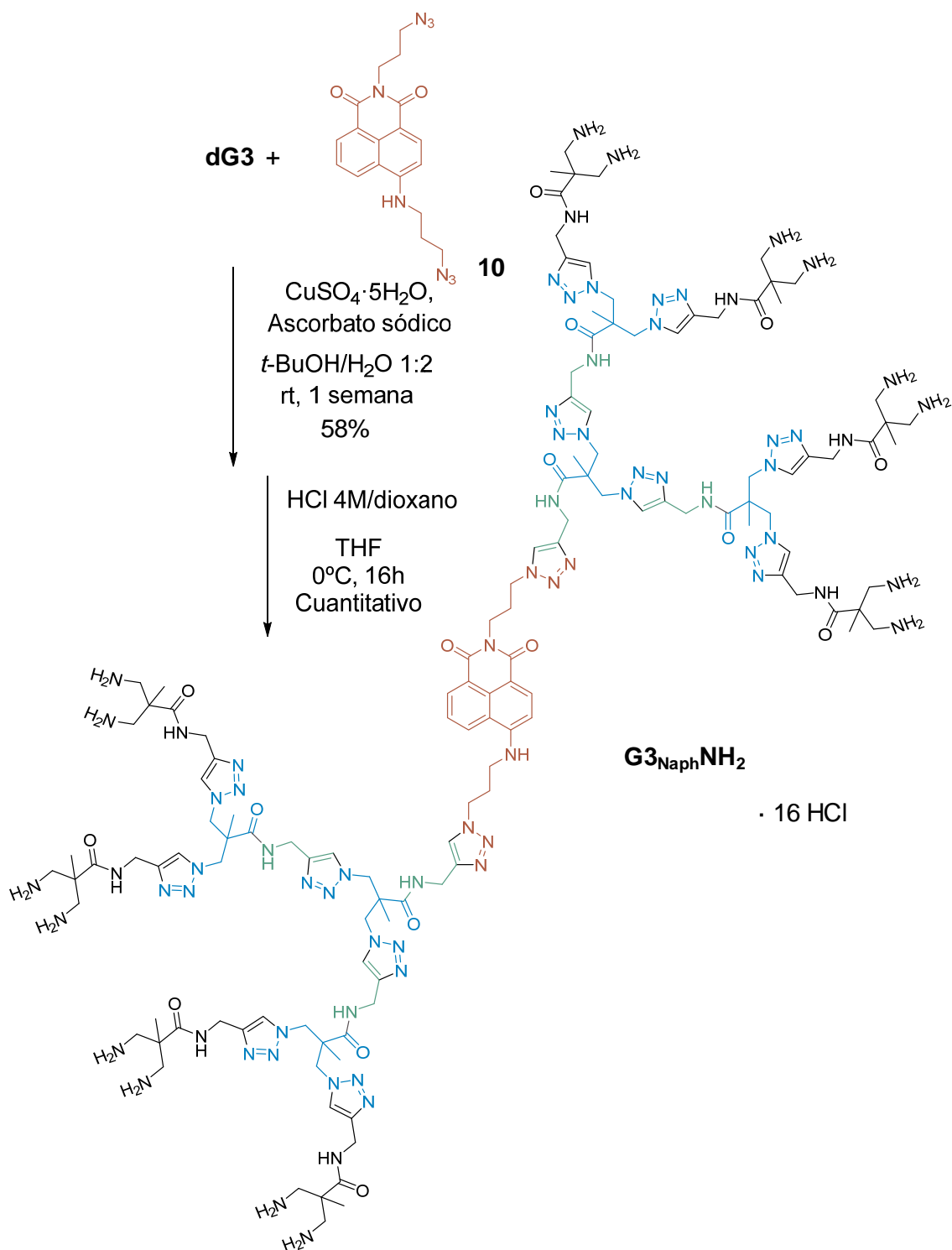


Figura 10. Síntesis de **G3_{Naph}NH₂**.

Todos los compuestos fueron caracterizados mediante técnicas de resonancia magnética. Se llevó a cabo experimentos de espectroscopía de masas siempre que fue posible pero desafortunadamente, no se pudieron obtener para los dendrímeros debido probablemente a la volatilidad de los grupos Boc en los dendrímeros tipo **Gx-NHBoc** y a la carga positiva de las estructuras finales en

los dendrímeros finales **G_x-NH₂**. Se obtuvieron espectros de infrarrojo de los productos tras las reacciones tipo *click* y en todos los casos, se confirmó la completa funcionalización de los compuestos indicada por la desaparición de la señal debida a los grupos azido de los productos de partida. Además, se realizaron experimentos de *diffusion ordered spectroscopy* (DOSY) a las estructuras dendriméricas finales. Mediante la representación gráfica de Stejskal-Tanner se calcularon los coeficientes de difusión y se confirmó la naturaleza monodispersa de los compuestos.

Debido a su naturaleza luminiscente, se llevó a cabo la caracterización fotofísica de **G₃NaphNH₂**. El espectro de absorción de una disolución 10⁻⁵M en agua mostró una banda a 447 nm mientras que el espectro de emisión presentó una λ_{max} a 550nm. El tiempo de vida medio resultó ser de 7.5 ns (λ_{em} = 550 nm).

Se estudiaron las posibles aplicaciones de **G₃NaphNH₂** como biomarcador bajo condiciones de excitación de uno y dos fotones. En colaboración con el grupo del Dr. Perez-Pomares y el Dr. Guadix del Departamento de Biología Animal de la Universidad de Málaga, bacterias *E. coli* (gramnegativa) y *P. subtilis* (grampositiva) se incubaron con **G₃NaphNH₂**. Las imágenes obtenidas mediante el microscopio confocal muestran una adhesión efectiva del compuesto a las paredes de las bacterias, mostrando fluorescencia bajo excitación de uno y dos fotones mientras que las bacterias control no presentaban ninguna fluorescencia.

A su vez, estudios bactericidas se llevaron a cabo en colaboración con el grupo del Dr. Díaz-Martínez y el Dr. Romero del Departamento de Microbiología de la Universidad de Málaga y en ellos no se pudo apreciar cambios en el crecimiento de bacterias *E. coli* y *P. subtilis* al aumentar la concentración de **G₃NaphNH₂** en el medio de 10 a 100 μM .

Síntesis de Complejos dendríticos de Pt(II) solubles en agua

Los complejos de platino han despertado gran interés gracias a sus excelentes propiedades fotofísicas¹⁷⁸ como su fotoestabilidad, un gran desplazamiento de Stoke,¹⁷⁹ la habilidad de emitir bajo excitación de dos fotones,¹⁸⁴ sus tiempos de vida, que permiten su uso en técnicas de Microscopía

basadas en el uso de fosforescencia en tiempo real (PLIM)¹⁸⁴ y la posibilidad de modificar su luminiscencia en función de la elección de los ligandos.^{180,181,182,183} Sus propiedades fotofísicas están íntimamente ligadas a las características de los centros metálicos, la estructura de los ligandos, el entorno y las interacciones intermoleculares. Sin embargo, las aplicaciones en bioimagen de estos compuestos se ven limitadas por el quenching y la baja solubilidad de éstos en medios acuosos, así como la tendencia a formar agregados.

Esto es debido en gran parte a que el Pt(II) tiene una configuración electrónica d^8 lo que resulta en complejos con geometría cuadrada plana.¹⁸⁶ La interacción entre los orbitales dz^2 , perpendiculares al plano de coordinación, da lugar a la formación de agregados que en algunos casos pueden ocasionar problemas en los procesos de purificación. Esta agregación puede ser más o menos controlada mediante la elección adecuada de ligandos, por ejemplo, puede evitarse insertando ligandos voluminosos.

A su vez, la síntesis de complejos de platino solubles en agua puede dar lugar a potenciales aplicaciones en bioimagen, donde las principales características deseables son un desplazamiento de Stoke grande, fotoestabilidad, solubilidad en agua y biocompatibilidad. La solubilidad de estos compuestos de platino en agua se ha conseguido en algunos casos modificando el ligando auxiliar con cadenas de TEG, aunque en estos casos se favorece la formación de hidrogeles y no se observa emisión de la especie monomérica a temperatura ambiente.²⁰⁶

Algunos de los problemas relacionados con estos complejos son la solubilidad en medios acuosos y la agregación, ambos importantes para algunas aplicaciones específicas. La inserción de los complejos en estructuras dendriméricas podría resolver dichos problemas, por lo que se propuso la inserción de una estructura dendrítica (**18**) con grupos amino en su periferia y una piridina como punto focal que se acoplará al complejo de platino. Este trabajo se ha llevado a cabo en colaboración con el grupo del Prof. Strassert del Centro de Nanotecnología de la Universidad de Muenster, que cuya principal línea de investigación es la síntesis y el estudio de nanomateriales organometálicos electroluminiscentes, siendo una de sus líneas la síntesis y el estudio de complejos de Pt (II).^{207,202,208}

Para ello, se ha diseñado la síntesis de un nuevo dendrón con un triple enlace como punto focal y cuatro grupos amino terminales protegidos (**13**) (Figura 11). El compuesto se preparó activando el grupo carboxílico del compuesto **5** con CDI y haciéndolo reaccionar con los grupos amino de **3**, obteniéndose un dendrón de segunda generación con el punto focal y los grupos terminales protegidos (**11**). El siguiente paso fue la desprotección del ácido carboxílico para obtener el compuesto **12**. Finalmente se introdujo un triple enlace mediante la reacción de este compuesto con propargilamina (**13**). Todos los compuestos fueron caracterizados mediante técnicas de resonancia magnética y espectroscopía de masas, obteniéndose con éxito el compuesto **13**.

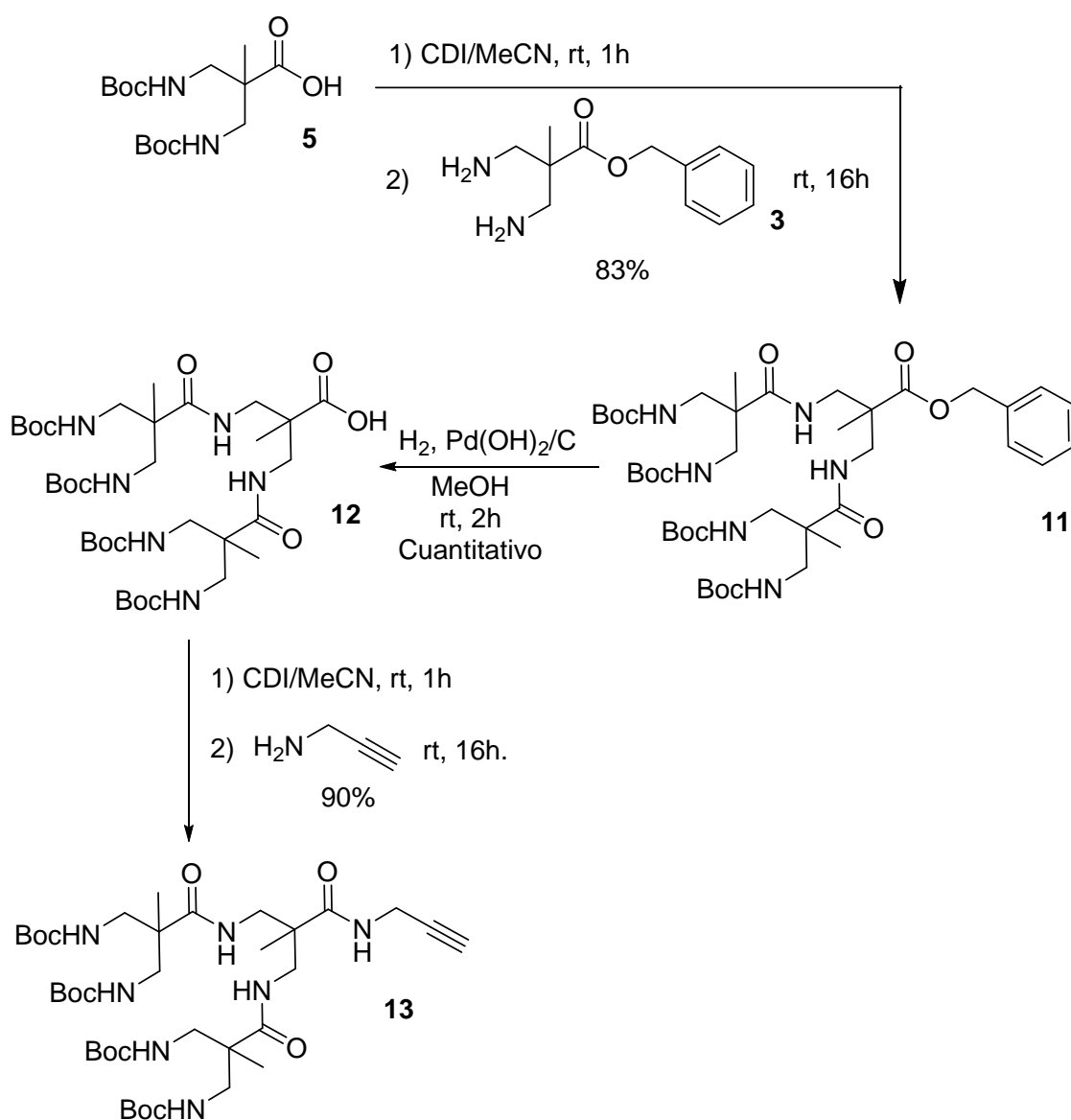


Figura 11. Síntesis de **13**.

Se propuso la síntesis de un derivado de piridina como punto focal de la estructura dendrítica final ya que el enlace entre el nitrógeno de la piridina y el platino había sido ampliamente estudiado por el grupo del Prof. Strassert.²¹² En primer lugar se sintetizó un bromo derivado de la piridina siguiendo la metodología previamente descrita.²¹⁵ El compuesto comercial ácido 3,5-piridinocarboxílico fue esterificado (**14**) y luego reducido para obtener la 3,5-bis(hidroximetil)piridina (**15**). La sustitución por bromos dio como resultado **16**. El último paso consistió en la sustitución de los bromos por grupos azido²¹⁴ para obtener **17** (Figura 12).

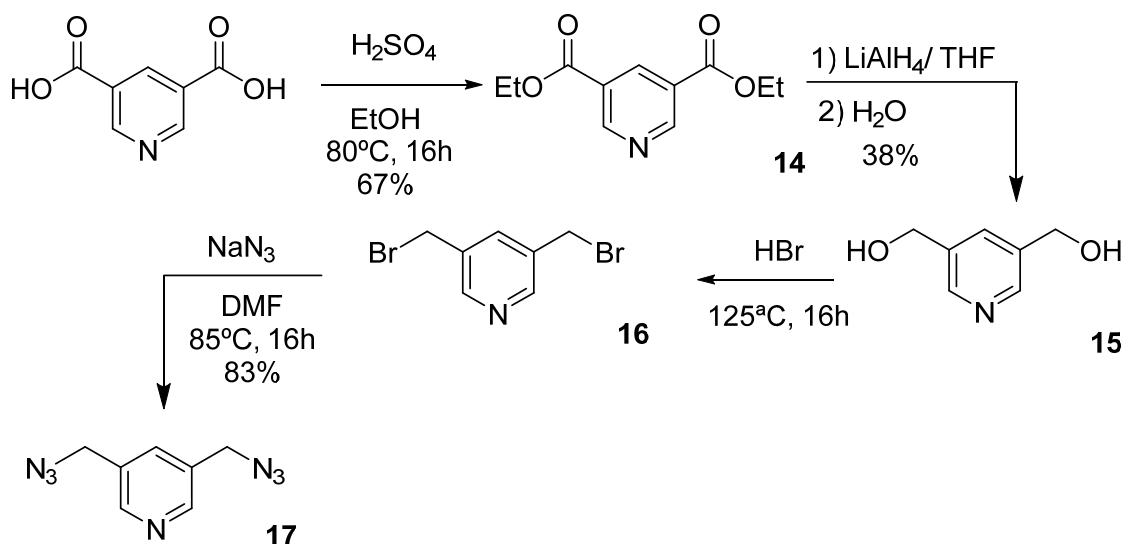


Figura 12. Síntesis de **17**.

La reacción *click* entre **13** y **17** dio como resultado la estructura dendrítica que se usaría como ligando auxiliar para formar el complejo de platino propuesto (Figura 13).

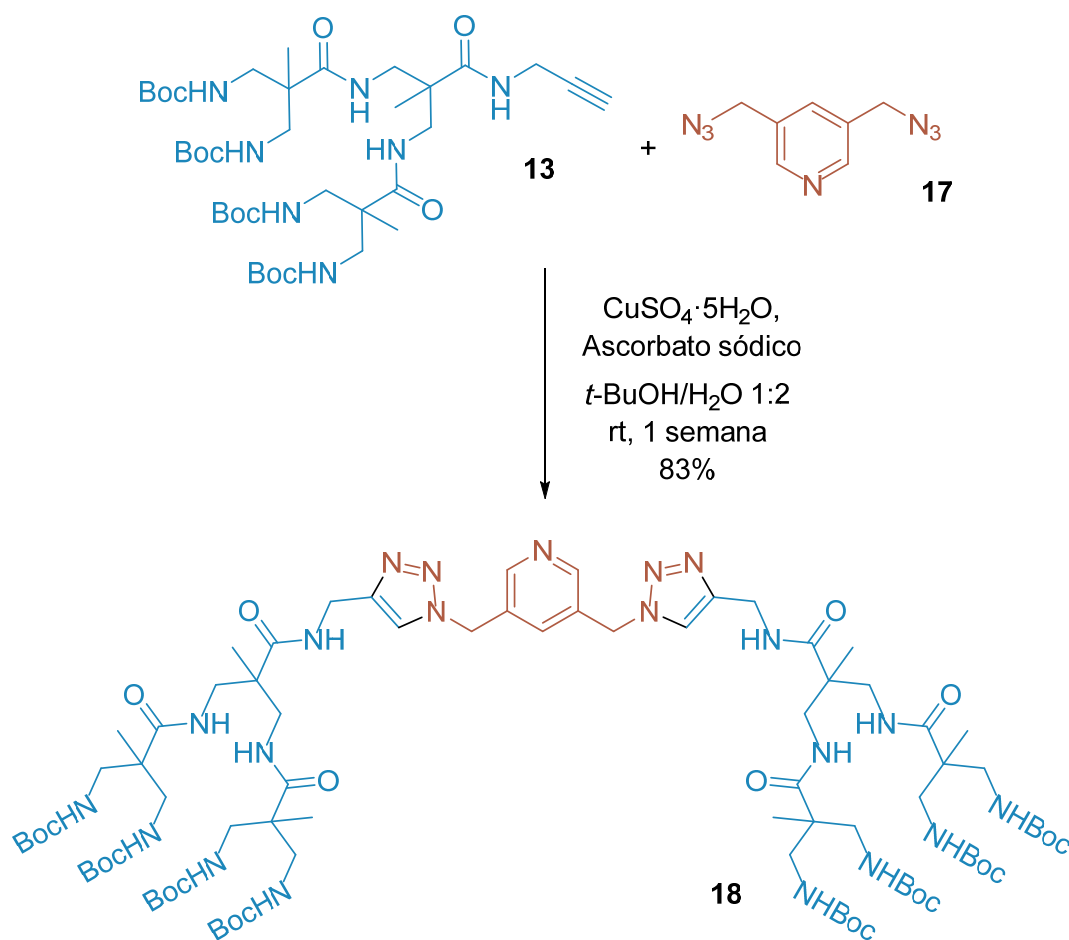
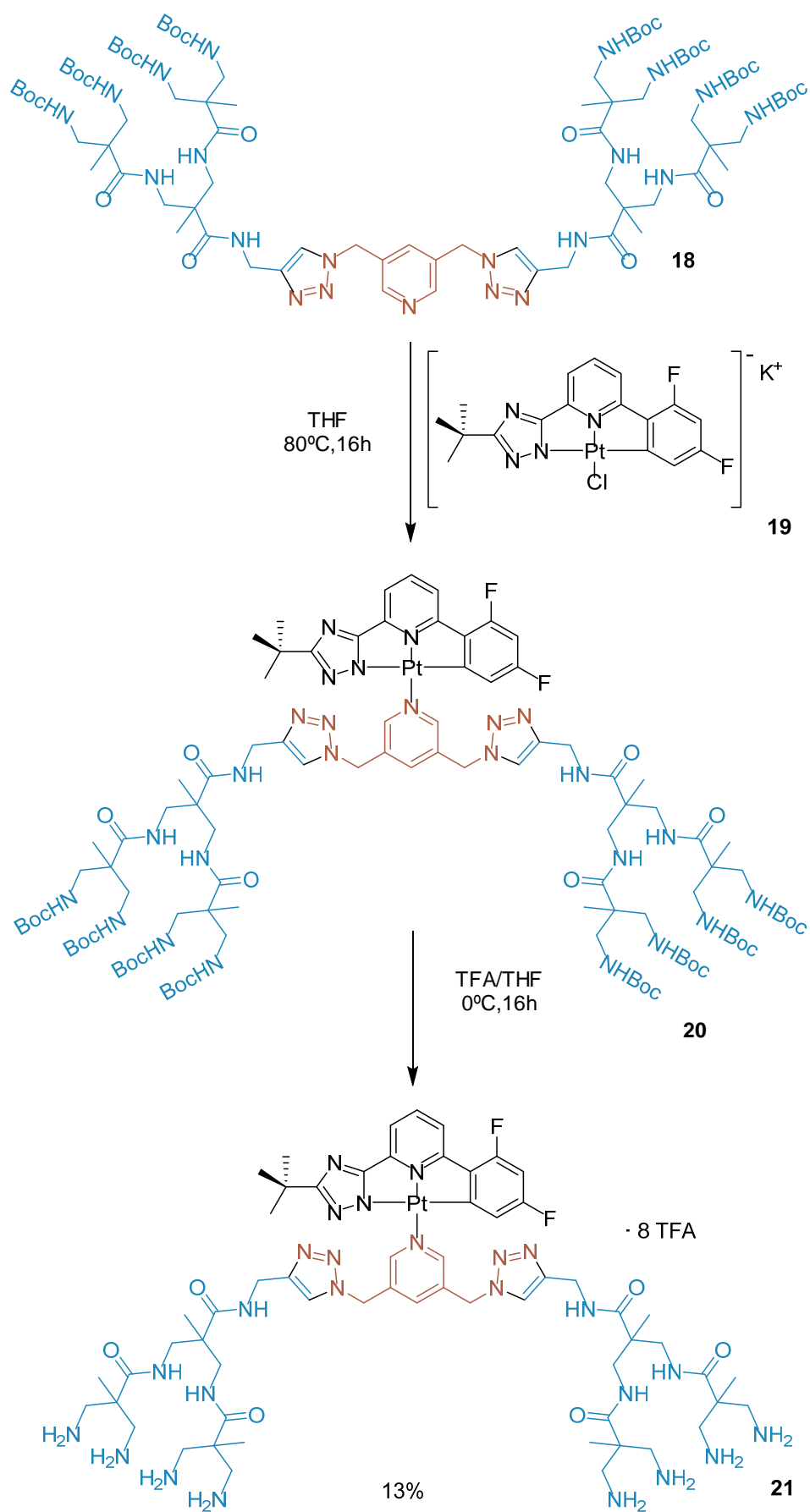


Figura 13. Síntesis de **18**.

El compuesto **18** fue caracterizado mediante técnicas de resonancia magnética y espectroscopía de masas. Además, se realizaron experimentos de infrarrojo y se comprobó que la banda debido a grupos azida desaparecía por completo tras la reacción *click*.

El grupo del Prof. Strassert facilitó el precursor de platino y la reacción con **13** se llevó a cabo usando THF como disolvente y calentando a reflujo durante 16 horas. Después de la eliminación del disolvente se procedió directamente a la desprotección de los grupos amino en presencia de TFA. El producto final (**21**), totalmente soluble en agua, fue purificado mediante cromatografía de exclusión (Figura 14).

Figura 14. Síntesis de **21**.

Desafortunadamente, debido a la labilidad del enlace entre la parte dendrítica y el compuesto de platino, no se pudo obtener un espectro de masas. Sin embargo, se llevaron a cabo experimentos DOSY de una disolución 10^{-3}M del compuesto en agua que confirmaron la presencia de una única especie.^{215,155}

Así mismo, se registraron los espectros de absorción, emisión y excitación de una disolución acuosa 10^{-5}M de **21**. En el espectro de absorción se observa una banda ancha a 260-360 nm y el espectro de emisión presenta una λ_{max} a 500 nm ($\lambda_{\text{exc}} = 350$ nm). Los rendimientos cuánticos de disoluciones 10^{-5}M en presencia y ausencia de oxígeno fueron de $\Phi_{\text{L}} = 0.05$ y $\Phi_{\text{L}} = 0.12$ respectivamente, mientras que los tiempos de vida calculados fueron 11 μs y 16 μs .

Se llevaron a cabo experimentos de emisión a diferentes concentraciones ($10^{-6} - 10^{-4}\text{M}$), viéndose a concentración 10^{-4}M una contribución despreciable de la emisión de agregados, caracterizados por una banda a 650 nm. Cabe destacar que complejos similares de platino, sin embargo, solo presentan emisión como resultado de la formación de estos agregados o excímeros.^{188,199,266}

En las medidas de emisión bajo excitación de dos fotones (TPE) se comprobó que el espectro de emisión obtenido ($\lambda_{\text{exc}} = 720$ nm) coincide con el obtenido bajo excitación de un fotón (OPE) ($\lambda_{\text{exc}} = 350$ nm). El cálculo de la sección eficaz (δ) mediante experimentos de fluorescencia excitada con dos fotones (TPEF) dio un resultado de 3.90 GM a 710 nm.

Por último, se llevaron a cabo estudios de fotoestabilidad de **21**, registrándose los espectros de emisión y excitación de una disolución acuosa 10^{-5}M a diferentes intervalos de tiempo durante 48 horas. En ellos, no se percibieron diferencias, confirmándose la estabilidad del compuesto en disolución acuosa durante al menos 48 horas a temperatura ambiente.

En colaboración con el grupo del Dr. Perez-Pomares y el Dr. Guadix del Departamento de Biología Animal de la Universidad de Málaga, se estudiaron las posibles aplicaciones de **21** como marcador multicanal. Para ello, bacterias *E. coli* (Gram negativas) fueron incubadas en presencia de **21** frente a otras bacterias control. Las imágenes de microscopía confocal fueron muy alentadoras ya que las bacterias incubadas con **21** presentaban una luminiscencia cuando eran excitadas a 405 nm en OPE y a 720 nm en TPE, que contrastaba claramente con la falta de

luminiscencia en las bacterias control. Las características de la luminiscencia que presentaban las bacterias incubadas con **21** coinciden con las del compuesto **21** en disolución, demostrándose que dicha luminiscencia es debida adhesión del compuesto a las bacterias. De forma análoga, se estudió la luminiscencia en bacterias *P. subtilis* (Gram positiva) y no llegándose a apreciar diferencias en el marcaje con respecto a los resultados obtenidos anteriormente con bacterias *E. coli*. La presencia de Pt en la membrana de bacterias *E. coli* fue confirmada por los resultados de análisis EDX.

Por último, en colaboración con el grupo del Dr. Díaz-Martínez y el Dr. Romero del Departamento de Microbiología de la Universidad de Málaga, se analizó el efecto bactericida de **21** en bacterias Gram negativas y Gram positivas. No se observaron cambios significativos en el crecimiento de bacterias *E. coli* en presencia de **21** en concentraciones desde 10 a 100 μM , sin embargo, el crecimiento *P. subtilis* se vio afectado a concentraciones de 100 μM de **21**.

Modificación de superficies de titanio con estructuras dendríticas funcionalizadas con el patrón RGD

El titanio es uno de los materiales más usados en prótesis debido a su biocompatibilidad, sus propiedades mecánicas, su resistencia a la corrosión, y la posibilidad, bajo las condiciones adecuadas, de formar conexiones estructurales y funcionales con la materia ósea.²¹⁸ Los trastornos musculoesqueléticos son uno de los problemas de salud más extendidos en el mundo debido al hecho de que nos encontramos frente a una población envejecida, por lo que la investigación en el campo de la ortopedia ha experimentado un crecimiento para impulsar el desarrollo de nuevos implantes con mejores tiempos de vida y menor riesgo de rechazo.

Cuando un biomaterial es implantado en el cuerpo humano, se pueden dar los siguientes procesos:

i) Proliferación y diferenciación de células óseas en la superficie del material que dará lugar a la oseointegración. Este es el resultado que se desea cuando se usan implantes.

ii) Respuesta inflamatoria y rechazo del implante.

iii) Formación de tejido fibroso en la superficie del material, impidiendo la oseointegración.

La topografía y las propiedades químicas de la superficie de estos materiales juegan un papel crucial en su biocompatibilidad. Diversos estudios señalan que la rugosidad de las superficies afecta a la morfología y el crecimiento celular,²²² favoreciéndose la adhesión de osteoblastos en superficies rugosas.²²³

Para favorecer la oseointegración y disminuir el riesgo de respuestas adversas, las investigaciones se han centrado tradicionalmente en el recubrimiento de la superficie de los implantes con materiales bioactivos, uno de los más usados desde los años ochenta siendo la hidroxiapatita (HA).²³¹

Sin embargo, recientes investigaciones han centrado sus esfuerzos en la inmovilización de moléculas con funciones biológicas, especialmente péptidos que participan en procesos de adhesión y crecimiento, en la superficie de estos materiales. Se ha demostrado la relación entre la adhesión mediada por integrinas (proteínas de la membrana que interaccionan con componentes de la matriz extracelular) con procesos de proliferación y diferenciación.²³⁶ Entre los patrones de péptidos que interaccionan específicamente con las integrinas, el patrón RGD ha sido ampliamente estudiado, cuyos primeros estudios en los años ochenta ya mostraron la importancia de esta secuencia péptida en los procesos de adhesión celular.^{237,238}

A su vez, las células mesenquimales (MSCs) son células multipotentes que poseen la capacidad de diferenciarse en diferentes tipos de células como osteoblastos, condrocitos y otras células de tejido conectivo. Desde los años ochenta, cuando se optimizó su aislamiento, su aplicación en ingeniería de tejidos ha sido ampliamente estudiada.^{239,240}

La secuencia péptida RGD puede actuar como promotor de la adhesión y proliferación de MSCs. Numerosos estudios se han centrado en la modificación de superficies con este patrón con la intención de mejorar la oseointegración.²⁴³ Tradicionalmente, las técnicas usadas en la modificación de superficies de biomateriales con RGD consisten en monocapas autoensambladas²⁵⁰ o en la

inmovilización de RGD en la superficie de polímeros.²⁵¹ El acoplamiento puede llevarse a cabo mediante métodos de adsorción o covalentes, siendo estos últimos los preferidos ya que presentan una unión más estable.

En los últimos años ha crecido el interés en el uso de dendrímeros como conector entre la superficie del biomaterial y los compuestos bioactivos ya que la posibilidad de modificar su naturaleza y controlar el número de grupos terminales los hacen altamente interesantes.

En este ámbito, nuestro grupo ha estudiado los efectos en la adhesión celular de MSCs en una superficie de poliestireno y la influencia que tiene la orientación del patrón RGD. Para ello, dos tetrapéptidos, RGD-Cys y Cys-RGD, se unieron a un dendrímero PAMAM funcionalizado con grupos maleimida. Los resultados confirmaron que la orientación influye en la respuesta celular, obteniéndose mejores resultados con RGD-Cys.¹²⁷ Además, nuestro grupo ha estudiado el uso de dendrímeros como una herramienta para controlar la densidad de RGD en una superficie y sus efectos en la adhesión de MSCs y la diferenciación condrogénica temprana.¹²⁸

Es por ello que en este trabajo se ha propuesto la modificación de superficies de titanio con estructuras dendríticas que posteriormente serían funcionalizadas con el tetrapéptido RGD-Cys.

Para este proyecto se ha usado el compuesto **12**, sintetizado anteriormente. Los discos de titanio (grosor 1 mm, diámetro 9 mm) fueron aportados por el grupo del Dr. Becerra y la Dra. Santos del Departamento de Biología Celular, Genética y Fisiología de la Universidad de Málaga. El primer paso fue el tratamiento de las superficies con una mezcla de ácido sulfúrico y peróxido de hidrógeno (**I**).²⁶⁰ A continuación, los discos fueron tratados con una disolución de APTMS en etanol, modificando su superficie con grupos amino (**II**) que reaccionaran en el siguiente paso con los grupos carboxílicos del compuesto **12** (Figura 15).

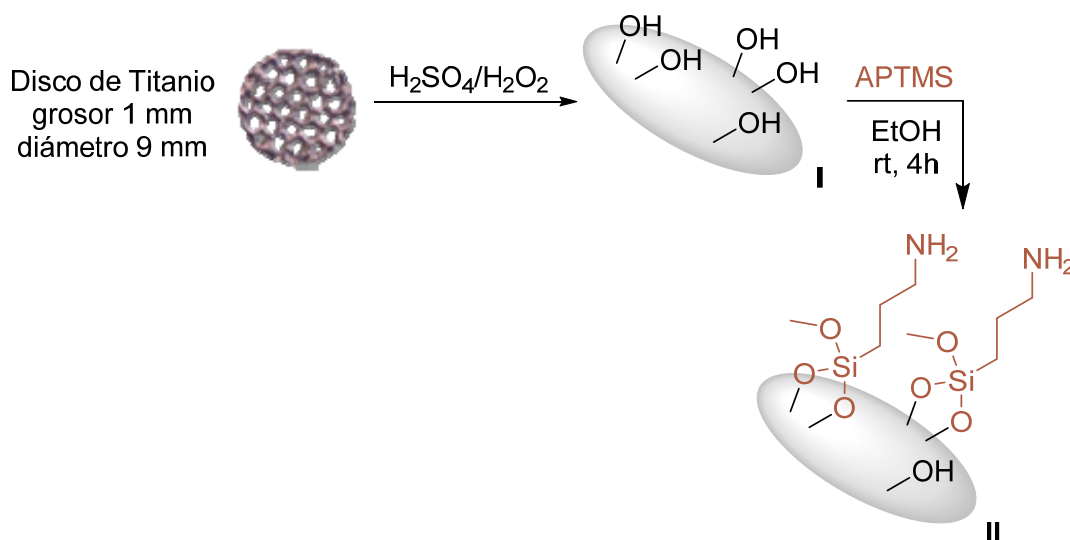


Figura 15. Preparación de los discos **II**.

La unión covalente de **12** a la superficie de los discos de titanio (**III**) se llevó a cabo mediante la formación de enlaces amida y usando CDI como agente activante (Figura 16).

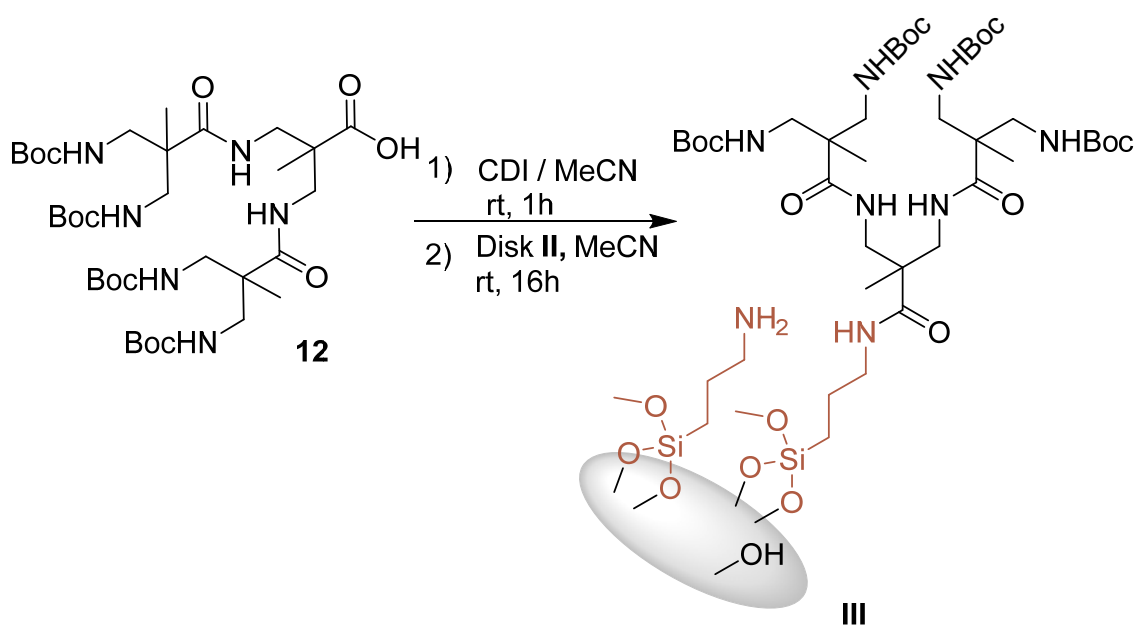


Figura 16. Preparación de los discos **III**.

Los discos (**III**) fueron tratados a continuación con glicidol con el objeto de bloquear los posibles grupos aminos que no hubieran reaccionado con **12**, (**IV**).

La desprotección de los grupos amino del dendrón (V) se realizó en presencia de ácido clorhídrico (Figura 17).

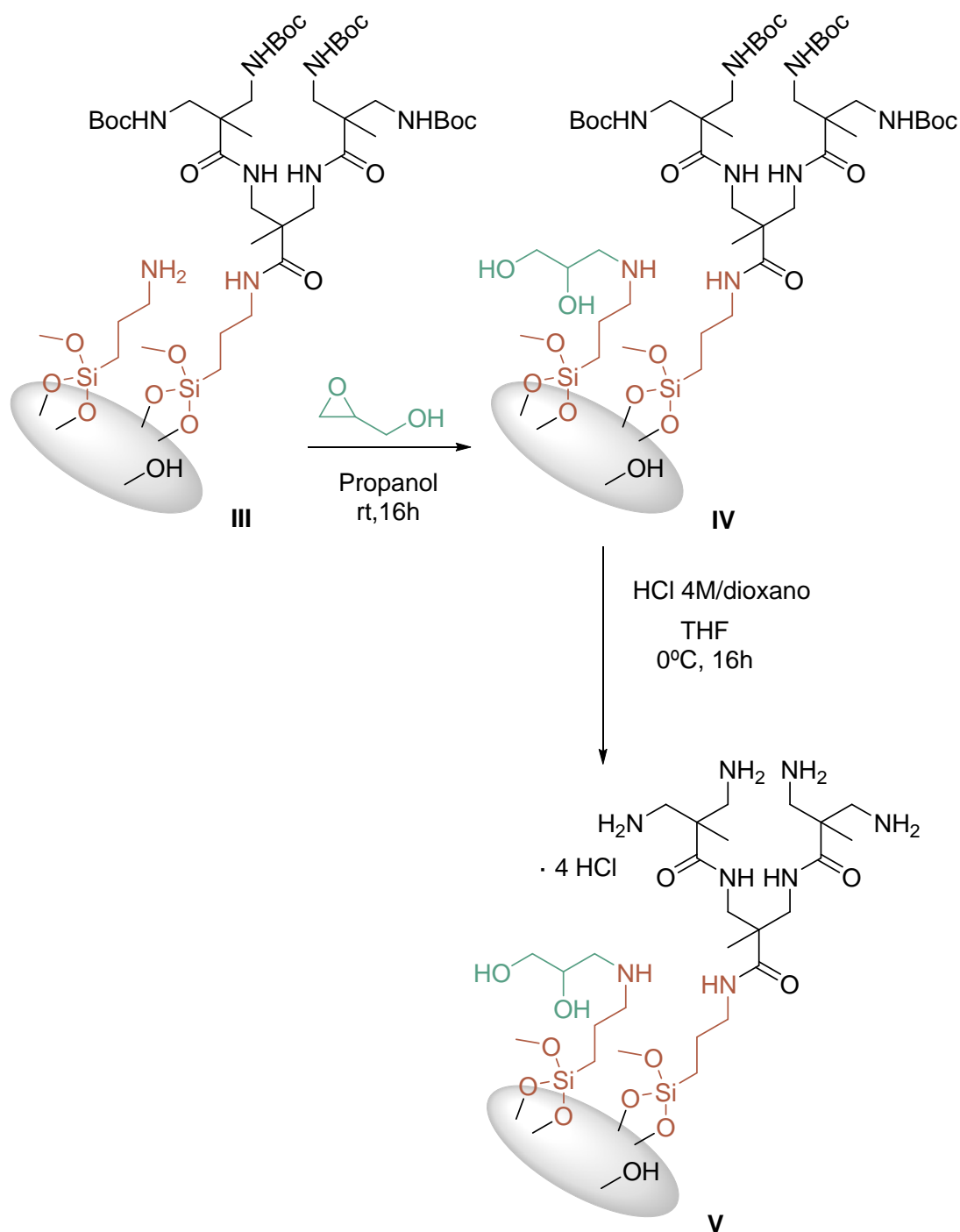


Figura 17. Preparación de los discos V.

La introducción del patrón RGD-Cys se llevó a cabo a través del grupo tiol terminal. Para ello, fue necesario la funcionalización de los discos con un grupo maleimida (VI) por lo que, siguiendo la experiencia del grupo,^{127,128} se sintetizó

un derivado de β -alanina (**22**). El paso final consistió en la inmersión de los discos **VI** en una disolución de RGD-Cys en PBS (Figura 18).

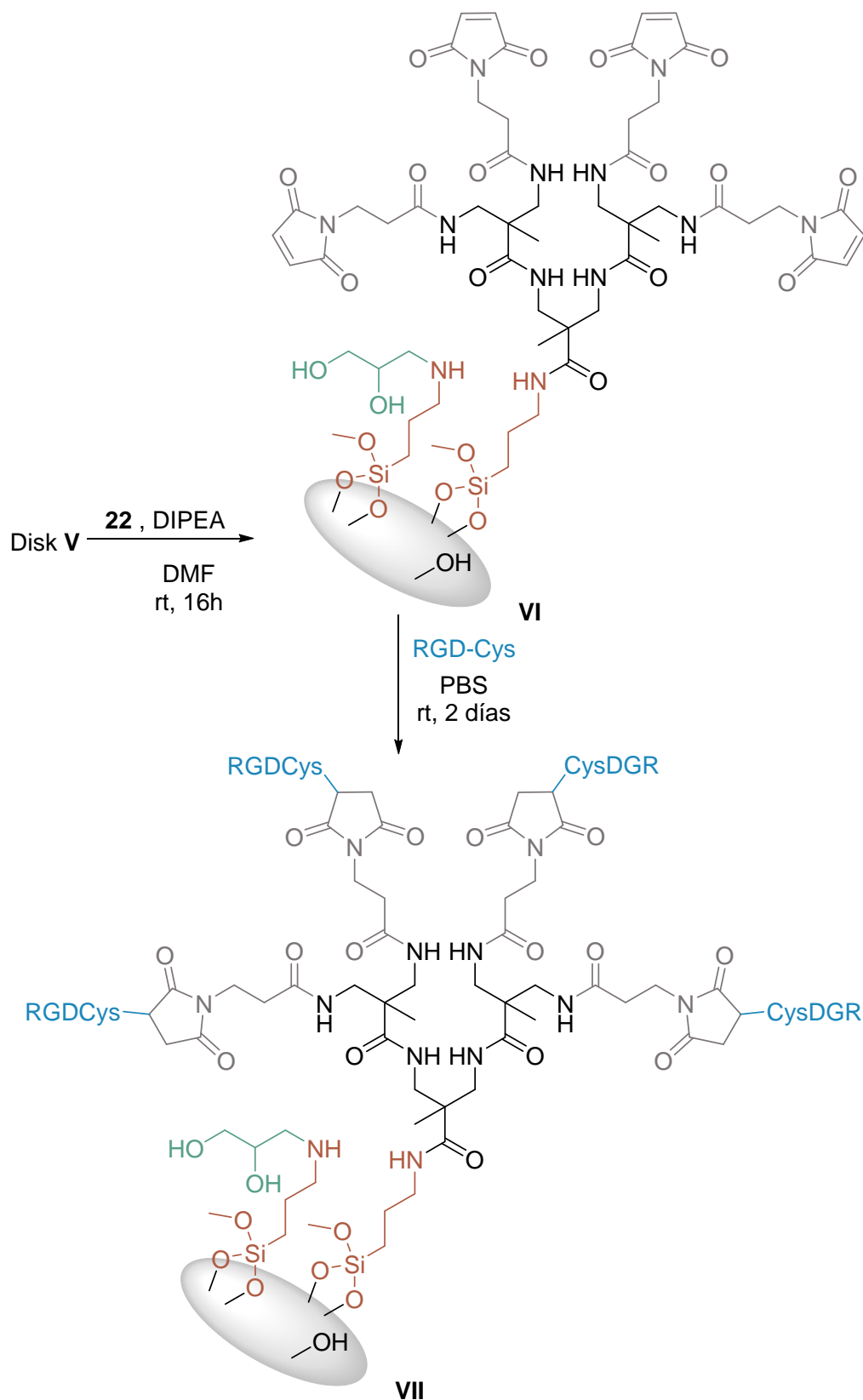


Figura 18. Preparación de los discos **VII**.

En todos los pasos de funcionalización de las superficies de titanio se llevó a cabo un control del número de grupos amino libres en los discos mediante el ensayo de ninhidrina.¹²⁴ La correcta inmovilización del péptido en la superficies de titanio vino corroborada por los experimentos de XPS. Los resultados obtenidos mediante esta técnica indicaron que la composición las superficies de titanio que no modificadas con el péptido (VI) estaba compuesta por titanio, oxígeno, nitrógeno y carbono mientras que tras la modificación (VII) los datos obtenidos confirmaron la presencia de azufre, presente únicamente en el péptido.

Tras estos resultados, se realizaron, en colaboración con el grupo del Dr. Becerra y la Dra. Santos del Departamento de Biología Celular, Genética y Fisiología de la Universidad de Málaga, ensayos con células pre-osteoblásticas. Se estudiaron la adhesión y proliferación de estas células en las superficies modificadas con el patrón RGD (VII) y su comparación con discos control no funcionalizados (VI).

En los estudios de adhesión no se apreciaron diferencias importantes entre los discos funcionalizados y los controles. Sin embargo, en los estudios de proliferación se apreció un aumento de ésta en los discos funcionalizados y parece apuntar a la formación de tejido sobre las superficies, lo que crearía una interfaz hueso-prótesis más favorable.